

UNC FILE COPY

AD-A202 878

UNITED STATES AIR FORCE

GRADUATE STUDENT SUMMER
SUPPORT PROGRAM

1986

PROGRAM TECHNICAL REPORT
UNIVERSAL ENERGY SYSTEMS, INC.

VOLUME 1 of 2

PROGRAM DIRECTOR, UES

RODNEY C. DARRAH

PROGRAM ADMINISTRATOR, UES

SUSAN K. ESPY

PROGRAM MANAGER, A.F.O.S.R.

MAJOR RICHARD KOPKA

JAN 28 1989

SUBMITTED TO

AIR FORCE OFFICE OF SCIENTIFIC RESEARCH

BOLLING AIR FORCE BASE

WASHINGTON, DC

DECEMBER 1986

Approved for Public Release
Distribution Unlimited

89

1 23 602

BEST

AVAILABLE COPY

DISCLAIMER NOTICE

**THIS DOCUMENT IS BEST QUALITY
PRACTICABLE. THE COPY FURNISHED
TO DTIC CONTAINED A SIGNIFICANT
NUMBER OF PAGES WHICH DO NOT
REPRODUCE LEGIBLY.**

REPORT DOCUMENTATION PAGE

REPORT SECURITY CLASSIFICATION UNCLASSIFIED			1b. RESTRICTIVE MARKINGS	
2a. SECURITY CLASSIFICATION AUTHORITY			3. DISTRIBUTION/AVAILABILITY OF REPORT APPROVED FOR PUBLIC RELEASE; Distribution Unlimited	
2b. DECLASSIFICATION/DOWNGRADING SCHEDULE				
4. PERFORMING ORGANIZATION REPORT NUMBER(S)			5. MONITORING ORGANIZATION REPORT NUMBER(S) AFOSR-TR- 87-0304	
6a. NAME OF PERFORMING ORGANIZATION Universal Energy Systems, Inc.		6b. OFFICE SYMBOL (If applicable)	7a. NAME OF MONITORING ORGANIZATION AFOSR/XOT	
6c. ADDRESS (City, State and ZIP Code) 4401 Dayton-Xenia Road Dayton, OH 45432			7b. ADDRESS (City, State and ZIP Code) Building 410 Bolling AFB, DC 20332-6448	
8a. NAME OF FUNDING/SPONSORING ORGANIZATION AFSOR		8b. OFFICE SYMBOL (If applicable) XOT	9. PROCUREMENT INSTRUMENT IDENTIFICATION NUMBER F49620-85-C-0013	
8c. ADDRESS (City, State and ZIP Code) Building 410 Bolling AFB, DC 20332			10. SOURCE OF FUNDING NOS.	
			PROGRAM ELEMENT NO. 61102F	PROJECT NO. 3396
11. TITLE (Include Security Classification) USAF Graduate Student Summer Support Program			TASK NO. D5	
12. PERSONAL AUTHOR(S) Rodney C. Darrah, Susan K. Espy				
13a. TYPE OF REPORT Annual		13b. TIME COVERED FROM _____ TO _____	14. DATE OF REPORT (Yr., Mo., Day) December 1986	
15. PAGE COUNT				
16. SUPPLEMENTARY NOTATION				
17. COSATI CODES			18. SUBJECT TERMS (Continue on reverse if necessary and identify by block number)	
FIELD	GROUP	SUB. GR.		
19. ABSTRACT (Continue on reverse if necessary and identify by block number) See Attached				
20. DISTRIBUTION/AVAILABILITY OF ABSTRACT CLASSIFIED/UNLIMITED <input checked="" type="checkbox"/> SAME AS RPT. <input type="checkbox"/> DTIC USERS <input type="checkbox"/>			21. ABSTRACT SECURITY CLASSIFICATION UNCLASSIFIED	
22a. NAME OF RESPONSIBLE INDIVIDUAL Major Richard W. Kopka, Program Manager			22b. TELEPHONE NUMBER (Include Area Code) 202-767-4970	22c. OFFICE SYMBOL XOT

I. INTRODUCTION

Universal Energy Systems, Inc. (UES) was awarded the United States Air Force Summer Faculty Research Program on August 15, 1984. The contract is funded under the Air Force Systems Command by the Air Force Office of Scientific Research.

The program has been in existence since 1978 and has been conducted by several different contractors. The success of the program is evident from its history of expansion since 1978.

The Summer Faculty Research Program (SFRP) provides opportunities for research in the physical sciences, engineering, life sciences, business, and administrative sciences. The program has been effective in providing basic research opportunities to the faculty of universities, colleges, and technical institutions throughout the United States.

The program is available to faculty members in all academic grades: instructor, assistant professor, professor, department chairman, and research facility directors. It has proven especially beneficial to young faculty members who are starting their academic research programs and to senior faculty members who have spent time in university administration and are desirous of returning to scholarly research programs.

Beginning with the 1982 program, research opportunities were provided for 17 graduate students. The 1982 pilot student program was highly successful and was expanded in 1983 to 53 students; there were 84 graduate students in the 1984 program.

In the previous programs, the graduate students were selected along with their professors to work on the program. Starting with the 1985 program, the graduate students were selected on their own merits. They were assigned to be supervised by either a professor on the program or by an engineer at the Air Force Laboratories participating in the program. There were 92 graduate students selected for the 1985 program.

Again in the 1986 program, the graduate students were selected on their own merits, and assigned to be supervised by either a professor on the program or by an engineer at the participating Air Force Laboratory. There were 100 graduate students selected for the 1986 program.

Follow-on research opportunities have been developed for a large percentage of the participants in the Summer Faculty Research Program in 1979-1983 period through an AFOSR Minigrant Program.

On 1 September 1983, AFOSR replaced the Minigrant Program with a new Research Initiation Program. The Research Initiation Program provides follow-on research awards to home institutions of SFRP participants. Awards were made to approximately 50 researchers in 1983. The awards were for a maximum of \$12,000 and a duration of one year or less. Substantial cost sharing by the schools contributes significantly to the value of the Research Initiation Program. In 1984 there were approximately 80 Research Initiation awards.

UNITED STATES AIR FORCE

GRADUATE STUDENT SUMMER SUPPORT PROGRAM

1986

PROGRAM TECHNICAL REPORT

UNIVERSAL ENERGY SYSTEMS, INC.

VOLUME 1 of 11

Program Director, UES
Rodney C. Darrah

Program Manager, AFOSR
Major Richard Kopka

Program Administrator, UES
Susan K. Espy

Submitted to

Air Force Office of Scientific Research

Bolling Air Force Base

Washington, DC

December 1986



Accession For	
NTIS CRA&I	<input checked="" type="checkbox"/>
DTIC TAB	<input type="checkbox"/>
Unannounced	<input type="checkbox"/>
Justification	
By	
Distribution	
Availability Codes	
Dist	Available for Special
A-1	

TABLE OF CONTENTS

<u>Section</u>	<u>Page</u>
Preface	i
List of 1986 Graduate Student Participants	ii
Participant Laboratory Assignment	xix
Research Reports	xxii

PREFACE

The United States Air Force Graduate Student Summer Support Program (USAF-GSSSP) is conducted under the United States Air Force Summer Faculty Research Program. The program provides funds for selected graduate students to work at an appropriate Air Force Facility with a supervising professor who holds a concurrent Summer Faculty Research Program appointment or with a supervising Air Force Engineer. This is accomplished by the students being selected on a nationally advertised competitive basis for a ten-week assignment during the summer intersession period to perform research at Air Force laboratories/centers. Each assignment is in a subject area and at an Air Force facility mutually agreed upon by the students and the Air Force. In addition to compensation, travel and cost of living allowances are also paid. The USAF-GSSSP is sponsored by the Air Force Office of Scientific Research, Air Force Systems Command, United States Air Force, and is conducted by Universal Energy Systems, Inc.

The specific objectives of the 1986 USAF-GSSSP are:

- (1) To provide a productive means for the graduate students to participate in research at the Air Force Weapons Laboratory;
- (2) To stimulate continuing professional association among the Scholars and their professional peers in the Air Force;
- (3) To further the research objectives of the United States Air Force;
- (4) To enhance the research productivity and capabilities of the graduate students especially as these relate to Air Force technical interests.

During the summer of 1986, 100 graduate students participated. These researchers were assigned to 25 USAF laboratories/centers across the country. This two volume document is a compilation of the final reports written by the assigned students members about their summer research efforts.

LIST OF 1986 GRADUATE STUDENT PARTICIPANTS

NAME/ADDRESS

DEGREE, SPECIALTY, LABORATORY ASSIGNED

Susan M. Abrams
University of Illinois
Dept. of Bioengineering
Chicago, IL 60680
(312) 996-8661

Degree: B.S., Human Factors
Engineering, 1984
Specialty: Zoology
Assigned: HRL/OT

William H. Acton
University of New Mexico
Dept. of Psychology
Albuquerque, NM 87131
(505) 277-4121

Degree: M.A., Applied Behavioral
Science, 1984
Specialty: Psychology
Assigned: AAMRL

Julie A. Albertson
Washington State University
Dept. of Mechanical Engineering
Pullman, WA 99164-2920
(509) 335-8654

Degree: B.S., Mechanical
Engineering, 1985
Specialty: Mechanical Engineering
Assigned: FJSRL

Jay H. Ambrose
University of Kentucky
Dept. of Mechanical Engineering
Lexington, KY 40506
(606) 257-2663

Degree: M.S., Mechanical
Engineering, 1985
Specialty: Mechanical Engineering
Assigned: APL

Mark R. Anderson
Purdue University
School of Aeronautics and
Astronautics
Grissom Hall
W. Lafayette, IN 47907
(317) 494-5154

Degree: M.S., Engineering,
Aeronautics and Astro-
nautics, 1984
Specialty: Engr. Aeronautics and
Astronautics
Assigned: FDL

Stanley F. Anton
Rutgers-The State University
of New Jersey
Psychology Department
Psychology Bldg.
Busch Campus
New Brunswick, NJ 08903
(201) 932-4036

Degree: M.S., Cognitive
Psychology, 1986
Specialty: Cognitive Psychology
Assigned: AAMRL

Christopher P. Antworth
Florida State University
Department of Chemistry
Box 13
Tallahassee, FL 32306
(904) 644-1274

Degree: B.S., Chemistry, 1980
Specialty: Chemistry
Assigned: ESC

Sherif A. Aziz
Wright State University
Systems Engineering
School of Engineering
130 Eng. and Math Bldg.
Dayton, OH 45435
(513) 873-2403

Degree: B.S., Systems and
Biomedical Eng., 1984
Specialty: Biomedical Engineering
Assigned: AAMRL

Alan H. Baginski
University of Lowell
Electrical Engineering
Lowell, MA 01854
(617) 452-5000

Degree: B.S., Electrical
Engineering, 1983
Specialty: Electrical Engineering
Assigned: RADC

Joseph M. Boroughs
University of New Mexico
Psychology Department
Albuquerque, NM 87131
(505) 277-4121

Degree: M.A., Psychology, 1981
Specialty: Psychology
Assigned: AAMRL

Dale T. Bracken
University of Georgia
Dept. of Psychology
302 Morris Hall
Athens, GA 30602
(404) 542-8362

Degree: B.S., Psychology, 1985
Specialty: Psychology
Assigned: HRL/ID

Angela M. Braun
Trinity University
Biology Department
715 Stadium Drive
San Antonio, TX 78212
(512) 736-7011

Degree: B.A., Biology, 1986
Specialty: Biology
Assigned: SAM

David A. Bridenstine
Arizona State University
Mechanical & Aerospace
Engineering
Tempe, AZ 85287
(602) 965-3291

Degree: M.S., Engineering, 1985
Specialty: Engineering
Assigned: ML

Paul E. Bussey
University of Colorado at
Colorado Springs
Austin Bluffs Parkway
Colorado Springs, CO 80933-7150
(303) 593-3351

Degree: B.S., Electrical
Engineering, 1986
Specialty: Electrical Engineering
Assigned: FJSRL

Timothy T. Clark
University of New Mexico
Mechanical Engineering
Albuquerque, NM 87131
(505) 277-2761

Degree: BSME, Fluid Dynamics, 1983
Specialty: Mechanical Engineering
Assigned: WL

Otis Cosby, Jr.
Meharry Medical College
School of Medicine
1005 D. B. Todd Jr. Blvd.
Nashville, TN 37208
(615) 327-6223

Degree: BS, Natural Science, 1983
Specialty: Natural Science
Assigned: SAM

Jennifer L. Davidson
Department of Mathematics
University of Florida
201 Walker Hall
Gainesville, FL 32611
(904) 392-0268

Degree: M.S., Mathematics, 1986
Specialty: Mathematics
Assigned: AD

Douglas W. DeHart
University of Wisconsin-Madison
Dept. of Engineering Mechanics
1415 Johnson Drive
Madison, WI 53706
(608) 262-3990

Degree: B.S., Engineering
Mechanics, 1985
Specialty: Engineering Mechanics
Assigned: RPL

Brian J. Doherty
Duke University
Biomedical Engineering Dept.
Durham, NC 27706
(919) 684-6185

Degree: B.S.E., Bioengineering, 1984
Specialty: Bioengineering
Assigned: AAMRL

Franklin J. Dunmore
Howard University
Dept. of Physics and Astronomy
2355 Sixth Street, N.W.
Washington, D.C. 20059
(202) 636-6241

Degree: B.S., Physics, 1982
Specialty: Physics
Assigned: ML

Michael P. Farr
Pennsylvania State University
312 Steidle Building
University Park, PA 16802
(814) 863-0154

Degree: M.S., Polymer Science, 1984
Specialty: Polymer Science
Assigned: ML

Christopher A. Feild
Dickinson College
Box 914
Carlisle, PA 17013
(717) 245-1533

Degree: B.S., Chemistry, 1986
Specialty: Chemistry
Assigned: ML

Michelle J. Ferry
Wright State University
Dayton, OH 45435
(513) 873-2855

Degree: B.S., Chemistry, 1984
Specialty: Chemistry
Assigned: AAMRL

Carl V. Frank
Univ. of Southern Mississippi
Computer Science Dept.
Southern Station, Box 9157
Hattiesburg, MS 39406-9157
(601) 266-3216

Degree: B.S., Computer Science,
1985
Specialty: Computer Science
Assigned: SAM

Beverley A. Gable
Ohio University
Psychology Dept.
1222 Carriage Hill
Athens, OH 45701
(614) 594-7167

Degree: B.S., Psychology, 1984
Specialty: Psychology
Assigned: AAMRL

Michael D. Garner
University of North Carolina at
Greensboro
Physics Dept.
Greensboro, NC 27412
(919) 379-5844

Degree: B.S., Physics, 1984
Specialty: Physics
Assigned: RADDC

Maurice B. Gilbert
Meharry Medical College
Medicine Department
1005 Dr. D.B. Todd Blvd.
Nashville, TN 37208
(615) 327-6111

Degree: B.S., Biology, 1982
Specialty: Biology
Assigned: SAM

Beverly E. Girten
Ohio State University
Exercise Physiology and
Physiological Chemistry Dept.
College of Medicine
333 W. 10th Avenue
Columbus, OH 43210
(614) 422-1462

Degree: M.S., Exercise
Physiology, 1983
Specialty: Physiology,
Assigned: AAMRL

Ellen S. Goldey
Miami University
Zoology Dept.
210 N. Main #4
Oxford, OH 45056
(513) 529-3451

Degree: B.S., Biology, 1984
Specialty: Biology
Assigned: AAMRL

Alfred W. Gordon
Atlanta University
Dept. of Biology
360 Westview Drive, S.W.
Atlanta, GA 30314
(404) 681-0251

Degree: B.A., Biology, 1976
Specialty: Biology
Assigned: SAM

Nadia C. Greenidge
New York University
Dept. of Anthropology
25 Waverly Place
New York City, NY
(212) 598-3258

Degree: M.S., Physical Anthropology
Specialty: Physical Anthropology
Assigned: AAMRL

Peggy J. Grigsby
Wright State University
Physics Department
Dayton, OH
(513) 873-2950

Degree: M.S., Mathematics, 1978
Specialty: Mathematics
Assigned: ML

Brad L. Halverson
Washington State University
Dept. of Civil and Environmental
Engineering
Sloan Hall 102
Structures Section
Pullman, WA 99164-2914
(509) 335-4921

Degree: B.S., Civil Engineering,
1985
Specialty: Civil Engineering
Assigned: WL

Charles R. Hammond
Vanderbilt University
Dept. of Mechanical and
Materials Engineering
P O Box 1592, Station B
Nashville, TN 37235
(615) 322-0892

Degree: M.S., Mechanical
Engineering, 1983
Specialty: Mechanical Engineering
Assigned: AEDC

Darren E. Hart
Texas A&M University
Dept. of Psychology
College Station, TX 77843
(409) 845-2581

Degree: B.A., Psychology, 1984
Specialty: Psychology
Assigned: HRL/MO

Peter V. Hlinomaz
University of Michigan-Dearborn
4901 Evergreen Road
Dearborn, MI 48128
(313) 593-5420

Degree: B.S., Electrical
Engineering, 1985
Specialty: Electrical Engineering
Assigned: RADC

Stephen Hom
Massachusetts Institute of
Technology
Mechanical Engineering Dept.
77 Massachusetts Avenue
Cambridge, MA 02139
(617) 253-5028

Degree: M.S., Structural
Engineering, 1977
Specialty: Structural Engineering
Assigned: ML

Jamal A. Hussein
University of Toledo
Mechanical Engineering Dept.
2801 W. Bancroft
Toledo, OH 43606
(419) 537-2620

Degree: M.S., Mechanical
Engineering, 1986
Specialty: Mechanical Engineering
Assigned: APL

David W. Jansen
Dept. of Zoology
Washington State University
Pullman, WA 99164-4220
(509) 336-3564

Degree: M.S., Zoology, 1980
Specialty: Zoology
Assigned: AAMRL

Karl K. Klett, Jr.
University of Wyoming
P O Box 3905
University Station
Laramie, WY 82071
(307) 766-6150

Degree: B.S., 1979
Specialty: Astrophysics
Assigned: AFGL

Raymond M. Kolonay
Ohio State University
Dept. of Civil Engineering
2070 Niel Avenue
Hitchcock Hall, Room 470
Columbus, OH 43210
(614) 422-2771

Degree: B.S., Civil Engineering,
1985
Specialty: Civil Engineering
Assigned: FDL

Craig A. Langenfeld
Ohio State University
Mechanical Engineering Dept.
305 Stonemill Road
Dayton, OH 45409
(513) 299-3218

Degree: B.S., Mechanical
Engineering, 1986
Specialty: Mechanical Engineering
Assigned: APL

Tieu-Binh Le
Wright State University
Chemistry Dept.
Dayton, OH 45435
(513) 873-2855

Degree: B.S., Chemistry, 1985
Specialty: Chemistry
Assigned: ML

Mark W. Lisee
University of Lowell
Dept. of Electrical Engineering
Box 2615
North Campus
1 University Avenue
Lowell, MA 01854
(617) 452-5000

Degree: B.S.E.E., expected 1988
Specialty: Electrical Engineering
Assigned: AFGL

Robert K. Littleton
University of Colorado
Physics Department
Austin Bluffs Parkway
Colorado Springs, CO 80903
(303) 593-3000

Degree: B.S., Chemistry, 1975
Specialty: Chemistry
Assigned: FJSRL

George A. Liu
Meharry Medical College
Dept. of Physiology
1005 18th Avenue, North
Nashville, TN
(615) 327-6413

Degree: B.A., Chemistry, 1986
Specialty: Chemistry
Assigned: SAM

Isabel Lopez
Wright State University
Dept. of Chemistry
Dayton, OH 45435
(513) 873-2855

Degree: M.S., Chemistry, 1985
Specialty: Chemistry
Assigned: AAMRL

Michael M. Lukes
Florida State University
Meteorology Dept.
Tallahassee, FL 32306
(904) 644-6205

Degree: B.S., Meteorology, 1973
Specialty: Meteorology
Assigned: ESC

Wayne R. Lundberg
Wright State University
Dept. of Physics and Mechanical
Engineering
3640 Col. Glenn Hiway
Dayton, OH 45435
(513) 873-2954

Degree: B.S., Physics, 1985
Specialty: Physics
Assigned: ML

William A. Marty
University of Oklahoma
Electrical Engineering and
Computer Science
202 West Boyd, Room 219
Norman, OK 73069
(405) 325-4721

Degree: B.S., Electrical
Engineering, 1985
Specialty: Electrical Engineering
Assigned: AL

Mary R. McGill
Eastern Kentucky University
Dept. of Chemistry
1661 Foxhaven #3
Richmond, KY 40475
(606) 624-9772

Degree: B.S., Chemistry, 1985
Specialty: Chemistry
Assigned: ESC

Jennifer McGovern-Weidner
University of Florida
Dept. of Psychology
114 Psychology Bldg.
Gainesville, FL 32611
(904) 392-0605

Degree: M.A., Gifted Education, 1983
Specialty: Psychology
Assigned: SAM

Dara C. Merenski
University of Dayton
Computer Science Dept.
300 College Park Drive
Dayton, OH 45469
(513) 229-2343

Degree: B.S., Systems Analysis, 1986
Specialty: Systems Analyst
Assigned: HRL/LR

Peter D. Meyer
University of Montana
Physics Department
Missoula, MT 59801
(406) 243-6535

Degree: B.A., Chemistry, 1984
Specialty: Chemistry
Assigned: AD

Douglas R. Moore
Univ. of Southern Mississippi
Dept. of Polymer Science
Southern Station Box 10076
Hattiesburg, MS 39406-0076
(601) 266-4868

Degree: B.S., Chemistry, 1977
Specialty: Chemistry
Assigned: ML

Eric V. Morris
Meharry Medical School
1005 18th Street, N.
Nashville, TN 37208
(615) 327-6000

Degree: B.S., Biological Sciences,
1984
Specialty: Pharmacology
Assigned: SAM

Russell Moy
Dept. of Chemical Engineering
The University of Michigan
2135 Dow Building
Ann Arbor, MI 48109-2136
(313) 764-3379

Degree: MSE, Chemical Engineering,
1982
Specialty: Chemical Engineering
Assigned: FJSRL

Glenn D. Munkvold
University of Texas at Austin
Dept. of Chemical Engineering
Austin, TX 78712
(512) 471-1046

Degree: B.S., Chemical Engineering,
1984
Specialty: Chemical Engineering
Assigned: SAM

Conrad R. Murray
Meharry Medical College
1005 D.B. Todd Blvd.
Nashville, TN 37208
(615) 327-6111

Degree: B.S., Pre-Medicine, 1983
Specialty: Medicine
Assigned: SAM

Victoria T. Nasman
Northwestern University
Psychology Department
CRESAP Laboratory
633 Clark Street
Evanston, IL 60201
(312) 492-7643

Degree: B.A., Psychology, 1983
Specialty: Psychology
Assigned: SAM

Sharon E. Navard
Univ. of Southwestern Louisiana
Dept. of Statistics
USL Box 44187
Lafayette, LA 70504
(318) 231-6772

Degree: M.S., Statistics, 1984
Specialty: Statistics
Assigned: AD

Bernadette P. Njoku
Meharry Medical College
School of Medicine
1005 D.B. Todd Blvd.
Nashville, TN 37208
(615) 327-4098

Degree: B.A., Chemistry, 1982
Specialty: Chemistry
Assigned: SAM

David P. Norton
Louisiana State University
Dept. of Electrical and
Computer Engineering
Baton Rouge, LA 70803
(504) 388-5488

Degree: M.S., Electrical
Engineering, 1986
Specialty: Electrical Engineering
Assigned: RADC

Roland L. Palmer
The University of Alabama-
Tuscaloosa
Psychology Department
Box 2968
University, AL 35486
(205) 348-5083

Degree: M.A., Psychology, 1985
Specialty: Psychology
Assigned: HRL/MO

Daniel S. Park
Univ. of Southern California
Aerospace Engineering
University Park
Los Angeles, CA 90089-0126
(213) 743-7177

Degree: MSAE, Aerospace
Engineering, 1985
Specialty: Aerospace Engineering
Assigned: FDL

April G. Parker
The Ohio State University
Dept. of Ceramic Engineering
177 Watts 2041 College Road
Columbus, OH 43202
(614) 422-2960

Degree: B.S., Ceramic
Engineering, 1985
Specialty: Ceramic Engineering
Assigned: ML

Deborah L. Parker
Tulane University
Psychology Department
2007 Percival Stern Hall
New Orleans, LA 70118
(504) 865-5331

Degree: M.A., Experimental
Psychology, 1985
Specialty: Psychology
Assigned: HRL/LR

Werner K. Perry
University of Florida
Computer and Info. Sciences
3117 S.W. 29 Avenue
Gainesville, FL 33312
(904) 374-8971

Degree: B.S., BEG-CIS, 1986
Specialty: Engineering
Assigned: AD

Frank M. Pitman
Clemson University
Mechanical Engineering Dept.
Clemson, SC 29631
(803) 654-5140

Degree: B.S., Mechanical
Engineering, 1985
Specialty: Mechanical Engineering
Assigned: FDL

Amy B. Powell
Texas A&M University
Psychology Department
College Station, TX 77843
(409) 845-0377

Degree: B.S., Psychology, 1984
Specialty: Psychology
Assigned: HRL/MO

Surya Raghu
Yale University
Dept. of Mechanical Engineering
Mason Laboratories
Box 2159
New Haven, CT 06520
(203) 436-8676

Degree: M.S., Engineering, 1980
M.S., M. Philosophy, 1986
Specialty: Aeronautical Engineering
Assigned: APL

Mark L. Ratcliff
University of Tennessee
Space Institute
Dept. of Mathematics
U.T.S.I. Upper E
Tullahoma, TN 37388
(615) 455-0631

Degree: B.A., Math, 1984
Specialty: Mathematics
Assigned: AFDC

Christopher Reed
University of Florida
Dept. of Engineering Sciences
Gainesville, FL 32611
(904) 392-0961

Degree: M.S., Engineering Science,
1984
Specialty: Aerodynamics
Assigned: AD

Gregg A. Reger
Univ. of Texas - San Antonio
Life Sciences Dept.
6900 Loop 1604 W.
San Antonio, TX 78285
(512) 691-4458

Degree: B.S., Dietics, 1981
Specialty: Dietics
Assigned: SAM

Anthony E. Restaino
State University of New York-
at Albany
Dept. of Atmospheric Science
1400 Washington Avenue
Albany, NY 12222
(518) 457-3987

Degree: B.S., Meteorology, 1984
Specialty: Meteorology
Assigned: AFGL

Dennis W. Richardson
Pennsylvania State University
Dept. of Electrical Engineering
322 Atherton Hall
University Park, PA 16802
(814) 862-7595

Degree: B.S., Electrical
Engineering, 1983
Specialty: Electrical Engineering
Assigned: AL

Kyle W. Ross
University of New Mexico
Dept. of Mechanical Engineering
Albuquerque, NM 87131
(505) 277-2761

Degree: B.S., Mechanical
Engineering, 1982
Specialty: Mechanical Engineering

Susan E. Sadofsky
Boston Universtiy
Math Department
111 Cummington Street
Boston, MA 02215
(617) 353-2560

Degree: M.A., Mathematics, 1986
Specialty: Mathematics
Assigned: AFGL

Yolman J. Salinas
Meharry Medical College
School of Medicine
1005 Dr. D.B. Todd Blvd.
Nashville, TN 37208
(615) 327-6308

Degree: M.S., Biochemistry, 1984
Specialty: Biochemistry
Assigned: SAM

William D. Schmidt
Indiana Univ. of Pennsylvania
Physics Department
Indiana, PA 15705
(412) 357-2100

Degree: B.S., Physics, 1983
Specialty: Physics
Assigned: AL

James P. Seaba
The University of Iowa
Mechanical Engineering Dept.
2228 Engineering Bldg.
Iowa City, IA 52242
(319) 353-6045

Degree: B.S., Mechanical
Engineering, 1984
Specialty: Mechanical Engineering
Assigned: APL

Laura Sewall
Brown University
Psychology Department
Box 1853
Providence, RI 02912
(401) 863-2727

Degree: B.S., Psychology, 1985
Specialty: Psychology
Assigned: HRL/OT

Loren T. Simpson
Davidson College
Mathematics Department
P O Box 2964
Davidson, NC 28036
(704) 892-8226

Degree: B.S., Mathematics, 1986
Specialty: Mathematics
Assigned: AFGL

Jim S. Sirkis
University of Florida
Dept. of Engineering Sciences
321 Aerospace Building
Gainesville, FL 32611
(904) 392-0961

Degree: M.S., Engineering
Mechanics, 1985
Specialty: Engineering Mechanics
Assigned: AD

Michael J. Slifker
Cornell University
Dept. of Computer Science
304 Kimball
Ithaca, NY 14850
(607) 255-5571

Degree: B.S., Computer Science, 1985
Specialty: Computer Science
Assigned: WL

Barry J. Stagg
Louisiana State University
Mechanical Engineering Dept.
Baton Rouge, LA 70803-6413
(504) 388-5792

Degree: B.S., Mechanical
Engineering, 1986
Specialty: Mechanical Engineering
Assigned: RPL

Martin A.P. Strnat
University of Dayton
Dept. of Biology
300 College Park Drive
Dayton, OH 45469
(513) 229-2135

Degree: B.S., Biology, 1984
Specialty: Biology
Assigned: AAMRL

John E. Swift
University of Oklahoma
School of Electrical Eng. and
Computer Science
202 West Boyd
Norman, OK 73069
(405) 325-4721

Degree: B.S., Electrical
Engineering, 1986
Specialty: Electrical Engineering
Assigned: AL

Moussa P. Tamer
Meharry Medical College
School of Medicine
1005 18th St.
Nashville, TN 37208
(615) 356-8756

Degree: B.S., Chemistry, 1983
Specialty: Chemistry
Assigned: SAM

Donald E. Tilton
University of Kentucky
Dept. of Mechanical Engineering
Lexington, KY 40506
(606) 257-2662

Degree: B.S., Mechanical
Engineering, 1985
Specialty: Mechanical Engineering
Assigned: APL

Shun P. Tschen
University of Iowa
Mechanical Engineering Dept.
Iowa City, IA 52242
(319) 353-5638

Degree: B.S., Mechanical
Engineering, 1985
Specialty: Mechanical Engineering
Assigned: APL

Cheryl A. Ulmer
Wright State University
Dayton, OH 45435
(513) 873-2210

Degree: B.S., Psychology, 1980
Specialty: Psychology
Assigned: HRL/LR

Joseph C. Varga
Kent State University
Dept. of Physics
Kent, OH 44242
(216) 672-2246

Degree: M.S., Physics, 1978
Specialty: Physics
Assigned: ML

Gregory L. Walker
University of Wisconsin-Madison
Engineering Mechanics Dept.
Engineering Building
7415 Johnson Drive
Madison, WI 53706
(608) 262-3990

Degree: B.S., Engineering
Mechanics, 1985
Specialty: Engineering Mechanics
Assigned: RPL

Mark M. Weislogel
Washington State University
Dept. of Mechanical Engineering
Pullman, WA 99164-2920
(509) 335-2727

Degree: B.S., Mechanical
Engineering, 1986
Specialty: Mechanical Engineering
Assigned: APL

Steven P. Wicelinski
Louisiana State University
Dept. of Chemistry
LSU Box 22023
Baton Rouge, LA 70893
(504) 388-5811

Degree: B.S., Chemistry, 1981
Specialty: Chemistry
Assigned: FJSRL

Celeste B. Williams
Auburn University
Dept. of Electrical Engineering
Broun Hall
Auburn, AL 36830
(205) 887-1843

Degree: B.S., Physics, 1984
Specialty: Physics
Assigned: RADC

Cornell L. Wooten
Texas Southern University
Math Department
3201 Wheeler
Houston, TX 77004
(713) 521-7011

Degree: B.S., Math and Mechanical
Engineering, 1985
Specialty: Mathematics
Assigned: AFGL

John S. Wroblewski
Univ. Southwestern Louisiana
Chemistry Department
P O Box 44370
Lafayette, LA 70504
(318) 231-6734

Degree: B.S., Chemistry, 1984
Specialty: Chemistry
Assigned: RPL

Jon D. Zobel, Jr.
University of Colorado at
Colorado Springs
Dept. of Electrical Engineering
Austin Bluffs Parkway
Colorado Springs, CO 80907
(303) 593-3351

Degree: B.S., Electrical
Engineering, 1986
Specialty: Electrical Engineering
Assigned: FJSRL

PARTICIPANT LABORATORY ASSIGNMENT

C. PARTICIPANT LABORATORY ASSIGNMENT (Page 1)

1986 USAF/UES GRADUATE STUDENT SUMMER SUPPORT PROGRAM

AERO PROPULSION LABORATORY (AFWAL/APL)
(Wright-Patterson Air Force Base)

- | | |
|-----------------------------|--------------------------|
| 1. Jay H. Ambrose | 5. James Phillip Seaba |
| 2. Jamal Ali Hussein | 6. Donald E. Tilton |
| 3. Craig Anthony Langenfeld | 7. Shun Peter Tschen |
| 4. Surya Raghu | 8. Mark Milton Weisloge1 |

ARMAMENT LABORATORY (AD)
(Eglin Air Force Base)

- | | |
|----------------------------|------------------------------|
| 1. Jennifer Lee Davidson | 4. Christopher William Perry |
| 2. Peter David Meyer | 5. Christopher William Reed |
| 3. Sharon Elizabeth Navard | 6. James Sanford Sirkis |

ARMSTRONG AEROSPACE MEDICAL RESEARCH LABORATORY (AAMRL)
(Wright-Patterson Air Force Base)

- | | |
|-----------------------------|--------------------------|
| 1. William Howard Acton | 8. Beverly Elaine Girten |
| 2. Stanley Francis Anton | 9. Ellen Sue Goldey |
| 3. Sherif Adel Aziz | 10. Nadia C. Greenidge |
| 4. Joseph Marshall Boroughs | 11. David W. Jansen |
| 5. Brian John Doherty | 12. Isabel Lopez |
| 6. Michelle Joanne Ferry | 13. Martin A.P. Strnat |
| 7. Beverley Ann Gable | |

ARNOLD ENGINEERING DEVELOPMENT CENTER (AEDC)
(Arnold Air Force Station)

1. Charles Reif Hammond
2. Mark Lindsay Ratcliff

AVIONICS LABORATORY (AFWAL/AL)
(Wright-Patterson Air Force Base)

- | | |
|------------------------------|--------------------------|
| 1. William Albert Marty | 3. William David Schmidt |
| 2. Dennis William Richardson | 4. John Edward Swift |

ENGINEERING SERVICE CENTER (ESC)
(Tyndall Air Force Base)

1. Christopher Paul Antworth
2. Michael Miles Lukes
3. Mary Ruth McGill

C. PARTICIPANT LABORATORY ASSIGNMENT (Page 2)

FLIGHT DYNAMICS LABORATORY (AFWAL/FDL)
(Wright-Patterson Air Force Base)

- | | |
|----------------------------|----------------------|
| 1. Mark Ronald Anderson | 4. Frank Mark Pitman |
| 2. Raymond Michael Kolonay | 5. Kyle W. Ross |
| 3. Daniel Suwhan Park | |

FRANK J. SEILER RESEARCH LABORATORY (FJSRL)
(USAF Academy)

- | | |
|------------------------|---------------------------|
| 1. Julie Ann Albertson | 4. Russell Moy |
| 2. Paul Eugene Bussey | 5. Steven Paul Wicelinski |
| 3. Robert K. Littleton | 6. Jon D. Zobel, Jr. |

GEOPHYSICS LABORATORY (AFGL)
(Hanscom Air Force Base)

- | | |
|----------------------------|-----------------------------|
| 1. Karl Kennedy Klett, Jr. | 4. Susan Ellen-Ann Sadofsky |
| 2. Mark Welson Lisee | 5. Loren Taylor Simpson |
| 3. Anthony Edward Restaino | 6. Cornell Leroy Wooten |

HUMAN RESOURCES LABORATORY/ID (HRL/ID)
(Lowry Air Force Base)

1. Dale Thomas Bracken

HUMAN RESOURCES LABORATORY/LR (HRL/LR)
(Wright-Patterson Air Force Base)

1. Dora C. Merenski
2. Deborah Lynn Parker
3. Cheryl Ann Ulmer

HUMAN RESOURCES LABORATORY/MO (HRL/MO)
(Brooks Air Force Base)

1. Daren Edward Hart
2. Roland Lavelle Palmer
3. Amy Beth Powell

HUMAN RESOURCES LABORATORY/OT (HRL/OT)
(Williams Air Force Base)

1. Susan Marci Abrams
2. Laura Sewall

MATERIALS LABORATORY (AFWAL/ML)
(Wright-Patterson Air Force Base)

- | | |
|----------------------------|----------------------------|
| 1. David Allen Bridenstine | 7. Tieu-Binh Le |
| 2. Franklin John Dunmore | 8. Wayne Randolph Lundberg |
| 3. Michael Patrick Farr | 9. Douglas Roger Moore |
| 4. Christopher Adam Field | 10. April Gayle Parker |
| 5. Peggy Jo Grigsby | 11. Joseph Charles Varga |
| 6. Stephen Hom | |

C. PARTICIPANT LABORATORY ASSIGNMENT (Page 3)

ROCKET PROPULSION LABORATORY (RPL)

(Edwards Air Force Base)

1. Douglas Wayne DeHart
2. Barry James Stagg

3. Gregory Lane Walker
4. John Stephen Wroblewski

ROME AIR DEVELOPMENT CENTER (RADC)

(Griffiss Air Force Base)

1. Alan Henry Baginski
2. Michael Dean Garner
3. Peter Vladimír Hlinomaz

4. David Paul Morton
5. Celeste Benay Williams

SCHOOL OF AEROSPACE MEDICINE (SAM)

(Brooks Air Force Base)

1. Angela Marie Braun
2. Otis Cosby, Jr.
3. Carl Von Frank
4. Maurice B. Gilbert
5. Alfred Wendell Gordon
6. George Albert Liu
7. Jennifer McGovern Weidner
8. Eric Van Morris

9. Glenn D. Munkvold
10. Conrad Robert Murray
11. Victoria Nasman
12. Bernadette Patricia Njoku
13. Gregg Allen Reger
14. Yolman John Salinas
15. Moussa Pierre Tamer

WEAPONS LABORATORY (WL)

(Kirtland Air Force Base)

1. Timothy Truman Clark
2. Bradlee Halverson
3. Michael Jude Slifker

RESEARCH REPORTS

1986 GRADUATE STUDENT SUMMER SUPPORT PROGRAM

<u>Technical Report Number</u>	<u>Title</u>	<u>Graduate Researcher</u>
Volume I		
1	The Effects of Fourier Limited Targets Upon Peripheral Perception	Susan M. Abrams
2	Studies of the Dimensionality of Subjective Workload and Standard Loading Levels in a Continuous Recall Task	William H. Acton
3	An Investigation of Unsteady Vorticity Production by a Pitching Airfoil	Julie A. Albertson
4	An Apparatus for Transient Saturation Measurements in a Heat Pipe	Jay H. Ambrose
5	Flight Control Synthesis with Practical Design Constraints	Mark R. Anderson
6	The Effects of Flow Rate and Edge Rate on the Perception of Self Speed	Stanley F. Anton
7	A Dispersion-Corrected HPLC/FACP Method for Measuring Sorption Isotherms of Substituted Aromatics on Soil Organic Matter	Christopher P. Antworth
8	Computer Simulation of the Cardio-vascular System Under +G _z Stress	Sherif A. Aziz
9	Inefficiencies of High Transmission Delays on Computer Protocols and their Applications	Alan H. Baginski
10	Cognitive Resources and Multi-Task Cost	Joseph M. Boroughs
11	Job/Task Difficulty and Job/Task Experience: A Literature Review	Dale T. Bracken, Jr.
12	Chlamydomonas Phototaxis as a Simple System for Testing the Effect of Drugs on Vision	Angela M. Braun
13	Research for the Development of an Executive System Prototype for Unified Life Cycle Engineering	David A. Bridenstine

14	Development of a High Speed Infrared Detection and Recording System with Resident Image Processing and Graphic Data Display for Support of Remote Defense Nuclear Agency High-Powered Pulsed Microwave Source Measurements	Paul E. Bussey
15	Modification of a Finite-Difference, 2-Dimensional Boundary Layer Code for Application to the Free Shear Layer of an Axisymmetric Jet	Timothy T. Clark
16	Mesopic Visual Function in Aircrew	Otis Cosby, Jr.
17	A Mathematical Classification of a Family of Edge Detectors	Jennifer L. Davidson
18	Design and Analysis of Models of Large Space Structures	Douglas W. DeHart
19	A Biomechanical Study of Anthropomorphic Head-Neck Systems	Brian J. Doherty
20	Materials Evaluation and Failure Analysis of Various Electronic Circuitry Components of Air Force Aircraft	Franklin J. Dunmore
21	Thermal Characterization of New Thermally Stable Matrix Materials	Michael P. Farr
22	Synthesis of Intermediates and Monomer of Polybenzothiazole	Christopher Feild
23	The Metabolism of t-Butylcyclohexane in Male Fischer 344 Rats	Michelle J. Ferry
24	Data Management Within the School of Aerospace Medicine	Carl V. Frank
25	The Effects of High Noise Levels and Obstruction to Articulation on the Acoustic-Phonetic Structure of Speech: A Preliminary Investigation	Beverley A. Gable
26	A Study of the Probability Distributions of the Long Term Variations of Acoustical Noise Over Time of Various Military Environments	Michael D. Garner
27	Exposure of Polycarbonate Lens to Natural Elements	Maurice B. Gilbert

28	Effects of Dobutamine Administration on Suspension Hypokinesia/Hypodynamia Deconditioning in Rats	Beverly Girten
29	Experimental Evidence Supporting a Pharmacokinetic Model of Uptake and Metabolism of Trichloroethylene in the Pregnant and Lactating Rat	Ellen S. Goldey
30	Effects of Acceleration Stress Upon Blood Lipid Levels	Alfred W. Gordon
31	Microfracture Patterns in the Lumbar Vertebrae of Macaca mulatta	Nadia C. Greenidge
32	Effects of Coherent Scattering on IR Absorption in Doped Semiconductors	Peggy J. Grigsby
33	A Modification of the ACSYS Preprocessor Code for use with the SAMSON2 Finite - Element Program	Brad L. Halverson
34	Automation of the Method of Optimal Design	Charles R. Hammond
35	Empirical Confidence Intervals for a Validity Coefficient Under Range Restriction: An Application of the Bootstrap	Daren E. Hart
36	An Analysis of Residual Output Noise from the R.A.D.C. Speech Enhancement Unit	Peter V. Hlinomaz
37	Knowledge for the ULCE Expert System	Stephen Hom
38	An Analytical Investigation for Designing an Energy Storage Container for Storing Lithium Hydride Between 300K and 1200K	Jamal A. Hussein
39	Modeling of Human Body Movement	David W. Jansen
40	Noise Analysis and Reduction for the AFGL Infrared Focal Plane Array Spectrometer	Karl K. Klett, Jr.
41	Structural Optimization Using Bending Elements	Raymond Kolonay
42	Swirling Flows in Dump Combustors	Craig A. Langenfeld

43	Thermal Stability Studies of Structure-Property Relationship of Various Silahydrocarbon Lubricants	Tieu-Binh Le
44	Computer Software Development in a Study of Executable Image Efficiency	Mark W. Lisee
45	Optimization of a Material to be used to detect Incident Microwave Radiation by IR Imaging	Robert K. Littleton
46	Synergistic Effects of Antimalarial Drugs and Hyperoxia on the Growth of Malaria Parasites in Culture	George A. Liu
47	The Metabolism of Isopropylcyclohexane in Male Fisher 344 Rats	Isabel Lopez
48	A Comparative Study and Evaluation of Four Atmospheric Dispersion Models with Present or Potential Utility in Air Force Operations	Michael M. Lukes
49	A Load-Balancing Modification to A. George's Incomplete Nested Dissection Algorithm for Mapping a Compact Irregular Quadrilateral Finite-Element Mesh onto the Hypercube Parallel Processing Architecture	Wayne R. Lundberg
50	Guide to ISPX: The Interactive Signal Processing Executive	William A. Marty
Volume II		
51	Polynuclear Aromatic Hydrocarbons in Particulate Turbine Engine Exhaust and From Combustion of Single Compound Fuels	Mary R. McGill
52	Electroencephalography and Online Analysis: An Evaluation of Some Available Choices	Jennifer McGovern-Weidner
53	Program Code: Style and Conventions	Dara C. Merenski
54	Synthesis and Time to Explosion Studies of Some Potential High Explosives	Peter D. Meyer
55	Polybenzimidazoles: Solubilization, Modification and Synthesis	Douglas R. Moore

56	MBTI Psychometric Study of United States Air Force Aircrew Personnel	Eric V. Morris
57	Chemical and Electrochemical Behavior of Aluminum Electrodes in Acidic 1-Methyl-3-Ethylimidazolium Chloride/Aluminum Chloride Room Temperature Molten Salt Electrolytes	Russell Moy
58	OBOGS Studies	Glenn D. Munkvold
59	Effects of Acceleration Stress Upon Blood Lipid Levels	Conrad R. Murray
60	Heart Rate Self-Regulation: The Effects of Increasing Cognitive Demands	Victoria Nasman
61	Modernization of Statistical Software	Sharon E. Navard
62	Visual Characteristics in Pilots with Central Serous Retinopathy	Bernadette P. Njoku
63	Residual Carrier Concentration Dependence on the Arsine Pressure for Gallium Arsenide Grown by Hydride-Based VPE	David P. Norton
64	Frequency and Temporal Information Processing	Roland L. Palmer
65	Parametric Numerical Simulation for Hypersonic Flow Over a Compression Ramp	Daniel S. Park
66	Characterization of Alkoxide Derived Zirconia Toughened Fused Silica	April G. Parker
67	On the Measurement of Variables Impacting the Performance of Flightline Maintenance Crews	Deborah Parker
68	Image Algebra Preprocessor and Image Algebra Executive	Werner K. Perry
69	Decentralized Control of Large Flexible Space Structures	Frank M. Pitman
70	Empirical Confidence Intervals for a Validity Coefficient Under Range Restriction: An Application of the Bootstrap	Amy B. Powell

71	Study and Control of Organ Pipe Type Oscillations in a Horizontal Combustion Tunnel	Surya Borbu
72	A Locally Implicit Numerical Method	Mark L. Ratcliff
73	Adaptive Grid Generation for Viscous Flow Problems	Christopher W. Reed
74	An Ultrastructural Study of Mossy Fiber Terminals Isolated from the Mammalian Brain	Gregg A. Reger
75	Response of Downslope and Florida Mesoscale Wind Systems to Physiographic Features	Anthony E. Restaino
76	Atmospheric Modeling for Operational Tactical Decision Aid	Dennis W. Richardson
77	An Experiment to Characterize the Turbulent Flow of a Circular Free Jet of Helium	Kyle Ross
78	Weather Attenuation	Susan E. Sadofsky
79	MBTI Psychometric Study of United States Air Force Aircrew Personnel	Yolman J. Salinas
80	Analytical Computer Modeling of the NPN BICFET Device	William D. Schmidt
81	Jet Diffusion Flame	James P. Seaba
82	Mechanisms of Chromatic Contrast	Laura Sewall
83	Computer Simulation of Physical Phenomena	Loren T. Simpson
84	A Discussion of Boundary Element Methods	Jim S. Sirkis
85	Automatic Program Generation from Specifications	Michael J. Slifker
86	A Study of the Use of Optical Combustion Diagnostics on Premixed Flames and Solid Rocket Propellant Flames	Barry J. Stagg
87	Expansion of USAF AAMRL/THT Electron Microscopy Division Capabilities with Respect to Specimen Preparation and Analysis	Martin A.P. Strnat

88	Translation of TRW's ADAPT-II to a Perkin-Elmer OS-32 Environment	John E. Swift
89	MBTI Psychometric Study of United States Air Force Aircrew Personnel	Moussa P. Tamer
90	High Power Density Evaporative Cooling	Donald E. Tilton
91	Visualization of Jet Diffusion Flames	Shun P. Tschen
92	The Effects of Stress and Crisis Conditions on Decision Making	Cheryl A. Ulmer
93	Numerical Calculations of Thermal and Dopant Diffusion in Ion-Implanted Laser-Annealed Silicon	Joseph C. Varga
94	Void and Boundary Layer Effect on the Stress Distribution Near Cylindrical Inclusions	Gregory L. Walker
95	Experimental Studies on Heat Pipe Coupling and Condensation Rates in Packed Beds of Spheres	Mark M. Weislogel
96	An Investigation of Prospective Media for Thin Film Fabrication of III-V Semiconductors	Steven Wicelinski
97	Study of Oxygen-Related Defects in Electron-Irradiated, Boron-Doped Silicon	Celeste B. Williams
98	A Study of the Finite Element Method in Limited Area Weather Prediction Modeling	Cornell L. Wooten
99	Synthesis and Polymerization of Dinitropropyl Vinyl Ether	John S. Wroblewski
100	Development of a High Speed Infrared Detection and Recording System with Resident Image Processing and Graphic Data Display for Support of Remote Defense Nuclear Agency High-Powered Pulsed Microwave Source Measurements	Jon D. Zobel, Jr.

1961 YEAR THE SUMMER SUPPORT PROGRAM

GRADUATE STUDENT SUMMER SUPPORT PROGRAM

sponsored by the

AIR FORCE OFFICE OF SCIENTIFIC RESEARCH

CONDUCTED BY THE

UNIVERSAL ENERGY SYSTEMS, INC.

FINAL REPORT

THE EFFECTS OF FOURIER LIMITED TARGETS UPON PERIPHERAL ADAPTATION

Prepared by:	Susan Abrams Garcia
Academic rank:	Graduate Student
Department and University :	Bioengineering, University of Illinois at Chicago
Research Location:	Human Resources Laboratory, Williams Air Force Base
USAF Researchers:	Dr. E. Martin/ Dr. G. Gerni
Date:	September 29, 1961
Contract No:	149620 - 65 - 2 - 1111

THE EFFECTS OF FOURIER-LIMITED TARGETS ON A DISCRIMINATION TASK

by

Susan Abramo Baroff

ABSTRACT

The effects of varying the bandwidth of a two-dimensional line figure, through its Fourier transform, was studied. It was found that by varying the presentation time (30, 45 and 60 ms. and the angle of presentation of stimuli (0.75, 10, and 15 degrees), that discrimination between two harmonically related figures could be altered. Three equal area targets of increasing complexity were used as stimuli. Three subjects were tested under 27 different conditions, which involved rating the similarity of two harmonically related figures. Preliminary analysis indicates that there is an interaction between presentation time and eccentricity; there is also evidence that discrimination is poorer for simple targets than for more complex targets. Further analysis has yet to be completed.

XXXXXXXXXXXX

I would like to thank the Air Force Office of Scientific Research for sponsorship of my research. Working at the Resource Laboratory proved to be an extremely rewarding experience. I would like to thank Dr. E. Martin, Dr. J. D. Lyon and Mr. Paul Wetzel for their help and assistance during the summer.

Finally, I would like to thank my husband, Mark, for his support, understanding and encouragement during my research.

I. Introduction

I received my B.S. from Tufts University in Medford, Massachusetts, studying human factors engineering. Currently, I am attending the University of Illinois at Urbana, where I am investigating the effects of figure complexity. I am also studying the effects of varying a two dimensional visual target, using its Fourier Transform, on perception and eye movement.

The research project at the Air Force Research Laboratory involved the perception of form in the periphery. Can the periphery encode form? Is the Fourier transform an effective method to describe the limitations of peripheral encoding ability?

The problem under investigation at Williams was very similar to the work I had researched at Illinois and Tufts University. Due to the research I have accomplished, I was assigned to work on the perception of form at the Human Resources Lab.

II. Summary of Research Effort

The objective of the perception research project was to devise a method by which visual information could be limited in the periphery while retaining the maximum information possible in normal perception. This experiment was an attempt to systematically reduce the peripheral information, by altering the Fourier bandwidth, without altering scene perception.

My individual objectives were: 1) Studying the effects of bandwidth limited Fourier target. Using a same-different four point rating scale, does the discriminability of a target change with increasing eccentricity and for increased time of

presented with the same target, and the results of the experiment vary with the complexity of the target.

III. Fourier Descriptors

A. Preliminary Analysis

In order to compare the effects of limiting the bandwidth of a target, a computer program was developed to allow the user to generate harmonically related forms. Three equal area forms were created. For each target, a series of narrow bandwidth variations were created. The highest bandwidth of each set was limited to the where the frequency of each additional harmonic was less than or equal to .05% of the power of the fundamental frequency (Abrams et al. 1966). It has been proven that there is a high correlation (.88) between perceived complexity and the ratio of equal area figures and their limited bandwidth.

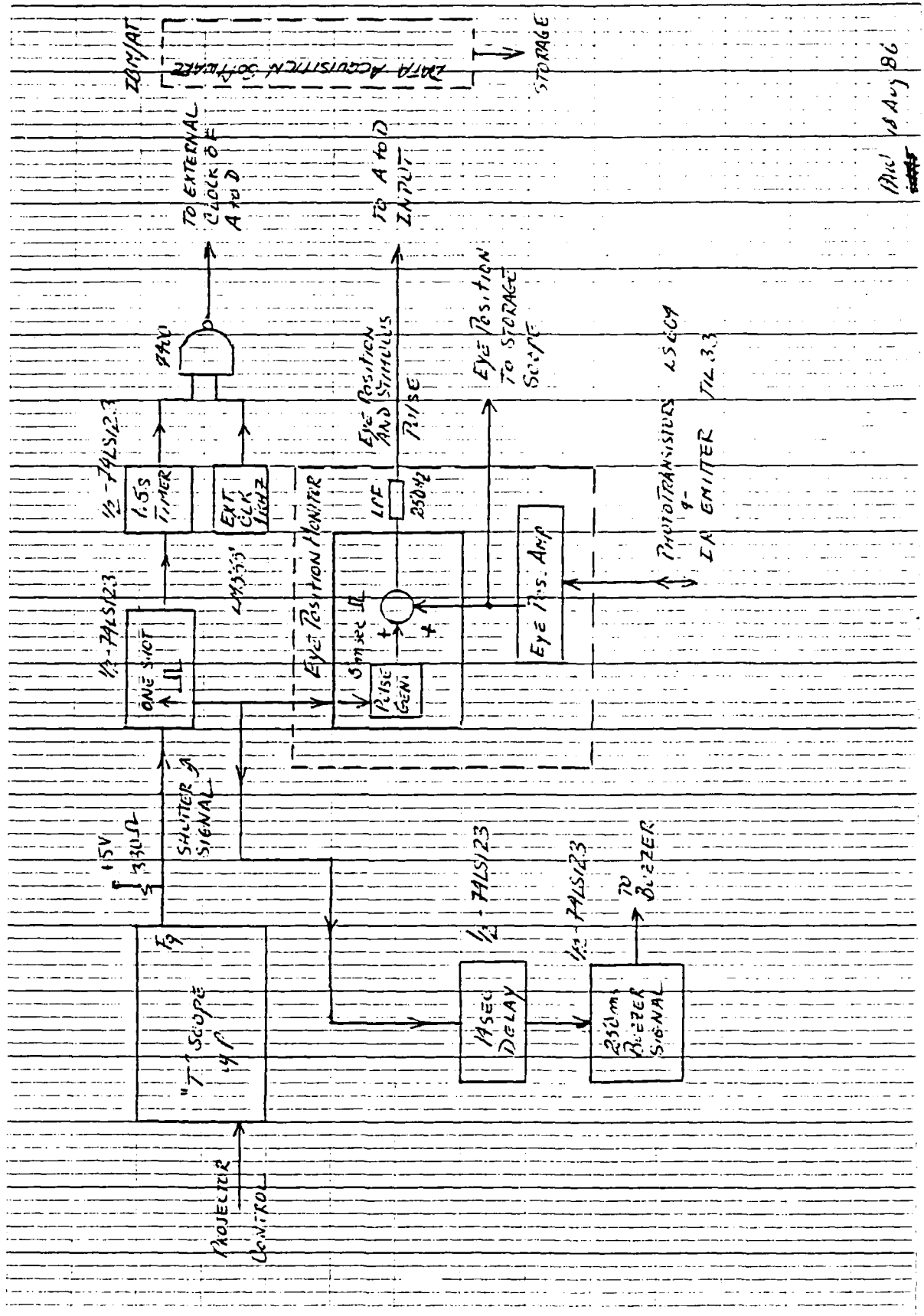
IV. Experimental Approach

A. Experimental controls

An important control of this experiment was that the targets be equally stimulated at all eccentricities; this was achieved by enlarging the figure by the Cortical Magnification factor (CMF) (Dow et al.) appropriate for the given presentation eccentricity. The CMF is used to describe the amount of cortical surface devoted to a given portion of visual space. The foveal receptive fields show much more overlap at any given electrode displacement distance than do more peripheral receptive fields. A point of light projected on the fovea is "registered" by many more cortical cells than a point of light projected onto the periphery, and a perifoveal point is seen by more cortical cells

[illegible]

The basic experiment was conducted as follows: Two target sets were presented at three equal eccentricities: 0.0°, 1.0°, and 2.0° degrees. The target was considered a "standard" target, which all other target in the series would be compared. There were two standards within each target set. Presentation of the images was controlled by the Gerald T. sector. This T. sector consisted of two Kodak slide projectors and a Gerald digital slide presentation system which could be set for presentation times of 10 ms - 10 seconds. In this experiment each target was presented at three different stimulus durations at each eccentricity. The stimulus durations were 30ms., 55 ms., and 100 ms. The subject was instructed to fixate upon a center point in all trials, approximately 0.5 degrees below the stimulus.



Rev 18 Aug 86

the subject was asked to make a similarity judgment between the current pair and the stimulus were about 10 seconds. Approximately 1.5 seconds after the time was announced, the pair is horizontally related, closely positioned, and/or related with the back lid projection screen. After each presentation, the subject was given 15 seconds in which to make a similarity rating of the similarity of the pair. The subject was then given the following chart with which to "mark" the pair as a pair:

- 4 - very similar/same
- 3 - similar
- 2 - different
- 1 - very different

The subject was allowed to give ratings of 1, 2, 3, or 4 for each presentation. Each stimulus pair was presented four times with a total of 40 random trials per session. After 10 trials, three subjects were tested under all 12 conditions.

In order to ensure that the judgments of the subjects were based upon peripheral processing, eye movements were monitored with an infrared eye tracking system. Any trial in which the subject deviated from the fixation point during the stimulus presentation was thrown out and repeated. In addition, in order to double check the experimenters accuracy, all eye movements were recorded on to an IBM computer during the stimulus presentation periods. (A complete flow chart is available in figure 1).

1. The experiment have not been completed. From a preliminary analysis, there appears to be an effect of time and eccentricity. The 10 ms. presentation appears to have been insufficient for the subjects to make out all of the details of the figure when it was presented at 10 and 15 degrees; the effect is less pronounced for the 1.75 degree presentation. In some cases, the effect seems to be more pronounced for the simple targets than for the more complex targets. Although in all cases the relative magnitudes of the added frequencies are approximately equal, about percentages of the fundamental, the subjects were able to discriminate the complex targets more easily than the less complex target. This may be due to the magnitude and the phase of the frequency added at each harmonic, but this analysis has not been completed. Further studies which concentrated upon the magnitude and phase of added frequencies as well as the complexity of the target could shed more light upon the visual systems' ability to discriminate form.

2. There seems to be no significant difference between the 45 ms and 300 ms presentation time. This may be due to the fact that these two intervals exceeded the necessary time for processing visual images into short term visual memory. Further studies which used masking techniques could be very interesting from a memory standpoint.

3. For all complexities of targets, there seems to be a slight decline in discrimination as the targets are presented further into the periphery, however a full analysis has yet to be completed. Further studies with larger presentation

presented in the present study. These results are preliminary and require further study. These studies could not be done due to equipment and time limitations.

4. From this preliminary analysis it appears as if there was greater difficulty in accurately discriminating between a standard and a test stimulus when the standard was the "power" of the form. The added frequencies in these larger bandwidth targets appear to carry less "information" to the subject; this may be due to the relatively high frequency and low magnitude of these added components. This must be further analyzed.

REFERENCES

1. Ariens, J., "Fourier transforms and their effects on perception and eye movements", in preparation.
2. Johnson, C.A., Keltner, C.L. and Galestry, J. "Effects of target size and eccentricity on visual detection and search." Visual Research, 1978, Vol. 18, pp. 1117 - 1121.
3. Kuh, F., "Elliptic fourier features of a closed contour", Computer Graphics and Image Processing, 18, 174-178, 1981.

1986 USAF-UES SUMMER FACULTY RESEARCH PROGRAM/
GRADUATE STUDENT SUMMER SUPPORT PROGRAM

Sponsored by the
AIR FORCE OFFICE OF SCIENTIFIC RESEARCH

Conducted by the
Universal Energy Systems, Inc.

FINAL REPORT

Studies of the Dimensionality of Subjective Workload and
Standard Loading Levels in a Continuous Recall Task

Prepared by:	William H. Acton
Academic Rank:	Graduate Student
Department and University:	Department of Psychology University of New Mexico
Research Location:	Harry G. Armstrong Aerospace Medical Research Laboratory, Wright Patterson AFB, Ohio
USAF Researcher:	Gary B. Reid and F. Thomas Eggemeier
Date:	August 1, 1986
Contract No:	F49620-85-C-0013

Studies of the Dimensionality of Subjective Workload and
Standard Loading Levels in a Continuous Recall Task

by

William H. Acton

ABSTRACT

Data from a study which employed Multidimensional Scaling techniques to suggest optimal workload rating scales were analyzed. The results indicated that two types of task characteristics were related to judgements of task similarity: overall task difficulty and requirements for central vs perceptual/motor processing. These conclusions were based on the multidimensional scaling results and on analyses in which univariate ratings were regressed onto the scaling results. In other research, parametric evaluation of the CTS Continuous Recall task showed that both task performance and subjective ratings of mental workload were significantly different for three levels of task difficulty produced by combinations of item complexity and number of items to be held in memory.

Acknowledgements

I thank the Air Force Systems Command, the Air Force Office of Scientific Research, and the Harry G. Armstrong Aerospace Medical Research Laboratory for sponsorship of my research. Special thanks go to Gary B. Reid and F. Thomas Eggemeier of AAMRL for their guidance and support. John Amell and William Perez of SRL also contributed their talents and insights to this work, and I am in their debt. Last, but certainly not least, I thank my family and friends in the Dayton area for giving me love and shelter during my stay; and my wife, Susan, for her patience and understanding throughout my absence from Albuquerque.

I. Introduction

I received an Master of Arts degree in Human Performance from Wright State University, Dayton, and am currently enrolled in a doctoral program in Cognitive Psychology at the University of New Mexico. My master's thesis was an investigation of the relative sensitivity of subjective workload rating scales to different types of task demands. Between the two academic programs I worked at AAMRL as an SRL support contractor, and was involved in both the behavioral and subjective workload metric development programs. Since I was familiar with the workload program, I was assigned to work at AAMRL.

II. Objectives of the Research Effort

I had two primary goals for the summer:

1. To complete the data analysis for a study begun last year at the AAMRL workload laboratory. The purpose of the study was to use Multidimensional Scaling (MDS) methods to help define an optimal set of workload rating scales.
2. To experimentally reevaluate the current Criterion Task Set (CTS) version of the Continuous Recall task. A number of CTS users have reported that the most demanding level of the current Continuous Recall task is too difficult to provide useful information. The objective of this study was to establish new loading levels for the task that would more readily lend themselves to dual task and other types of performance assessment research.

III. Data Analysis for the MDS Study

A major issue in the use of workload rating scales concerns the number and types of scales that should be used to provide a complete description of load. Generally, correlations between different scales are moderate, so it is difficult justify selection of any specific scale or set of scales. Derrick (1981) used Multidimensional Scaling (MDS) methods to help explain dissociation between different categories of workload metrics, and commented on the utility of different rating devices for explaining the scaling solution obtained. MDS uses data on the proximity of rating stimuli to produce a scaling solution that is depicted in an n-dimensional space. The purpose of this research (begun last year at AAMRL) was to evaluate the utility of MDS for defining the smallest possible number of scales that provide a complete description of operator workload.

In the study, 24 subjects performed each of sixteen tasks on four consecutive workdays. In the fourth session, subjects also rated the tasks on eleven separate rating scales designed to assess various aspects of the subjective experience of mental work, such as emotional stress, effort, memory demands, etc. In a fifth and final session, all possible pairs of the tasks were rated for the similarity of the mental work they entailed. These similarity ratings were the data from which the multidimensional scaling solution was

derived.

At the point when I began the summer program, the only analysis that had been completed was the MDS scaling itself. The results suggested that ratings of task similarity were best scaled in a two dimensional space. The three dimensional scaling model did not fit the similarity data much more closely, and the third dimension could not be identified in an intuitively satisfying way.

The method used to identify the two observed scaling dimensions was a traditional one: MDS scale values for the experimental tasks were regressed onto scores from the unidimensional ratings obtained in the fourth session. The results were as follows:

<u>Rating Scale</u>	<u>Regr. Wts. Dimension</u>		<u>Mult. Corr</u>	<u>p</u>
	<u>1</u>	<u>2</u>		
Time Pressure	-.59	-.72	.52	.008
Perceptual Load	-.19	-.56	.44	.02
Display Complexity	.07	-.34	.14	.36
Memory Load	-.54	-.13	.18	.27
Cognition	-.72	-.45	.77	.0001
Effort	-.48	-.81	.76	.0001
Response Demand	-.42	-.66	.84	.0001
Emotional Stress	-.41	-.83	.75	.0001
Overall Difficulty	-.21	-.89	.61	.002
Fatigue	-.25	-.74	.80	.0001
Estimated Performance	.12	.77	.76	.0001

Multiple correlations for the perceptual load, display complexity, and memory load scales were nonsignificant at the $p=.01$ level. All other scales were significantly related to the location of task stimuli within the scaling solution space. Ratings of

overall difficulty were most closely related to task locations on Dimension 2 of the MDS solution, although several other types of ratings were also more closely related to Dimension 2 than Dimension 1, including emotional stress, effort, fatigue, and time pressure. Only unidimensional ratings of cognition, defined by requirements for thinking, calculating, analyzing and deciding, produced a larger regression weight on scaling Dimension 1.

To clarify these findings, stepwise multiple regression analyses were performed in which univariate ratings were treated as predictor variables and MDS task scale values as dependent variables. As expected, ratings of overall difficulty were the best single predictors of Dimension 2 scale values, accounting for 84% of the variance. The cognition scale was the best single predictor of Dimension 1 scale values, but accounted for only 53% of the variance. However, the combination of cognition and perceptual load ratings was an excellent predictor of task values on Dimension 1, accounting for 89% of the variance.

In the only other major analysis, normalized performance scores were regressed onto each of the univariate rating scales. Two of the scales were significantly related to performance but did not interact with subject: emotional stress ($F=6.38$, $p=.012$) and overall difficulty ($F=4.99$, $p=.026$). These scales were good predictors of performance and were used in

roughly the same way by all subjects.

IV. Recommendations

Although univariate ratings of cognition were significantly related to one of the MDS derived dimensions, they were not good predictors of task performance, and might not be good indices of workload. However, primary task performance itself is not always a good index of workload. To determine the value of ratings of cognition and overall difficulty for workload assessment, they would have to be explicitly compared to other workload metrics such as secondary tasks or appropriate physiological measures. A logical extension to this study would be to experimentally perform this sort of comparison.

Another limitation of this research arises from the restricted number of stimuli that can be employed with MDS methodology. Since the number of required paired comparisons increases exponentially with the number of stimuli, it is generally impractical to include more than 16-20 rating items. Unfortunately, it may be impossible to adequately represent the universe of human tasks in such a small set. Also, the types of tasks employed in this study may have been different in crucial ways from the sorts of tasks performed in real-world work settings. It might therefore be valuable to compare these findings with MDS dimensions derived from similar research in operational AF systems.

V. Empirical Evaluation of the Continuous Recall Task

The other major goal for the summer was to reevaluate the current Criterion Task Set (CTS) version of the Continuous Recall Task. The CTS is a battery of standardized loading tasks with empirically determined training characteristics and information processing requirements. The battery was intended for application to a wide range of theoretical and practical problems in human performance assessment such as workload metric evaluation and measurement of environmental stressor effects. The tasks which compose the battery were selected so as to collectively impose demands on a wide range of basic mental capacities. The current Continuous Recall task is intended to impose requirements on short term memory functions, and consists of three demand levels which vary in the number and complexity of items which must be retained.

Recently, users of the CTS have reported that the most difficult level of the task, which requires that four digit items be compared to items three back in the stimulus series, is too demanding. Error rates are so high that performance approaches chance levels, and this may affect the workload actually imposed by inducing the subject to employ load reducing strategies. Such strategy shifts may undermine the ordering of the current loading conditions. That is, the highest level of the task may not necessarily impose the greatest demand, if a load shedding strategy is adopted.

To provide data for establishing a more moderate "high demand" condition, and to evaluate the intrusiveness of subjective workload ratings on task performance, a parametric study was conducted. The method employed in the study was in keeping with the standard experimental procedures that are used in all CTS parametric research. Subjects performed a variety of candidate demand conditions which were produced by factorially combining two variables known to influence performance and subjective rating of workload: number of digits in the to-be-remembered items (one, two, and three digits), and number of items to be simultaneously stored (comparison of each stimulus to the stimulus one, two and three positions back in the series).

All nine demand conditions were performed twice in four separate sessions conducted on consecutive workdays. In all sessions but the first, task conditions were randomly ordered within the 18 three-minute trials. In the first two sessions, summary reaction time and percent correct data were presented after each trial so that subjects could maintain an appropriate balance between speed and accuracy. SWAT ratings (see Reid, Shingledecker and Eggemeier, 1981) were produced in one of the last two sessions (randomly determined) so that otherwise identical conditions could be compared to determine the intrusiveness of ratings. To avoid rating bias, feedback was not made available in the last two sessions.

VI. Results

Mean reaction times and percent correct response scores for the nine memory demand conditions are shown below. The values in the table represent means taken across both replications in each of the last two sessions. Collapsing in this way seemed justified in light of the fact that differences in performance on the task in the SWAT rating and non-rating conditions were negligible: mean reaction times in the rating conditions were 2.329 sec, compared to 2.188 sec in the rating conditions, a difference of less than 2/10 sec. Percent correct scores were 94.01 and 93.93 for the same conditions, respectively. If further statistical analyses indicate that these differences are statistically reliable, decisions about new task loading levels may need to take this into account.

<u>Number Back</u>	<u>Number Digits</u>	<u>(msec)</u>	<u>%C</u>
1	1	968	98.50
	2	916	97.40
	3	1065	98.70
2	1	2286	96.78
	2	2128	97.95
	3	2558	94.89
3	1	3212	95.86
	2	3551	87.38
	3	3649	77.93

The number back variable clearly had a greater impact on reaction times than did the number of digits

in the stimuli. However, within the three back conditions, percent correct scores were greatly influenced by the number of digits. Errors were at 5% or less for all conditions except 2 digits - 3 back and 3 digits - 3 back.

VII. Recommendations

The fact that errors are considerably increased for two and three digit numbers in the three back condition suggests that these conditions may not be suitable for the revised version of the Continuous Recall task. Since the motivation for this research was to eliminate strategy shifts that may result from overload, it would seem logical to recommend selection of final task levels from among the conditions producing roughly homogeneous percent correct scores. Another potential difficulty with the two and three digit versions of the three back condition was indicated by a comment made by one of the subjects in the study. She noted that to make successful performance possible, one can memorize only one of the digits, and ignore the others. While this could also be done in the one and two back conditions, subjects did not report doing so, perhaps because high accuracy could be maintained in these conditions without resorting to a truncating strategy.

As in all CTS research, selection of three loading levels should be based on pairwise statistical comparison of all condition means, both for performance and subjective data. Unfortunately, I was not able to

complete the paired-comparisons in time to include them in this report. However, the initial summary statistics presented above suggest that it will be possible to discriminate three significantly different levels of task demand that will be within an acceptable range of workloads.

References

1. Derrick, W.L., The Relationship Between Processing Resource and Subjective Dimensions of Operator Workload, Proc. Human Factors Society Annual Meeting, Rochester, N.Y., October 1981, pp 532-536.
2. Reid, G.B., Shingledecker, C.A. and Eggemeier, F.T., Application of Conjoint Measurement to Workload Scale Development, Proc. Human Factors Society Annual Meeting, Rochester, N.Y., October 1981, pp 522-526.

1986 USAF-UES Summer Faculty Research Program/
Graduate Student Summer Support Program

Sponsored by the

AIR FORCE OFFICE OF SCIENTIFIC RESEARCH

Conducted by the

Universal Energy Systems, Inc.

Final Report

An Investigation of Unsteady Vorticity Production by a Pitching Airfoil

Prepared By:	J.A. Albertson
Academic Rank:	Graduate Student
Department & University:	Department of Mechanical Engineering Washington State University
Research Location:	Frank J. Seiler Research Laboratory, Aerospace Mechanics Directorate, United States Air Force Academy
USAF Researcher:	Major John M. Walker
Date:	September 2, 1986
Contract No.:	F49620-85-C-0013

An Investigation of Unsteady Vorticity Production by a Pitching Airfoil

by

T.R. Troutt
J.A. Albertson

Abstract

This research investigation concentrated on developing insight into the unsteady aerodynamics produced by pitching airfoils in uniform airstreams. The specific experimental situation addressed involved a two-dimensional NACA 0015 airfoil which was pitched at constant rates through angles of attack from 0-60 degrees. The experimental results analyzed included high speed motion picture flow visualizations and simultaneous pressure measurement from eighteen chord locations distributed over the surface of the airfoil. The research techniques employed involved both the development of simple analytical procedures for computation of the vorticity generation rates by the surface of the pitching airfoil and digital image techniques for enhancing and quantifying interpretations of the visualization results. The analytical results demonstrate that the nondimensional parameter $\alpha^+ = \dot{\alpha}c/U$, where $\dot{\alpha}$ is the airfoil pitching rate, c is the airfoil chord length, and U is the free stream velocity, should be the primary parameter for predicting the relative influence of pitching rate and free stream velocity on the unsteady aerodynamics around an airfoil. This result agrees closely with experimental findings. The results from the image analysis techniques show that the initiation of the dynamic stall vortex on the airfoil top surface corresponds closely to a halt in the increase in lift as a function of attack angle curve. The subsequent fast growth of the dynamic stall vortex is found to accompany a rapid decrease in the lift on the airfoil.

I. Introduction

My previous related research interests have been in the areas of turbulent free shear flows and reattaching separated flows. The dominant proportion of my efforts in these areas has involved the acquisition and analyses of experimental data with the objective of developing improved understanding of the role of quasi deterministic flow structures in the development of these turbulent flows. Representative publications associated with these previous efforts are given in references 1, 2, 3, 4, 5.

The unsteady aerodynamic research pursued by graduate student, Ms. Julie Albertson, and myself this summer was a natural extension of my previous experience involving separated and turbulent flows. The specific area studied this summer involved the analysis of unsteady separation phenomena created by pitching airfoils in a uniform airstream. The motivation behind this work involves the interest of the U.S. Air Force in developing improved understanding of the aerodynamics produced by unsteady maneuvering of high performance aircraft.

II. Objectives of the Research Effort

The primary goal of this research program was to improve understanding of dynamic stall phenomena associated with airfoils undergoing rapid accelerations or pitching motions. This goal was pursued through two avenues involving analyses of experimental data acquired previously by the aeromechanics directorate at the Seiler Research Laboratory. The two research avenues followed were: 1. The development of a simple analytical technique to understand and quantify the vorticity generation

rates from the unsteady surface motions and instantaneous surface pressure gradients; 2. The development and application of digital image analysis techniques to enhance both qualitative and quantitative interpretations of flow visualization results.

One goal which was proposed in my original objectives statement was to perform additional focussed experiments to supplement and extend previous studies in this area. Because of some delays in getting a new wind tunnel facility and associated peripherals into working status no additional experiments were performed. It is hoped at this time that additional experiments employing the new wind tunnel facility at the Seiler Research Laboratory could be performed at a somewhat later time with the support of the mini grant associated with the USAF-UES Summer Faculty Research Program. A grant application concerning this work is in preparation.

III. Approach

III.1 Vorticity Generation Analysis

The first avenue of investigation concerned the application of Morton's (6) vorticity generation analysis to the problem of vorticity production by a pitching airfoil.

Morton's analysis shows that the vorticity generation in a homogeneous fluid may only take place at rigid boundaries and that the generating mechanisms are the tangential surface pressure gradient and the tangential surface acceleration of the boundary.

This deduction can be mathematically represented by the equation

$$\frac{d\Gamma_z}{dt} = \rho^{-1} \left(\frac{\partial p}{\partial s} \right)_0 + \frac{dU_s}{dt} \quad (1)$$

where $d\Gamma_z/dt$ is the flux of z direction vorticity from the surface (the z axis is tangential to the surface and normal to the s direction), ρ is the fluid density, $\left(\frac{\partial p}{\partial s}\right)_0$ is the tangential pressure gradient along the rigid surface in a direction normal to the z axis, and dU_s/dt is the tangential acceleration of the rigid surface. This equation explicitly separates the effects of the fluid dynamics through the pressure gradient from the effects of the rigid surface acceleration on the vorticity generation rate at the surface. Although the surface pressure gradient is dependent upon the flow and cannot easily be obtained for turbulent flows, except from experiments, the surface acceleration term can be easily calculated for specific experimental situations.

For the case of an airfoil pitching about a fixed pivot the surface acceleration term can be given by the following relation

$$\frac{dU_s}{dt} = r_0 [\dot{\alpha}^2 \cos(\theta + \xi) + \ddot{\alpha} \sin(\theta + \xi)] \quad (2)$$

where r_0 is the radial distance from the pivot point to the specified surface position, $\dot{\alpha}$ is the airfoil rotation rate, θ is the angle between the chord axis and r_0 , ξ is the angle of the local surface tangent and $\ddot{\alpha}$ is the rotational acceleration. A diagram showing the various geometrical quantities and the employed coordinate system is given in figure 1.

For the specific airfoil experiments evaluated thus far, $\dot{\alpha}$ was maintained constant during the measurements so equation (2) reduces simply to

$$\frac{dU_s}{dt} = r_0 \dot{\alpha}^2 \cos(\theta + \xi) \quad (3)$$

The surface acceleration term for a specific airfoil geometry pitching about at a fixed pivot at a constant rotation rate is thus solely

dependent on $\dot{\alpha}^2$. Competition between the pressure gradient term and the surface acceleration term with respect to vorticity generation for constant density flow can therefore be scaled by $\dot{\alpha}^2 c^2 / U^2$ or $\dot{\alpha} c / U$ where c is the chord length of the airfoil and U is the free stream velocity. This nondimensional parameter has in fact been noted previously by Walker and Helin (7) as the primary controlling factor in their pitching airfoil experiments. This parameter was assigned the symbol α^+ by Walker and Helin (7) and will therefore be referred to as such throughout the rest of this report.

Figure 2 shows the computed values of the vorticity flux density from the top surface of a NACA 0015 airfoil as a function of chord position for various values of the parameter α^+ . For these curves the hinge position was located on the airfoil chord at $0.25 c$ from the leading edge. This hinge position was used for the bulk of the pitching airfoil experiments conducted at the Seiler Laboratory. The results show that both positive and negative vorticity is produced by the top surface of the airfoil with a zero vorticity flux located approximately at the hinge chord location because the sum of the two angles ($\theta + \xi$) goes through 90° in this vicinity. Since the NACA 0015 is a symmetric airfoil the bottom surface vorticity production is a negative of the top surface generation rate, and the total instantaneous vorticity generation produced by the tangential surface acceleration of the pitching airfoil will be identically zero at all times. In addition one can also conclude from Morton's (6) discussion that the total vorticity production from the tangential surface pressure gradient will also identically cancel at all times such that no net vorticity is created by the body.

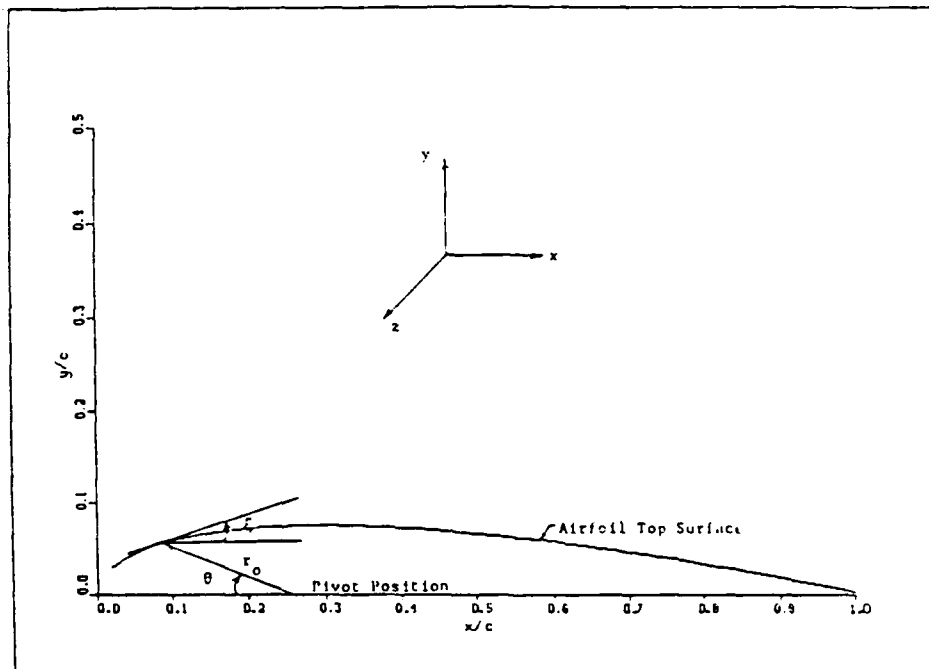


Figure 1. Schematic of Airfoil Geometry and Coordinate System.

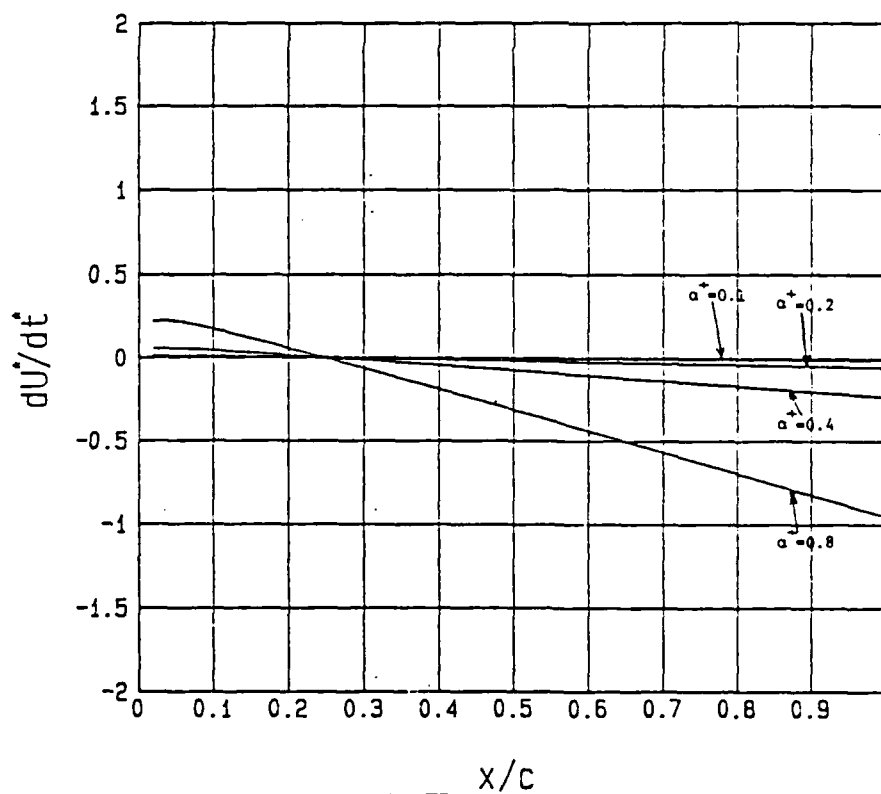


Figure 2. Tangential Surface Acceleration Curves for Pitching Airfoil at Various α Values with Pivot at $x_h = 0.25 c$.

$$U^* = U_s/U, \quad t^* = tU/c. \quad 3-6$$

Vorticity generation from the tangential surface acceleration for the upper surface pitching about various hinge positions is shown in figure 3. As the hinge position is moved down the chord the relative amounts of positive and negative vorticity generation change with the zero flux position corresponding closely to the pivot location.

The determination of the vorticity generation by the tangential surface pressure gradients is considerably more complex than the surface acceleration analysis since the surface pressure gradient depends directly on the flow character. To evaluate this generation term point surface pressure measurements from previous experimental results provided by Major J.M. Walker, Chief of the Mechanics Directorate at the Seiler Research Laboratory were analyzed. The raw surface pressure data was obtained from 18 pressure transducers located at various downstream position along the airfoil surface.

Typical surface pressure measurements are shown for a value of $\alpha^+ = 0.2$ at various attack angles in figures 4a-d. Both the instantaneous coefficient of pressure curve and its tangential surface gradient are shown in each figure. The surface pressure gradients at all angles of attack are positive over most of the airfoil top surface. According to equation (1) these positive gradients will produce positive z direction vorticity. This positive vorticity production will tend to induce reversed or separated flow close to the airfoil. This is, of course, the situation that arises in steady aerodynamics as the attack angle nears the stall angle, and the separation region spreads over the airfoil surface. For pitching airfoils this result is avoided by apparently preventing the spread of the separation region over the entire upper airfoil surface.

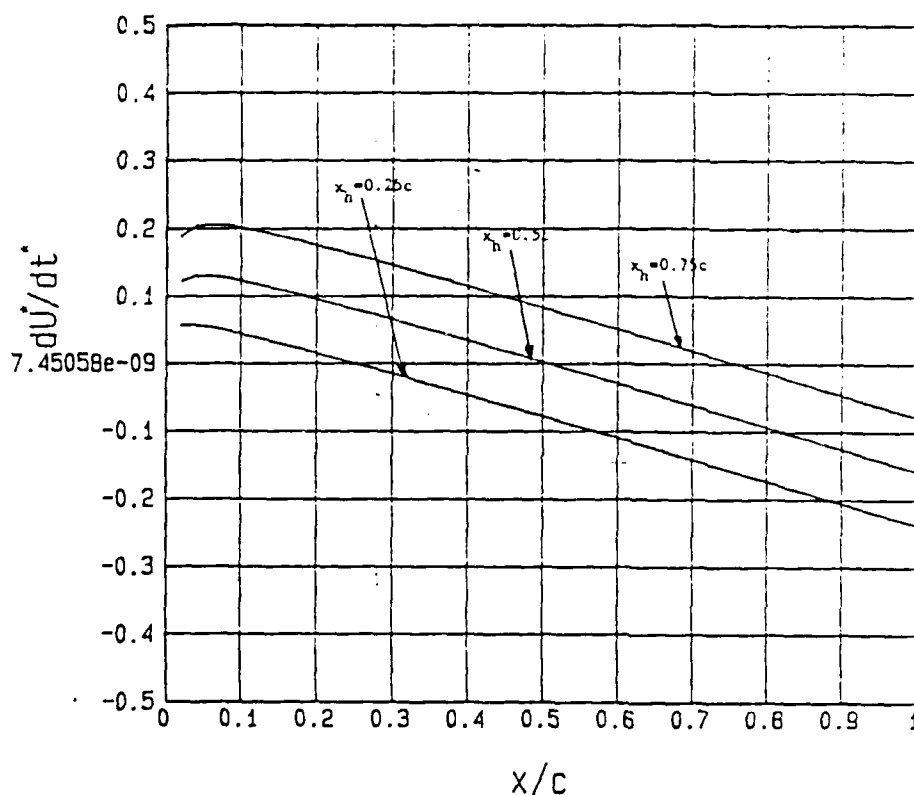


Figure 3. Tangential Surface Acceleration Curves for Pitching Airfoil with Various Pivot Locations, $\alpha^+ = 0.2$.

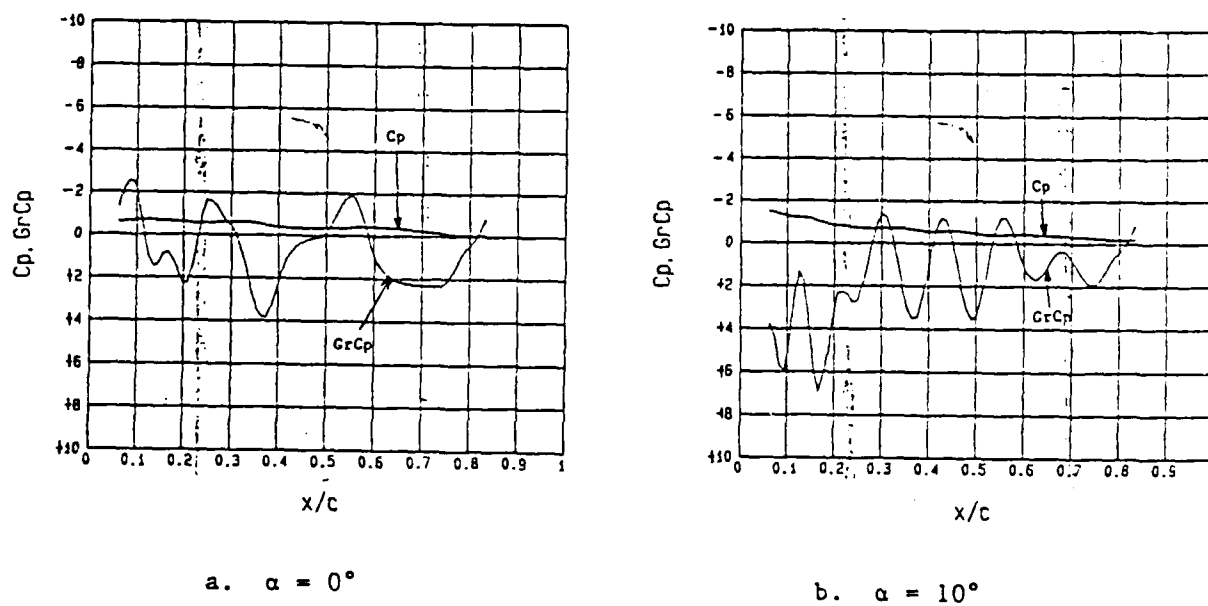
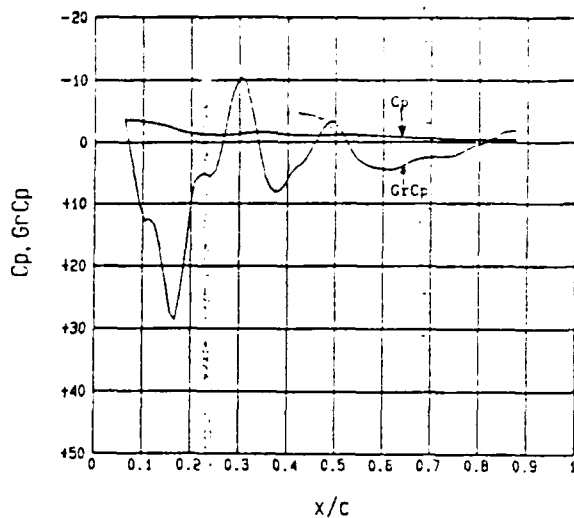
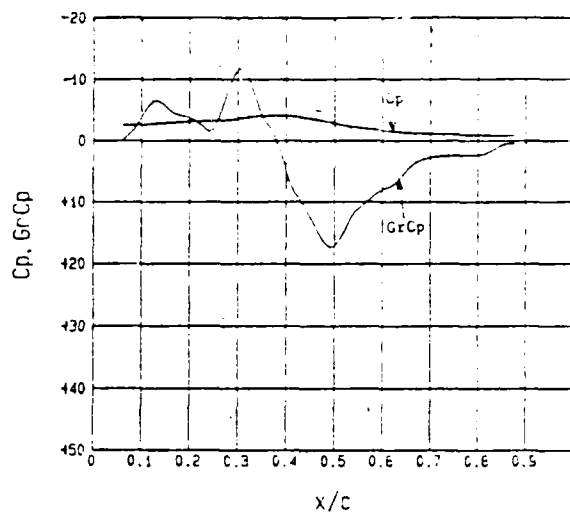


Figure 4. Tangential Surface Pressure Gradients for Pitching Airfoil, $\alpha^+ = 0.2$.



c. $\alpha = 20^\circ$



d. $\alpha = 40^\circ$

Figure 4. Tangential Surface Pressure Gradients for Pitching Airfoil, $\alpha^+ = 0.2$.

A comparison of the two vorticity generation terms can now be made. The negative z vorticity produced by the surface acceleration term downstream of the pivot location will tend to counteract the positive vorticity produced by the surface pressure gradients. However, for cases involving relatively low α^+ values (0.1 - 0.4) it would not appear that the surface acceleration values are of comparable magnitude to the levels of pressure gradient encountered even at moderately low angles of attack. The large influence of the airfoil pitching motion on the maximum coefficient of lift observed by Walker, Helin and Chou (8) can thus apparently not be explained easily through a simple superposition of vorticity generation terms. Since the pressure gradient term is a product of the fluid dynamics of the system small changes in the boundary conditions must be reflected as large effects in the flow through the nonlinearity of high Reynolds number flow. It therefore appears that well designed experiments are needed which better separate

the individual vorticity generation terms so that their separate effects can be better understood.

III.2 Image Analysis of Flow Visualization Experiments

The influence of airfoil pitching motion on the development of stall formation and the relationship between dynamic stall vortex growth and lift and pressure drag over the airfoil were studied using digital image analysis of flow visualization results previously obtained. The subject of the flow visualization was also a two dimensional NACA 0015 airfoil driven at constant pitching rates over attack angles from zero to 60 degrees in a uniform air stream. The digital image analysis techniques were performed using an International Imaging System 570. Photographs obtained from high-speed motion film taken at α^+ values of 0.1 and 0.2 were studied over angles of attack between the formation of the stall vortex and its eventual detachment from the airfoil surface.

The major objective of the image analysis technique was to clearly determine the stall vortex boundary from each photograph. Once this vortex boundary was defined the vortex growth and position could then be quantified as a function of attack angle.

The first step in the image analysis procedure employed an imaging technique which enhanced the contrasts between light and dark areas of the smoke streakline flow over the airfoil. The resulting image from this technique was then used to determine the leading and upper edges of the stall vortex at each attack angle.

Determination of the trailing edge of the stall vortex was somewhat more difficult since this edge merged with the thin turbulent separation region covering the remaining portion of the airfoil. This difficulty

was overcome by tracking the trailing edge of the dynamic stall vortex backwards in time from its eventual departure from the airfoil surface. Enhanced flow visualization pictures from four attack angles are displayed in figure 5 for an $\alpha^+ = 0.1$. The development of the dynamic stall vortex region with increasing attack angle is readily apparent in these figures.

The vortex area growth as a function of attack angle was quantified using an image analysis program to color the vortex region. A 6 x 6 pixel grid was then placed over the artificially colored area. The number of grid squares associated with the colored region were then computed to produce a reasonably accurate vortex area estimate. For each α^+ value the area measurement was initiated when the dynamic stall vortex was first discernable on the top surface of the airfoil. The area measurement was then continued until the vortex became clearly detached from the airfoil surface or the maximum attack angle was reached.

The relationship between the vortex location and the pitching motion of the airfoil was determined from measurements of the vortex center on an axis perpendicular to the chord. The vortex center was defined to be halfway between the leading and trailing edges of the stall vortex at each angle of attack and was obtained from the digitally enhanced images used in the vortex growth measurements. The vortex growth and location data obtained were then plotted as a function of angle of attack.

Vortex growth as a function of α plots at constant α^+ values but differing $\dot{\alpha}$ and U values are shown in figures 6a and b, for α^+ values of 0.1 and 0.2 respectively. The curves for $\alpha^+ = 0.1$ in figure 6a indicate similar growth rates at constant α^+ for each vortex if allowance is made



$\alpha = 24.7$



$\alpha = 25.3$



$\alpha = 28.7$



$\alpha = 29.3$

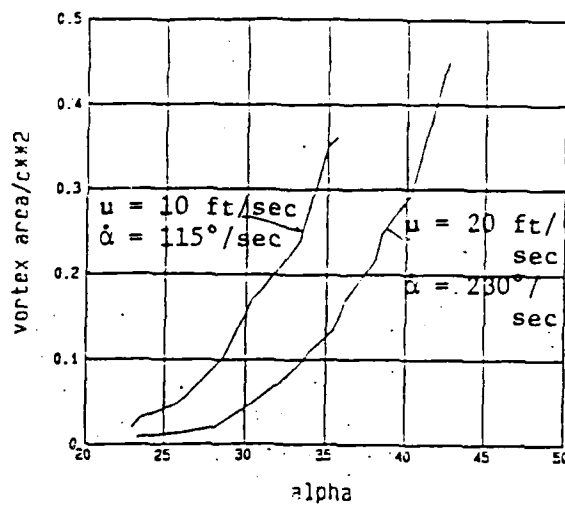
Figure 5. Enhancement of dynamic stall vortex boundaries. $\alpha^+ = 0.1$,
 $u = 10^{11}$ /sec.

for the slightly different vortex initiation angles. The $\alpha^+ = 0.2$ curves in figure 6b also show similar growth rates which appear slightly slower than the $\alpha^+ = 0.1$ curves.

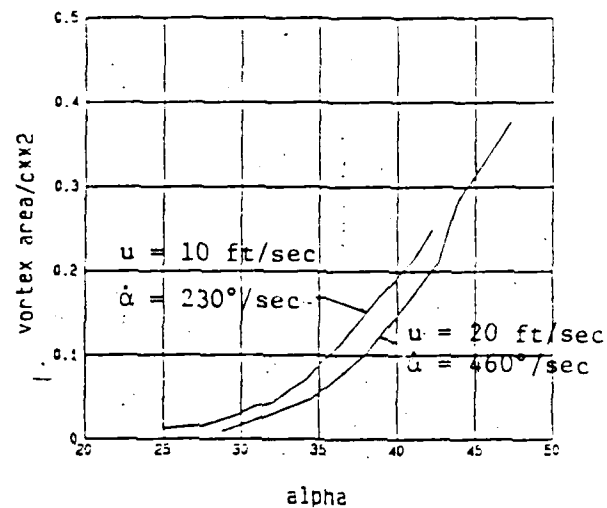
Figure 7 shows experimentally measured lift coefficients as a function of α for an $\alpha^+ = 0.2$ from a similar airfoil. These data were furnished by W.D. Siuru from analyses of experiments performed by the Seiler Laboratory Aeromechanics group. The lift coefficient curves indicate that a general reduction in slope occurs near an attack angle of 24° which corresponds closely to the observation of the vortex initiation discussed previously. The curve acquires a negative slope near an attack angle of 38° which also corresponds closely to the initiation of the fast vortex growth previously mentioned.

Figure 8, also from Siuru's analyses, displays the experimentally measured pressure drag coefficient as a function of α for an $\alpha^+ = 0.2$. The drag coefficient increases up to approximately 40° and then begins a steady decrease. The beginning of this decrease appears to correspond closely to the detachment of the stall vortex from the airfoil surface shown previously.

Plots of the stall vortex center location as a function of attack angle are shown in figures 9a and b for $\alpha^+ = 0.1$ and 0.2 respectively. The similarity of the curves at constant values of α^+ indicates again the importance of α^+ as a parameter for this unsteady flow. In addition, the attack angle at which the stall vortex center moves into the $x/c = 0.25$ position coincides with the angle at which the stall vortex growth rate undergoes a rapid increase for both α^+ values of 0.1 and 0.2 . This result indicates that a possible connection between the pivot location and the dynamic stall vortex behavior may exist. Further experiments are needed to clarify this possibility.



a. $\alpha^+ = 0.1$



b. $\alpha^+ = 0.2$

Figure 6. Dynamic stall vortex area versus angle of attack.

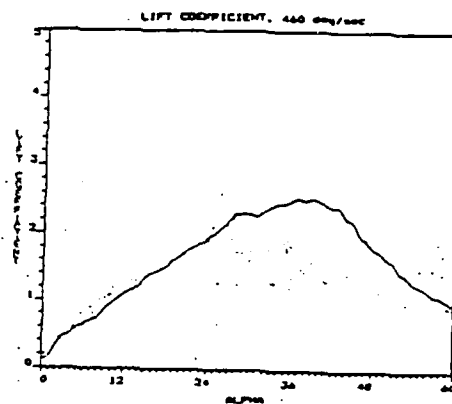


Figure 7. Lift coefficient versus angle of attack.
 $\alpha^+ = 0.2$, $u = 20$ ft/sec

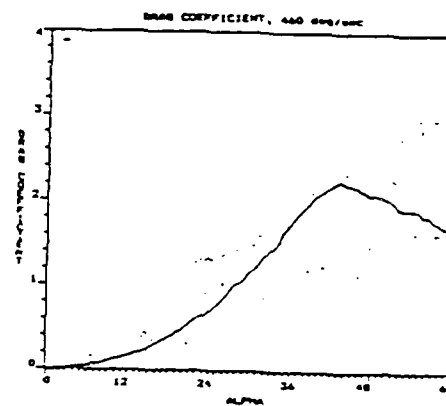
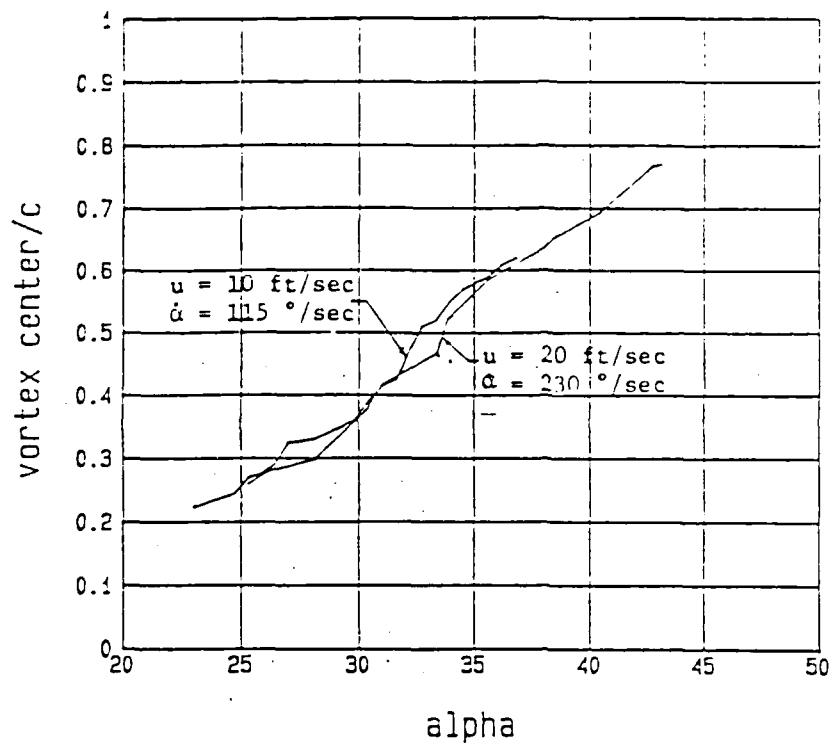
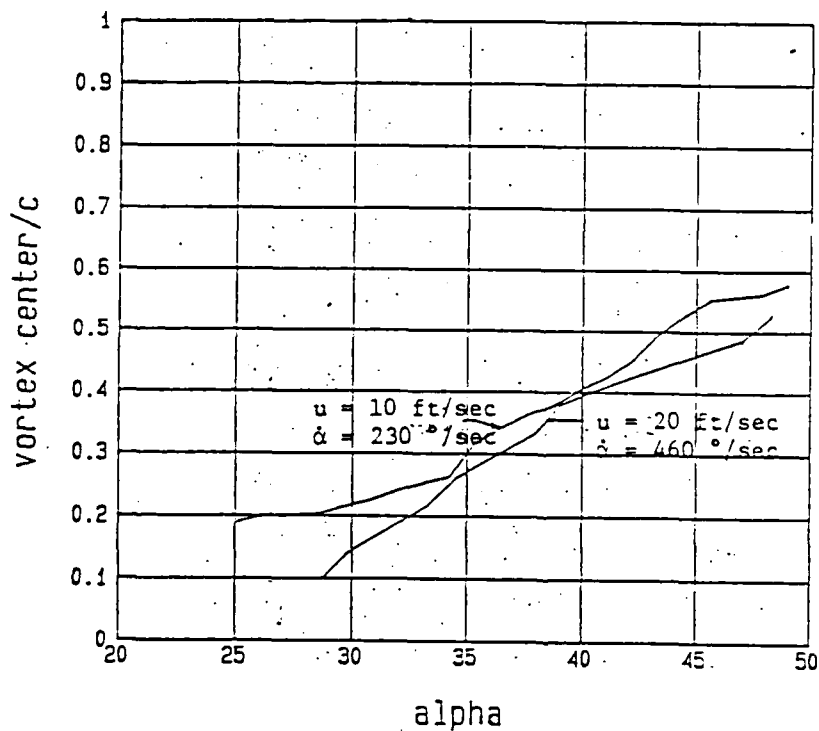


Figure 8. Drag coefficient versus angle of attack.
 $\alpha^+ = 0.2$, $u = 20$ ft/sec



a. $\dot{\alpha} = 0.1$



b. $\dot{\alpha} = 0.2$

Figure 9. Dynamic stall vortex position along the airfoil versus angle of attack.

IV. Conclusions

The following conclusions from this study apply to a NACA 0015 airfoil pitching at constant rates.

1. The nondimensional parameter α^+ was shown to be associated with the ratio of vorticity generation rates by unsteady surface motions and surface pressure gradients.
2. The maximum value of lift obtained by the pitching airfoil occurs near the angle of attack at which the dynamic stall vortex becomes apparent.
3. The rapid growth of the dynamic stall vortex with increasing attack angle was found to coincide with decreasing values of lift.
4. The departure of the dynamic stall vortex from the airfoil surface was found to coincide with a decrease in the pressure drag.

V. Recommendations

This study has shown that important insights into the nature of unsteady vorticity production from pitching airfoils can be developed through the use of simultaneous flow visualization and point sensor measurements of flow variables. In addition the use of digital image analyses techniques was shown to enhance and clarify interpretations from the visual information. It is recommended that the analysis techniques employed here be used on certain additional focussed experimental situations to further examine the effects of unsteady vorticity production on airfoils. Three experimental studies which appear to have

high potential for further analyses using the technique employed in this research are:

1. A study of airfoils subjected to translational accelerations such that the effects of vorticity generation from surface pressure gradients and unsteady surface motions can be more explicitly separated.
2. A study of airfoils for which the pivot location is changed to determine if the surface distribution of the vorticity generation from the unsteady acceleration term is an important factor.
3. A study of airfoils pitching at low α^+ values to determine how small values of unsteady motion are able to cause large changes in the aerodynamic forces on the airfoils.

VI. References

1. Browand, F.K. and Troutt, T.R., "A Note on Spanwise Structure in the Two-Dimensional Mixing Layer," J. of Fluid Mech., 97, 1980, 771-781.
2. Troutt, T.R. and McLaughlin, D.K., "Experiments on the Flow and Acoustic Properties of a Moderate Reynolds Number Supersonic Jet," J. of Fluid Mech., 116, 1982, 123-156.
3. Troutt, T.R., Scheelke, B. and Norman, T.R., "Organized Structures in a Reattaching Separated Flow Field," J. of Fluid Mech., 143, 1984, 413-427.
4. Browand, F.K. and Troutt, T.R., "The Turbulent Mixing Layer: Geometry of Large Vortices," J. of Fluid Mech., 158, 1985, 487-504.
5. Bhattacharjee, S., Scheelke, B. and Troutt, T.R., "Modifications of Vortex Interactions in a Reattaching Separated Flow," AIAA J., 24, 4, 1986, 623-692.
6. Morton, B.R., "The Generation and Decay of Vorticity," Geophys. Astrophys. Fluid Dynamics, 28, 1984, 277-308.

7. Helin, H.E. and Walker, J.M., "Interrelated Effects of Pitch Rate and Pivot Point on Airfoil Dynamic Stall," AIAA Paper 85-0130, The Aerospace Sciences Conference, Reno, NV, Jan. 1985.
8. Walker, J., Helin, H., and Chou, D., "Unsteady Surface Pressure Measurements on a Pitching Airfoil," AIAA Paper 85-0532, AIAA Shear Flow Control Conference, Boulder, CO, March 1986.

1986 USAF-UES SUMMER FACULTY RESEARCH PROGRAM/
GRADUATE STUDENT SUMMER SUPPORT PROGRAM

Sponsored by the
AIR FORCE OFFICE OF SCIENTIFIC RESEARCH
Conducted by
UNIVERSAL ENERGY SYSTEMS, INC.
FINAL REPORT

AN APPARATUS FOR TRANSIENT SATURATION MEASUREMENTS
IN A HEAT PIPE

Prepared by	J.H. Ambrose
Academic Rank:	Graduate Student
Department and	Mechanical Engineering
University:	University of Kentucky
Research Location:	Aero Propulsion Laboratory, Aerospace Power Division, Power Technology Branch, Nuclear/Thermal Technology Group
USAF Researcher:	Dr. J.E. Beam
Date:	July 14, 1986
Contract No.:	F49620-C-0013

An Apparatus for Transient Saturation Measurements in a Heat Pipe

by

J. H. Ambrose

ABSTRACT

This report describes the design and fabrication of an apparatus which will be used to obtain direct measurements of the liquid distribution in a heat pipe wick during transient and steady state operation. Attenuation of x-rays by the liquid in the wick will be utilized for measuring the saturation as a function of time and position.

Saturation measurements have been made in heat pipes in the past using radiography. However, all cases of detailed measurements were limited to the case of steady state operation. Real time neutron imaging systems are still under development and these present the most promise for imaging of liquids through metals. X-ray radiography is usually not very useful because the metals attenuate x-rays strongly while liquids attenuate x-rays very weakly.

To facilitate accurate saturation measurements using x-ray radiography, a special heat pipe was designed with beryllium walls which are relatively transparent to x-rays. Thus, the attenuation of the wall material has been kept very low, enabling the use of very low energy x-rays. A synthetic fabric is used as the wicking material and it too is fairly transparent. The liquid attenuates x-rays strongly enough to be seen through the wall and wick material. Transient measurements will be accomplished by taking rapid exposures of the apparatus at short time intervals, and determining the saturation distribution with a recording microphotodensitometer.

ACKNOWLEDGEMENTS

The work described in this report was performed at the Air Force Aero-Propulsion Laboratory, Wright Patterson AFB, Ohio, under the sponsorship of the Air Force Systems Command and Air Force Office of Scientific Research. The author sincerely acknowledges the guidance provided by his SFRP supervising professor, L. C. Chow and also that provided by Dr. J. E. Beam. The technical assistance provided by Mr. D. Reinmuller at the Air Force Aero Propulsion Laboratory Thermal Lab and Mr. Harold Kamm, Universal Technology Corporation, at the Air Force Materials Laboratory Nondestructive Evaluation Lab is appreciated.

I. INTRODUCTION:

Heat pipes will play a major role in thermal energy management for future Air Force space missions. As such the transient behavior of such devices should be well understood so that thermal control systems can be designed to operate effectively over a wide range of loading conditions.

During the 1985 AFOSR/UES summer program, the author investigated transient heat pipe response [1]. The analytical and experimental investigation focused on dryout and rewetting of a heat pipe subjected to a pulsed heat input. The analytical model was a simple one-dimensional model to predict the liquid movement in the wick during dryout and rewetting. The experimental work consisted of measuring the transient external temperature profile of a screen wick, water heat pipe subjected to pulsed heat loads. Considering the highly simplified nature of the one-dimensional model, the agreement between theory and experiment was good.

Although the simplified model of transient response provided useful information, it is the author's goal to obtain a more detailed understanding of the mechanisms involved in transient response of the heat pipe. The actual heat and mass transfer processes occurring in the heat pipe wick during transient operation are definitely more complex than those of the model. A slightly more refined finite element model was developed in which the wick pores were modeled as a series of capillary tubes with semi-spherical menisci. This allowed the liquid pressure to be related to the amount of liquid present in any area of the wick. This saturation dependence of the capillary pumping is central to the problem of modeling the wick as finite elements. The capillary tube model proved to be too crude to describe the actual dependence. To accurately model the saturation dependence of the pumping requires more study. If the finite element model is to be compared with experiment, a detailed measurement of the liquid movement in the wick is also necessary.

II. OBJECTIVES OF THE RESEARCH EFFORT:

The goal of the author's research project was to develop an experiment which would enable direct measurement of the liquid saturation in the wick of a heat pipe as a function of both position and time. The operating conditions within the heat pipe apparatus should closely resemble those in actual heat pipes which would be useful for thermal control systems. This experiment should also provide for detailed measurement of internal temperatures of the wick and vapor core of the heat pipe. From this experiment, valuable information should be attainable regarding the transient behavior of the heat pipe working fluid under a variety of operating conditions.

III. ALTERNATIVE METHODS:

Several methods of obtaining a direct measurement of the saturation in the heat pipe wick were considered. The relative difficulty and merits of each of the methods were assessed. A major consideration was whether a given method could be implemented while still maintaining an apparatus which resembled an actual heat pipe in operation. The different alternatives which were considered are outlined below. Advantages and disadvantages of each method is discussed.

a. Neutron Radiography:

Neutron radiography is an excellent candidate for imaging of some fluids within metal containers. This is a result of the very high absorption of thermal neutrons by fluids such as hydrogen, water and lithium. Neutron images of water and lithium heat pipes have been used successfully in the past to determine position of the working fluid [2,3]. These were images of a steady state phenomena. To obtain satisfactory transient measurements would require very large fluxes of neutrons or new imaging techniques such as those used for real time neutron imaging. Because very high neutron fluxes are impractical and real time neutron imaging

is still in the developmental stages [4], neutron radiography was ruled out as a viable candidate for transient measurements.

b. Capacitance:

Capacitance measurements have been used to measure working fluid distribution [5] in heat pipe wicks. This method relies on the change in capacitance between two electrodes produced by the presence of a dielectric fluid. This method allows good transient response because the capacitance is measured instantaneously. It is difficult to obtain detailed local measurements with this technique because it would require many electrodes within the heat pipe. Also, the requirement that the wick form a nonconducting path inhibits the use of metallic wall materials.

c. Attenuation of Laser Beam:

This method would allow local, transient measurements to be made in a grooved or transparent wicked heat pipe. The probable boiling which would occur in the wick would seriously affect the accuracy of such a measurement. Vapor bubbles in the wick would provide many reflecting interfaces oriented at all arbitrary angles to the incident beam, making accurate measurement of liquid amounts impossible.

d. X-ray Radiography:

This method is difficult to apply to imaging of fluids because of their low attenuation of x-rays. Conventional heat pipe wall materials such as steel and copper attenuate much greater than the working fluid. However, if a weakly attenuating wall and wick material were selected, an accurate measurement of the working fluid distribution could be obtained.

c. X-ray Diffraction:

X-ray Diffraction has long been used for the measurement of thin coatings on metals [6]. The collimated beam of x-rays is directed at an angle onto the surface and is partially reflected from the substrate material. The beam is attenuated as it passes through the coating material. This method could be applied to measuring liquid amounts within a wick. However, because of the low diffracted intensity, the measurement must involve counting the x-ray quanta rather in order to be accurate. The method is thus only useful for one local measurement per detection device.

After considering the above methods for obtaining the transient saturation measurement, x-ray radiography was selected as the most feasible for obtaining saturation measurements as a function of both position and time.

IV. DESIGN OF HEAT PIPE APPARATUS:

Having selected x-ray radiography as the most viable method, the task of designing an apparatus consisted of determining the best geometry and materials. The design must resemble a conventional heat pipe in operation, and also allow the x-ray attenuation of the working fluid to be at least as great as that of the other elements. The heat pipe design is shown in figure 1. The different elements of the heat pipe design are described in the subsections that follow.

a. Wall Material:

The wall material of the heat pipe is most important, because the conventional heat pipe wall materials such as steel and copper would absorb (at least two orders of magnitude) more x-rays than

the working fluid. Beryllium was chosen for the wall material because it is very transparent to x-rays and also is a strong metal and a good conductor of heat. There are some disadvantages to using beryllium but it was felt that all of these could be overcome. Beryllium has not been applied as a heat pipe material to date, and hence compatibility with working fluids is not known. Much information exists on the corrosion of beryllium in water, and from this, it would appear to be incompatible. The corrosion of beryllium by water can be controlled by using high purity water, but even at the lowest corrosion rates reported (<0.1 mils per year, defilmed weight loss, [7]) the evolution of hydrogen from the oxidation reaction would be significant. If the outgassing is enough to affect the performance of the heat pipe in a short time (days) then two courses of action may be taken. The first is to change working fluids. Candidate fluids other than water which will be considered include freon, methanol, ethanol and acetone. The other action is to electroplate the beryllium with a layer of copper or other more compatible metal. The electroplating of beryllium has been investigated extensively [7] and can be accomplished without undue problems. The plating would have to thin, of one micron or less with copper, to ensure that it will not attenuate x-rays too strongly.

b. Wick Material:

The wick material would also represent a larger x-ray absorber than the working fluid if a conventional metal screen wick were used. Synthetic screening fabrics were chosen because they are identical to the metal screens in geometry but are much weaker absorbers of x-rays. The screens are made of polyester, teflon or polypropylene monofilaments and are available in a wide variety of meshes and thread diameters. The temperature rating of the fabrics ranges from 121 °C for polypropylene to 260 °C for teflon and is suitable for low temperature heat pipes such as

water. The major difference between the synthetic fabric and metallic screens is their lower thermal conductivity. However, Phillips [8] has shown that the thermal conductivity of the solid phase has only a weak effect on the effective conductivity of fluid saturated screen wick samples. Water will wet only the polyester wicks but the other liquids mentioned above will wet all three types of wick material.

c. External Heat Load:

It is important to obtain detailed measurement of the saturation in the evaporator section of the heat pipe because this is where the significant variations will occur. The method of heat input usually used for heat pipe tests are nichrome or other metallic electrical resistance heaters and these would greatly interfere with radiography in the heated region. Two alternatives were available to provide heat input without greatly reducing the incident x-ray intensity. The first was to construct a very thin resistive element of a low atomic number material. The second was to use radiant heat input, allowing a gap through which x-rays could pass unabsorbed. The second method is advantageous because it does not absorb x-rays. Problems arise in the measurement of the radiative heat input, where a small error in temperature on one surface can produce a large error in the calculated heat flux value. An electric resistance heater was chosen because it would facilitate accurate measurement of the heat input. The heater is fabricated from thin (0.035") graphite strips which are relatively low absorbers. The ends of the graphite strip are coated with aluminum by a flame-spray process to provide good electrical contacts and thus ensure more uniform heating. Very thin (0.001") mica sheet will be placed between the graphite heater and the beryllium wall to provide electrical insulation.

The heat flux rejected from the condenser is lower than the heat flux input to the evaporator because of the condensers larger

area. Heat removal will be accomplished with forced air convection. This method has been proven effective for cooling heat pipes with moderate heat transport rates.

d. Temperature Measurements:

It is important to have detailed temperature measurements but at the same time not to upset the flow of working fluid with the measurement probes. To accomplish this, many very fine thermocouples will be fed through the heat pipe wall and imbedded in the wick at regularly spaced locations. The layout of the thermocouples is shown in figure 2. The positioning minimizes the intrusion into the liquid and vapor flow. The very fine diameter wires are difficult to seal with conventional feedthroughs. Therefore a special feedthrough was constructed by sealing the wires into a 1/8" tube with epoxy and then feeding this through a conventional compression seal.

V. EXPERIMENTAL PROCEDURE:

This section describes the method which will be used to obtain the saturation measurements. The key elements of the experimental apparatus are:

1. Heat pipe
2. X-ray machine
3. Data logger
4. Power supply
5. Coolant flow
6. X-ray shutter mechanism
7. X-ray film and advance mechanism

The heat pipe is first cleaned, purged and filled with the

appropriate amount of pure degassed working fluid. It is then positioned between the x-ray tube and the film. Thermocouple readings are taken with the data logger. Power input to the graphite heater is via the low voltage, high current DC power supply. The experiment is controlled remotely from outside of the x-ray facility.

Measurements may be made under transient operating conditions by using the shutter to expose the x-ray film for a period of approximately two seconds. Power input to the x-ray tube is at 15 kilovolts peak to obtain the best resolution of the working fluid. At least 10 mA of tube current is used because of the short exposure times. The x-ray film is then advanced by the remotely controlled advance mechanism so that an unexposed section of film is in place. Subsequent exposures may be made at intervals of as little as a few seconds. The time and duration of each exposure is noted for comparison with power input and temperature readings from the data logger. A feedback loop will be programmed into the data logger to prohibit condensate from forming on the unwicked walls of the heat pipe. This feedback control will compare the vapor temperature to that of the unwicked walls, and will turn on low power heating foils attached to the walls as necessary. In this way the unwicked walls will be maintained at the vapor temperature.

Once the test is completed, the x-ray film must be developed and processed to obtain the saturation data. X-rays of completely saturated and completely dry wicks are taken as calibration standards for the densitometer. Each exposure is scanned by the recording micro photodensitometer along several different lines. The photodensitometer is a double-beam type in which a single beam of light is split, passes through both the film sample and reference wedge, and is received by a photomultiplier. Any difference in intensity causes movement of the reference wedge to the corresponding density location, and the recording pen is connected to the wedge. In this way, relative exposure of exact locations on the film may be recorded on a chart. The exact density of the film at any location is related directly to the amount of the incident x-ray beam which was not attenuated by the apparatus. By

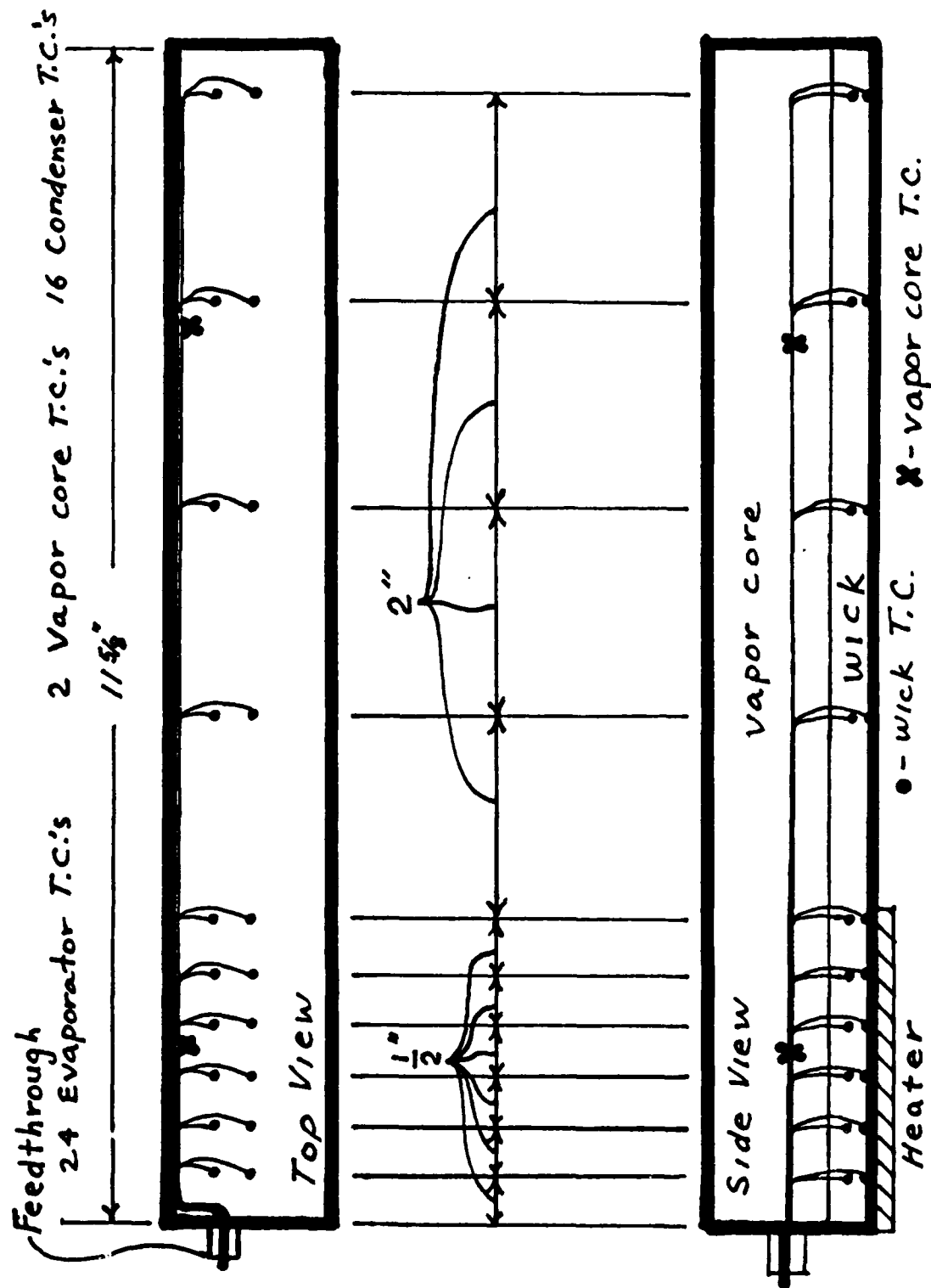
comparison with the calibration standards, the chart of density vs. location is converted to one of saturation vs. location for a given time.

VI. RECOMMENDATIONS:

The apparatus and experimental technique described in this report might be applied to investigation of other thermal management topics of interest to the Air Force. One such area is the investigation of melting and freezing of thermal storage salts. Another area is a study of the effectiveness of condensate removal obtained with various wicked radiator surfaces.

REFERENCES

1. Ambrose, J.H., "Prediction of Heat Pipe Rewetting Behavior," Final Report, 1985 USAF-UES Summer Faculty Research Program/Graduate Student Summer Support Program.
2. Moss, R.A., and A.J. Kelly, "Neutron Radiographic Study of Limiting Planar Heat Pipe Performance," Intl. J. Heat and Mass Transfer, Vol. 13, pp. 491-502, 1970.
3. Merrigan, M.A., E.S. Keddy, and J.T. Sena, "Transient Performance Investigation of a Space Power System Heat Pipe," AIAA Paper No. 86-1273, Presented at the AIAA/ASME 4th Joint Thermophysics and Heat Transfer Conference, Boston, Mass., June 2-4, 1986.
4. Matsumoto, G., M. Tamaki, K. Ohkubo, and Y. Ikeda, "Real-Time Imaging of Working Fluids in Heat Pipes by Neutron Television," Proc. 5th Intl. Heat Pipe Conf., Tsukuba, Japan, 1984.
5. Shishido, I. and S. Ohtani, "Working Fluid Distribution within Heat Pipe Wick," Proc. 5th Intl. Heat Pipe Conf., Tsukuba, Japan, 1984.
6. Friedman, H., and L.S. Birks, "Thickness Measurement of Thin Coatings by X-Ray Absorption," Review of Scientific Instruments, Vol. 17, No. 3, March, 1946.
7. White, D.W., and J.E. Burke, Eds., The Metal Beryllium, Cleveland, Ohio, The American Society for Metals, 1955.
8. Phillips, J.R., L.C. Chow, and W.L. Grosshandler, "Thermal Conductivity of Layered Cloth Heat Pipe Wicks," to be presented at the ASME Winter Annual Meeting, Anaheim, CA., November, 1986.



NOT TO SCALE

FIGURE 2

Direct
Saturation
Measurement
Apparatus

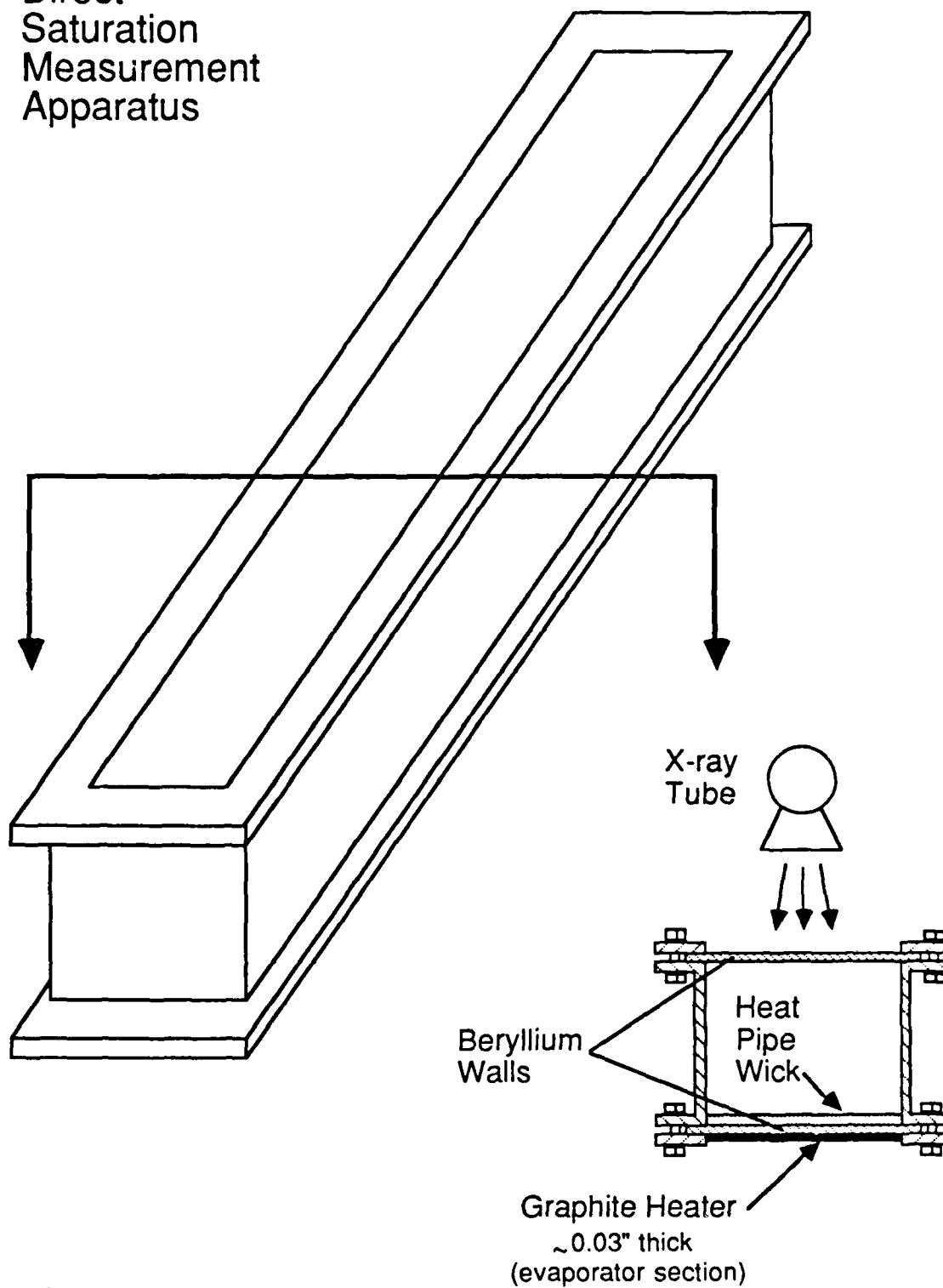


FIGURE I

1986 USAF-UES SUMMER FACULTY RESEARCH PROGRAM/
GRADUATE STUDENT SUMMER SUPPORT PROGRAM

Sponsored by the
AIR FORCE OFFICE OF SCIENTIFIC RESEARCH
Conducted by the
Universal Energy Systems, Inc.

FINAL REPORT

FLIGHT CONTROL SYNTHESIS
WITH PRACTICAL DESIGN CONSTRAINTS

Prepared by:	Mark R. Anderson
Academic Rank:	Doctoral Candidate
Department and	School of Aeronautics and Astronautics
University:	Purdue University
Research Location:	Flight Dynamics Laboratory (AFWAL/FIGCB) Wright Patterson AFB, OH
USAF Research:	Frank L. George
Date:	July 30, 1986
Contract No.:	F49620-85-C-0013

FLIGHT CONTROL SYNTHESIS
WITH PRACTICAL DESIGN CONSTRAINTS

by

Mark R. Anderson

ABSTRACT

Of the many requirements a flight control system must meet, the most important issues relevant to preliminary design are: closed-loop performance, stability robustness, and control law complexity. For the flight control problem, closed-loop performance is defined by how well the augmented vehicle dynamics meets given airworthiness specifications. However, these specifications must be met within the constraints imposed by the control surface actuation hardware. The apparent design trade-off between meeting flying qualities specifications within actuation constraints is discussed.

ACKNOWLEDGMENTS

I would like to thank the Air Force Systems Command and the Air Force Office of Scientific Research for sponsorship of my research effort. This program gave me the unique opportunity to broaden my education outside of the university environment. I would also like to thank the staff of the Wright Patterson AFB Flight Dynamics Laboratory, Control Dynamics Branch, especially my Air Force supervisor, Mr. Frank L. George, for their friendly guidance and encouragement.

Finally, and most importantly, I would like to thank my wife, Donna, for her boundless patience and understanding throughout the summer.

I. INTRODUCTION:

I received a Master's Degree in Engineering from Purdue University in December, 1984. Since that time I have been studying techniques to address handling qualities objectives in flight control design as part of my doctoral research requirements. Preliminary research in this area, reported in Ref. [1], led to a proposed flight control law synthesis strategy which forms the basis for work this summer.

Because the problem area encompasses both aircraft handling qualities specifications and flight control synthesis methods, I was assigned to the Air Force Flight Dynamics Laboratory (AFWAL/FIGCB) for the summer research period.

II. OBJECTIVES OF THE RESEARCH EFFORT:

A simplified block diagram of the design strategy proposed in Ref. [1] is shown in Fig. #1. This diagram represents the various parts of a design program beginning with the desired handling qualities specifications to a simple, low-order dynamic compensator required to meet the primary design objectives of closed-loop performance and stability robustness. With the backbone of the design procedure defined, the primary goal for this summer was to explore the potential weaknesses in the program by identifying theoretical gaps which might occur in use. This objective was accomplished primarily through an intensive literature review of methods available to address the requirements of each section (or block) of the proposed design

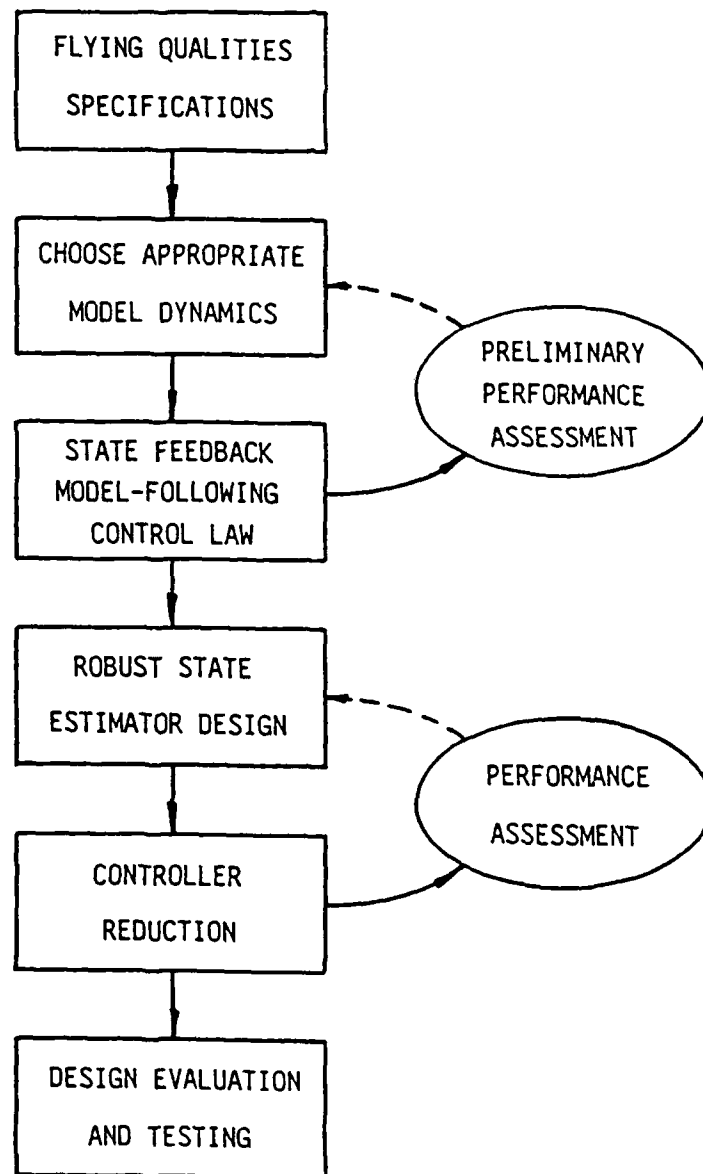


Fig. #1 - Proposed Flight Control Design Procedure

procedure.

Some of my specific objectives were:

1. Pinpoint the advantages and disadvantages of the various model-reference design algorithms available in literature.
2. Determine if "perfect" or "exact" model-following is necessary to meet the design objectives of the flight control designer.
3. Investigate the effects of non-linear elements (i.e., actuator hardware constraints) on the design process results.
4. Determine if model-reference design methods or specification models can be tailored to minimize the dynamic complexity of the resulting controller.

Detailed analysis and significant conclusions from this summer research period will be published in an Air Force Flight Dynamics Laboratory Technical Memo (Ref. [2]). The remainder of this final report constitutes a brief summary of the major results of this research.

III. MODEL-REFERENCE DESIGN TECHNIQUES:

From a pilot's perspective, a good airplane is one in which the pilot can perform his mission adequately, safely, and predictably. Including these desired characteristics in aircraft design invariably leads to defining specifications which the aircraft must meet to assure the pilot can complete his mission.

These specifications form the basis for the flight control designer's objectives. Whether they are incorporated directly in some

mathematical representation (i.e., frequency or time domain requirements) or they exist only in the mind of the designer, these properties must be incorporated into the design process.

One class of multivariable control synthesis techniques which readily accepts the definition of desired dynamic characteristics (as opposed to simple regulating or tracking design methods) is generally known as model-reference or model-following design techniques. These methods use some mathematical description of the desired model dynamics, to derive the appropriate control law which will allow the plant vehicle to behave similarly.

Over the summer research period, much of the available model-reference design literature was reviewed in order to evaluate the ease in which each algorithm could be used to address important flight control design objectives. Table #1 includes a general grouping of algorithms studied with regard to objectives important in this specific research problem. Details of this evaluation will be included in Ref. [2], Appendix A.

In general, it was found most model-reference design algorithms can be placed in one of two groups depending on their block diagram structure. One group includes designs requiring dynamic control system elements in the feedback path only, as shown in Fig. #2. The other group consists of designs which may require both feedforward and feedback control elements. This structure is shown in Fig. #3. One can see in Table #1 (Column 5) the structure of the resulting control system has a significant impact on the control effort required in implementation. This trend results from the generally higher feedback

Table #1 - Model-Reference Algorithm Comparison

MODEL-FOLLOWING (MF) TECHNIQUE	REF.*	FEEDBACK ONLY STRUCTURE	FEEDFWD/ FEEDBACK STRUCTURE	PERFECT MF POSSIBLE	CONTROL EFFORT REQ'D.	ALGORITHM COMP. EFFORT	STABILITY GUARANTEE	REQ'D. ACTUATOR BANDWIDTH
STATE SPACE IMPLICIT MF	15-18	X		X	LO	LO		
STATE SPACE FEEDFWD CONTROL	36-37, 39-40		X	X	HI	LO		
EIGENSPACE ASSIGN.	19-23	X		X	LO	LO		
TRANSFER MATRIX MATCHING	27-29	X		X	LO	HI		
OPTIMAL QUADRATIC IMPLICIT MF	7-14	X		X	LO	LO	X	X
OPTIMAL QUADRATIC EXPLICIT MF	8,9,12,14, 17,22, 31-33,35		X		HI	LO	X	X
OPTIMAL QUADRATIC EXPLICIT MF W/ERROR RATE WEIGHTING	8,14,34,35		X	X	HI	LO	X	X

*Reference list from Ref. [2]

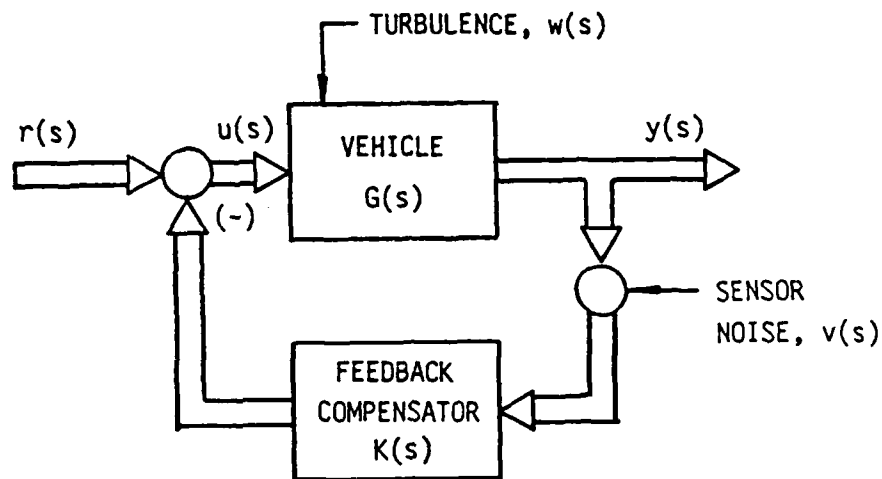


Fig. #2. - Model-Matching with Feedback Compensation Only

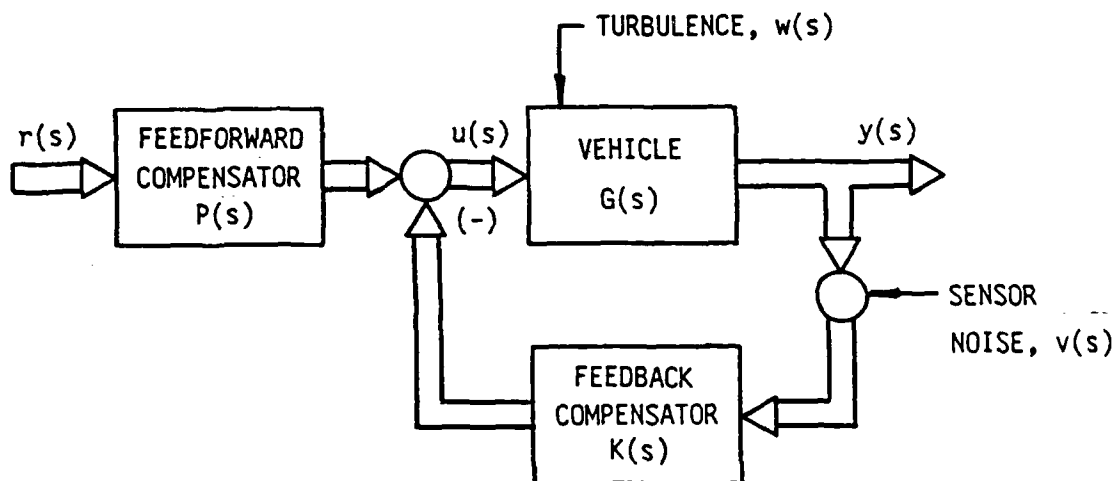


Fig. #3. - Model-Following with Feedback and Feedforward Compensation

gains required to force the augmented vehicle to "follow" the model dynamics, represented in the feedforward compensator of Fig. #3. An in-depth analysis of this effect is presented in Ref. [3].

Of particular interest are algorithms which can provide "perfect" or "exact" model-following. These algorithms, represented by an 'X' in the fourth column of Table #1, result in feedforward and/or feedback compensation which will allow the augmented vehicle to behave exactly like the specified model dynamics. In practical application, perfect model-following is very difficult to achieve in the presence of finite bandwidth control surface actuation hardware. However, solution methods and closed-loop properties of perfect model-following systems should be understood since they provide an "ideal" which actual designs can approach. A detailed analysis of perfect model-following constraints and synthesis techniques are included in Ref. [2], Appendix B. Conditions for perfect model-following are derived as well as solutions for state feedback and state feedforward/ feedback structures.

When perfect model-following is not possible due to limitations of control surface actuation hardware, a reasonable approximation is required which can effectively balance model-following fidelity with actuation control effort. Of the model-reference design techniques discussed in Table #1, the quadratic optimal model-following formulation can address this apparent design trade-off through the cost functional formulation. It is worth noting both the quadratic optimal implicit model-following and explicit model-following with error rate weighting algorithms can provide perfect model-following, when possible. Therefore, if properly defined, these algorithms will converge to the

solutions (and closed-loop properties) discussed in Ref. [2], Appendix B. The application of quadratic optimal model-following techniques to flight control design is covered in detail in Ref. [3].

IV. ACTUATION CONSTRAINTS AND IMPLEMENTATION

The technical paper cited in Ref. [3] includes a succinct discussion on the effect of finite actuator bandwidth on the flight control design process. Control surface actuator rate and deflection limits are addressed by including the turbulence response characteristics of the quadratic optimal control law designs.

The effect of a non-linear actuator deflection rate limit saturation on system stability margins is studied in Ref. [2], Appendix C. This study led to the definition of regions within the frequency domain in which stability robustness with respect to actuator rate saturation can be measured. The designer can use these regions as a guide in designing a control system less likely to be affected by actuator rate limiting. The study also considered a method using designed actuator cross-coupling in the analysis.

Once the state feedback control law has been designed using the recommended model-following design methods, proper measurement-based implementation is required. Ref. [1] recommended using robust state estimation methods[4,5] to derive a full-order dynamic feedback control law equivalent to the state feedback control law. These methods will retain the stability robustness properties of the state feedback system.

Several controller reduction schemes are available which might

reduce the dynamic order of the full-order compensator defined above. However, because controller reduction methods approximate the full-order controller, some closed-loop properties may be altered by the reduction process. Namely, flying qualities requirements may not be met when the reduced-order compensator is implemented.

A method is proposed in Ref. [2], Appendix D which combines quadratic optimal model-following, robust state estimation and a balanced controller reduction technique so the low-order control law might be "tuned" to regain desired flying qualities. Hopefully, dynamic compensators resulting from the design methodology will be simple enough that the experienced designer can use conventional feedback design rules to effectively tune the controller for "optimal" closed-loop performance.

V. RECOMMENDATIONS:

1. Although excellent results can be obtained using model-following techniques to meet handling qualities objectives, the designer must still use experience as a guide in choosing appropriate quadratic cost function weightings. Specific relationships between quadratic weightings and their effect on equivalent closed-loop handling qualities parameters could prove helpful to the inexperienced user.
2. State feedback control laws should directly incorporate handling qualities objectives within the constraints of actuation hardware. Similar methods which incorporate constraints of measurement sensor hardware on robust state estimator development process should be

investigated. For example, many current aircraft flight control systems use very low bandwidth angle-of-attack probe measurements for stability augmentation. One would expect that low bandwidth sensor dynamics would affect not only stability robustness properties but also closed-loop performance unless they were included in the design process.

3. Once an equivalent full-order dynamic compensator has been defined, controller reduction techniques can be used to reduce the dynamic order of the control law, thereby reducing the control law complexity. However, the reduction process must retain properties which define both the stability margins as well as the handling qualities of the system. It has not been determined which reduction procedure will produce the best results under these conditions frequency-weighted reduction techniques[6] may offer the best solution since the weighting process can accent a specific frequency range (i.e., the gain crossover region).
4. The sensitivity of the final reduced-order control law designs to operating point changes should be investigated for both the feedback only and the feedback/feedforward model-following design structures. Specific circumstances under which either control structure is preferable in flight control design can then be defined.
5. It is hoped that a thorough investigation of the areas recommended above will completely define an efficient multivariable synthesis methodology which can incorporate a variety of design specifications as well as hardware limitations. Once defined, the true merit of the design procedure will be revealed by exercising the methodology

on relevant design problems. While longitudinal dynamics were studied in Ref. [3], a lateral-directional case study should be completed using these methods. Other applications in the aerospace industry, such as engine control and flight simulator design, might also be considered.

REFERENCES

- [1] Schmidt, D.K. and Anderson, M.R., "Flight Control Synthesis to Meet Handling Qualities Specifications," Final Report under WS-AD-2038, McDonnell Aircraft Co., St. Louis, MO, Feb. 1986.
- [2] Anderson, M.R., "Flight Control Synthesis with Practical Design Constraints," AFFDL-TM (to be published), Aug. 1986.
- [3] Anderson, M.R. and Schmidt, D.K., "Formulating an Integrated Flight Control Law Synthesis Strategy," AIAA Paper No. 86-2711, AIAA Aircraft Systems Design and Technology Meeting, Dayton, OH, Oct. 1986.
- [4] Doyle, J.C. and Stein, G., "Robustness with Observers," IEEE Trans. on Automatic Control, Vol. AC-24, No. 4, Aug. 1979, pp. 607-611.
- [5] Rynaski, E.G., "Flight Control System Design Using Robust Output Observers," AGARD CP-321, Advances in Guidance and Control Systems, Portugal, Oct. 1982, pp. 14-(1-8).
- [6] Bacon, B.J. and Schmidt, D.K., "A Multivariable Frequency-Weighted Order Reduction Method," AIAA Paper No. 86-1998, AIAA Guidance and Control Conf., Williamsburg, VA, Aug. 1986.

1986 USAF-UES SUMMER FACULTY RESEARCH PROGRAM
GRADUATE STUDENT SUMMER SUPPORT PROGRAM

Sponsored by the
AIR FORCE OFFICE OF SCIENTIFIC RESEARCH

Conducted by the
Universal Energy Systems, Inc.

FINAL REPORT

The Effects of Flow Rate and Edge Rate
on the Perception of Self Speed

Prepared by:	Stanley Anton
Academic Rank:	Graduate Student
Department and	Department of Psychology
University:	Rutgers University
Research Location:	Armstrong Aerospace Medical Research Laboratory, Human Engineering, Wright-Patterson Air Force Base
USAF Researcher:	Dr. Rik Warren
Date:	September 15, 1986
Contract No:	F49620-35-C-0013

The Effects of Flow Rate and Edge
Rate on the Perception of Self Speed

by

Stanley Anton

ABSTRACT

An experimental design was developed to determine the individual effects of flow rate and edge rate on the perception of egospeed. Flow rate and edge rate, normally linked in the environment, were tested separately by holding one constant while varying the other. A computer generated flow field consisting of earth tone textured blocks was devised which could independently cause the flow rate and the edge rate to accelerate or decelerate. Subjects were instructed to pedal on an exercise bicycle at the same rate as the moving flow field. Preliminary results suggest that the dominant effect on the perception of egospeed is flow rate, at least for viewing durations of 30 seconds. One recommendation is to have the subject actively control the rates of change of the flow field by his own motion.

Acknowledgments

I would like to thank the Air Force Systems Command, the Air Force Office of Scientific Research and the Armstrong Aerospace Medical Research Laboratory for providing me all the support to conduct research during my 10 week fellowship. In particular I would like to thank my summer supervisor, Rik Warren, and my research colleague, Kim Reardon, for making my summer stay as intellectually stimulating and rewarding as possible.

I. INTRODUCTION: I received my master of science from Rutgers - The State University of New Jersey in the field of visual perception. My area of special interest is in motion perception. My master's thesis was on the perception of motion in depth. Furthermore, my particular expertise is in the perception of self-motion, also known as egomotion.

The research being conducted in Dr. Rik Warren's laboratory at Armstrong Aerospace Medical Research Laboratory is an analysis into the stimulus conditions which give rise to the perception of egospeed.

Since my background and interests were similar to the type of research being conducted by Dr. Warren, I was granted a summer fellowship to work on the problem of egospeed.

II. OBJECTIVES OF THE RESEARCH EFFORT: The overall objective of the egospeed research is to determine the relative contributions of two known factors which influence the perception of egospeed, namely, flow rate and edge rate.

My individual objectives were:

1. To supervise the design of a computer-generated display which has the capability of presenting separately variable flow rates and variable edge rates which are normally linked together.
2. To design an experimental procedure which ultimately will be used in a formal investigation of the problem.
3. To collect preliminary data which are based on a more

quantitative description of the results than had previously been gathered in other studies.

III. DEFINITION OF FLOW RATE AND EDGE RATE: Flow rate is defined as the observer's velocity scaled in eyeheights per second. Therefore it is a function of both how fast the observer is moving and his altitude. In the present case we are concerned only with travel over level ground which reduces flow rate solely to a function of velocity. Edge rate is defined as the number of texture edge elements traversed per second. Optically this would mean the number of optical edges which move past the fixed retina per second.

In order to demonstrate how flow rate and edge rate are normally linked, it will be assumed that the observer is traveling at a constant altitude over level terrain in which equally spaced edges are present. If the observer then moves at a constant velocity, both flow rate and edge rate will be constant and the perception of egospeed will be constant. If, however, the observer accelerates, then not only will his velocity increase and thus his flow rate, but he will also pass more edges per second than a moment before. His perception of egospeed will be one of acceleration. But again, here both flow rate and edge rate could have contributed to this perception. The same holds true for deceleration except that here the perception of egospeed

is one of slowing down.

IV. BASIS OF RESEARCH: Stimulus information is constantly bombarding our sensory organs. In the case of vision, light rays impinge upon the retina under the conditions of eyes open and sufficient lighting, while the specific light pattern depends on the location of the eyes relative to a light emitting source or reflecting surface. The type of information available becomes all the more complex when either we move relative to the environment or the environment moves relative to us. However, this does not mean that just because the information is available it is necessarily used by the visual system. In the case of the information available through flow rate and edge rate, one, both, or neither may contribute to the perception of egospeed. Furthermore, even if they both contribute they may do so in varying degrees.

The purpose of the current research is to investigate the individual influences of flow rate and edge rate on the perception of egospeed. Research has already been directed at the contributions of both but the results have been contradictory and inconclusive.

Denton (1976, 1980) has shown that edge rate alone will affect the perception of egospeed. In one study he held velocity constant while reducing the spacing between the edges along a simulated rectilinear track while subjects

viewed the display for 250 seconds. He found that this had the effect of perceived acceleration. However, Warren (1982) found a strong effect of flow rate on ego-speed perception especially when the exposure duration was no greater than 6.5 seconds.

The above results are apparently contradictory and suggest that a rigorous comparison of flow rate and edge rate needs to be made. In order to do so, a display would have to be created which could isolate flow rate from edge rate to test each independently.

The purpose of the present series of experiments is to test whether observers are affected more by flow rate or edge rate in their ability to detect changes in self velocity. In order to do this, an exercise bicycle was hooked up to an IRIS 3020 graphics computer which generates the moving displays. The observer's task would then be to pedal at a velocity which is equivalent to the velocity of the moving display. Therefore, only if the observer perceived a change in the speed of the display would a change in bike pedalling velocity be expected. So, for example, if the display depicted a constant flow rate but an accelerating edge rate a quantifiable measure of the perceived edge rate acceleration could be determined by noting how much, if any, pedal acceleration took place.

V. METHOD: The first task was to generate a display which

could separately present variable flow rates and variable edge rates. This was accomplished through a program run on the IRIS computer which was hooked up to a rear projector that presented the displays onto a 2.4 meter x 1.8 meter screen. The displays depicted flat, rectilinearly textured planes. The moving displays are under computer control and can also be activated by the observer's own pedalling motion.

The display consisted of textured blocks that simulated a sidewalk which extended to optical infinity. The blocks are earthtone colors to simulate a more realistic scene. The observer sits four feet in front of the display while being horizontally centered and vertically three fourths of the way up the display. The horizon line is at eye level.

Since the purpose of my research was to test the feasibility of running these experiments under such conditions certain factors had to be determined. Before investigating the influence of flow rate and edge rate, a preliminary study was conducted to see if pedalling at a constant velocity for a period of time in the laboratory was possible. Different time durations were used to see the optimal time that the observer could pedal comfortably at a constant rate while still being able to collect sufficient data per trial. It was determined that 30 seconds was suitable. However, this was true only for the condition in which the

observer was instructed to pedal at a comfortable rate. Another condition in which the instruction was to pedal at a walking rate proved to be impossible and should be discontinued. However, only a narrow range of tension was set on the wheel. A different tension level may facilitate the ability to pedal at a walking rate.

A second factor which had to be controlled for was the position of the eyes during a trial. Five different eye conditions were employed. They were: (1) Fixating the horizon; (2) Fixating the middle of the flow field; (3) Fixating the bottom of the flow field; (4) Tracking from top to bottom and (5) Free viewing. The results of this preliminary study indicated that by fixating the horizon line it became difficult to see the moving elements. Also, tracking from top to bottom was too difficult a task and was a distraction to the main task. Therefore, these two eye conditions are not recommended. However, either of the three other conditions proved satisfactory and either could be employed.

With the above parameters set, an investigation into the effects of variable flow rates and edge rates on perceived motion could be made. One important feature of the program used to generate these variable rates is that flow rate can be made to accelerate or decelerate while edge rate is held constant and conversely edge rate can be made

to accelerate or decelerate while flow rate is held constant.

Since the bulk of my appointment time was spent in refining the experimental design and specifying the particular elements to be incorporated into the computer program, little data could be collected on the central problem. However, a preliminary study was conducted. In this study two observers were run separately and were instructed to sit comfortably on the exercise bicycle. Each observer was instructed to begin pedalling to keep pace with the moving display as soon as it appeared. The observer was instructed to notice any change in the display's velocity and to reflect those changes by appropriately adjusting his pedalling rate. The observer was allowed free viewing since it is the most natural viewing condition. He was told that each trial would last 30 seconds and to stop pedalling after the trial ended. Each observer was run for 25 trials. In five of the trials the flow rate was constant while the edge rate accelerated. In another five trials the flow rate was constant while the edge rate decelerated. In the third set of five trials the edge rate was held constant while the flow rate accelerated. In the fourth set of five trials the edge rate was held constant while the flow rate decelerated. In the final five trials both flow rate and edge rate were held constant. The trials were randomly presented. For the acceleration trials the flow and edge rates for the

textured blocks were increased by 2.0 percent over the previous block and for the deceleration trials the rates were decreased by 2.0 percent. This means that for the acceleration trials a block's velocity moving down the screen would be 2.0 percent faster than the previous block's velocity for flow rate acceleration and the block's size would be 2.0 percent smaller than the previous block's size for edge rate acceleration. For the deceleration trials a block's velocity moving down the screen would be 2.0 percent slower than the previous block's velocity for flow rate deceleration and the block's size would be 2.0 percent larger than the previous block size for edge rate deceleration. The initial edge block size was set at two meters long. The initial velocity was set at 20 meters per second.

There was a 60-second rest period between each trial. At the conclusion of each trial the observer received feedback about his performance with a graph which showed his velocity as a function of time.

The following conclusions can be reached: (1) When flow rate is held constant and edge rate accelerates little, if any, perceived acceleration is reported; (2) When flow rate is held constant and edge rate decelerates there is a small but noticeable perceived display deceleration; (3) When edge rate is held constant and flow rate accelerates a very large

display acceleration is reported and (4) When edge rate is held constant and flow rate decelerates a fairly noticeable deceleration is reported.

Tentatively it can be concluded that flow rate exerts a much greater influence on the perception of speed than edge rate. However, these results are very preliminary and should be taken as such. In fact, one of the strong points of this design is that quantifiable data can be collected. Therefore, firm conclusions cannot be reached until such measures are recorded.

VI. RECOMMENDATIONS: (1) The procedure in which the observer is instructed to pedal at a velocity equivalent to the velocity of the flow field should be continued. It forces the observer to attend to the display which is critical to the success of the experiment. It also has the advantage of attaining a quantifiable measure of the observer's perceived velocity of the display. This, in turn, allows the experimenter to graph the relative influences of flow rate and edge rate under the conditions of one being held constant while the other is variable.

(2) In one sense the procedure used in these initial studies involved active participation on the part of the observer. The observer's task was to pedal at the velocity he perceived the flow field to be moving at. However, in another sense the observer was acting passively. Normally,

when one locomotes through the environment, he controls where he is going and how fast he is getting there. In the present experiments, the displays were preset so that no action on the observer's part influenced what happened in his visual field. In order to realistically simulate what takes place during real locomotion, the movement of the display should be contingent upon the observer's own movement.

REFERENCES

1. Denton, G.G., "The Influence of Adaptation on Subjective Velocity for an Observer in Simulated Rectilinear Motion," ERGONOMICS, Vol. 19, No. 4, pp.409-430.
2. Denton, G.G., "The Influence of Visual Pattern on Perceived Speed," PERCEPTION, Vol. 9, pp. 393-402.
3. Warren, R., D.H. Owen, and L.J. Hettinger, "Separation of the Contributions of Optical Flow Rate and Edge Rate to the Perception of Egospeed Acceleration," Wright-Patterson Air Force Base, 1982.

1986 USAF-UES SUMMER FACULTY RESEARCH PROGRAM/
GRADUATE STUDENT SUMMER SUPPORT PROGRAM

Sponsored by the
AIR FORCE OFFICE OF SCIENTIFIC RESEARCH

Conducted by the
Universal Energy Systems, Inc.

FINAL REPORT

A DISPERSION-CORRECTED HPLC/FACP METHOD FOR MEASURING SORPTION
ISOTHERMS OF SUBSTITUTED AROMATICS ON SOIL ORGANIC MATTER

Prepared by:	Chris Antworth
Academic Rank:	Research Assistant
Department and	Chemistry Department
University:	Florida State University
Research Location:	Headquarters Air Force Engineering and Services Center, Environics Division, Tyndall Air Force Base, FL
USAF Research:	Mr. Thomas Stauffer
Date:	August 8, 1986
Contract No:	F49620-85-C-0013

A DISPERSION-CORRECTED HPLC/FACP METHOD FOR MEASURING SORPTION
ISOTHERMS OF SUBSTITUTED AROMATICS ON SOIL ORGANIC MATTER

by

Chris Antworth

ABSTRACT

A High Performance Liquid Chromatography (HPLC) method was developed in order to study the sorption of substituted aromatics on various fractions of soil organic matter (SOM). Isotherms were calculated from the desorption branch of a single breakthrough curve via the Frontal Analysis by Characteristic Point (FACP) technique. Using nonretained solutes, a dispersion correction was incorporated into the calculations and the resulting dispersion-corrected HPLC/FACP method was shown to produce isotherms similar to those generated by the conventional Frontal Analysis (FA) method. The FACP technique, however, greatly reduces analysis times.

Sorption isotherms of a number of substituted aromatic compounds, each representing a different type of specific solute polarity, were determined on several SOM fractions. The resulting K_d values indicate that each SOM fraction possesses a unique set of active sites. These results imply that the sorption of relatively polar organic compounds cannot be adequately explained by the hydrophobic model, and suggest a series of experiments to determine at what level of solute water solubility the hydrophobic model needs revision.

ACKNOWLEDGEMENTS

We would like to thank the Air Force Office of Scientific research for providing the opportunity and financial support to conduct the research summarized in this report through the Summer Faculty and Graduate Student Research Program. We would especially like to thank the staff of the Environics Division, Air Force Engineering and Services Center, Tyndall AFB, for all of their support and encouragement. Mike Henley and Sgt. Dan Stork deserve special mention for their technical expertise and helpful attitude. This project was formulated as a result of many helpful discussions with our sponsor, Tom Stauffer, and we appreciate his many efforts to help us succeed. Finally, we must acknowledge the contribution of Bill Macintyre (URRP), who provided not only a number of useful technical suggestions but also a most generous amount of good humor.

SECTION I

INTRODUCTION

The source, transport and fate of organic pollutants in groundwater is currently a subject of major interest to environmental scientists. Organics in groundwater are of particular concern to the U.S. Air Force because of the potential for aquifer contamination from Air Force operations. Two classes of nonionic organic chemicals pose the greatest threat from routine operations:

- (1) cleaning solvents and degreasers such as trichloroethylene and tetrachloroethane
- (2) jet fuel components such as benzene, nitrobenzene, toluene and naphthalene.

In recognition of the potential for polluting groundwaters at and/or near Air Force installations, the Environics Division, Air Force Engineering and Services Center, Tyndall AFB has launched an extensive program to study the behavior of these compounds in groundwater. One aspect of this subject the Environics Division has identified as particularly important is the sorption of nonionic organics onto soil and aquifer materials. The objective of this research effort was to develop a rapid and sensitive High Performance Liquid Chromatographic (HPLC) method for quantifying the sorptive characteristics of various components of soil and aquifer media.

I and my research group at Florida State University have been studying the surface chemistry of heterogeneous geological materials for a number of years. This effort is an extension of my graduate work in the Biogeochemical Laboratories at Indiana University. Although the heterogeneity of natural soils and sediments makes their molecular characterization difficult, we have made significant progress using innovative chromatographic approaches combined with modern, state-of-the-art spectroscopy. In the research activity summarized in this report, Chris Antworth, a graduate student working under my

direction, and myself have attempted to combine our knowledge of organic geochemistry and experience with physico-chemical chromatographic techniques to develop a routine method applicable to one of the Air Force's primary environmental research projects.

SECTION II

OBJECTIVES OF THE RESEARCH EFFORT

The primary objective of our research activity was to develop a rapid and sensitive HPLC method for characterizing interactions between nonionic organic solutes and soil organic matter (SOM). It has long been recognized that the sorption of sparingly soluble organic compounds onto soils is dominated by the natural organic carbon fraction of the soil. However, accurate characterization of organic solute - soil organic matter interactions at the molecular level has proven to be a difficult and largely unobtained goal to date. With the development of our HPLC method, which is capable of producing large amounts of data in a relatively short period of time, we sought to address the following questions regarding organic solute - soil organic matter interactions.

- (1) What role do the various SOM fractions play in the sorption of nonpolar and polar, functionalized solutes?
- (2) Can the "specific sorptivity" of SOM be described as the sum of the sorptivities of its various fractions?

- (3) Does SOM differ significantly in its sorptivity, or is the driving force for sorption the tendency for nonionic organics to remove themselves from water?
- (4) At what level does water solubility or hydrophobicity begin to dominate the sorption process.

SECTION III

EXPERIMENTAL

Solutes. Chemical compounds were initially investigated for their utility as "solute probes" for this work based on their acidic, basic and dipolar characteristics. Using a molecular polarity scale developed for analytical HPLC, we chose compounds which represented one apex (acid, base or dipole) of the Snyder Selectivity Triangle (1). In this way we isolated the important polar interactions responsible for any sorption phenomena. The solutes which proved most effective in this regard and which were chosen as polar probes were: o-cresol (2-methylphenol, proton donor), aniline (proton acceptor) and nitrobenzene (dipole interactor). In addition, benzene was used as an indicator of the extent of nonspecific dispersion interactions. Phenol, resorcinol (1,3-dihydroxybenzene), potassium benzoate and calcium chloride were all used at various times as nonretained, conservative solutes for void volume and dispersion correction calculations. Note that all solutes except calcium chloride are aromatic. This allows sensitive detection with a

conventional HPLC UV monitor.

All solutes were of analytical reagent grade or better. Aniline and nitrobenzene were further purified by distillation, with distillate fractions having boiling ranges of <2 C collected for use in sorption studies.

Soil Organic Matter. Soil material used in these studies was obtained from a commercial supplier. The soil itself is an organic rich material commonly referred to as "Minnesota Peat". An organic rich soil was chosen for these initial studies so that the organic matter would not have to be concentrated by removal from the inorganic matrix. The organic carbon content of the total soil organic matter was estimated to range from 20-40%.

The initial soil material was fractionated into various organic chemical fractions according to a standard extraction protocol (2) used by organic geochemists to isolate the primary components of soil and sedimentary organic matter: lipids, humic/fulvic acids and nonextractable humin (3). We initially intended to study each fraction separately. However, it was not possible to retain the humic/fulvic acid fraction in the sorption columns once they had been removed from the organic matrix because of their relatively high water solubility. We therefore analyzed the total soil organic matter, sequentially extracted each fraction and analyzed the residue remaining after each extraction phase. Data is available for three residues: total SOM, SOM - lipids, and SOM - lipids - humic/fulvic acids (or humin). In

view of the changes in chemical behavior of the humic/fulvic acid fraction once it had been removed from the organic matrix, we feel this approach is actually more representative of natural conditions in soils and sediments.

Experimental Apparatus. The instrument used for these studies was a modified Waters HPLC. The system consisted of a Waters 6000 pump, Valco 6-port HPLC injector valve and Waters 440 UV absorbance detector. Short, precision-bore (0.007" I.D.) connecting tubing was used throughout.

The primary modification of the system involved the use of large volume sample loops in the injector rather than the conventional small volume (5-50 uL) loops used in analytical HPLC. By filling the larger loops with a probe solution of known concentration with the valve in the FILL position and then switching to the INJECT position, a sharp step function change in solute concentration occurs in the column. This technique simulates a Frontal Analysis (FA) injection.

Each SOM fraction was lyophilized, frozen with liquid nitrogen and gently crushed in a mortar and pestle. The resulting material was size sorted and the 38-53 micron subfraction isolated. These 38-53 micron particles were then mechanically mixed with 37-44 micron pellicular silica gel to produce a 5% (w/w) mixture and the resulting mixture dry-packed in 75mm x 4.6mm I.D. stainless steel columns. The pellicular silica gel used in this work is a nonporous, low surface area adsorbent. Initial adsorption experiments demonstrated essentially no uptake of the solute probes by the silica gel, and it is thus considered an inert support

matrix.

Isotherm Calculations. Isotherms were calculated from the desorption branch (diffuse rear boundry) of single solute breakthrough curves by the Frontal Analysis by Characteristic Point (FACP) method (4). A sufficient volume of probe solution was injected to produce an equilibrium concentration of solute throughout the column. The injection valve was then returned to the FILL position, reintroducing pure water. This time is taken as t_0 for calculation purposes.

Individual points on isotherms are calculated from the diffuse rear boundry using the governing equation (4)

$$q(C) = \frac{1}{M} \int_0^C (V - V_0) dC \quad (1)$$

where $q(C)$ is the concentration of adsorbed solute in equilibrium with the mobile phase concentration (C) , M the mass of adsorbent, V the retention volume and V_0 the void volume of the system.

The FACP technique, in contrast to the more conventional FA method, does not take into account dispersional broadening of the front that occurs in the column. In order to refine the FACP technique we have introduced a dispersion correction which employs the diffuse rear boundry of a nonretained solute breakthrough curve. Isotherm points are now calculated using equation 2, where S is a sensitivity factor (umoles/unit area), F the volumetric flow rate and the subscripts tp and cp refer to test probe and correction probe respectively.

$$q(C) = \frac{S \cdot F}{M} \cdot (\text{Area}_{tp} - \text{Area}_{cp}) \quad (2)$$

This method of isotherm calculation is depicted in Figure 1.

Solutes were determined to be nonretained by comparing their retention volumes with those of calcium chloride and column void volumes determined gravimetrically (5). These comparisons agreed within 3%.

SECTION IV

RESULTS AND DISCUSSION

A. RELIABILITY OF THE HPLC/FACP METHOD

Before beginning extensive studies of organic solute - SOM interactions a series of experiments were conducted to determine the reliability of the dispersion-corrected HPLC/FACP technique. We use the term "reliability" here to mean the extent to which this technique produces isotherms similar to those produced by conventional and accepted procedures. These initial experiments addressed two major uncertainties associated with the FACP method: (1) Does the dispersion correction adequately account for dispersion? (2) What effect does flow rate have on isotherm results?

The first question was addressed by comparing isotherms determined by the FA, corrected FACP (C-FACP) and uncorrected FACP (U-FACP) methods. Comparisons for cresol (weakly retained) and aniline (strongly retained) sorbed on the humin fraction are summarized in Figure 2 and Table 1. K_d values

were calculated from an exponential fit of sorption data (a Freundlich isotherm). Figure 2 and Table 1 indicate that the dispersion correction significantly improves the accuracy of the FACP calculation, assuming the FA isotherm to be the primary standard for comparison. The improvement is more significant for the less strongly retained solute (cresol). This is an entirely expected result since, for strongly sorbed solutes such as aniline, broadening of the rear boundry is dominated by sorption rather than dispersion effects.

The effects of mobile phase flow rate on calculated isotherms was studied by generating FACP isotherms (again, cresol and aniline on humin) at 0.2, 0.5, 1.0 and 2.0 mL/min. In addition, van Deemter (6) curves were also calculated. A van Deemter curve describes the kinetic efficiency of a chromatographic system by fitting Height Equivalent of a Theoretical Plate (HETP, or H) data to equation 3

$$H = A + B/v + Cv \quad (3)$$

where v represents mobile phase linear velocity and A , B and C are constants characteristic of a particular system. A minimum in a van Deemter plot, given by B/C , corresponds to the velocity at which sorption, desorption and diffusion kinetics are optimally balanced.

van Deemter plots and the corresponding isotherms for cresol and aniline on humin are displayed in Figures 3 and 4, respectively. K_d values calculated from the isotherms are

summarized in Table 2. It appears that a van Deemter minimum is observed for cresol at 0.3 cm/min (0.2 mL/min). No such minimum is observed for aniline, however, and this is probably due to its greater affinity for the humin fraction. (Note that the van Deemter minimum is equal to B/C , and C is proportional to K_d).

The data of Table 2 indicate that, when operated near the van Deemter minimum (i.e. cresol), the HPLC/FACP method results in isotherms substantially similar to those produced at the actual minimum. As mobile phase velocities deviate from optimum, however, significant variations (10-15%) in K_d will result, particularly for strongly retained solutes.

B. CHARACTERIZATIONS OF SOLUTE INTERACTIONS WITH SOM

FRACTIONS

It is generally accepted that, when the organic matter content of soils approaches some level (~1%, ref 7), SOM dominates the sorption of sparingly soluble organic solutes. When such a situation exists the distribution coefficient can be approximated with equation 4

$$K_d = K_{oc} * f_{oc} \quad (4)$$

where K_{oc} is the organic carbon partition coefficient and f_{oc} the fraction of organic matter. Reported K_{oc} 's are generally within 3-5 for a particular solute regardless of the nature of SOM. This has led several workers to conclude that hydrophobicity, and not affinity for SOM, drives the sorption process (8).

The variations observed in K_{oc} values have led us to

believe that, at some level of water solubility, the driving force for sorption becomes the solute's affinity for SOM and not its hydrophobicity. Such a hypothesis further leads to the conclusion that a somewhat soluble organic solute should exhibit different affinities for different types of SOM.

To test these assumptions we have determined K_d values for the sorption of polar solutes on the major chemical fractions of soil and sedimentary organic matter. These K_d values are summarized in Table 3, which reveals significant differences in the sorptive characteristics of the three SOM fractions. One of the most significant differences occurs in the uptake of aniline when lipids are removed. This indicates that the relative abundance of acidic active sites increases and, possibly, some acidic sites are activated with lipid removal. It is also interesting to note that aniline uptake does not decrease substantially with removal of the humic/fulvic acid fraction. This would indicate that, when these materials are bound to the SOM matrix, their acidic functional groups are not "free" but are probably involved in cross-linking reactions.

The steady decrease in benzene uptake probably reflects the removal of hydrophobic groups from SOM with each extraction phase. The essentially constant uptake of cresol is an indication that few basic active sites are present in SOM. The similarity in K_d 's of benzene and cresol on humin probably reflects a complete lack of basic sites in this material.

SECTION V

RECOMMENDATIONS

The results presented in this report, although preliminary, raise a number of interesting and important questions. However, the most significant result of the research is undoubtedly the demonstration of the utility of the HPLC/FACP method for characterizing organic solute - soil organic matter interactions. This method provides a rapid and reliable technique for addressing basic questions in sorption phenomena - questions which would be difficult to address by conventional batch methods because of their inherent slowness and imprecision.

Recommendations for further studies using the HPLC/FACP technique include the following.

1. Comparison of batch and dynamic (chromatographic) methods, particularly the effects of mobile phase flow rate.
 2. Parallel studies of less soluble organic compounds.
 3. Chemical and spectroscopic characterization of the SOM fractions.
 4. Correlation of K_d , K_{oc} and water solubilities (or octanol-water partition coefficients) for a group of organic compounds varying widely in solubility.
- At what point does the hydrophobic model break down?

REFERENCES

1. Snyder, L.R., J. Chromatogr., 92,223(1974).
2. Hatcher, P.G., I.A. Breger, L.W. Dennis and G.E. Maciel, in Aquatic and Terrestrial Humic Materials, R.F. Christman and E.T. Gjessing, eds., Ann Arbor Science, Ann Arbor, MI, 1983, p 37.
3. Tissot, B.P. and D.H. Welte, Petroleum Formation and Occurrence, Springer-Verlag, New York, 1984, p 70.
4. Glueckauf, E., J. Chem. Soc., 1302(1947).
5. Jacobson, J., J. Frenz and C. Horvath, J. Chromatogr., 316,53(1984).
6. Knox, J.H., J. Chromatogr. Sci., 15,352(1977).
7. McCarty, P.L., M. Reinhard and B.E. Rittman, Environ. Sci. Tech., 15,40(1981).
8. Rao, P.S.C., A.G. Hornsby, D.P. Kilcrease and D. Nkedi-Kizza, J. Environ. Qual., 14,376(1985).

Table 1. Effect of Dispersion Correction on Calculated K_d

Solute	K_d (umoles/g)		% Deviation from FA
	C-FACP	U-FACP	
cresol	9.33	10.58	2.6
aniline	27.83	30.61	5.8
			10.0

Table 2. Effect of Flow Rate on Calculated K_d

Solute	K_d (umoles/g)		% Deviation (.5 - .2)
	0.2	2.0	
cresol	9.90	9.99	-3.5
aniline	28.35	32.77	11.2

Table 3. Comparison of SOM Fractions

Material	K_d (umoles/g)		
	Cresol	Aniline	Benzene
SOM	9.08	31.5	21.0
SOM - Lipids	12.1	40.8	22.8
Humic	9.60	33.9	16.40
Silica Gel		6.07	0.07

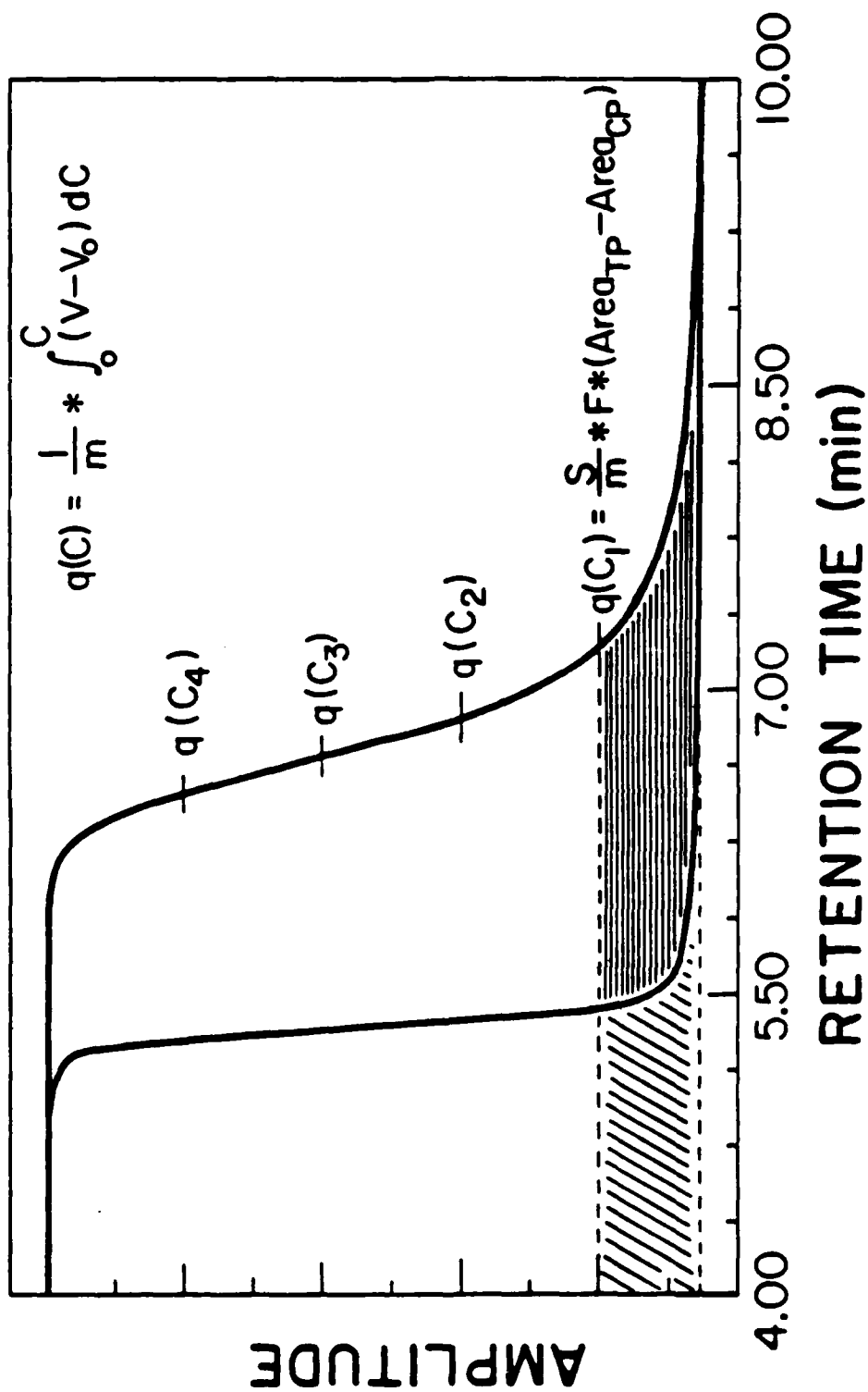
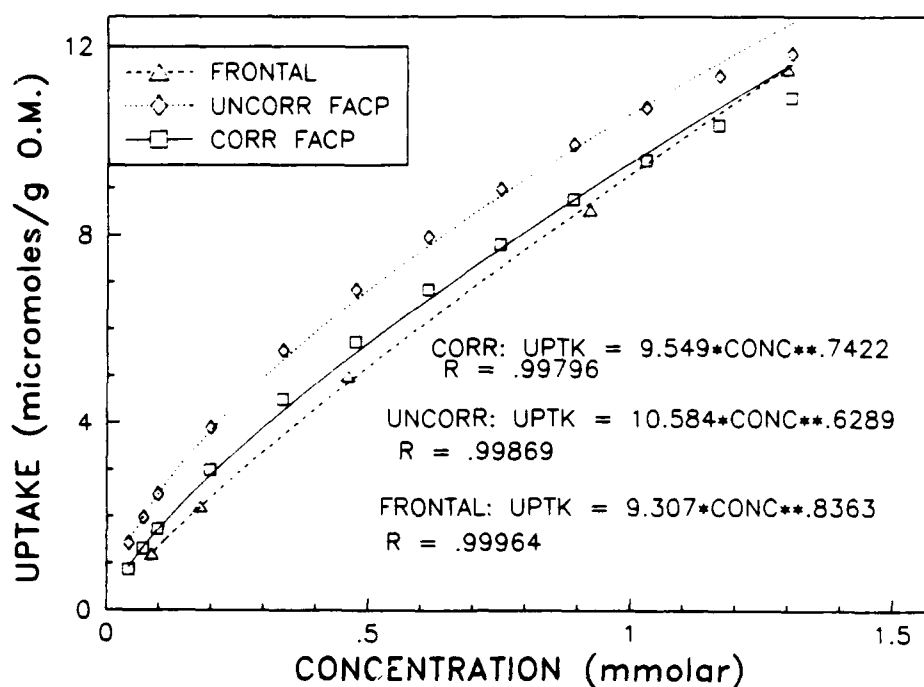


Figure 1. Calculation of Isotherms by the Dispersion Corrected HPLC/FACP Method

CRESOL, HUMIN



ANILINE, HUMIN

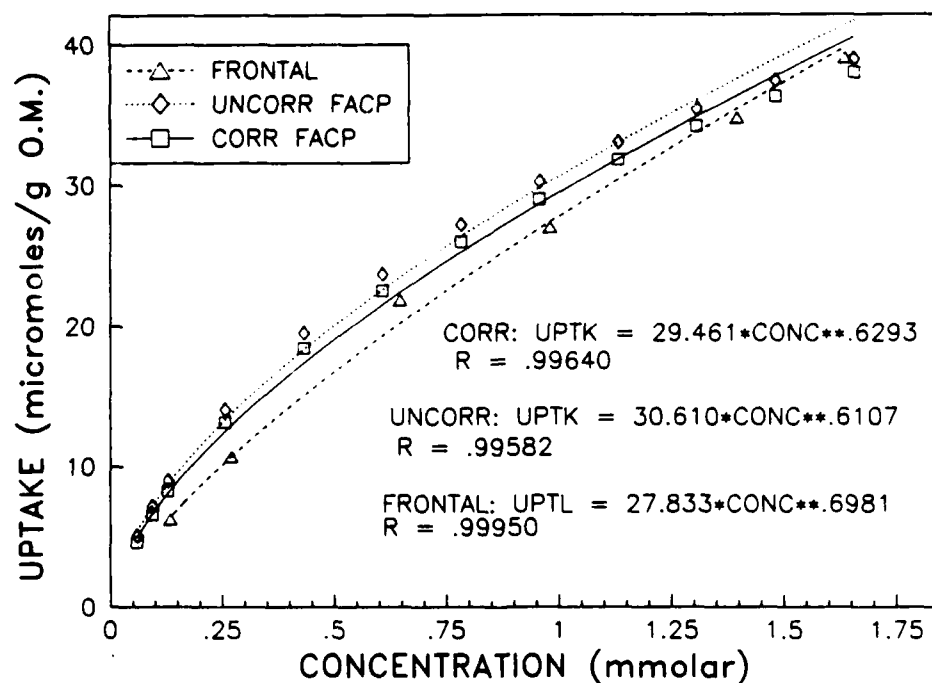
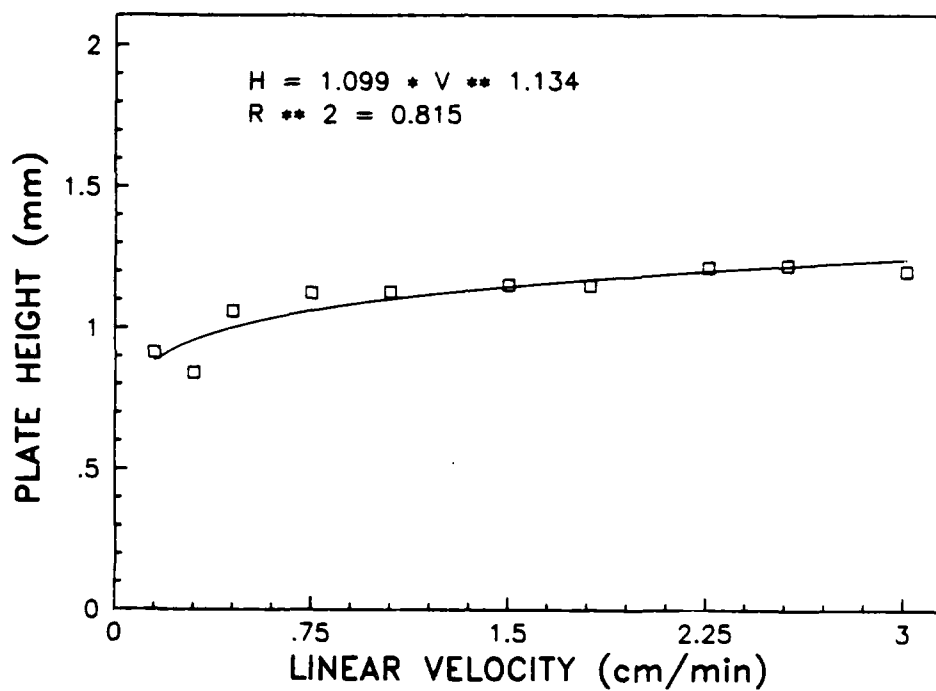


Figure 2. Effect of Dispersion Correction on Calculated Isotherms

VAN DEMPTER PLOT, CRESOL/5% HUMIN



o-CRESOL

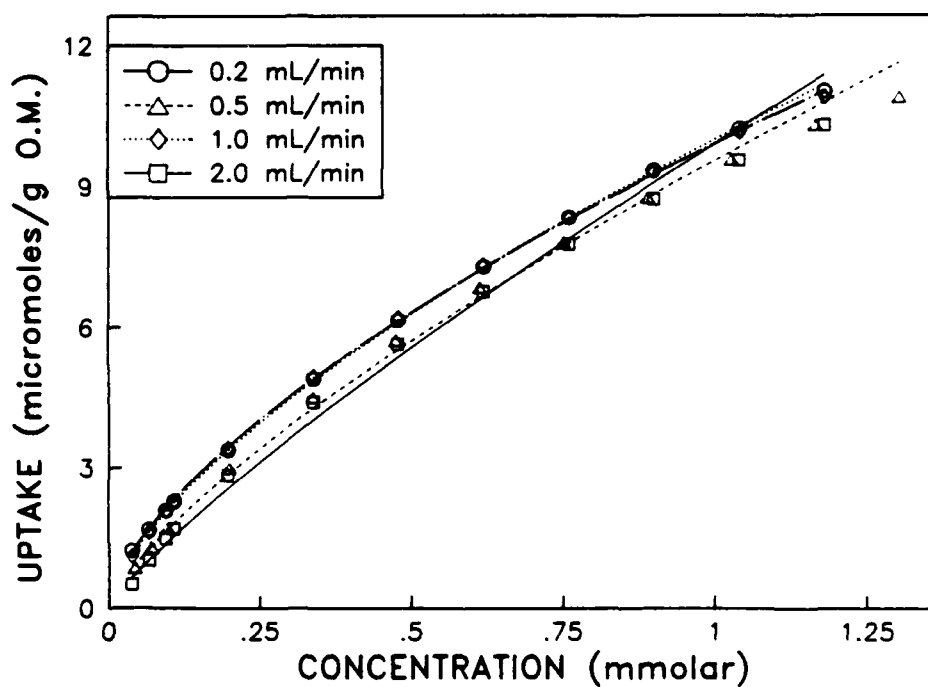
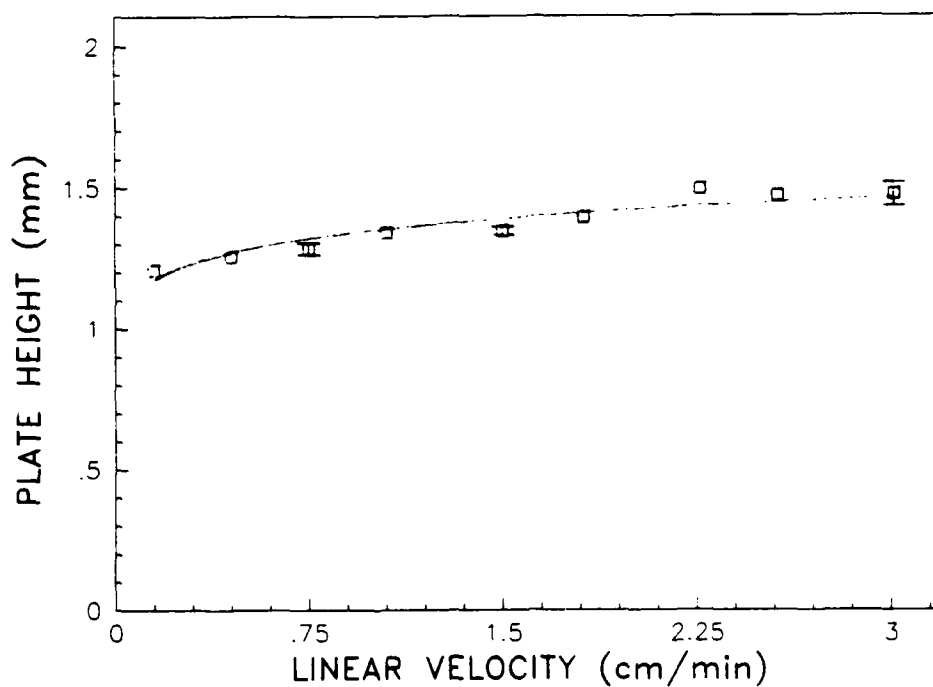


Figure 3. Effect of Flow Rate on Calculated Isotherm of a Slightly Retained Solute.

VAN DEMPTER PLOT, ANILINE/5% HUMIN



ANILINE

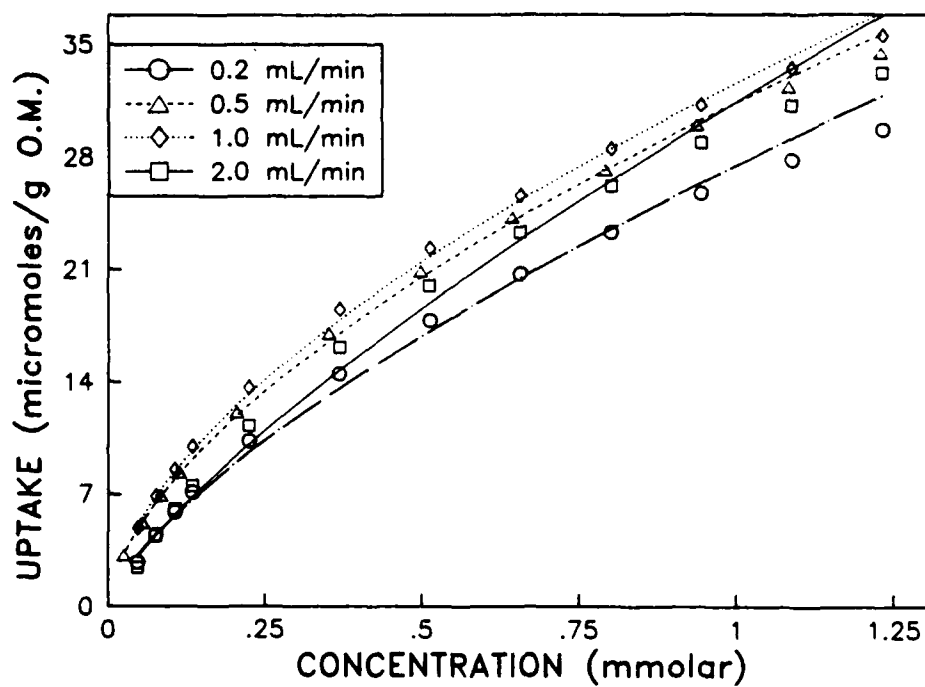


Figure 4. Effect of Flow Rate on Calculated Isotherm of a Strongly Retained Solute.

1986 USAF-UES SUMMER FACULTY RESEARCH PROGRAM/
GRADUATE STUDENT SUMMER SUPPORT PROGRAM

Sponsored by the
AIR FORCE OFFICE OF SCIENTIFIC RESEARCH

Conducted by the
Universal Energy Systems, Inc.

FINAL REPORT

Computer Simulation of the Cardiovascular System Under +G Stress

Prepared by:	Sherif A. Aziz
Academic Rank:	Graduate Student
Department and	Department of Electrical Systems Engineering
University:	Wright State University
Research Location:	Armstrong Aerospace Medical Research Laboratory, Bioengineering and Biodynamics Division Acceleration Effects Branch Wright Patterson Air Force Base
USAF Researcher:	Dr. Daniel W. Repperger
Date:	August 22, 1986
Contract No:	F49620-85-C-0013

Computer Simulation of the Cardiovascular System Under +G_z Stress

by

Sherif A. Aziz

ABSTRACT

A state-variable model of the cardiovascular system under +G_z stress was implemented. The model (which includes simulation of the arterial and venous systems, heart, baroreceptor control of the heart and venous tone, and inputs for acceleration force and externally applied pressure) was used to study the impairment of cerebral function during +G_z stress. It was found that even though eye level blood pressure decreases significantly during G_z stress, cerebral blood flow is maintained due to a compensatory mechanism which compares favorable with the experimental results found in the literature. This model will be used to investigate the effectiveness of anti-G suits. Finally, a preliminary design of a closed-loop control system for an anti-G suit was carried out. It was found that it is possible to control both the rise time (which is needed for the improvement of G-valve) and the overshoot of the suit pressure. More work needs to be done both in the simulation and design areas.

Acknowledgements

The author hereby expresses his gratitude to the Air Force Systems Command, the Air Force Office of Scientific Research and the Universal Energy Systems for providing him with the opportunity to spend a very worthwhile and interesting summer at the Armstrong Aerospace Medical Research Laboratory, Wright Patterson Air Force Base, Ohio. He appreciates the hospitality and excellent working conditions provided by Dr. Robert E. Van Patten and the Acceleration Effects Branch (AAFML/BBS).

The author would like to thank Dr. Daniel W. Repperger for his conscientious coordination of this research effort, making sure that the author felt welcome. He would like to thank several members of the AAFWAL/BBS branch, Mr. J.W. Frazier, Lt. Edward Hade, Mr. David Ratino and Mr. Lawrence Gould for their help during the course of this research. Last, but not least, he would like to express his thanks to Dr. Henning von Gierke and Dr. Ints Kaleps for many helpful discussions.

Finally, he would like to thank Dr. Kuldip S. Rattan for his help and guidance during the course of this research and Suzy McGovern of the College of Engineering and Computer Science, Wright State University for her careful and professional typing of this report.

I. Introduction

I received my B.S. in Systems and Biomedical Engineering from Cairo University. I am currently working on my M.S. in Electrical Systems Engineering at Wright State University. I have always been interested in the application of Control Theory to Biological Systems.

The Harry G. Armstrong Aerospace Medical Research Laboratory (AAMRL) at Wright Patterson Air Force Base has been involved in studying the effects of high onset rate, high sustained $+G_z$ forces on pilots. They are working on developing new control schemes to increase $+G_z$ tolerance.

During the ten week appointment, I worked on the implementation of a Cardiovascular Model which should aid in the design of an Anti-Gravity suit controllers and the prediction of the benefits of different control schemes.

II. Objectives of the Research Effort

The overall objective of this research is to study existing methods of increasing $+G_z$ tolerance to acceleration forces and to propose a control strategy to improve the design of existing g-suits. We feel this can be done if the effects of the $+G_z$ forces on the cardiovascular system and the existing methods of improving $+G_z$ tolerance are better understood. Our objectives were:

- 1) To study existing mathematical models of the cardiovascular system under $+G_z$ forces. Develop a computer simulation of one of the models and study the effects of $+G_z$ forces on the cardiovascular responses such as eye and leg level pressures and flows.
- 2) Study the existing protective mechanism such as g-suits and straining maneuvers and develop a computer model of the g-suit.
- 3) Propose a closed-loop control strategy to improve the design of the existing g-suit.

III. Implementation of the Cardiovascular Model:

The cardiovascular model chosen for our purpose was the one developed by Chu [1] and is explained briefly in Dr. Rattan's final report. The model was implemented using the computer-aided design package, MATRIX_x [2].

3.1. MATRIX_x:

MATRIX_x is a powerful programmable matrix calculator with excellent graphical capabilities. With it you can solve complex, large-scale matrix problems.

3.2. SYSTEM BUILD:

System Build is a capability in MATRIX_x which provides an interactive, menu-driven graphical environment for building, modifying and editing complex computer simulation models. Simulating system performance under both nominal and strained environment is easily accomplished with System Build.

3.2.1 BASIC BUILDING UNIT - A BLOCK:

System Build basic building unit is the block. System Build has a large library of different types of blocks. The main block categories are:

1. SUPER BLOCK
2. GAIN BLOCK
3. PIECE-WISE LINEAR FUNCTIONS
4. DYNAMIC BLOCK
5. TRIGNOMETRIC FUNCTIONS
6. USER CODE BLOCK
7. CO-ORDINATE TRANSFORMATION
8. SIGNAL SOURCES
9. LOGICAL FUNCTIONS

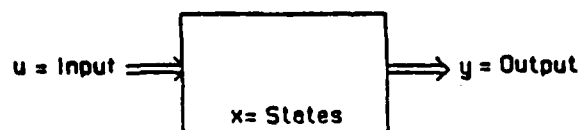


Fig. 1 General Architecture of a Block

The system prompts the user for the type of block, block name, block parameters, number of inputs and number of outputs. The next step is to determine the simulation time duration and the input forcing functions. Once that has been done, the model is ready to run.

3.2.2. SUPER-BLOCK:

A very important type of block is the SUPER-BLOCK. This block can have up to six other blocks interfaced in any way. The most important advantage of a SUPER BLOCK is that it can contain other SUPER BLOCKS. This permits the nesting of SUPER-BLOCKS as seen in Fig. 2.

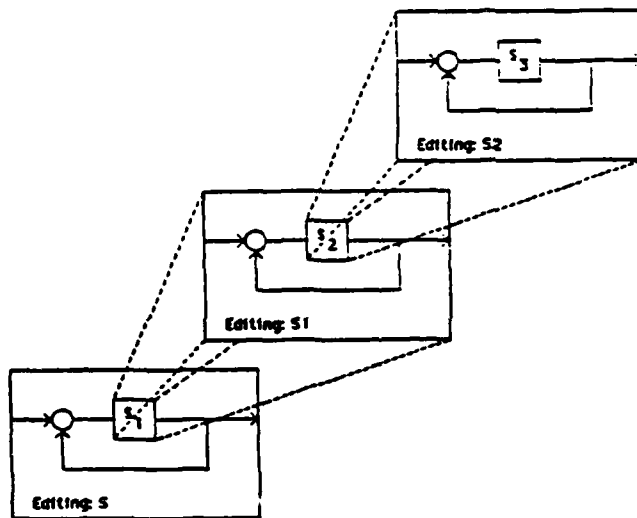


Fig. 2 Nesting SUPER-BLOCKS

This nesting property makes it possible to implement complex systems that contain any number of blocks.

3.3 Modeling of an A Segment in the Arterial Tree Using System-Build:

Each segment of the arterial tree is modeled by two nested super blocks. Fig. 3 shows an A element of the arterial tree.

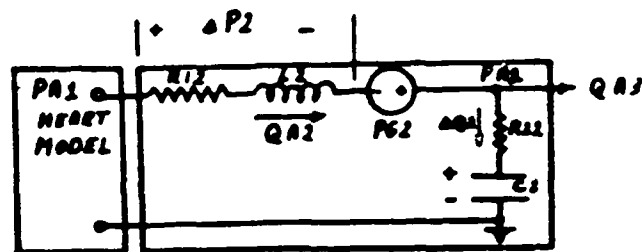


Fig. 3 A Element of the Arterial Tree

The equations used to implement such a segment are:

$$\Delta P_n = P_{n-1} + PG_n - P_n \quad (1)$$

$$\Delta Q_n = Q_n - Q_{n+1} \quad (2)$$

$$\frac{dQ_n}{dt} = \frac{\Delta P_n - Q_n \cdot R1_n}{L_n} \quad (3)$$

$$\frac{dV_n}{dt} = \Delta Q_n \quad (4)$$

where V_n is the volume of blood in the segment. Figs. 4 and 5 show an example of such a segment. The segment shown is A2.

SUPER-BLOCK SEGA2 has the following inputs and outputs:

INPUTS:

PA1 : Pressure of segment A1
QA3 : Flow in segment A3
G : Gravitational profile

OUTPUTS:

PA2 : Pressure of segment A2
QA2 : Flow through segment A2
VA2 : Volume of segment A2

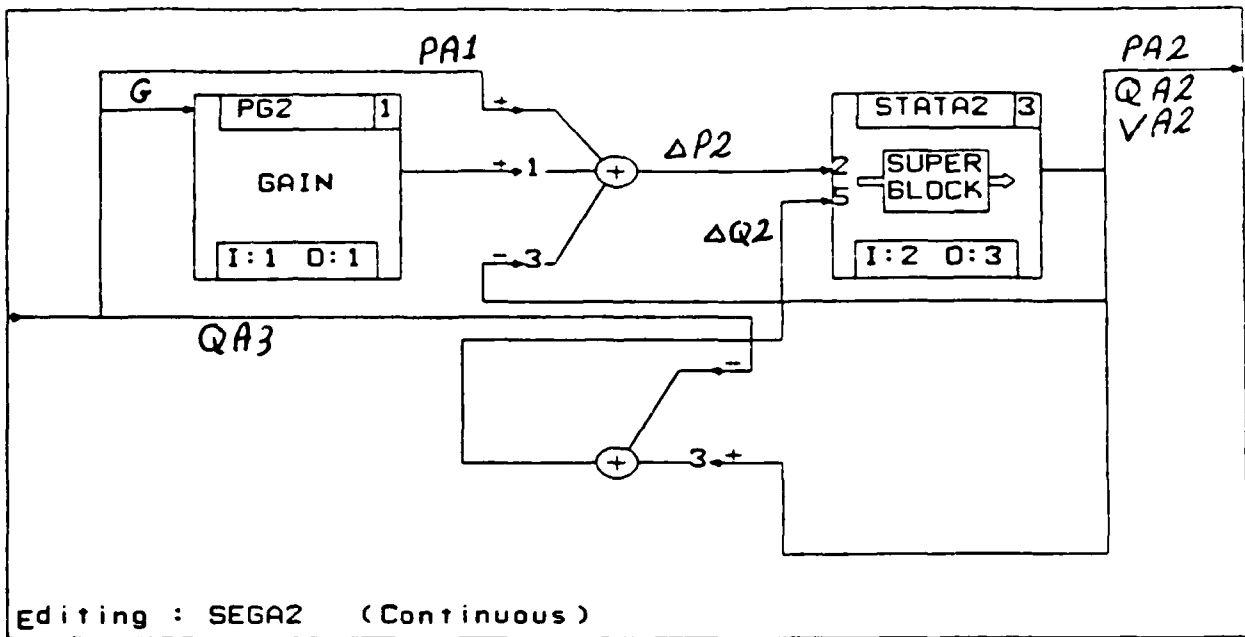


Fig. 4 Segment A2

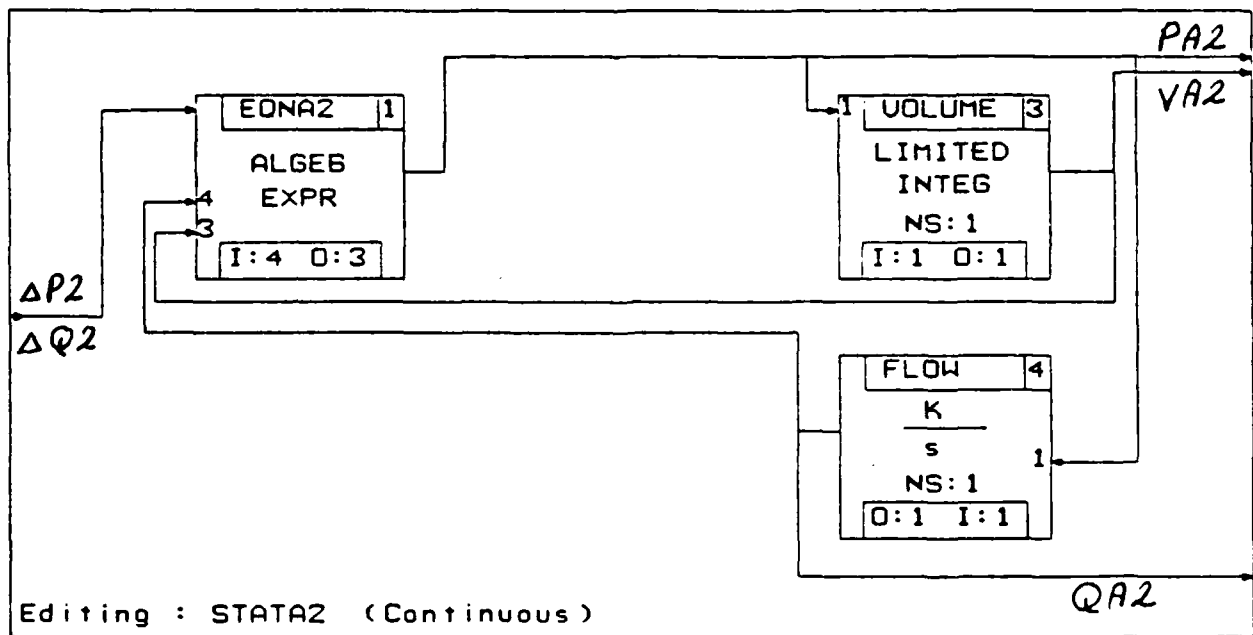


Fig. 5 State A2

These outputs are used to interface the segment with the surrounding segments. Internally, SEGA2 calculates ΔP_2 and ΔQ_2 and sends them as inputs to the SUPER-BLOCK STATA2. STATA2 then forms the differential equations \dot{Q}_n and \dot{V}_n in the block EQNA2. The differential equations are then integrated using the integrator FLOW and limited integrator VOLUME.

3.4. Interfacing an A Segment with the Rest of the Model

As an example of this case, we take segment A2:

- SEGA2 is first interfaced with the Ascending Aorta in SUPER-BLOCK AAORTA as shown in Fig. 6.
- The Ascending Aorta is interfaced with the rest of the arterial tree in SUPER-BLOCK ARTERI (Fig. 7).
- The arterial tree is interfaced with the rest of the Cardiovascular Model in SUPER-BLOCK CIRCUL (Fig. 8).
- The G-Profile and G-Suit models are then added to the Cardiovascular Model in SUPER-BLOCK GSTRES (Fig. 9).

3.5 MODEL SIMULATION:

The total number of SUPER-BLOCKS needed in the model is 90. The pressure, volume and flow from each segment is available as output resulting in a total number of 99 outputs.

The integration algorithm used in the simulation is Variable Step Kutta Merson. The time increment chosen is 0.0025 sec. and the relative and absolute tolerance are taken to be 0.001.

IV. Results

Figs. 10, 11, 12 and 13 show the output of the model for a +6 G_z profile. For more discussion on these results, refer to Dr. Rattan's final report.

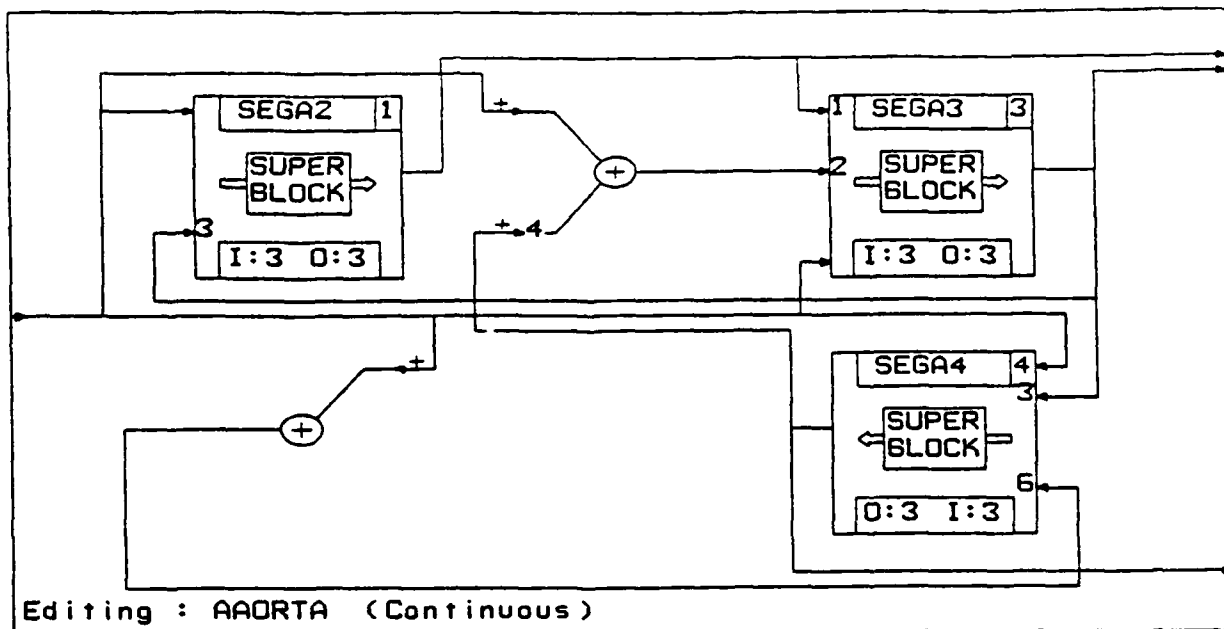


Fig. 6 Ascending Aorta

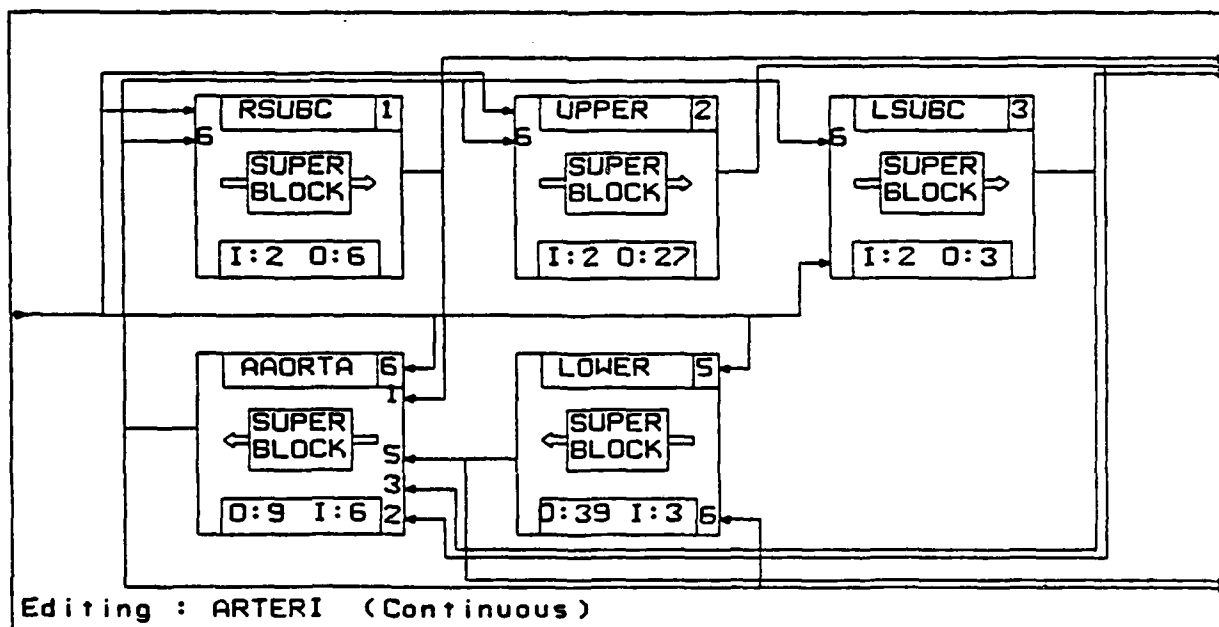


Fig. 7 Arterial Tree

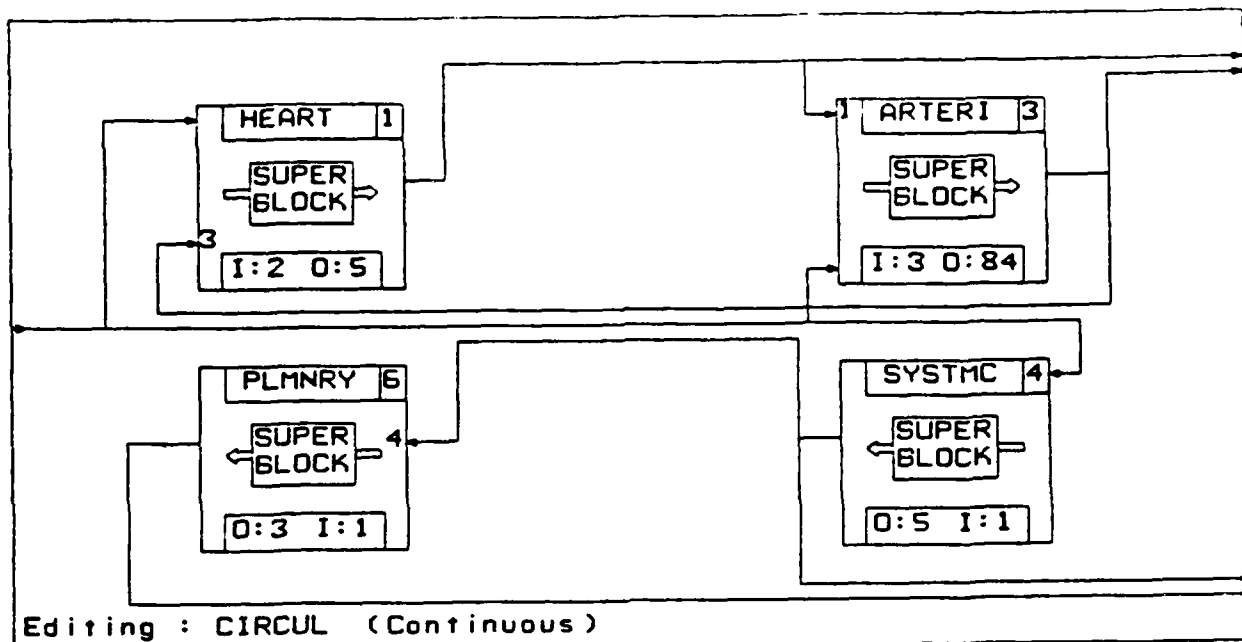


Fig. 8 Circulatory System

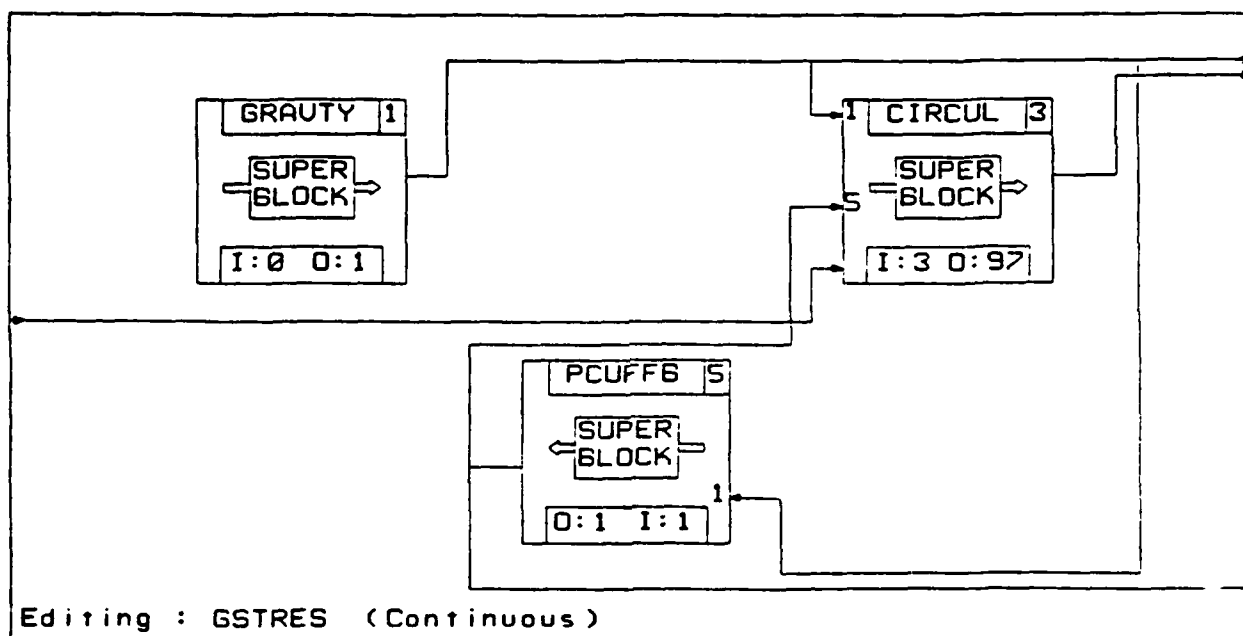


Fig. 9 Model of Circulatory System Under G Stress
and Compensation of Anti-Gravity Suit

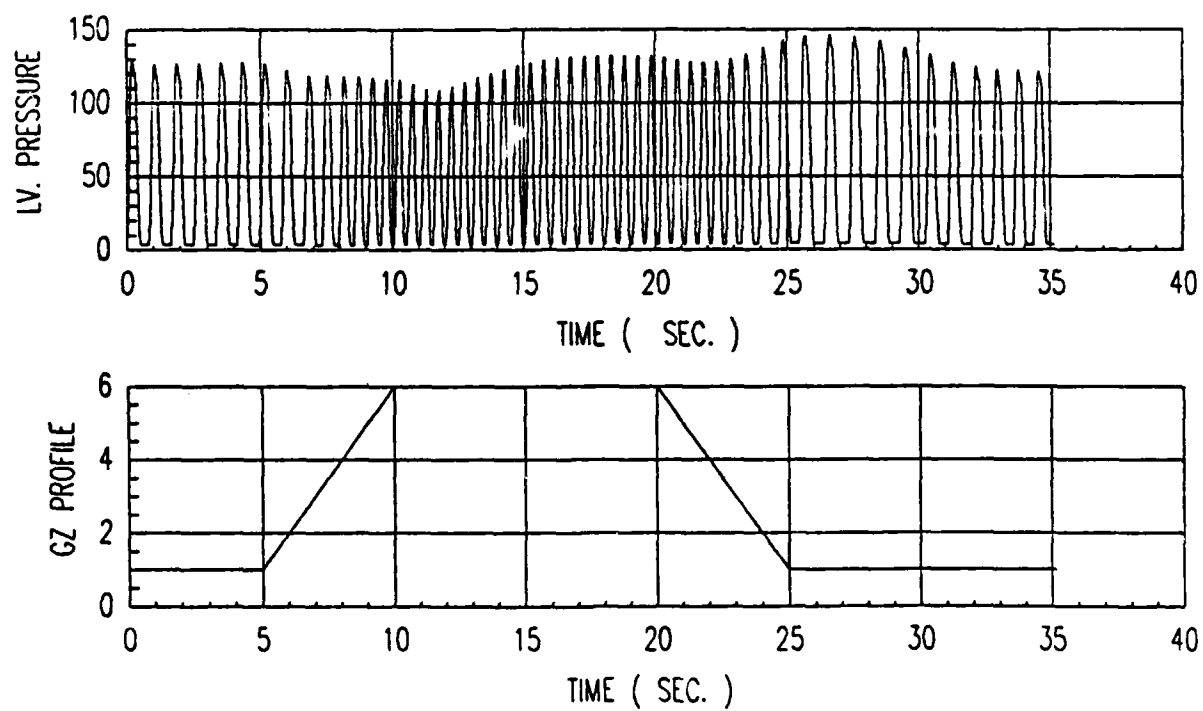


Fig. 10 Model Results for 6 +G_z Profile

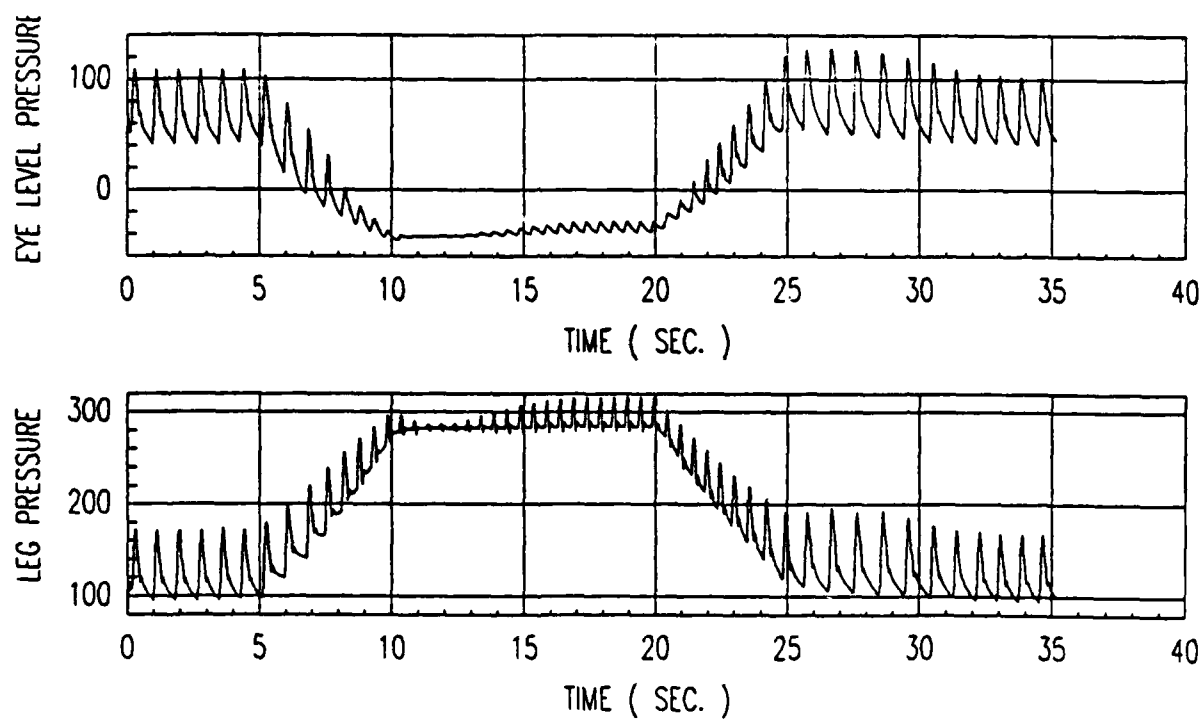


Fig. 11 Model Results for 6 +G_z Profile

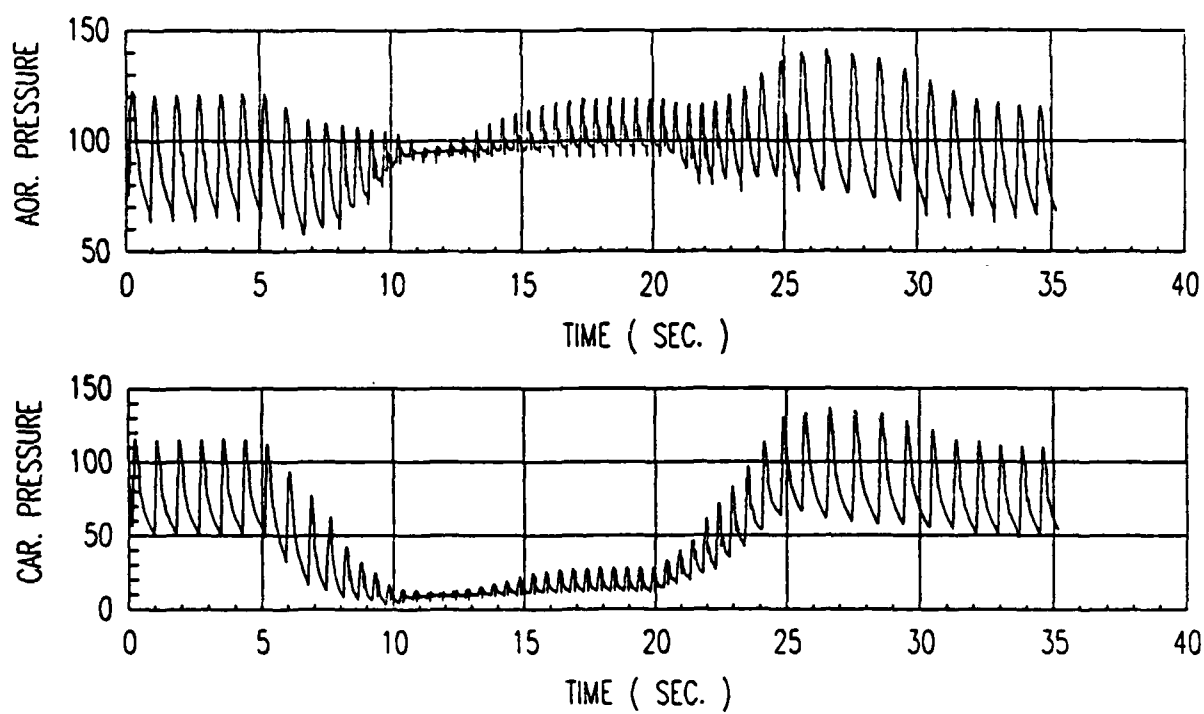


Fig. 12 Model Results for 6 +G_z Profile

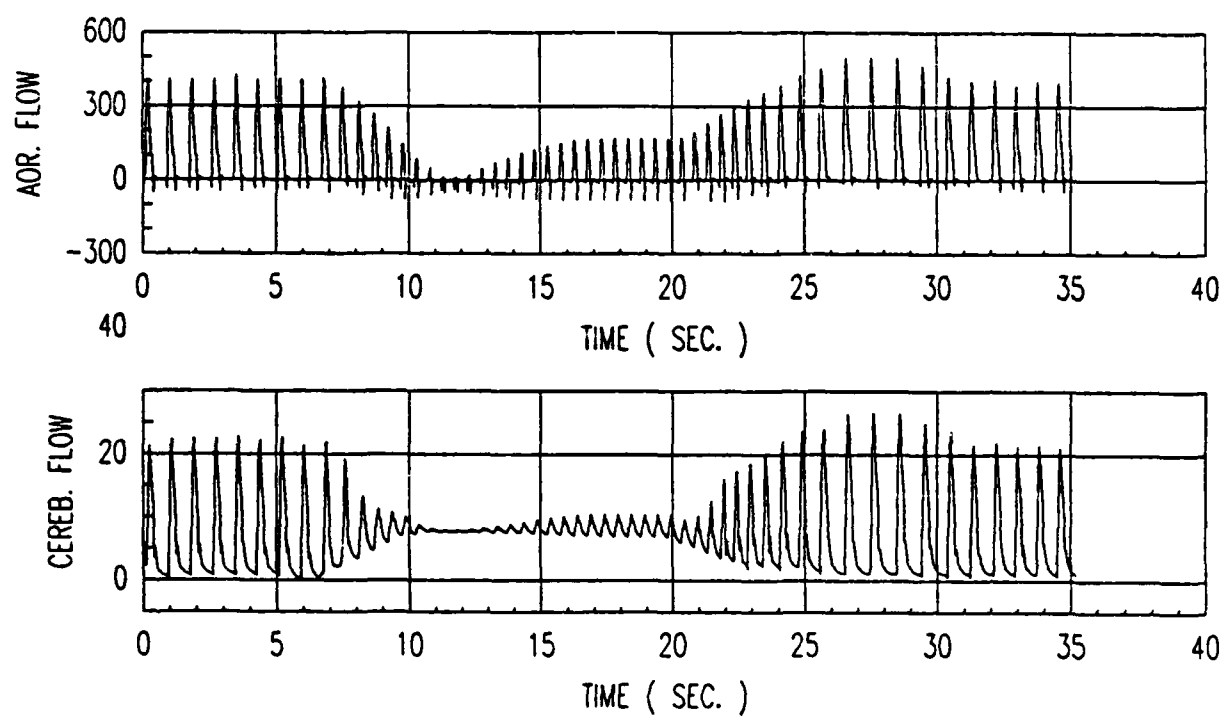


Fig. 13 Model Results for $6 + G_z$ Profile

V. Recommendation for Future Work

1. The computer simulation of the cardiovascular system we have developed takes approximately 24 hours of CPU time for the G-profile shown in Fig. 14

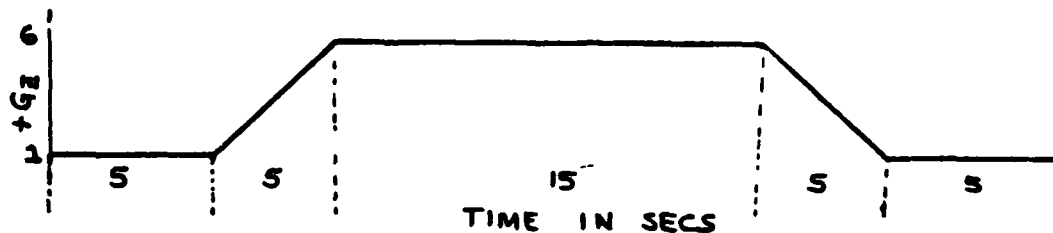


Fig. 14 +G_z Profile

In order to effectively use this simulation, it is important that the simulation be speeded up. A new version of MATRIX_x released recently has an option called HYPER-BUILD. Our initial study indicates that this option may speed up our simulation by a factor of approximately 10.

2. Present computer simulation assumes all the resistances, inductances and capacitances of the arterial tree to be fixed. The simulation should be modified to include the nonlinear effects of these variables.
3. Modify the cardiovascular model and computer simulation to include G-suits and study their effects.
4. The present cardiovascular model assumes the leg as a peripheral element B. To study the effects of sequential G-suit, the multielement arterial tree should be modified to include the thigh and calf parts of the leg.
5. The lumped venous model needs to be replaced by a multielement model in order to get more accurate blood distribution under acceleration stress or external applied force.
6. To study the effects of various maneuvers, such as M1, L1, the model needs to include external pressure sources around the thoracic area.
7. Study the technique of pulsating G-suit synchronized with the heart.

8. Obtain a multivariable transfer function model using the state-space representation of the multielement arterial tree.
9. The proposed closed-loop servo controller designed is just a preliminary design. Time-domain and frequency-domain techniques should be used to design an optimal controller. The effort should be made to design a multivariable control system which should include eye level pressure and heart rate as inputs.

References

1. Chu, C., "A Mathematical Model of the Cardiovascular System Under +Gz Stress." Ann Arbor, Michigan. University Microfilm International, 1984.
2. "MATRIX User's Guide." Integrated Systems, Inc., 1986.

1986 USAF+UES Summer Faculty Research Program/
Graduate Student Summer Support Program

Sponsored by the
Air Force Office of Scientific Research

Conducted by the
Universal Energy Systems, Inc.

Final Report

Inefficiencies of High Transmission Delays on
Communication Protocols and their Applications

Prepared by:	Alan H. Baginski
Academic Rank:	Graduate Student
Department and University:	Department of Electrical Engineering University of Lowell
Research Location:	The Rome Air Development Center, Command and Control Division, Distributed Systems Section, Griffiss AFB, NY
USAF Researcher:	Thomas F. Lawrence
Date:	September 30, 1986
Contract No.:	F49620+85=C+0013

Inefficiencies of High Transmission Delays on
Computer Protocols and their Applications

by

Alan H. Baginski

ABSTRACT

The performance of the Transmission Control Protocol (TCP) was studied in order to find inefficiencies in a high transmission delay environment. It was determined that improvements to the TCP could be made in the connection set up procedure, the window size assignment algorithm, and the handling of transmission errors so that the delays may be minimized. The performance of a process synchronization application using a communication protocol such as the TCP was also studied for inefficiencies in the context of a high delay environment. A hierarchical mutual exclusion algorithm was proposed. The benefits that these results could bring to the performance of the Cronus distributed operating system is discussed.

Acknowledgements

Many thanks to the Air Force Office of Scientific Research for sponsoring this effort. I would also like to thank Tom Lawrence, Tony Newton, and Craig Prohazka for helping me complete this effort as well as for their time, advice, and helpfulness. Finally, thanks to the Rome Air Development Center and, especially, the COTD section for their friendliness and for providing an excellent work environment.

I. Introduction

I received a BSEE from the University of Maryland. I am currently a candidate for a Master's degree in Computer Engineering at the University of Lowell concentrating in computer software.

Since the Cronus distributed operating system project sponsored by the Distributed Systems section at the Rome Air Development Center is using existing communication protocols, the suitability of these protocols for this application is in question. The study of the effect of high delays on protocol performance is a small part of this larger problem.

II. Objectives of the Research Effort

The ultimate objectives of the research will be to determine the efficiency of the communication protocols used with the Cronus distributed operating system designed by Bolt Beranek and Newman, Inc. and to recommend changes in the protocols or introduce new communication protocols for distributed operating system applications.

My individual objectives were a subset of the overall objectives. These objectives were to study the efficiency of these communication protocols in a high transmission delay environment that might be found with communication between Cronus clusters and to recommend improvements. Another objective was to determine if high transmission delays in the Cronus cluster architecture would affect the performance of distributed operating system applications using the communication protocols and to recommend improvements.

III. High Transmission Delays

The performance of a computer network with constant and relatively low communication delays and the performance of the applications which use the computer network should be predictable and efficient. The performance of a network and its applications is not so predictable, however, if nodes in the network are geographically remote from other nodes because some communications delays will be high. The Cronus distributed operating system with clusters of nodes at BBN in Cambridge, MA and at the Rome Air Development Center in Rome, NY is an example of such a network. The effects of high delays on the performance of the TCP protocol and a synchronization application will be examined.

To understand the effects of a high transmission delay on the efficiency of a communication protocol, consider the throughput of a communication line with the following characteristics where bits sent must be acknowledged by the receiver:

- D - transmission delay in seconds
- T - transmit time per bit
- A - bit acknowledge processing time

The time needed to transmit one bit is the transit time (T), the bit acknowledge time (A), and twice the transmission delay (D) to send the bit and to return the acknowledgement. Since only one transit time was used to transmit useful information, the bandwidth utilized (BW) is:

$$BW = \frac{T}{T + A + 2D} \quad (1)$$

If the sender is allowed to transmit up to W unacknowledged bits the bandwidth utilized is increased to

$$\begin{aligned}
 BW &= \frac{WT}{T + A + 2D} && \text{for } WT \leq T + A + 2D \\
 &= 1 && \text{for } WT > T + A + 2D
 \end{aligned}
 \tag{2}$$

where W is called the window size. Bandwidth utilization is maximized when the time it takes to send a window of bits, WT , is greater than or equal to the time needed for the initial bits sent to be acknowledged, $(T + A + 2D)$. In this case, the sender can continuously send bits since there will never be more than W unacknowledged bits at any time. From (2), it is seen that as delay increases the window size must double the increase in delay in order to utilize the same percentage of bandwidth. If the window size is not large enough to keep the sender continuously transmitting, messages sent on the communication line will experience a delay greater than twice the transmission delay of the line.

Even if the communication protocol is optimal, the delay for sending messages is still twice the transmission delay. This message delay could be quite large and have adverse effects on the performance of applications using the communication protocol when compared to a low delay case. These effects occur when applications are interactive in nature and the delays are additive. The effects are at a minimum when applications are not interactive and the delay must be incurred only once. Therefore, applications of a communications network which are interactive must be modified so that the degree of interactivity is minimized in cases where there are high transmission delays.

IV. TCP Inefficiencies in a High Delay Environment

The TCP is an end to end, reliable, connection oriented protocol which provides a process to process communication service. The TCP accepts streams of data octets from the user and, at its control, segments the octets to send to the receiving TCP. Each of these octets is assigned a sequence number. Reliability is achieved through the use of acknowledgement messages containing the sequence number that the receiver expects to see next. Unacknowledged octets must be retransmitted until acknowledged. To prevent a fast sender from overloading a slow receiver, flow control is provided by the receiver advertising a window of acceptable sequence numbers starting from the acknowledgement sequence number. The window size will expand and contract depending on the load on the receiving TCP from this and other connections. Connections are established through a handshake procedure to ensure reliability and to pass initial sequence numbers and window sizes.

In a high transmission delay environment, several TCP features such as the connection set up procedure, the window mechanism, and the handling of transmission errors operate inefficiently. These inefficiencies will be examined and solutions will be proposed.

TCP Connection Set Up

The TCP requires a three way handshake procedure to initiate a connection between processes. During this procedure, messages are exchanged to initialize the sequence numbers and window sizes for both directions of transmission. No user data may be transmitted. Therefore, regardless of the duration or the size and number of messages of a connection, a round trip transmission delay is incurred before any

useful data can be transmitted.

This inefficient handshake procedure is tolerable for small transmission delay connections because the round trip delay is small when compared to message transmission times. As transmission delays increase, the connection set up time will be a greater percentage of the message transfer time. In addition, the round trip delay caused by the connection set up procedure does not take into account to the normal message delay which, of course, will be longer with high transmission delays. There are two ways to eliminate the inefficiency of the TCP connection set up procedure. The first is to provide permanent connections to processes which are distant to each other. The second is to allow data to be sent during the connection set up request.

Permanent Connections

Processes which have high transmission delays, exchange messages frequently, or require the lowest possible delay could be assigned permanent connections. Every message that would normally require a new connection and messages that depend on this message will be delivered one round trip transmission delay time sooner. In order to make sure the connection is healthy during the times the connection is inactive, messages confirming the current window size and sequence number should be sent periodically.

Providing permanent connections to processes does not come without a cost. TCP resources must be dedicated to a probably lightly used connection at all times. The TCP must allocate some of its memory to provide a non-negligible window size to the connection. It is also possible that lower level protocol resources must also be dedicated. This does not seem to be the case with the IP protocol.

Connection Initiation Requests with User Data

If user data could accompany a connection request and if other data segments could be sent before the connection request is acknowledged, the round trip delay caused by the three way handshake procedure can be eliminated. Of course, if the receiving TCP does not have the buffers to accept the data or there are errors in the connection request or data, the data should be ignored. Sending data to a receiving TCP which has not advertised a window size suggests changing several aspects in the window size concept.

One such change would be to require TCPs to set aside memory for its idle connection ports in the event the TCP receives a connection set up request accompanied by user data. The memory which should be set aside is not negligible since these connections may be high transmission delay connections. As discussed above, the window size for a connection must be at least an amount of data in which the time it takes to transmit this amount is greater than the time it takes to acknowledge the initial segment of the data in order to allow the sender to continuously transmit. The set aside memory would be replenished by not advancing the window from existing connections or from the closing of connections. Care must be taken to ensure that it is unlikely that the set aside memory is over requested if several TCPs initiate connections simultaneously. When this occurs, data must be rejected and eventually retransmitted. If this happens frequently, so much data is retransmitted that performance deteriorates more than the performance improves by allowing data to be transmitted before connections are acknowledged.

A possible solution to reduce the probability that data is rejected

is to introduce a long delay service bit in connection initiation messages that would indicate whether a connection will use the set aside memory. A tradeoff could now be made between the amount of TCP memory set aside for future connections and the number or type of connections that will be allowed to use the set aside memory.

Window Size

The transmission delay is minimized if the window size is large enough so that the sender can continuously transmit data segments. This window size becomes larger for high delay connections. Since the TCP does not distinguish between high and low delay connections in assigning window sizes, high delay connections will routinely receive insufficient window sizes. An algorithm which allows a TCP to optimally assign window sizes based on transmission delay is needed to improve the performance of high delay connections.

An efficient manner to inform the receiving TCP of the proper window size is in the connection set up request. A field in the connection set up request indicating the transmission delay between TCPs or the time stamp of the message in which the delay can be calculated could be introduced. The optimal window size producing the least delay and use the least resources can now be determined. From the optimal window sizes of all the connections and which connections are using the set aside memory, a TCP can optimally assign window sizes for each connection from its capacity. For example, high delay connections would normally be given larger window sizes than low delay connections. Those connections which request large window sizes and use the set aside memory would be guaranteed its optimal window size.

Transmission Errors

To minimize the delay of a message, transmission errors must be minimized and those that do occur must be detected by the sender as soon as possible. In order for a transmission error to not increase the transmission delay of a message, the error must be detected by the sender before it has transmitted its window of unacknowledged bits. If the sender has a window of unacknowledged bits outstanding, it must wait for knowledge of which data is in error or for the advancement or enlargement of the window to continue transmitting useful data. In a high transmission delay environment, this waiting is proportionately longer than for low transmission delay environments.

By assuming that lower level services are not one hundred percent reliable, the number of transmission errors cannot be reduced unless duplicate data segments are sent along different routes. This will increase the probability that one copy of the data arrived at the receiver properly. This solution is not feasible, however, since communication costs would rise sharply and any reduction in delay resulting in fewer transmission errors would be more than offset by the increase in delay caused by transmitting two copies of all data.

To detect transmission errors at the sender as soon as possible, a negative acknowledgement scheme at each site along the transmission path including the destination site is needed. At each site in the route, the data segment should be copied as it is retransmitted. Currently, the IP protocol will test the header checksum and only retransmit if it is correct. There is no checking of the data and there are no negative acknowledgements. If there is an error, the header should be returned to the sender with a negative acknowledgement. If there is an error in the header, it will be impossible to correctly determine and notify the

source of the message and the data must timeout before it can be retransmitted. Receiving negative acknowledgements may allow the sending TCP to retransmit a data segment and possibly have the data acknowledged and the window advanced before the sender has completely sent its originally allotted window.

V. Process Synchronization Inefficiencies in a High Delay Environment

Eventhough the communication protocols may be efficient, high delays may still exist in a network. For the same reasons that communications protocols may be inefficient, applications using these protocols may become inefficient as transmission delays increase.

A common application of a distributed operating system is to provide mutual exclusion among a number of processes on different nodes in a network. Four traditional methods - distributed, centralized, ring, and token request- have been used to provide this application function and all are useful depending on the number of processes, the network architecture, the scheduling algorithm, and the performance desired. When there are high transmission delays and, possibly, many processes which require mutual exclusion, each of these synchronization methods becomes inefficient in some manner. The Cronus distributed operating system with clusters of nodes at BBN and the Rome Air Development Center is example of a network architecture that would exhibit this behavior. The four synchronization methods and their inefficiencies in the presence of high transmission delays will be discussed and an improved synchronization method using a hierarchical combination of the traditional methods is proposed. For this application, it is assumed that there are n processes, one per node, of which only one may be in its critical section at any one time.

Distributed Synchronization Method

In the distributed synchronization application, a process that wishes to enter its critical section sends a request message to each of the other processes. When the requesting process receives replies from all the other processes, it may enter its critical section. Each critical section entry request, therefore, generates $2(n-1)$ messages. If a process is in its critical section or has requested to enter and has higher priority when it receives a critical section request from another process, it waits until it exits its critical section before replying. Otherwise, it replies immediately.

This algorithm works efficiently when there are only a few processes with low transmission delays between them. The communication costs in providing mutual exclusion is low because the number of messages will be low. The performance of the algorithm will be good because the amount of time that elapses when one or more processes wishes to enter its critical section while no other process is in its critical section will be minimized. To see that this is true, there are two cases to consider - contention for mutual exclusion and no contention for mutual exclusion. In the contention case, the wasted time when no process is in its critical section is the time between one process leaving its critical section and the next process entering. In the distributed synchronization method, this time is one message delay from the process leaving its critical section to the process entering. In the no contention case, the time wasted is the time between a critical section request and the critical section entry. In the distributed synchronization method, this time is two message delays - one to request the critical section and one to receive all the replies.

In either case, these messages are low delay messages.

As the number of processes increase and high message delays are present such as in the RADC-BBN Cronus architecture, the communication costs of the algorithm increase and its performance deteriorates. The communication costs rise because the number of messages rise due to the increase in processes and, on average, half of them will be high delay messages between the clusters. The performance of the algorithm decreases with contention because half of the time the process leaving its critical section and the process entering will be in different clusters. If there is no contention the deterioration of performance is worse since the both of the two messages delays will be high delay messages. This is because the request for the critical section must always reach processes in the other cluster and these processes must reply.

Centralized Synchronization Method

In the centralized synchronization method, a coordinator process ensures that only one process is in its critical section at any time. A process wishing to enter its critical section must send a request message to the coordinator process. The process may enter its critical section when it receives a permission message from the coordinator. The process must notify the coordinator upon exiting its critical section with a release message so that the coordinator may allow other processes to enter their critical sections. Therefore, the centralized synchronization algorithm requires three messages per critical section request- a request, permission, and release message.

This algorithm works efficiently for networks that exhibit centralized control and have a large number of nodes that have low

transmission delays between them. The communication costs are low since only three messages are required per critical section entry. The performance is rather predictable and good because the time wasted when processes could be in there critical sections but are not is two message delays for both the contention and no contention cases - a release or request message to the coordinator from a process and a permission message from the coordinator to a process.

In the Cronus architecture, the performance will be poor and unpredictable. Zero, one, or both of the message delays will be high delay messages depending on the location of the coordinator and of the processes involved. In the no contention case, the process requesting the critical section may or may not be in the same cluster as the coordinator process. In the contention case, the process leaving its critical section and the process entering may or may not be in the same cluster or in the cluster of the coordinator process. On the average, the time wasted will be one high delay message and one small delay message. Also, the algorithm will not be fair in the no contention case because processes in the same cluster as the coordinator process will receive better service. Communication costs are still low, however, since there will be only three messages per critical section request regardless of the number of processes.

Ring Synchronization Method

In the ring synchronization method, the nodes of the network are arranged in a physical or logical ring. A token "message" is passed around the ring from node to node whether or not the processes at these nodes want to enter their critical section.

This algorithm works well in a "high" contention environment since

only a few token messages are needed before the token arrives at a node whose process wishes to enter its critical section. In a no contention case, the algorithm is poor since on average $n/2$ token message delays are required for the token to arrive at a node whose process wants to enter its critical section. The communication costs for this algorithm can be significant if no process wishes to enter its critical section for long periods of time since token messages will be uselessly passed around the ring.

In the RADC-BBN Cronus architecture, the performance of the algorithm may still be satisfactory if there is high contention. Only one of the possibly several message delays will be a high delay message. This message would correspond to passing the token to the other cluster. The performance of the algorithm for little or no contention will be extremely poor since there will almost always be a long message delay before a process enters its critical section. In some cases there would be two long message delays if a cluster did not contain any process which wants to enter its critical section and it was passed the token.

Token Request Synchronization Method

This synchronization method is similar to the ring synchronization method except that the token is not passed to another node unless the process at that node requests it. This is accomplished by having each process that wants to enter its critical section send messages to all the other processes in a manner similar to the distributed synchronization method. Every process saves enough information from these request messages to determine the priority of each critical section request. After a process leaves its critical section, it sends the token to the next process to enter its critical section. If there

are none, the process keeps the token until there is one.

The token request method requires a higher communication cost than the ring method but higher performance is achieved. The communication costs are higher since each critical section request generates n messages- $(n-1)$ for the request and one to receive the token- whereas the ring method usually will require only a few messages. The performance is superior in the token request method because only one message delay time is wasted to pass the token if there is contention or two message delay times wasted to request the token and to have it passed if there is no contention.

If there are high transmission delays and more nodes, communication costs rise because there are more messages and half of them will be high delay messages. The algorithm's performance will be poor if the next process to enter its critical section is in a different cluster as the process currently in its critical section. The performance will be good if both processes are in the same cluster. Notice that the token request synchronization method performs just as well as the distributed synchronization method in the contention case except that communication costs are lower in the token request method. This is due to the fact that there are $(n-1)$ reply messages with the distributed method while only one reply- the passing of the token- in the token request method.

Combined Hierarchical Synchronization Method

To improve upon the four traditional synchronization methods for a network with many nodes and a cluster architecture, the amount of intercluster, high transmission delay communication must be reduced. That is, the actions of requesting to enter a critical section or changing the process which is in its critical section should not require

intercluster communication as much as possible. The combination of the traditional synchronization methods in a hierarchical manner exhibits this behavior.

This synchronization method ensures only one process will be in its critical section by ensuring that only one cluster is in its "critical section" and only one process in this cluster is in its critical section. Therefore, one of the traditional synchronization methods can be used for mutual exclusion of the clusters and one for the processes within the clusters. The choice of synchronization methods depends on the number of objects requiring mutual exclusion and whether a distributed or centralized control policy is naturally present in the network. For example, a large number of processes in a cluster will require many messages with the distributed synchronization method but few with the centralized method. If the network was part of a distributed operating system, providing synchronization by centralized control would probably be inefficient.

The hierarchical synchronization method improves performance and reduces communication costs by allowing several processes in a cluster to enter their critical sections before allowing processes in other clusters to enter theirs. Therefore, much of the communication to change the process in its critical section will be intracluster low delay messages. Occasionally, there will be high delay intercluster messages but only for the purpose of changing the cluster in its "critical section" and this will happen infrequently in comparison with the amount of low delay intracluster messages. This synchronization method does not allow a first come first serve mutual exclusion as do the traditional synchronization methods, but the method is fair in terms of the amount of time a process will have to wait, on average, to enter its critical section.

VI. Recommendations

This research assumed a high transmission delay for messages between TCP layers in, for example, two Cronus distributed operating system clusters. The actual performance of the TCP for the Cronus clusters in Rome, NY and Cambridge, MA should be measured to determine if the performance of the protocols between the clusters and, therefore the performance of the distributed operating system, suffers from high transmission delays.

If these high delays do occur, several communication protocol changes should be made. First, the round trip delay caused by the TCP connection initiation procedure should be modified to reduce or eliminate its effect. Second, and probably most important, it must be ensured that these high delay connections are ensured a large enough window size so that the transmitting TCP is not constantly waiting for the receiving TCP. Finally, if a cause of the poor performance of the TCP is a high transmission error rate, a negative acknowledgement scheme should be implemented so that the sending TCP does not have to wait for data segments to timeout.

Several changes should also be made in the structure of the applications using the communication protocols if high delays are present. These changes should minimize the amount of high transmission delay communication between Cronus clusters for example. A hierarchical structure proved to be efficient in a process synchronization application. Applying this structure to other distributed operating system applications should be attempted.

References

1. Ricart, G and A. K. Agrawala, "An Optimal Algorithm for Mutual Exclusion in Computer Networks," Communications of the ACM, Vol. 24, No. 1, pp. 9-17.
2. Postel, J, "Transmission Control Protocol - DARPA Internet Program Protocol Specification," RFC 793, USC/Information Sciences Institute, September 1981.
3. Postel, J, "Internet Protocol - DARPA Internet Program Protocol Specification," RFC 791, USC/Information Sciences Institute, September 1981.
4. Peterson, J L and A. Silberschatz, Operating Systems Concepts, Addison-Wesley Publishing Company, 1985.

1986 USAF-UES SUMMER FACULTY RESEARCH PROGRAM/
GRADUATE STUDENT SUMMER SUPPORT PROGRAM

Sponsored by the
AIR FORCE OFFICE OF SCIENTIFIC RESEARCH
Conducted by the
Universal Energy Systems, Inc.

FINAL REPORT

COGNITIVE RESOURCES AND MULTI-TASK COST

Prepared by:	Joseph M. Borroughs
Academic Rank:	Graduate Student
Department and	Psychology
University:	University of New Mexico
Research Location:	Harry G. Armstrong Aerospace Medical Research Laboratory, Human Engineering Division, Technology Development Branch
USAF Researcher:	Dr. John Forester
Date:	September 19, 1986
Contract No.:	F49620-85-C-0013

COGNITIVE RESOURCES AND MULTI-TASK COST

by

Joseph M. Boroughs

ABSTRACT

The construct of cognitive resources is reviewed with special emphasis on the need to develop design principles and guidelines for reducing multi-task cost. Although the concept of cognitive resources has been widely accepted by cognitive psychologists it does not represent the only manner in which multi-task interference can be viewed. The number of alternative views is numerous, however, and no relevant alternative theories have been developed. It is recommended that the Air Force initiate a program of basic research which aims to identify those aspects of tasks which are the greatest causes of multi-task cost.

ACKNOWLEDGEMENTS

I would like to thank the Air Force Systems Command and the Air Force Office of Scientific Research for sponsorship of my research. The environment and facilities of the Armstrong Aerospace Medical Research Laboratory were excellent and inspiring. Mr. Walt Summers deserves thanks for the warm and supportive atmosphere he fostered for me at the Technology Development Branch. Finally, I would like to thank Dr. John Forester for many exciting hours of discussion.

I. INTRODUCTION:

My graduate work in cognitive psychology at the University of New Mexico is advised by Dr. Peder Johnson. I have worked closely with him on research concerning attention which has employed dual-task and priming methodologies. Additionally I have pursued independent research in tachistoscopic word and letter recognition. Presently, I am conducting a general review of the literature in visual attention and perception in preparation for advancing my dissertation research proposal.

Dr. John Forester and several other researchers at the Armstrong Aerospace Medical Research Laboratory are interested in establishing a program of basic research into questions of attention and performance in multi-task environments. The initial phase of this endeavor comprises review of relevant empirical and theoretical work on the topic with the objective of reformulating some of the basic issues. Dr. Forester knew of my background and present objectives, and I was awarded the opportunity to work with him in developing this project.

II. OBJECTIVES OF THE RESEARCH EFFORT:

Dr. Forester and I agreed upon three objectives which would meet his needs in developing a research proposal as well as facilitating my goal of reviewing literature per-

herent to my dissertation proposal. First, I was to survey the recent psychological research literature for articles relevant to attention and performance in multi-task environments. Second, I was to read as many of these articles as time would permit and to recommend articles important to the proposed research effort. Third, I was to meet frequently with Dr. Forester in order to brief him on the information I was encountering and to discuss whatever issues arose concerning the development of the research program. These objectives remained unchanged throughout the research period.

I successfully covered a large territory in reading as well as in discussions. In this report I present a concise overview of the points which were most influential in shaping my recommendations. In the following sections I outline the basic problem area of multi-task cost, review the theory of cognitive resources, and discuss issues which motivate the recommended strategy toward the problem.

III. THE PROBLEM OF MULTI-TASK COST:

Two simple facts converge to create a serious problem for the Air Force. Fact 1: Timesharing several tasks generally results in poorer performance on all the tasks when compared to doing each task separately. This decrement in task performance is called multi-task cost. Fact 2: Many jobs in the Air Force inevitably involve multi-task

environments. Pilots are prototypical since they usually must perform several tasks concurrently, and this basic aspect of flying simply cannot be eliminated by task restructuring. Consideration of these two basic facts leads to an unfortunate conclusion: the intrinsic multi-task nature of many Air Force jobs is itself a factor which limits human performance. Since human limitations often represent the limits of whole systems, reducing multi-task cost and thereby improving human performance is a highly desirable objective.

Achieving this goal requires the development of design principles and guidelines for structuring tasks which occur in combination. The number of possible alternative ways to structure the various tasks is large even for an environment consisting of only two or three tasks, and trying all the combinations for each environment in need of improvement is simply infeasible. Human factors researchers in the Air Force have looked to basic research in cognitive psychology for theory and data which would allow tasks and combinations of tasks to be structured in a principled manner. What cognitive psychology presently offers is resource theory, and no viable alternatives appear to be forthcoming. This theory is briefly described in the following section.

IV. RESOURCE THEORY:

A major evolutionary shift is visible in the brief 30-year history of cognitive psychology. The first modern attempts to understand the mind were structural. Research sought to establish the basic parts of the mind and how they interacted. Eventually most psychologists became disenchanted with this approach and came to think more in terms of processes. The concept of cognitive resources is very much a part of the process view of the mind, and the increasing usage of the term has paralleled the shift away from structural accounts of cognition. Presently the term enjoys widespread acceptance and is often used interchangeably with "attention", "capacity", and sometimes "effort." The position taken here is that "resources" is a key concept within a general theory of cognitive performance, and its meaning is best understood within that theoretical context, whereas the other terms mentioned have connotations extraneous to that context. The enthusiasm of cognitive psychologists for the concept of resources is not merely due to congruence with current trends, however. The theory surrounding the concept is itself simple and powerful.

The process view of the mind assumes that all important behavior depends upon the execution of cognitive processes. The fact that humans are capable of a wide variety of behavior depends upon the fact that we possess a

repertoire of basic cognitive functions which can be assembled into an essentially infinite number of different cognitive processes. At any moment behavior reflects only a tiny fraction of our capabilities because only a small number of all the processes we can execute are actually in progress. The major challenge for the process view is to articulate how processes are controlled so as to result in adaptive behavior.

Resource theory consists of a set of closely interrelated notions that collectively represent a response to this challenge. The first notion naturally posits the existence and basic function of cognitive resources. In order for any process to execute it must have access to some minimum amount of resources. Further investment of resources improves the quality of the output of the process. Eventually a limit is reached when the process has access to all the resources it can effectively utilize, and at that point the quality of the output will depend solely on the quality of the input (or data) that the process is manipulating (Norman & Bobrow, 1975). The second notion is that we have control over the deployment of our resources. Acting out an intention to do something amounts to selectively allocating resources to those processes which are required to accomplish the objective. The third notion is that the resources invested in one process are unavailable

for use by any other processes, and the fourth notion is that the supply of resources is limited at any moment in time. The joint effect of these two ideas is that whenever several processes are executing simultaneously it is because each process has access to part of the available resource pool. If most of the resources are committed, then improved performance in one process can only be obtained at the expense of performance on some other task.

The four notions comprising resource theory were borrowed from macroeconomics and when dovetailed with the process view of the mind they form a simple package. The power of the theory comes from the fact that several major characteristics of cognitive performance emerge in a very straightforward way from this package. Three characteristics are presented here: task difficulty, task selection and/or prioritization, and multi-task cost. First, what does it mean for one cognitive task to be more difficult than another? Strict process views slaved to the computer metaphor have some trouble providing a satisfactory answer. Resource theory, by contrast, simply posits the quite reasonable view that one task is more difficult than another when its processes require a greater investment of resources in order to produce an output (of acceptable quality). A related spinoff of this account is that when the quality of performance in a task is increased, the task

is generally more difficult. All this fits very well with our intuitions about difficulty. Second, the issue of task selection and/or prioritization is an essential aspect of control which resource theory handles easily with the notion of allocation. Again the side effects are just what we would want: if several tasks are attempted at once, the relative importance of each task can be taken into account by differential allocation to the underlying respective processes. Finally, multi-task cost comes about because the supply of resources is limited. When more than one task at a time is attempted, then the supply of resources must be divided among the base processes, and this typically results in poorer performance on each task because the resource allotment is less than would have been possible if each task were performed separately.

The theory of cognitive resources seems to have a good deal going for it. It fits nicely with the process view of mind, it is quite simple, and it readily fits our understanding of basic aspects of cognitive performance in an intuitive manner. It is not surprising, given this, that the theory has been a good catalyst for research ideas. It provides a comfortable framework for thinking about "how things might work", and hundreds of experiments owe their inspiration and interpretation to the theory.

V. THE CRUCIAL ISSUE:

Since resource theory seems to be "the only game in town", I thought it was important to assess whether it has an "Achilles' heel" -- any weakness which would undermine the useful application of the theory to the practical problem of multi-task cost. In my opinion such a weakness does exist. The problem arises from research motivated by an issue which is as old as resource theory itself. The basic question is whether cognitive resources are all alike or whether there are several different kinds. This issue is crucial because its implications affect both the strategy appropriate for reducing multi-task cost within real work environments and the appeal of resource theory itself.

If a single, undifferentiated pool of resources exists, then the practical problem of multi-task cost can be approached simply, but with modest expected results. If several concurrent tasks suffer poorer performance because they cannot obtain their optimal share of the resources, then the problem can be reduced exactly to the extent that each task can be made easier (so it uses fewer of the available resources). No concern need be displayed over particular task combinations so long as obvious sources of peripheral interference are avoided. Each task simply needs to be structured so its performance in isolation is maximal. Presumably then, each task is making the best

possible use of the available resources, and joint performance will necessarily be the best that can ever be obtained. The only way this outcome could be prevented would be if some tasks have very different functions for the marginal utility of resources given different structurings. Notice that this sort of explanation is post hoc since the functions are hypothetical. No use can be made of this possibility in a predictive manner, so it does not constrain the question of proper design. In sum, if one kind of resource exists, then structuring the whole multi-task environment is not really required. Multi-task cost is inevitable and all that can be done is to make the component tasks as easy as possible.

On the other hand, if resources are of several distinct kinds, each with its own limited supply, the problem of reducing multi-task cost is much more complex, but the possible benefits are considerable. Say the cognitive system has N different kinds of resources, and the quality of output for any given process depends upon variations in the supply of at least some and perhaps all of the different kinds of resources. Each process could be thought of as having a resource profile which describes how it utilizes each resource to produce a certain quality of output. Different processes could have very different profiles. Since external tasks can be restructured so as to change the

nature of their underlying processes, there is no profile for a task, per se, but rather a collection of profiles corresponding to the various ways the task could be accomplished. Reducing multi-task cost would involve the selection of a process profile for each component task in a way that it best fits with the profiles selected for the other tasks. Good fits would imply little or no multi-task cost, whereas poor fits could result in dismal concurrent performance. Obtaining a good fit is clearly a problem of designing the whole multi-task environment, and great benefits can result when compared to mixing the task structures without regard for their complex interactions.

It is clear that very different prospects emerge for the reduction of multi-task cost depending on whether resources are alike or different. The issue is also crucial to resource theory itself. As mentioned previously, the main force of the theory comes from the combination of its simplicity with the straightforward and intuitive manner in which it accounts for some basic characteristics of cognitive performance. Recall that the theory provides a mechanism for the control of cognitive processes by virtue of the resources invested in them, and also details how simultaneous processes interact via differential allocation and competition for the limited supply of resources. If this picture is complicated by introducing several kinds of

resources, then tough questions rather than easy answers emerge. For example, is the quality of output of a process controlled by joint allocation of all its needed resources, or are only some "critical" resources manipulated? Are all the kinds of resources allocatable will equal ease? Is a given level of output quality obtained only with a particular combination of resource allocations, or are several combinations possible? If variety in control is possible, what determines which "mix" is picked? Clearly a system with multiple resources could exert control in a wide variety of ways, and some specification is required before the behavior of the system is fathomable. What is troubling is that no particular specification seems "natural"; all are just speculation. Whatever specification is articulated will necessarily be fairly complex relative to the original resource view. Similarly, the new theory would have to make an account of the basic characteristics of cognitive performance, and this would also seem more contrived than the original theory. If the data rule out the possibility of a single resource, then there is good reason to suspect that the whole resource perspective will seem less compelling.

As it turns out there are many studies which bear upon the crucial issue. Wickens(1980,1984) argues persuasively that certain patterns of results from dual-task studies are

inconsistent with the hypothesis of a single, undifferentiated pool of cognitive resources. He identified four such patterns which he labels perfect timesharing, difficulty insensitivity, structural alternation effects, and the uncoupling of difficulty and structure. Without describing each of these patterns in detail, suffice it to say that dual-task interference effects are more complex than can be accounted for by a single-resource model of the cognitive system. I think Wickens has done excellent work in this connection, and the issue is settled: one resource is not enough. What remains is to consider what to do in light of this discovery. Wickens chose to develop a multiple resource theory which has turned out to be extremely influential among human factors researchers. Another possible course of action, however, is to question the resource perspective altogether.

Navon(1985) has done exactly that. Rather than assume multiple resources, he argues for the plausibility of a cognitive system without resources. Resource theory is a theory, and the concept of cognitive resources is a theoretical concept which should require empirical support like any other theoretical concept. Although multi-task cost is usually interpreted in terms of resources, other explanations may work just as well. Navon briefly describes some alternative sources of dual-task

interference: cross talk between tasks, difficulty in making non-habitual transitions, matching indeterminacy, and temporary disablement. Each of these could result in multi-task cost, but they are not resource accounts. It is important to realize that Navon is not offering a well-formed alternative theory of cognitive function. Rather, he is trying to show that the concept of resources is not coextensive with the process view of the mind. Other possible mechanisms of process interaction exist and should be developed. Given this, it should be clear that the evidence Wickens offers against a single-resource model is not automatically evidence in favor of a multiple-resource model. The patterns of data he denominates argue against any single-factor account of dual-task interference effects. The conservative conclusion is that the data show that multi-task cost is multiply determined. The exact nature of the determinants is hardly constrained -- they could be resource-like or they might not be. Wickens(1984) was aware of this limitation when he noted that his theory might be empirically indistinguishable from Kahneman's 1973 theory which proposed a single pool of resources plus several additional specific sources of interference.

How does this conservative evaluation of the evidence bearing on the crucial issue relate to the practical problem of reducing multi-task cost? I think there are two

important conclusions to be drawn. The first is that if multi-task costs are multiply determined, then the problem is both complex as well as likely to produce benefits. The second is that the resource perspective should not be assumed when approaching this problem. In order to formulate design principles and guidelines all of the major causes of multi-task cost must be correctly identified. Some of the causes might be well described within a resource view, but others might not. The failure to discover these other causes because of a theoretical bias could prove disastrous to the project. How these conclusions might be implemented is briefly discussed in the next section.

VI. RECOMMENDATIONS:

My most fundamental recommendation is that the Air Force should sponsor a program of basic research focused on the issue of multi-task cost. Several justifications apply. First, the problem is serious and widespread. Second, reducing multi-task cost is possible. There are several studies in which concurrent performance shows very little multi-task cost, and there are many studies which show substantial costs. When a range of variation like this exists, there is the opportunity to move toward the desirable pole. Third, to devise design principles and

guidelines an appropriate data base is required. Although much relevant research has been conducted, it serves more to delineate what that data base should be like rather than actually being useful as a part of it. In order to extract the desired principles and "rules of thumb" from the data base, it must provide information of the right type. In this case, the right type of information is how well various components of task structure fit together. Relevant components of task structure need to be identified, and then these components need to be tested in multi-task environments to discover "what goes with what". It is important to recognize that no theoretical basis whatsoever need be assumed, and I recommend a strictly functional approach. The objective is to find out what to do and what to avoid rather than attempting to confirm or disprove any theory.

References

- Kahneman, D. (1973). Attention and effort, Englewood Cliffs, NJ: Prentice-Hall.
- Navon, D. (1985). Attention division or attention sharing? In Posner, M.I. and Marin, O.S.M. (Eds.), Attention and performance XI, Hillsdale, NJ: Lawrence Erlbaum Associates.
- Norman, T.A., & Bobrow, D.J. (1975). On data-limited and resource-limited processes. Cognitive Psychology, 7, 44-64.
- Wickens, C.D. (1980). The structure of attentional resources. In R. Nickerson (Ed.), Attention and performance VIII, Hillsdale, NJ: Lawrence Erlbaum Associates.
- Wickens, C.D. (1984). Processing resources in attention. In R. Parasuraman and D.R. Davies (Eds.), Varieties of Attention, Orlando, FL: Academic Press.

1985 USAF-UES Summer Faculty Research Program/

Graduate Student Summer Support Program

Sponsored by the

Air Force Office of Scientific Research

Conducted by the

Universal Energy Systems, Inc.

Final Report

Job/Task Difficulty and Job/Task Experience:

A Literature Review

Prepared by:	Dale Bracken Jr.
Academic Rank:	Summer Fellow
Department and	Department of Psychology
University:	University of Georgia
Research Location:	Air Force Human Resources Laboratory Brooks Air Force Base
USAF Researcher:	Lt. Col. Michael Dickinson
Date:	September 5, 1986.
Contract No.:	F49620-85-C-0013

Job/Task Difficulty and Job/Task Experience:

A Literature Review

by

Dale Bracken Jr.

ABSTRACT

Industrial/organizational as well as human factors literature conceptualizes job/task difficulty and job/task experience through a variety of definitions. It is necessary to organize the various definitions of job/task difficulty and job/task experience in order to better understand their impact on a study. This review examines the various concepts of job/task difficulty and job/task experience as literature has related them to measures of job/task performance. Job/task difficulty definitions were collapsed and categorized into a conceptual scheme of organization. Job/task difficulty measures were classified along two dimensions: Definitional referent which refers to whether job/task difficulty is defined in terms of characteristics intrinsic to the task or the performer; and measurement objectivity/subjectivity which is concerned with the extent of human judgment involved in the measurement of difficulty. Job/task difficulty as well as job/task experience literature finds the particular variables to affect performance in a variety of ways. Future research on difficulty and experience must employ psychometrically sound measures to examine the relation between difficulty, experience, and performance.

Aknowledgements

The author would like to thank the Air Force Office of Scientific Research and all those involved in the IDE Branch of the Air Force Human Resource Laboratory, Brooks Air Force Base, Texas for providing me the opportunity to further my education.

Special thanks to Dr. Charles E. Lance for his support and guidance throughout the summer.

I. Introduction

An ultimate goal of the Joint-Service Job Performance Measurement/Enlistment Standards Project is to link enlistment standards to measures of on-the-job performance. It has been suggested that measures of job/task difficulty and job/task experience may be utilized as surrogate job performance measures in place of other more expensive and time consuming methods. The purpose of this report is to examine how human factors and industrial/organizational literature has historically linked the issues of job/task difficulty and job/task experience to job/task performance.

II. Objectives of the Research Effort

Recent job performance measurement research has focused on social/cognitive information processes involved in performance rating (DiNisi, Cafferty, & Meglino, 1984). Research on the prediction of performance continues to focus upon human aptitudes (Waldman & Avolio, 1986). Rhodes (1983), Weeks (1984), Maier and Hiatt (1985), and Maier and Mayberry (1986), have discussed other factors, among them being job/task difficulty and job/task experience that may be crucial in: (a) determining the level of incumbent job performance; and (b) further defining the relationship between recruit aptitudes and job performance.

Occasional research has attempted to address the issues of job/task experience and job/task difficulty as they relate to performance; however, the definitions and conceptualizations of literature regarding job/task difficulty and job/task experience are varied. The primary goal of this literature review is to

present the variety of conceptualizations of job/task difficulty and job/task experience in a format that may clear some of the confusion and provide insight to the job/task difficulty-job/task experience relation to performance.

III. The Difficulty of Defining "Difficulty"

According to Locke, Shaw, Saari, and Lathem (1981) "A difficult task is one that is hard to do." (p. 126). Several other more precise definitions of job/task difficulty will be examined in this section. The plan is to: (a) review the various definitions of job/task difficulty; (b) provide a conceptual scheme for organizing these various representations; (c) review various theoretical predictions regarding the relation between job/task difficulty and job/task performance; (d) discuss job/task difficulty in the context of situational constraints that may have direct effects on employee performance and, in addition, may serve to moderate the relationships between aptitudes and job/task performance; and (e) review predictions concerning the potential moderating effects of job/task difficulty on the aptitude and performance relation.

III.1 Definitions of Job/Task Difficulty

Table 1 lists nine distinct conceptualizations of the nature and appropriate measurement of job/task difficulty found in this review of industrial/organizational and engineering psychological literature.

Insert Table 1 About Here

III.1.1 Normative job/task difficulty is defined in terms of the amount and relevant resources which are required for success at a task (Terborg, 1977). Normative task difficulty, therefore, is calculated as the proportion of individuals who are successful on a particular task. A larger proportion of individuals are successful on easier tasks. Relatively fewer individuals are successful at more difficult tasks.

III.1.2 Unanchored subjective ratings scales is a method of defining and measuring job/task difficulty that involves obtaining difficulty ratings from subject matter experts (SMEs). These subjective ratings range on a continuum from extremely easy to extremely difficult; however, these ratings do not allow generalizability of difficulty indices across studies (Ryan-Jones, 1979).

III.1.3 Manipulated primary and secondary task characteristics notions of job/task difficulty are most often found in human factors research. Thus, a researcher might adjust the difficulty level of a primary task by varying the complexity of required responses, or the number of responses necessary for a subject to achieve a pre-determined criterion of success. Cambell and Ilgen (1976), for example, manipulated the difficulty of various chess problems by varying the number of moves needed to achieve checkmate. In other studies, the difficulty of a primary task is manipulated by varying demands incurred by a secondary task. For example, Drory

(1985) introduced voice communication as a secondary task in conjunction with the primary task of operating a driving simulator. Decrements primary task performance measures such as steering wheel reversals, tracking, and brake reaction time indicated the extent of the difficulty manipulation. Note that a secondary task may also be used in a somewhat different context. Often, the secondary task is performed and measured concurrently with the primary task. Performance decrement on the secondary task is used to infer primary task difficulty (Wierwille, Rahimi, & Casali, 1985).

III.1.4 Ability requirements definitions of difficulty, (e.g. Fleishman, 1978) defined abilities as relatively enduring attributes of the individual performing the task. Fleishman (1978) maintained that the importance of various abilities increases as the difficulty of the task increases. That is, individual differences in ability play a relatively smaller role in determining performance on relatively easy tasks whereas with more difficult tasks, variance in task performance increases due to individual differences in abilities.

III.1.5 Job/Task Learning Difficulty. The U. S. Air Force has for some time been concerned with the relations between job/task difficulty and job/task performance. Mead & Christal (1970), Fugill (1973), Burtch, Lipscomb, and Wissman (1982), and Weeks (1984) have conceptualized job/task difficulty in terms of the average time required for a typical recruit to learn to perform a given task at an acceptable level of performance. At a higher level of aggregation, job learning difficulty indices have also been developed and are referred to as measures of the

average task difficulty per unit time (ATDPUT) (Burtch, et al., 1982).

III.1.6 Production Standards. Locke et al, (1981), distinguished between task difficulty and goal difficulty by proposing that task difficulty refers to the nature of the work to be accomplished while goal difficulty specifies a certain level of task proficiency against a standard. In a sense, task difficulty assumes a "quantity to be produced" posture whereas goal difficulty is referenced to performance intentions and some prior performance standard.

III.1.7 Perceived job complexity. Difficulty is sometimes defined in terms of literature relating to employee perceptions of job complexity. Although this literature has tended to focus on relations between employees' task perceptions and levels of satisfaction, occasional research has investigated relations between complexity and performance. Task difficulty in this sense is defined as the extent to which employees perceive their job to be characterized as high in Hackman and Oldham's (1976) core job dimensions (i.e., variety, autonomy etc.).

III.1.8 Self ratings of perceived workload are often obtained in human factors research (e.g., Moray, 1982). For example, perceived workloads of pilots have been measured on the Cooper (1957), and Cooper-Harper (1969) scales. These scales were developed to measure the handling characteristics of an aircraft. If a pilot chooses to say that the aircraft was difficult to fly, he is in effect stating that the task of flying imposes a very heavy workload.

III.1.9 Physiological Measures. Wierwille and Conner (1983), Wierwille, Rahimi, and Casali (1985), and others have investigated the relationship between various physiological indicators and manipulated task complexity. This approach assumes that pulse rate, pulse rate variability, respiration rate, pupil diameter, and voice pattern will covary with and indicate the actual difficulty of the primary task.

III.2 Classifications of Job/Task Difficulty

Approaches to defining and measuring job/task difficulty are diverse. We attempted to provide a conceptual scheme for organizing the many job/task difficulty concepts.

Insert Figure 1 About Here

Figure 1 represents a classification of the various job/task difficulty definitions along two dimensions: Definitional Referent and; Measurement Objectivity/Subjectivity. The Definitional Referent dimension concerns the question: for each approach to job/task difficulty, is difficulty defined in terms of characteristics intrinsic to the task itself or in terms of characteristics of the performer of the task? The Measurement Objectivity/Subjectivity dimension concerns the question: to what extent is human judgment involved in the measurement of difficulty?

The majority of the conceptualizations and measurements of job/task difficulty define difficulty in terms of characteristics

of the performer which are assessed objectively (quadrant I). Normative task difficulty is included here since it incorporates objective data describing the performance of individuals who might perform a given task. The ability requirements approach also focuses upon the performer and his/her characteristics as measured by standardized and objective tests. Performance on secondary tasks is also generally objectively measured (e.g. reaction time or tracking) and indicates the amount of attention that a person is able to devote to the primary task. Finally, physiological indicators of job/task difficulty are included in this cell because measures of individuals' biological responses usually involve little subjectivity.

Quadrant II includes objective measures of job/task difficulty defined in terms of characteristics intrinsic to the task. Primary and secondary task manipulation studies fall within this cell because experimental manipulations are generally defined quite explicitly as the job/task performance measures themselves. The goal setting literature speaks of job/task difficulty in terms of a "quantity to be produced" standard, thus this definition also falls into quadrant II.

Quadrant III includes definitions of job/task difficulty that lead to subjectively derived measures of characteristics intrinsic to the task. SME relative ratings is one example of task intrinsic difficulty measures obtained from the respondents' judgments. Field research on perceived job characteristics also involves subjective ratings of the complexity of incumbents' tasks. Still another definition that falls within quadrant III involves studies containing self ratings of perceived workload.

Again, individual's perceptions provide the basis for subjective ratings of the difficulty of the task. The Hackman & Oldham (1976) and Loher, Noe, Moeller, & Fitzgerald (1985) research on perceived job characteristics also involves measures of the person describing the "difficulty" of the task.

Finally, quadrant IV contains subjective ratings of characteristics intrinsic to the task performer(s). The notion of job/task learning difficulty is perhaps the most difficult to classify. There is certainly rationale for learning difficulty to be included within quadrant IV. Of all the conceptualizations of "job/task difficulty" identified in this literature review, the learning difficulty approach was the only one that opted to operationalize task difficulty in terms of subjectively derived measures (subject matter expert ratings) and in terms of characteristics intrinsic to the task performers (time for the typical subject to learn to perform a task to an acceptable performance level, Weeks, 1984). Still, there exists an equally strong rationale for the inclusion of learning difficulty within quadrant III (task/subjective). Learning difficulty is often viewed as the military assuming one person whose performance will vary directly as a function of the task difficulty itself. This notion of learning difficulty is represented through the work of Mead & Christal (1970), and Fugill (1973).

Our conceptual schema for organizing the various notions of job/task difficulty clears some of the confusion; however, it is important to understand that some of the quadrants of figure 2 may still be considered somewhat heterogeneous.

III.3 Relations Between Job/Task Difficulty and Performance

Along with the variety of job/task difficulty definitions exists a variety of theoretical rationale for the relations between job/task difficulty and job/task performance. Observed correlations between job/task difficulty and job/task performance are inconsistent across studies but relationships predicted often vary as a function of the definition of job/task difficulty chosen by the particular study.

Rationale for a positive relation between job/task difficulty and job/task performance have been offered (Sales, 1970, and McGinn, Day, & Burke, 1984). Sales (1970) contended that people translate work into goals. If workers are presented with higher work levels, these are translated into goals that call for more work to be completed thus, task difficulty may be positively related to performance under a "quantity produced" conceptualization of task difficulty. McGinn et al. (1976) tested Sales' hypothesis by examining over a dozen distributions of goal setting effects. The results reinforced the notion of a positive linear relationship between setting specific difficult goals and task performance.

Many studies find a negative relationship between job/task difficulty and job/task performance. Rationale for such a negative relationship has been offered by many including: Casali & Wierwille (1983), Drory (1985), Hagman & Rose (1983), McGrath (1976), and Weeks (1984). Weeks (1984), for example, contended that the most difficult specialties in the armed services should have the highest aptitude requirement

minima. Weeks (1984) assumes a strong positive relation between aptitude and performance such that as a job or task difficulty level increases, performance should decrease for all recruits of comparable aptitude levels.

Hagman and Rose (1983) examined the effect of task repetition on retention and performance. The underlying hypothesis of the study was that the more difficult tasks would result in relatively decreased performance. Performance errors did decrease, however, through task repetition.

Human factors research also hypothesizes a negative relation between job/task difficulty and job/task performance. Casali and Wierwille (1983) found that difficulty (manipulated through increased workload of a secondary communications task) led to a significant performance decrement on a tracking task. Also, Drory (1985) made a communications task more difficult by adding a secondary vigilance task and performance suffered with increased levels of difficulty.

Finally, McGrath's work in the area of job stress suggests an inverse relation between difficulty and performance (McGrath 1976). McGrath defined task difficulty as the extent to which requirements of a task fall below, meet, or exceed the performance of the person. He proposed a negative monotonic relationship between task difficulty (that is, all other things being equal, the more difficult the task, the poorer the performance).

Still others have hypothesized that a curvilinear or "inverted U" relationship exists between job/task difficulty and job/task performance. Wiener, Curry, & Faustina (1984) argued

that for any task there is an optimal workload level that yields the highest level of performance. Any increase or decrease in the "optimal level" of task demand will result in a performance decline. McGrath (1976) explained the "inverted U" hypothesis by including stress, task difficulty, and performance as follows: Task difficulty bears a negative monotonic relationship with performance. Arousal, on the other hand, is shown to bear a positive relation with performance. Performance is highest at moderate levels of both task difficulty and arousal. On extremely difficult tasks, performance is depressed by task difficulty (McGrath, 1976). On extremely easy tasks, arousal plays the major role in task performance. Figure 2 shows this hypothesized relationship.

Insert Figure 2 About Here

Relations observed between job/task difficulty and job/task performance have ranged from positive to negative with no clear trend apparent. The association is further complicated by the presence of extraneous variables which may be responsible for the varied conclusions arrived at by literature concerning difficulty and performance. Some extraneous variables have been referred to as situational constraints.

III.4 Situational Constraints

Many have argued that, as one situational influence upon behavior, job/task difficulty exerts direct effects on job/task performance. Most have agreed that the relationship is inverse.

Peters and O'Conner (1980), and Terborg, Richardson and Pritchard (1980) have considered the effects of other situational variables on performance in the context of situational constraints. These constraints include job related information, tools and materials, budgetary support, time availability, and work environment. A general proposition is that changes in the severity of situational constraints will result in changes in performance.

Two general themes in the situational constraint literature seem equally applicable to the literature relating to job/task difficulty: (a) environmental variables, in conjunction with ability, can affect employee performance; and (b) situational variables may moderate relationships between aptitude and performance (Sohnieder, 1978).

III.5 Interactive Effects

Interactive effects have been suggested between aptitude, job/task difficulty and performance. Maier and Hiatt (1985), for instance, suggested that the relations between aptitudes and performance may vary as a function of occupation. Occupations may, in turn, be rank ordered by occupational difficulty. Schmidt, Hunter, and Pearlman (1981) examine the moderating effects of job/task differences upon relations between abilities and performance in the interest of demonstrating validity generalization. However, mean differences were found in validity coefficients across occupational groups and these differences were quite reliable. Though occupational difficulty was not explicitly indexed, differential job requirements (e.g., information

processing) may imply differences in job difficulty.

In accordance, Terborg (1977) also suggested a moderate level of task difficulty is optimal for differentiating abilities when performance is the dependent criterion. Very hard tasks as well as very simple tasks were shown to be of little value in obtaining differentiation of abilities.

In conclusion, literature relating to job/task difficulty is characterized by a diverse array of conceptualizations. Observed relations between job/task difficulty and job/task performance range from positive to negative with arguments for the possibility of curvilinear relations. Situational variables have been suggested as moderating relationships between aptitude and performance. Finally, it has been proposed that job/task differences, including differences in difficulty, may moderate relations between abilities and performance.

IV Experience

Literature relating to job/task experience contains an interesting mixture of theories and concepts. Measures taken as indicators of job/task experience are varied and include such variables as age, job tenure, years of service to an organization, years in career, and number of times a task has been performed. Five general themes emerge from the job/task experience literature: (a) the effects of age on performance; (b) economic issues; (c) changes in relations between performance and job related abilities and skills over time; (d) the presumed relationship between job/task experience and job/task

performance; and (e) interactions between job/task experience and job/task difficulty in determining performance.

IV.1 Age and Performance

Age/performance relations are not well understood but do relate peripherally to this review. Rhodes (1983) provided a comprehensive review of relations between age and performance and concluded that existing results are mixed. Schwab and Heneman (1978) suggested that age stereotypes may not have as strong an impact upon performance changes as has been previously reported and Waldman and Avolio (1986) suggested that the type of performance measure used may be responsible for some of the inconsistent results. Waldman and Avolio (1986) showed that performance declined with age in the eyes of the employees' supervisors but this decline was less evident when objective performance reports were used.

IV.2 Economic Issues

A number of studies in the economics literature have correlated experience and salary. In efforts to determine the relation between experience and productivity, Marcus and Quester (1985) pointed out that this earnings slope is too often used as the dependent variable in lieu of a more tangible output measure. Maranto and Rodgers (1984), and Medoff and Abraham (1981) note the requisite assumption that more experienced workers are highly paid because they are more productive. Some studies in the economics literature have, however, related experience measuring to direct measures of performance. These

studies will be discussed in section IV.4.

IV.3 Temporal Changes in Abilities

Temporal change in abilities is another theme seen in the job/task experience literature. Fleishman (1972), for instance, presented what has come to be known as a "changing-task" model. This model proposes that abilities which contribute to performance change over time. Earlier, Corballis (1965) introduced a concept known as the "changing subject" model. The changing-subject model assumes that practice on the criterion task systematically and significantly affects the ability levels of the subjects. The changing-subject model contends that individual differences in skill learning can be measured at all stages of practice. Perhaps the most important difference between the changing-subject model and the changing-task model lies in the fact that the changing-task model is able to be examined through factor analysis. The changing-subject model is historically examined through regression procedures. Long term implications of combining the two models are discussed by Dunham (1974). The complex changing-subject changing-task model is the logical combination of the previous models and employs concepts of ability change from both the changing task and the changing subject models and is characterized by maximum prediction ability. This is the only model that is capable of predicting changes in abilities from initial performance to late performance. Currently, many training programs are reviewed and their tasks restructured as a result of the examination of

findings directly attributable to the implimentation of the changing-subject changing-task model.

IV.4 The Effects of Experience on Performance

Proposed relations between job/task exeprience and job/task performance range from positive to negative to arguments for curvilinear relations. These results are further complicated by research that suggests little, if any, association between experience and performance.

Early research cited skill level as an another factor that, along with experience, influenced measures of job success. Jay and Copes (1957) measured experience as the number of months on a job and found a small positive average correlation between experience and job proficiency. Employee skill level however, had a stronger affect on performance than did experience.

Stewart and Sparks (1966) suggested that the proficiency of chemists increased with years of work. They showed that the patents issued per man-year, increased significantly with an increases in years of service as a chemist. Giniger, Dispenzieri, and Eisenberg (1983) analyzed the relation between experience and performance of factory employees while holding age constant and found significant partial correlations between experience and performance for both speed and skill jobs. Hunter and Hunter (1984) conducted a meta-analysis using age, education, and experience as the predictor variables with training and proficiency measures as the criterion variables. Estimates of correlations between experience measures and

measures of training success and overall proficiency were small and positive (.18 and .15 respectively). Maier and Hiatt (1985) also found a positive relationship was found between experience and performance. Scores on a written performance test tended to increase uniformly with experience.

Other studies suggest a negative relationship between job/task experience and job/task performance. Medoff and Abraham (1980) cautioned that, although there seems to be a positive relation between experience and earnings, there is either zero or a negative relation between work experience and relative rated performance. Tiffin (1947) suggest two possible reasons for a negative relation between job experience and performance: (a) the more capable employees historically transfer out of the job or are promoted; and (b) employees with long tenure may actually be less competent than the younger employees with less tenure.

Mathews and Cobb (1974) argue for a curvilinear relation between job/task experience and job/task performance suggesting that performance increases with experience up to five years of experience on the job and five years of job experience yields the highest positive correlation with performance among air traffic controllers. Inversely, controllers with over fifteen years of experience show a decrement in performance.

Spiker, Harper, and Hayes (1985) also found a curvilinear association between job experience and job performance. Spiker et al. (1985) operationalized experience as the number of times a task had been performed. Performance of automotive mechanics was shown to improve markedly as an optimal point of

experience was approached. The proficiency range peaked and declined gradually as the mechanics' experience increased past the "optimal point". Research that suggests a performance decline with a great amount of experience often cites such variables as lack of motivation, carelessness, and false confidence as factors responsible for the measures of decreased proficiency.

Katz (1978) examined an implicit assumption to the curvilinear relation between job/task experience and job/task performance. Katz proposed three stages of job longevity: (a) a Learning Stage characterized by the individual becoming preoccupied with learning the tasks and exhibiting behaviors and attitudes that are expected in the new setting; (b) a Responsive Stage in which employee satisfaction is most associated with job dimensions that would yield top proficiency and performance. The implicit inference is that high satisfaction should yield top performance; and (c) an Unresponsive Stage during which a career begins to "wind down" and the job is no longer satisfying. Katz' model thus predicts an increase in performance early in one's career followed by a gradual decline.

Finally, there are a number of studies that find no significant relationship between experience and performance. Cobb (1968) measured experience by the length of service of air traffic controllers and concluded that: (a) experience (independent of age) tended to exhibit negligible relations with performance; and (b) age and experience do not interact to determine performance. Taylor and Vineberg's (1973) work with the U.S. Army utility testing project led them to

conclude that, with respect to experience, mean job sample scores for "inexperience actives" (those who remained in the army after testing and were initially considered more experienced at their jobs) did not differ significantly from the scores for "inexperience separates" (those who left the army after completion of the utility testing project). The U.S. Army utility testing project provided little evidence in the way of any clear relationship between job/task experience and job/task performance.

Maier and Mayberry (1986) performed a feasibility study to analyze the effects of job/task experience (time in service) on job performance. Performance was expected to increase with time in service. They found however, that hands-on test scores increased only modestly, and many times not at all, during the first term of enlistment.

Job/task experience literature has indicated positive, negative and curvilinear relations with job/task performance. One reason for the diverse findings is represented by the definitions of job/task experience and the measures of performance that the researcher chooses to incorporate in the study. More specifically, any research concerning job/task experience must initially examine the overall rationale for why and how experience should have any effect on performance.

Secondly, if job/task experience is considered to be a possible measure of performance, the researcher must clarify what is meant by "experience" (i.e., tenure, time in a particular field, the number of times a task is performed etc.) and why the

particular definition of experience was chosen for the study.

Finally, there seems to be a reliable notion throughout industrial/organizational and human factors literature that experience is something more than the amount of time spent in one place. In accordance with this notion, the Air Force must develop meaningful and psychometrically sound measures of experience to replace the currently utilized but empty demographics of time spent on a given task. It would be well advised for any Air Force research concerning job/task experience to further examine the various conceptualizations of job/task experience provided by the literature and to choose the measure of experience that would seem to be the most reliable surrogate measure of job/task performance.

results lies in the fact that experience research, on the whole, is sparse and fragmented. Perhaps clear trends of the relation between job/task experience and job/task performance will result as work on job/task experience measures and performance measures proliferates.

V. Recommendations

Job/task difficulty and job/task experience literature must be further reviewed to determine the feasibility of difficulty and experience as surrogate measures of job/task performance in the armed services. Currently, research regarding job/task difficulty and job/task experience remains fragmented. Presumably, clear trends concerning the relation of job/task difficulty and job/task experience will arise as research

proliferates. Perhaps, analysis of these trends can aid the armed services in developing a more reliable, less expensive, and less time consuming measure of job/task performance that can be used in conjunction with the Walk Through Performance Testing.

References

- Burtch, L.D., Lipscomb, D.J., & Wissman, D.J. (1982). Aptitude requirements based on task difficulty: Methodology for evaluation (AFHRL-TR-81-34). Brooks Air Force Base, Texas: Manpower and Personnel Division, Air force Human Resources Laboratory, January 1982.
- Campbell, D.J., & Ilgen, D.R. (1976). Additive effects of task difficulty and goal setting on subsequent task performance. Journal of Applied Psychology, 61, 319-324.
- Casali, J.G., & Wierwille, W.W. (1983). A comparison of rating scale, secondary-task, physiological, and primary-task workload estimation techniques in a simulated flight task emphasizing communications load. Human Factors, 25, 623-641.
- Cobb, B.B. (1968). Relationships among chronological age, length of experience, and job performance ratings of air route traffic control specialists. Aerospace Medicine, 39, 119-124.
- Cooper, G.E. (1957). Understanding and interpreting pilot opinion. Aeronautical Engineering Review, 16, 47-52.
- Cooper, G.E., & Harper, R.P. (1969). The use of pilot ratings in the evaluation of aircraft handling characteristics. Washington, DC; NASA, Report No. TN-D-5153.
- DeNisi, A.S., Cafferty, T.P., & Meglino, B.M. (1984). A cognitive view of the performance appraisal process: A model and research propositions. Organizational Behavior and Human Performance, 33, 360-396.

- Drory, A. (1985). Effects of rest and secondary task on simulated truck-driving task performance. Human Factors, 25, 201-207.
- Dunham, R.B. (1974). Ability-skill relationships: An empirical explanation of change over time. Organizational Behavior and Human Performance, 12, 372-382.
- Fleishman, E.A. (1972). On the relation between abilities, learning, and human performance. American Psychologist, 27, 1017-1032.
- Fleishman, E.A. (1978). Relating individual differences to the dimensions of human tasks. Ergonomics, 21, 1007-1019.
- Fugill, J.W.K. (1973). Task difficulty and task aptitude benchmark scale for the administrative and general career fields (AFHRL-TR-73-13). Lackland Air Force Base, Texas: Personnel Research Division, Air Force Human Resources Laboratory, October 1973.
- Giniger, S., Dispenzieri, A., & Eisenberg J. (1983). Age, experience, and performance on speed and skill jobs in an applied setting. Journal of Applied Psychology, 68, 469-475.
- Hackman, J.R., & Oldham, G.R. (1976). Motivation through the design of work: Test of theory. Organizational Behavior and Human Performance, 16, 250-279.
- Hagman, J.D., & Rose, A.M. (1983). Retention of military tasks: A review. Human Factors, 25, 199-213.
- Hunter, J.E., & Hunter R.F. (1984). Validity and utility of alternative predictors of job performance. Psychological Bulletin, 96, 72-98.
- Jay, R., & Copes, J. (1957). Seniority and criterion measures

- of job proficiency. Journal of Applied Psychology,
41, 58-60.
- Katz, R. (1978). The influence of job longevity on employee reactions to task characteristics. Human Relations, 31, 703-725.
- Kemp, N.J., & Cook, J.D. (1983). Job longevity and growth need strength as joint moderators of the task design-job satisfaction relationship. Human Relations, 36, 883-898.
- Kozlowski, S.W.J., & Hults, B.M. (1986). Joint moderation of the relation between task complexity and job performance for engineers. Journal of Applied Psychology, 71, 196-202.
- Locke, E.A., Shaw, K.N., Saari, L.M., & Latham, G.P. (1981). Goal setting and task performance: 1969-1980. Psychological Bulletin, 90, 125-152.
- Loher, B.T., Noe, R.A., Moeller, N.L., & Fitzgerald, M.P. (1985). A meta-analysis of the relation of job characteristics to job satisfaction. Journal of Applied Psychology, 70, 280-289.
- Maier, M.H., & Hiatt, C.M. (1985). On the content and measurement validity of the hands-on job performance tests (CRM 85-79). Alexandria, VA: Marine Corps Operations Analysis Group; Center for Naval Analysis, August 1985.
- Maier, M.H., & Mayberry, P.W. (1986). Improving the design of the marine corps job performance measurement project. Program for 10th Psychology in the DOD Symposium, April 1986.
- Marcus, A.J., & Quester, A.O. (1985). Factors in the productivity of military personnel. Monthly Labor Review, 108, 33-35.

- Maranto, C.L., & Rodgers, R.C. (1984). Does work experience increase productivity? A test of the on-the-job training hypothesis. Journal of Human Resources, 16, 341-357.
- Mathews, J.J., & Cobb, B.B. (1974). Relationships between age, ATC experience, and job ratings of terminal air traffic controllers. Aerospace Medicine, January 1974, 56-60.
- Mead, D.F., & Christal, R.E. (1970). Development of a constant standard weight equation for evaluating job difficulty AFHRL-TR-70-44. Lackland AFB TX: Personnel Division, Air Force Human Resources Laboratory, November.
- Medoff, J.L., & Abraham, K.G. (1981). Are those paid more really more productive? The case of experience. Journal of Human Resources, 15, 186-216.
- Medoff, J.L., & Abraham, K.G. (1980). Experience, performance, and earnings. Quarterly Journal of Economics, 95, 734-736.
- Moray, N. (1982). Subjective mental workload. Human Factors, 24 25-40.
- Peters, L.H., & O'Connor, E.J. (1980). Situational constraints and work outcomes: The influences of a frequently overlooked construct. Academy of Management Review, 5, 391-397.
- Rhodes, S.R. (1983). Age related differences in work attitudes and behavior: A review of conceptual analyses. Psychological Bulletin, 73, 328-367.
- Ryan-Jones, D.L. (1979). A comparison of expert ratings of task difficulty with an independent criterion TR-418. Alexandria, VA: U.S. Army Research Institute for the Behavioral and Social Sciences, November.

- Schneider, B. (1978). Person-situation selection: A review of some ability-situation interaction research. Personnel Psychology, 31, 281-297.
- Schwab, D.P., & Heneman, H.G. (1978). Age stereotyping in performance appraisal. Journal of Applied Psychology, 63, 573-578.
- Spiker, V.A., Harper, W.R., & Hayes, J.F. (1985). The effect of job experience on the maintenance proficiency of army automotive mechanics. Human Factors, 27, 301-311.
- Stewart, N., & Sparks, W.J. (1966). Productivity of research chemists as related to age and experience. Personnel and Guidance Journal, 45, 28-35.
- Taylor, E.N., & Vineberg, R. (1973). Role of selection and growth in performance of experienced men: Some evidence from a study of four army jobs (TR 73-4). Alexandria, VA: Human Resources Research Organization, February 1973.
- Terborg, J.R. (1977). Validation and extension of an individual differences model of work performance. Organizational Behavior and Human Performance, 18, 188-216.
- Terborg, J.R., Richardson, P., & Pritchard, R.D. (1980). Person-situation effects in the prediction of performance: An investigation of ability, self esteem, and reward contingencies. Journal of Applied Psychology, 65, 574-583.
- Tiffen, J. (1947). Industrial Psychology. New York, New York: Prentice-Hall, Inc., rev. ed., 1947.
- Waldman, D.A., & Avolio, B.J. (1986). A meta analysis of age differences in job performance. Journal of Applied Psychology,

71, 33-38.

Weeks, J. (1984). Occupational learning difficulty: A standard for determining the order for aptitude requirement minimums (AFHRL-SR-84-26). Brooks Air Force Base, Texas: Manpower and Personnel Division, Air Force Human Resource Laboratory, November 1984.

Wiener, E.L., Curry, R.E., & Faustina, M.L. (1984). Vigilance and task load: In search of the inverted U. Human Factors, 26, 215-222.

Wierwille, W.W., & Connor, S.A. (1983). Evaluation of 20 workload measures using a psychomotor task in a moving-base aircraft simulator. Human Factors, 25, 1-16.

Wierwille, W.W., Rahimi, M., & Casali, J.G. (1985). Evaluation of 16 measures of mental workload using a simulated flight task emphasizing mediational activity. Human Factors, 27, 489-502.

TABLE I

Definitions of Difficulty

1. Normative Job/Task Difficulty (Terborg, 1977)
2. Unanchored Subjective Ratings Scales (Ryan-Jones, 1979)
3. Manipulation of Primary and Secondary Tasks (Campbell and Ilgen (1976), Drory (1985)
4. Ability Requirements (Fleishman, 1978)
5. Learning Difficulty (Fugill, 1973, Burtch, Lipscomb, and Wissman, 1982, and Weeks, 1984)
6. Task Difficulty vs Goal Difficulty (Locke et al, 1981)
7. Job/Scope Complexity (Hackman and Oldham, 1976)
8. Self Ratings of Percieved Workload (Moray, 1982)
9. Physiological Indicators (Wierwille and Conner, 1983, and Wierwille, Rahimi, and Casali, 1985)

FIGURE 1

DIFFICULTY CHARACTERISTICS INTRINSIC TO THE:

	<u>PERFORMER</u>	<u>TASK</u>
<u>OBJECTIVE MEASURES</u>	(Quadrant I) Normative Job/Task Difficulty Ability Requirements Physiological Indicators Secondary Task Performance	(Quadrant II) Production Standards Primary Task Manipulation Secondary Task Manipulation
<u>SUBJECTIVE MEASURES</u>	(Quadrant IV) Learning Difficulty*	(Quadrant III) Unanchored Subjective Ratings Scales Job/Scope Complexity Self Ratings Of Perceived Workload

FIGURE 1 CLASSIFICATION OF JOB/TASK DIFFICULTY DEFINITIONS
ALONG TWO DIMENSIONS: DEFINITIONAL REFERENT, AND
MEASUREMENT OBJECTIVITY/SUBJECTIVITY

*
See text for explanation of ambiguity inherent in Learning
Difficulty

FIGURE 2

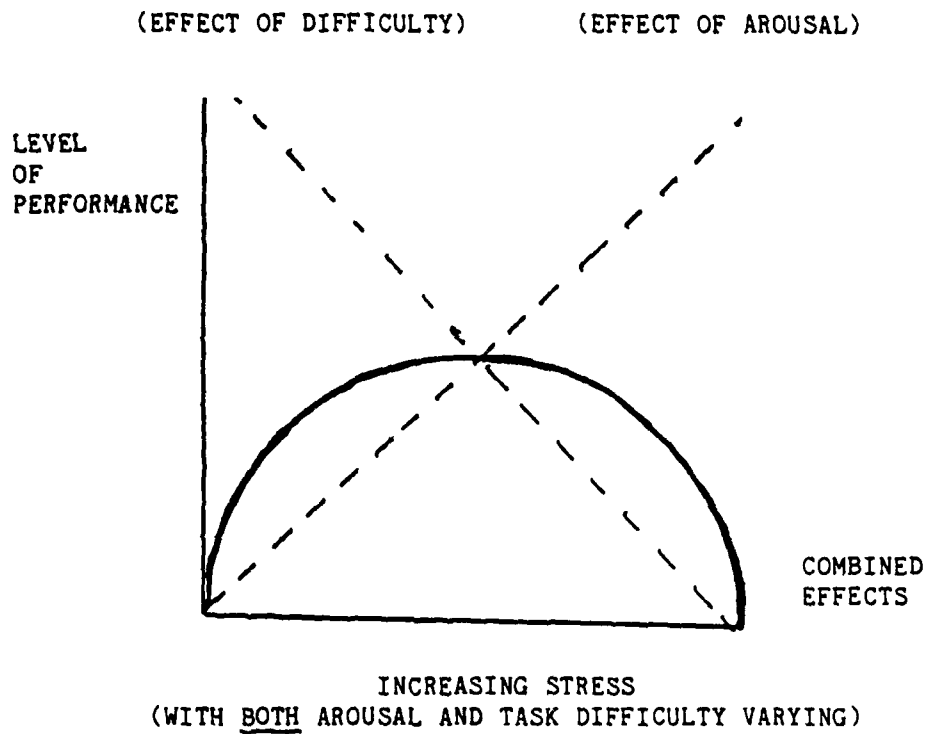


FIGURE 2 DIAGRAM OF THE INVERTED U RELATION AS A HYPOTHETICAL FUNCTION OF TASK DIFFICULTY AND AROUSAL (MCGRATH, 1976)

1986 USAF-UES SUMMER FACULTY RESEARCH PROGRAM/

GRADUATE STUDENT SUMMER SUPPORT PROGRAM

Sponsored by the
AIR FORCE OFFICE OF SCIENTIFIC RESEARCH
Conducted by
Universal Energy Systems, Inc.

FINAL REPORT

CHLAMYDOMONAS PHOTOTAXIS AS A SIMPLE SYSTEM
FOR TESTING THE EFFECT OF DRUGS ON VISION

Prepared by: Angela M. Braun
Academic Rank: Bachelor of Arts, Biology
Department: Biology Department
University: Trinity University

Research Location: Opthamology Branch,
Clinical Sciences Division
School of Aerospace Medicine
Brooks Air Force Base, Texas 78235-5301

USAF Researcher: Dr. John Taboada

Date: September 15, 1986

Contract No. F49620-85-C-0013

CHLAMYDOMONAS PHOTOTAXIS AS A SIMPLE SYSTEM FOR
TESTING THE EFFECT OF DRUGS ON VISION

by

Angela M. Braun

ABSTRACT

The major goal of this program is to develop, refine, and characterize the phototaxis system in Chlamydomonas reinhardtii and then employ it in the goal of finding and quantifying the effect of drugs which may enhance dark or color vision in pilots. A major problem associated with the testing of drugs which may affect vision in animals or man is that the drugs may affect more than one tissue, organ, or organ system. The advantage of first testing the effect of the drugs on the ability of a phototactic alga such as Chlamydomonas to swim toward the light is the inherent simplicity of the system in which the investigator can control the variables. Chlamydomonas is a simple, single-celled alga whose phototaxis apparatus biochemically mimics the fundamental vision system of man.

Major emphasis of our research team, Ms. Angela Braun, Dr. Taboada and Dr. Moyer has been the simplification of the procedure for producing phototactic cells and improve the method for measuring phototaxis. Eight Strains of Chlamydomonas reinhardtii were placed under phototaxis-inducing conditions and the growth and phototactic ability of the strains compared in different phases of their growth curves. Various means of measuring phototaxis were investigated. We were successful in simplifying and shortening the procedure for developing phototactic cells and in developing a simple and rapid method for quantifying the phototactic ability of algal cells to any wavelength of light between 400 and 700 nanometers.

Because of the large amount of data generated and the size limitation of the final report, the final reports of Ms. Braun and Dr. Moyer have been cooperatively blended to provide enough space to include all of the figures and legends.

ACKNOWLEDGEMENT

I would like to thank the Air Force Systems Command, the Air Force office of Scientific Research, and Universal Energy Systems for providing me the opportunity to participate in a valuable research experience at the Clinical Sciences Division, School of Aerospace Medicine, Brooks Air Force Base, Texas. My thanks are particularly directed to Dr. John Taboada and Sergeant Mario Villanea of the Laser Spectroscopy Clinical Application Laboratory and Robotic Vision Laboratory Ophthalmology Branch for their help and for making my brief stay very pleasant as well as informative and productive.

My thanks also to Capt. Paul Barnicott, and Sgt. Raul Canales, Flight Medicine Branch, Clinical Sciences Division, Brooks AFB for their permission and aid in the use of their model ZBI Coulter Counter and Diluter. I also wish to thank Ms. Bonnie Fridley for aid in the use of the Aerospace Library and Mr. Joe Franzello (Aeromedical Library) for performing a computer search on phototaxis in algae.

My special thanks to Dr. Rex Moyer, UFOSR-UES summer faculty research collaborator for his direction and support in this research endeavor. My thanks also to Trinity University personnel, Ms. Peggy Henry, Administrative Secretary for Dr. William Stone in the Biology Department for typing, to Mr. Jesse Villalobos, Biology Department, for purchase of chemicals and equipment and for helping to set up algae culturing apparatus, to Mr. Tom Nixon, physical plant, for set-up of lighted incubators and environmental chambers, to Ms. Sophia Wu, Thorman Laboratory, for other technical assistance, and to Ms. Beth Burgener, Biology Department, for washing glassware. My thanks to Dr. Tom Koppenheffer, Chair of the Biology Department and Dr. Ed Roy, Dean of the Division Science, Mathematics and Engineering for their continuing support of my research.

My personal thanks to Dr. John Taboada, Clinical Science Division, Brooks AFB, for being an excellent research collaborator.

I. INTRODUCTION

I graduated from Trinity University in May of 1986, with a Bachelor of Arts degree in Biology. During the one and one half years of my undergraduate work, I gained useful research experience working under the direction of Dr. William H. Stone in his immunogenetics laboratory at Trinity. Although my training previous to this program did not involve the field of microbiology, I believe my research experience will be useful in the technical aspect of this research effort. My lack of knowledge in the area of microbiology will be compensated by my research collaborator, Dr. Rex Moyer, a microbiologist who initiated this research project in 1985 during his AFOSR-UES summer faculty fellowship.

II. OBJECTIVES OF THE RESEARCH EFFORT

The major goal of this 1986 Summer Fellowship is to develop phototaxis in Chlamydomonas reinhardtii algae in order to find and quantify the effect of drugs which may enhance dark or color vision in man.

The overall research plan has three component phases:

Phase I. Establish Phototaxis System using Chlamydomonas reinhardtii.

Phase II. Refine and Characterize the Phototaxis System; Isolate a Collection of Phototaxis Mutants.

Phase III. Testing the Effect of Drugs on Phototaxis in Chlamydomonas reinhardtii.

Phase I was completed during Dr. Moyer's 1985 Summer Faculty Research Fellowship. Phase III is to be accomplished in the future and Phase II is my goal for my 1986 Fellowship and Dr. Moyer's 1985 Mini-grant. Phase II had four goals: (1) Simplify the procedure for producing phototactic cells; (2) Develop methods for the synchronization of the growth of Chlamydomonas; (3) Improve the laser doppler method for measuring phototaxis; and (4) Isolation of temperature-sensitive phototaxis mutants.

III. MATERIALS AND METHODS

See Dr. R.C. Moyer's report.

IV. RESULTS: (Continuation from Dr. Moyer's report)

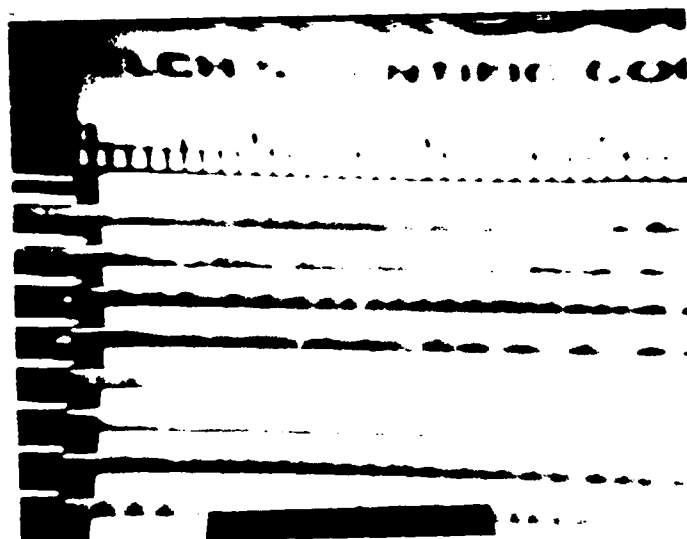
C. Techniques for assessing phototaxis.

As described in Materials and Methods, five different techniques have been tried to measure the phototaxis of the algal cells.

Only two of these were studied in any detail because they immediately showed some promise: the diffraction grating method and the spectrophotometer method.

1. Diffraction Grating method.

The 100 μ l capillaries were filled with an algal suspension and were placed on a stable, vibration-free surface. The visible spectrum illuminated the complete capillary. Within six minutes the algae began to form alternating bands of dense algal suspension separated by areas virtually devoid of cells. The poloroid photograph shown below shows this banding.



- 1102 - banding
- 1101 - no banding, graining
- 1010 - banding
- 1009 - banding
- 656 - minimal banding
- 654 - no bands
- 125 - banding
- 124 - banding

Strains 654 and 1101 did not produce bands under these conditions but all the other strains did. Initially we suspected that the banding was a response to specific wavelengths of light. This was subsequently disproved by rotating the platform securing the capillaries by 90° so that a capillary was illuminated with narrow wavelength band rather than the complete spectrum. Under these conditions, the bands form also. We also illuminated the capillaries at a 45° angle with respect to the light. Bands also formed under these conditions. The banding of the algal cells, although likely to be phototaxis related, was not wavelength-specific. Therefore, this technic was abandoned in favor of the

spectrophotometer method in which the wavelength of light the cells were exposed to could be accurately regulated.

2. Spectrophotometer method.

As indicated in Materials and Methods, the Spectrophotometer turned out to be the most useful method of quantifying phototaxis. Although this technique was finally adopted late in the summer, it did provide a rapid and simple way of comparing the phototactic ability of the different algal strains and also of comparing the phototaxis of the algal cells under different conditions of growth.

D. Algal Phototaxis.

Algal phototaxis was measured by placing the side-arm containing the cells of the culture flask into the light path and taking an initial reading. Then, without disturbing the flask or changing the wavelength setting, turbidity readings were taken at 30 second intervals for 3 or 4 minutes. If the culture was phototactic, it would steadily increase in turbidity for 3 or 4 minutes as the algal cells crowded into the light path. Such an experiment is shown in Fig. 6 (See Dr. Moyer's report for Figs. 1-5). Strain 1009 was grown in a liquid shake culture in HSA broth for 24 hours. An assay was run at 25 nm intervals between 400 and 700 nm. Each assay was run for 3 minutes. The culture was mixed between each phototactic assay. The Δ O.D. was the difference between the initial OD and the maximum OD recorded after 3 minutes of exposure to light at the given wavelength. The initial OD varied with the wavelength selected from a high at 400 nm (O.D.₄₀₀ = 1.05) to a low of below 0.5 for wavelengths of 550, 575, 600, and 700 nm. The wavelengths that stimulated the greatest phototactic response in strain 1009 were 475 nm with a Δ O.D. of 0.50 and 675 nm with a Δ O.D. of 0.483. Because the same culture would yield different initial O.D.'s for the various wavelengths, we normalized the data by obtaining the ratio between maximum O.D. at a given wavelength after the cells have phototaxed for 3 (or 4) minutes, and the initial O.D. at that same wavelength before the cells have begun to phototax. We have expressed this ratio as OD max/OD int. This is shown in Fig. 7 and more clearly shows the wavelengths

stimulating the greatest phototactic response, 475 and 675 nm. The OD max/OD int method of plotting the phototactic activity of the algae to various wavelengths of light clearly normalizes the curves by relating all of the initial O.D. values to 1.0. However, the question of whether all the *C. reinhardtii* strains behaved the same or whether initial turbidity which reflects population density influences phototaxis remained unknown. To answer these questions, a phototaxis action spectrum of 4 algal strains was performed: 124, 125, 1009, and 1010. To test if initial turbidity influenced the action spectrum, strain 125 was tested at two initial OD₆₀₀ readings; OD₆₀₀ = 0.63 and OD₆₀₀ = 0.48. The data were obtained as described in Figs. 6 and 7 but are not shown. The cultures were 24 hour liquid shake cultures. Fig. 8 shows the phototactic action spectra for these strains for the wavelengths between 400 and 700 nm. In Fig. 8, the phototaxis is expressed as Δ OD. In Fig. 9, phototaxis is expressed as OD max/OD int. Both figures clearly show a significant difference in wavelengths stimulating phototaxis between the strains tested. When the Δ OD method of quantifying phototaxis is used to compare the two different concentrations of strain 125, one sees very little difference. However, when phototaxis is expressed as OD max/OD int, differences between the strains as well as the between different concentrations of strain 125, are magnified. Under these two methods of expressing phototaxis, the maxima vary in some cases as shown below.

WAVELENGTH/MAXIMA OF PHOTOTAXIS OF STRAINS 124, 125, 1009 and 1010
EXPRESSING PHOTOTAXIS BY Δ OD AND BY OD MAX/OD INT.

STRAIN	Δ OD		OD max/OD int	
	Maxima(nm)		Maxima (nm)	
124	475	675	475	700
125 OD ₆₀₀ =0.63	400-500?	650	500	600
125 OD ₆₀₀ =0.48	450	650-675?	475	675
1009	475	675	475	675
1010	425	650	450-500?	650-700?

Under the conditions of this experiment, strain 124 showed distinct bimodal phototaxis maxima at 475-500 nm and 675-700 nm whereas the other strains showed a rather broad phototactic response to all the wavelengths. The maxima recorded above were not pronounced. The phototaxis action spectra of the two different dilutions of strain 125 suggested that phototaxis was greater in the more dilute culture. Additional studies need to be done with this system.

Fig. 10 shows the comparison of the two ways of expressing phototaxis for one strain (1009). This was a 24 hr shake culture. The ΔOD and OD max/OD int scales in Fig. 10 were adjusted so that at 400 nm they were the same. The two different plots tend to separate with the OD max/OD int plot being greater as the wavelength increases.

Several phototaxis action spectrum experiments were performed with strains 125 and 1009 soon after harvest from HSA agar plates. Specifically, spectra were determined on 0 hr and 3 hr HSA liquid shake cultures. The phototaxis was poor. It thus was important to determine when during the growth of the cells in liquid culture that phototaxis developed. Figs. 11 and 12 show the results of phototaxis assays of strain 125 over a 30 hr HSA liquid shake culture period. Because of the time required for each assay, only two wavelengths were tried. These were 475 and 675 nm which were judged to be the nominal phototaxis action spectrum maxima for strain 125 at dilute cell concentration when plotted as OD max/OD int. Fig. 11 shows the change in phototaxis of the strain 125 cells with respect to time in culture when the phototaxis is expressed as ΔOD . Fig. 12 shows the same data but with phototaxis expressed as OD max/OD int. When phototaxis is expressed as ΔOD , it appears that phototaxis steadily increases with culture age with maximal phototaxis occurring at 20 to 28 hours culture age. Review of Figs. 3, 4, and 5 (Moyer's report) show that at 20-30 hrs culture age turbidity is near stationary phase for strain 125. There is insufficient data in Fig. 5 to draw any conclusions about cell numbers/ml at 20 to 30 hrs for strain 125. This needs further research. When phototaxis is expressed as OD max/OD int, several new properties of 125 cell cultures emerge.

First, it appears that phototaxis is greater in response to light at 675 nm than at 475 nm. Secondly, that 125 cells freshly removed from agar culture are poorly phototactic, but improve dramatically by two hours in liquid shake culture. Finally, it appears that phototaxis occurs in waves, i.e., at 16 hrs, 22 hrs, and 26 hrs.

The maxima of the phototaxis action spectra in these studies are different from published values, i.e., 500 nm (Foster, et al. 1985). Thus it is of interest to determine if the phototaxis action spectra are related to the absorption spectrum of chlorophyll, the carotenoids, or rhodopsin. This was tested as follows. Liquid shake cultures were centrifuged at 1,000 rpm as described in Materials and Methods. The cell pellet was extracted with 3 ml of acetone. The extract was again centrifuged at 1,000 rpm for 10 min and the cell pellet discarded. The acetone cell extract was placed in a glass cuvette and the absorption spectrum determined between 300 and 750 nm against an acetone blank. Figs. 13 and 14 show the resultant spectra of the acetone soluble extract. Extracts from all the strains were qualitatively similar with absorption maxima at 433 and 663 nm. These values are similar to published values for chlorophyll a of 430 nm and 670 nm. It is known that the maxima vary according to the solvent in which the pigment is dissolved. Rhodopsin is reported to have an absorption maximum of 500 nm. Although more data are needed to draw definitive conclusions, these preliminary data do support that the phototactic action spectra more nearly reflect the absorption spectrum of chlorophyll a than they do rhodopsin.

V. DISCUSSION

After considerable investment of time and effort in overcoming problems associated with the growth medium, and optimal growth conditions, possible contaminants, and testing various techniques of assessing phototaxis, we were able to pursue our stated research goals. The goals receiving highest priority were the simplification of the Foster procedure for producing phototactic cells and the development of a procedure for measuring phototaxis. Although more research in both of these areas is warranted, we feel we have accomplished these goals but not in

exactly the way anticipated. Instead of developing a laser-doppler method of assessing phototaxis, we utilized a spectrophotometric method. With this technique of assessing phototaxis, we were able to compare the phototactic ability of the 8 algal strains under various conditions of growth. These studies are not yet complete. We also discovered an interesting banding of algal cells in 100 μ l capillary tubes when exposed to spectral light that disappeared when the cells were exposed to white light.

We have observed that the various algal strains possess a mean cell volume which varies over two-fold from the smallest to the largest cells. Thus the mean size of the algal cells seems to be an important factor in the relationship between cell number and culture turbidity. The mean cell volume, represents a composite of all the cell volumes within the population and has limited use. We feel that studies of the cell size distribution of the algal populations is in order and should clarify some of the vagaries of growth and phototaxis.

We have studied two ways of expressing the quantification of phototaxis. At present we are not in a position to choose one or the other.

In studies of the phototactic ability of four different algal strains to a number of wavelengths between 400 and 700 nm, we observed that different strains yield different phototaxis action spectra. These spectra are influenced by how the phototaxis is expressed but that is not the whole answer.

Finally, we have studied the phototaxis to two wavelengths during the growth of a liquid shake culture and observed that phototaxis increased with the cell growth.

We have done preliminary experiments which suggest that the phototaxis action spectra of the algal strains is related to the absorption spectrum of chlorophyll a and not rhodopsin.

VI. RECOMMENDATIONS

The results presented in these reports appear to be novel and setting the stage for publication. We feel that efforts should be directed toward repeating the data to obtain verification and then prepare a manuscript for publication.

In repeating the experiments, we feel that a subset of the

strains used should be studied more intensely. To date we have studied a number of parameters independently of each other in all or most of the algal strains, i.e., cell number, turbidity, phototaxis, mean cell volume, culture time, etc. Now it is time to try to relate these culture parameters to each other in a fewer number of strains:

Through a number of qualitative studies of the phototaxis of the 8 algal strains, most of which have not been reported here, we had concluded that strain 125 was the most phototactic under the widest range of conditions. Strain 125, however, also appears to be quite erratic and has proven recalcitrant to yielding reproducible results regarding its growth and phototactic properties. Some of our experiments indicated that other strains may be better models. We interpret these results to indicate that it is still too premature to select a single strain for intensive study and as the strain to use in mutagenesis studies. We had observed a number of indications that we can by no means yet control or are even aware of all the factors that influence growth and phototaxis of these 8 algal strains. To proceed ahead with developing mutants of phototaxis at this point is premature and to do so now, may result in problems later on.

One of the characteristics of the algae that needs further study is the mean cell volume. A study was conducted comparing the morphology of the algal cells at various stages of the growth curve of the cultures (data not shown in these reports). The morphology was assessed by observing with a microscope the living algal cells in a hanging drop and also in stained smears. We observed more large volume cells and more cells devoid of pigment late in the growth phase. It also appeared that the smaller cells were more motile. We do not yet know the relationship between the cell volume of the cells and their phototactic ability. I had purchased a Coulter Cell Counter with a Channelizer attachment which has been standing idle in need of repairs. With this apparatus functional we will be able to obtain a cell-size distribution for all the strains and thus be able to relate them to phototaxis.

The Trinity Biology Department has recently acquired a Gilford programable recording spectrophotometer. This instrument is quite advanced and hopefully can be adapted to generating data of greater accuracy much more rapidly than with our present Bio-Tech spectrophotometer. We feel it is important to verify our completed experiments with the Gilford spectrophotometer.

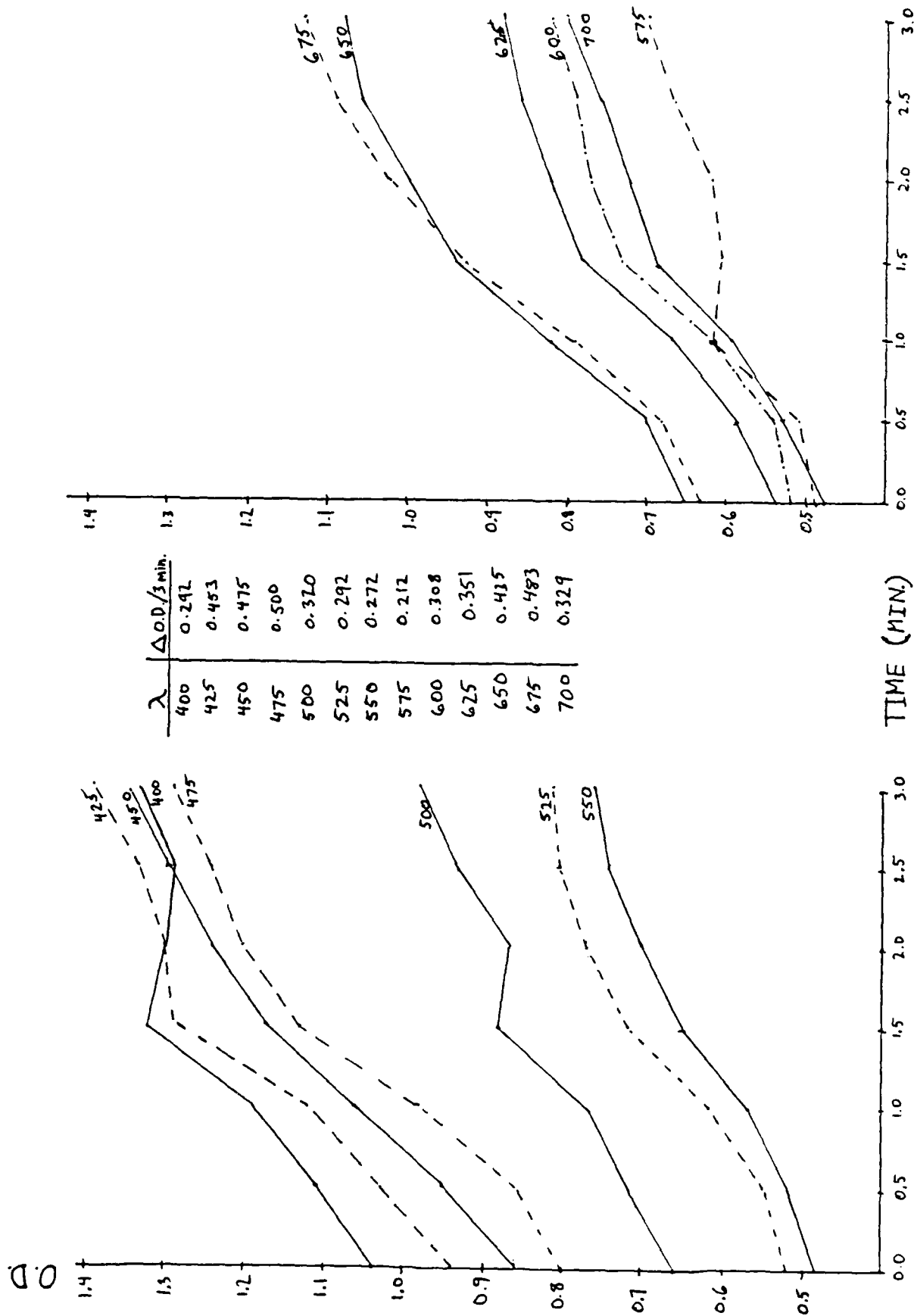


Fig. 6. Phototaxis assays of *C. reinhardtii* strain 1009 grown for 24 hrs in a liquid shake culture in HSA broth.
Data expressed as $\Delta O.D.$

Fig. 7. Phototaxis assays of *C. reinhardtii* strain 1009 grown for 24 hr in a liquid shake culture in HSA broth.
Data expressed as $\frac{\text{Max O.D.}}{\text{Int. O.D.}}$

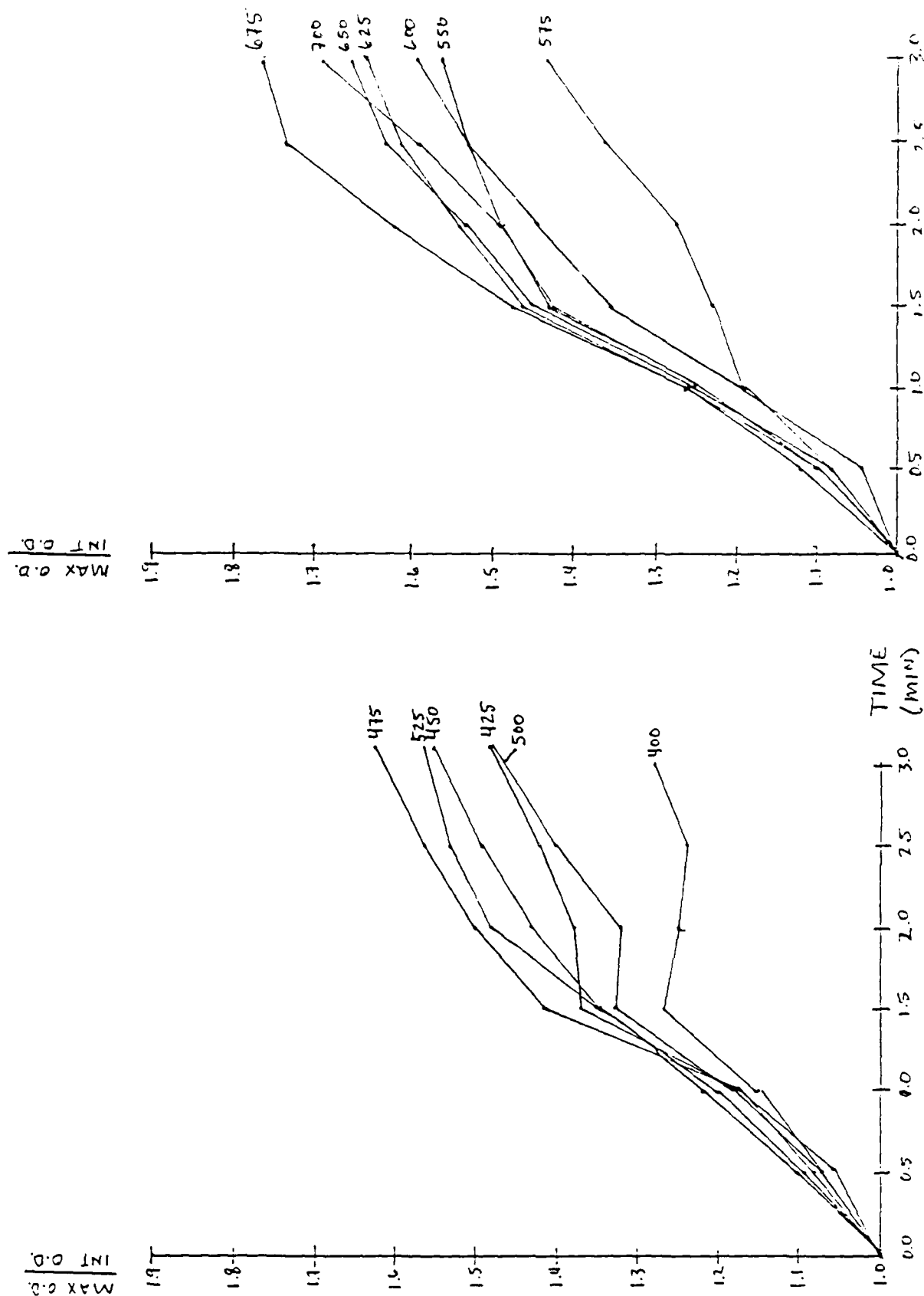
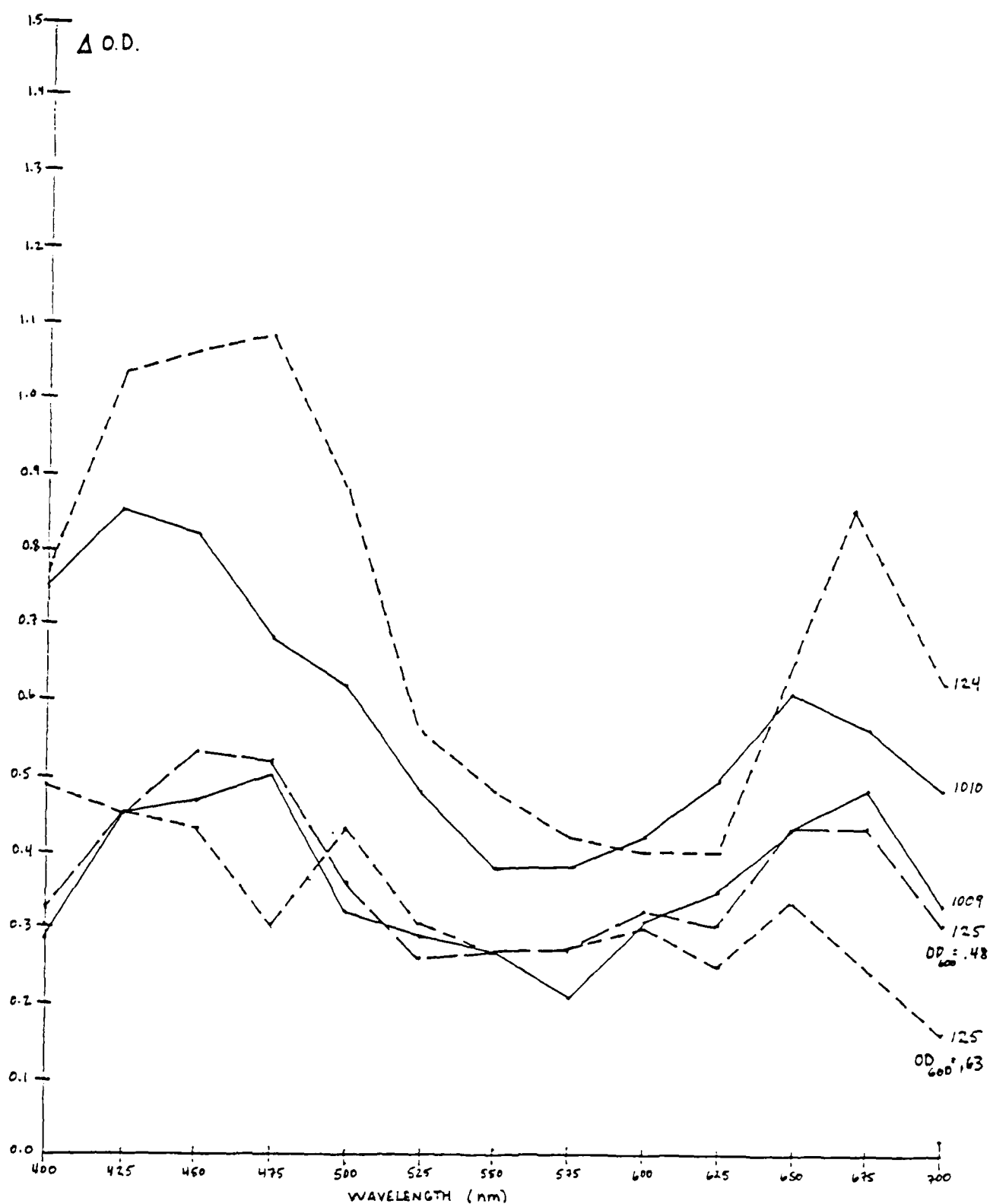


Fig. 8. Phototaxis Action spectra expressed as ΔOD of *C. reinhardtii* strains 124, 125, 1009, and 1010.



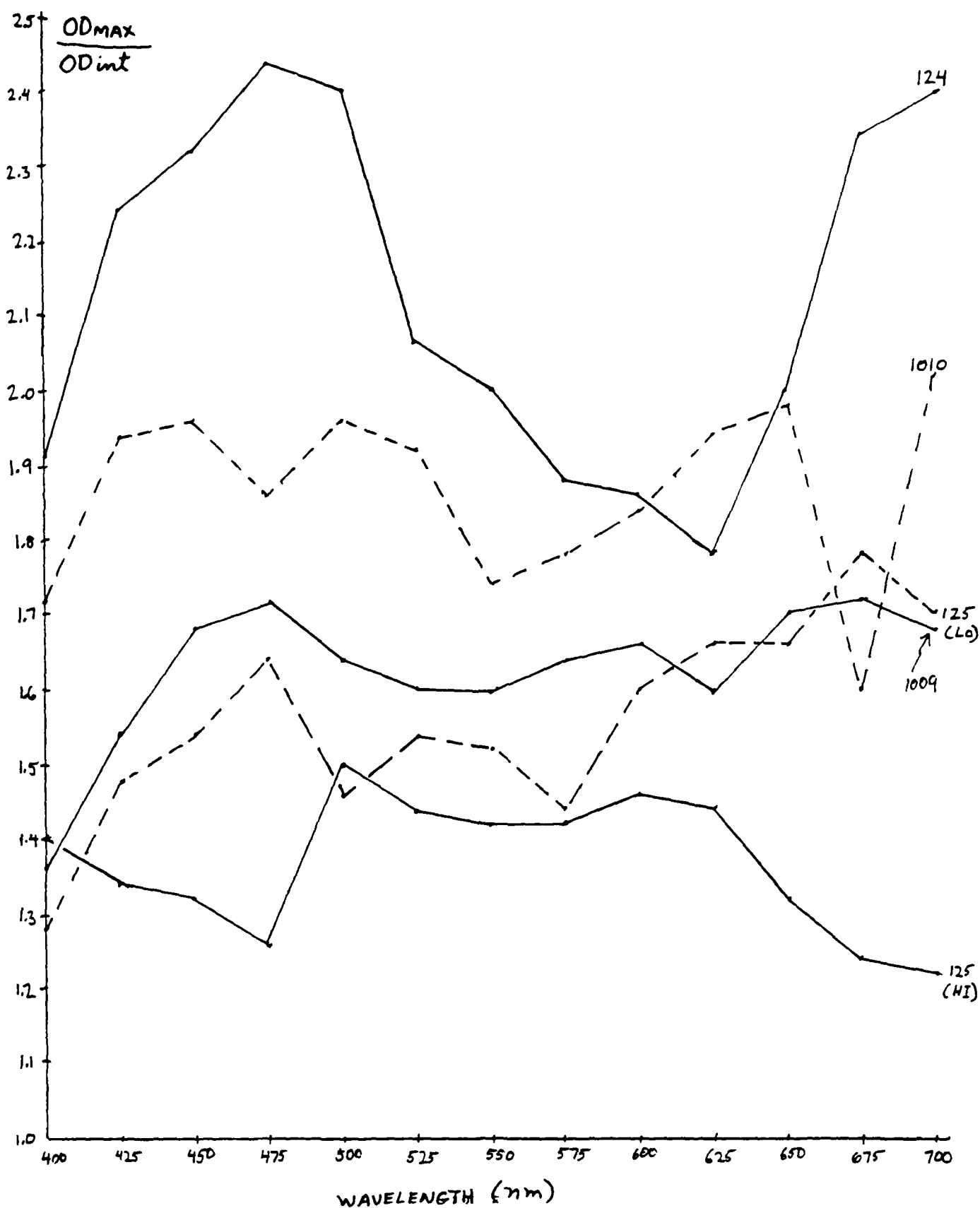


Fig. 9. Phototaxis action spectra expressed as OD Max/OD int of *C. reinhardtii* stains 124, 125, 1009 and 1010.

Fig. 10. The phototaxis action spectrum of C. reinhardtii strain 1009 with phototaxis expressed both as ΔOD and as OD Max/OD int.

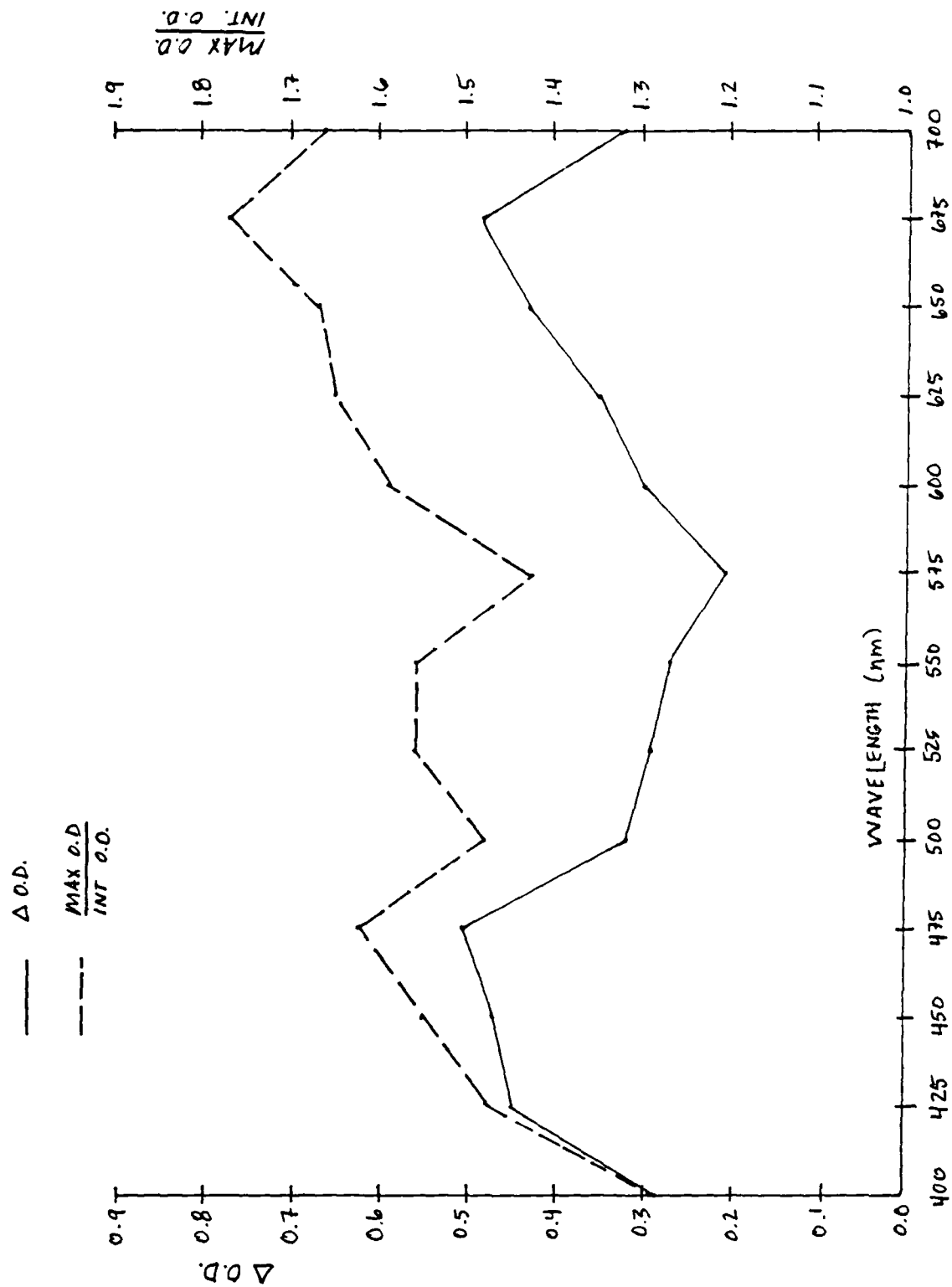


Fig. 11. Phototaxis of *C. reinhardtii* strain 125 to 475 and 675 nm light over a 28 hr period in HSA liquid shake culture. Phototaxis is expressed as ΔOD .

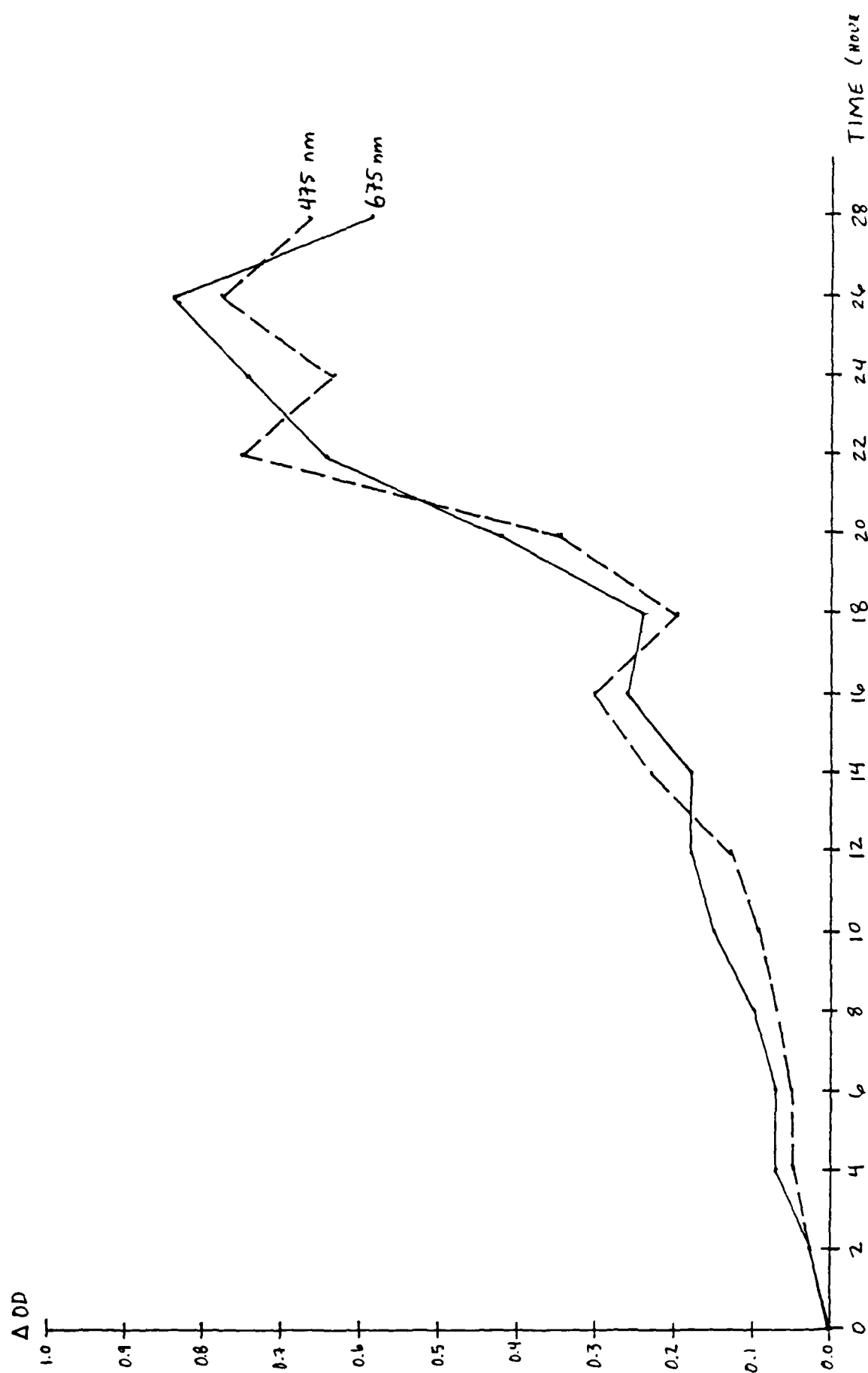


Fig. 12. Phototaxis of *C. reinhardtii* strain 125 to 475 and 675 nm light over a 28 hr period in HSA liquid shake culture. Phototaxis is expressed as OD MAX/OD INT.

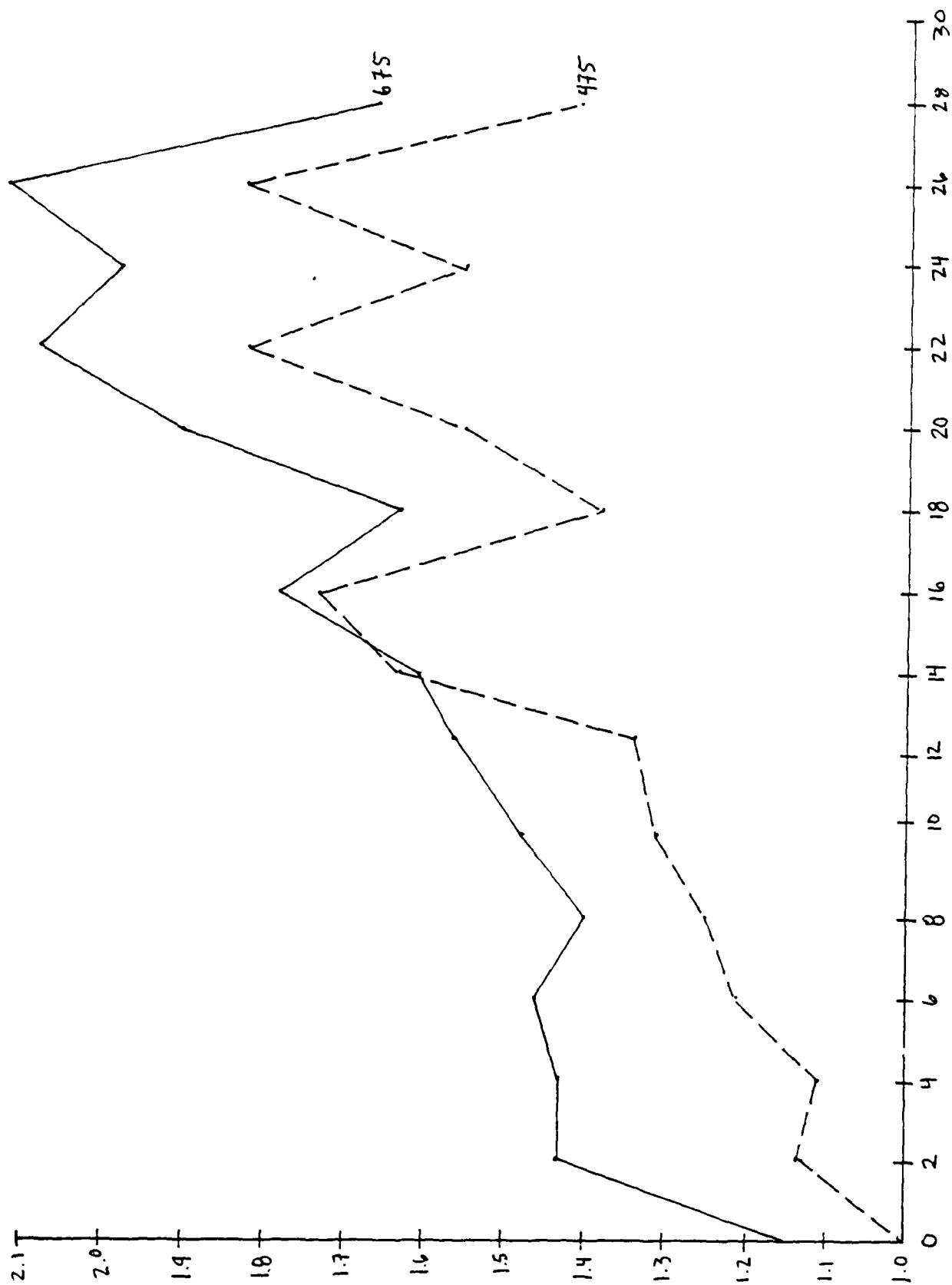
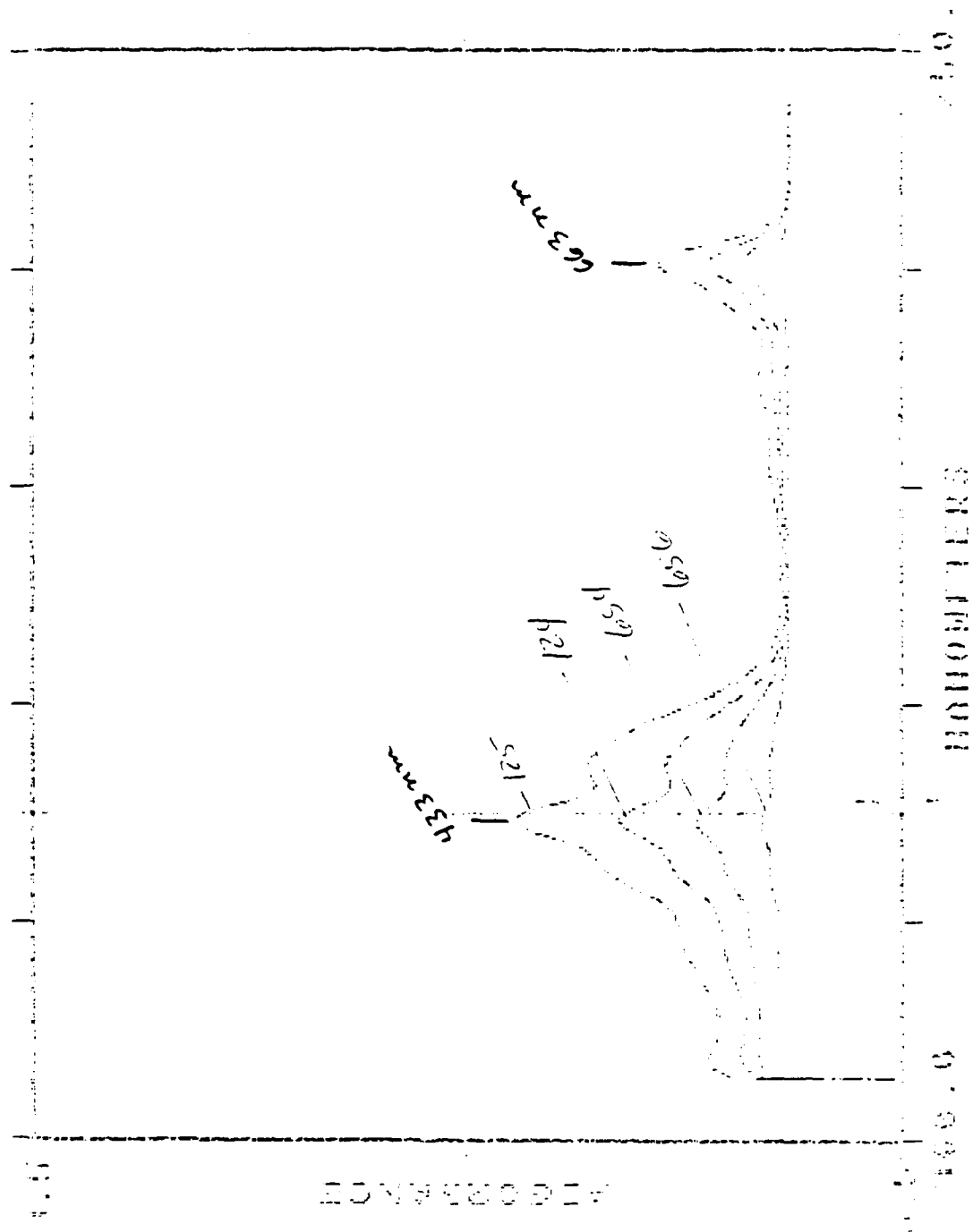


Fig. 13. Absorption spectrum of an acetone extract of C. reinhardtii strains 124, 125, 654, and 656.

5.0
 4.0
 3.0
 2.0
 1.0
 0.0



8/25/86

WAVELENGTH =

WAVELENGTH = 1.2, 3.4

SAMPLE 1 / 1009

A 433.5
0.5592

SAMPLE 2 / 1010

A 433.0
1.6561
B 663.0
0.6804

SAMPLE 3 / 1101

A 433.0
1.0377
B 662.5
0.4399

SAMPLE 4 / 1102

A 434.0
0.4499

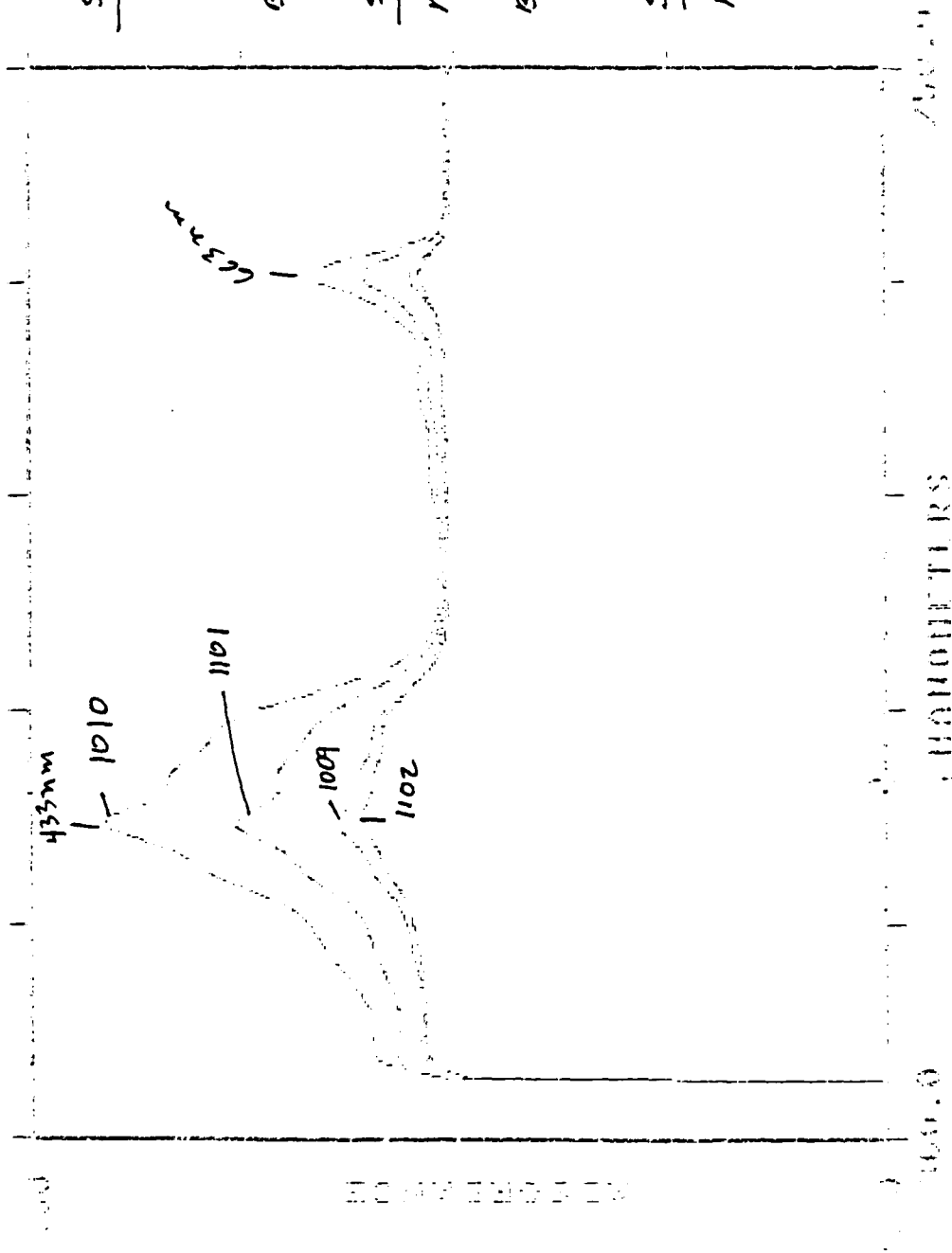


Fig. 14. Absorption spectrum of an acetone extract of *C. reinhardtii* strains 1009, 1010, 1101, and 1102.

WPAFB-TR-80-100

Technical Report

Final Report

Research for the Development of an Engine with a

Variable Geometry

Engine for the Development of an

Engine

Research for the Development of an Engine with a

Variable Geometry

Prepared by: David Allen Bridenstine
Academic Rank: Master of Science Candidate
Department and: Mechanical and Aerospace Engineering
University: Arizona State University
Research Location: WPAFB AFWAL MLT

WPAFB Researcher: Major Steven Lee Cole

Date: 27 September 1980

Contract No: F49620-80-C-0013

Copy on this page does not
permit fully legible reproduction

$$f_{\text{max}} = \frac{1}{2\pi} \sqrt{\frac{1}{L(C_1 + C_2)}} = \frac{1}{2\pi} \sqrt{\frac{1}{L(C_1 + C_2 + C_3 + C_4)}} = \frac{1}{2\pi} \sqrt{\frac{1}{L(C_1 + C_2 + C_3 + C_4 + C_5 + C_6 + C_7 + C_8 + C_9 + C_{10})}}$$

1. *Phylogenetic relationships*—The phylogenetic relationships among the 10 species of *Phrynosoma* were determined using the parsimony method of Farris (1993) as implemented in the computer program PAUP (Phylogenetic Analysis Using Parsimony; version 4.0; Farris and Neeland, 1999). The parsimony method was chosen because of the lack of a priori knowledge of the relative importance of the different characters used in this study. The parsimony method was also chosen because of the lack of a priori knowledge of the relative importance of the different characters used in this study. The parsimony method was also chosen because of the lack of a priori knowledge of the relative importance of the different characters used in this study.

1. *Chlorophyll a* and *Chlorophyll b* were determined by the method of Lichtenthaler and Whistler (1973).

As a result of the above, the following is suggested:

It is generally well understood that the life cycle of a product includes manufacturability criteria early in the life cycle. This concept is one driving force in the development of CAD/CAM. It is logical to extend this notion to include considering all aspects of engineering simultaneously from the onset. This paper identifies key issues in the development of a system capable of integrating knowledge from all aspects of the life cycle throughout the engineering process. The fundamental component of the system that does this engineering in parallel is the Executive System containing meta-level knowledge. The problem is reformulated as the Executive System. Research issues and the architecture of an Executive System are discussed. This paper then proposes and describes a prototype system that could be developed for continuing research. The development of this prototype would involve research in fundamental issues of a general system. The prototype is a materials and process selector for a well defined class of geometric shapes.

Annual Report

I would like to thank the staff members of the Division of General Services for their cooperation and assistance in the preparation of this report. The Division of General Services has been very helpful in providing the necessary information for the preparation of this report.

The Division of General Services has been very helpful in providing the necessary information for the preparation of this report.

The Division of General Services has been very helpful in providing the necessary information for the preparation of this report. The Division of General Services has been very helpful in providing the necessary information for the preparation of this report.

I received my Master's from Utah State University and was transferred to Arizona State University for my dissertation.

My dissertation work involved a study of the effect of Arizona State University's computer system referred to as IADNDK. This work is that of a computer system that would have the engineer as the user in parallel, that is, total integration of the design and engineering process as a product is developed integrating ideas from manufacturing, inspection, maintenance, etc. from the very beginning of the design process.

Major Steven LeClair at the materials laboratory has been working on his concept of Unified Life Cycle Engineering that also involves integrated engineering.

Because of these similarities, it was determined that I could assist Major LeClair in his work at WPAFB and pursue my doctorate research.

II. Objectives of the Research Effort

The fundamental goal for this research was to do preliminary work on the meta-level control method referred to as EXPROM (EXpert Product Manager). The following research objectives were accomplished:

- 1) Research existing projects that relate to this work
- 2) Examine resources and tools for use in this project
- 3) Propose an architecture for a prototype system
- 4) Develop a method of measuring system performance

III. THE DESIGN OF AN AUTOMATIC DESIGN SYSTEM

Early in this research effort it was decided that each person involved in the project had their own expectations as to what a unified life cycle design system should consist of. The general consensus was that the system should be generic so that it applied to a wide range of design and that the system should interact with the user so that much of the information processing would be done with human intervention. During the course of the project it was quickly determined that few systems could be both generic and automated.

In the trend to automate the engineering process, researchers are developing expert systems for a wide range of domains of engineering. The areas of diagnosis, repair, and classification have received most of the attention with application specific expert systems such as FANUC [11], TURBOMAC [12], and EX [13]. Relatively few knowledge-based systems have been developed for the design task. A brief description of some of the design systems follows.

RI-XCON [14] is an expert system developed on a VAX-11-780s. The system uses abstraction to reduce the search space and is forward-chained. It can generate GPCB and uses about 600 rules.

XENIE [15] is an Expert System for the design of integrated circuits for electronic components. This system uses an architecture described by J. R. Dixon and M. H. H. that will be discussed later.

An Expert System for the design of VLSI integrated circuits uses the same architecture as XENIE.

An Expert System for the design of integrated circuits uses the same architecture as XENIE.

...the design process. The design process is a sequence of steps that lead from the initial problem statement to the final design. The design process is a sequence of steps that lead from the initial problem statement to the final design.

All of the design systems mentioned above are designed to assist the designer in the design process. They are designed to assist the designer in the design process.

The design process is a sequence of steps that lead from the initial problem statement to the final design. The design process is a sequence of steps that lead from the initial problem statement to the final design.

EXADS is a design system that is designed to assist the designer in the design process. It is designed to assist the designer in the design process.

EXADS is a design system that is designed to assist the designer in the design process. It is designed to assist the designer in the design process.

Most expert systems were designed for use in a specific application. Some of the expert systems listed above are actually test cases illustrating the utility of the design architecture for implementing the design process. These systems would be used for systems in which the design process is of primary interest in understanding the design process and gaining insight into the design process.

Dixon and Simons use what they refer to as the Evaluate-Redesign Architecture to develop expert systems for design [10]. The design process is realized as a series of modules or functions, each with their own knowledge base and inference engine. The process begins with the initial problem statement and continues until the final design is reached.

The design process is a complex one, involving many steps and decisions. The design process is a hierarchical one, starting with the user's requirements and moving through various levels of abstraction and detail. The design process is a iterative one, involving many cycles of design, evaluation, and redesign. The design process is a collaborative one, involving many people and teams. The design process is a dynamic one, evolving as more information is gathered and more decisions are made. The design process is a creative one, requiring imagination and innovation. The design process is a challenging one, requiring persistence and determination. The design process is a rewarding one, providing a sense of accomplishment and satisfaction. The design process is a vital part of many industries and professions, and it is one that is constantly evolving and improving.

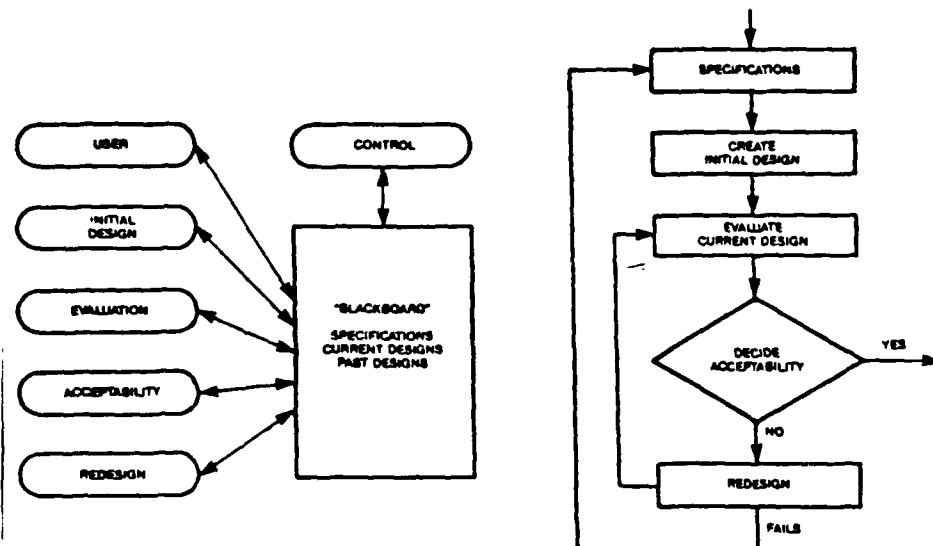
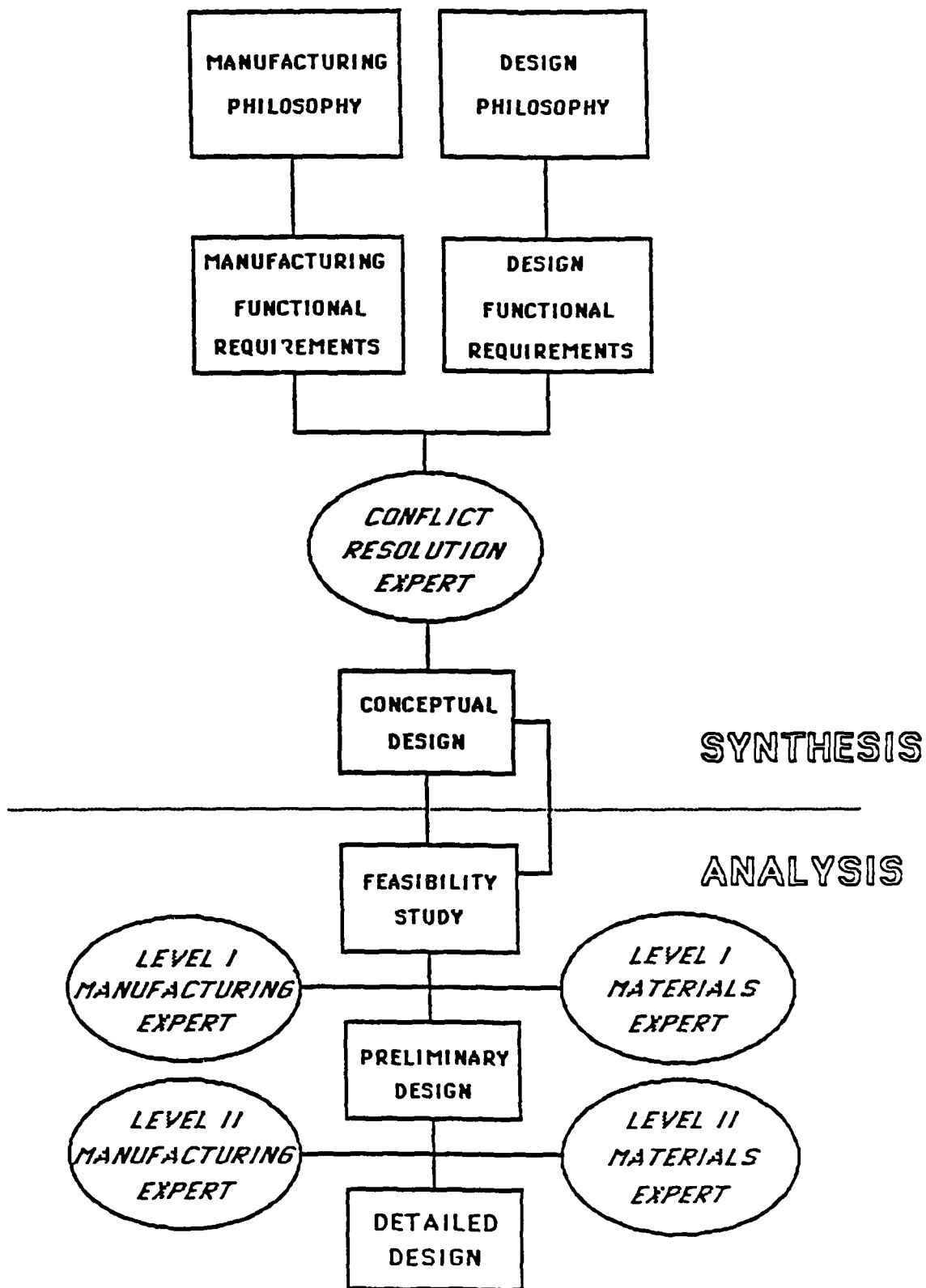


Figure 1: Overview of the Architecture of the Design System. In Design from Idea and Vision.

[illegible]

Both of the architectures mentioned above are based on the use of a hierarchical collection of specialists. The literature contains other expert systems that use the structure of a hierarchy of specialists. For example,

Bryan Greenway and James K. Hinkle, project manager, proposed a materials selection system. Similar to expert systems that integrate design and manufacturing, included in that work are a materials database and manufacturing process database. It was concluded that such work is not representative of the capabilities



13-9

the system will be able to:

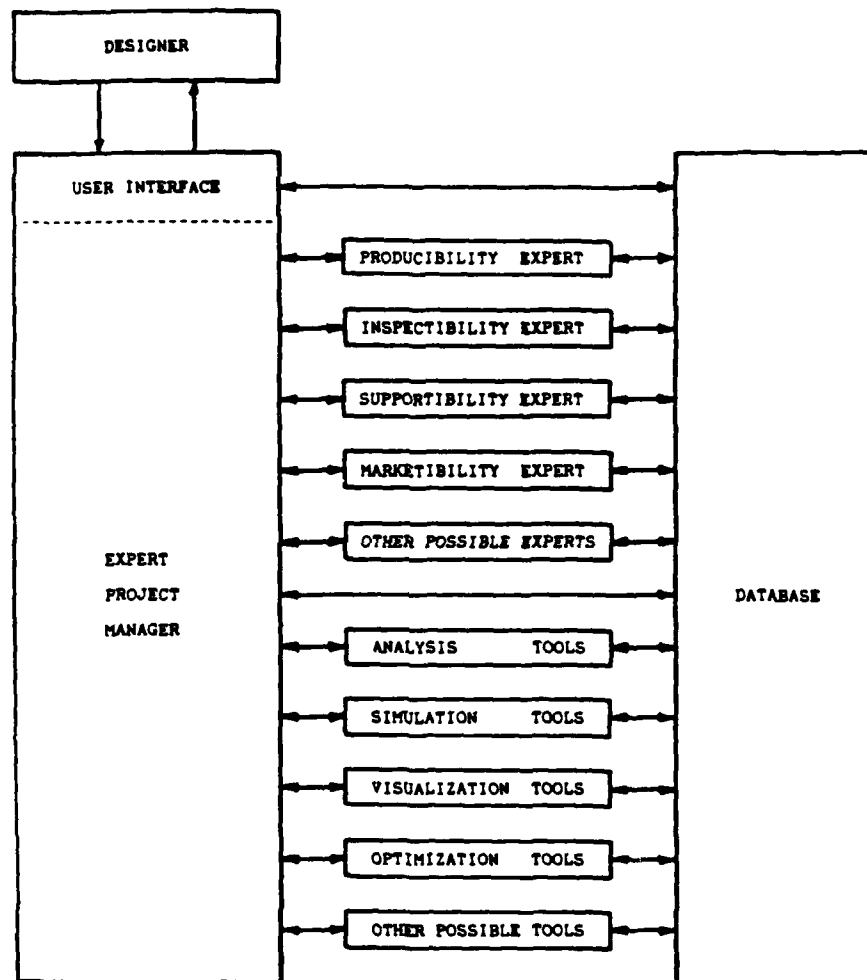
The system should be able to learn from the user's experience. There will be separate expert modules for each aspect of the life cycle of the product. Some of these modules are:

DESIGN :	Design, Detail Design, Drawing, Assembly
INSPECTIBILITY:	Assembly, Inspection, Production
PERFORMANCE:	Stress, Strength, Fatigue, Vibration, Corrosion
SUPPORT:	Disassembly, Repair, Preventative Maintenance
INSPECTIBILITY:	Access, Probability of Detection of flaws
BUSINESS:	Market, Security, Environmental, Environmental Impact

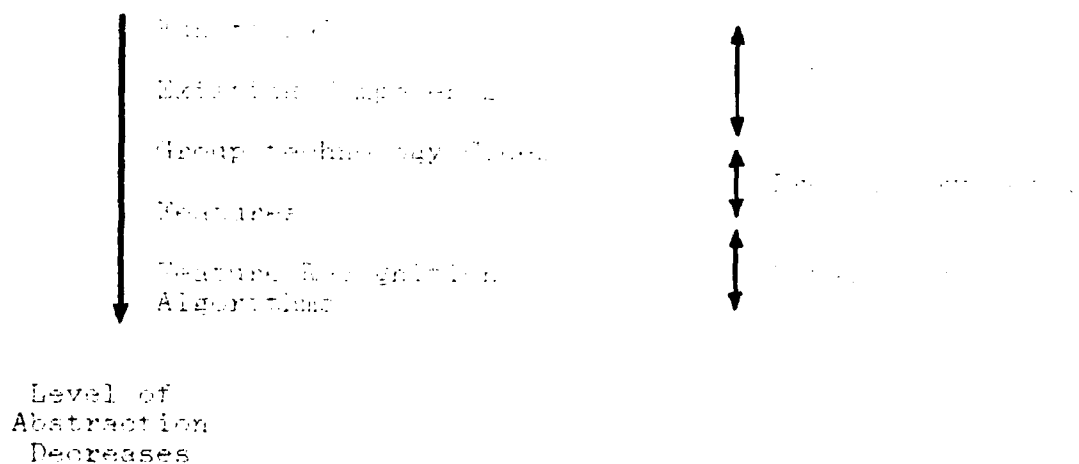
Each of these modules will have similar structures. They will have separate knowledge bases but may either share a common inference engine or reside on different computers.

The system will also consist of a collection of databases. It would be well to have some common data for all the various dissimilar databases in the system. The user, EXPROM and each of the other expert modules should have controlled access to the databases.

The system will also contain several analytical packages to assist in computational extensive problems. Examples include finite element analysis, optimization, statistics and visualization routines. The following figure illustrates the architecture proposed.

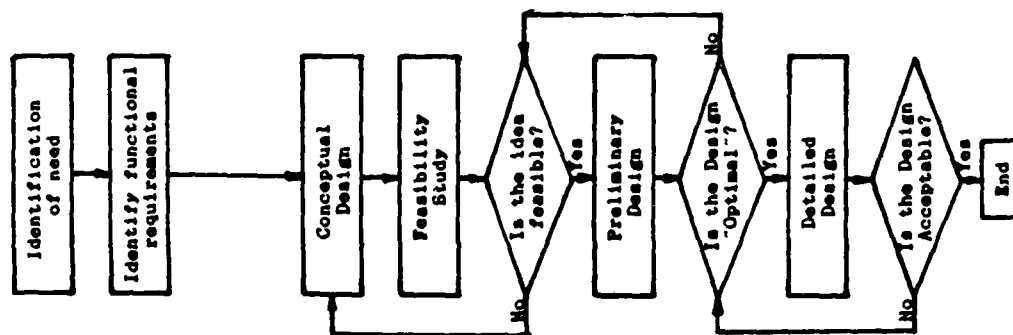


the system is designed to be able to handle the problem of abstraction. The process of abstraction is considered as the process of reducing the level of abstraction. The process of abstraction is considered as the process of reducing the level of abstraction. The process of abstraction is considered as the process of reducing the level of abstraction.

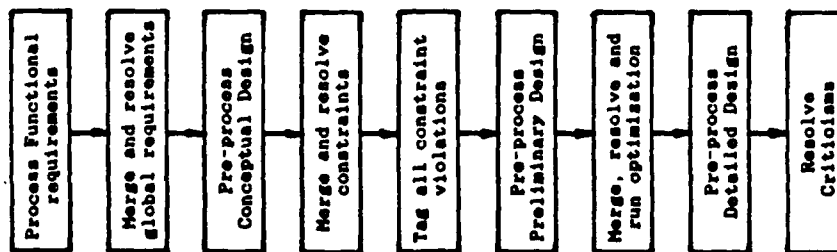


To understand this architecture, we need to develop a 'flow chart' showing what the designer, KALM, and the expert module is doing. The expert modules are designed similarly and that have one common flow chart. In general, the system generates constraints first then, or second, characteristics that should be considered as part of some objective function. It is difficult to show a parallel structure using flow charts. As an example, three flow charts that follow each other in parallel. For example, KALM may begin to process a constraint and then difference with parts that are in the system. The flow chart is the flow chart.

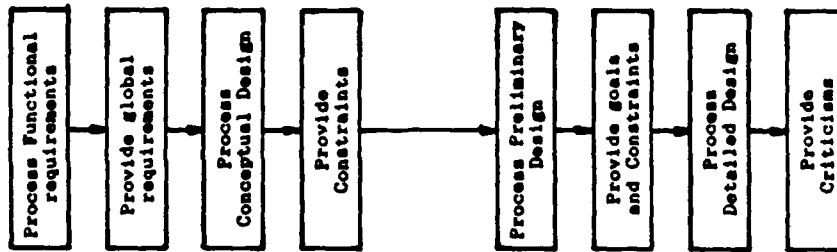
DESIGNER



EXPERT PROJECT MANAGER



TYPICAL EXPERT



the 1990s, the number of people in the world who are illiterate has increased from 1.2 billion to 1.5 billion. The number of illiterate people in the world is expected to reach 1.7 billion by the year 2015. The number of illiterate people in the world is expected to reach 1.7 billion by the year 2015.

[illegible]

- 1) The system will consider the building of a piece. Some specifications limiting the building of some well defined assembly will be allowed.
- 2) The single piece will have a constant cross section so that specification is limited to a two dimensional description and length.
- 3) The cross section shall be completely described using a maximum of two features from a small library of features.
- 4) The library of features will be limited to a circle and a rectangle parallel with the X and Y axes.

The specification above does not require the designer to design a specific object, it is more abstract. The designer could be developing, for example, a device for rotating a beam, pipe, shaft, rectangular or triangular, wheel, etc. or many other objects that fit within the above stated limitations. I believe this approach is more desirable for general systems than specifying exact dimensions.

The first three sub-panels appear to have been
too closely identified as a single entity. The
panels suggested that the person in question
had been the one who identified the person. It
is indeed the case that the person in question
was the one who identified the person. It is
the task of the system to consider the person.

- This description is completely descriptive of the system that will produce useful information and does not give a general concept as the definition is abstract. This will be an example of a material selection scenario:

1. The Executive expert system obtains some goals and goals from a representative of each factor in the life cycle. In the case of multiple goals, it chooses the preemptive rank by preference and then the relative placement of numerical weights or values and the value to be extracted. All of this information will be extracted by deduction when possible or by direct input.

REPRESENTATIVE	CONSTRAINTS	ADVANTAGES
DESIGN	Non-mag. E. E.	Simple, rugged
PRODUCIBILITY	Machine limits	
INTELECTABILITY	X-ray insensitive	
PERFORMANCE	corrosion	
SUPPORTABILITY	-	Wear resistant
ECONOMICS	Available	Low cost

- II. Using the constraints, a list of candidate materials is directly obtainable using boolean operations on the relational database. If there is a contradictory conflict resolution takes place.
- III. The Executive System must then rate the materials proposed by the representation of a simplified description of the Archimedean ratings. The selection of the materials is made by the conflict resolution.

REFERENCES

- [1] J. C. Marshall and J. Knapton, 'The Use of Expert Systems for Design Capabilities in the Design of Mechanical Components', in *Proceedings of the 1984 Computers in Engineering Conference*, pp. 319-321.
- [2] J. L. Dwyer and J. W. Thomas, 'The Use of Expert Systems in the Design of Mechanical Components', in *Proceedings of the 1984 Computers in Engineering Conference*, pp. 322-324.
- [3] M. Ali and B. Chandrasekaran, 'Expert Systems for Design Automation and Planning', in *Proceedings of the 1984 Computers in Engineering Conference*, pp. 325-327.
- [4] J. L. Dwyer and M. J. Dwyer, 'Expert Systems for Design Automation and Planning', in *Proceedings of the 1984 Computers in Engineering Conference*, pp. 328-330.
- [5] V. M. Kulkarni, J. R. Dixon, 'Expert Systems for Design: The Design of Heat Fins as an Example of Conflicting Subgoals and the use of Dependencies', in *Proceedings of the 1985 Computers in Engineering Conference*, pp. 146-150.
- [6] J. R. Dixon and M. K. Simmons, 'An Architecture for Application of Artificial Intelligence to Design', in *Proceedings of the 1985 Design Automation Conference*, pp. 634-640.
- [7] M. Vaghul, J. R. Dixon, G. E. Elam, and M. K. Simmons, 'Expert Systems in a CAD Environment: Injection Molding Part Design as an Example', in *Proceedings of the 1985 Computers in Engineering Conference*, pp. 77-82.
- [8] D. G. Brown and B. Chandrasekaran, 'Expert Systems for a Class of Mechanical Design Activity', in *Proceedings of the WG5.2 Working Conference on Knowledge Engineering for Computer Aided Design*, Budapest, Hungary, 1984.
- [9] J. R. Zumsteg, D. Pecora, and V. J. Lee, 'A Prototype Expert System for the Design and Analysis of Composite Material Structures', in *Proceedings of the 1984 Computers in Engineering Conference*, pp. 151-153.
- [10] T. R. Thompson, J. R. Dixon, and A. J. Miller, 'An Expert System Approach to Pipe Synthesis', in *Proceedings of the 1984 Computers in Engineering Conference*, pp. 154-156.

1986 USAF-UES SUMMER FACULTY RESEARCH PROGRAM/
GRADUATE STUDENT SUMMER SUPPORT PROGRAM

Sponsored by the
AIR FORCE OFFICE OF SCIENTIFIC RESEARCH

Conducted by the
Universal Energy Systems, Inc.

FINAL REPORT

Development of a High Speed Infrared Detection and Recording
System with Resident Image Processing and Graphic Data
Display for support of Remote Defense Nuclear Agency
High-Powered Pulsed Microwave Source Measurements

Prepared by:	Paul E. Bussey
Academic Rank:	Graduate student
Department and	Department of Electrical Engineering
University:	University of Colorado at Colorado Springs
Research Location:	The University of Colorado at Colorado Springs, and the Frank J. Seiler Research Laboratory, NH, United States Air Force Academy
USAF Researcher:	Dr. Ronald M. Sega
Date:	August 8, 1986
Contract No:	F49620-85-C-0013

Development of a High Speed Infrared Detection and Recording
System with Resident Image Processing and Graphic Data
Display for Support of Remote Defense Nuclear Agency
High-Powered Pulsed Microwave Source Measurements

by

Paul E. Bussey

ABSTRACT

Infrared detection and measurement of electromagnetic field strengths is used at the University of Colorado at Colorado Springs (UCCS). In each experiment, the measurements are of steady-state, continuous wave (CW) conditions. However, Seiler Labs was asked to support the test of a pulsed microwave source to be conducted by the Defense Nuclear Agency (DNA) at the Air Force Weapons Laboratory (AFWL) in late July or early August, 1986; the AGA Thermovision 780 system that is used by UCCS is not suited for such tests. Subsequent investigation revealed that an appropriate and affordable system could not be obtained for the test. At that point, a means of adapting the present system at UCCS to support the test was pursued. The resulting system consists of the AGA system, and a modified IBM PC/AT to store the data and do all of the necessary data/image processing at the remote test site. The effort was a three phase group effort, including hardware development, software development, and detection material

Acknowledgments

I would like to thank the Air Force Systems Command and the Air Force Office of Scientific Research for sponsorship of my research. I would also like to thank the Frank J. Seiler Research Laboratory, specifically Captain Dan Fredal, along with the University of Colorado at Colorado Springs Department of Electrical Engineering with special thanks to my faculty sponsor Dr. Ron Sega and his cohort Dr. John Norgard. I am extremely grateful to Don Metzger, Kent Cedola, and Rodger Fulton for the software they have donated to this project. Finally, the completion of this project would not have been possible without my friends Jon Zobel, Alex Sapp, and especially Chad McAllister for acquisitioning equipment and materials for me.

I. Introduction

I received my Bachelor of Science degree in electrical engineering from the University of Colorado at Colorado Springs with emphasis on electromagnetics, and I am continuing to pursue this area in graduate school at UCCS. Having worked in the electromagnetics laboratory for over a year with Dr. Sega and Dr. Norgard, I was very familiar with the infrared techniques for detecting electric fields currently under development. I was also quite familiar with the data processing software used in conjunction with the infrared camera system. Thus, I was asked by Dr. Sega to create a new data processing software package to be used on an IBM PC-AT, which was to be interfaced directly to the infrared camera system.

II. Objectives of the Research Effort

The overall objective of our summer project was to support tests by the Defense Nuclear Agency of high-power pulsed microwave sources using infrared detection techniques. The duration of the experiment was to be approximately two seconds, with the pulse-width of the source being on the order of nanoseconds. The infrared data acquisition equipment was originally only capable of recording one frame of infrared information (128x128 pixels, each pixel is represented by eight bits. Only 112 of the horizontal pixel represent valid data) per second, while this data acquisition speed is acceptable for continuous wave measurements, it is far from adequate for making transient measurements for the pulsed source. It was thus determined that interfacing the AGA infrared system to an IBM PC-AT, data acquisition speeds of about six frames per second could be reached, and that this would be adequate for transient measurements.

My personal tasks included writing the software for data acquisition, data processing, graphic data display, and the calibration of an absorbtive screen material for the extraction of electric field strength from the isotherm units generated by the infrared camera system.

III. Data Acquisition

In order for the PC to obtain the data generated by the infrared system, an interface card was designed and built, and controlling software was written by Captain Fredal and Jon Zobel. By calling these software routines, the direct memory access (DMA) controller is first initialized to prepare for data storage. A trigger pulse with user programmable delay is then generated which can be used to initiate the firing of the microwave source. After this, the data from the infrared camera system is then collected and stored in the PC's memory by the DMA controller.

My task was to write a main program which could call these routines, as well as other routines which would display a false-color image of any of the stored frames of data (to ensure that the data collected was good), and store the data on disk. The main program was written to be menu-driven, and user-friendly.

The false-color image routine displays a false-color image of a 112 x 128 frame of pixels; each pixel is eight bits, giving a possible range of 0 to 255 for the pixel values. This range is divided into ten levels as follows: 0 to 25, 26 to 50, 51 to 75, 76 to 100, 101 to 125, 125 to 150, 151 to 175, 176 to 200, 201 to 225, and 226 to 255. Each of these levels is assigned a corresponding color.

Thus, the procedure plots the frame taking one pixel at a time, determining which level it is in, and then placing a box of corresponding color in the appropriate place. The color scale used is based in the color spectrum of light, with dark purple representing the low range (0 to 25), moving through the blues to green to yellow to orange representing the high range (226 to 255).

To store the data on disk, a file is created to contain fields of data, and the desired images are then placed in this file. Any type of disk storage device can be used with this routine, including hard drives, RAM disks, and floppy drives.

IV. Data Processing

In order to obtain more accuracy from the data collected by the acquisition system described above, I wrote several data processing and data extraction routines. These routines include statistical averaging of multiple frames, combining frame by frame averages of pixel blocks to form a time history of the specified pixel block, and extracting several rows or columns from a frame (either previously averaged, or raw data), and averaging them together.

The statistical averaging of multiple frames routine was designed to be the workhorse of most of the data processing. From this, three-dimensional surfaces and contour maps can be plotted, and data can be "cleaned up" before extracting rows or columns of information. This subroutine operates by first averaging a given pixel from all of the frames selected; the standard deviation about this average is then calculated. The pixels are then scanned one by one to determine if they are within plus or minus one standard deviation of the average; if they are, then they are included in a new average, if not, they are discarded. By using this method, the accuracy of the data is greatly increased, and the sample size of the data can remain fairly small.

The routine to form a time history of an averaged

pixel block was designed so that the infrared camera system could be used as a tool for making transient measurements, which was the original purpose of this project. From this, a two-dimensional plot is created which shows the thermal response of the pixel block with respect to time.

The routine to extract several rows or columns from a frame of data and average them together (which we have termed "slicing") was designed so that the data collected with this system could be compared with data collected using more conventional means such as calibrated dipoles and loops. This also can be used to produce a two dimensional plot, this time showing the thermal response of the screen material along a horizontal or vertical strip.

The main program which controls these routines is also responsible for setting up global variables, and calling the various graphics programs used to display the data. This program is also menu-driven, and user-friendly.

V. Graphics Display

After processing, the data can be displayed in several formats. When a display format is chosen, the data and default plot values are set in specific memory locations. The chain-and-execute feature of Turbo Pascal is then used to run the desired graphics program without having to exit the data processing program. This feature proved to be quite useful because the size of the object code is limited by Turbo Pascal to 64K; the total object code for the data processing program and the graphics programs combined is 100K. By using the chain-and execute feature, all 100K of software can be accessed by the 29K data processing program.

Once the desired graphics program has been entered, an initial plot is made using the default values. After this, however, the user can change these defaults, and add extra features very simply. A help screen is available (by typing "help") to show the various changes and additions which can be made, and the commands necessary to implement them. When the user is finished with a particular plotting session, he can return to the data processing program by typing "end".

1. Two Dimensional Plotting

This program is used to plot the data generated by

the time history and slicing routines. After the initial plot, the features available to the user are as follows:

- a) help : show help screen
- b) new : clear the screen
- c) color (number) : set color for subsequent commands
- d) limits x [y] (min) (max) : set limits for x [y] axis
- e) scale x [y] (factor) : set x [y] multiplication factor
- f) offset x [y] (offset) : set x [y] offset
- g) label with (label) : add texts anywhere on screen
- h) label x [y] (label) : set label for x [y] axis
- i) label plot (label) : set title label for plot
- j) draw axes : draw the axes and labels
- k) draw line x1 y1 x2 y2 : draw a line from (x1,y1) to (x2,y2)
- l) plot : plot the data
- m) print : print the screen
- n) end : end the plotting session

These commands can be entered at any time during the plotting session.

2. Three Dimensional Surface Plotting

This program does 3-d surface plots. It scans the data from the "front" to the "back", and decides whether the lines to the new data point are hidden or not. By doing this, and then projecting the point from a three-dimensional location to a two-dimensional screen

location, a gridded surface map is formed. After the initial plot, the features available to the user are as follows:

- | | |
|-------------------------------|-------------------------------------|
| a) help | : show the help screen |
| b) new | : clear the screen |
| c) color | : set color for subsequent commands |
| d) limits x [y/z] (min) (max) | : set limits for x [y/z] axis |
| e) theta (value) | : set viewing angle from x axis |
| f) phi (value) | : set viewing angle from y axis |
| g) magnify (factor) | : set magnification for plot |
| h) dB z | : toggles z axis in dB on/off |
| i) label with (label) | : add text anywhere on screen |
| j) label x [y/z] (label) | : set label for x [y/z] axis |
| k) label plot (label) | : set title label for plot |
| l) draw axes | : draw axes and labels |
| m) frame margins | : draw 3-d frame around plot |
| n) plot | : plot the data |
| o) print | : print the screen |
| p) end | : end the plotting session |

3. Contour Map Plotting

This program does contour maps. It scans through the frame four adjacent pixels at a time and determines

whether or not any contours cross on or between these points; if a contour does cross between the points, then the actual position of the contour is extrapolated linearly between the points, and the contour is plotted. After the initial plot, the features available to the user are as follows:

- | | |
|-----------------------------|-------------------------------------|
| a) help | : show the help screen |
| b) new | : clear screen |
| c) color | : set color for subsequent commands |
| d) limits x [y] (min) (max) | : set limits for x [y] axis |
| e) label with (label) | : add text anywhere on screen |
| f) label x [y] (label) | : set label for x [y] axis |
| g) label plot (label) | : set title label for plot |
| h) draw axes | : draw axes and labels |
| i) plot | : plot the data |
| j) print | : print the screen |
| k) end | : end plotting session |

VI. Recommendations

The calibration of a new detection screen for the extraction of electric field strength was not performed because a suitable new screen material has not yet been found; this needs to be done as soon as the new screen material has been chosen.

Although the data processing/graphics display software works fine as it is, there is still room for modifications to be made. Some suggestions for further improvement are:

- 1) Allow the user to add a grid with row and column numbers to the false-color image to aid in selecting row or column numbers for slicing.
- 2) Allow the user to change the increment size in the surface plotting routine to enable faster display of the data.
- 3) Add a routine to the data processing program which enable the user to subtract one frame from another, so that background noise could be recorded initially, and then later subtracted from any measurements.
- 4) Allow the user to put more than one slice or time history plot on a graph.

Many other improvements are possible, but these should serve as good examples of what could be done.

Because the program listings are about 40 pages, I have not included them with this report. However, they are available upon request by writing to the Frank J. Seiler Research Laboratory, or the UCCS Electromagnetics

laboratory.

VII. References

1. Turbo Pascal Version 3.0 Reference Manual, Borland International, 1985
2. Norton, Peter, Programmer's Guide to the IBM PC, Microsoft Press, 1985.

1986 USAF-UES SUMMER FACULTY RESEARCH PROGRAM/
GRADUATE STUDENT SUMMER SUPPORT PROGRAM

Sponsored by the
AIR FORCE OFFICE OF SCIENTIFIC RESEARCH

Conducted by the
Universal Energy Systems, Inc.

FINAL REPORT

MODIFICATION OF A FINITE-DIFFERENCE, 2-DIMENSIONAL
BOUNDARY LAYER CODE FOR APPLICATION TO THE
FREE SHEAR LAYER OF AN AXISYMMETRIC JET

Prepared by: Timothy T. Clark
Academic Rank: Graduate Student
Department: Department of Mechanical Engineering
University: University of New Mexico
Research Location: The Air Force Weapons Laboratory
Kirtland Air Force Base, New Mexico
USAF Research: Dr. Bruce Masson
Date: August 25, 1986
Contract No.: F49620-85-C-0013

MODIFICATION OF A FINITE-DIFFERENCE, 2-DIMENSIONAL
BOUNDARY LAYER CODE FOR APPLICATION TO THE
FREE SHEAR LAYER OF AN AXISYMMETRIC JET

by

Timothy T. Clark

ABSTRACT

An existing finite-difference, 2-dimensional boundary layer code was modified so that it could be applied to the free shear layer of an axisymmetric jet. The governing equations and boundary conditions of the free shear layers of the jet were derived. These equations were non-dimensionalized and scale factors were found. The non-dimensionalized equations were expressed in stream-function form and the result was expressed as finite-difference equations. The derived finite-difference equations and the boundary conditions formed the basis of modifications to the code. The code was exercised and the results compared to similarity solutions. The comparisons indicated that the code yielded reasonable results.

LIST OF PARAMETERS

- b - Total viscosity (non-dimensional)
- C_0 - Constant relating radial growth of the jet to axial velocity (Ft^2/S)
- C_1 - Constant relating radial growth of the jet to axial position
(non-dimensional)
- J - Momentum of the jet ($\text{lbm} \cdot \text{Ft}^2/\text{S}^2$)
- r - Radial position (Ft)
- r_0 - Radius of the jet nozzle (Ft)
- r^* - Radial scale factor (Ft)
- R - Non-dimensional radial position
- u - Radial (cross-stream) velocity (Ft/S)
- u^* - Radial velocity scale factor (Ft/S)
- U - Non-dimensional radial velocity
- w - Axial (streamwise) velocity (Ft/S)
- w^* - Axial velocity scale factor (Ft/S)
- W - Non-dimensional axial velocity
- z - Axial position (Ft)
- z^* - Axial scale factor (Ft)
- Z - Nondimensional axial position
- Re^* - A Reynolds number-like scale factor (non-dimensional)

- ϵ - Eddy viscosity (Ft^2/S)
- ρ - Fluid density (Slugs/Ft^3)
- ν - Kinematic viscosity (Ft^2/S)

NOTE: A prime will denote differentiation with respect to R, e.g.,

$$U' \equiv \partial U / \partial R.$$

I. Introduction

I received my Bachelor of Science degree in Mechanical Engineering from the University of Maryland in 1983. During the period from 1983 to 1986 I was employed by MPR Associates, a consulting engineering firm in the field of power generation. I am currently enrolled as a graduate student of Mechanical Engineering at the University of New Mexico.

The research problem at the Air Force Weapons Laboratory involved the effects of turbulence on the optical properties which influence beam propagation. Professor Truman, of the University of New Mexico has studied the modelling of turbulent flows. My work at the Air Force Weapons Laboratory was performed under the guidance of Professor Truman.

II. Objectives of Research Effort

The overall objective of the research effort is to predict the behavior of an optical beam traversing a turbulent medium. To accomplish this, measurements will be made to characterize the behavior of an axisymmetric, turbulent jet and to document the effect of this turbulence on the propagation of a laser beam through the jet. These measurements will be compared to the results of numerical evaluations of various turbulence models to determine the suitability of each turbulence model for predicting the behavior of the optical properties of the jet medium.

My individual objectives were to:

- identify a suitable computer code for predicting the behavior of turbulent shear layers using various turbulence models,
- modify the computer code as necessary to apply it to the problem of predicting the behavior of free shear layers in an axisymmetric, turbulent jet, and

- verify the computer code by comparison of the computed results to similarity solutions for a laminar jet and for a turbulent jet using a simple eddy-viscosity model.

III. Computer Code

The computer code of Cebeci and Bradshaw¹ was selected for adaptation to the problem of predicting the behavior of free shear layers in an axisymmetric jet. This code solves for 2-dimensional laminar and turbulent boundary layers by using a finite-difference approach. Keller's box method is used to solve the differenced equations. This method is second order accurate, unconditionally stable and permits the use of non-uniform grid spacing while maintaining its accuracy². Additionally, this method solves the block-tridiagonal form of the finite-difference equations, thus permitting efficient solution^{1,2}.

IV. Governing Equations

In order to apply the computer code of Cebeci and Bradshaw to the problem of predicting the behavior of the free shear layers of a turbulent axisymmetric jet, the finite-difference equations and the boundary conditions of the code had to be modified. These modifications reflected the differences between the governing equations of the free shear layers of an axisymmetric jet, and the governing equations of the shear layers in a 2-dimensional boundary layer.

To determine which of the Navier-Stokes equations govern the behavior of an axisymmetric jet, the following assumptions were made:

1. The axial (streamwise) momentum of the jet is large compared to the radial (cross-stream) momentum (i.e., the radial momentum will be neglected).
2. The tangential velocity and momentum of the jet are negligible (i.e., no swirl).
3. The fluid is assumed to be incompressible (i.e., the Mach number is less than 0.3).
4. The jet is assumed to be steady.
5. There is no pressure gradient.

As a result of these assumptions, the governing equations were found to be the continuity equation and the axial momentum equation. Based on these assumptions, the axial momentum equation and the continuity equation were found to have the following form (in cylindrical coordinates)³:

Continuity

$$\frac{1}{r} \frac{\partial ru}{\partial r} + \frac{\partial w}{\partial z} = 0 \quad (1)$$

Axial Momentum

$$u \frac{\partial w}{\partial r} + w \frac{\partial w}{\partial z} = \nu \left\{ \frac{1}{r} \frac{\partial}{\partial r} \left(r \frac{\partial w}{\partial r} \right) + \frac{\partial^2 w}{\partial z^2} \right\} - \left\{ \frac{1}{r} \frac{\partial}{\partial r} (r \overline{w'u'}) \right\} \quad (2)$$

(Note that u and w are time-mean velocities and u' and w' are the fluctuating components of velocity.) The applicable boundary conditions are:

$$\text{at } r = 0, u = 0, \frac{\partial w}{\partial r} = 0$$

$$\text{at } r = \infty, w = 0$$

The last term of equation (2) represents the Reynolds stress,

$$\tau = -\rho \overline{u'w'} \quad (2.a)$$

The equations were next expressed in non-dimensional form, and scale factors were determined from order of magnitude evaluations. Also, the Reynolds stress was expressed in terms of an eddy viscosity⁴, defined as

$$\epsilon \frac{\partial w}{\partial r} = -\overline{u'w'} \quad (3)$$

The resulting equations in non-dimensional form are

Continuity

$$\frac{1}{R} \frac{\partial RU}{\partial R} + \frac{\partial W}{\partial Z} - \frac{W}{Z} - \frac{R}{Z} \frac{\partial W}{\partial R} = 0 \quad (4)$$

Axial Momentum

$$(UZ - RW) \frac{\partial W}{\partial R} + W \left(Z \frac{\partial W}{\partial Z} - W \right) = \frac{1}{R} \frac{\partial}{\partial R} \left\{ \frac{b}{R^*} R \frac{\partial W}{\partial R} \right\} \quad (5)$$

The non-dimensional parameters (in upper-case letters) are related to the dimensional parameters (in lower-case letters) by the scale factors (designated with asterisks) as follows.

$$w = Ww^* \quad (6.a)$$

$$u = Uu^* \quad (6.b)$$

$$r = Rr^* \quad (6.c)$$

$$z = Zz^* \quad (6.d)$$

The parameter b in equation (5) represents the non-dimensional, total viscosity

$$b = 1 + \epsilon/\nu, \quad (7)$$

where ϵ is the eddy viscosity.

On the basis of the order of magnitude evaluation, and the similarity solution for a turbulent jet^{5,6}, the scale factors were taken as follows.

$$r^* = C_1 z \quad (8.a)$$

$$w^* = \frac{C_0}{r^*} \quad (8.b)$$

$$z^* = \frac{C_1}{r_0} \quad (8.c)$$

$$u^* = \frac{C_0}{z^*} \quad (8.d)$$

$$Re^* = \frac{C_0 C_1}{\nu} \quad (8.e)$$

In the case of turbulent flow, the coefficient C_1 is based on experimental data and is taken as 0.0848.⁵ In the case of laminar flow, Re^* is taken as 1, and C_1 is then calculated from equation (8.e). The coefficient C_0 is a function of the jet momentum, J , and is expressed as follows.

$$C_0 = \frac{1}{2} \sqrt{\frac{3}{2\pi}} \sqrt{\frac{J Re^*}{\rho b}} \quad (9)$$

To further simplify the equations, they were expressed in stream-function form. In this form the continuity equation is identically satisfied and the axial momentum equation becomes

$$\left[\frac{b}{Re^*} R \left(\frac{f'}{R} \right)' \right]' + \left(\frac{f'}{R} \right)^2 R + \left(\frac{f'}{R} \right) f = Z \left\{ R \left(\frac{f'}{R} \right) \frac{\partial}{\partial Z} \left(\frac{f'}{R} \right) - \left(\frac{f'}{R} \right)' \frac{\partial f}{\partial Z} \right\} \quad (10)$$

where the stream function $\Psi(R, Z)$ is related to the dimensionless stream function f as follows.

$$\Psi(R, Z) = w^* r^{*2} f(R, Z) \quad (11)$$

To facilitate finite-differencing, equation (10) was expressed as a set of first-order ordinary differential equations. These equations are shown below.

$$F_1 = f \quad (12.a)$$

$$F_2 = \frac{f'}{R} \quad (12.b)$$

$$F_3 = \left(\frac{f'}{R} \right)' \quad (12.a)$$

$$\left[\frac{b}{Re^*} RF_3 \right]' + F_2^2 R + F_2 F_1 = 2 \left\{ RF_2 \frac{\partial F_2}{\partial Z} - F_3 \frac{\partial F_1}{\partial Z} \right\} \quad (12.d)$$

Finite-differencing of equations (12.a-d) was performed in a manner similar to that demonstrated by Cebeci and Bradshaw⁷. The details of the differencing procedures are not presented here. The resulting linearized differential equations and the boundary conditions are presented below.

Equations (12.b) and (12.c) become

$$(r_1)_j = F_{1,j-1}^n - F_{1,j}^n + h_j \frac{1}{2} \left\{ F_{2,j}^n + F_{2,j-1}^n \right\} \frac{1}{2} \left\{ R_j + R_{j-1} \right\} \quad (13.a)$$

$$(r_3)_{j-1} = F_{2,j-1}^n - F_{2,j}^n + h_j \frac{1}{2} \left\{ F_{3,j}^n + F_{3,j-1}^n \right\} \quad (13.b)$$

The momentum equation (12.d) becomes

$$\begin{aligned} (S_1)_j \delta F_{3,j} + (S_2)_j \delta F_{3,j-1} + (S_3)_j \delta F_{1,j} + (S_4)_j \delta F_{1,j-1} \\ + (S_5)_j \delta F_{2,j} + (S_6)_j \delta F_{2,j-1} = (r_2)_j \end{aligned} \quad (14.a)$$

$$\begin{aligned} (r_2)_j = R_j^{n-1} - \left[\frac{1}{h_j Re^*} \left\{ b_j^n R_j F_{3,j}^n - b_{j-1}^n R_{j-1} F_{3,j-1}^n \right\} \right. \\ + \frac{\alpha_1}{2} \left\{ F_{3,j}^n F_{1,j}^n + F_{3,j-1}^n F_{1,j-1}^n \right\} + \frac{\alpha_2}{2} \left\{ (F_{2,j}^n)^2 R_j + (F_{2,j-1}^n)^2 R_{j-1} \right\} \\ \left. + \frac{\alpha}{2} \left\{ (F_{1,j}^n F_{3,j}^{n-1} + F_{1,j-1}^n F_{3,j-1}^{n-1}) - (F_{1,j}^{n-1} F_{3,j}^n + F_{1,j-1}^{n-1} F_{3,j-1}^n) \right\} \right] \quad (14.b) \end{aligned}$$

$$(S_1)_j = \frac{1}{h_j Re^*} \left\{ b_j^n R_j \right\} + \frac{\alpha_1}{2} F_{1,j}^n - \frac{\alpha}{2} F_{1,j}^{n-1} \quad (14.c)$$

$$(S_2)_j = \frac{1}{h_j Re^*} \left\{ -b_{j-1}^n R_{j-1} \right\} + \frac{\alpha_1}{2} F_{1,j-1}^n - \frac{\alpha}{2} F_{1,j-1}^{n-1} \quad (14.d)$$

$$(S_3)_j = \frac{\alpha_1}{2} F_{3j}^n + \frac{\alpha}{2} F_{3j}^{n-1} \quad (14.e)$$

$$(S_4)_j = \frac{\alpha_1}{2} F_{3j-1}^n + \frac{\alpha}{2} F_{3j-1}^{n-1} \quad (14.f)$$

$$(S_5)_j = \alpha_2 F_{2j}^n R_j \quad (14.g)$$

$$(S_6)_j = \alpha_2 F_{2j-1}^n R_{j-1} \quad (14.h)$$

$$R_{j-\frac{1}{2}}^{n-1} = \alpha \left\{ (F_3 F_1)_{j-\frac{1}{2}}^{n-1} - (F_2 R)_{j-\frac{1}{2}}^{n-1} \right\} - L_{j-\frac{1}{2}}^{n-1} \quad (14.i)$$

$$L_{j-\frac{1}{2}}^{n-1} = \left[\frac{1}{h_j \text{Re}^*} \left\{ (b R F_3)_j^{n-1} - (b R F_3)_{j-1}^{n-1} \right\} + (F_3 F_1)_{j-\frac{1}{2}}^{n-1} + (F_2^2 R)_{j-\frac{1}{2}}^{n-1} \right] \quad (14.j)$$

$$\alpha = \frac{1}{2K_n} \left\{ Z^n + Z^{n-1} \right\} \quad (14.k)$$

$$\alpha_1 = 1 + \alpha \quad (14.l)$$

$$\alpha_2 = 1 - \alpha \quad (14.m)$$

Boundary conditions: At $R = 0$, $F_1 = 0$, $F_3 = 0$

At R Large, $F_2 = 0$

The finite-difference equations and boundary conditions were implemented as modifications to the code of Cebeci and Bradshaw. Additional modifications were made to the input and output routines to make them consistent with the required data for the jet.

V. Verification of the Modified Computer Code

The modified computer code was installed on a mainframe computer and exercised to verify that the code was performing correctly. Both a laminar

jet and a turbulent jet were evaluated. The results of these evaluations are discussed below.

Note that for the laminar jet, the growth rate of the jet, as indicated by the coefficient C_1 , decreases as the momentum of the jet increases (see equations (8.e) and (9)). As the momentum of the jet, and thus the Reynolds number increase, the jet becomes turbulent. The transition Reynolds number was calculated by substitution of the turbulent value of C_1 into the turbulent similarity solution for C_0 and setting the eddy viscosity to zero⁵. Solving through yields a Reynolds number of 70 at the transition from laminar to turbulent flow.

The laminar jet was taken to have a Reynolds number (as defined below) of approximately 70.

$$R_j = \frac{w(2r_0)}{v} = 70 \quad (15)$$

The computed results at approximately 50 nozzle diameters downstream of the nozzle are compared to the similarity solution in Figure 1. The comparison indicates that the computed results for laminar flow are consistent with those predicted on the basis of similarity far downstream.

The turbulent jet was taken to have a Reynolds number of 43×10^5 . Additionally, a constant value of eddy viscosity was assumed for the purpose of comparing the computed results to those predicted by similarity. The computed results at approximately 50 nozzle diameters downstream of the nozzle are compared to the similarity solution in Figure 2. As shown, the comparison indicates that the computed results for turbulent flow are also consistent with the those predicted on the basis of similarity far downstream.

The results of the comparisons of the computed results to the similarity solution for both turbulent and laminar jets indicate that the modified code is yielding reasonable results. This provides confidence that the changes to the code were implemented correctly.

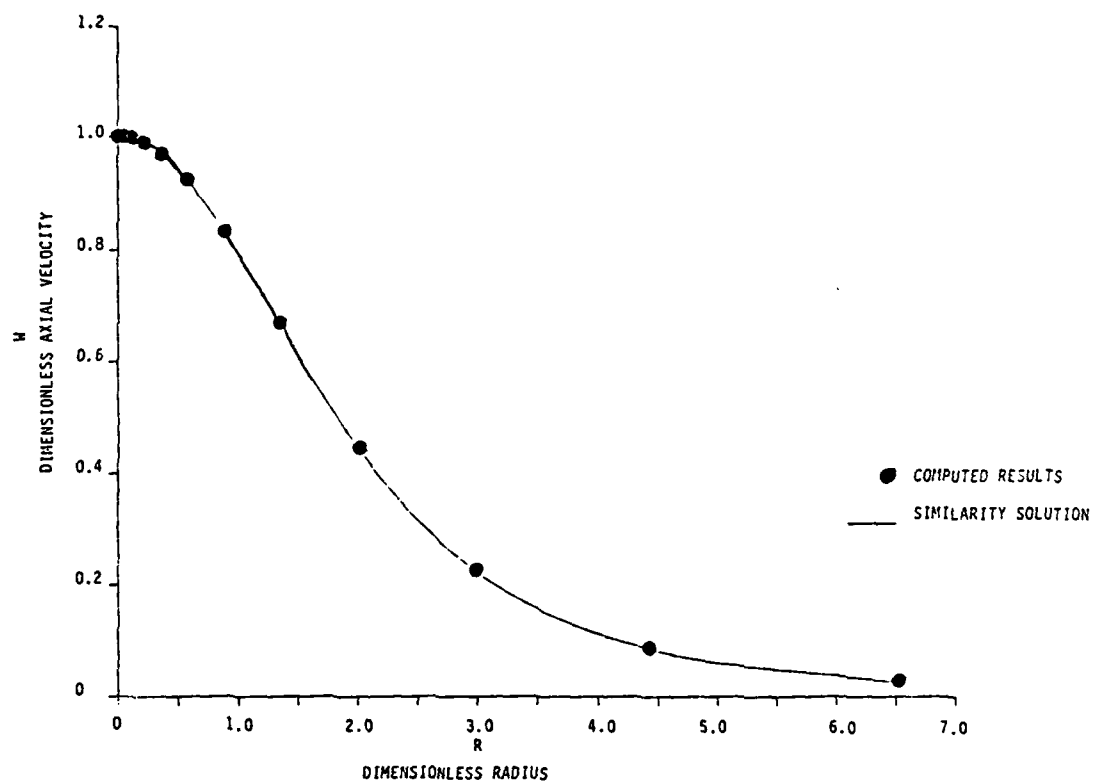
VI. Recommendations

The modified code is intended as a tool for use in the evaluation of various turbulence models. More specifically, the modified code is intended to be used in conjunction with the various turbulence models, and the computed results are to be used for correlation with test data to determine which turbulence models best predict phenomena which effect the optical properties of the jet medium. Therefore, it is recommended that further use of this code be made to evaluate turbulence models. The models which show the greatest promise of predicting aero-optical interaction, and which should be evaluated with the modified code are:

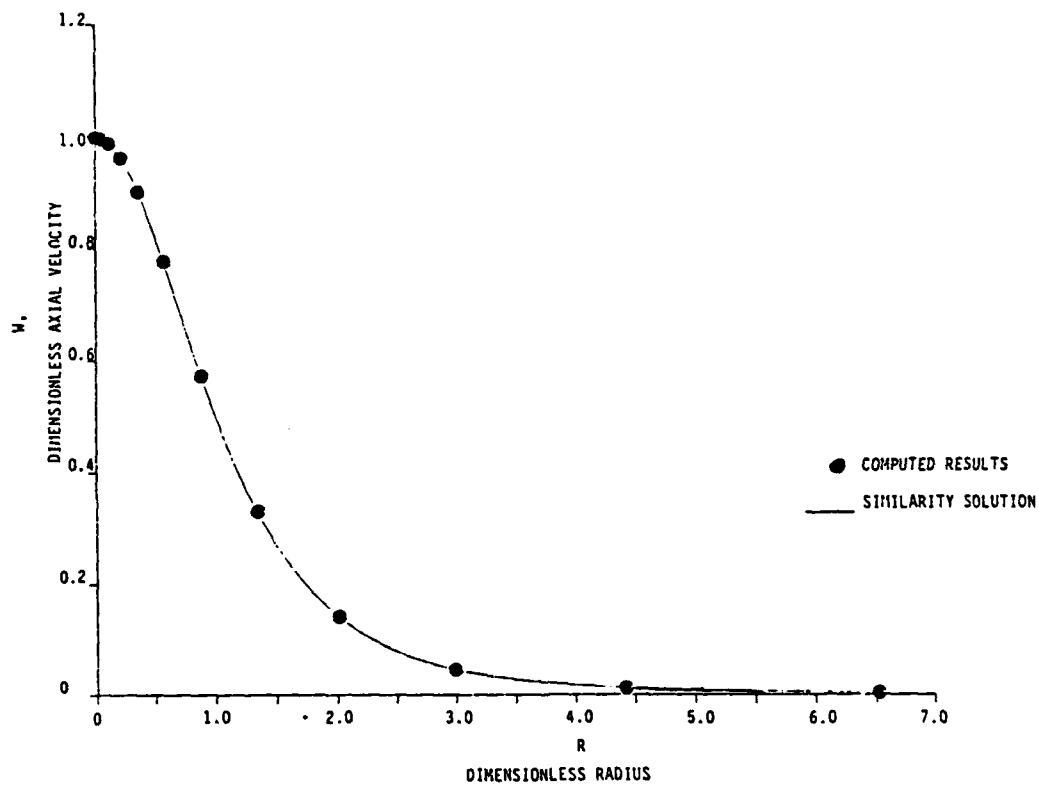
1. a two-equation, turbulent kinetic energy-rate of dissipation model with multiple time scales^{9,10} and
2. a Reynolds stress transport model^{11,12,13}.

ACKNOWLEDGMENTS

I would like to thank the Air Force Office of Scientific Research for Sponsorship of my research, and the Air Force Weapons Laboratory for their support. In particular, I would like to thank Dr. Bruce Masson, Captain Martin Trout, Captain Steve Rinaldi and Captain Rich Charles for their technical support and guidance. In addition, I would like to thank Professor Truman of the University of New Mexico for his guidance and insight.



LAMINAR JET VELOCITY PROFILE
AT 50 DIAMETERS DOWNSTREAM
OF NOZZLE
FIGURE 1



TURBULENT JET VELOCITY PROFILE
AT 50 DIAMETERS DOWNSTREAM
OF NOZZLE

FIGURE 2

REFERENCES

1. Cebeci, T. and P. Bradshaw, Momentum Transfer in Boundary Layers, Hemisphere Publishing Corporation, Washington, 1977, Appendices 7A and 8A, pp. 223-231, 259-271.
2. Bradshaw, P., T. Cebeci and J.H. Whitelaw, Engineering Calculation Methods for Turbulent Flow, Academic Press, 1981, p. 88.
3. White, F.M., Viscous Fluid Flow, McGraw-Hill Book Company, New York, 1974, Appendix B, p. 672.
4. Cebeci and Bradshaw, p. 159.
5. Cebeci and Bradshaw, pp. 204-205.
6. Wood, P.E. and L.G. Leal, "Similarity Solutions of Free Shear Flows with Mean Reynolds Stress Turbulence Models," Numerical Heat Transfer, Vol. 6, 1983, pp. 235-244.
7. Cebeci and Bradshaw, pp. 214-218.
8. Schetz, J.A., Foundations of Boundary Layer Theory for Momentum, Heat and Mass Transfer, Prentice-Hall, Inc., New Jersey, 1984, pp. 220-254.
9. Wilcox, D.C., Multiscale Model for Turbulent Flows, AIAA-86-0029, presented January 1986, Reno, Nevada.
10. Hanjalic, K., B.E. Launder and R. Schiestel, "Multiple-Time-Scale Concepts in Turbulent Transport Modelling," Turbulent Shear Flows - 2, Springer-Verlag, New York, 1980, pp. 36-49.
11. Vandromme, D. and W. Kollmann, "Second Order Closure for Variable Density Free Shear Layer," Turbulent Shear Flows - 3, Springer-Verlag, New York, 1982, pp. 275-290.
12. Janicka, J. and J.L. Lumley, "Second-Order Modelling in Non-Constant Density Flows," FDA-81-01, Sibley School of Mechanical and Aerospace Engineering, Cornell University, Ithaca, New York, January 1981.

1986 USAF--UES SUMMER FACULTY RESEARCH PROGRAM/

GRADUATE STUDENT SUMMER SUPPORT PROGRAM

Sponsored by the

AIR FORCE OFFICE OF SCIENTIFIC RESEARCH

Conducted by the

UNIVERSAL ENERGY SYSTEMS , INC.

FINAL REPORT

**MESOPIC VISUAL FUNCTION
IN AIRCREW**

Prepared by:	Otis Cosby , Jr.
Academic Rank:	Sophomore Medical Student
Department and	The Medical School of
University:	Meharry Medical College
Research Location:	Aerospace Vision Lab, Ophthalmology Branch, Division of Clinical Scien- ces, School of Aerospace Medicine
USAF Research:	Lt. Colonel Robert E. Miller
Date:	September 20, 1986
Contract Number:	F49620-85-C-0013

MESOPIC VISUAL FUNCTION IN AIRCREW

by

Otis Cosby, Jr.

ABSTRACT

Mesopic vision may prove to be a more important component of the visual system during USAF night missions than scotopic vision. Ninety aircrew members were tested using the Nyktometer (mesopic vision tester) under mesopic conditions, both with and without glare. The subjects were placed into one of three age categories: 1) Less than 29, 2) 30-39, 3) 40 and above. There appeared to be a weak correlation between age and Nyktometer performance.

ACKNOWLEDGEMENT

First, I would like to thank the Air Force Systems Command, Air Force Office of Scientific Research, and Universal Energy Systems for their sponsorship and conduct-ion of the program and allowing me to have the opportunity to return as a summer fellow.

I wish to express my appreciation for the help and the guidance that Lt.Colonel Robert Miller offered to me as serving as my preceptor. It was again a pleasure to work with him and his staff in the Aerospace Vision Lab.

Special thanks go to Colonel Thomas Tredici, the staff of the Ophthalmology Branch, and Mr. Billy Jackson for their assistance with this project.

1. INTRODUCTION

I would like to make a few comments on my particular abilities and what led me to work in the area of vision research.

I developed an interest in the medical field in high school. Upon graduation, I entered Towson State University where I received a bachelor's degree in the natural sciences. During this period, I spent countless hours of volunteer work at The Johns Hopkins Hospital and served as president of the hospital's Medical Explorers Post for three years. In addition, I participated in a summer enrichment program for pre-medical students at the University of Maryland before entering the medical school of Meharry Medical College (which I am attending now).

Because of my lack of research exposure prior to going to medical school, I decided to explore the opportunities available at Meharry. After talking to professors and visiting both basic and clinical laboratories on campus, I became enthused with the projects underway in the Department of Pediatrics. This led to my present assignment, activation and deactivation of the enzyme glutathione-S-transferase, which involves investigative work during the academic school year.

Later, I was informed by Dr. James Mrotek (associate professor of physiology) who has spent several summers of research at Brooks Air Force Base, about the Graduate Student Summer Support Program. With his assistance, I was able to procure a position proved to be an invaluable experience since I plan to pursue a career in ophthalmology.

And now that I was able to receive a second appointment in this exciting program, I further strengthened my knowledge base and abilities to conduct a research project successfully.

II. OBJECTIVES OF THE RESEARCH EFFORT

- 1) To prepare the data collected from the Nyktometer studies for the statistician.
- 2) To take the results obtained by the statistician and express them in graphical form.
- 3) To prepare a paper for publication, including the introduction, methods, and results.

III. INTRODUCTION TO NIGHT VISION

Let's discuss some of the basic principles involved in night vision.

Night vision (or scotopic vision) differs in a number of ways from day vision (or photopic vision). The retina of the eye contains photoreceptors, namely rods and cones, which are responsible for receiving light stimuli and in turn generating nerve impulses which are carried to the brain and interpreted as visual images. Rods tend to be activated in the presence of low illumination (night vision), whereas cones are more active in high illumination (day vision). However, both rods and cones play an important role during conditions of moderate illumination, and this is referred to as mesopic vision. Because of the type of photoreceptor involved, scotopic vision is not sensitive to colors, but all colors will be seen as shades of gray. In photopic vision, colors can be recognized and visual acuity is much greater. In addition, dark adaptation

time (which is the time required for eye adjustment at low illumination) in scotopic vision is longer (about 30 minutes) than that required in photopic or mesopic vision (between five to ten minutes). Hence, these and other parameters make night vision a distinct and unique part of the overall visual process.

IV. THE NYKTOMETER

The basis of my study on night vision focused on the reliability of the German-made instrument, the Rodenstock Nyktometer, as a tool for assessing night vision (or mesopic vision) in aircraft pilots.

The Nyktometer has several key features. A screen is provided to prevent the entry of ambient light. This allows for suitable testing even in a room that is moderately illuminated. Equipped with a deviating mirror, the Nyktometer is able to project light from the illumination source onto the 3° test field of a test type carrier (two types are available), the background luminance being .032cd/m² (.01mL) without glare and 0.1cd/m² (.03mL) with glare. These test type carriers have 12 different levels of contrast each, six with glare and six without glare. Positions one through six correspond to contrast values of .96, .79, .63, .50, .40, and .32, respectively. In addition, minus lenses may be inserted if twilight myopia is suspected, and the aiming optics of the Nyktometer allows the patient to view the test types at a distance of four (4) meters.

Other features include its ability to be easily transported and its capability of testing both monocular and binocular

vision.

Ninety flyers were tested in my study. First, they were allowed to dark adapt for five minutes. Then they were asked to indicate the directions of the key hole (which correspond to the 12 positions of the test type carrier) according to clock hours. This was done for both monocular and binocular vision. Those flyers who normally wore glasses were asked to wear them during the testing. None of these flyers had a diagnosed pathological eye condition, nor were their pupils dilated just prior to the experiment.

V. RESULTS OF THE EXPERIMENT

The participants in this project consisted of a random sample of flyers who were referred to the ophthalmology branch of Brooks Air Force Base for a routine eye examination. The subjects were placed into one of three age categories: 1) Less than 29, 2) 30-39, 3) 40 and above. The age range was from 21 to 64. Approximately 30 subjects were in each group. The visual acuity for both near and far vision averaged about 20/20.

The results from the Nyktometer were recorded according to the number of correct responses from the total number attempted (both monocularly and binocularly). Also, data was recorded separately for the positions on the test type carrier without glare (positions one to six) and with glare (positions seven to twelve). For the Less than 29 age group, the mean correct number of responses was 5.2 (standard deviation -1.2) for no glare and

with glare was 3.6 (s.d.-1.4). The 30 to 39 age group had a mean of 5.1 for no glare (s.d.-1.0) and 3.2 (s.d.-1.6) for with glare. The average number of correct responses for the 40 and above age group was 5.0 (s.d.-1.1) for no glare and 2.4 (s.d.-1.8) for with glare. Thus, there is no significant difference in the mean number of correct responses among the groups.

Most of the subjects did better when they viewed the keyhole binocularly, rather than monocularly.

VI. RECOMMENDATIONS

With a statistical analysis of the data collected a baseline could be established which would serve as an aid in further Nyktometer studies. In our study, we were mainly concerned with the relationship between age and Nyktometer performance; however, we also looked at the effects of the total number of flying hours, rating (e.g. if the subject were a pilot, navigator, or other), and visual acuity. These and other variables may require further study in order to evaluate the potential use of the Nyktometer by the USAF.

Because of our time limitations, some of the goals that we originally established could not be fulfilled; but an extensive computer analysis will be done, and hopefully a publication on this work will be forthcoming.

REFERENCES

1. Sagawa, K., Takeichi, K., "Spectral luminous efficiency functions in the mesopic range", Journal of Optical Society of America, 3, January, 1986, pp.71-75.
2. Tredici, T. J., "Scotopic Vision," USAF School of Aerospace Medicine, Brooks AFB, Texas, 1984.
3. "Rodenstock Nyktometer", a pamphlet supplied with the Nyktometer, undated.

1986 USAF-UES SUMMER FACULTY RESEARCH PROGRAM/
GRADUATE STUDENT SUMMER SUPPORT PROGRAM

Sponsored by the
AIR FORCE OFFICE OF SCIENTIFIC RESEARCH

Conducted by the
Universal Energy Systems, Inc.

FINAL REPORT

MATHEMATICAL CLASSIFICATION OF A FAMILY OF EDGE DETECTORS

Prepared by:	Jennifer L. Davidson
Academic Rank:	Graduate Student
Department and University:	University of Florida Department of Mathematics
Research Location:	Air Force Armament Laboratory, Eglin AFB Advanced Seeker Division Electro-Optical Terminal Guidance Branch
USAF Researcher:	Mr. Neal Urquhart
Date:	August 8, 1986
Contract No:	F49620-85-C-0013

A MATHEMATICAL CLASSIFICATION OF A FAMILY OF EDGE DETECTORS

Jennifer L. Davidson

ABSTRACT

A mathematical classification of a family of edge detectors is presented. The nine edge detectors under consideration are of the enhancement/threshold type. Edge detection is an important part of the image processing sequence, as it is a heavily used segmentation routine. Presently there does not exist a classification scheme which completely accounts for the behavior of all existing edge detection techniques. This report defines two types of edge "enhancers," using the structure of the Image Algebra in which to embed the definition. The classification depends on the two distinct parts of every edge detector: the masks, and the function of the image and the masks. Eight of the edge detectors could be classified as one of the two enhancers, while the logarithmic edge detector was left unclassified. The Image Algebra was used as it is capable of expressing all image to image transformations and can be used as a general purpose algebra for presenting image processing concepts. Determination of criterion and image measures for optimizing edge detection using the enhancer definition is discussed, and suggestions for further research are given. The principle behind classifying edge detectors and using the classification to specify and evaluate image measures is to develop a method which in principle could be implemented in an automated target recognition (ATR) system.

I. BACKGROUND. Jennifer L. Davidson is currently pursuing her Ph.D in Applied Mathematics at the University of Florida. She received her M.S. in Mathematics in May, 1986. She has worked in the area of image processing since the summer of 1984, when she participated in the Graduate Student Summer Support Program at Eglin AFB, Florida, working in the Image Processing Laboratory. Her course work at the University of Florida includes complex analysis, numerical methods, statistics, and image processing.

II. INTRODUCTION. Solutions of the problem of automatic target recognition (ATR) is of obvious importance in a variety of military applications. A general approach in modeling the ATR system is to first segment the image into regions, attach previously defined labels to the regions, determine a list of relations between the regions, and deduce from that list the target or object of interest. Figure 1 gives a flowchart of this approach.

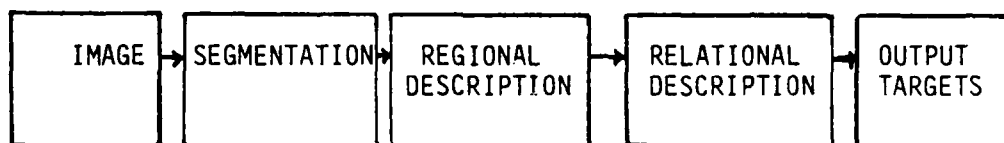


Figure 1.

Segmentation is an important first step. The information extracted here is passed on to successive steps in the processing sequence, and how much or how little gets passed on is determined by the segmentation algorithm. Many types of segmentation techniques exist, one of which is edge-based segmentation. This technique is a collection of algorithms which locates boundaries of objects in the image. After a collection of boundary or edge

points are chosen, a thinning algorithm can be applied to narrow the edge width as desired, usually to one or two pixels. Then a linking technique which links disconnected edges together is often applied. These linked edges are the output of the edge segmentation scheme. Since this is the initial stage of the processing, it is crucial that the boundaries output from the segmentation algorithm be as close as possible to the true boundaries that exist in the image, so the maximum amount of exact information is passed on to successive steps in the processing. Thus an accurate edge-segmentation algorithm is an essential block of the processing scheme.

There are of course other edge-segmentation techniques [7]. In [5] there is a discussion on image recognition systems, of which (edge) segmentation is a part. The purpose of this paper is to discuss one part of the edge segmentation algorithm: determination of the edge points.

Methods of edge detection can be divided into two main categories: 1) the edge fitting method; and 2) the enhancement/thresholding method [7]. Edge detection methods of type (2) were the only ones investigated mainly because of the 10-week time restriction. The Heuckel detector is the main edge-fitting detector used in the field. It is complicated to code, and has serious shortcomings [1]. Thus it was decided to omit the study of these types of detectors.

Although there does not exist a standard definition of an "edge" in the literature, the basic concept of an edge which is used in design of edge detectors is fairly uniform. One model uses a step function, and the edge point occurs where the discontinuity of the function is located. Another model uses a ramp function, with the edge point most often occurring at the base of the ramp [2] See Figure 2, solid lines. There are variations of these models, indicated by the dotted lines in Figure 2.

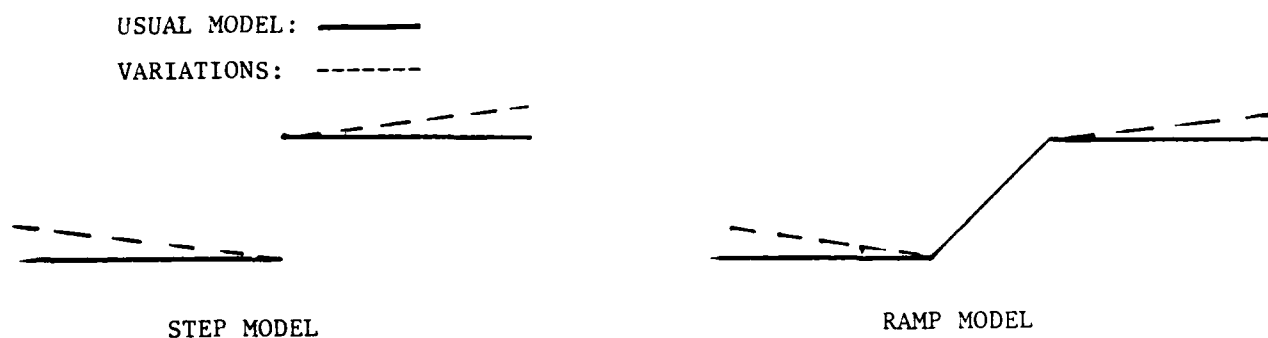


Figure 2.

However, for the purposes of digital image processing, the distinction between these models become irrelevant. This is because the purpose of an edge detector is to detect and characterize intensity variations of a significant nature in a neighborhood of a pixel p , and the discrete nature of the surface in a neighborhood of p allows either model to be used with equivalent results.

There are different ways to characterize variations in magnitude of a collection of pixels in a neighborhood of p , which depend both on the masks used and the mathematical function of the masks and the image. A rigorous definition of an edge detector was constructed using a two-part approach. This is discussed in section VI.

III. Research Objectives. The research done this summer is concerned with the first step of edge segmentation, that is, determination of edge points. A good edge detector reduces the need for complicated thinning and linking algorithms, so there is strong motivation to use the best edge detector for the job. The primary goal of this research effort was to define an edge detector in mathematically rigorous terms and express several of the more popular edge detection techniques presently used in image processing in

terms of this definition. A second goal was to develop criterion and measures of an image such that if an image measure satisfied certain criterion then certain edge detectors would be more useful than others on all images with that image measure. The definition of the edge detector would be used in determining and evaluating these criterion and measures. However, the second goal was not researched in great depth, and a total lack of articles in the literature on this subject indicates that this area needs to be investigated in much more detail. The edge detection techniques were also translated into the Image Algebra in order to facilitate the investigation into the properties of each technique. The edge detectors investigated were:

1. Sobel
2. Prewitt
3. Roberts'
4. Kirsch
5. Gradient
6. $\nabla^2 G$, Laplacian of the gaussian
7. $\frac{\partial^2 f}{\partial n^2}$, the second directional derivative in the direction of the gradient
8. logarithmic edge detector
9. a geometric edge detector

IV. The Edge Detection Techniques. This section gives a brief discussion of the edge detectors and their formulation in the Image Algebra. The two template operators from the Image Algebra used are $+$ and \vee , which are defined as follows:

$$A \oplus T = \{(x, c(x)) : c(x) = \sum_{y \in \mathcal{N}(x)} a(y) t_x(y) \text{ , } x \in X \}$$

$$A \otimes T = \{(x, c(x)) : c(x) = \bigvee_{y \in \gamma(x)} a(y) t_x(y), x \in X\}$$

1. Sobel. $E(A) = [(A \oplus S)^2 + (A \oplus T)^2]^{\frac{1}{2}}$ where

$$S(x) = \begin{bmatrix} -1 & 0 & 1 \\ -2 & 0 & 2 \\ -1 & 0 & 1 \end{bmatrix}$$

$$T(x) = \begin{bmatrix} -1 & -2 & -1 \\ 0 & 0 & 0 \\ 1 & 2 & 1 \end{bmatrix}$$

2. Prewitt. $E(A) = [(A \oplus S)^2 + (A \oplus T)^2]^{\frac{1}{2}}$ where

$$S(x) = \begin{bmatrix} -1 & 0 & 1 \\ -1 & 0 & 1 \\ -1 & 0 & 1 \end{bmatrix}$$

$$T(x) = \begin{bmatrix} -1 & -1 & -1 \\ 0 & 0 & 0 \\ 1 & 1 & 1 \end{bmatrix}$$

3. Roberts'. $E(A) = [(A \oplus S)^2 + (A \oplus T)^2]^{\frac{1}{2}}$ where

$$S(x) = \begin{bmatrix} -1 & 0 \\ 0 & 1 \end{bmatrix}$$

$$T(x) = \begin{bmatrix} 0 & -1 \\ 1 & 0 \end{bmatrix}$$

4. Kirsch. $E(A) = \bigvee_{i=1}^8 |A \oplus T_i|$, where

$$T_1(x) = \begin{bmatrix} -3 & 5 & 5 \\ -3 & 0 & 5 \\ -3 & -3 & -3 \end{bmatrix}$$

$$T_2(x) = \begin{bmatrix} 5 & 5 & 5 \\ -3 & 0 & -3 \\ -3 & -3 & -3 \end{bmatrix}, \text{etc.}$$

5. Gradient.

Define $f: R \rightarrow R^2$ by $f(r) = (|r|, 180\chi_{<0}(r))$, χ being the characteristic function. Let $A(i) = (0, \theta(i)) + f(A \oplus M(i))$, $i=1, \dots, 6$, where $M(i)$ are the masks as below, and $\theta(i)$ are the degrees associated with $M(i)$. Then $E(A) = \bigvee_{i=1}^6 A(i)$. The gradient is the only edge detector in this report

which associates two values with every pixel: an edge magnitude and an edge direction. Each $M(i)$ approximates the gradient in one of twelve directions, the direction being $\theta(i)$ or $\theta(i)+180 \pmod{360}$ degrees, depending on whether the magnitude is positive or negative, respectively.

M(1)-M(6)

1	1	1
0	0	0
-1	-1	-1

180°

-1	0	1
-1	0	1
-1	0	1

90°

-7	.8	1
-1	0	1
-1	-8	7

120°

.7	1	1
-.8	0	.8
-1	-1	-.7

150°

1	1	7
8	0	-.8
-.7	-1	-1

210°

1	.8	-.7
1	0	-1
.7	-.8	-1

240°

The next two detectors, $\nabla^2 G$ and $\frac{\partial^2}{\partial n^2}$ have the same basic theory behind them: Where the rate of change of magnitude is the greatest is where the first derivative has a maximum. Where the first derivative has a maximum is where the second derivative is zero. Thus, the zeros of these two detectors are where edges are located.

6. $\nabla^2 G$. This is the Laplacian of an image which has been convolved with a Gaussian distribution. The detector is formulated in the continuous case but is easily discretized.

$$\nabla^2 (G(s,t) \otimes A(s,t)) = \int_{-\infty}^{\infty} \int_{-\infty}^{\infty} \frac{1}{\pi \sigma^4} \left[1 - \frac{(x^2 + y^2)}{2\sigma^2} \right] e^{-\frac{(x^2 + y^2)}{2\sigma^2}} a(x-s, y-t) dx dy$$

The Image Algebra code is:

$E(A) = A \oplus H$, where H is a translation invariant template defined by:

$$A(x) = X; H(x) = \{(i,j,h(i,j)) : h(i,j) = \frac{1}{\pi \sigma^4} \left[1 - \frac{i^2 + j^2}{2\sigma^2} \right] e^{-\frac{(i^2 + j^2)}{2\sigma^2}}, x \rightarrow (i,j) \in X\}$$

7. $\frac{\partial^2}{\partial n^2}$. This is the second directional derivative in the direction of the gradient. It also is presented in the continuous form:

$$\frac{\partial^2 f}{\partial n^2} = \frac{f_x^2 f_{xx} + 2f_x f_y f_{xy} + f_y^2 f_{yy}}{f_x^2 + f_y^2}$$

Using approximations for the partials gives the discrete form of this detector. For example, if

$$T(x) = \begin{bmatrix} 1 & 2 & 1 \end{bmatrix}$$

$$Z(x) = \begin{bmatrix} -1 & 0 & 1 \\ 0 & 0 & 0 \\ 1 & 0 & -1 \end{bmatrix}$$

$$S(x) = \begin{bmatrix} 1 \\ 2 \\ 1 \end{bmatrix}$$

$$U(x) = \begin{bmatrix} -1 & 0 & 1 \end{bmatrix} \quad W(x) = \begin{bmatrix} -1 \\ 0 \\ 1 \end{bmatrix}$$

$$\text{then } E(A) = \frac{(A + U)^2 (A + T) + 2(A + U)(A + W)(A + Z) + (A + W)^2 (A + S)}{(A + U)^2 + (A + W)^2}$$

The last two detectors are different in structure from the previous seven:

8. Logarithmic. $E(A) = \ln(A) - \left[\left(\frac{1}{4} \ln(A) \right) \oplus T \right]$, where $T(x) = \begin{bmatrix} & 1 & \\ 1 & 0 & 1 \\ & 1 & \end{bmatrix}$

9. Geometric [8]. $E(A) = [(A \oslash T - A \oslash S)^2 + (A \oslash U - A \oslash W)^2]^{1/2}$

$$T(x) = \begin{bmatrix} 2 & 1 & 2 \end{bmatrix}$$

$$S(x) = \begin{bmatrix} 1 & 2 & 1 \end{bmatrix}$$

$$U(x) = \begin{bmatrix} 2 \\ 1 \\ 2 \end{bmatrix}$$

$$W(x) = \begin{bmatrix} 1 \\ 2 \\ 1 \end{bmatrix}$$

V. The Edge Detector Definition. The definition consists of two parts, a template definition and an operator definition. Since all image-to-image transforms, including edge detection techniques, can be expressed in the Image Algebra, it was decided to use the Image Algebra as a means of writing the definition of an edge detector. It also facilitates the writing of mathematical properties as the notation is succinct and expresses the operations clearly with much less writing.

Definition. A differential edge mask or differential edge template with respect to the convolution operator \oplus is a template T satisfying:

1. $A \oplus T = 0$ for a constant image A .

$$2. (kA) \oplus T = k(A \oplus T)$$

$$3. (A + B) \oplus T = A \oplus T + B \oplus T$$

Note that it immediately follows from 1 and 3 that $(K + A) \oplus T = A \oplus T$ for any constant image K .

Definition. A differential edge operator is a function $E: R^X \rightarrow R^X$ such that

1. $E(A) = 0$ if A is a constant image
2. $E(kA) = kE(A)$, $k \geq 0$
3. $E(K + A) = E(A)$, K a constant image

The majority of the edge detectors investigated during this research were differential edge operators having differential edge masks. Two of the detectors, however, were different in their basic structures: the logarithmic and the geometric. The following definition distinguishes this difference for the geometric detector.

Definition. A template T is an edge mask with respect to the convolution operator \otimes , or simply, a lattice edge mask, if T satisfies:

1. $T \geq 0$
2. $(kA) \otimes T = k(A \otimes T)$, for A, T , $k \geq 0$
3. $(A + B) \otimes T \leq A \otimes T + B \otimes T$, $A, B, T \geq 0$

Remark: Note that $(K + A) \otimes T = k(I \otimes T) + A \otimes T$ where $I = \{(x,1): x \in X\}$.

The geometric edge detector is a differential edge operator with a lattice edge mask. That it is a differential operator is not obvious. Upon checking the 3 operator conditions above, it is found that the geometric detector does satisfy them all. Henceforth a differential edge

operator with differential edge templates will be called a differential edge enhancer. A differential edge operator with lattice edge templates will be called a lattice edge enhancer. The geometric edge detector is the only lattice edge enhancer presented here; all the others are differential edge enhancers except for the log edge detector.

The log operator does not fit any of the above definitions. The world is not so nice as to make all detectors quickly classifiable. This edge detector has a mask which satisfies only two parts of the mask definition, and one part of the differential operator. What differential mask properties it satisfies are:

1. $(kA) \oplus T = k(A \oplus T)$
2. $(A + B) \oplus T = A \oplus T + B \oplus T$

The operator properties it satisfies are:

1. $E(A) = 0$, A a constant image
2. $E(kA) = E(A)$, $k \geq 0$

At this point a few things can be mentioned. The first seven edge detectors are algebraic function; the log edge detector involves a transcendental function, the logarithm. The geometric detector uses a lattice operation. Thus, it is reasonable to believe that the following conjecture is true:

Conjecture. Let $T(1), \dots, T(n)$ be n edge templates of either type, differential or lattice. Suppose that $E(T(1), \dots, T(n))$ is an Image Algebra transform involving only $\oplus, \otimes, +, \vee, **, *$ and algebraic operations. Then E is a differential edge enhancer.

All the edge detectors studied this summer exemplify this conjecture. If this conjecture is true, then it is a good classification of a type of image operators. That needs to be investigated more thoroughly.

A table of properties of the edge templates and operators is given on the following page. It also lists what type of edge template and edge enhancer each edge detector technique is.

VI. History of Previous Research. There has been much research done on edge detectors [1], [2], [3], [4], [5], [6], [7], [9]. In Pattern Recognition and Scene Analysis Duda gives a brief but clear discussion on edge detection. In a recent article, "On Edge Detection," [9], edge detection is approached from the aspect of numerical differentiation. In the context of this summer's research, Torre and Poggio's work shows that if the edge operator E is a differential edge enhancer, then looking for edges using E requires a smoothing of the image with a Gaussian prior to edge detection. The next paragraph is a short discussion on this topic.

Numerical differentiation is well-known to be an inverse problem. We are looking for a solution $f(x)$ in $g(x) = Af(x)$ where Af is the integral operator

$$\int_{-\infty}^x f(z) dz = \int_{-\infty}^{\infty} u(x-z) f(z) dz$$

$u(x)$ = unit step function. If we are given the data points $g(x)$, and we could determine $f(x)$, then $\frac{d}{dx}g(x) = f(x)$, thus solving our problem of finding the derivative. In Torre's paper, it is shown that numerical differentiation is an ill-posed problem in the sense of Hadamard, and that the problem can be transformed to a well-posed problem, that is, regularized, by convolving the data with a cubic spline. Since the Gaussian distribution is very similar to a cubic spline, this explains in part why filtering with a Gaussian is successful prior to application of an edge detector [9], [6].

However, not all edge detectors can be classified in terms of a

<div> <div>DETECTOR</div> <div>PROPERTY</div> </div>	SOBEL	PREWITT	ROBERTS	KIRSCH	GRADIENT	$\nabla^2 G$	$\frac{\delta^2}{\delta n^2}$	LOG	GEOMETRIC
EDGE MASK OPERATION	+	+	+	+	+	+	+	+	v
*****	*****	*****	*****	*****	*****	*****	*****	*****	*****
$A \oplus T = 0$	X	X	X	X	X	X	X		
$(kA) \oplus T = k(A \oplus T)$	X	X	X	X	X	X	X	X	
$(A + B) \oplus T = A \oplus T + B \oplus T$	X	X	X	X	X	X	X	X	
*****	*****	*****	*****	*****	*****	*****	*****	*****	*****
$T \geq 0$									X
$(kA) \otimes T = k(A \otimes T)$									X
$(A + B) \otimes T \leq A \otimes T + B \otimes T$									X
*****	*****	*****	*****	*****	*****	*****	*****	*****	*****
$A \text{ const} = E(A) = 0$	X	X	X	X	X	X	X	X	X
$E(kA) = kE(A)$	X	X	X	X	X	X	X		X
$E(K + A) = E(A)$	X	X	X	X	X	X	X		X
*****	*****	*****	*****	*****	*****	*****	*****	*****	*****
EDGE TEMPLATE TYPE	DIFF	DIFF	DIFF	DIFF	DIFF	DIFF	DIFF		LATTICE
*****	*****	*****	*****	*****	*****	*****	*****	*****	*****
EDGE ENHANCER TYPE	DIFF	DIFF	DIFF	DIFF	DIFF	DIFF	DIFF		LATTICE

TABLE OF EDGE TEMPLATE AND EDGE OPERATOR PROPERTIES

partial differential operator or a discretization of one; for example the geometric, log, and rolling ball algorithms are not approximations to partial differential operators. Thus, viewing edge detection as a problem in numerical differentiation is not a complete representation of the problem of detecting edges. For the case of partial differential operators, Torre's work characterizes the problem of detection of edges, and gives one approach for "optimum" design of an edge operator. Marr and Hildreth [6] discuss edge detection entirely in the context of filtering with different Gaussian distributions and taking the Laplacian of the result to locate edges. It is shown in [3] that this particular edge detector does not detect certain types of edges ideally. In general, any given theory of edge detection does not give a satisfactory classification scheme for all existing edge detectors. A long-range goal is to construct a theory of edge detectors which is very general and can apply to any existing edge detector or any derived in the future.

VII. Recommendations. Implementation of most of these edge detectors has been accomplished using the Image Algebra Preprocessor available in the Image Processing Laboratory at Eglin, AFB. This saved much time in encoding the algorithms. In the case of the enhancers having differential edge templates, the differential edge enhancers, a smoothing filter such as a Gaussian convolution should be applied to the data prior to using the edge enhancer. However, it is still unclear whether a smoothing filter prior to edge detection is a valid procedure for the remaining two detectors, the logarithmic and geometric detectors. This is because the mask associated with each is not a differential edge template and thus the detector cannot be treated as a partial differential operator. This

too needs further investigation.

This summer's research has classified a certain type of image operators, namely, edge enhancement techniques. The edge templates and edge operators each preserve specific properties, and for each edge detector the effect of each property should be able to be quantized. This information could be used in determining image measures by which to select an edge operator that will give the most useful results.

Two avenues of research could provide very useful contributions: 1. investigation into surface complexity measures, and 2. investigation into statistical measures. To determine surface complexity measures, which measure the complexity of a surface, properties from differential geometry will be applied. Much pure mathematical research has been done in differential geometry, with very few applications in image processing. There has been much work on statistical measures of images but specific application to surface configuration will be consolidated.

These two measures, or a combination of them, could be used in classifying the surface complexity of an image, and correlations between these measures and the quantized effects of the properties of an edge detector might be able to be found. Since not much research has been done in this area, the results could be extremely beneficial not only to edge detection but to other areas of image processing.

ACKNOWLEDGEMENTS

The author would like to express her appreciation and gratitude to the Air Force Systems Command, the Air Force Office of Scientific Research, and Universal Energy Systems for providing the opportunity to spend a very educational and interesting summer at the Air Force Armament Laboratory, Eglin AFB, FL. In particular she would like to thank the staff of the Electro-Optical Terminal Guidance Branch of the Advanced Seeker Division. Their hospitality and support made this summer research a very pleasant experience. Special thanks are due Mr. Neal Urquhart for his support of this research project, and for his continued encouragement. Also, appreciation is extended to the Image Processing Lab personnel for their time and expertise in assisting with our inevitable problems with the computer.

VII. REFERENCES

1. Abdou, I., "Quantitative Methods of Edge Detection," Ph.D. thesis, Image Processing Institute, University of Southern California, 1978.
2. Abdou, I., and Pratt, W., "Quantitative Design and Evaluation of Enhancement/Thresholding Edge Detectors," Proc. IEEE, 67, No. 5, May 1979.
3. Berzins, V., "Accuracy of Laplacian Edge Detectors," Computer Vision, Graphics, and Image Processing, 27, 1984.
4. Duda, R. and Hart, P., Pattern Classification and Scene Analysis, Wiley-Interscience, NY, 1973.
5. Hall, E., Computer Image Processing and Recognition, Academic Press, NY 1979.
6. Marr, D. and Hildreth, E., "Theory of Edge Detection," Proc. R. Soc. Lond. B, 207, 1980.
7. Pratt, W., Digital Image Processing, Wiley-Interscience, NY, 1978.
8. Ritter et al., Program Review Meeting, University of Florida, July 1986.
9. Torre, V. and Poggio, T., "On Edge Detection," IEEE Trans. on PAMI, PAMI-8, No. 2, March 1986.

1985 USAF-UES Summer Faculty Research Program

Graduate Student Summer Support Program

Sponsored by the

Air Force Office of Scientific Research

Conducted by the

Universal Energy System, Inc.

Final Report

Design and Analysis of Models of

Large Space Structures

Prepared by:	Douglas W. DeHart
Academic Rank:	Teaching Assistant
Department and	Department of Engineering Mechanics
University:	University of Wisconsin - Madison
Research Location:	AF Rocket Propulsion Laboratory, DY58, Edwards AFB, CA
USAF Research:	2 Lt Tim Strange
Date:	11 September 1986
Contract No.:	F49620-85-C-0013

DEVELOPING ANALYSIS OF MODELS OF
LARGE SPACE STRUCTURES

by

Douglas W. Denhart

ABSTRACT

The first step in designing any large structure is to develop a model of the structure and test that model under simulated loading conditions. Much of the analysis of the models can be done using computer programs such as a finite element program which creates a finite element picture of the model and analyzes it when subjected to a variety of loading conditions. This is especially true for large space structures which cost a lot of money to build and to test in their natural environment. The main concern in designing large space structures is damping out internal vibrations which may cause severe deformations when the vibrations hit the natural frequencies of the structure. It is then essential to know what the natural frequencies of the structure are.

ACKNOWLEDGMENTS

I would like to thank the Air Force Systems Command, Air Force Office of Scientific Research, and the Rocket Propulsion Laboratory for their sponsorship of my research this summer. I would also like to thank the members of my division, DYSS, including 2lt Tim Strange, 1lt Eric Dale, 1lt Waid Schlaegel, Mr. Joe Hildreth and Dr. Alok Das for their help and support in my research. Also I would like to thank Mr. Kevin Slimak and Mr. Wayne Roe for their guidance.

I. Introduction

I have received my B.S. from the University of Wisconsin at Madison in Engineering Mechanics with emphasis in Aerospace Engineering. I have completed a year of work towards my M.S. degree in Engineering Mechanics. During that year I have taken numerous classes in the field of Aerospace Engineering particularly in the area of structures and dynamics. I also have some knowledge in the area of vibrations.

The particular research problem encountered at the Air Force Rocket Propulsion Laboratory was the design of a model of a generic large space structure, whether it be a space-based radar structure or a space-based laser structure. The model had to meet certain specifications as stated later in the report.

In order to design the model, they needed someone familiar with the design and analysis of structures and also someone familiar with the internal dynamics of large structures. With my background in Engineering Mechanics, I fit the qualifications.

II. Objective of the Research Effort

The objective of my research this summer was to design and analyze some models of large space structures. In order

to do so I had to do the following:

A. I first had to become acquainted with the main frame computer systems which I would be using to design and analyze the models. These computer systems were the VAX 750, the CDC and the PRIME.

B. Second, I had to learn how to use a computer modeling program to draw the structural models. This program was called PATRAN and was used on the PRIME system.

C. Third, I had to learn how to use a finite element program to analyze the models of the structures. This program was called NASTRAN and was used on either the CDC or the VAX 750 systems.

D. The fourth objective was a personal objective which was to learn about military life of an Air Force officer. This was important due to the fact that I am going on active duty around January 1987. I wanted to see what I probably would be doing on active duty.

III. Designing the Models

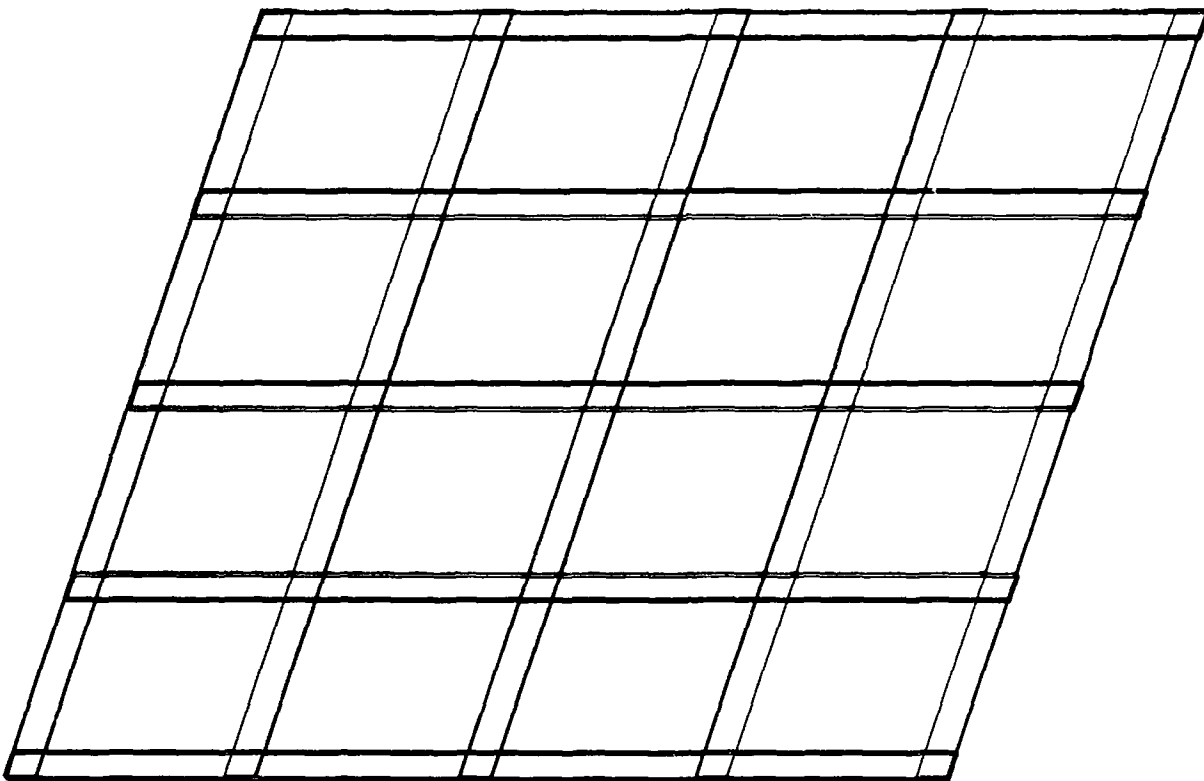
In order to design anything, one first needs to know what the object will be used for. This model that I designed is a generic model of a grid work for a large space structure. The structure could support a radar system or maybe a laser system. It might even be a part of a space station.

I was first given a list of certain specifications that the model had to fulfill. Some of these are:

- A. First natural frequency less the 1.0 hertz.
- B. Very stiff in the in-plane directions.
- C. Moderate stiffness in the out-of-plane directions.
- D. The displacement in the out-of-plane direction had to be between 1 and 2 inches.
- E. Since 24 sensors would be attached to the model to measure accelerations, the model's weight had to be high so the sensor/model weight ratio was low.
- F. The first 20 frequencies had to be less than 20 hertz.
- G. Finally the modal shapes for each eigenvector had to be significantly larger in the out-of-plane (z) direction compared to the in-plane (x,y) directions.

After I received the list of specifications, I had to learn how to run the computers in order to construct and analyze the structure. The first program that I learned was PATRAN. In using PATRAN I developed a computer drawing of what the grid structure would look like (see fig.1). Besides creating a computer drawing from PATRAN, I was also able to create NASTRAN data cards to run on the finite element program, NASTRAN.

My next step was to learn how to use NASTRAN. In the actual designing of the grid, I made a list of possible dimensions that probably could be used. For the material, I chose aluminum since it was fairly stiff and very light weight. For each of the possible dimensions on the list, I ran the NASTRAN program and received output from it (see



Y

X

Z

(Fig. 1)

table 1 and fig.2). From the data available, I chose grid structure number nine to be the actual grid. The first and main reason why I chose that particular structure was, for the first 25 mode shapes, the deflection in the z-direction was greater than the x or y directions for all except for number 18. This is crucial because the grid should be extremely stiff in the x and y directions and should not have large deflections.

The second reason is the first frequency fit into the range. The third reason is the weight of the structure is just large enough for the weight of the sensors not to affect the performance of the model, but not too large to make the structure too heavy to be realistic.

Attached is a listing of the first 120 frequencies of the grid and a copy of the coding program used to run NASTRAN.

IV. Designing Other Model

The second model designed is a prototype for a space-based radar system being constructed at the Jet Propulsion Laboratory. For this model I was given a rough drawing of what it should look like and some rough dimensions. The structure is 24 ft. in diameter, 12 ft. high and weighs 100 lbs. From this I created a computer drawing of the structure (see fig. 3). As I did with the grid structure, I created data cards along with the drawing.

Using these data cards, I created a NASTRAN program and

Table 1

GRID #	DIMENSIONS	WEIGHT	1ST FREQ	GENERALIZED STIFFNESS	EIGENVECTOR WHEN X OR Y > Z
1	1.5 X 0.25 (STIFFENED BARS) 1.0 X 0.125 (OTHER BARS)	14.11	0.30422	3.6538	12, 24
2	1.5 X 0.25 (STIFFENED BARS) 1.5 X 0.125 (OTHER BARS)	16.32	0.3012	3.5812	17
3	2.0 X 0.50 (ALL BARS)	56.01	0.8273	27.0225	9, 21, 23-25
4	0.30 X 0.50 (ALL BARS)	11.02	0.70298	19.5093	3, 7, 9, 14, 25
5	0.25 X 1.0 (STIFFENED BARS) 0.125 X 1.0 (OTHER BARS)	11.91	0.8733	30.1069	1, 4, 5, 9, 11
6	0.25 X 1.0 (STIFFENED BARS) 1.0 X 0.125 (OTHER BARS)	11.91	1.0105	40.315	6, 16, 19-21
7	2.0 X 0.25 (ALL BARS)	29.55	0.40035	6.32771	17
8	1.5 X 0.25 (ALL BARS)	22.93	0.392	6.070	12, 23
9	2.0 X 0.25 (STIFFENED BARS) 2.0 X 0.125 (OTHER BARS)	20.72	0.3108	3.81358	18

Generalized Stiffness vs Frequency

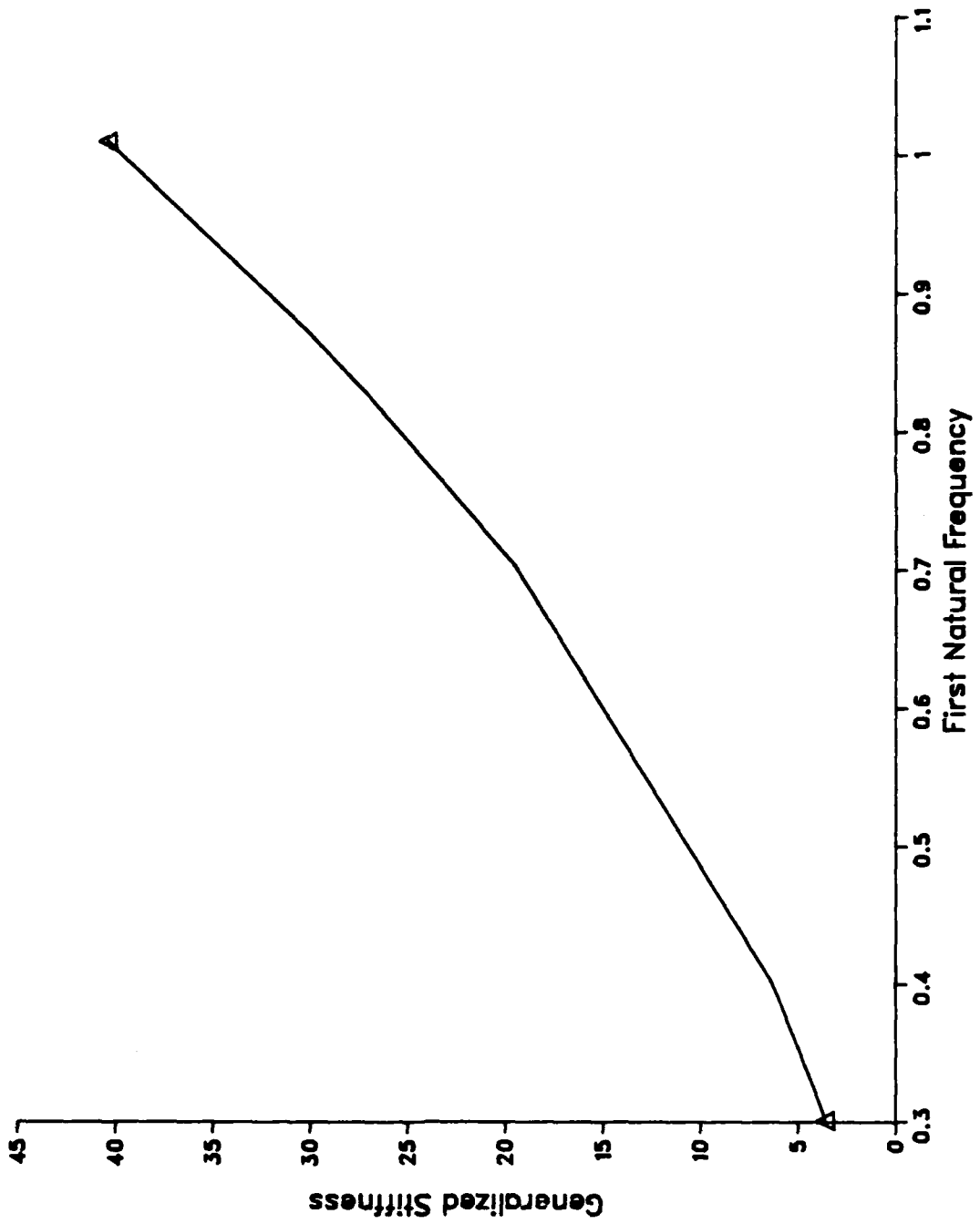
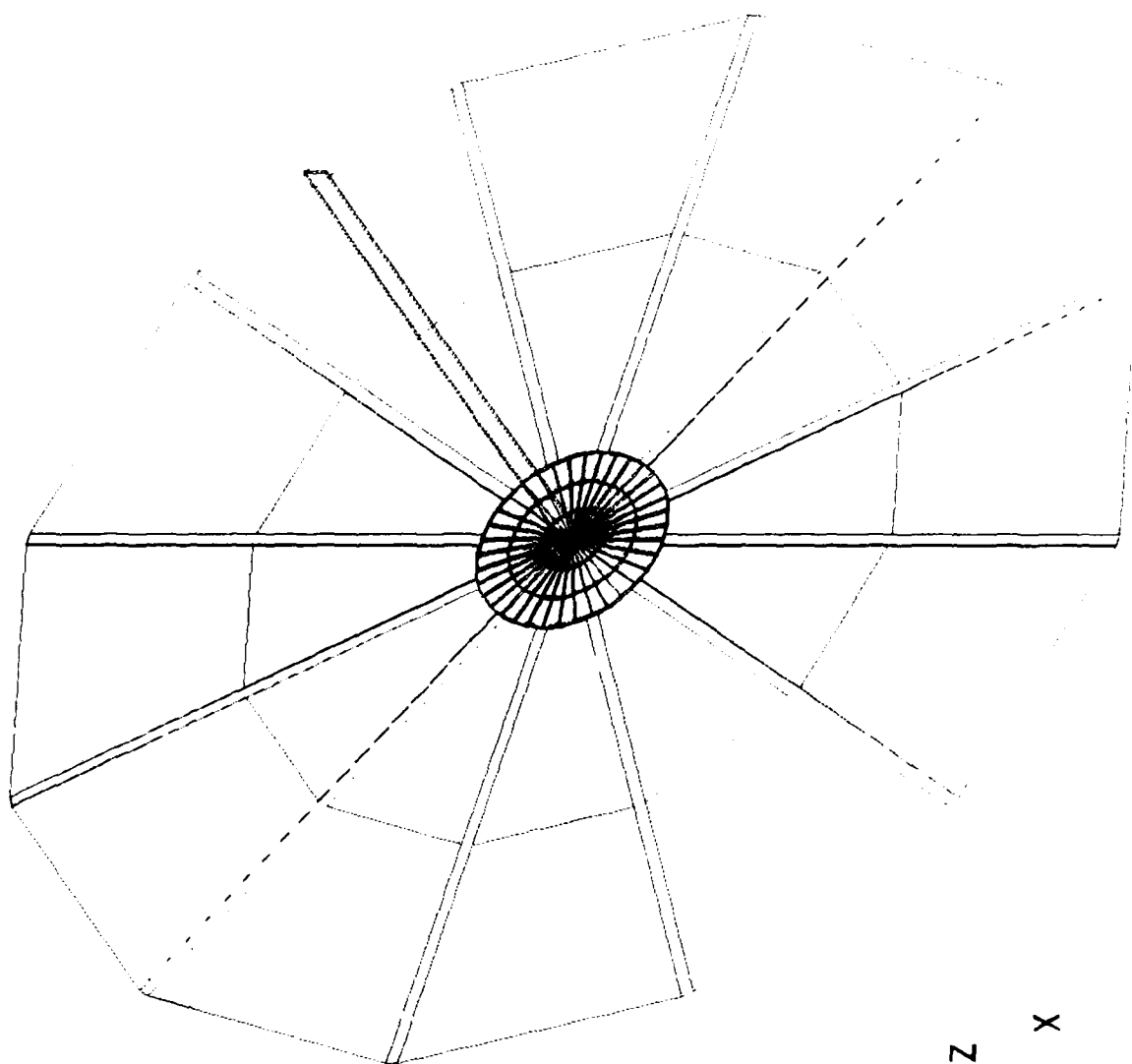


(Fig. 2)



Y
Z
X

(Fig. 3)

analyzed the prototype. For the prototype I also found out what the frequencies would look like. A listing of the first 200 frequencies are also attached.

V. Other Accomplishments

While I was at the Lab, I revised a communication link between the program PATRAN and the program NASTRAN. When I first arrived, I found out that this link last worked about four years ago. Since then people had to type NASTRAN bulk data cards into the computer. With this communication link, all one has to do is to render a computer drawing of the model and then run a program which translates the drawing into the data cards.

VI. Recommendations

The result of my 10 weeks of research is the design of a generic space structure. The structure is in the process of being constructed at the Air Force Rocket Propulsion Laboratory. Also, testing facilities are also being constructed. The construction should be completed by the end of October and testing of the grid should begin in November. The results of the tests will be compared to the theoretical results produced from the finite element program. When the results of the test are in, I hope to receive a copy and will submit a copy if UES desires.

As for the communication link, I hope it is being used

as much as I used it. The people at the Rocket Lab considered the link to be very helpful in the design of their structures.

REFERENCES

1. Nastran Users Manual, Washington D.C., Scientific and Technical Office NASA, 1983.
2. Patran-G Users Manual, Santa Ana, CA, Software Products Division PDA Engineering, 1984.
3. Beer, Ferdinand P. and E. Russell Johnston Jr., Mechanics of Materials, New York, NY, McGraw-Hill Co., 1981.

REAL EIGENVALUES

Grid

MODE NO.	EXTRACTION ORDER	EIGENVALUE	FACIAN FREQUENCY	CYCLIC FREQUENCY	GENERALIZED MASS	GENERALIZED STIFFNESS
1	120	3.813533E-00	1.932540E-00	3.102741E-01	9.999999E-01	3.813533E-00
2	119	2.614130E-01	5.112556E-00	8.107563E-01	1.000000E-00	2.614130E-01
3	118	1.130162E-02	1.063091E-01	1.571962E-00	9.999999E-01	1.130162E-02
4	117	2.135414E-02	1.461306E-01	2.325740E-00	1.000000E-00	2.135414E-02
5	116	3.478458E-02	1.865063E-01	2.968339E-00	9.999999E-01	3.478458E-02
6	115	5.440933E-02	2.332581E-01	3.712417E-00	9.999999E-01	5.440933E-02
7	114	7.664147E-02	2.768420E-01	4.408076E-00	9.999999E-01	7.664147E-02
8	113	8.677628E-02	2.945721E-01	4.688235E-00	1.000000E-00	8.677628E-02
9	112	1.206423E-03	3.473360E-01	5.528023E-00	1.000000E-00	1.206423E-03
10	111	1.643240E-03	4.053690E-01	6.431647E-00	1.000000E-00	1.643240E-03
11	110	1.776114E-03	4.214397E-01	6.707420E-00	9.999999E-01	1.776114E-03
12	109	2.262500E-03	4.756574E-01	7.570323E-00	9.999999E-01	2.262500E-03
13	108	2.281372E-03	4.776371E-01	7.601830E-00	1.000000E-00	2.281372E-03
14	107	2.662277E-03	5.159726E-01	8.211959E-00	1.000000E-00	2.662277E-03
15	106	3.746932E-03	6.12119E-01	9.742222E-00	9.999999E-01	3.746932E-03
16	105	3.863405E-03	6.215630E-01	9.892482E-00	9.999999E-01	3.863405E-03
17	104	4.786395E-03	6.918378E-01	1.101094E-01	1.000000E-00	4.786395E-03
18	103	6.632539E-03	8.144225E-01	1.236194E-01	1.000000E-00	6.632539E-03
19	102	9.644516E-03	9.820630E-01	1.563005E-01	1.000000E-00	9.644516E-03
20	101	1.170188E-04	1.081752E-02	1.721622E-01	9.999999E-01	1.170188E-04
21	100	1.254367E-04	1.119985E-02	1.752512E-01	9.999999E-01	1.254367E-04
22	99	1.610515E-04	1.269061E-02	2.015773E-01	9.999999E-01	1.610515E-04
23	98	1.704902E-04	1.305721E-02	2.078120E-01	9.999999E-01	1.704902E-04
24	97	2.344922E-04	1.531216E-02	2.437154E-01	1.000000E-00	2.344922E-04
25	96	2.491345E-04	1.578400E-02	2.512101E-01	1.000000E-00	2.491345E-04
26	95	3.068431E-04	1.751123E-02	2.756998E-01	0.0	0.0
27	94	3.205000E-04	1.751368E-02	2.831051E-01	0.0	0.0
28	93	3.214542E-04	1.752997E-02	2.833644E-01	0.0	0.0
29	92	3.521371E-04	1.871596E-02	2.975737E-01	0.0	0.0
30	91	4.751530E-04	2.179822E-02	3.469304E-01	0.0	0.0
31	90	4.783512E-04	2.167124E-02	3.480916E-01	0.0	0.0
32	89	4.957162E-04	2.226469E-02	3.543534E-01	0.0	0.0
33	88	5.431377E-04	2.330532E-02	3.709156E-01	0.0	0.0
34	87	6.400280E-04	2.529877E-02	4.026425E-01	0.0	0.0
35	86	6.555545E-04	2.561051E-02	4.076040E-01	0.0	0.0
36	85	6.859773E-04	2.619135E-02	4.168515E-01	0.0	0.0
37	84	7.198143E-04	2.682935E-02	4.270024E-01	0.0	0.0
38	83	7.519515E-04	2.742228E-02	4.364391E-01	0.0	0.0
39	82	8.810415E-04	2.968234E-02	4.724091E-01	0.0	0.0
40	81	1.024664E-03	3.216619E-02	5.119407E-01	0.0	0.0
41	80	1.076223E-03	3.280736E-02	5.221452E-01	0.0	0.0
42	79	1.334579E-03	3.633999E-02	5.814534E-01	0.0	0.0
43	78	1.410271E-03	3.756110E-02	5.978035E-01	0.0	0.0
44	77	1.458563E-03	3.819510E-02	6.078939E-01	0.0	0.0
45	76	1.600412E-03	4.000764E-02	6.367414E-01	0.0	0.0
46	75	1.604173E-03	4.009238E-02	6.374534E-01	0.0	0.0
47	74	1.827798E-03	4.344832E-02	6.915015E-01	0.0	0.0
48	73	2.355772E-03	4.857506E-02	7.787085E-01	0.0	0.0
49	72	2.420578E-03	4.920293E-02	7.864964E-01	0.0	0.0
50	71	2.545547E-03	5.049601E-02	8.036490E-01	0.0	0.0
51	70	3.145635E-03	5.609436E-02	8.727854E-01	0.0	0.0
52	69	3.526344E-03	5.928303E-02	9.451102E-01	0.0	0.0
53	68	3.625208E-03	6.020970E-02	9.582671E-01	0.0	0.0
54	67	4.525722E-03	6.728092E-02	1.076305E-02	0.0	0.0
55	66	4.770379E-03	6.906773E-02	1.099250E-02	0.0	0.0
56	65	5.481129E-03	7.403505E-02	1.178304E-02	0.0	0.0
57	64	5.659541E-03	7.522593E-02	1.197258E-02	0.0	0.0
58	63	6.521564E-03	8.075807E-02	1.255305E-02	0.0	0.0
59	62	7.156179E-03	8.423029E-02	1.330115E-02	0.0	0.0
60	61	7.441235E-03	8.626603E-02	1.372966E-02	0.0	0.0
61	60	8.029625E-03	9.06817E-02	1.426135E-02	0.0	0.0
62	59	8.180508E-03	9.044616E-02	1.439495E-02	0.0	0.0
63	58	8.695584E-03	9.327156E-02	1.484463E-02	0.0	0.0
64	57	9.262062E-03	9.623961E-02	1.531701E-02	0.0	0.0
65	56	9.734474E-03	9.866343E-02	1.570277E-02	0.0	0.0
66	55	1.108179E-06	1.052701E-03	1.675426E-02	0.0	0.0
67	54	1.211733E-06	1.100797E-03	1.751972E-02	0.0	0.0
68	53	1.554360E-06	1.250744E-03	1.990621E-02	0.0	0.0
69	52	1.718324E-06	1.310848E-03	2.086280E-02	0.0	0.0
70	51	2.160944E-06	1.470015E-03	2.339601E-02	0.0	0.0
71	50	2.367013E-06	1.538510E-03	2.448615E-02	0.0	0.0
72	49	2.784520E-06	1.668688E-03	2.655795E-02	0.0	0.0
73	48	2.842588E-06	1.685849E-03	2.682112E-02	0.0	0.0
74	47	3.612533E-06	1.900693E-03	3.025046E-02	0.0	0.0
75	46	3.826764E-06	1.956212E-03	3.123405E-02	0.0	0.0
76	45	4.434018E-06	2.105711E-03	3.351342E-02	0.0	0.0
77	44	4.909190E-06	2.215669E-03	3.526347E-02	0.0	0.0

REAL EIGENVALUES

MODE NO	EXTRACTION ORDER	EIGENVALUE	RADIAN FREQUENCY	CYCLIC FREQUENCY	GENERALIZED MASS	GENERALIZED STIFFNESS
78	43	3.009165E-06	2.244609E-03	3.57275E-02	0.0	0.0
79	42	3.389793E-06	2.321593E-03	3.69493E-02	0.0	0.0
80	41	3.830709E-06	2.414686E-03	3.843092E-02	0.0	0.0
81	40	3.923626E-06	2.434261E-03	3.874246E-02	0.0	0.0
82	39	4.436534E-06	2.540971E-03	4.044081E-02	0.0	0.0
83	38	6.406187E-06	2.570291E-03	4.09081E-02	0.0	0.0
84	37	7.476623E-06	2.734341E-03	4.251825E-02	0.0	0.0
85	36	8.335268E-06	2.887086E-03	4.554940E-02	0.0	0.0
86	35	9.066151E-06	3.011003E-03	4.792163E-02	0.0	0.0
87	34	9.387460E-06	3.063894E-03	4.876342E-02	0.0	0.0
88	33	9.966552E-06	3.156965E-03	5.024497E-02	0.0	0.0
89	32	9.975184E-06	3.188352E-03	5.026672E-02	0.0	0.0
90	31	1.138021E-07	3.373455E-03	5.369020E-02	0.0	0.0
91	30	1.254653E-07	3.556196E-03	5.659861E-02	0.0	0.0
92	29	1.309604E-07	3.618645E-03	5.759571E-02	0.0	0.0
93	28	1.345773E-07	3.673932E-03	5.847245E-02	0.0	0.0
94	27	1.396714E-07	3.737264E-03	5.949040E-02	0.0	0.0
95	26	1.552386E-07	3.902417E-03	6.210890E-02	0.0	0.0
96	25	1.753607E-07	4.187505E-03	6.664797E-02	0.0	0.0
97	24	1.855591E-07	4.311254E-03	6.861573E-02	0.0	0.0
98	23	1.875355E-07	4.330538E-03	6.892265E-02	0.0	0.0
99	22	1.966763E-07	4.434065E-03	7.057033E-02	0.0	0.0
100	21	2.027777E-07	4.502640E-03	7.166174E-02	0.0	0.0
101	20	2.151772E-07	4.671163E-03	7.434356E-02	0.0	0.0
102	19	2.316629E-07	4.813137E-03	7.660245E-02	0.0	0.0
103	18	2.340330E-07	4.837696E-03	7.694322E-02	0.0	0.0
104	17	2.462144E-07	4.962000E-03	7.897267E-02	0.0	0.0
105	16	2.530786E-07	5.030672E-03	8.006463E-02	0.0	0.0
106	15	2.593517E-07	5.092720E-03	8.105515E-02	0.0	0.0
107	14	2.628745E-07	5.127304E-03	8.120352E-02	0.0	0.0
108	13	2.911667E-07	5.395430E-03	8.587094E-02	0.0	0.0
109	12	2.945778E-07	5.427502E-03	8.638137E-02	0.0	0.0
110	11	3.055141E-07	5.527333E-03	8.747023E-02	0.0	0.0
111	10	3.179537E-07	5.638740E-03	8.974332E-02	0.0	0.0
112	9	3.241142E-07	5.693147E-03	9.060925E-02	0.0	0.0
113	8	3.259782E-07	5.709450E-03	9.066872E-02	0.0	0.0
114	7	3.411760E-07	5.841027E-03	9.296284E-02	0.0	0.0
115	6	3.638611E-07	6.155657E-03	9.860492E-02	0.0	0.0
116	5	4.312494E-07	6.566925E-03	1.045156E-01	0.0	0.0
117	4	4.952555E-07	7.038136E-03	1.120154E-01	0.0	0.0
118	3	5.041023E-07	7.100016E-03	1.130003E-01	0.0	0.0
119	2	5.169172E-07	7.189695E-03	1.144275E-01	0.0	0.0
120	1	5.581225E-07	7.470762E-03	1.189005E-01	0.0	0.0

Grid coding

C\$type grid.dat
 NASTRAN NLINES=85, TITLEDPT=0, SYSTEM(76)=1
 ID GRID,CT1

APP DISP

SOL 3

TIME 30

CEND

DISP=ALL

METHOD=100

BEGIN BULK

GRID	1		0.	0.	0.			
GRID	2		15.	0.	0.			
GRID	3		30.	0.	0.			
GRID	4		45.	0.	0.			
GRID	5		60.	0.	0.			
GRID	6		0.	15.	0.			
GRID	7		15.	15.	0.			
GRID	8		30.	15.	0.			
GRID	9		45.	15.	0.			
GRID	10		60.	15.	0.			
GRID	11		0.	30.	0.			
GRID	12		15.	30.	0.			
GRID	13		30.	30.	0.			
GRID	14		45.	30.	0.			
GRID	15		60.	30.	0.			
GRID	16		0.	45.	0.			
GRID	17		15.	45.	0.			
GRID	18		30.	45.	0.			
GRID	19		45.	45.	0.			
GRID	20		60.	45.	0.			
GRID	21		0.	60.	0.	123456		
GRID	22		15.	60.	0.	123456		
GRID	23		30.	60.	0.	123456		
GRID	24		45.	60.	0.	123456		
GRID	25		60.	60.	0.	123456		
CBAR	1	90	1	2				+B01
+B01			0.	0.	-.125	0.	0.	-.125
CBAR	2	90	2	3				+B02
+B02			0.	0.	-.125	0.	0.	-.125
CBAR	3	90	3	4				+B03
+B03			0.	0.	-.125	0.	0.	-.125
CBAR	4	90	4	5				+B04
+B04			0.	0.	-.125	0.	0.	-.125
CBAR	5		6	7				+B05
+B05			0.	0.	-.0625	0.	0.	-.0625
CBAR	6		7	8				+B06
+B06			0.	0.	-.0625	0.	0.	-.0625
CBAR	7		8	9				+B07
+B07			0.	0.	-.0625	0.	0.	-.0625
CBAR	8		9	10				+B08
+B08			0.	0.	-.0625	0.	0.	-.0625
CBAR	9		11	12				+B09
+B09			0.	0.	-.0625	0.	0.	-.0625
CBAR	10		12	13				+B10
+B10			0.	0.	-.0625	0.	0.	-.0625
CBAR	11		13	14				+B11
+B11			0.	0.	-.0625	0.	0.18-16	-.0625
CBAR	12		14	15				+B12
+B12			0.	0.	-.0625	0.	0.	-.0625
CBAR	13		16	17				+B13

+B14		0.	0.	-.0625	0.	0.	-.0625	
CBAR	15	18	19					+B15
+B15		0.	0.	-.0625	0.	0.	-.0625	
CBAR	16	19	20					+B16
+B16		0.	0.	-.0625	0.	0.	-.0625	
CBAR	17	90	16	21				+B17
+B17		0.	0.	.125	0.	0.	.125	
CBAR	18	90	11	16				+B18
+B18		0.	0.	.125	0.	0.	.125	
CBAR	19	90	6	11				+B19
+B19		0.	0.	.125	0.	0.	.125	
CBAR	20	90	1	6				+B20
+B20		0.	0.	.125	0.	0.	.125	
CBAR	21		17	22				+B21
+B21		.0	.0	.0625	.0	.0	.0625	
CBAR	22		12	17				+B22
+B22		.0	0.	.0625	.0	.0	.0625	
CBAR	23		7	12				+B23
+B23		0.	0.	.0625	0.	0.	.0625	
CBAR	24		2	7				+B24
+B24		0.	0.	.0625	0.	0.	.0625	
CBAR	25		18	23				+B25
+B25		0.	0.	.0625	0.	0.	.0625	
CBAR	26		13	18				+B26
+B26		0.	0.	.0625	0.	0.	.0625	
CBAR	27		8	13				+B27
+B27		0.	0.	.0625	0.	0.	.0625	
CBAR	28		3	8				+B28
+B28		0.	0.	.0625	0.	0.	.0625	
CBAR	29		19	24				+B29
+B29		0.	0.	.0625	0.	0.	.0625	
CBAR	30		14	19				+B30
+B30		0.	0.	.0625	0.	0.	.0625	
CBAR	31		9	14				+B31
+B31		0.	0.	.0625	0.	0.	.0625	
CBAR	32		4	9				+B32
+B32		0.	0.	.0625	0.	0.	.0625	
CBAR	33	90	20	25				+B33
+B33		0.	0.	.125	0.	0.	.125	
CBAR	34	90	15	20				+B34
+B34		0.	0.	.125	0.	0.	.125	
CBAR	35	90	10	15				+B35
+B35		0.	0.	.125	0.	0.	.125	
CBAR	36	90	5	10				+B36
+B36		0.	0.	.125	0.	0.	.125	
PBAR	90	100	.500	2.6042-3166.67-39.5964-3				
CONM2	51	1		4.7926-3				
CONM2	52	2		4.7926-3				
CONM2	53	3		4.7926-3				
CONM2	54	4		4.7926-3				
CONM2	55	5		4.7926-3				
CONM2	56	6		4.7926-3				
CONM2	57	7		4.7926-3				
CONM2	58	8		4.7926-3				
CONM2	59	9		4.7926-3				
CONM2	60	10		4.7926-3				
CONM2	61	11		4.7926-3				
CONM2	62	12		4.7926-3				
CONM2	63	13		4.7926-3				
CONM2	64	14		4.7926-3				
CONM2	65	15		4.7926-3				
CONM2	66	16		4.7926-3				
CONM2	67	17		4.7926-3				

CUR#12	10	20							
BAROR		100			0.	0.	1.		1
PBAR	100	100	0.25	325.52-683.333-31.2508-3					
MAT1	100	10.0+6	3.7+6	.32	3.0435-3				
EIGR	100	GIV				25			
+EIG	MASS								+EIG
PARAM	COUPMASS1								
PARAM	GRDPNT	13							
ENDDATA									

Radar

REAL EIGENVALUES

MODE NO.	EXTRACTION ORDER	EIGENVALUE	RADIAN FREQUENCY	CYCLIC FREQUENCY	GENERALIZED MASS	GENERALIZED STIFFNESS
1	108	1. 215871E-06	1. 102663E-03	1. 734947E-04	1. 000000E+00	1. 215871E-06
2	107	3. 481018E-04	1. 863749E-02	2. 469431E-03	9. 999999E-01	3. 481018E-04
3	198	6. 904771E-01	8. 309493E-01	1. 322497E-01	9. 999999E-01	6. 904771E-01
4	197	2. 288938E-00	1. 312924E-00	2. 407893E-01	1. 000000E+00	2. 288938E-00
5	196	2. 448864E-00	1. 364883E-00	2. 490391E-01	9. 999999E-01	2. 448864E-00
6	195	5. 228366E-00	2. 286606E-00	3. 639246E-01	9. 999999E-01	5. 228366E-00
7	194	1. 724233E-01	4. 132431E-00	6. 608831E-01	9. 999999E-01	1. 724233E-01
8	193	1. 908103E-01	4. 362190E-00	6. 952190E-01	1. 000000E+00	1. 908103E-01
9	192	6. 031195E-01	7. 773943E-00	1. 239057E-00	9. 999999E-01	6. 031195E-01
10	191	1. 456334E-02	1. 206869E-01	1. 623792E-00	1. 000000E+00	1. 456334E-02
11	190	1. 462132E-02	1. 209032E-01	1. 624743E-00	0. 0	0. 0
12	189	2. 261153E-02	1. 903042E-01	2. 352346E-00	0. 0	0. 0
13	188	3. 444794E-02	1. 836016E-01	2. 932940E-00	0. 0	0. 0
14	187	4. 302574E-02	2. 121995E-01	3. 377264E-00	0. 0	0. 0
15	186	6. 186644E-02	2. 487296E-01	3. 936635E-00	0. 0	0. 0
16	185	9. 118560E-02	3. 019743E-01	4. 606073E-00	0. 0	0. 0
17	184	9. 627824E-02	3. 102574E-01	4. 932765E-00	0. 0	0. 0
18	183	1. 010433E-02	2. 176740E-01	5. 049122E-00	0. 0	0. 0
19	182	1. 018462E-02	3. 191233E-01	5. 079168E-00	0. 0	0. 0
20	181	1. 391231E-02	3. 989523E-01	6. 349326E-00	0. 0	0. 0
21	180	1. 892553E-03	4. 350389E-01	6. 923255E-00	0. 0	0. 0
22	179	2. 081344E-03	4. 562394E-01	7. 251273E-00	0. 0	0. 0
23	178	4. 238974E-03	6. 567089E-01	1. 046336E-01	0. 0	0. 0
24	177	4. 459111E-03	6. 677638E-01	1. 062782E-01	0. 0	0. 0
25	176	1. 000495E-04	1. 000248E-02	1. 991943E-01	0. 0	0. 0
26	175	1. 303192E-04	1. 141573E-02	1. 816973E-01	0. 0	0. 0
27	174	1. 320183E-04	1. 148992E-02	1. 828677E-01	0. 0	0. 0
28	173	1. 344412E-04	1. 159488E-02	1. 849382E-01	0. 0	0. 0
29	172	1. 360003E-04	1. 249001E-02	1. 967844E-01	0. 0	0. 0
30	171	1. 794150E-04	1. 329439E-02	2. 131815E-01	0. 0	0. 0
31	170	1. 823255E-04	1. 350278E-02	2. 149034E-01	0. 0	0. 0
32	169	1. 993533E-04	1. 412676E-02	2. 249344E-01	0. 0	0. 0
33	168	2. 004272E-04	1. 415723E-02	2. 253192E-01	0. 0	0. 0
34	167	4. 434490E-04	2. 105520E-02	2. 331517E-01	0. 0	0. 0
35	166	4. 495126E-04	2. 120171E-02	3. 274357E-01	0. 0	0. 0
36	165	4. 501503E-04	2. 121628E-02	3. 274675E-01	0. 0	0. 0
37	164	8. 323212E-04	2. 419538E-02	4. 646621E-01	0. 0	0. 0
38	163	1. 091552E-03	3. 303918E-02	5. 238349E-01	0. 0	0. 0
39	162	1. 162942E-03	3. 418979E-02	5. 441473E-01	0. 0	0. 0
40	161	1. 373429E-03	3. 709981E-02	5. 896251E-01	0. 0	0. 0
41	160	1. 503662E-03	3. 677716E-02	6. 171576E-01	0. 0	0. 0
42	159	1. 577972E-03	4. 120284E-02	6. 227792E-01	0. 0	0. 0
43	158	1. 810764E-03	4. 225343E-02	6. 772388E-01	0. 0	0. 0
44	157	2. 161212E-03	4. 770388E-02	7. 577023E-01	0. 0	0. 0
45	156	2. 323272E-03	4. 820633E-02	7. 672310E-01	0. 0	0. 0
46	155	2. 333512E-03	5. 023472E-02	8. 011019E-01	0. 0	0. 0
47	154	2. 351153E-03	5. 675155E-02	8. 026778E-01	0. 0	0. 0
48	153	3. 225722E-03	5. 677782E-02	8. 036459E-01	0. 0	0. 0
49	152	3. 373152E-03	5. 721989E-02	8. 126191E-01	0. 0	0. 0
50	151	3. 473152E-03	5. 721989E-02	8. 126191E-01	0. 0	0. 0
51	152	4. 123267E-03	6. 421790E-02	1. 022053E-02	0. 0	0. 0
52	200	4. 367084E-03	6. 608393E-02	1. 031738E-02	0. 0	0. 0
53	151	6. 003141E-03	7. 747994E-02	1. 233131E-02	0. 0	0. 0
54	150	6. 123537E-03	7. 825303E-02	1. 243436E-02	0. 0	0. 0
55	149	6. 359421E-03	8. 099023E-02	1. 289000E-02	0. 0	0. 0
56	148	7. 373208E-03	8. 586738E-02	1. 366622E-02	0. 0	0. 0
57	147	1. 196283E-06	1. 093748E-03	1. 740734E-02	0. 0	0. 0
58	146	1. 238620E-06	1. 112933E-03	1. 771288E-02	0. 0	0. 0
59	145	1. 253656E-06	1. 119668E-03	1. 782007E-02	0. 0	0. 0
60	103	1. 254080E-06	1. 119857E-03	1. 782306E-02	0. 0	0. 0
61	106	1. 254137E-06	1. 119882E-03	1. 782348E-02	0. 0	0. 0
62	144	1. 280752E-06	1. 131703E-03	1. 801161E-02	0. 0	0. 0
63	102	1. 662636E-06	1. 289440E-03	2. 052208E-02	0. 0	0. 0
64	101	1. 662638E-06	1. 289441E-03	2. 052209E-02	0. 0	0. 0
65	143	1. 833564E-06	1. 354092E-03	2. 153104E-02	0. 0	0. 0
66	142	2. 072676E-06	1. 439679E-03	2. 291320E-02	0. 0	0. 0
67	141	2. 262692E-06	1. 504223E-03	2. 394046E-02	0. 0	0. 0
68	140	2. 342732E-06	1. 530599E-03	2. 436023E-02	0. 0	0. 0
69	100	2. 351091E-06	1. 597213E-03	2. 542044E-02	0. 0	0. 0
70	99	2. 351111E-06	1. 597220E-03	2. 542054E-02	0. 0	0. 0
71	139	2. 646786E-06	1. 626893E-03	2. 589283E-02	0. 0	0. 0
72	138	3. 152185E-06	1. 775439E-03	2. 823699E-02	0. 0	0. 0
73	98	3. 152245E-06	1. 776312E-03	2. 827092E-02	0. 0	0. 0
74	97	3. 153346E-06	1. 776329E-03	2. 827116E-02	0. 0	0. 0
75	137	3. 182502E-06	1. 784237E-03	2. 839702E-02	0. 0	0. 0
76	136	3. 337763E-06	1. 826755E-03	2. 907689E-02	0. 0	0. 0
77	135	3. 343412E-06	1. 828900E-03	2. 910148E-02	0. 0	0. 0

REAL EIGENVALUES

MODE NO.	EXTRACTION ORDER	EIGENVALUE	RADIAN FREQUENCY	CYCLIC FREQUENCY	GENERALIZED MASS	GENERALIZED STIFFNESS
78	199	3.383834E-06	1.829520E-03	2.927687E-02	0.0	0.0
79	96	3.450148E-06	1.837458E-03	2.956235E-02	0.0	0.0
80	134	3.782033E-06	1.944745E-03	3.095157E-02	0.0	0.0
81	94	3.941201E-06	1.959898E-03	3.119275E-02	0.0	0.0
82	95	3.841212E-06	1.959901E-03	3.119275E-02	0.0	0.0
83	133	4.039723E-06	2.009921E-03	3.198895E-02	0.0	0.0
84	93	4.394225E-06	2.093254E-03	3.322472E-02	0.0	0.0
85	92	4.384272E-06	2.093899E-03	3.322472E-02	0.0	0.0
86	132	4.723373E-06	2.173333E-03	3.455491E-02	0.0	0.0
87	91	4.743240E-06	2.179057E-03	3.468077E-02	0.0	0.0
88	90	4.743240E-06	2.179057E-03	3.468077E-02	0.0	0.0
89	89	5.063912E-06	2.250225E-03	3.581344E-02	0.0	0.0
90	88	5.364124E-06	2.316458E-03	3.686131E-02	0.0	0.0
91	87	5.364124E-06	2.316458E-03	3.686131E-02	0.0	0.0
92	86	6.022252E-06	2.454034E-03	3.937198E-02	0.0	0.0
93	85	6.022252E-06	2.454034E-03	3.937198E-02	0.0	0.0
94	84	6.264475E-06	2.502893E-03	4.003477E-02	0.0	0.0
95	83	6.334423E-06	2.516227E-03	4.036255E-02	0.0	0.0
96	82	6.334423E-06	2.516227E-03	4.036255E-02	0.0	0.0
97	131	6.495812E-06	2.546708E-03	4.053355E-02	0.0	0.0
98	130	6.122438E-06	2.550032E-03	4.053355E-02	0.0	0.0
99	81	1.400912E-07	3.742376E-03	5.957074E-02	0.0	0.0
100	80	1.400912E-07	3.742376E-03	5.957074E-02	0.0	0.0
101	129	1.403176E-07	3.745898E-03	5.981782E-02	0.0	0.0
102	128	1.412146E-07	3.757823E-03	5.980809E-02	0.0	0.0
103	78	2.113638E-07	4.597454E-03	7.317032E-02	0.0	0.0
104	79	2.113638E-07	4.597454E-03	7.317032E-02	0.0	0.0
105	127	2.531255E-07	5.031198E-03	8.007336E-02	0.0	0.0
106	77	2.655827E-07	5.133472E-03	8.202006E-02	0.0	0.0
107	76	2.655827E-07	5.133472E-03	8.202006E-02	0.0	0.0
108	126	2.799020E-07	5.286523E-03	8.414240E-02	0.0	0.0
109	74	3.013542E-07	5.489614E-03	8.737000E-02	0.0	0.0
110	75	3.013542E-07	5.489614E-03	8.737000E-02	0.0	0.0
111	73	3.141753E-07	5.609132E-03	8.920844E-02	0.0	0.0
112	71	4.423755E-07	6.648895E-03	1.059135E-01	0.0	0.0
113	72	4.423755E-07	6.648895E-03	1.059135E-01	0.0	0.0
114	125	4.441187E-07	6.634891E-03	1.059135E-01	0.0	0.0
115	70	4.472317E-07	6.690325E-03	1.061003E-01	0.0	0.0
116	124	4.542294E-07	6.735762E-03	1.074685E-01	0.0	0.0
117	68	4.935444E-07	7.563422E-03	1.200080E-01	0.0	0.0
118	69	4.935444E-07	7.563422E-03	1.200080E-01	0.0	0.0
119	67	4.935444E-07	7.563422E-03	1.200080E-01	0.0	0.0
120	66	4.935444E-07	7.563422E-03	1.200080E-01	0.0	0.0
121	65	5.047526E-07	7.623775E-03	1.217897E-01	0.0	0.0
122	63	5.247406E-07	7.843232E-03	1.250642E-01	0.0	0.0
123	64	5.247406E-07	7.843232E-03	1.250642E-01	0.0	0.0
124	62	5.247406E-07	7.843232E-03	1.250642E-01	0.0	0.0
125	61	5.247406E-07	7.843232E-03	1.250642E-01	0.0	0.0
126	60	5.247406E-07	7.843232E-03	1.250642E-01	0.0	0.0
127	123	5.702288E-07	7.851732E-03	1.251225E-01	0.0	0.0
128	59	5.801357E-07	7.916670E-03	1.262234E-01	0.0	0.0
129	58	5.801357E-07	7.916670E-03	1.262234E-01	0.0	0.0
130	57	7.547102E-07	8.687640E-03	1.382621E-01	0.0	0.0
131	56	7.547102E-07	8.687640E-03	1.382621E-01	0.0	0.0
132	54	9.327151E-07	9.687762E-03	1.522700E-01	0.0	0.0
133	55	9.327151E-07	9.687762E-03	1.522700E-01	0.0	0.0
134	53	9.842305E-07	9.920839E-03	1.537080E-01	0.0	0.0
135	52	1.008428E-06	1.004205E-04	1.598242E-03	0.0	0.0
136	51	1.008428E-06	1.004207E-04	1.598242E-03	0.0	0.0
137	49	1.051000E-06	1.025183E-04	1.631629E-03	0.0	0.0
138	50	1.051000E-06	1.025193E-04	1.631643E-03	0.0	0.0
139	48	1.093029E-06	1.043480E-04	1.643933E-03	0.0	0.0
140	47	1.093029E-06	1.043487E-04	1.643944E-03	0.0	0.0
141	46	1.123263E-06	1.059841E-04	1.686789E-03	0.0	0.0
142	45	1.123263E-06	1.059842E-04	1.686791E-03	0.0	0.0
143	44	1.148611E-06	1.071756E-04	1.705732E-03	0.0	0.0
144	43	1.269273E-06	1.126631E-04	1.763085E-03	0.0	0.0
145	42	1.269273E-06	1.126634E-04	1.763094E-03	0.0	0.0
146	41	1.492221E-06	1.221563E-04	1.944181E-03	0.0	0.0
147	40	1.492221E-06	1.221577E-04	1.944200E-03	0.0	0.0
148	39	1.638773E-06	1.287836E-04	2.045687E-03	0.0	0.0
149	38	1.638773E-06	1.287838E-04	2.045690E-03	0.0	0.0
150	37	1.718155E-06	1.310784E-04	2.096178E-03	0.0	0.0
151	122	2.344723E-06	1.521216E-04	2.437145E-03	0.0	0.0
152	121	2.676675E-06	1.676078E-04	2.692215E-03	0.0	0.0
153	120	3.042295E-06	1.745991E-04	2.778201E-03	0.0	0.0
154	119	4.579272E-06	2.140064E-04	3.406018E-03	0.0	0.0

REAL EIGENVALUES

QPE NO.	EXTRACTION ORDER	EIGENVALUE	RADIAN FREQUENCY	CYCLIC FREQUENCY	GENERALIZED MASS	GENERALIZED STIFFNESS
155	118	4.811902E-08	2.193606E-04	3.491232E-03	0.0	0.0
156	36	5.104833E-08	2.239388E-04	3.599927E-03	0.0	0.0
157	34	5.186710E-08	2.277435E-04	3.624630E-03	0.0	0.0
158	39	5.186740E-08	2.277442E-04	3.624661E-03	0.0	0.0
159	33	5.423684E-08	2.328880E-04	3.706528E-03	0.0	0.0
160	32	5.424021E-08	2.328955E-04	3.706647E-03	0.0	0.0
161	31	5.779005E-08	2.403936E-04	3.826015E-03	0.0	0.0
162	30	5.779005E-08	2.403936E-04	3.826033E-03	0.0	0.0
163	29	6.168547E-08	2.483656E-04	3.932261E-03	0.0	0.0
164	28	6.168557E-08	2.483724E-04	3.932570E-03	0.0	0.0
165	27	6.474432E-08	2.544492E-04	4.049624E-03	0.0	0.0
166	26	6.474432E-08	2.544496E-04	4.049672E-03	0.0	0.0
167	25	6.590421E-08	2.567184E-04	4.085502E-03	0.0	0.0
168	117	6.165937E-08	2.837610E-04	4.548022E-03	0.0	0.0
169	116	8.415422E-08	2.901637E-04	4.618099E-03	0.0	0.0
170	115	1.971241E-07	3.963283E-04	6.308723E-03	0.0	0.0
171	114	1.627135E-07	4.032913E-04	6.420013E-03	0.0	0.0
172	24	2.822223E-07	5.312395E-04	8.455200E-03	0.0	0.0
173	22	2.846411E-07	5.337266E-04	8.464522E-03	0.0	0.0
174	23	2.846411E-07	5.337266E-04	8.464522E-03	0.0	0.0
175	21	2.924123E-07	5.407320E-04	8.606335E-03	0.0	0.0
176	20	2.924123E-07	5.407320E-04	8.606335E-03	0.0	0.0
177	19	3.037123E-07	5.511010E-04	8.771043E-03	0.0	0.0
178	18	3.037123E-07	5.511010E-04	8.771043E-03	0.0	0.0
179	17	3.162982E-07	5.624045E-04	8.930944E-03	0.0	0.0
180	16	3.162982E-07	5.624045E-04	8.930944E-03	0.0	0.0
181	113	3.162982E-07	5.624045E-04	8.930944E-03	0.0	0.0
182	112	3.253871E-07	5.704271E-04	9.078629E-03	0.0	0.0
183	19	3.264929E-07	5.713995E-04	9.094042E-03	0.0	0.0
184	14	3.264944E-07	5.713996E-04	9.094063E-03	0.0	0.0
185	13	3.304506E-07	5.749423E-04	9.148995E-03	0.0	0.0
186	111	4.705143E-07	6.859405E-04	1.091708E-02	0.0	0.0
187	12	7.782103E-07	8.525027E-04	1.404547E-02	0.0	0.0
188	10	7.822345E-07	8.542384E-04	1.407465E-02	0.0	0.0
189	11	7.822345E-07	8.542384E-04	1.407473E-02	0.0	0.0
190	9	7.912572E-07	8.696458E-04	1.415513E-02	0.0	0.0
191	8	7.912572E-07	8.696458E-04	1.415513E-02	0.0	0.0
192	7	8.057125E-07	8.877620E-04	1.428823E-02	0.0	0.0
193	6	8.057125E-07	8.877620E-04	1.428823E-02	0.0	0.0
194	5	8.227905E-07	9.070780E-04	1.443155E-02	0.0	0.0
195	4	8.227905E-07	9.070780E-04	1.443155E-02	0.0	0.0
196	3	8.370575E-07	9.149132E-04	1.456123E-02	0.0	0.0
197	2	8.370575E-07	9.149132E-04	1.456123E-02	0.0	0.0
198	1	8.427506E-07	9.180363E-04	1.461100E-02	0.0	0.0
199	110	2.184599E-13	4.674076E-06	7.429022E-15	0.0	0.0
200	109	1.520117E-17	3.673341E-09	5.722541E-17	0.0	0.0

1986 USAF-UES GRADUATE STUDENT SUMMER SUPPORT PROGRAM

Sponsored by the
AIR FORCE OFFICE OF SCIENTIFIC RESEARCH

Conducted by the
Universal Energy Systems, Inc.

FINAL REPORT

A BIOMECHANICAL STUDY OF ANTHROPOMORPHIC HEAD-NECK SYSTEMS

Prepared by:	Brian J. Doherty
Academic Rank:	Graduate Student
Department:	Biomedical Engineering Department
University:	Duke University
Research Location:	AAMRL/BBM Wright-Patterson Air Force Base
USAF Researcher:	Dr. Ints Kaleps
Date:	September 22, 1986
Contract No.:	F49620-85-C-0013

A BIOMECHANICAL STUDY OF ANTHROPOMORPHIC HEAD-NECK SYSTEMS

by

Brian J. Doherty

ABSTRACT

Hybrid II, modified Hybrid II, and Hybrid III anthropomorphic manikin head-neck assemblies were studied. Preparations were made to measure the kinematic and dynamic responses of these mechanical head-neck assemblies to abrupt decelerations imparted to the base of the neck by a pendulum test apparatus according to existing DOT specifications for Part 572 dummy compliance testing and recommended procedures for Hybrid III compliance testing. Measurements were made of the geometric and inertial properties of the pendulum and the modified Hybrid II and Hybrid III test specimens. The actual execution of these tests is planned for the upcoming year. The measured geometric and inertial properties and pendulum test performance standards were analyzed to determine inputs for both the Articulated Total Body (ATB) Model and the AAMRL Head-Spine Model (HSM). Data sets, which represent the Hybrid II head-neck system, were developed for the HSM and ATB Model. Simulations of the Hybrid II pendulum tests were performed and compared to experimental results to verify the assumptions used to define the Hybrid II head and neck structures and validate these data sets. More modeling work still needs to be done. Some additional tuning of the Hybrid II data sets is suggested. Modified Hybrid II and Hybrid III data sets need to be developed. Simulations of modified Hybrid II and Hybrid III pendulum tests need to be performed and compared to experimental results to validate these data sets.

ACKNOWLEDGEMENTS

I would like to express my appreciation to the Air Force Systems Command, the Air Force Office of Scientific Research, and Universal Energy Systems for sponsorship of my research. I thank Dr. Ints Kaleps for his guidance, encouragement, and criticism of my research. I also thank the BBM staff, especially Dr. Eberhardt Privitzer and Louise Obergefell for their assistance and patience with modeling tasks and Capt. Gary Chestnut for his assistance with the experimental aspects of this project. Several members of the SRL staff deserve special recognition and thanks; these include Dick White, Jennifer McKenzie, Jeff Setticerri, Jeff Eastup, and Gene McGregor. Dr. Bob Beecher of UDRI was also very helpful with the anthropometric aspects of this study. Overall, the laboratory proved to be a very stimulating and enjoyable work environment.

In addition, appreciation is expressed to Steve Goldner of Humanoid Systems and James Blaker of the Transportation Research Center of Ohio for their technical assistance.

I. INTRODUCTION

I received the B.S.E. degree from the University of Pennsylvania in Bioengineering, with a minor in Mechanical Engineering. As an undergraduate, I worked in the Head Injury Laboratory at the Hospital of the University of Pennsylvania. My Senior Thesis involved studies on strain detection within a physical model of the head. Recently, I received a Master's degree in Biomedical Engineering from Duke University, where I performed Modal Analysis on the human head.

The research problem at AARML/BBM was an investigation of the geometric, inertial, and mechanical properties of the head-neck systems of several anthropomorphic test dummies. These dummies are used in the evaluation and design of aircrew ejection seats. Both experimental work and computer simulation were included in this research effort. The problem under investigation at AAMRL/BBM was, therefore, very similar to the problems I had studied previously. Because of this similarity, I was assigned to work at AAMRL/BBM.

II. OBJECTIVES OF THE RESEARCH EFFORT

One goal of the AAMRL/BBM research program is to develop a durable, servicable, and biofidelic anthropomorphic dummy head-neck system with repeatable and reproducible biomechanical responses. Another goal is to develop data sets for the Articulated Total Body (ATB) Model and the AAMRL Head-Spine Model (HSM) which accurately predict the head-neck kinematics and dynamics of existing dummies in crash environments. To accomplish these goals, it was desired to measure, analyze, and simulate the kinematic and dynamic responses of Hybrid II, modified Hybrid II, and Hybrid III mechanical head-neck assemblies to abrupt decelerations imparted to the base of the neck by a pendulum test apparatus.

My individual objectives were:

- (1) to measure the geometric and inertial properties of the modified Hybrid II and Hybrid III head-neck systems and the pendulum test apparatus
- (2) to setup the test apparatus and instrumentation to measure the desired responses of these mechanical head-neck assemblies according to existing DOT specifications for Part 572 dummy compliance testing and recommended procedures for Hybrid III compliance testing
- (3) to analyze the measured geometric and inertial properties and pendulum test performance standards to determine inputs for both the HSM and the ATB Model.
- (4) to compare simulations of the pendulum tests to experimental results to verify the assumptions used to define the head and neck structures and validate the HSM and ATB Model data sets.

III. RATIONALE

In recent years, there has been an increasing awareness of both the serious consequences that can occur with head and neck injuries and the effectiveness of biomechanical studies to reduce the likelihood of these injuries. Two sources of information about head and neck injury and prevention are: (1) experiments with human surrogates; and (2) analysis of mathematical models. Information from dummy tests is limited. The use of inanimate devices reduces the repeatability problems associated with animals and cadavers but raises questions as to biofidelity. Attempts to improve human surrogate biofidelity are well documented. When a new manikin design is incorporated into a crash test program, data bases are generated which describe their geometric and inertial properties and mechanical behavior. Performance evaluations are conducted to ensure uniformity of results among different specimens and laboratories. Compliance tests are developed. Mathematical modeling is an accepted technique of scientific research. Once validated by comparison with experimental results, mathematical models are useful, economical, and versatile engineering tools. They can, in lieu of direct experimentation with actual physical systems, evaluate the effects of varying parameters on the responses of systems to a wide variety of input conditions. In particular, with validated data sets for the Hybrid II, modified Hybrid II, and Hybrid III head-neck systems, any environment or test, where the head and/or neck is in jeopardy, could be simulated.

It was expected that the proposed systematic study of the geometric, inertial, and kinematic and dynamic properties of mechanical head-neck assemblies would provide useful information to those interested in injury prevention and crashworthiness.

IV. BACKGROUND

Experimental Studies

Hybrid II, modified Hybrid II, and Hybrid III mechanical head-neck assemblies were chosen as specimens for this study.

The Hybrid II was the first GM dummy design to have acceptable repeatability and good durability and serviceability. The Hybrid II head-neck assembly is a fairly simple system. The head is a hollow aluminum casting, with a rear cap to allow access to the instrumentation inside. This instrumentation consists of a mutually orthogonal array of three uniaxial accelerometers; this array is mounted at the head CG. Both pieces of the head are covered with a rubber skin. The neck is a right circular cylinder of butyl rubber. It is solid, except for a small hole through the middle. Metal plates are molded into each end to facilitate head-neck and the neck-thorax attachment.

The AAMRL modified Hybrid II accommodates a load cell, for measuring neck axial and shear loads and moments about the occipital condyles, and a nodding joint at the occipital condyles. These modifications required alterations of both the head and the neck. A large hole was cut in the transverse bulkhead, the load cell and nodding joint were added between the base of the head and the top of the molded neck, and the accelerometer array was mounted on top of the load cell. Also, the solid molded neck was shortened in order to keep the overall height the same as that specified by DOT for Part 572 dummies. Another modification is the use of head accelerometers and an aluminum mounting plate unlike the devices supplied by Humanoid Systems. These modifications are significant and will probably alter the bending properties and overall performance of the head-neck system.

The Hybrid III head-neck system is a measurable improvement over the Hybrid II and modified Hybrid II systems in terms of component biofidelity in frontal impacts. The Hybrid III design represents state-of-the-art knowledge of human geometry, weight, inertia, and biomechanical response. The head is a hollow two-piece precision casting of 356 aluminum with T6 heat treatment. The thickness of the vinyl skin is specified and closely controlled to assure biomechanical fidelity and repeatable head response in hard-surface impacts. As in the modified Hybrid II, a load cell and nodding joint connect the head and neck. The molded neck is constructed of alternate layers of aluminum and 75-durometer (shore hardness) butyl rubber elastomer; the rubber layers are asymmetric to give different responses in flexion and extension. A steel cable runs through the center of the neck to provide axial strength. An adjustable bracket connects the neck to the thorax. The AAMRL Hybrid III dummy was modified to include head accelerometers and a steel mounting plate, unlike the devices supplied by Humanoid Systems, and an occipital condyle pin replacement, which permits attachment to the three-potentiometer unit. These modifications should not significantly alter the bending properties and performance of the head-neck system.

The head-neck pendulum test consists of a pendulum drop. At the bottom of the pendulum's swing, the arm impacts a block of honeycomb; this produces a near-square wave pendulum deceleration pulse. The head-neck system, which is mounted to the end of the pendulum, does not undergo any impact. The environmental test conditions, instrumentation requirements, and test procedures (including the pendulum geometric and inertial properties and strike plate deceleration pulse and impact velocity) are specified. For the Hybrid II dummy, the head rotation, chordal displacement of the head center of gravity, and maximum allowable

head acceleration are also specified. Hybrid II test procedures and performance standards are described in the Code of Federal Regulations, Title 49, Part 572. For the Hybrid III dummy, the moments at the occipital condyles and D-plane rotation are specified by recommended Hybrid III test procedures and performance standards, which are based on the General Motors Calibration Test Procedure, evaluation testing performed by the Transportation Research Center of Ohio for the NHTSA Vehicle Research and Test Center, and the Society of Automotive Engineers (SAE) Engineering Aid #23, written by the Dummy Testing Equipment Working Group. Currently, there are no DOT specifications for Hybrid III compliance testing.

The instrumentation used in a typical pendulum test consists of piezoresistive accelerometers, a six-axis load cell, a three-potentiometer device or high-speed 16mm camera, and a velocimeter with a photocell sensor. A triaxial accelerometer measures the pendulum arm deceleration 65.25 inches from the pivot point of the pendulum along the pendulum arm centerline. Three single-axis accelerometers measure the Hybrid II head accelerations. A two- or three-potentiometer unit or a high-speed 16mm camera measures head rotation and displacement data in order to obtain a complete description of head motion in the mid-sagittal plane. A six-axis load cell measures forces and moments at the modified occipital condyle pin of the Hybrid III manikin. A velocimeter-photocell device measures the pendulum velocity just prior to impact.

Theoretical Studies

Two types of mathematical models were selected for this study: (1) an internal body structure model; and (2) a whole-body gross-motion simulator model. Internal body structure models have been successfully

implemented at AAMRL for military applications (e.g., the dynamic responses of head-spine subsystems to +Gz accelerations). Numerous applications of whole-body gross-motion simulator models, involving automobile, pedestrian, and motorcycle crash victims, are documented in the literature.

Description of the Head-Spine Model

The Head-Spine Model (HSM) is a three-dimensional computer model which represents the human body by a collection of rigid bodies connected by deformable elements (Belytschko et al., 1976). The deformable elements can be beam elements, spring elements, hydrodynamic elements, or elastic surfaces. The rigid bodies generally represent bones (e.g., the head, vertebrae, pelvis, and ribs); the deformable elements represent soft tissues (e.g., viscera, ligaments, and intervertebral discs).

The mathematical model is a matrix structural analysis program. The program integrates the equations of motion in time, either implicitly or explicitly. The analysis accommodates large displacements of the rigid bodies, nonlinear material properties, and viscous forces.

The data base defines the structure to be modeled. It consists of the geometric and inertial properties of the rigid bodies, the geometric, inertial, and material properties of the deformable elements, the connectivity data, boundary conditions, constraints, and global coordinate system definition. The model inputs are defined in a separate subroutine called ICIF that is linked with the code prior to execution.

Description of the Articulated Total Body Model

The Calspan three-dimensional Crash Victim Simulator (CVS) Model is a digital computer program developed at Cornell Aeronautical Laboratory (McHenry and Naab, 1967) for the DOT for the study of human and dummy

dynamics during automobile crashes. Originally, its validity was determined from comparisons of predicted responses with those measured in sled tests and full-scale automobile crash tests using anthropometric dummies (McHenry and Naab, 1967; Bartz, 1972). The formulation, however, was of sufficient generality to allow application of this model to problems involving other impact environments. The Articulated Total Body (ATB) Model is a modified version of the CVS which accommodates specific Air Force applications such as vibration loading, encumbrance effects on crewman performance, and ejection from disabled aircraft (e.g., retraction, head-canopy impacts, windblast, parachute-opening shock).

The primary component of this program is the body dynamics model. The body dynamics model contains and solves the equations of motion and constraint. These equations are formulated from Euler's rigid body equations of motion with Lagrange-type constraints. This model differs from most other three-dimensional occupant models, which are formulated from Lagrange's equations of motion. Variation of the number of segments and joints is permitted within the formulation. In most applications, the crash victim is represented by fifteen rigid body segments connected by fourteen joints. The resulting simultaneous first-order ordinary differential equations are solved using a Vector Exponential Integrator. The three-dimensional rotational equations are integrated using quaternions (also known as Euler Parameters).

V. SFRP RESEARCH

As part of the SFRP at AAMRL, Paver and Doherty conducted experimental and theoretical studies of the Hybrid II, modified Hybrid II, and Hybrid III dummy head-neck assemblies and the Part 572 and recommended Hybrid III dummy head-neck compliance tests. Measurements were made of the geometric and inertial properties of the test specimens and apparatus. Mounting plates, test fixtures, and apparatus modifications were made. All transducers were wired; some were calibrated. The test specimens and apparatus were assembled for the Part 572 tests. A test plan was written. The measured geometric and inertial properties and Part 572 pendulum test specifications were analyzed to determine inputs for both the HSM and the ATB Model. Data sets which represent the Hybrid II head-neck system were developed for the HSM and ATB Model. The pendulum test was simulated to validate these data sets.

Experimental Studies

The inertial properties of the dummy head and neck segments were determined experimentally using balsa wood holding boxes, a C & S electronic scale, a moment table, a Space Electronics Model #KGR1000-3 Mass Properties Torsion Pendulum, a Hewlett-Packard HP85 microcomputer, and a Micro Control Systems perceptor three-dimensional digitizer linked to the AAMRL Perkin Elmer computer. The scale was used to determine the segment-box weight to the nearest 0.01 lbs. The moment table, which had two parallel knife edges, was used to measure the segment-box center of gravity (CG) location. One knife edge was placed on the scale and the other on a fixed stand. With the scale tared to zero, the first moment about the fixed blade edge was read directly from the scale. Then, using

the known distance between the knife edges, the exact location of the CG of the segment-box combination was calculated. The torsion pendulum was used to determine the moment of inertia of the segment-box combination about its CG. By performing this task with the segment-box in six different orientations, the inertia tensor elements at the CG were determined. Using these tensor elements and data obtained from the perceptor, the principal moments of inertia, and the direction cosines of the respective principal axes were determined. The effects of the box were removed and the inertial properties of the segment were calculated relative to specified points on the segment.

The geometric and inertial properties of the pendulum were also measured. The weight was determined with a high-capacity scale. A knife edge was used to measure the CG location. The torsion pendulum and HP85 microcomputer were used to determine the relevant moment of inertia. Although the pendulum was designed using the Part 572 specifications as a model, some differences exist. The estimated effects of the differences were negligible with respect to the dynamics of the head-neck system.

Simulating the Part 572 Head-Neck Pendulum Test with the Head-Spine Model

An HSM data set, which represents the Hybrid II head-neck system, was developed. The Part 572 head-neck pendulum compliance test was simulated to validate this data set. Since the head is connected directly to a cylindrical rubber neck and the base of the neck is connected directly to the pendulum arm during a test, the corresponding HSM was made up of two elements. A rigid body represented the head; a beam element represented the neck. The pendulum arm was not explicitly defined; the boundary conditions of the node at the base of the neck were made to reflect the presence of the pendulum.

For this simulation, it was necessary to describe the geometric and inertial properties of the head separately from those of the neck. Since the Part 572 specification requires that the head and neck properties be defined by the SAE Recommended Practice J963 (i.e., the head and upper neck are lumped together; the upper torso and lower neck are lumped together), this data was inappropriate. Instead, values for these parameters were abstracted and/or derived from Hubbard and McLeod (1977) and the Hybrid II Performance Evaluation Report (1973), where the geometric and inertial properties of the head are described separately from those of the neck.

The coordinate system was defined so that the positive x axis was the A-P direction, the positive y axis was the L-R direction, and the positive z axis was the S-I direction. The pendulum arm was free to rotate about the y axis only. Since the response is measured only from the time of impact to the time the head returns to the pre-impact position, the end of the pendulum (i.e., the base point) does not rotate during the test. The motion of this point was modeled as a pure translation in the x direction; no translations in the y and z directions or rotations about the x or z axes were allowed for this point. All other points were allowed to translate and rotate in the x-z plane.

A trapezoidal acceleration pulse with a 20 G constant peak acceleration was the excitation for the model. This pulse complied with Part 572. The initial condition was the pendulum strike plate impact velocity specified in Part 572. These two quantities were not included in the data set itself; they were inputs to the subroutine ICIF. This subroutine is called by the model after it reads the data set.

The data set was tuned to make the HSM head-neck response comply with the Part 572 head-neck pendulum test performance standards. Part 572 specifies the response in three ways: head rotation vs. time, chordal displacement vs. time, and peak head acceleration. Since the inertial properties of the Hybrid II head and neck are well documented, these constants remained fixed; they were not used to tune the data set. The stiffness and damping of the neck, however, are not as well documented. The values used initially for axial, bending, and torsional stiffness and damping were calculated from a material specification abstracted from a Sierra blueprint. The response of the model did not comply with Part 572 using these initial values; it was necessary to increase the amplitude and decrease the period of the response. The material properties of the neck were varied in a systematic manner to bring the response of the model into compliance with Part 572. It was discovered that a decrease in the bending stiffness increased both the amplitude and the period of the motion. A decrease in the bending damping increased the amplitude but had little effect on the period. Changes in the axial and torsional stiffness and damping had no effect on the performance of the head-neck system in bending. The final data set resulted in the correct period of rotation but slightly low amplitudes. The peak head acceleration was also slightly low. Both of these deficiencies may have resulted from the fact that the input acceleration pulse was trapezoidal, with a 20 G constant peak acceleration; actual acceleration pulses show a peak of 25-30 G's. These deficiencies may also have resulted from the initial condition specification; the actual neck velocity should be higher than the pendulum strike plate velocity. A more realistic excitation and initial condition would give the head a higher-amplitude rotation and higher peak accelerations.

Simulating the Part 572 Head-Neck Pendulum Test with the ATB Model

ATB data sets, which represent the Hybrid II head-neck system, were developed. The Part 572 head-neck pendulum test was simulated to validate these data sets. Initially, three segments were defined. Ball-and-socket joints were specified between the head and neck and between the neck and pendulum. A pin joint was specified between the pendulum and the vehicle. The geometric and inertial properties of the Hybrid II head and neck and the joint characteristics of the neck were abstracted from operational data sets at AAMRL/BBM. The pendulum geometric and inertial properties and joint characteristics were measured or estimated.

Two types of ATB simulations were performed. The first type were full-drop simulations where time zero represented the initial release of the pendulum. The second type were simulations of only the impact phase where time zero was the time just prior to the impact of the pendulum against the aluminum honeycomb.

The full-drop simulations were used to determine the relative angular orientation and velocity of the head and neck with respect to the pendulum just prior to impact. It was discovered that the time to impact and the initial striking velocity could be varied by changing the joint viscous coefficient of the pendulum pivot. The required simulation time varied from 750 to 1250 msec, depending on the specified impact velocity. Only the final 150 msec corresponded to the impact phase.

The impact phase simulations revealed a problem in the specification of the pendulum-honeycomb contact. Three approaches were considered:

- (1) The pendulum was defined as a segment with an attached ellipsoid and the honeycomb was defined as a plane. Plane-ellipsoid contact resulted.

(2) The pendulum was defined as a segment with an attached plane and the honeycomb was defined as an ellipsoid. Plane-ellipsoid contact resulted.

(3) The pendulum acceleration specified by Part 572 was input by defining the pendulum as the vehicle and attaching the neck to the vehicle. No contacts were defined.

Since the contact forces were defined in terms of the penetration between contact surfaces and since the strike plate was located at a distance almost equal to the major axis length of the pendulum ellipsoid, contact was not observed at the right point in space if the dimensions of the pendulum and honeycomb were defined correctly. Hence, both the amount of penetration and the contact time were low. One fix for this problem was to make the contact ellipsoid attached to the pendulum or honeycomb large enough so that the minor axis occurred at the strike plate location. This resulted in unrealistic graphics which were later modified in the AMRLVIEW input deck.

VI. RECOMMENDATIONS

The following are recommendations for future experimental studies:

- (1) Execution of modified Hybrid II and Hybrid III pendulum tests according to existing DOT specifications for Part 572 dummy compliance testing and recommended procedures for Hybrid III compliance testing. Some tests will be designed to assess the effects of three-potentiometer devices, in two different mounting configurations, on head-neck kinematics and dynamics.
- (2) Expansion of the test program to include other impact directions and deceleration profiles to obtain a comprehensive evaluation of the manikin head-neck responses.

The following are recommendations for future theoretical studies:

- (1) Continue tuning the proposed Hybrid II data sets.
- (2) Develop and validate data sets of the modified Hybrid II and Hybrid III head-neck systems. As a preliminary effort, the data sets would not contain detailed representations of every part of the neck. Instead, the effects of the nodding blocks, central cable, and the layered construction of the Hybrid III neck would be lumped together.
- (2) Develop and validate data sets which incorporate the occipital condyle nodding joint into the neck description. This joint is part of both the modified Hybrid II and III head-neck systems. Experimental determination of the torque-angle characteristics of the joint will be required.
- (3) Develop and validate Hybrid III data sets which incorporate the layered aluminum-butyl rubber construction of the neck.

REFERENCES

1. Bartz, J.A.: Development and Validation of a Computer Simulation of a Crash Victim in Three Dimensions. Proceedings of the 16th Stapp Car Crash Conference, SAE PAPER #720961, 1972.
2. Belytschko, T.; Schwer, L.; Schultz, A.: A Model for Analytical Investigation of Three-Dimensional Head-Spine Dynamics.
NTIS Report #AD-A025-911, April 1976.
3. Hubbard, R.P.; McLeod, D.G.: Geometric, Inertial, and Joint Characteristics of Two Part 572 Dummies for Occupant Modeling.
Proceedings of the Twenty-First Stapp Car Crash Conference, SAE PAPER #770937, 1977.
4. McHenry, R.R.; Naab, K.N.: Computer Simulation of the Crash Victim -- A Validation Study. Proceedings of the 10th Stapp Car Crash Conference, SAE PAPER #660792, 1967.
5. Miller, J.S.: Performance Evaluation of the General Motors Hybrid II Anthropomorphic Test Dummy, NTIS Report #PB-224-005, Department of Transportation Report #DOT-HS-800-919, September 1973.

1986 USAF-UES SUMMER FACULTY RESEARCH PROGRAM

GRADUATE STUDENT SUMMER SUPPORT PROGRAM

Sponsored by the

AIR FORCE OFFICE OF SCIENTIFIC RESEARCH

Conducted by the

Universal Energy Systems, Inc.

FINAL REPORT

MATERIALS EVALUATION AND FAILURE ANALYSIS OF VARIOUS ELECTRONIC
CIRCUITRY COMPONENTS OF AIR FORCE AIRCRAFT

Prepared by:	Franklin J. Dunmore
Academic Rank:	Bachelor of Science Degree Holder and Master of Science Candidate
Department and University:	Department of Physics and Astronomy Howard University
Research Locat:	Air Force Wright Aeronautics Laboratories Materials Laboratory, Materials Integrity Branch, Electric/Electronic Failure Analysis Laboratory
USAF Research:	Dr. Bill Dobbs
Date:	August 15, 1986
Contract No. :	F49620-85-C-0013

MATERIALS EVALUATION AND FAILURE ANALYSIS OF VARIOUS ELECTRONIC
CIRCUITRY COMPONENTS OF AIR FORCE AIRCRAFT

by

Franklin J. Dunmore

ABSTRACT

This report contains the objectives, procedures and results of the work that was done by the author on failure analysis of various aircraft electronic components and related apparatus. Section III deals with the electrostatic discharge and surface resistivity test of a pair of antistatic gloves for handling electrical overstress sensitive electronic components (for example, field effect transistors). Section IV deals with solder strength tests and solder joint flaw inspections of printed circuit boards of F-15 aircraft. Section V deals with the study of the growth mechanism of Tin Whiskers. Section VI deals an accelerated lifetime study through thermal-shock treatment of Printed Circuit Boards of C-5B aircraft and of a newly designed Printed Circuit Board (PCB) from Manufacturing Technology Division.

/NP/

I. INTRODUCTION:

I am a Master's Degree Candidate in Physics at Howard University in Washington D.C. optics and solid state physics are my fields of interest. Electronics failure analysis has important applications of solid state physics and materials science. My previous knowlege of physics, chemistry and microelectronics is why I was selected for this assignment at the

ACKNOWLEDGEMENTS

I would like to thank the Air Force Systems Command and the Air Force Office of Scientific Research for their sponsorship of my research and learning experience. I would also like to thank Air Force Wright Aeronautics Laboratories, the Materials Laboratory, the Systems support Division, and the Electronic Failure Analysis Laboratory.

My personal thanks goes to Dr. Bill Dobbs, Failure Analysis Lab Senior Engineer, T.D. Cooper, Materials Integrity Branch chief, and Ron Williams, Technical Area Manager. Personal thanks goes to George Slenski, Eddie White, Paul Jarusiewicz and 1st Lt. Michael Marchese of the Failure Analysis Lab as well as Dale Hart, Rick Reibel and John Zigenhagen of the University of Dayton Research Institute for their assistance at the Failure Analysis Lab. Thanks goes to secretaries Sherri Swihart and Abbey Beam for their help.

Failure Analysis Lab and this knowledge was very useful in learning and performing the techniques of materials evaluation and failure analysis.

II. OBJECTIVES

The summer research goal and objective was to learn about and gain experience in failure analysis techniques. Not having previous experience in this very important field, the experience that was gained in the practical applications previous physics training will be of great help in advancing a future career in applied physics. During the summer these projects were received to be completed: Electrostatic Overstress/Electrostatic Discharge (EOS/ESD), surface resistivity, and chemical resistance test of antistatic glove material; solder joint testing of Printed Wire Boards (PWB's) from F-15 aircraft; Tin Whisker location, morphology study, and origination mechanism study; and the resoldering and thermal shock of IC chips and PCBs.

III. CHEMICAL RESISTANCE, SURFACE RESISTIVITY AND EOS/ESD TESTS OF OAK TECHNICAL INC. ANTISTATIC GLOVE MATERIAL

A. Chemical Composition and Resistance Test

The glove material was shown through chemical analysis to consist of polyvinyl chloride (PVC) with an organic ester dioctyl phthalate (DOP) mixed in throughout as a plasticizer for elasticity. Silicon and calcium were found in the material as the possible, but unlikely surface conductive agents(Ca being hydrophilic, may cause a somewhat conductive surface film). The actual conductive are proprietary information that the manufacturer would not disclose. Unfortunately, the chemical analysts could not ascertain the conductive compound.

Since many chemical solvents are used in failure analysis work as well as other work with electronic components, it is desirable that the glove material remain unchanged by contact with the chemicals (hence the name chemical resistance). Sections of the glove were immersed in various common solvents and ultrasonically vibrated 30 seconds for surface cleaning purposes. Then the sample sections were inspected. Results of this test are in Table 1.

The material failed the chemical resistance test with all test solvents except, marginally, for methanol. Chemical analysis showed that the DOP plasticizer was 30% washed out in the non-methanol cases, and that was enough to cause the effects of the first four of the chemicals listed in table 1.

B. Surface Resistivity Test

Important articles that need low surface resistivity are antistatic gloves that are used for protection of electronic circuitry components from electrical overstress from electrostatic discharges from 5 to 15 kV. that can easily cause total failure of such devices. These discharges are emitted from a person's touch because flesh as a relative insulator accumulates much static charge. Low surface resistivity gloves allow accumulated charge to dissipate sufficiently rapidly such that dangerous build ups of static charge cannot occur.

1. A surface resistivity test was conducted using a Hewlett-Packard 16008A Resistivity Cell connected to a Hewlett-Packard 4329A High Resistance Meter. The sample was an approximately 3 by 3 in. square sheet from the wrist area of the glove that was not chemically treated. The sample was placed so that contact was made on the annular ring electrodes of the resistivity cell without excessively stretching the sample.

2. From test voltages ranging from 25 to 1000 volts, the surface resistivity mean was calculated to be 170 gigaohms/square (with the largest value of 174 and the smallest value of 164). There was no systematic variation of surface resistivity with respect to test voltage. The mean value of surface resistivity compares quite favorably with the value claimed by OAK, 450 gigaohms/square. This amount of surface resistivity allows static charge to be dissipated in time, but still the glove insulates the hand from electrical current at relatively low voltages.

C. Electrostatic Overstress/Electrostatic Discharge Test

1. An electrostatic discharge test was conducted using Federal Test Method Standard 4046.1, no. 101C as the model for the test. The discharge time measurement was done for the glove being positively and negatively charged to the voltages of 0.5, 1.0, 1.5, 2.0, 2.5, and 3.0 kilovolts. This was done using an x-y plotter with the decay time as the horizontal axis and the accumulated charge as the vertical axis. The accumulated charge versus decay time plots for positive voltage and negative voltages are at the Failure Analysis Laboratory. A 5 kilovolt DC power supply was not available. The measured discharge time was the time interval necessary for the accumulated charge to decay to 10% of maximum. The results for both the positive and negative voltages are shown in tables 2 and 3 respectively.

2. Semi logarithmic plots were made for the discharge time versus test voltage for positive and negative voltages, and are shown in figures 2 and 3 respectively. The decay time versus test voltage data plots were extrapolated to 5 kilovolts using exponential curve fitting of the data points (since the $t=0$ voltage-axis is an asymptote to the negative

exponential curve that is formed by the data points). The extrapolation was done to determine the data points at the Federal Test standard two second mark, where the static charge must dissipate to ten percent of its time equals zero value. The correlation coefficient for data table 1 is 0.93, that for data table 2 is 0.96

IV. SOLDER JOINT STRENGTH TESTS

Solder joints are a major source of failure in integrated circuit systems. Open circuits due to solder joint (SJ) cracks and pores (air bubbles) causing PCBs to be jarred loose can easily cause total failure (circuit never works) or the even more serious intermittent failures, where the circuit operates at first, then fails. Each PCB section tested was manufactured by Hughes Aircraft Inc. for the F-15 and had 15 SJs on each of 2 sides of one IC chip carrier. Only one side (15 SJs for each) were tested.

A. Visual Pre-Inspection and Thermal-cycling

Untreated SJ's were inspected visually for small cracks that may weaken SJ strength. No anomalies were found. Then 2 of the PCBs were put through thermal-cycling. Thermal-cycling replicates the transition from the high temperatures of operation to the cold temperatures of high altitude flight. This cycling induces thermal stress causing strains that can cause SJ cracks. PCB1 was not put through any thermocycling. PCB2 was put through 10 thermal cycles and PCB3 was put through 106 thermal cycles, both from -55 degrees celsius to +125 degrees celsius.

B. SJ Pull Strength Test

Here was determined the amount of pull force (in grams) and stress (lbs./in. sq.) needed to detach the SJ heel from the solder pad.

Extensive tables of these values are available in the failure analysis lab. The instrument used was a Chatillon Digital Force Gauge and the minimum failure force required was 300 grams. The vast majority of SJs passed this test, but PCB3 showed 2 cracked SJs after thermal-cycling. The subsequent pull test showed that these SJs failed at 100 grams, with the cycling induced cracks directly responsible for the failures. Microscope photographs (micrographs) of the cracks and other photographs of the 3 PWBs and their SJs are available at the lab. The results of the pull test are in table 5.

C. Post SJ Pull Inspection

After SJ pull tests the SJ pads were inspected by naked eye, stereo microscope and Zeiss high magnification microscope, and micrographs as well as photographs were taken. These pictures are at the lab. The anomalies looked for were off-center SJ bonds and porosity at the SJ heel. There is a substantial but not complete correlation between SJ heel porosity and SJ strength failure (SJ pull strength under 300g). Some passing SJs had substantial porosity, some did not, vice versa for those with low porosity. There was a stronger correlation between off-center bonds and pull strength. Extensive tables of off-centeredness and SJ pad porosity are at the lab. In this specific group of three PCBs, the expected weakening of SJs by thermal-cycling did not make itself apparent in Table 5. This was because PCBs 2 and 3 were inherently better soldered than PCB 1.

V. TIN WHISKERS

Tin Whiskers have been a recurring problem in electronic circuitry for nearly three decades since the development of integrated circuitry . The whiskers, ranging from a few to several hundred microns in length and

from a small fraction of one to two microns in diameter, grow spontaneously from the inside of tin coated lids that seal IC dies, and tinned switch contacts. Vibrations cause these whiskers to fall from their roots and then rest on the circuitry, causing very serious short circuits that may (and often do) lead to failure of the IC devices. And short circuits across open switch contacts can also occur.

Soon after the discovery of the tin whisker problem, a solution was found, replacing tin plating with cadmium plating. But it was discovered in the early seventies that cadmium was a serious environmental pollutant, so tin was brought back. The main method used today to reduce the number of whiskers growing on tin lids is annealing (heating just below the melting point of tin) for hours in order to relieve the stresses in the plating that arise when melted tin cools then hardens.

Stress relief has long been thought to be the cause of whisker growth, though whiskers still grow in metal plating, be it at a slower rate, after annealing. Stress relief phenomenon also does not explain the fact that most whiskers are single crystals. The extrusion of metal into cylindrical whiskers by stress will produce amorphous structured tin, not tin with definite crystal structure. Corrosion has recently been thought to play a role in a theory under consideration by Dr. Dobbs. Hydrogen chloride, present in the tinning process, may not be completely removed before tinning is completed. Chlorine being very corrosive may react with tin (corrode tin), with the ensuing chemical reaction thermal energy being a source for whisker growth as well as potential energy from stress. From the chemical corrosion process may come the explanation for whiskers having definite crystal structure.

1. Individual whiskers were located and documented in their original tin lids using a Zeiss high magnification microscope. Then all of the whiskers were micrographed with a Scanning Electron Microscope (SEM) at magnification from 50X to 2000X, for the purpose of morphology study of individual whiskers. Individual whiskers were the transplanted to special grids that would be placed in a Transmission Electron Microscope (TEM) in order to do an electron channeling study of the objects. Electron channeling is a method of electron diffraction through a metal crystal in order to obtain the crystal morphology of a metal specimen. Other whisker samples were placed on slides for X-ray topography and X-ray diffraction study.

2. At the point in time that this report is being written, none the crystal diffraction results have yet arrived.

VI. ACCELERATED LIFETIME STUDY OF PCBs THROUGH THERMAL-SHOCK

A new PCB design was formulated by Manufacturing Technologies division that had a surface solder mount for IC chips instead of the standard plated through hole that mechanically held the chip to the PCB. this has been contraversial because of the problem of ceramic chip carriers having a very diferent coefficient of expansion than that of the organic epoxy resin of the PCB surface. This difrence in coefficients leads to stress causing strain that causes SJ cracks and the problems that come with them. In order to judge in a controlled test the likelihood of this happening the IC carriers were removed by heating the standard PCB to the melting point of solder (the IC carriers were empty of Ics so that heat dammage was not a concern). Then the carriers were resoldered on the surface mount PCB.

The operation of PCBs leads to heating due to current in circuits. An aluminum heat sink sandwiched between the two layers of lamination in order to dissipate heat has also been disputed as to whether the thermal expansion problem is improved or worsened by it.

1. The Man. Tech. boards are to put through Thermal-shock in order to test the likelihood of SJ cracks occurring during operation. Thermal-shock procedure is to switch specimens quickly between two air or fluid filled chambers, this test using air filled chambers, one at -55 deg. C. the other at +125 deg. C. for one half hour a piece, making one cycle, for 100 cycles according to Military Standard 202F.

Two other PCBs, manufactured by Lockheed, that were submitted for thermal-shock analysis, having had problems with solderability (the ability of solder to adhere on the surface of the epoxy resin lamination). Thusly either too much or too little solder was placed on the solder pads over the plated through holes. Lack of solder will increase the probability of SJ cracks, as will excess solder to a lesser extent. The results of thermal-shock analysis will determine if the Lockheed PCBs will be purchased by the Air Force.

2. At the 56 cycle point, SJ cracks first appeared at the base of the chips of the Man. Tech. board. The sides that had the greatest number of cracks were those that had the smallest amount of solder most like the original board. The SJs that had substantially more solder avoided cracks. The Lockheed PCBs also had the appearance of new SJ cracks at the 56 cycle point. At the 69 cycle point, the next smaller sized chip carriers on the Man. Tech. PCBs began to have SJ cracks, as well as the joints with more solder. On the Lockheed boards, cracks found before continued to get larger. The three PCBs had these SJ cracks, both before and after

thermal-shock, photographed and documented.

VII. RECOMMENDATIONS

A. With regard to section III., these recommendations can be put forth.

1. The OAK antistatic gloves should not be used near chemical solvents.
2. These gloves should not be the primary means of antistatic protection, but in combination with other common anti electrical overstress procedures (e.g. conductive to ground wrist straps and table mats).
3. A conductive surface coating, such as a detergent type substance or a carbon black should be place on the surface of the gloves in order obtain low surface resistivity and provide continued EOS/ESD protection.

B. With regard to section IV.

1. In Air Force operational systems subject to the extreme environmental and mechanical stresses that the F-15 is subject to, mechanical durability of solder joints is of utmost importance. More resources must in general be devoted to the quality control solder joints with special consideration given to the centering of SJs and procedures to prevent porosity of SJs, such as non-corrosive solder flux.

C. With regard to section V.

1. Since there is not an experimentally verified theory that explain all important aspects of metal whisker growth, and since metal whisker growth has the potential of being a problem in future more densely packed ICs; research on the specific growth mechanism of whiskers, like the research begun during this summer at the materials lab, is recommended for the future in electronics.

D. With regard to section VI.

1. At this point, the results show that fatigue (SJ cracks) are still a serious problem in the Man. Tech. surface mount board. The main problem is that the ceramic chip carrier has a different coefficient of expansion than the epoxy lamination surface. In the future, a chip carrier must be developed to that has the same expansion coefficient as the lamination surface.

TABLE 1

SOLVENT	CONDITION
Freon-ethanol	crisp, stiff, lossed all resilience
Freon-trimathylene	"same"
Freon-acetone	"same"
Isoprpyl-alcohol	"same"
Methanol	"same" but to a much lesser extent

TABLE 2

TEST VOLTAGE V (KV.)	DECAY TIME T (SECS.)
+0.5	16.3
+1.0	10.0
+1.5	12.5
+2.0	9.2
+2.5	7.0
+3.0	5.5

TABLE 3

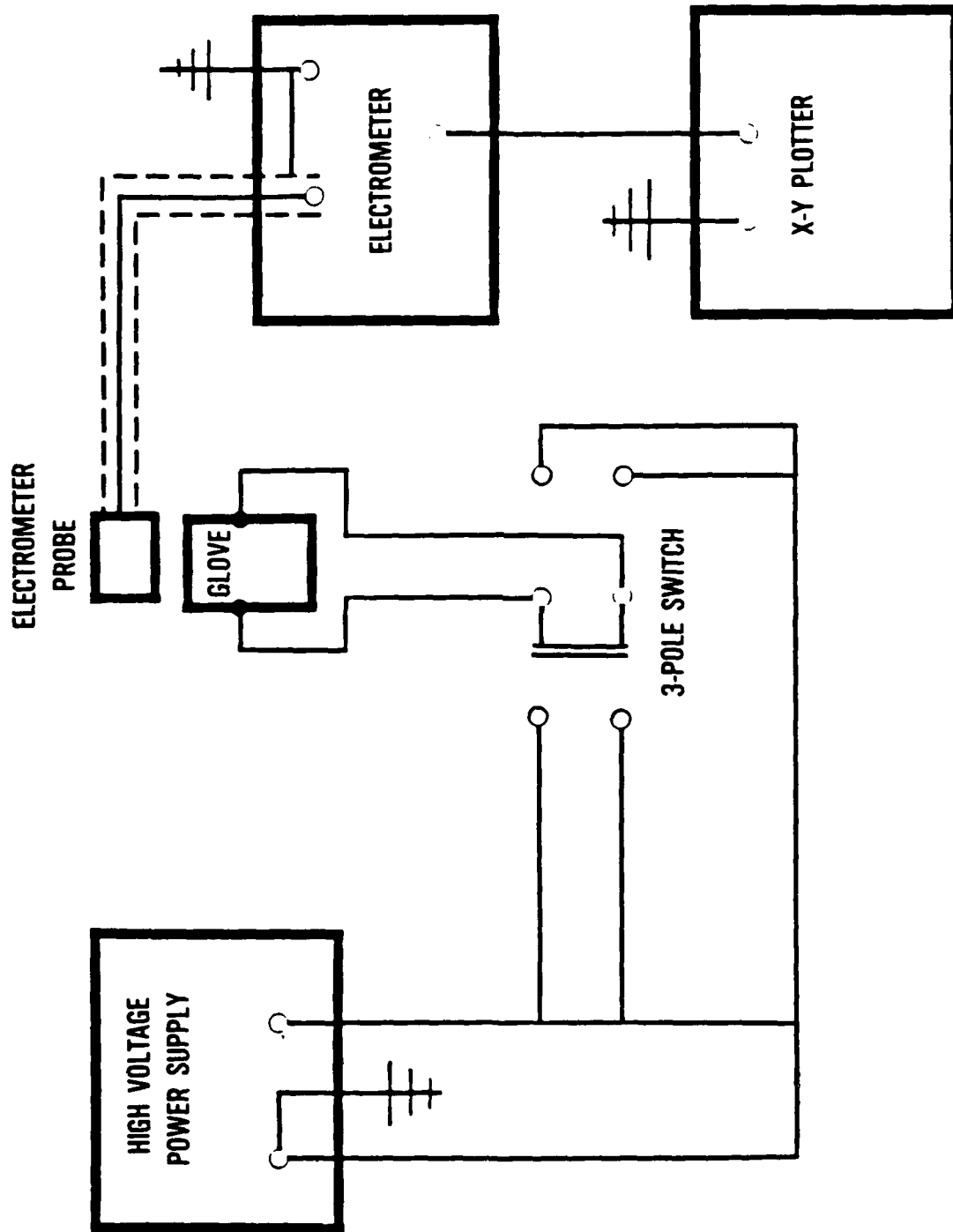
TEST VOLTAGE V (KV.)	DECAY TIME T (SECS.)
-0.5	26.0
-1.0	18.5
-1.5	12.0
-2.0	12.0
-2.5	9.7
-3.0	8.2

TABLE 4
EXTRAPOLATED DATA POINTS

V (KV.)	T (SECS.)
+5.0	2.7
+5.75	2.0
-5.0	3.2
-6.05	2.0

TABLE 5

	MEAN	STAN. DEV.	HI	LO
PCB1	960g	540g	1900g	200g
PCB2	1420g	650g	2200g	600g
PCB3	1700g	320g	2100g	100g



ELECTROSTATIC DISCHARGE RATE MEASUREMENT SET UP

FIGURE 1

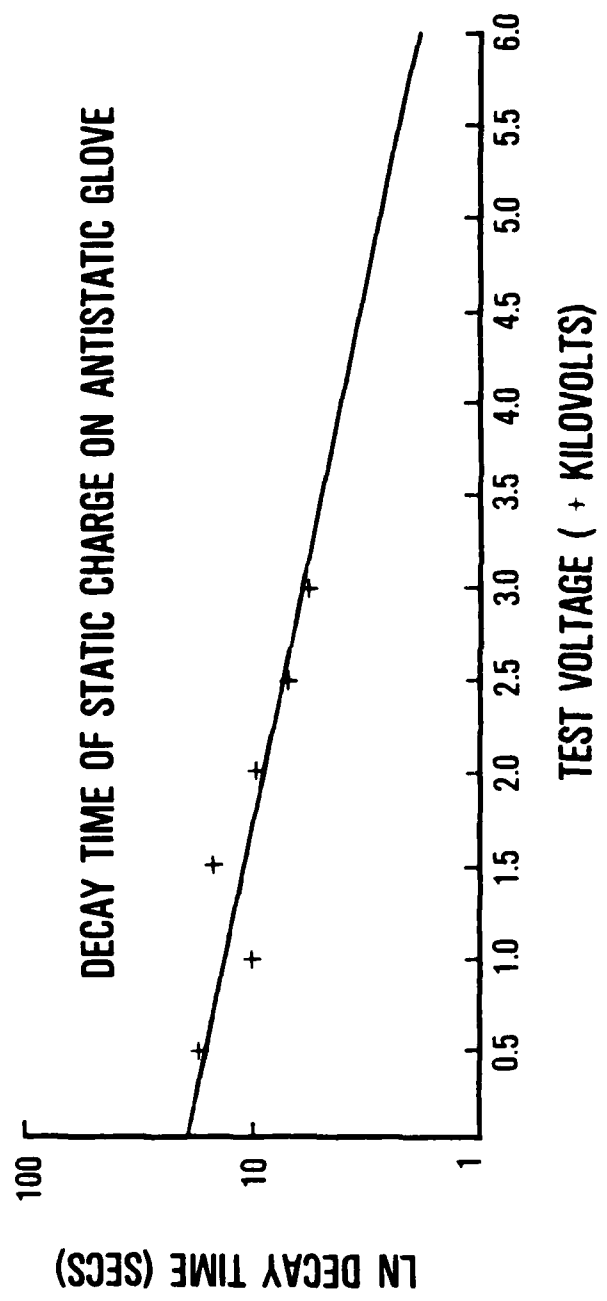


FIGURE 2

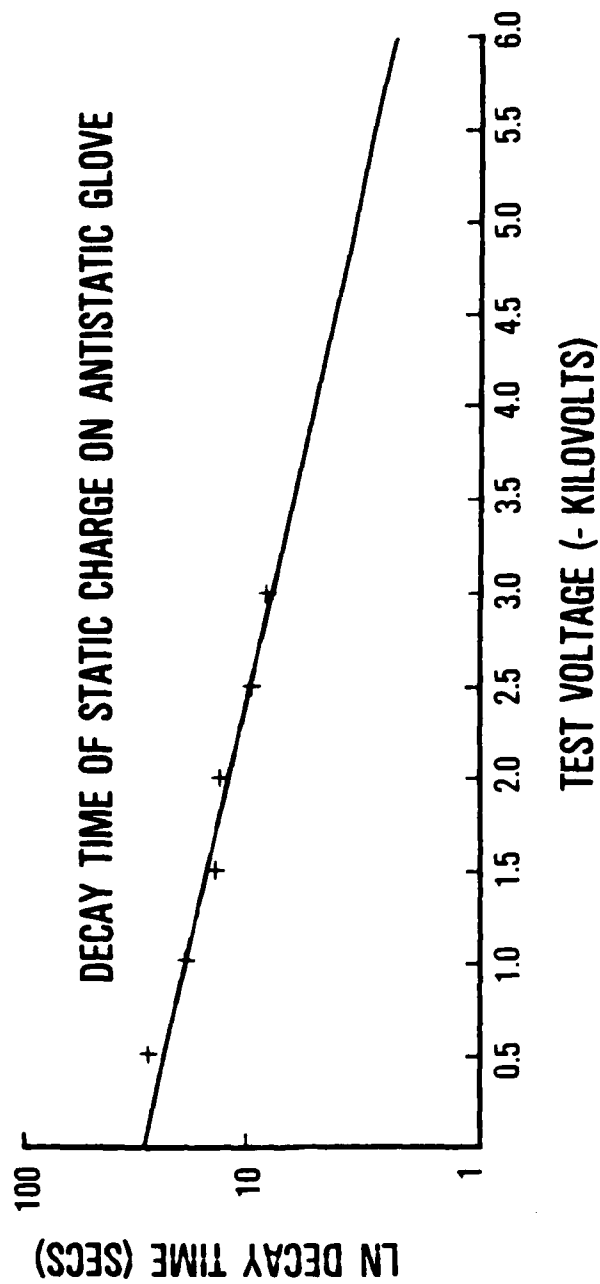


FIGURE 3

REFERENCES

1. Huntsman and Yenni, "Test Methods for Static Control Products," Electrical Overstress/Electrostatic Discharge Symposium Proceedings Vol. IV. 1982
2. Devaney, Hill and Seippel, Failure Analysis , Mechanisms and Photo Atlas, Failure Analysis recognition and Training Services Inc. Monrovia Ca. 1983.
3. Doyle and Morris (Editors) Microelectronics Failure Analysis Techniques, a procedural Guide. U.S.A.F. , General Electric and ITT Research Institute.
4. Hada, Marikawa and Togami, "Study of Tin Whiskers on Electromagntic Relay Parts," Proc. 26th Annual National Relay Conference, Oklahoma State University, Stillwater Oklahoma, April 1978 pp. 9-1 9-15
5. Furuta and Hamamura, "Growth Mechanism of Proper Tin Whisker", Japanese Journal of Applied Physics. Vol 8., No. 12 December 1969 pp. 1404-1410
6. Lane, Pease and Yew, "Electron Channeling Patterns in the SEM," ETEC Corporation publication, Hayward California.
7. Military Specification 8170B, Amendment 3, June 9, 1983

8. Federal Test Method 4046.1, Method 101 C, Change Notice 1, October
8,1982

9. Military Standard 202F, Method 107G, April 1 1980

1986 USAF-UES SUMMER FACULTY RESEARCH PROGRAM

GRADUATE STUDENT SUMMER SUPPORT PROGRAM

Sponsored by the

AIR FORCE OFFICE OF SCIENTIFIC RESEARCH

Conducted by the

Universal Energy Systems, Inc.

FINAL REPORT

Thermal Characterization of New Thermally Stable Matrix Materials

Prepared by:	Michael P. Farr
Academic Rank:	Graduate Student
Department and	Material Science Department of
University:	The Pennsylvania State University
Research Location:	Air Force Wright Aeronautical Laboratories Material Laboratory, Polymer Branch Properties Group
USAF Researcher:	Dr. Ivan Goldfarb
Date:	8/27/86
Contract No:	F49620-85-C-0013

THERMAL CHARACTERIZATION OF NEW THERMALLY STABLE MATRIX
MATERIALS

by

Michael F. Parr

ABSTRACT

Two different systems were studied, a 1:1 molar ratio of BCB/BMI and an oligomer of BCB. As part of the 50 gm evaluation thermal analysis of both systems and their constituents was performed. The BCB/BMI system had some type of impurity which affected the curing reaction. A large portion of the work was spent cleaning the system. Since the BCB oligomer system was pure, a large portion of the 50 gm evaluation was able to be completed. The oligomer system has promising properties for use as a high performance matrix material. Unfortunately, not enough work was completed on the BCB/BMI to make an estimation of its possible usefulness.

ACKNOWLEDGEMENTS

I would like to thank the Air Force Systems Command and the Air Force Office of Scientific Research for sponsorship of my research. I would also like to extend my appreciation and thanks to the staff of the Polymer Branch of the Materials Laboratory for making my summer such a positive experience. Finally, I would like to offer a special thanks to Dr. Ivan Goldfarb, Ms. Lisa Denny and Mr. Bill Olick for their assistance and guidance in my research.

I. INTRODUCTION

I am presently finishing my masters degree in Polymer Science at the Pennsylvania State University (PSU). The research performed has been concerned the with thermal analysis of unique isomers of common polymers (specifically poly vinylidene chloride). A large portion of the project dealt with the thermal stability and the kinetics of decomposition of the isomeric polymers.

The Polymer Branch of the Air Force Materials Laboratory is involved in synthesis and characterization of new high performance polymers for Air Force type applications. When a new polymer is developed, it progresses through a series of scale up steps. The final step is an extensive 50 gm evaluation to determine the usefulness of the material.

A large portion of the evaluation deals with thermal analysis of different polymer systems. Although the analysis differs in some areas, the general concepts are quite similar to the work I have been doing at PSU. In order to complete as many evaluations as possible, I was assigned to work on two 50 gm evaluations.

II. OBJECTIVES

The overall objectives of the project is to develop new, less water absorbant, thermally stable matrix materials for Air Force uses. My personal objectives were to:

- 1) Perform parts of the 50 gm evaluations of two different

polymer systems, 1:1 molar ratio BCB/BMI and BCB oligomer.

2) Develop a curing mechanism for the BCB/BMI system.

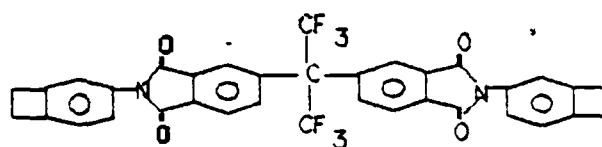
3) Compare the properties of the BCB/BMI 1:1 system with different molar ratios. Also to ascertain why all the systems seem to have the same thermal stability.

III CHEMISTRY OF THE SYSTEMS

To be able to grasp the significants of the thermal results a brief overview of the chemistry of the systems is required. The two compounds used in the investigation are highly conjugated and are end capped with reactive groups. The synthesis of the monomers has been published several times¹⁻³. The first monomer,

Bis-2,2-(N-4-Benzocyclobutenyl phthalimide),

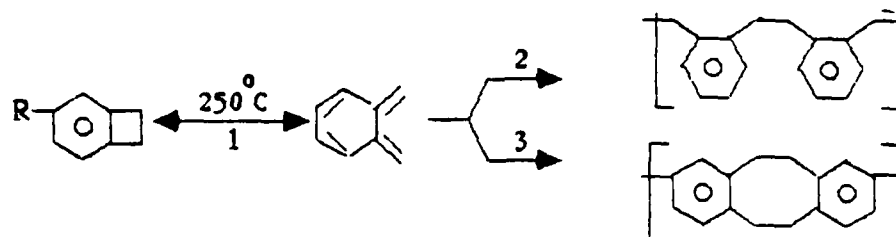
hexafluoropropane (abbreviated BCB₇, may



BCB

undergo several homo reactions. At approximately 250 °C the cyclobutene rings open forming diene end groups (Fig. 1).

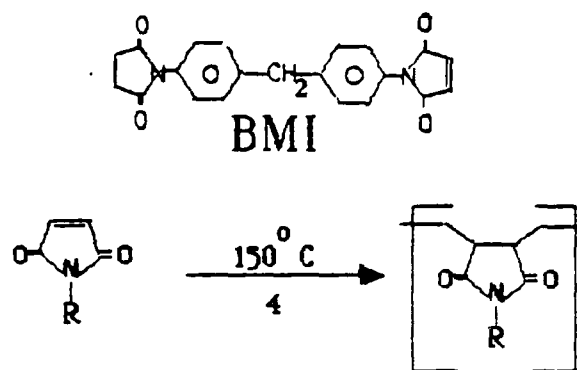
From this point the diene can go on to react two ways.



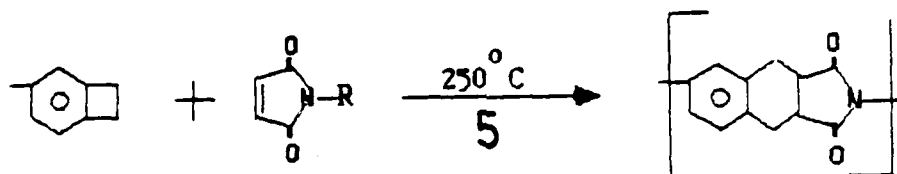
First, the diene can react to form linear chains (Reaction 2). Second, two dienes may react to form an eight membered

ring (Reaction 3). These are the types of reactions which form polymer from the BCB oligomer.

The other monomer, 1,1'-(Methylene di-4,1-phenylene)bismaleimide (abbreviated BMI), only undergoes one reaction upon heating; the thermal radical polymerization of one double bond of the imide end group (Reaction 4)⁴. The



mixing of the two monomers presents the possibility of another reaction. It has long been known that dienes in the presences of a dienophile will under go



cycloaddition (Reaction 5). This reaction is made use of in the copolymerization of the two monomers. It is assumed that reaction 5 is the preferred reaction of the co-system polymerization.

IV. EXPERIMENTAL

The 1:1 molar ratio BCB/BMI comonomers and the BCB oligomer were provided by S.A. Ian and F.E. Arnold of AFWAL/MLRF using the procedure outlined in previous

articles¹⁻³. The co-system was found to contain contaminants which affected the cure reaction, the BCB oligomer seemed free of contaminants.

Differential Thermal Analysis (DSC) was performed on a DuPont Thermal Analysis System. All experiments were done using a heating rate of 10 °C/min and a nitrogen atmosphere. In addition, the thermal kinetics were obtained using the method outlined by Goldfarb et al³. Data used in the kinetic analysis was collected using a Perkin Elmer DSC II using heating rates from 5 °C/min to 80 °C/min.

Cure rheology data was determined using a Rheometrics Dynamic Spectrometer (RDS). The 25 mm parallel plate experiments provided information on the viscosity profile and possible gelation time of the different systems. Two types of experiments were performed on the BCB/BMI system: a temperature sweep at 2 °C/min, and two time sweeps isothermal at 150 °C and 170 °C. These experiments could not be performed on the BCB oligomer system due to high glass transition temperature (160 °C) and fast reaction at temperatures around 200 °C.

Torsion Impregnated Cloth Analysis (TICA), which has been previously described⁴, supplies information on vitrification times and dynamic mechanical Tg's of the resins before and after cure. Since the BCB/BMI sample was contaminated, TICA was only performed on the BCB oligomer. The temperature scans were run at 2 °C/min with a nitrogen atmosphere.

Twenty samples of BCB oligomer, each weighing 1.63 g, were compression molded into dogbone tensile testing samples. The following cure cycle was used to prepare the dogbones. Samples were deaerated for one hour at 100 °C. Next, each sample was placed in a mold which was preheated to 200 °C, in a computerized controlled press. The curing process contains three stages. First, so that the material may soften and fill the mold; the sample is held at 365 °F with a pressure of 600 psi for fifteen minutes. Next, the temperature is raised to 430 °F for 45 minutes to cure the polymer. This step is accompanied by a decrease in pressure to 260 psi. Finally, postcuring is completed at 500 °F for fifteen minutes at minimal pressure. All the samples were stored in a desiccator until testing. Due to the time restriction of the summer only preliminary tensile testing was done. These test were done on a Instron model 1102.

V. RESULTS AND DISCUSSION

(A) POLYMER FROM BCB OLIGOMER

The investigation of the BCB oligomer system covered three areas. First, thermal analysis was performed. The analysis including DSC and kinetics of both the monomer and the oligomer. Second, rheometrics studies were carried out on the oligomer system. Finally, some preliminary work was carried out on the mechanical properties of the system.

In order to obtain data needed for other work the first step is to accomplish thermal analysis of the system. The analysis consist of determining relevant thermal parameters.

such as T_g uncured, T_g cured, the cure temperature, and reaction kinetics. By comparing DSC traces of the monomer with the oligomer several interesting facts are brought to light. First, as expected due to the increase in molecular weight; the oligomer has a higher T_g than the monomer (150 C to 230 C). These numbers are used to base temperature parameters for the rheometric studies. Second, the polymerization peaks for both systems are approximately the same in height and position. And the oligomer trace shows a cured T_g of 293 C.

Kinetic results show approximately the same energy of activation for both samples. The oligomer has an average energy of activation of 31 kcal/mole, while the monomer is 33 kcal/mole. Also, the general trends of the energies throughout the reaction are same. There seems to be an induction period from 0-60% conversion, after which there is a decline in energies. The activation energy of breaking a butene ring and forming a diene has been reported to be 32.3 kcal/mole. One explanation for the trends seen, is that the diene, formed by the opening of the butene ring, must reach a certain initial concentration. The polymerization reaction needs less energy and could explain the apparent drop off in energy at the latter conversions. The kinetic data also provided a reaction window plot from which the extent of reaction can be predicted versus time.

With an understanding of the thermal properties of the system, rheometric work can be done. The first step is to

run parallel plate experiments to obtain a viscosity profile. Unfortunately, due to the high T_g (150 C), the system does not soften enough before beginning to cure so as to be able to obtain a viscosity profile. Fortunately though, good data was acquired from the TICA experiments. The cure scan showed the system had an uncured T_g of 166 C and a vitrification maxima of 239 C (Plot 1). The cooling scan showed the cured polymer had a T_g of 180 C. It should be noted that there are several discrepancies between the DSC and TICA results. These differences are largely due to the nature of the techniques.

The last piece of work performed using the BCB oligomer was the optimization of a cure cycle and preliminary testing of the tensile samples. The cure cycle used is described in the experimental section. It was felt that this cycle produced the optimum cured sample. Preliminary tensile testing (Plot 2) yielded a tensile strength of 9715 psi and a elongation to break of 4.68%. These numbers compare well with those of epoxy systems in the literature (tensile strength 8000-10,000, elongations 2-5%). It should be noted that these results are for BCB samples which have not been uncured. These properties should increase on postcuring.

(B) BCB/EMI 1:1 MOLAR RATIO CO-SYSTEM

The major thrust of the project was to be characterizing the system. Due to problems of contamination, which affected the reaction mechanism, very

little work was done on the 50 gm evaluation and the cure mechanism. No work at all was done on a comparison of the properties of the different molar ratios. Instead, using thermal analysis along with viscosity profiles I attempted to ascertain if the contaminants affecting the reaction had in fact been removed.

Thermal analysis, in particular DSC, is very useful in determining the presence of side reactions. In some earlier work on the BCB/BMI system* only one major exotherm (centered around 255 C) was present on the DSC trace. Upon scaling up the synthesis process of the co-system to 50 grams, some type of contaminant or unreacted species must have been introduced to the system. Results from DSC work on the 50 gm sample indicated a second peak centered around 174 C. Furthermore, the peak was not present in either of the DSC traces of the individual monomers. The BMI monomer has a crystalline melting endotherm which leads into a shoulder on the main polymerization peak. It is quite possible that either the melting endotherm is masking the exotherm or that crystallinity inhibits the reaction.

In an attempt to ascertain the origin of the contaminants, the BMI, which was felt to contain the contaminant, was repurified and mixed with a sample of BCB used in the 50 gm sample. DSC analysis still indicated the presence of a low temperature exotherm. Finally, both monomers were repurified. The analysis of this sample showed only the main exotherm, indicating that the system

was now at levels as pure as the original polymer was indicated.

Viscosity data indicates what seems to be a decrease in processing properties with an increase in purity of the system (Plot 3). The relatively high "minimum viscosity" and speed with which the 30 gm sample began curing was quite unexpected. These results also seemed to indicate some type of secondary reactions. Analysis of the other samples were even more unexpected. With higher purity samples, the temperature at which the "minimum viscosity" was reached showed a continued decrease. In addition, the system began curing quicker as sample purity improved. This type of behavior would indicate that impurities, what ever they were, inhibited to some extent the cure reaction. Inhibition, in this case, yields more favorable processing conditions. The behavior of the system is quite puzzling and merits further investigation.

7. RECOMMENDATIONS

A. BCB OLIGOMER

The BCB oligomer system seems to have promise. Several aspects of the project still need some work.

1) The rest of the 50 gm evaluation needs to be completed. This entails the finishing of the mechanical properties and the Torsion Bar testing.

2) The processing of the material would profit from a investigation into two areas of the synthesis of the oligomer. First, if the molecular weight distribution could be controlled, the Tg of the oligomer may be tailored, raised or lowered, for a given processing need. Also, since properties vary widely with molecular weight, a quality control of the molecular weight distribution is needed.

B. BCB/BMI

There are several areas of investigation left on this project.

1) The 50 gm evaluation needs to be completed. processing , mechanical properties etc.

2) A greater understanding is needed of exactly what reaction(s) are taking place in the system. An indepth study of the curing mechanism is definitely needed.

3) Finally, no work at all was done on the different molar ratios. Due to the unusual properties demonstrated in a previous work². An indepth investigation into the differences and similarities between these systems should be performed.

References

1. F.E. Arnold and L.S. Tan, 31st SMPPE Symp., 963 (1985).
2. L.S. Tan and F.E. Arnold, ACS Polymer Preprints, 26 (2), 173 (1985).
3. L.S. Tan, E.J. Soloski and F.E. Arnold, ACS Polymer Preprints, 37 (1), 453 (1986).
4. P.O. Towany and R.H. Snyder, Chem. Abs., 43, 1 (1961).
5. I.J. Goldfarb and W.W. Adams, ACS Organic Coatings and Plastics, 45, 133 (1981).
6. C. Y-C. Lee and I.J. Goldfarb, Polym. Eng. Sci., 21 787 (1981).

PLOT 1

1.0E+09 808 OUTLINER CURE RUN

20:12:19

○ 6' VS TIME (2 C/MIN)
 = 6" VS TIME (2 C/MIN)

LOG MODULUS

1.0E+06

0.0E+00

5.0E+01

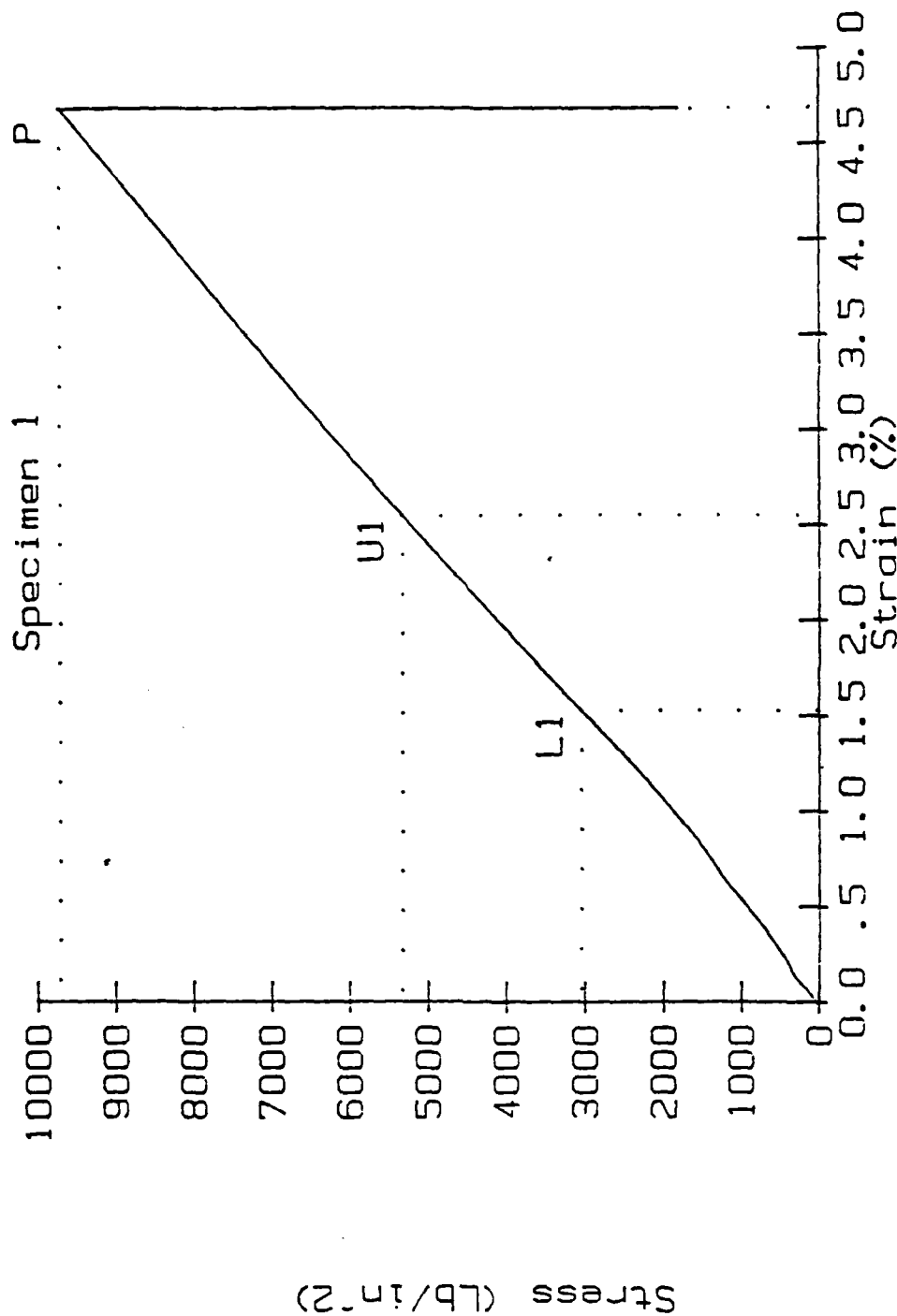
1.0E+02

1.5E+02

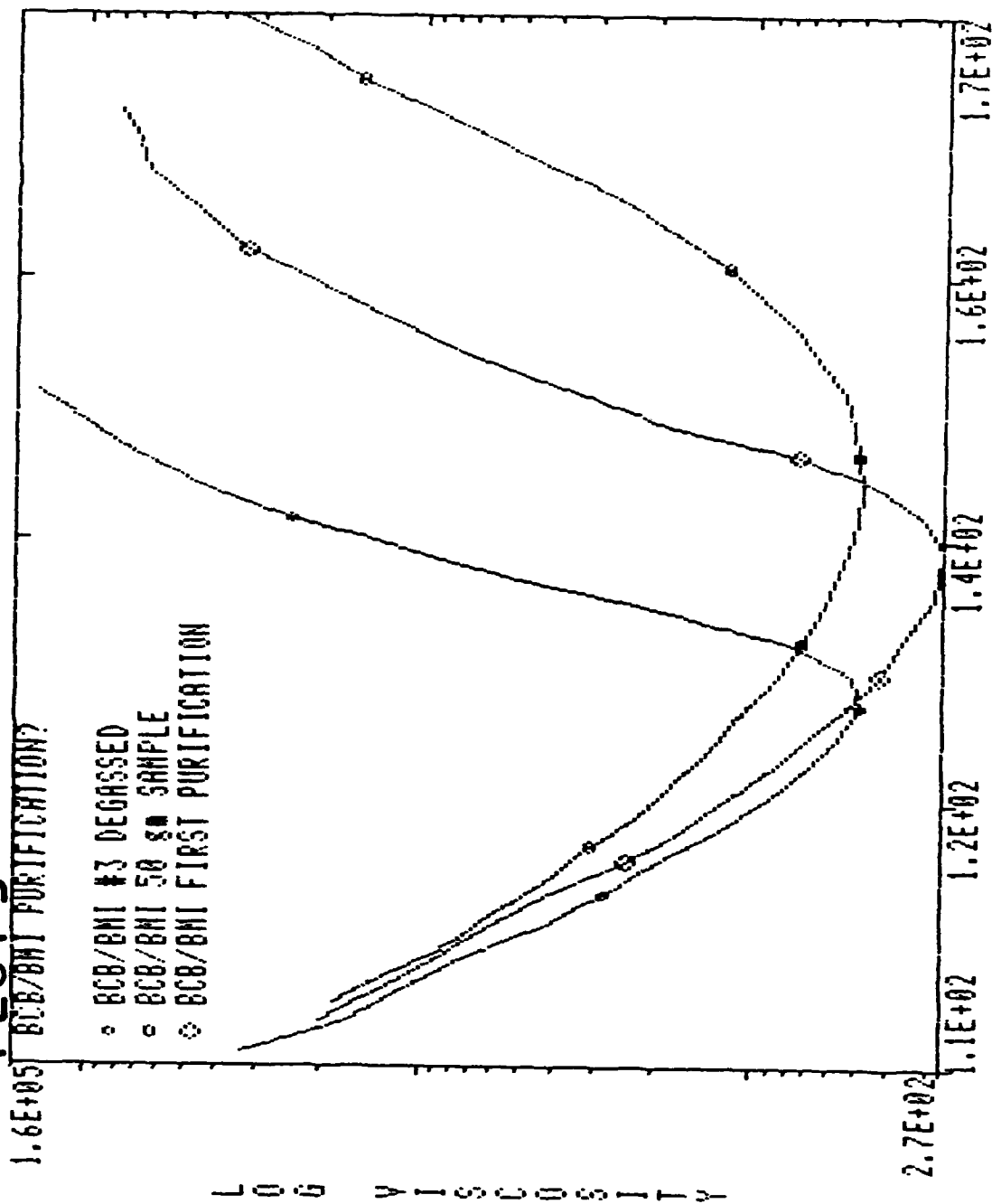
2.0E+02

GENERAL PURPOSE TENSILE TEST

PLOT 2



PLOT 3



1986 USAF-UES SUMMER FACULTY RESEARCH PROGRAM/
GRADUATE STUDENT SUMMER SUPPORT PROGRAM

sponsored by the
AIR FORCE OFFICE OF SCIENTIFIC RESEARCH

Conducted by the
Universal Energy Systems, Inc.

Final Report

Synthesis of Intermediates and Monomer of Polybenzothiazoles

Prepared by:	Christopher A. Feild
Academic Rank:	Graduate Student
Department and	Department of Chemistry
University:	Cornell University
Research Location:	Materials Laboratory, Polymer Branch, Wright- Patterson Air Force Base
USAF Research:	Mr. Bruce Reinhardt
Date:	August 26, 1986
Contract No.:	F49620-85-C-0013

Synthesis of Intermediates and Monomer of Polybenzothiazole

by

Christopher A. Feild

ABSTRACT

Intermediates in the synthesis of polybenzothiazole were prepared purified, and characterized by appropriate methods. Previously devised reaction routes were employed. Some optimization of yields was done in scale-up. One monomer was prepared. Finally, attempts to prepare intermediates with long chain alkyl substituents were made.

ACKNOWLEDGMENTS

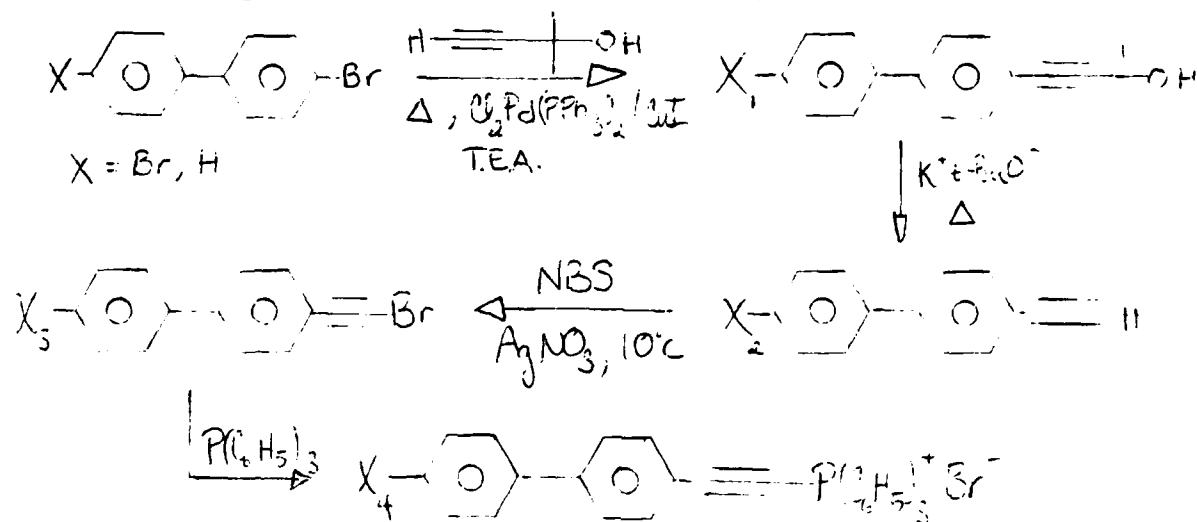
I would like to thank the Air Force Systems Command, and the Air Force Office of Scientific Research for giving me the opportunity to research areas of interest to the Air Force. Additionally, I would like to thank Bruce Reinhardt, Marilyn Enroe, Dan Evans and all the people of the Polymer Branch at Wright-Patterson Air Force Base for all their help, and for making my stay such an enjoyable and rewarding experience. Thank You.

I. INTRODUCTION: As a recent graduate of Dickinson College (B.S.), I will be attending Cornell University this fall to pursue a doctorate in chemistry. While at Dickinson, I was able to take several advanced courses including an advanced organic, instrumental analysis, and an independent research course related to the spectroscopy of some gold(I) polymers. There I was able to operate a Varian 60 MHz NMR, a Hewlett-Packard GC-Mass Spectrometer, a Nicolet FT-IR, and a Perkin-Elmer UV/VIS Spectrophotometer, among other spectroscopic tools. Having a strong interest in polymer chemistry, I felt confident to work at the Polymer Branch of Wright-Patterson AFB.

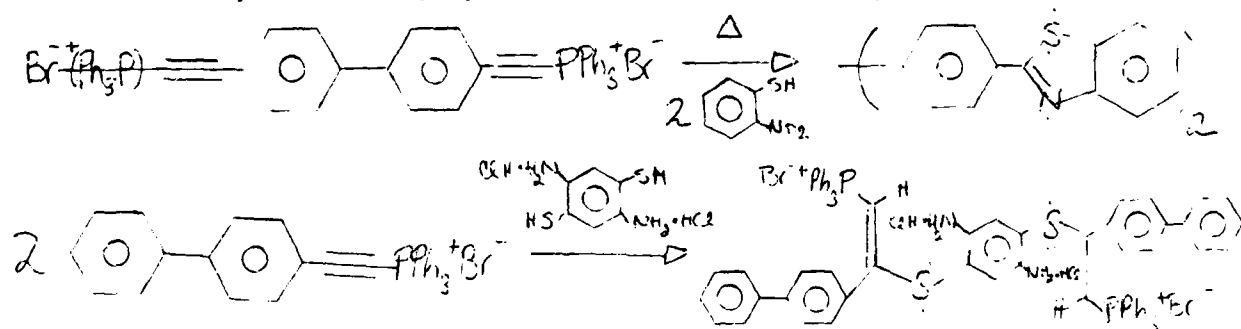
II. OBJECTIVES OF THE RESEARCH EFFORT: Preliminary goals were set at synthesizing the polybenzothiazole monomer and solving problems encountered with scale-up. The objectives were expanded to include alternative reaction routes, analogs of model compounds and synthesis of intermediates with alkyl/alkoxy substituents.

III. DESCRIPTION: A primary concern in these syntheses has been the use of mild reaction conditions. Traditionally, substituted acetylenes have been prepared via reaction with an alkali metal in ammonia. However, in a large scale synthesis, this is impractical. Acetylations of alkyl and aryl halides under room conditions have been prepared in good yield by Sonogashira et al (1) using $\text{Cl}_2\text{Pd}(\text{P}(\text{C}_6\text{H}_5)_3)_2$ / CuI catalysts in diethylamine. Much work has been done by the Air Force in this area, in order to explore new catalysts and improve syntheses. (2,3) Use of an acetone protection group on acetylene allows only mono-substitution and prevents use of acetylene gas; deprotection occurring easily with mild base to give acetone plus the desired product. The acidic proton can be replaced by bromine using NBS and AgNO_3 catalyst. Treatment with $\text{P}(\text{C}_6\text{H}_5)_3$ will convert the compound to the triphenylphosphine bromide salt.

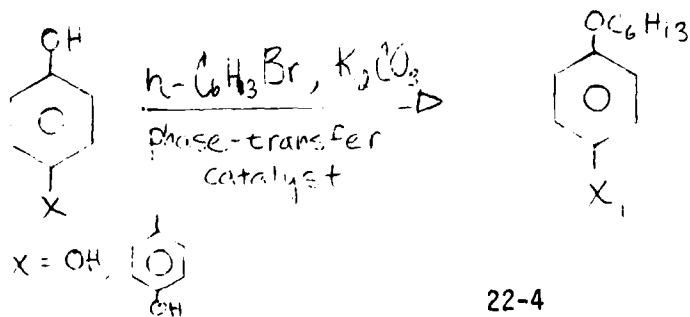
Using either 4-Bromobiphenyl or 4,4'-Bisbromobiphenyl as the initial aryl halide, the reaction sequences performed are outlined below. In the case of the latter reagent, the final product is the polybenzothiazole monomer.



Two model compounds were prepared from the above final products:



Attempts to prepare intermediates with long chain alkyl or alkoxy substituents were carried out with hydroquinone and p,p'-hydroxybiphenol in the presence of a new phase transfer catalyst recently reported in the literature. (4)



IV. EXPERIMENTAL: Synthesis of 4,4'-bis(2-methyl-3-butyne-2-ol)biphenyl:

To a 31 3NRBF equipped with mechanical stirrer, gas inlet, and claison adapter with thermometer and condenser, 97.97g (0.3140 m) 4,4'-bis-bromobiphenyl were dissolved in 1500 mls of triethylamine. The solution was flushed with nitrogen for 15 minutes. Successively, 1.68g (2.39E-03 m) $\text{Cl}_2\text{Pd}(\text{PPh}_3)_2$ and 0.130 g (6.83E-04 m) CuI were added as catalysts, and 66 mls (0.678 m) 2-methyl-3-butyne-2-ol were added. Under nitrogen, the mixture was heated to 50 C and allowed to react for 24 hours. The solution was then vacuum filtered hot to remove triethylamine salts. The filtrate was evaporated to give a brown solid. The triethylamine salts were extracted with water, filtered, and the solid dried. Both solid portions were combined and recrystallized from toluene with decolorizing charcoal to give fluffy white crystals. (60-75% yield)

Synthesis of 4,4'-bisethynylbiphenyl: An apparatus consisting of a 31 3NRBF, thermometer, gas inlet, and Dean-Stark adapter with condenser was assembled. Under nitrogen, 2400 mls of toluene were added to the flask and dried by removal of about 300mls of the azeotrope by distillation. Cooling to 90 C, 61.02g (0.192 m) 4,4'-bis(2-methyl-3-butyne-2-ol)biphenyl were dissolved in a minimum of dry THF and added to the flask, followed by 21.43g (0.192 m) Potassium tert-butoxide. The reaction was stirred at 90 C under nitrogen for 24 hours. The solution was filtered hot through a Buchner funnel with a one inch layer of silica. The filtrate can be evaporated and the solid chromatographed with a 5% CH_2Cl_2 in hexane eluent on a silica column to further purify, if recrystallization from 95% ethanol is unsuccessful.

Synthesis of 4,4'-bis(bromoethynyl)biphenyl: In a 3l RBF equipped with a drying tube, 20.80g (0.103m) 4,4'-bisethynylbiphenyl were dissolved in 2500 mls of acetone. The flask was wrapped in foil to prevent catalyst decomposition, and then cooled in an ice bath to about 10 C. Then, 36.61 g (0.206m) NBS and 3.98g (0.024m) pulverized AgNO₃ were added, and the ice bath removed. Completeness of the reaction can be monitored by TLC. After two hours the mixture was poured into two 4l beakers containing 1250 mls ice water. After melting, the solutions were vacuum filtered and the precipitate dried. The precipitate was then dissolved in a minimum of CH₂Cl₂ and vacuum filtered through a frit with a layer of silica. The filtrate was roto-evaporated to give a light green solid (78% yield).

Synthesis of 4,4'-bis(triphenylphosphinebromide ethynyl)biphenyl: To a 2l RBF equipped with a drying tube, 44.49g (0.1236m) 4,4'-bis(bromoethynyl)biphenyl and 64.84 (0.2472m) triphenylphosphine were dissolved in 1100 mls of CH₂Cl₂ and the reaction continued for 5 days. The volume of solution was reduced and 1500 mls acetone were added. Upon partial evaporation, the product precipitated and was collected by filtration under nitrogen. The yellow solid was dried under high vacuum over P₂O₅. (22-40% yield).

The following monofunctional compounds were prepared under identical conditions to the analogous difunctional compounds above, except 4-bromobiphenyl was the starting material and a 1:1 mole ratio of reagents was used:

4-(2-methyl-3-butyne-3-ol)biphenyl

4-ethynylbiphenyl

4-bromoethynylbiphenyl

4-triphenylphosphinebromide ethynylbiphenyl

Model Compounds

Synthesis of 4,4'-bis(benzothiazole)biphenyl: In a 100 mls 3 NRBF equipped with a gas inlet and condenser, were combined 3.70g (4.18×10^{-3} m) 4,4'-bis(triphenylphosphinebromide ethynyl)biphenyl and 1.39g (0.011m) o-aminothiophenol in 20 mls of dry NMP. The reaction was stirred 24 hours under nitrogen at room temperature. (Isolation of the intermediate salt can be done at this step.) Ring Closure was accomplished by heating the mixture to 130 C in an oil bath for 24 hours. After cooling, the product was precipitated from methanol and vacuum filtered. The crude crystals were recrystallized from xylenes to give light yellow crystals with a metallic sheen (M.P. 311 sub?, 74% yield).

Synthesis of a model compound from 4-triphenylphosphinebromide ethynyl biphenyl and 2,5-diamino-1,4-dithiophenol hydrochloride: To a 250 mls 3 NRBF equipped with gas inlet, were added 1.78g (0.007m) 2,5-diamino-1,4-dithiophenol hydrochloride in 60 mls of dry NMP. The solution was gently heated to 60 C to dissolve. Then, 7.59g (0.014m) 4-triphenylphosphine bromide ethynylbiphenyl were added and the mixture stirred under nitrogen 24 hours at room temperature. The salt intermediate was isolated by precipitating into 1500 mls xylenes, and vacuum filtering under nitrogen. The precipitate was dissolved in a minimum of CH_2Cl_2 and reprecipitated in diethyl ether. Vacuum filtering under nitrogen, the product was dried under high vacuum over P205 to give an orange-brown solid (76% yield).

Attempt to prepare Benzoxazolebiphenyl: Combining 1.21g (0.011m) 2-aminophenol dissolved in 30 mls NMP and 5.74g (0.011m) 4-triphenylphosphinebromide ethynylbiphenyl in a 100 mls 3 NRBF equipped with condenser and gas inlet, the mixture was heated to 70 C for 1 hour. The heat was removed but the reaction continued for several hours. The mixture was poured into

diethyl ether to precipitate the salt intermediate, but on standing oiled, presumably due to water from the air. On removal of the ether, a brown oil remained. Unsuccessful.

Attempts to prepare intermediates with alkoxy substituents:

Synthesis of p-dihexoxybenzene: The following reaction was performed five times varying the solvent as each proved unsuccessful. Solvents used include: toluene, chlorobenzene, triethylamine, n-bromohexane, and tris-(3,6-dioxaheptyl)amine. To a 50mls 3 NRBF equipped with gas inlet, and Dean-Stark adapter with condenser, were added 25 mls of the appropriate solvent, 1.98g (0.018m) hydroquinone, 3.4 mls n-bromohexane, 0.24g tris-(3,6-dioxaheptyl)amine, and 1.24g K₂CO₃. The mixture was heated to reflux for 24 hours. The mixture was poured into water. Using a separatory funnel, the aqueous layer was removed and washed with additional solvent. The organic layers were combined and washed with a 10% KOH solution. The aqueous layer was removed. The organic layer was dried with MgSO₄, filtered and the solvent roto-evaporated to give a brown oil in all cases.

Synthesis of 4,4'-bis(hexoxy)biphenyl: To a 100 mls 3 NRBF equipped with gas inlet, and Dean-Stark adapter with condenser, were added 50 mls chlorobenzene, from which 10 mls were azeotropically distilled. Then, 5.26g (0.028m) p,p'-hydroxybiphenol, 5.3 mls bromohexane, 0.38g tris(3,6-dioxaheptyl)amine and 1.94g K₂CO₃ were added, and the reaction heated to reflux under nitrogen for 2 days. The mixture was poured into water. The organic layer was removed and the aqueous layer extracted with additional chlorobenzene. The organic layers were combined and washed with 10% KOH, separated, dried with MgSO₄, and filtered. The filtrate was roto-evaporated and the solid obtained recrystallized from hexane (M.P. 126-129 C, 3.3% yield).

V. RECOMMENDATIONS: Most reactions performed had reasonably good yields (60-75%). However, in forming the triphenylphosphine salt, the yield dropped considerably as batch size increased. It is suggested that the filtrate obtained on isolation of the final product be retained, and excess triphenylphosphine be added. Since the major side product will be the half salt, addition of PPh_3 could shift the equilibrium and improve yield.

All of the syntheses attempting to prepare intermediates with alkoxy substituents failed. As suggested in the literature (4), the sodium phenate salt should be formed, then reacted with the bromohexane. (William's type synthesis).

REFERENCES

1. Sonogashira, K., Yasuo, T., Hagihara, N., "A Convenient Synthesis Of Acetylenes: Catalytic Substitution of Acetylenic Hydrogen With Bromoalkenes, Iodoarenes, and Bromopyridines," Tetrahedron Letters, 50, 1975, pp. 4467-4470.
2. Ishuzi, K., Prabhu, U.D.G., Draney, D., Marvel, C.S., "New Acetylene-Terminated Quinoxaline Oligomers," AFWAL-TR-82-4006 Final Report, March 1982, pp. 1-33.
3. Harrison, J.J., Selwitz, C.M., "Low Cost Routes to Acetylenic Intermediates," AFML-TR-79-4183 Final Report, December 1979, pp.1-67.
4. Soula, G., "Tris(polyoxalkyl)amines (Trident), a New Class of Solid-Liquid Phase-Transfer Catalysts," J. Org. Chem., 1985, 50, 3717-3721.

1986 USAF-UES SUMMER FACULTY RESEARCH PROGRAM/
GRADUATE STUDENT SUMMER SUPPORT PROGRAM

Sponsored by the
AIR FORCE OFFICE OF SCIENTIFIC RESEARCH

Conducted by the
Universal Energy Systems, Inc.

FINAL REPORT

THE METABOLISM OF t-BUTYLCYCLOHEXANE
IN MALE FISCHER 344 RATS

Prepared by: Michelle J. Ferry
Academic Rank: B.S.
Department and Chemistry
University: Wright State University
Research Location: Toxic Hazards Division, AAMRL
 Wright-Patterson Air Force Base
USAF Researcher: Major Henningson
Date: September 21, 1986
Contract No: F49620-85-C-0013

THE METABOLISM OF t-BUTYLCYCLOHEXANE
IN MALE FISCHER 344 RATS

By

Michelle J. Ferry

ABSTRACT

The study of metabolism of t-butylcyclohexane in male Fischer 344 rats was undertaken. The cyclic hydrocarbon was shown to be mildly nephrotoxic, causing the formation of hyaline droplets in the proximal tubule cells. Identification of the urinary metabolites confirmed the presence of cis-4-t-butylcyclohexanol, trans-4-t-butylcyclohexanol, 2-methyl-2-cyclohexylpropionic acid, and four stereoisomers of 4-t-butyl-1,2-cyclohexandiol. Two other major metabolites have not been identified. Kidney homogenate extract analysis showed no metabolites to be present.

ACKNOWLEDGMENTS

I would like to acknowledge the assistance of Dr. M. Paul Serve, Mrs. K.O. Yu, Isobel Lopez, SSgt. B. Hancock, Maj. Henningson, Col. Bruner, and others at the Toxic Hazards Division of AAMRL. I would also like to acknowledge the sponsorship of the Air Force Systems Command, Air Force Office of Scientific Research and Universal Energy Systems, Inc.

I. INTRODUCTION

In the early seventies, the American Petroleum Institute sponsored a study to research the physiopathological effects of gasoline inhalation. The research found a high incidence of renal carcinomas in male rats. Female rats did not display this type of renal damage. The Toxic Hazards Division of the Harry G. Armstrong Aerospace Medical Research Laboratory (AAMRL), along with others, instigated extensive research to explore the nephrotoxicity caused by hydrocarbons. Additionally, AAMRL became interested in the identification of the metabolites of hydrocarbons to perhaps elucidate the mechanism of hydrocarbon nephrotoxicity.

Compounds known to produce kidney damage include Stoddard Solvent (a mixture of aliphatic hydrocarbons with some naphthenes and benzene derivatives), the branched aliphatic hydrocarbon, 2,2,4-trimethylpentane.¹ Documented research on cyclic hydrocarbons include JP-4, JP-5, and JP-10 which are used as fuels, and cis- and trans-decalin which is a solvent.^{2,3} Cyclohexane has been shown to cause kidney damage in lethal doses but does not appear effect the kidney in low doses. The main effect caused by inhalations has been symptoms relating to the depression of the central nervous system.⁴ The

toxicity of methylcyclohexane was found to be similar to cyclohexane.⁵

At puberty, the male rat is unique in that the liver produces a low molecular weight protein, alpha 2u globulin (MW 26,000). This protein is produced mainly under the influence of testosterone, and is major urinary protein of young adult male rats. It is readily filtered through the kidney glomeruli, and resorbed in the tubules.⁶

Exposure to hydrocarbons has been shown to disrupt the resorption process of the protein in the tubules. Hyaline droplets, cysts composed of alpha 2u globulin, have been found in male rats exposed to hydrocarbons.⁷

To compliment other research of cyclic hydrocarbons, t-butylcyclohexane was chosen for study. The boiling point of t-butylcyclohexane is 171.5 °C, therefore can not exhaled like cyclohexane and must be metabolized by the body.

Having received a B.S. in chemistry from Wright State University, and working towards a Masters degree with an emphasis in organic chemistry and toxicology, this writer was chosen to undertake the t-butylcyclohexane research. The study included characterizing and separating the metabolites.

II. OBJECTIVES

The purpose of this research was to analyze qualitatively the metabolism products of the hydrocarbon, t-butylcyclohexane, by male Fischer 344 rats. Another objective of this study was to identify the physiological and histopathological effects, if any, caused by the exposure to the compound. By comparison to other hydrocarbons and their metabolites, correlations could possibly be determined relating to the mechanism of nephrotoxicity. The relevance of these findings and their application to man could be important.

III. PATHOPHYSIOLOGICAL EFFECTS.

Eight male rats (306 +/- 9 g) were administered t-butylcyclohexane orally with a dose of 1.0 ml/kg body weight for a period of fourteen days. Also, four male rats (311 +/- 5 g) were dosed with water in a similar matter for use as controls. Feed and water were available ad libitum. Following the initial dosing, rats were placed in metabolism cages for the first 48 hours for urine collection. After fourteen days, the rats were sacrificed by anesthetic overdose. One kidney was used for histopathologic study; the other was used for metabolite extraction.

During the dosing period the weight of the exposed male rats fluctuated. The greatest weight loss occurred after the first dose and the rats slowly gained weight with some variations. At the end of the dosing period, the average weight was 305 +/- 10 g, only slightly less than the original weight. The four rats used as controls slowly gained weight, reaching a final weight of 321 +/- 7 g.

The kidney histopathological study was completed by the Pathology Branch of AAMRL. Mild hyaline droplet formation was found in the exposed male rats. Also, mild cell degeneration had occurred in the proximal tubules. Therefore, t-butylcyclohexane can be considered to be mildly nephrotoxic.

IV. IDENTIFYING THE METABOLISM PRODUCTS

The urine from the exposed and control animals was collected and frozen until it was processed. Likewise, one kidney was removed after the dosing period and frozen. An aliquot from the collected urine was acidified with 5.0 N hydrochloric acid to a pH of 4 and 0.4 ml of glucuronidase/sulfatase (calbiochem) was added. The solution was placed in a water bath at 37 °C and agitated for 18 hours. After cooling to room temperature, the solution was filtered through a silica (Clin-Elut) column

using neat methylene chloride as the eluent. The kidney was homogenized in 2.0 ml of distilled water and processed in the same manner.

The methylene chloride extracts of the urine and kidney metabolites on a Hewlett-Packard model 5880A gas-liquid chromatograph fitted with a flame-ionization detector. The column utilized was a 15 meter carbowax 20M fused silica capillary column with an internal diameter of 0.25 mm. The temperature program maintained the oven temperature at 100 °C for one minute after sample injection, then raised 5 °C/min to a final temperature of 180 °C where it was held for 25-30 minutes. The injection port temperature was 200 °C and the detector temperature was 250 °C. Helium was used as the carrier gas. A Hewlett-Packard gas chromatograph/mass spectrometer model 5985 was used for metabolite identification. The mass spectrometer was a quadrupole instrument and operated in the electron impact mode at a voltage of 70eV and an ion source temperature of 200 °C.

Comparing the gas chromatograph and mass spectra data of the urine and the kidney metabolites with data from purchased or synthesized compounds, the metabolites were identified. Gas chromatograph and gas chromatograph/mass spectrometer analysis of the urine confirmed the presence of nine major metabolites in the male rat. (See figure 1).

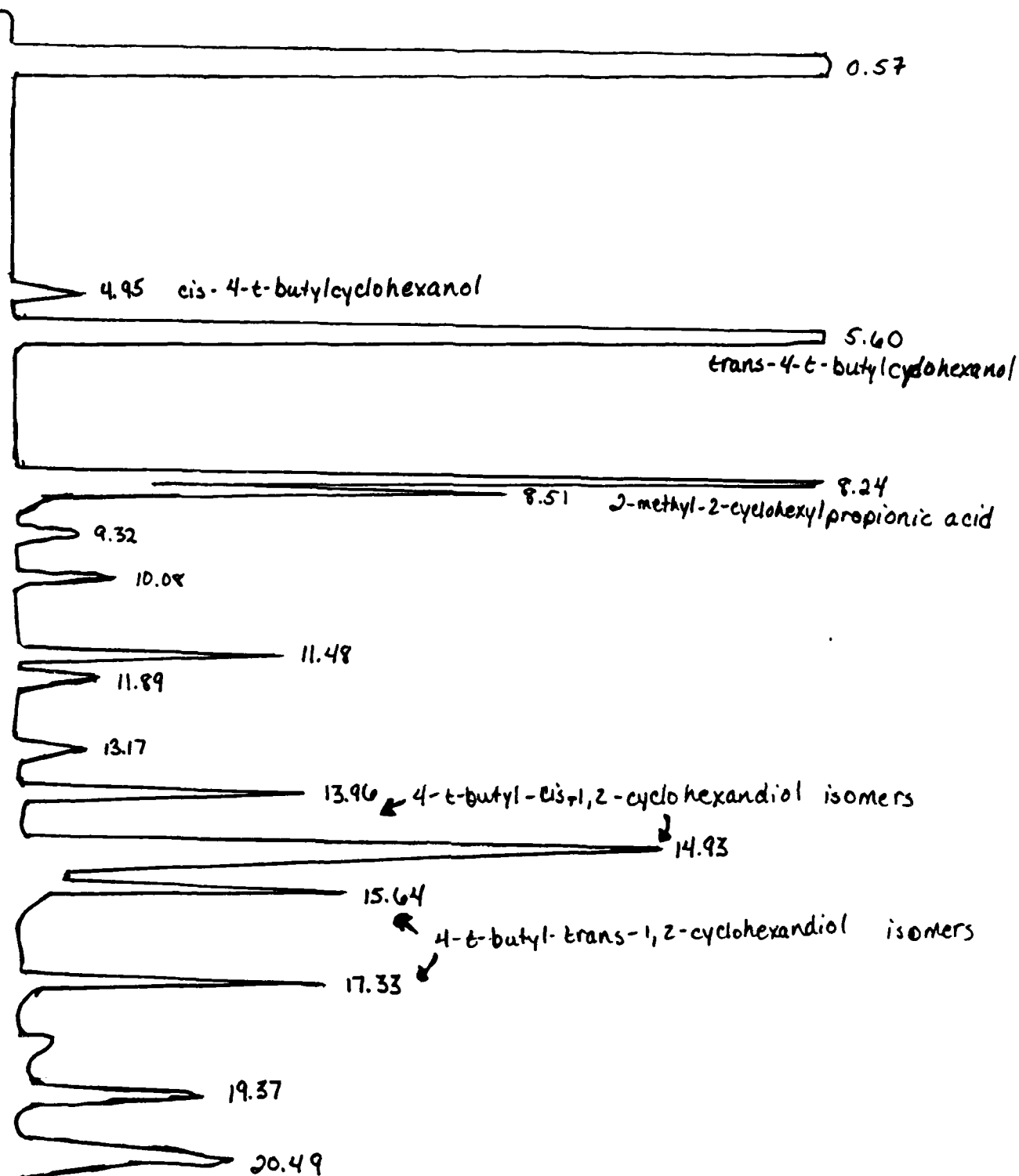


Figure 1: Representative GC Tracing of Male Rat
Dosed with t-Butylcyclohexane

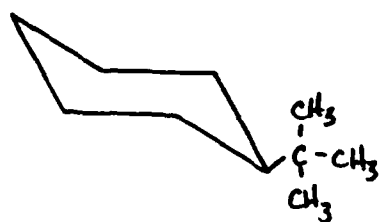
The compounds identified were cis-4-t-butylcyclohexanol, trans-4-t-butylcyclohexanol, 2-methyl-2-cyclohexylpropionic acid, two stereoisomers of 4-t-butyl-cis-1,2-cyclohexandiol, and two stereoisomers of 4-t-butyl-trans-1,2-cyclohexndiol. In the chair formation of cyclohexane, the bulky t-buytl group must occupy the equatorial position because of steric hindrance in the axial position. The two hydroxy groups occupy either the axial or the equatorial positions giving the four different isomers. See figures 2-6.

Two major metabolites were not identified. Referring to figure 1, they are the last peaks at 19.37 and 20.49 minutes. The molecular ion peaks from mass spectra data are 170 and 142, respectively.

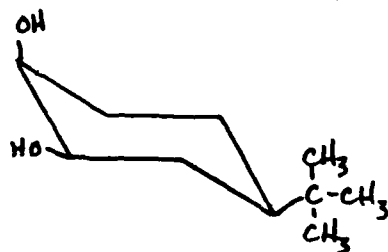
Analysis of the kidney extracts did not show the presence of any metabolites.

V. RECOMMENDATIONS

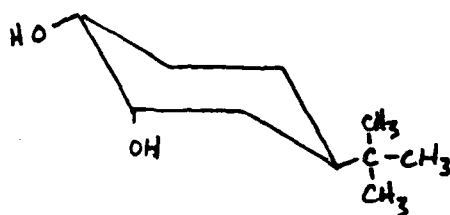
By looking at the structure of the metabolites of hydrocarbons, one can perhaps discover more about the biochemical mechanism of metabolism. Comparison of this study to other hydrocarbon studies could lead to the ability to foretell the sites that will undergo metabolism in untried compounds and predict the renal toxicity.



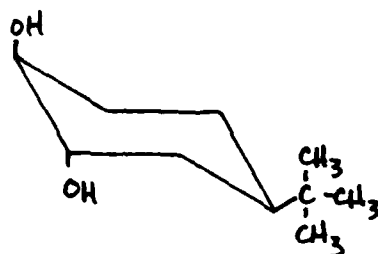
4-*t*-butylcyclohexane
Figure 2



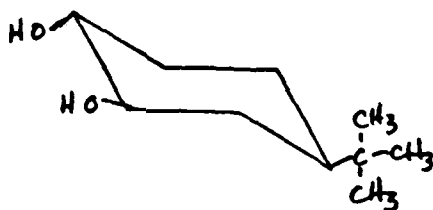
cis-4-*t*-butyl-cis-1,2-cyclohexandiol
Figure 3



trans-4-*t*-butyl-cis-1,2-cyclohexandiol
Figure 4



cis-4-*t*-butyl-trans-1,2-cyclohexandiol
Figure 5



trans-4-*t*-butyl-trans-1,2-cyclohexandiol
Figure 6

Further research on t-butylcyclohexane should include studying the effect of enzyme induction and inhibition on metabolism. Additionally, one should study the metabolism of this hydrocarbon in other species of laboratory animals. Research in this area could prove beneficial to man in assessment of the hazards of hydrocarbons.

REFERENCES

1. Olson, C.T., K.O. Yu, D.W. Hobson, and M.P. Serve, Biochem. and Biophys. Rsch. Comm., Vol 130, No.1, 1985.
2. Inman, R.C., K.O. Yu, and M.P. Serve, Proceed. of 13th Conf. on Environ. Toxic., University of California, Irvine, November 1982, pp. 350-363.
3. Olson, C.T., K.O. Yu, and M.P. Serve, "Metabolism of Nephrotoxic Cis- and Trans-Decalin in Fischer 344 Rats." In publication.
4. Treon, J.F., W.E. Crutchfield, and K.V. Kitzmiller, J. Ind. Hyg. Toxicol., Vol. 25, 1943, pp. 199.
5. Ibid.
6. Roy, A.K., J. Endro., Vol 56, 1973, pp. 295-301.
7. Kloss, M.W. and G.S. Bus, CITT Activities, Vol. 5, No. 5, 1985.

1986 USAF-UES SUMMER FACULTY RESEARCH PROGRAM/
GRADUATE STUDENT SUMMER SUPPORT PROGRAM

Sponsored by the
AIR FORCE OFFICE OF SCIENTIFIC RESEARCH

Conducted by the
Universal Energy Systems, Inc.

FINAL REPORT

DATA MANAGEMETN WITHIN THE SCHOOL OF AEROSPACE MEDICINE

Prepared by:	Carl V. Frank
Academic Rank:	Bachelor of Science
Department and	Computer Science and Statistics
University:	University of Southern Mississippi
Research Location:	USAF School of Aerospace Medicine Clinical Science Divison Brooks Air Force Base, Texas
USAF Researcher:	Mr. William Nixon
Date:	September 10, 1986
Contract No.:	F49620-85-C-0013

DATA MANAGEMENT WITHIN THE SCHOOL OF AEROSPACE MEDICINE

by

Carl V. Frank

ABSTRACT

The report contains a summary of an investigation of human-computer interaction and its effect on the data within the United States Air Force School of Aerospace Medicine (USAFSAM). Data for the investigation was gathered primarily by interviewing staff personnel and observations by the researcher. After examining the data it was determined that there are areas that need improvement. These areas are centered around data validation and resource management. Suggestions were made to acquire new hardware and software, only after the School's present needs and growth requirements are understood.

ACKNOWLEDGEMENTS

I would like to thank the Air Force Systems Command and the Air Force Office of Scientific Research for sponsorship of my research. I would also like to thank the Brooks Air Force Base School of Aerospace Medicine, particularly, the entire Clinical Sciences Division for providing the environment in which the research could be conducted. I would like to thank individually Dr. Clifford Burgess, my supervising professor, as well as several members of the divisional staff, namely, Dr. Bryce Hartmann, Col Gil Tolan, Mr. William Nixon, Mr. William Besich, Mr. Tim DeCelles, Sgt. Walker, and AIC Campbell for the guidance necessary for my research.

I. Introduction

I received my Bachelor's Degree in Computer Science from Henderson State University in Arkadelphia, Arkansas. At this time I am working on my Master's Degree in Computer Science at the University of Southern Mississippi in Hattiesburg, Mississippi. My graduate project is to be in the area of user interfaces or computer aided instruction.

My computer science background and interests were similar to the areas of interest of the United States Air Force School of Aerospace Medicine (USAFSAM). I was therefore assigned to the database group within the Clinical Science Division (NG) of USAFSAM located at Brooks Air Force Base, San Antonio, Texas.

II. Objectives of the Research Effort

The primary objective was to gather and study information concerning the methods for the acquisition, transformation, validation, storage, retrieval, and analysis of patient data within the Clinical Science Division (NG) of the United States Air Force School of Aerospace Medicine (USAFSAM). The secondary objective was to examine the human-computer interactions and determine their effect on the areas mentioned above.

The final objective was to use the results from the first two objectives to make suggestions for improvement and where appropriate suggestions for further study.

III. Data Collection

The main means of obtaining data for this study was from a series of interviews with the personnel who transcribe, compile, and enter the data into the databases; as well as the personnel who maintain the databases, retrieve and analyse data.

The initial interviews, on the average, lasted about one hour. They consisted of the person being interviewed describing his or her job duties; as well as any problems or areas of concern that he or she felt existed. I then would ask questions to complete the interview. Specifically, the questions concerning computer usage, availability of resources, and any suggestions to handle the problems perceived by the person being interviewed.

After the initial interview I would summarize the interview and make a return appointment. This enabled me to ensure that my observations of the interview coincided with the views of the person interviewed.

Other sources of information for this study included guided tours of base facilities, Digital Equipment's VAX Utility Monitor, and informal branch meetings.

IV. Observations

In the interview process I encountered about six different computer systems, plus a variety of

microcomputers in use. The users expressed different levels of acceptability towards these different systems. In large, the microcomputers were preferred over the large minicomputers and mainframes for a number of reasons. The main reason for this was the response time. On the large multi-user machines there was a poor response time. Many users stated that the VAX 780 that they used was unbearably slow (one user complained that it took as long as five minutes to log-on or log-off). Microcomputers, on the other hand, being single user oriented have very good response time. Another reason for this shift from the minicomputers and mainframes to the microcomputers is that some of the researchers felt that the data repositories (databases) maintained on the larger machines contained erroneous or "dirty" data. As opposed to "cleaning" the data in the repositories, researchers simply maintained their own data on microcomputers. The data analysts (statisticians) agreed that the repositories do in fact contain erroneous data. This indicates that further data validation techniques should be employed.

This shift to microcomputers presents another problem, the subsequent loss of data due to the lack of data archiving facilities for microcomputers. For example, for any given study tests will be given, and data will be collected on the microcomputer, analyzed, and a paper will be composed from the results. After

the paper has been produced, in many cases, the disks are reformatted and used for something else. Even in the cases where the principal investigator saves back-up copies of the data it is generally unavailable to the rest of the School. This is a serious problem due to the nature of the data. The data generated at the School is unique in many ways because the subjects are healthy, physically fit individuals, and is not duplicated at any other institution. One mission of the School is to detect disease before symptoms develop. Therefore accurate data needs to be preserved to ensure national security.

Another problem observed was resource management. As noted earlier, many users complained of poor response time, this was due partly to the large number of users forced to use that particular machine. I was using another VAX 780 and in many instances I was the only user on the system. While on the system, I used the DEC VAX Monitor Utility to monitor the central processing unit (CPU), 80 - 90 percent idle was not uncommon. There were also personnel who had no computer support at all, though they desired it. This indicates that the resources available are not distributed equitably.

I seem to have painted a dismal picture, this is not the case. I have merely limited my descriptions to the areas in need of improvement. In fact, the staff

at USAFSAM, in which I had any contact with, performed in a professional manner and should be commended on the degree of testing and research which is accomplished with the facilities on hand.

V. Recommendations

There is no single solution to obliterate the problems mentioned above, it will take a coordinated effort comprised of several partial solutions.

An important part of this effort will have to be additional hardware and software. It is advisable to first conduct a full study of the School's computer system needs and determine projected growth requirements. This is opposed to the current method of using existing equipment until a point is reached where it is imperative that the equipment be upgraded or replaced, whereupon six to eight months later the new or upgraded equipment is itself obsolete. After the needs of the School are fully understood, the task of supplying the appropriate hardware and software can then be undertaken.

Another component that would be of considerable effectiveness, especially in the area of resource distribution, is that the computer/database support for the entire School be handled by one agency. A logical choice would be NGS. There would be no conflict of interest in this, as NGS's tasks are service oriented. NGS could develop, distribute, and maintain the School's

resources in an unbiased manner according to need. This would preclude the "hording" of resources that presently exist.

An on-screen forms management package could be developed that could provide all the data validation needed by the School. This package would utilize table look-ups, range checking, and cross field checks.

Once the data validation problem is solved, the next step is to develop a simple query language or natural language processor. This will allow users with no database experience to access the data. The query language or natural language processor should be developed with the people who are to use the database in mind, primarily the doctors and technicians. Therefore, they should have a large role in its development stage with inputs and criticisms.

For these recommendations to be implemented effectively further study is indicated, primarily in regard to the School's computer system needs. After the School's needs have been realistically defined the other recommendations that I have mentioned, as well as those that would emerge from a study of this nature could be implemented concurrently.

1985 USAF-UES Summer Faculty Research Program/
Graduate Student Summer Support Program

Sponsored by the
Air Force Office of Scientific Research
Conducted by the
Universal Energy Systems, Inc.

Final Report

The Effects of High Noise Levels and Obstruction to
Articulation on the Acoustic-Phonetic Structure
of Speech: A Preliminary Investigation

Prepared by:	Beverley A. Gable
Academic Rank:	Graduate Student
Department and	Department of Psychology
University:	Ohio University
Research Location:	Biological Acoustics Branch, Biodynamics and Bioengineering Division, Armstrong Aerospace Medical Research Laboratory, Aerospace Medical Division.
USAF Research:	Dr. Thomas Moore
Date:	September 20, 1986
Contract No.:	F49620-85-C-0013

SPEECH PRODUCED UNDER HIGH SUSTAINED ACCELERATION

Beverley A. Gable
Department of Psychology
Ohio University, Columbus, OH

ABSTRACT

The purpose of this study was to obtain preliminary data concerning the acoustic-phonetic structure of speech produced under high sustained acceleration. Acoustical measurements were made of a set of Air Force vocabulary words as spoken by two subjects at 1G and 6Gz. There were differences in both the durational and spectral characteristics of speech, though not always consistently for the two speakers. At 6Gz, vowel formants tended to centralize, and fundamental frequency in stressed syllables increased for both speakers. For one speaker, word durations increased consistently under acceleration while for the other speaker, the durational differences were inconsistent. Duration differences were primarily a function of changes in vowel duration. [Sponsored in part by the Air Force Office of Scientific Research/AFSC, United States Air Force, under Contract F49620-85-C-0013.]

Acknowledgments

I would like to thank the Biological Acoustics Branch, Biodynamics and Bioengineering Division, Armstrong Aerospace Medical Research Laboratory, Aerospace Medical Division (AMD). I would like to thank Dr. Zinny S. Bond, Dr. Thomas J. Moore, and Dr. Charles W. Nixon for giving me the opportunity and guidance to carryout this research.

Finally, I would like to thank Mark J. Schirtzinger for his support and encouragement throughout the summer.

I. Introduction.

The acoustical structure of normal speech has been the focus of many investigations. Bond (1985) defined normal speech as, "speech produced with minimal distraction or disturbance of the speaker." A good understanding of normal speech has been formed, yet ordinary discourse usually involves speech that is effected by circumstances such as high noise levels, distraction, and physical exertion of the speaker. Therefore, there is a need for investigating speech produced in adverse circumstances. There are only a few such investigations.

A study by Dreher and O'Neill (1957) examined speech produced under high levels of white noise. A pannel of listeners were presented spondee words and sentences produced by speakers who were exposed to high noise levels. The signal to noise ratio was 4 dB. The results showed that speech produced under noise was more intelligible than speech produced in quiet. There was no difference between speech produced at different noise levels, 70 to 100 dB SPL. Dreher and O'Neil reported that the intensity and duration of speech were greater under noise than in quiet.

Results by Ladefoged (1967) were not consistent with the results by Dreher and O'Neil (1957). Speech was produced by speakers under levels of noise which were high enough to mask the auditory feedback by bone conduction.

The exact level of masking noise was not reported, but Bond (1985) estimated that it was approximately 120 dB SPL. The results showed that the length and quality of vowels were affected. Furthermore, results showed a shift to a lower quality of voice and pitch pattern. Ladefoged did not test the intelligibility of the speech, but he did mention that the speech appeared intelligible yet disorganized.

Pisoni et al., (1984) investigated the acoustical changes in speech under noise (80 to 100 dB SPL). Results showed that as noise increased, there was an increase in intensity, fundamental frequency, word duration, and variability of F0. Furthermore, at higher frequencies, there was an increase in the relative distribution of energy in the speech spectrum. Vowel formants shifted towards more centralized positions; F1 rose while F2 and F3 dropped. Pisoni et al. did not assess the intelligibility of the speech produced under high levels of noise.

Bond (1985) reviewed these three studies and concluded: It would seem, therefore, that the presence of masking noise at some levels causes speakers to change their speech towards more intelligible but that masking beyond these levels cause speech to become disorganized and undoubtedly less intelligible. It is also possible of course, that the differences between the results represent the effects of noise on different speakers.

Bond also concluded that data was scarce regarding how adverse conditions cause changes in the acoustical structure of speech and subsequently affect intelligibility. Thus, there is a need for further research. The present study addressed the following questions proposed by Bond(1985):

1. What are the acoustical changes in speech under adverse conditions, specifically speech produced under high levels of noise, or with obstruction to articulation as produced by an oxygen mask?
2. How variable are speaker reactions to adverse speaking conditions?

II. Objectives.

This investigation examined speech samples of four speakers produced in different noise environments with and without obstruction to articulation as produced by oxygen masks. This was done to obtain the effects of both listening to noise and wearing an oxygen mask on the acoustic-phonetic structure of speech. Such data provide information about human speech production under adverse conditions. Therefore, the data are relevant to an understanding of speech production in general. The data may also be relevant to testing automatic speech recognition systems.

III. Method.

The speakers were four male volunteers. Each speaker participated in three speaking conditions and one

speaker participated in seven additional speaking conditions. Before the actual experiment, the speakers were familiarized with the materials to be recorded. After each recording, the speakers were debriefed.

Speech Materials. Ten of the words developed by CID served as isolated word samples. The words were all two syllables long and contained a number of different vowels and consonants. To "avoid incidental fatigue effects on the speakers while speaking in adverse circumstances" (Bond, 1985) the recordings were kept short. The ten spondaic words selected were the following: baseball, birthday, drawbridge, duckpond, headlight, mousetrap, mushroom, oatmeal, padlock, schoolboy.

Recording Materials. The recordings were made using a TEAC Tascam 44 4-channel tape recorder. Speakers wore either an oxygen mask (Gentex Regular) with microphone (M-101) or a headset (H-157) with boom microphone (M-167).

Noise Conditions. Three speakers were asked to produce speech while listening to pink noise at 95 dB SPL and no noise. The fourth speaker was asked to produce speech while listening to pink noise at 85, 95, and 100 dB as well as no noise. The fourth subject was also asked to produce loud speech in a second no noise condition.

Mask Conditions. Three speakers produced speech while wearing an oxygen mask and again listening to pink noise at 95 dB SPL and no noise. The fourth subject produced

speech while wearing an oxygen mask and again listening to pink noise at 85, 95, and 100 dB SPL and no noise. The fourth speaker also produced loud speech while wearing an oxygen mask and listening to no noise.

A total of three different speaking conditions were recorded for three speakers: 95 dB pink noise, no-noise, and 95 dB pink noise with an oxygen mask. A total of ten different speaking conditions were recorded for the fourth speaker: 85 dB noise, 95 dB noise, 100 dB noise, no-noise, loud speech, 85 dB noise with oxygen mask, 95 dB noise with oxygen mask, 100 dB noise with oxygen mask, no-noise with oxygen mask, loud speech with oxygen mask.

Each speaker recorded two repetitions for each of the ten spondaic words. Thus, for three speakers, twenty tokens were obtained in each of three different noise-mask conditions; a total of 60 tokens. Similarly, for the fourth speaker, twenty tokens were obtained in each of ten different noise-mask conditions; a total of 200 tokens.

Measurements: The measurements were made in a similar manner to those made by Bond, Moore, and Anderson (1986). Both repetitions of all ten words were digitized at 16 KHz using a 6.4 KHz anti-aliasing filter and 16 bit resolution. All tokens were stored on disk. The tokens were recorded and analyzed using a computer program called SPIRE (Zue and Cyphers, 1985) on the Symbolics 3670 computer. The

boundaries for each segment were located on the display of the wide-band spectrogram and waveform. The segmentation was done in the manner described by Peterson and Lehiste (1960). Segmentation was difficult at times for three reasons. First, the boundaries were occasionally indistinct. Second, the recording quality was occasionally obscure. Third, there was an occasional presence of noise. The following measurements were taken:

1. The duration of each word.
2. The first, second and third formants for each vowel.
3. The fundamental frequency for each vowel.
4. The total energy for each vowel.
5. The duration of each vowel.
6. The frequency of each fricative.
7. The total energy of each fricative.
8. The duration of each fricative.
9. The closure duration of each stop consonant.
10. The voice onset time for each stop consonant.

IV. Results.

Statistical Analyses. For all four speakers, the frequency, duration, and amplitude of the two vowels in each of the ten words were submitted to a $3 \times 4 \times 10 \times 2$ (noise by subject by word by syllable) Multivariate Analysis of Variance, MANOVA. The noise factor consisted of the following conditions: 95 dB pink noise, no-noise, and 95 dB pink noise with oxygen mask.

The multivariate test for the Syllable main effect was significant, $p < .001$. Furthermore, the univariate tests indicated a significant difference for Frequency, $F(1,240) = 1321.221$, $p < .001$, Duration, $F(1,240) = 132.685$, $p < .001$, and Amplitude, $F(1,240) = 242.579$, $p < .001$.

The multivariate test for the Word main effect was significant, $p < .001$. The univariate tests indicated a significant difference for Frequency, $F(9,240) = 7.686$, $p < .0001$, Duration, $F(9,240) = 12.088$, $p < .001$, and Amplitude, $F(9,240) = 7.069$, $p < .001$.

The multivariate test for the Speaker main effect was significant, $p < .001$. And, the univariate tests indicated a significant difference for Frequency, $F(3,240) = 724.950$, $p < .001$, Duration, $F(3,240) = 6.903$, $p < .001$, and Amplitude, $F(3,240) = 65.646$, $p < .001$.

The multivariate test for the Noise main effect was significant, $p < .001$. And, the univariate tests indicated a significant difference for Frequency, $F(2,240) = 335.373$, $p < .001$, Duration, $F(2,240) = 9.768$, $p < .001$, and Amplitude, $F(2,240) = 102.720$, $p < .001$.

The multivariate test for the Word by Syllable interaction was significant, $p < .001$. The univariate tests indicated a significant difference for Frequency, $F(9,240) = 4.081$, $p < .001$, Duration, $F(9,240) = 8.812$, and Amplitude, $F(9,240) = 7.951$, $p < .001$.

The multivariate test for the Speaker by Syllable interaction was significant, $p < .001$. And, the univariate tests indicated a significant difference for Frequency, $F(3,240) = 34.076$, $p < .001$, Duration, $F(3,240) = 4.534$, $p < .004$, and Amplitude, $F(3,240) = 3.173$, $p < .025$.

The multivariate test for the Speaker by Word interaction was significant, $p < .001$. Also, the univariate tests indicated a significant difference for Frequency, $F(27,240) = 1.892$, $p < .006$, and Amplitude, $F(27,240) = 1.657$, $p < .026$.

The multivariate test for the Noise by Syllable interaction was significant, $p < .001$. The univariate tests indicated a significant difference for Frequency, $F(2,240) = 83.163$, $p < .001$, Duration, $F(2,240) = 5.070$, $p < .007$, and Amplitude, $F(2,240) = 6.211$, $p < .002$.

The multivariate test for the Noise by Speaker interaction was significant, $p < .001$. The univariate tests indicated a significant difference for Frequency, $F(6,240) = 27.069$, $p < .001$, Duration, $F(6,240) = 2.827$, $p < .011$, and Amplitude, $F(6,240) = 8.305$, $p < .001$.

The multivariate test for the Noise by Speaker by Syllable interaction was significant, $p < .001$. Furthermore, the univariate tests indicated a significant difference for Frequency, $F(6,240) = 8.441$, and Amplitude, $F(6,240) = 3.122$, $p < .006$. There was also a

marginal difference for Duration, $F(6,240) = 2.098$, $p < .054$.

Also, for all four subjects, the word durations of the ten words were submitted to a 3×4 (noise by subject) MANOVA. Again, the noise factor consisted of the following conditions: 95 dB pink noise, no-noise, 95 dB with oxygen mask. The main effect for noise was significant, $F(2,228) = 4.899$, $p < .008$. Also, the main effect for subject was significant, $F(3,228) = 19.155$, $p < .001$. Furthermore, the noise by subject interaction was significant, $F(6,228) = 4.124$, $p < .001$.

For the fourth subject only, the frequency, duration and amplitude of the two vowels in each of the ten words were submitted to a $2 \times 5 \times 10 \times 2$ (mask by noise by word by syllable) MANOVA. The mask factor consisted of the mask and no mask conditions. The noise factor consisted of the 85 dB, 95 dB, 100 dB, no noise and loud conditions.

The multivariate test for the Syllable main effect was significant, $p < .001$. Furthermore, the univariate tests indicated a significant difference for Frequency, $F(1,200) = 4132.783$, $p < .001$, Duration, $F(1,200) = 259.389$, $p < .001$, and Amplitude, $F(1,200) = 542.364$, $p < .001$.

The multivariate test for the Word main effect was significant, $p < .001$. Also, the univariate tests indicated a significant difference for Frequency,

$F(9,200) = 16.639$, $p < .001$, Duration, $F(9,200) = 16.550$, $p < .001$, and Amplitude, $F(9,200) = 19.412$, $p < .001$.

The multivariate test for the Noise main effect was significant, $p < .001$. And, the univariate tests indicated a significant difference for Frequency, $F(4,200) = 169.777$, $p < .001$, Duration, $F(4,200) = 3.318$, $p < .012$, and Amplitude, $F(4,200) = 36.469$, $p < .001$.

The multivariate test for the Mask main effect was significant, $p < .001$. And, the univariate tests indicated a significant difference for Frequency, $F(1,200) = 439.916$, $p < .001$, and Amplitude, $F(1,200) = 195.782$, $p < .001$.

The multivariate test for the Word by Syllable interaction was significant, $p < .001$. Furthermore, the univariate tests indicated a significant difference for Frequency, $F(9,200) = 9.066$, $p < .001$, Duration, $F(9,200) = 21.611$, $p < .001$, and Amplitude, $F(9,200) = 24.783$, $p < .001$.

The multivariate test for the Noise by Syllable interaction was significant, $p < .001$. Also, the univariate tests indicated a significant difference for Frequency, $F(4,200) = 15.010$, $p < .001$, and Amplitude, $F(4,200) = 13.755$, $p < .001$.

The multivariate test for the Noise by Word interaction was significant, $p < .013$. Also, the univariate tests indicated a significant difference for

Amplitude, $F(36,200) = 1.797$, $p < .006$.

The multivariate test for the Mask by Syllable interaction was significant, $p < .001$. And, the univariate tests indicated a significant difference for Frequency, $F(1,200) = 146.065$, $p < .001$, and Duration, $F(1,200) = 5.778$, $p < .017$.

The multivariate test for the Mask by Word interaction was significant, $p < .001$. And, the univariate tests indicated a significant difference for Amplitude, $F(9,200) = 4.144$, $p < .001$.

The multivariate test for the Mask by Noise interaction was significant, $p < .001$. Also, the univariate tests indicated a significant difference for Frequency, $F(4,200) = 108.474$, $p < .001$, and Amplitude, $F(4,200) = 17.111$, $p < .001$.

The multivariate test for the Noise by Word by Syllable interaction was significant, $p < .024$. Furthermore, the univariate tests indicated a significant difference for Amplitude, $F(36,200) = 1.773$, $p < .007$.

The multivariate test for the Mask by Word by Syllable interaction was significant, $p < .001$. Also, the univariate tests indicated a significant difference for Frequency, $F(9,200) = 2.258$, $p < .020$, and Amplitude, $F(9,200) = 4.072$, $p < .001$.

The multivariate test for the Mask by Noise by Syllable interaction was significant, $p < .001$. And, the

univariate tests indicated a significant difference for Frequency, $F(4,200) = 27.279$, $p < .00$, and Amplitude, $F(4,200) = 5.767$, $p < .001$.

Also, for the fourth speaker only, the word durations of the ten words were submitted to a 2×5 (mask by noise) MANOVA. The mask factor consisted of the mask and no-mask conditions. The noise factor consisted of the 85 dB, 95 dB, 100 dB, no-noise, and loud speech conditions. The main effect for mask was significant, $F(1,191) = 4.247$, $p < .041$. The main effect for noise was also significant, $F(4,191) = 2.531$, $p < .042$ and the mask by noise interaction was significant, $F(4,191) = 2.847$, $p < .025$.

V. Discussion on the Data for All Four Speakers.

Formants. The formants became more centralized in high noise conditions. Further analysis is required to fully understand the formant shifts.

Word Duration. See figure 1. Word durations increased with increased noise. Also, word durations increased with the use of an oxygen mask. The difference between the noise and the noise with mask conditions varied between subjects. Speakers two and four had similar results; the no-noise condition had shorter word durations than the two noise conditions. Furthermore, the 95 dB noise condition had a longer word duration than the 95 dB with mask condition. Speaker four had longer word durations overall than speaker two.

Speaker one differed from the other three speakers by decreasing word duration with increased noise; the 95 dB noise condition had a shorter word duration than the no-noise condition. Why is unclear.

Speaker three differed from the other three speakers by increasing word duration with the use of an oxygen mask; the 95 dB with mask condition had longer word durations than the 95 dB condition.

Fundamental Frequency. See figure 2. The F0 for the first three speakers was similar, except that in the 95 dB conditions speaker two had a higher F0 than speakers one and three. Speaker four had a higher F0 than the other three speakers in all three conditions.

Results indicated that the F0 increased with noise, however, the use of an oxygen mask attenuated the effects of noise on F0. The same results were found for the second syllable. There was one difference. For the second syllable, Speaker one had a higher F0 for the 95 dB with mask condition than for the 95 dB noise condition.

Vowel Duration. See figure 3. Significant individual differences occurred in the vowel duration data, however, there were some consistencies. Vowel durations were shorter for the no-noise conditions than for the noise conditions. One exception was speaker one who had mixed results. The results on noise and noise with an oxygen mask are mixed, however, speakers two and four had longer vowel durations for the

95 dB noise condition than for the 95 dB and mask condition.

Amplitude. See figure 4. For both the first and second syllable, amplitude increased with an increase in noise; the amplitude was higher for the 95 dB noise condition than for the no-noise condition. Furthermore, obstruction to articulation (wearing an oxygen mask) attenuated the effects of high noise; the amplitude was higher for the 95 dB noise condition than for the 95 dB noise with mask condition. For subject three, there was no difference in amplitude between the 95 dB and 95 dB with mask conditions.

VI. Discussion on the Data for Speaker Four Only.

Word Duration. See figure 5. For the no-mask condition, word duration increased with increasing noise, except at 100 dB SPL where a decrease occurred. The word duration for the loud condition and the no-noise condition were similar and were much shorter than the word durations for the high noise conditions. This indicates that the increase in word duration for the high noise conditions was not simply due to an attempt to speak loud. This does not mean that word duration and amplitude were not correlated; they probably were. Further analysis using a Sphericity test would indicate whether or not duration, amplitude, and frequency were correlated.

For the mask condition, the results were less clear. Word duration increased with increased noise from 85 dB

to 100 dB, however, the word duration for the no-noise condition was as high as that for the 100 dB noise condition. The loud condition had the shortest word duration of all five conditions.

The results showed differences between the mask and no-mask conditions. The largest difference was at the 85 dB noise level. Word duration was much longer for the no-mask condition than for the mask condition. Also, at 95 dB, the word duration was longer for the no-mask condition than for the mask condition. Conversely, the mask condition had longer word durations than the no-mask condition at 100 dB and no-noise, the difference is small.

Fundamental Frequency. See figure 6. For the no-mask condition, the F0 for the vowel in the first syllable increased with increasing noise, except at 100 dB where a decrease occurred. The F0 for the loud condition was similar to the F0 at 85 dB.

The pattern of results for the second syllable was the same as the pattern for the first syllable. The only difference was that the second syllable had a lower F0 across all noise conditions.

For the mask condition, the F0 for both the first and second syllable increased with increasing noise. The difference, however, between no-noise, 85 dB, and 95 dB was small. The loud condition was similar in F0 to the 100 dB condition.

Differences were found between the mask and no-mask conditions. For the first syllable, the no-mask condition had a higher F0 than the mask condition at no-noise, 85 dB, 95 dB, and loud. Conversely, the mask condition had a higher F0 than the no-mask condition at 100 dB. For the second syllable, the no-mask condition had a higher F0 than the mask condition only at 95 dB and loud. The mask condition had a higher F0 at no-noise, 85 dB, and 100 dB.

Vowel Duration. See figure 7. In the no-mask condition, the vowel duration for the first syllable was longer in high noise conditions than in quiet. The vowel duration was nearly the same length for all three high noise levels.

For the second syllable, the vowel duration was longer in high noise conditions than in quiet. Also, the vowel duration was longer for the 95 dB condition than for the 85 dB and 100 dB conditions.

In the mask condition, there was no difference in the vowel duration of the first syllable between speech in noise and in quiet. The five noise conditions had nearly the same vowel duration. The 100 dB condition had the longest vowel duration.

For the second syllable, the vowel duration increased with increases in already high noise. The no-noise condition had a longer vowel duration than the 85 dB and 95 dB noise conditions.

Amplitude. See figure 8. The no-mask conditions had

higher amplitudes than did the mask conditions.

One exception was the second syllable for the no-noise condition which showed the reverse. Amplitude also increased with increasing noise.

VII. Further Research.

The present results are based on only four speakers. Therefore, caution should be excersized when making generalizations. The results indicated that the changes in the acoustic-phonetic structure of speech produced under high levels of noise are relatively systematic. The changes under obstruction to articulation are not as clear as the changes under high levels of noise, but they are still somewhat systematic.

The recomendations made after studing speech under high acceleration (Bond, Moore, & Anderson, 1986). apply to the present research on noise and obstruction to articulation. The changes in speech should be taken into account when attempts are made to introduce automatic speech recognition technology into the flight environment. For example, the recognizer trained under quiet conditions with no obstruction to articulation may perform poorly when used under high noise conditions and conditions in which an oxygen mask is used. As Bond, Moore and Anderson suggested, research defining the systematic changes in the acoustic-phonetic structure of speech may lead to the developement of compensatory

algorithms for automatic speech recognition technology in the cockpit.

Further analysis on the present data should include post hoc comparisons between the means of those conditions which the ANOVAs indicated a significant difference. Also, the vowel formants, consonants and fricatives under the different conditions should be analyzed.

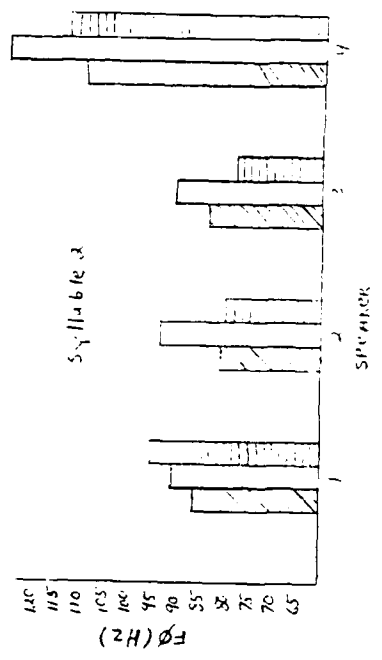
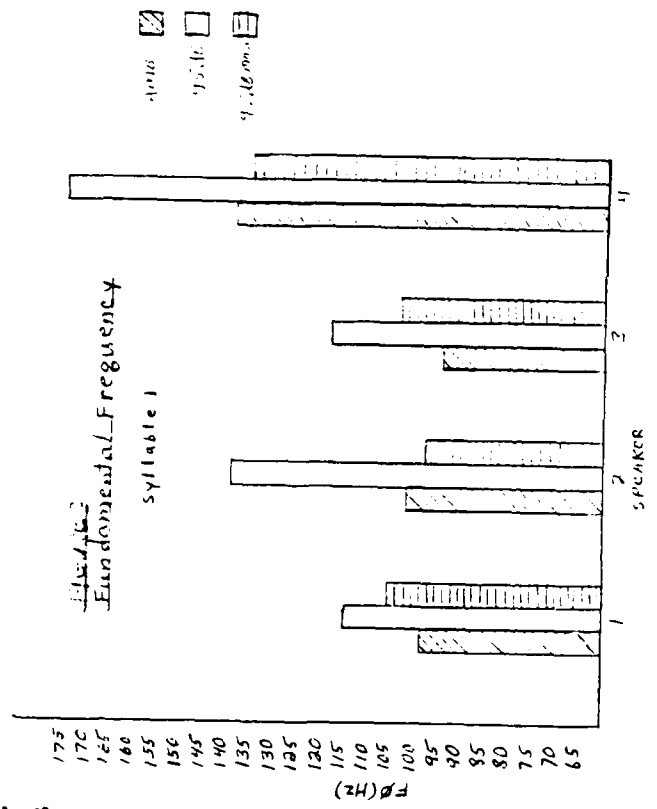
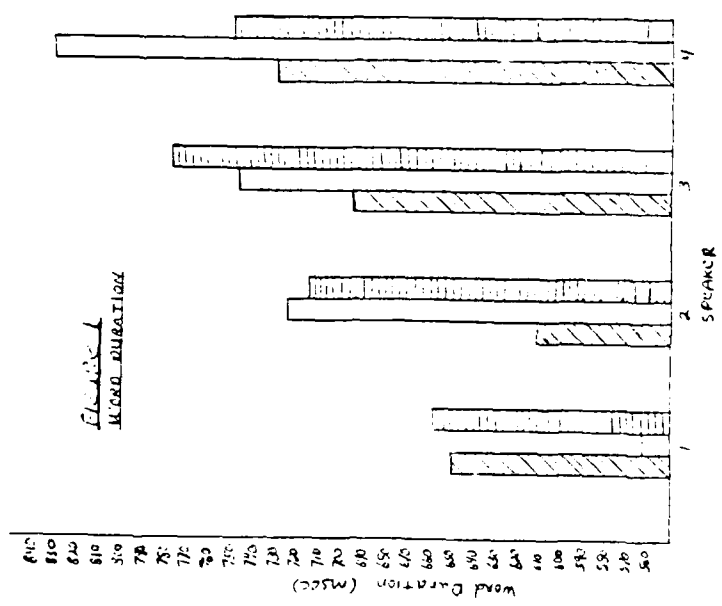
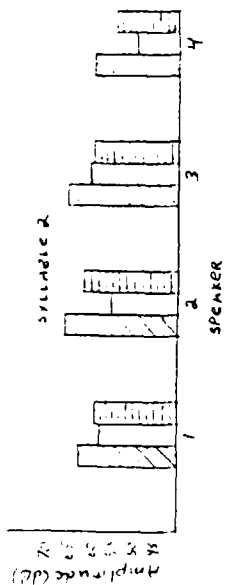
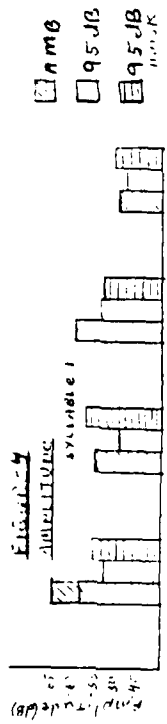
Further research on the effects of noise and obstruction to articulation on speech should address two additional questions outlined by Bond (1985):

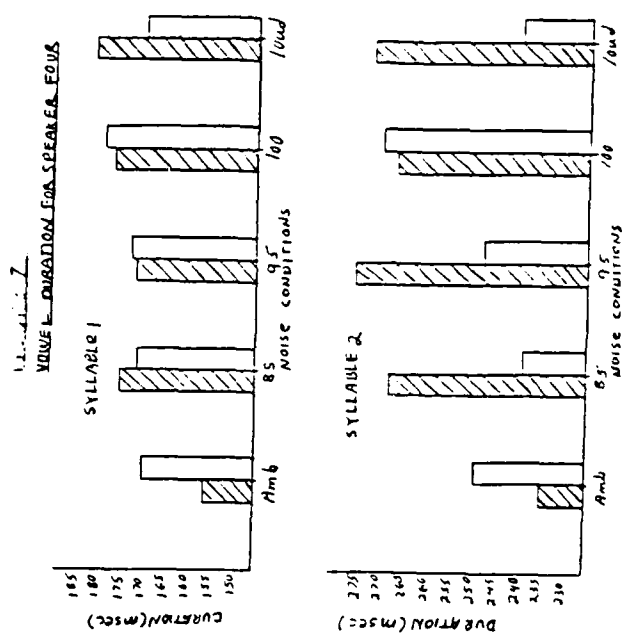
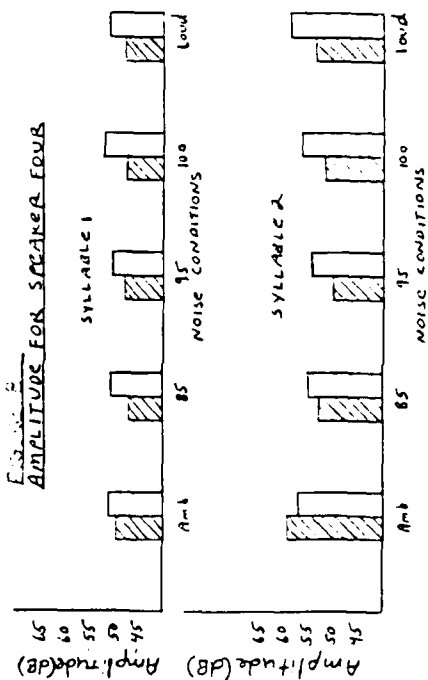
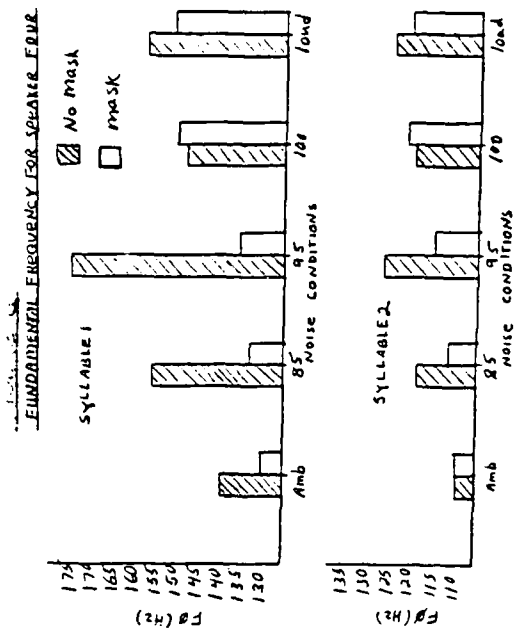
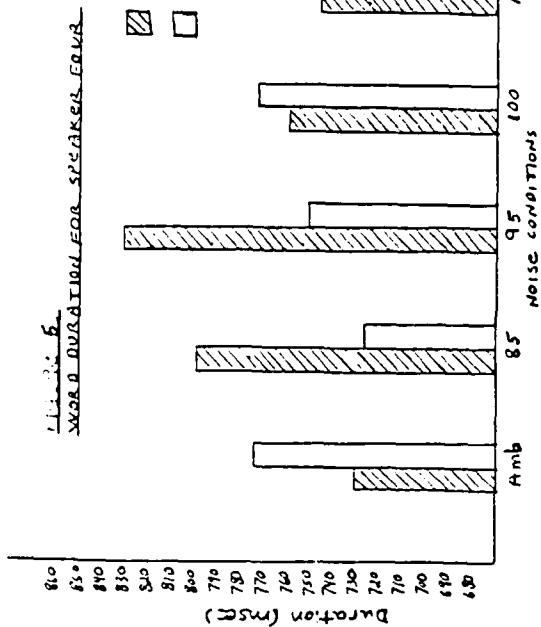
1. Is speech affected differently when the units of production are different, such as words, sentences, or longer texts?
2. What are the effects of noise and obstruction to articulation on the intelligibility of speech?

Further research should address other adverse speaking circumstances, such as vibration. Systematic changes in the acoustic-phonetic structure of speech under vibration may be found and need to be taken into account by automatic speech recognition technology.

References

- 1 Bond, Z. S. "Speech Produced Under Adverse Circumstances: Acoustic Structure and Intelligibility," A Proposal, Unpublished manuscript, (1985).
- 2 Bond, Z. S., Moore, T.J. and Anderson, T.R. "The effects of High Sustained Acceleration on the Acoustic Phonetic Structure of Speech: A Preliminary Investigation," (1986), Aerospace Medical Research Laboratory Technical Report AAMRL-TR-86-011.
- 3 Dreher, J. and O'Neill, J. "Effects of Ambient Noise on Speaker Inteelibility for Words and Phrases," Journal of the Acoustical Society of America, (1957), 29, 1320-1323.
- 4 Peterson, G. E. and Lehiste, I. "Duration of Syllable Nuclei in English," Journal of the Acoustical Society of America, (1960), 32, 693-703.
- 5 Pisoni, D. B., Bernacki, R. H., Nusbaum, H. C. and Yuchtman, M. "Acoustic-Phonetic Correlates of Speech Produced in Noise," ICASSP-IEEE International Conference on Acoustics, Speech, and Signal Processing, (1985) 1581-1584.
- 6 Kassel, R. H. "A User's Guide to SPIRE," Massachusetts Documentation, (1986), Speech Communication Group, Research Laboratory of Electronics, Massachusetts Institute of Technology.





1986 USAF-UES Summer Faculty Research Program/
Graduate Student Support Program

Sponsored by the
Air Force of Scientific Research

Conducted by the
Universal Energy Systems, Inc.

Final Report

A Study of the Probability Distributions of the Long
Term Variations of Acoustical Noise Over Time
of Various Military Environments

Prepared by: Michael D. Garner
Academic Rank: Research Assisant
Department and Physics
University: University of North Carolina at Greensboro
Research Location: The Speech Processing Center,
Hanscom Air Force Base,
(Boston), Mass.
USAF Researcher: Anton Segota
Date: August 29, 1986
Contract No: F49620-85-C-0013

A Study of the Probability Distributions of the Long
Term Variations of Acoustical Noise Over Time
of Various Military Environments

by

Michael Garner

Abstract

The probability distributions of the long term variations of acoustic noise over various Air Force military platforms were studied. It was found that the acoustical noise environments of aircraft such as the E-4B, EC-135, HC130 and F-15 have nearly Gaussian distributions. From the F-15 recordings the noise environments of several flight configurations were studied. All the flight configurations had identical nearly Gaussian distributions. On the other hand aircraft such as the EC-130 and P-3C have very non-Gaussian distributions. The turbo powered helicopter HH-53 was found to have an almost Gaussian distribution, but was slightly skewed toward lower variations in the acoustical noise intensity.

Acknowledgements

I would like to thank the Air Force Systems Command and the Air Force Office of Scientific Research for the sponsorship of my research. I would also like to thank the staff of the RADC/EEV Speech Processing Facility for their assistance and cooperation.

I. Introduction

I received my M.S. in physics from the University of North Carolina at Greensboro in the spring of 1986. The area of my research involved developing numerical methods for suppressing electronic noise in digital flat images acquired with an image intensification and integration system.

The research problem at the RADC/EEV Speech Processing Facility involved the degradation of the performance of narrowband digital voice processors in background acoustic noise. The Air Force utilizes digital voice communications to operate over a large variety of military platforms. Various noise reduction and suppression methods have been tried to solve this problem for specific platforms and processors. Only recently has research been directed at characterization and categorizing noise environments of interest to the Air Force as they affect narrowband voice processors and noise reduction techniques¹.

The problems that noise character has on the type of noise reduction and suppression methods used were similar to the problems I had encountered during my research at Greensboro. Therefore, because of this similarity I was assigned to work on further noise characterization and categorizing of aircraft noise environments at the Speech Processing Facility at Hanscom Air Force Base in

Massachusetts.

II. Objectives of the Research Effort

The overall objective of the acoustic noise characterization and categorization is towards formulation of design parameters, as a function of the specific aircraft, for future speech compression algorithms that are intended to perform in Air Force noise environments.

My individual objectives were:

1. Study the probability distributions of the long term variations of acoustical noise over time of various military environments.
2. Categorize the military environments into groups based on their probability distributions.

III. Sources of Data and Analysis Methods

The sources of data are those present in the RADC Speech Processing Facility's acoustic noise data base. This data base consist of acoustic noise recordings made with high-quality microphones and recording equipment aboard several aircraft of different types.

For this study the primary analysis tools were:

1. The Map 300 and the supporting software Mapin for the analog to digital conversion of the analog recordings.
2. Computer software developed in Fortran for computing the probability distributions.
3. The QIOLIB subroutines for file management support

for the computer software.

4. The Interactive Laboratory System (ILS) software used in conjunction with the Textronics graphics terminal for permanent record documentation.

Each aircraft position was sampled using the Map 300 at 16K HZ and then low pass filtered at 7600 HZ. A total of 81,920 samples were taken of each aircraft position. The probability distributions of the long term variations of these records were then computed using the computer software and supporting QIDLIB subroutines. Permanent records were made using the ILS software and Textronics terminal.

The next section surveys the probability distributions for various aircraft and aircraft positions.

IV. Probability Distributions of the Long Term Variations Over Time of Aircraft Acoustical Noise Environments

In this section we illustrate the noise probability distributions of various military aircraft contained in the RADC/EEV speech processing facility data base. The probability distributions were set to a bin resolution of 256 bins over the lowest and highest variation in intensity. All plots are relative to each other for direct comparison purposes.

Each figure has a overlaid Gaussian distribution. The Gaussian distribution was created from a Gaussian noise generator in the RADC/EEV Speech Processing Facility and

was sampled 16K HZ and low pass filtered at 7600 HZ with the Map 300. The relative standard deviation of the Gaussian distribution was 31.40. The Gaussian distribution was smoothed to prevent confusion with the aircraft distributions.

A. Acoustical Noise Distribution in the E-4B

The probability distribution (figure 1) is based on recordings made by Ketron Corp. in June 1982 aboard the E-4B Advanced Airborne Command Post in the battle staff area. The E-4B is based on the commercial Boeing 747 airframe and is the successor to the EC-135 as a strategic command and control platform.

B. Acoustical Noise Distribution in the EC-135

The probability distribution (figure 2) is based on recordings made by Ketron in July 1982 aboard the EC-135 in the battle staff area. It's primary function is command and control. The airframe is similiar to a commercial Boeing 707.

C. Acoustical Noise Distribution in the EC-130

The probalility distribution (figure 3) is based on recordings made in 1984 by RADC/EEV personnel aboard the EC-130 in the Airborne Communications, Command, and Control (ABCCC) position. The EC-130 is a multi-engine turboprop aircraft. It's primary function is command and control.

D. Acoustical Noise Distribution in the HC-130

The HC-130 is a search and rescue variant of the same

basic airframe as the EC-130. The probability distributions (figures 4 and 5) are based on recordings aboard the HC-130 made simultaneously with two microphones a few feet apart to include any significant variations due to position.

E. Acoustical Noise Distribution in the P-3C

The probability distributions (figure 6) is based on a recording made in 1978 by Ketrion Corp. aboard the P-3C. The P-3C is a long-range anti-submarine patrol aircraft developed for the US Navy by commercial Lockheed Electra.

F. Acoustical Noise Distribution in the HH-53 Helicopter

The probability distribution (figure 7) is based on a recording made in 1984 recording made in 1984 by RADC/EEV personnel aboard the HH-53 helicopter. The HH-53 helicopter is a search and rescue helicopter with main and tail rotors powered by a turbine engine.

G. Acoustical Noise Distribution in the F-15

The F-15 is a twin engine single-seat air-superiority fighter. The probability distributions (figures 8,9,and 10) are based on recordings made in 1976 aboard an F-15 at Wright-Patterson Air Force Base. These recordings were made over a variety of aircraft configurations for comparison purposes.

In the next section we categorize the different aircraft noise environments into groups.

Figure 1: E-4B Battle Staff Position

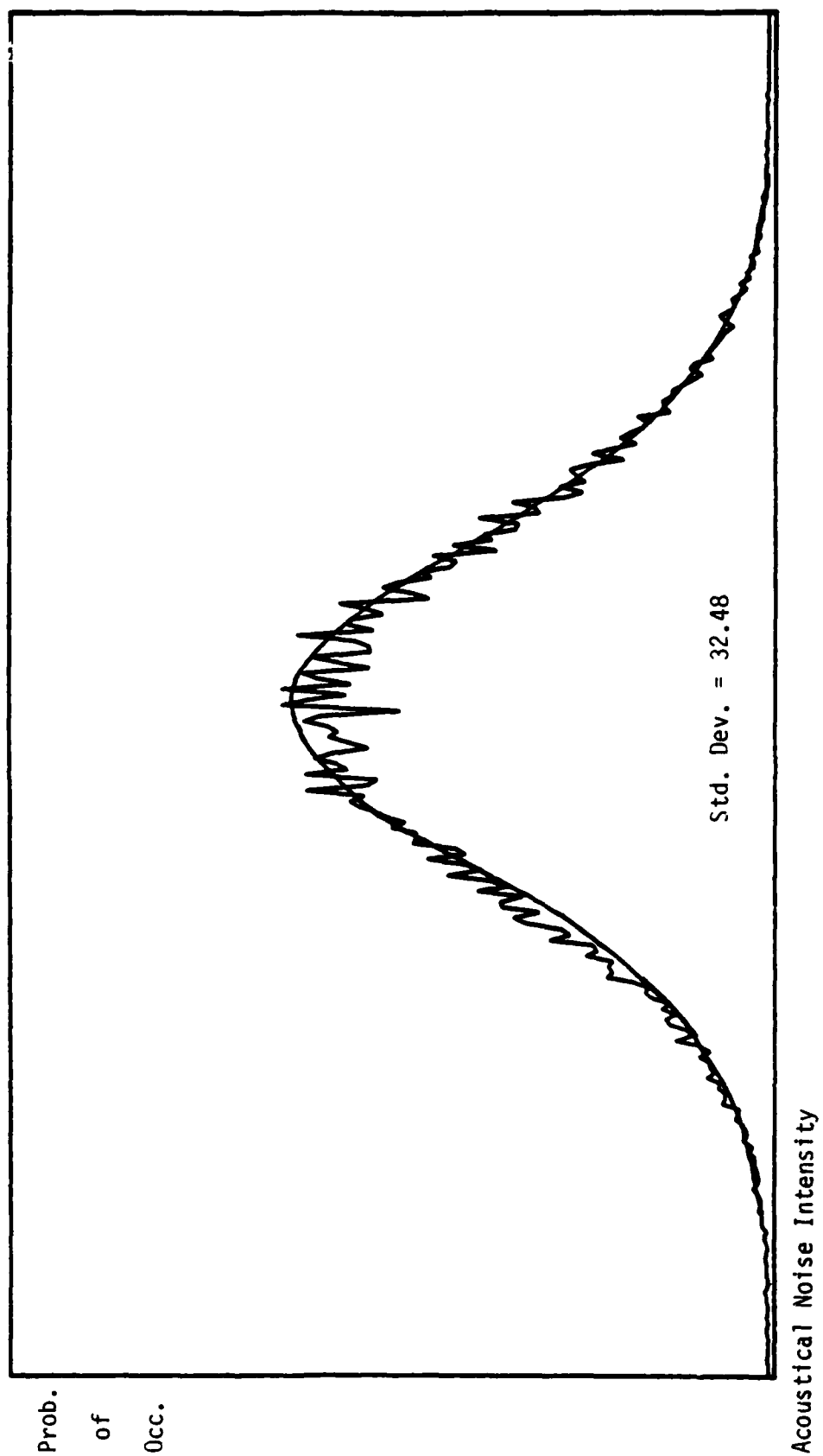


Figure 2: EC-135 Battle Staff Position

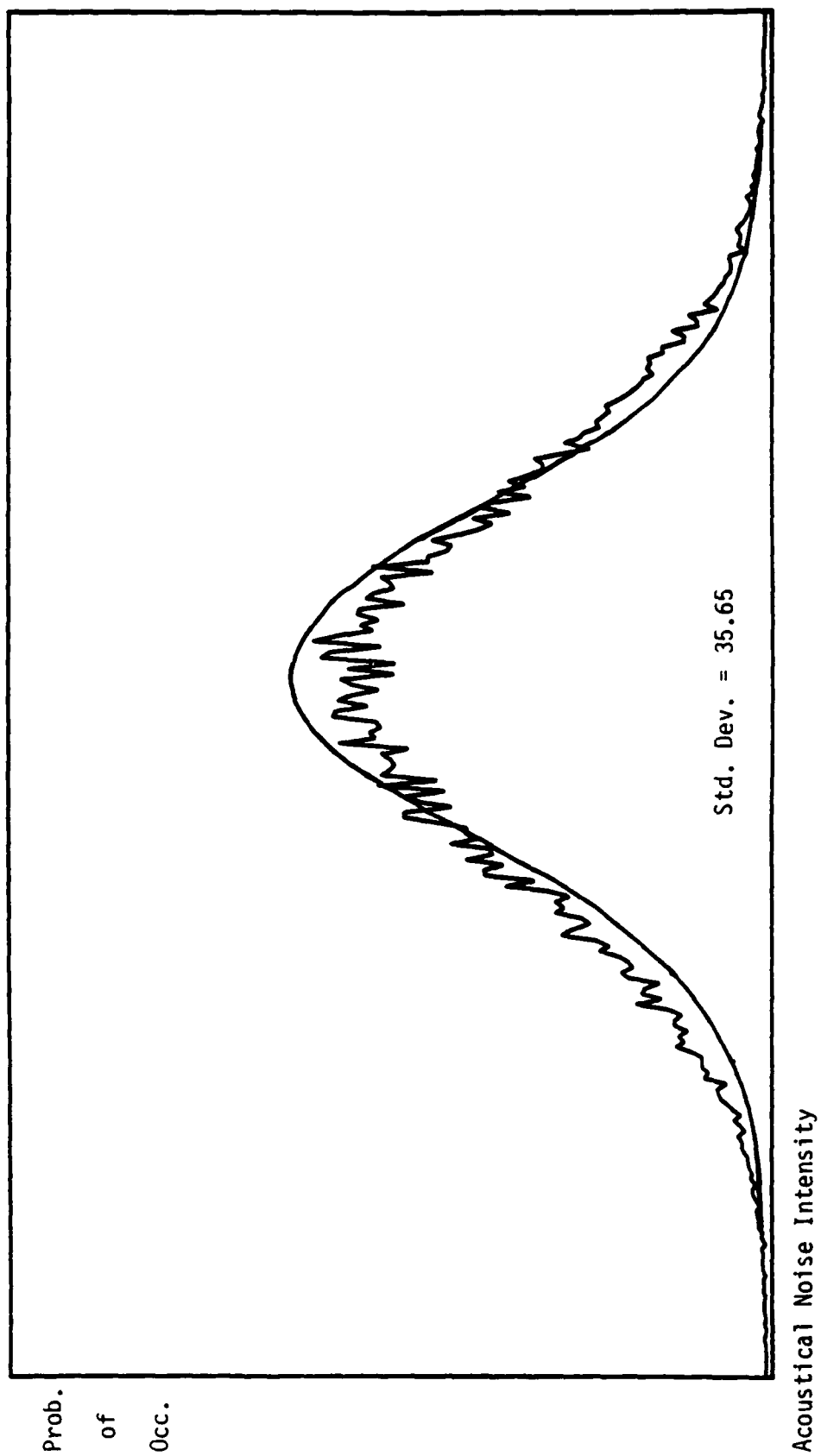


Figure 3: EC-130 ABCCC Position

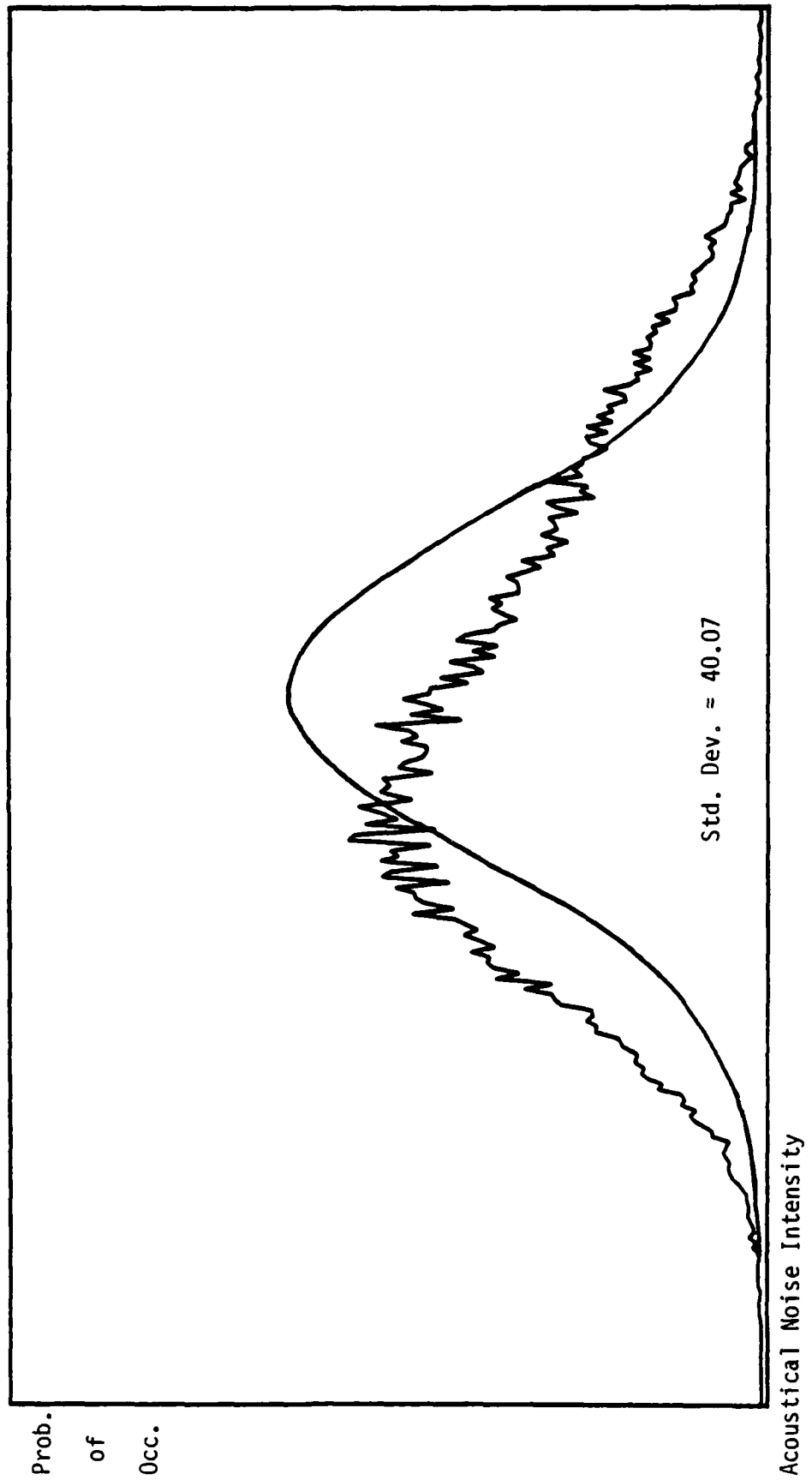


Figure 4: HC-130 Channel A

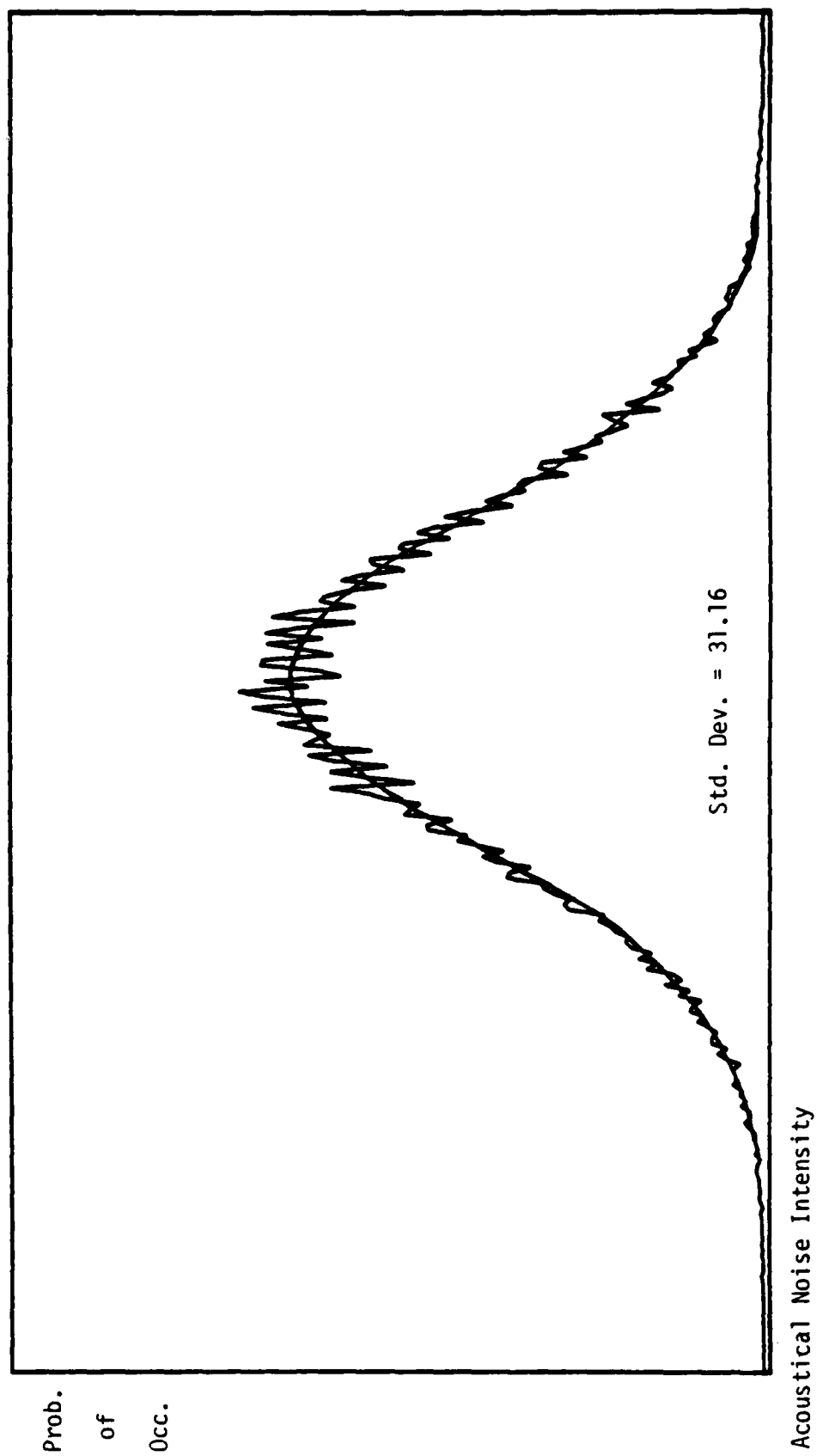


Figure 5: HC-130 Channel B

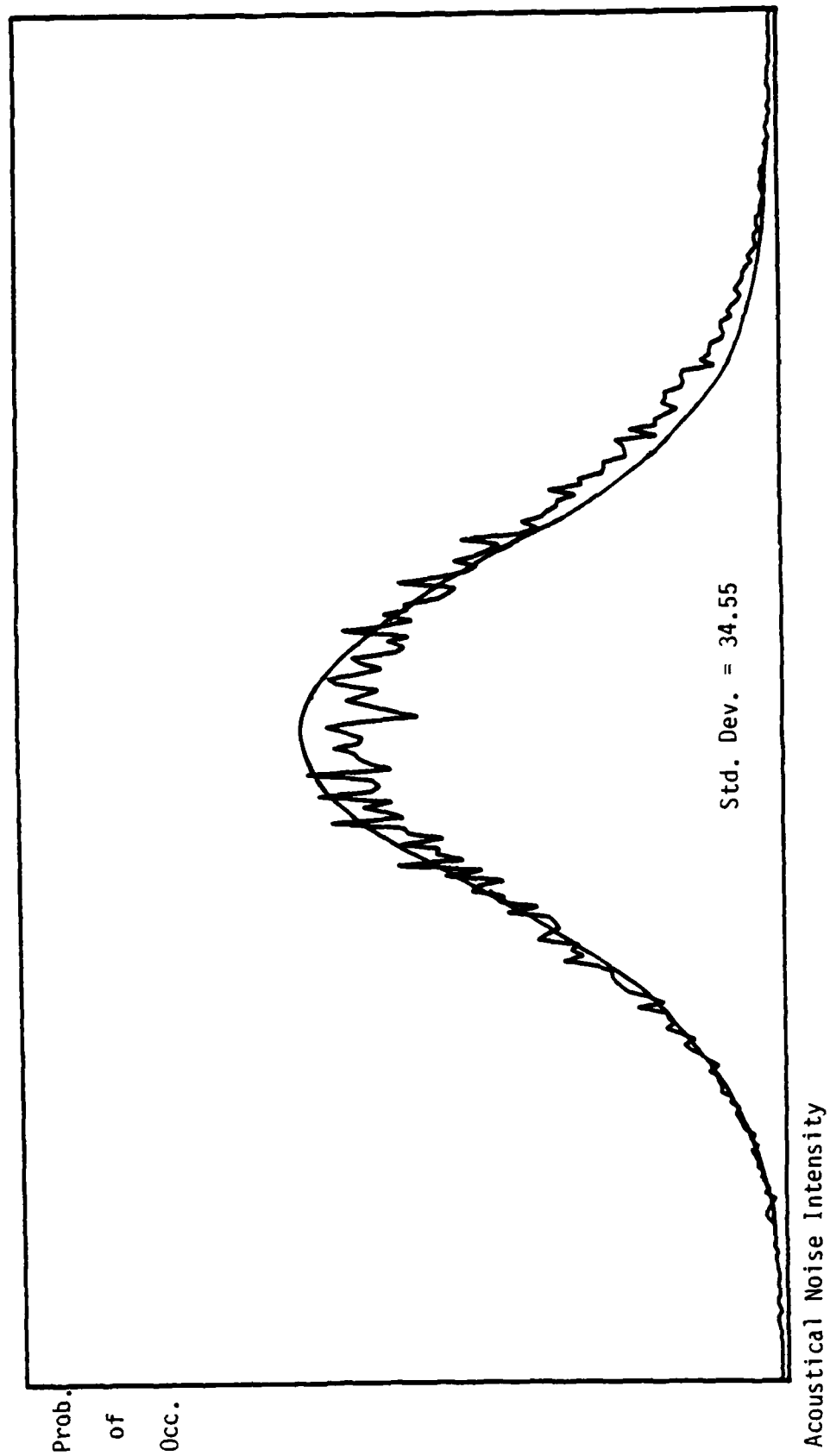


Figure 6: P-3C

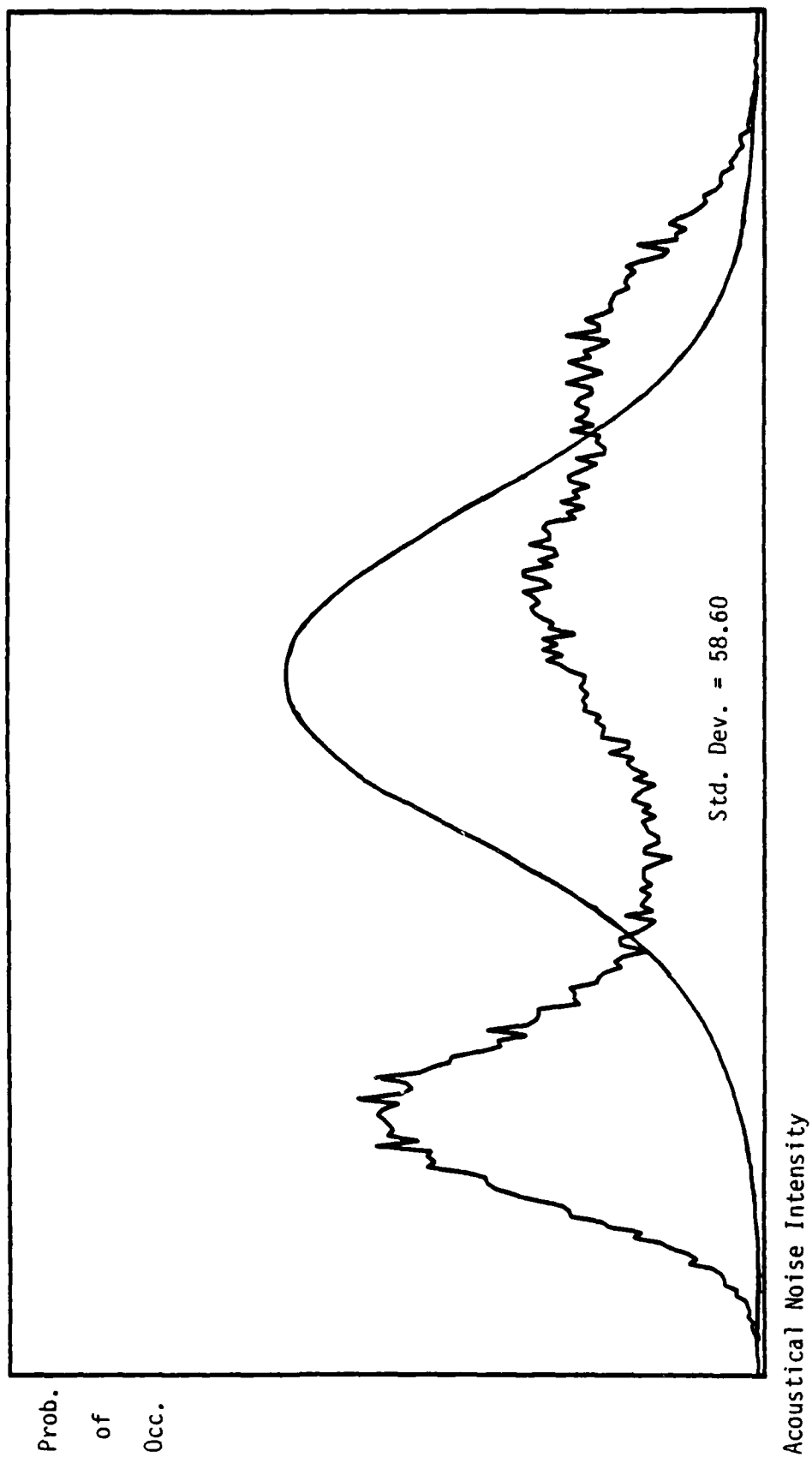


Figure 7: HH-53

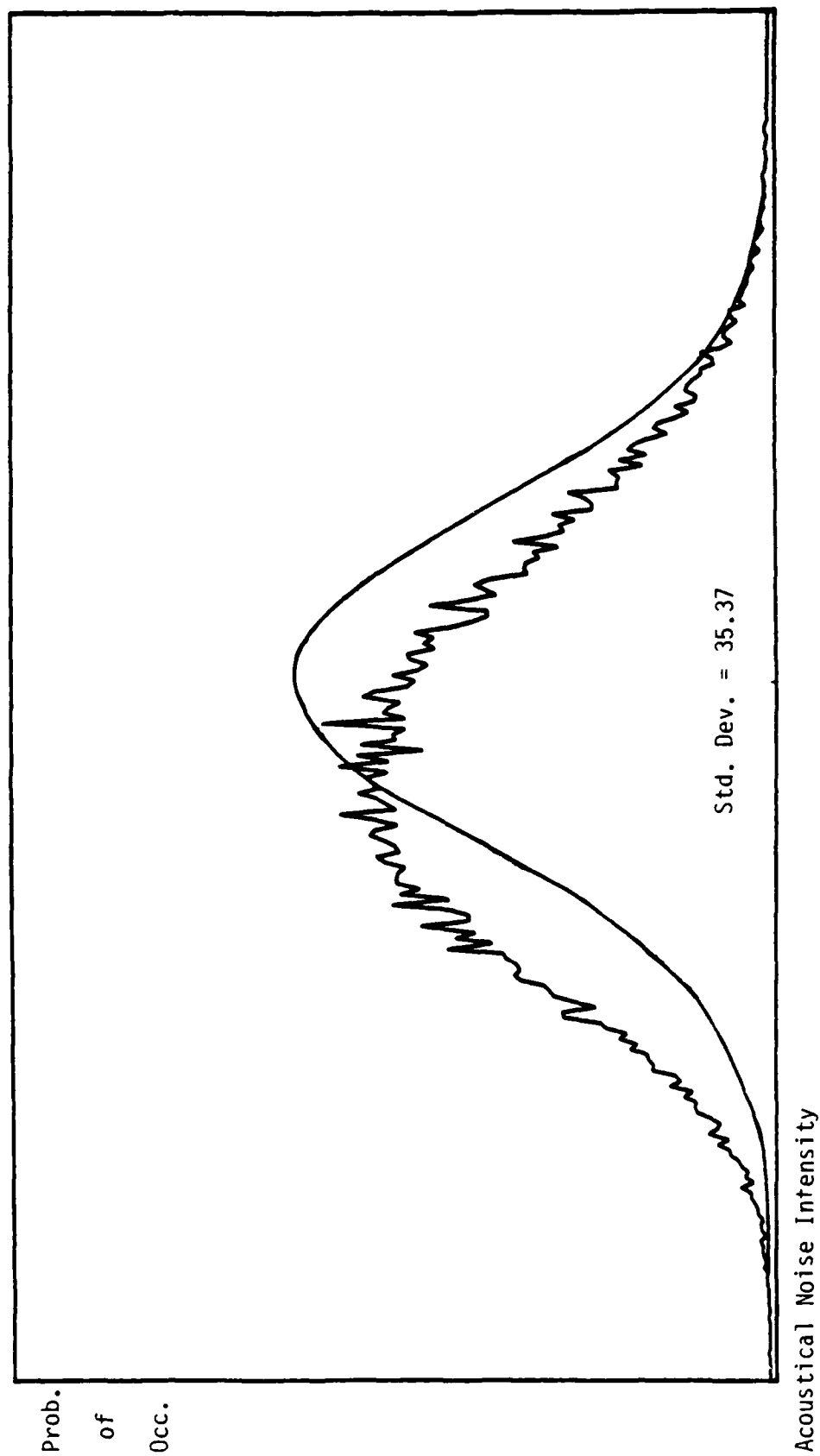


Figure 8: F-15 Climbing 15-20 kft, 0.9 mach.

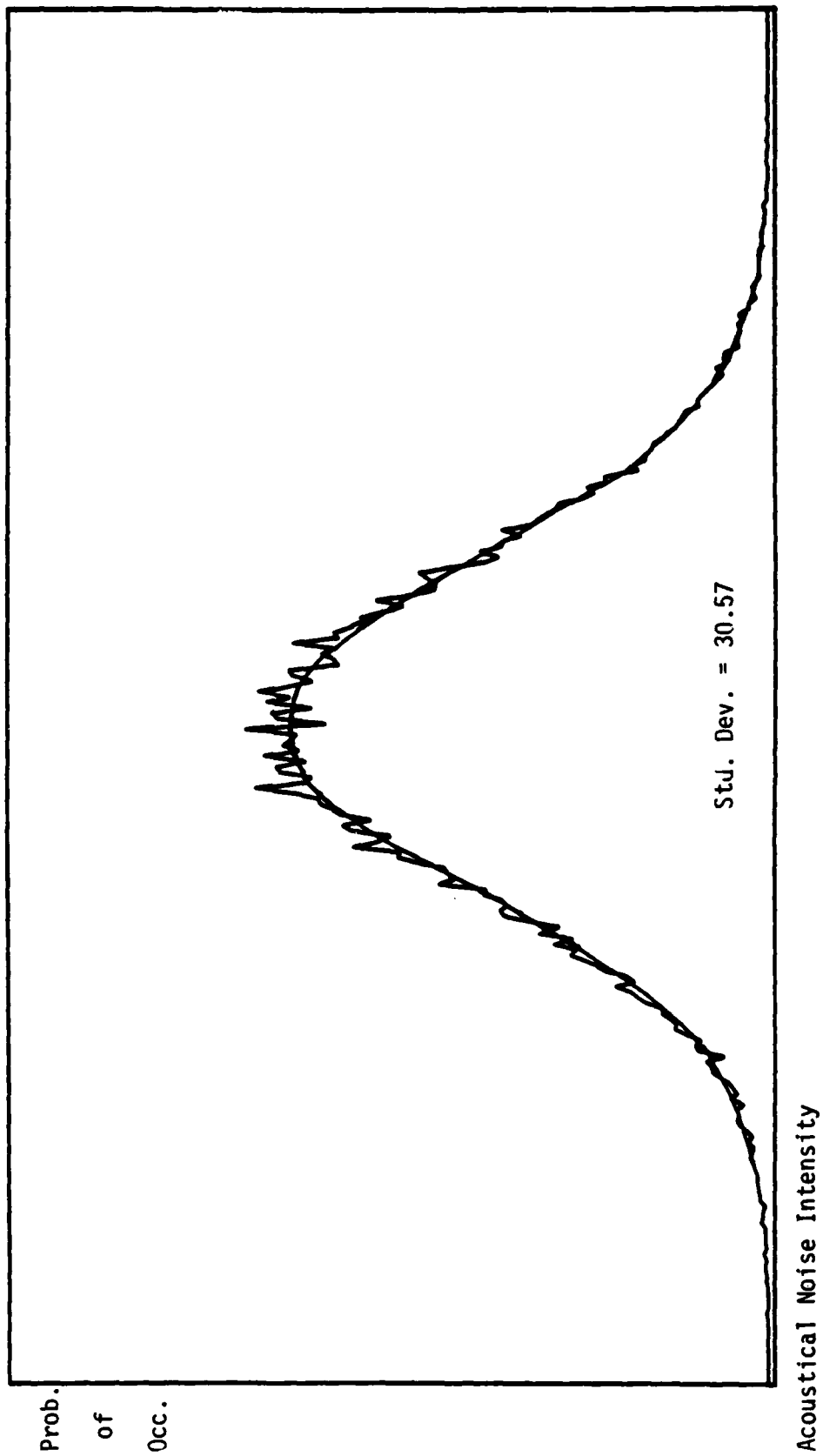


Figure 9: F-15 Level flight 25,000 ft., 0.9 mach, 90% power.

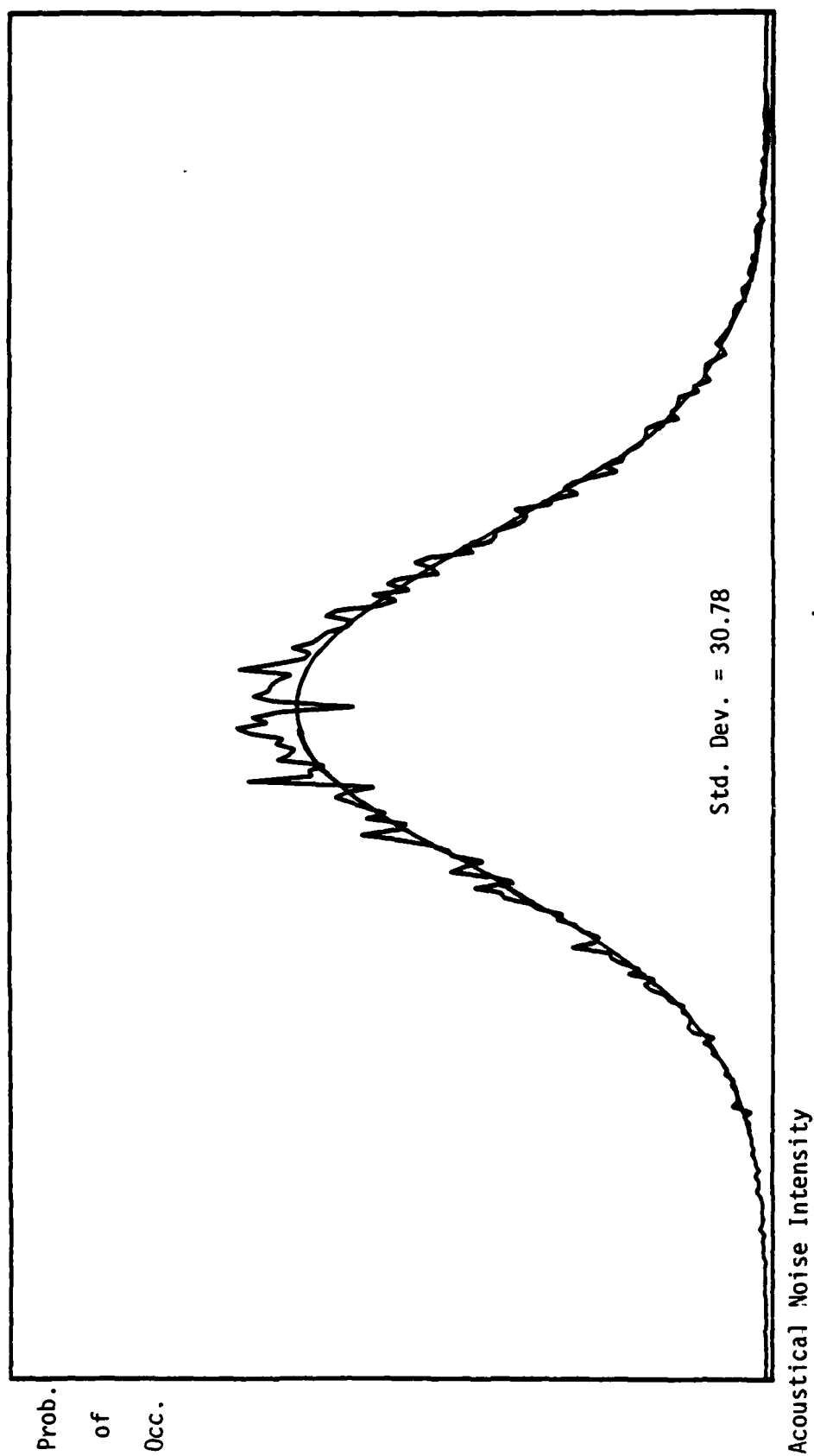
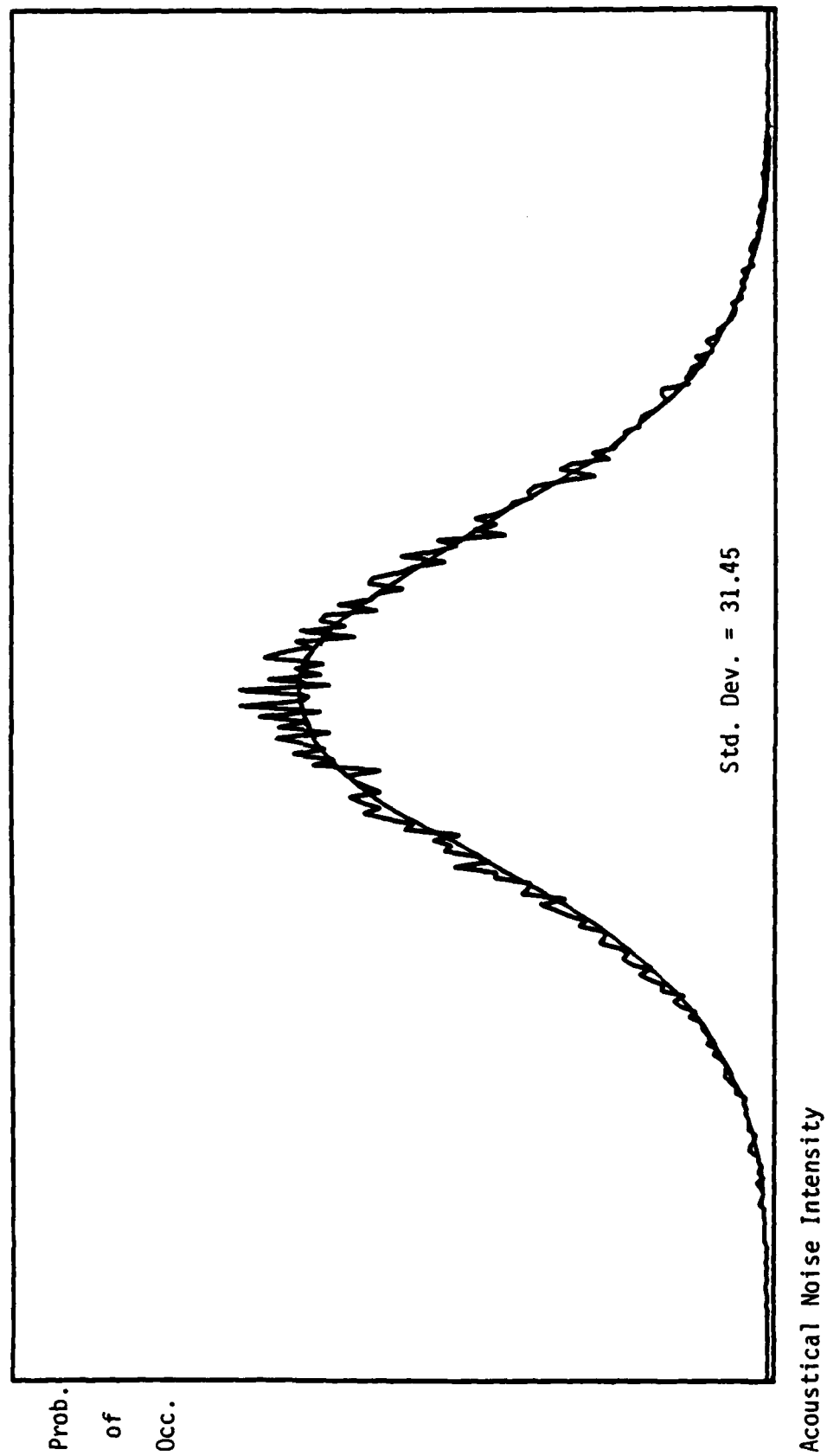


Figure 10: F-15 Level flight 25,000 ft., 1.3 mach.



V. Categorization of Different Probability Distributions of Aircraft Acoustical Noise Environments

Direct comparison of the probability distributions and their standard deviations imply a grouping into three categories.

Category one is defined as all aircraft that display a near Gaussian distribution and standard deviation. In this category fall aircraft such as the E-4B, EC-135, HC-130, and F15.

Category two is defined as all aircraft that display a non-Gaussian distribution and standard deviation. In this category fall the respective positions in aircraft such as the EC-130 and P-3C.

Category three defines the turbine powered helicopter HH-53. The HH-53 displayed an almost Gaussian distribution, but was slightly skewed toward lower variations in the acoustical noise intensity.

In the next section we will discuss recommendations for further study of the long term variations of the acoustical noise environments.

VI. Recommendations

1. Compute the probability distributions over the range of 100 to 3800 hz at a sampling frequency of 8khz since most narrowband processors operate in this range and sampling frequency.

2. Much more work is needed to characterize and categorize the acoustical noise environments before meaningful formulation of design parameters can occur for future speech compression algorithms.

References

1. La Follette, Philip A., "Acoustic Noise Characterization", Arcon Corporation, R86-01W, Research and Development for Digital Voice Processing (DVP)", May 30, 1986, pp. 38-66.

1986 USAF-UES Summer Faculty Research Program/

GRADUATE STUDENT SUMMER SUPPORT PROGRAM

Sponsored by the

AIR FORCE OFFICE OF SCIENTIFIC RESEARCH

Conducted by the

Universal Energy Systems, Inc.

FINAL REPORT

EXPOSURE OF POLYCARBONATE LENS TO

NATURAL ELEMENTS

Prepared by:	Maurice B. Gilbert
Academic Rank:	Medical Student II S1P II
Department and University:	School of Medicine Meharry Medical College
Research Location:	Ophthalmology Branch USAF School of Aerospace Medical Division Brooks Air Force Base, TX 78235-5000
USAF Research:	Lt. Col. Robert E. Miller II
Date:	August 8, 1986
Contract No:	F49620-85-C-0013

EXPOSURE OF POLYCARBONATE LENS TO
NATURAL ELEMENTS

by

Maurice B. Gilbert

ABSTRACT

Polycarbonate optics endure varied types of exposure when utilized by personnel. They function to increase visual acuity and serve as protectors of individuals eyes. Sixty (60) polycarbonate lenses are being tested for effects due to natural weathering on the integrity of the lens.

Initial readings for each lens have been performed. After one (1) year's exposure comparative measurements will be taken to evaluate changes in the lenses. The intention is to generate base-line data for life-expectancy of the polycarbonate lens.

ACKNOWLEDGMENTS

I would like to thank the Air Force Systems Command and the Air Force Office of Scientific Research for allowing me the opportunity to conduct research at the School of Aerospace Medicine at Brooks Air Force Base. The Ophthalmology Branch allowed for hands-on application and correlation with medical training. I would like to thank the members of the Ophthalmology Branch for their guidance and support, Lieutenant Colonel Robert E. Miller II, Major William Woessner, Captain William Flynn, Airman First Class Trevor Abbott, and Airman Tina Balderson. To Captain Flynn, good luck in your medical education.

I. INTRODUCTION

I am a graduate of Morehouse College in Atlanta, Georgia. Where, I received my Bachelor's of Science in Biology. Currently, my studies are continuing at Meharry Medical College in Nashville, Tennessee obtaining a Doctor of Medicine. Having completed a majority of the Basic Science curriculum has given me an in depth understanding of function in the human body.

The Aerospace Medical Division which is inclusive of the Department of Ophthalmology is involved in the support of research concerning the welfare of Air Force personnel. They are involved in maintaining and conducting research in visual optics. A problem under consideration by the Ophthalmology Branch is the life-expectancy of polycarbonate plastics which are utilized as eye shields for flight and ground personnel. How are the lenses which are manufactured from polycarbonate effected by heat, weather, and solar radiation? What would be an appropriate maintenance schedule? What additional factors should be considered by the manufacturer who supplies the lenses?

Questions being considered by the Ophthalmology Branch are valid. My assignment is to examine medical aspects and conduct testing of the lenses.

II. OBJECTIVES OF THE RESEARCH EFFORT

The overall objective of the weathering experiment is to determine and document what factors effect the life expectancy of the polycarbonate lens. It is our goal to understand it's limitations in real word situations.

III. EXPERIMENTAL PROTOCOL

Lens Specimen

A total of sixty (60) polycarbonate optical lenses are being utilized in weathering tests. Thirty will be exposed to the elements, while the other thirty will serve as controls for a period of one (1) year. The lenses were manufactured at the Dudly Plant of the Gentex Corporation.

Stress Patterns

The stress patterns were observed by Major Woessner. Orientation of two polarizing filters show the area where the greatest amount of stress exists for each lens. (9)

Measurement of Curvature

Measurement of the surface curvature of each lens was accomplished with the use of a VIGOR GA - 760 lens measure.

Table 1.

Transmittance of Lens

Measurement of spectral transmission was accomplished with a CARY 17 Recording Spectrophotometer. Transmission was measured in the ultra violet, visible and infra red spectra.

Table 2.

Exposure to Environment:

Thirty polycarbonate optical lenses were placed in an exposure rack and placed on the roof on Friday, 20 June 1986 at 10:45 a.m. The rack was positioned toward the south at an angle of approximately 30 degrees. The controls were placed in a box and maintained on a laboratory shelf.

Weather Data:

Climate measurement will be collected from the Kelly Air Force Base weather station. We will collect data for one (1) year concerning humidity, temperature and general weather conditions. The weather station will collect the data and report to us the monthly averages.

Curvature of Lens (diopters)

<u>LENS NUMBER</u>	<u>CONTROL</u>	<u>WEATHER - EXPOSED</u>
1.	6.0	6.0
2.	5.8	5.2
3.	5.8	5.8
4.	7.6	7.9
5.	6.6	6.3
6.	6.4	6.1
7.	7.0	7.0
8.	6.0	5.8
9.	6.2	6.0
10.	7.0	6.8
11.	5.2	5.0
12.	6.0	6.0
13.	6.0	6.0
14.	6.0	6.0
15.	6.0	5.8
16.	6.0	5.8
17.	6.0	6.0
18.	6.0	5.8
19.	6.0	6.0
20.	6.8	6.5
21.	7.0	6.8
22.	6.0	6.0
23.	5.2	5.0
24.	6.0	6.0
25.	5.8	6.2
26.	5.4	5.5
27.	6.0	6.0
28.	5.4	5.4
29.	7.0	6.9
30.	6.4	6.2

NOTE: Time Clock calibrated for glass
N = 1.53

$$F = \frac{N - 1}{d}$$

Table 1.

PERCENT TRANSMISSION

Highest Minus Sphere (Lens Number 2)

<u>nm</u>	<u>Control</u>	<u>Weather-exposed</u>
400	69.0	71.0
500	84.6	93.5
600	85.0	94.0
700	86.5	96.0
800	86.0	-
900	-	-
1000	-	-

Highest Plus Sphere (Lens Number 4)

<u>nm</u>	<u>Control</u>	<u>Weather-exposed</u>
400	40.0	64.0
500	45.5	100.0
600	45.0	100.0
700	46.2	-
800	45.0	100.0
900	-	-
1000	-	-

Plano (Lens Number 12)

<u>nm</u>	<u>Control</u>	<u>Weather-exposed</u>
400	80.0	82.0
500	99.0	96.0
600	99.7	94.5
700	-	100.0
800	-	-
900	-	-
1000	-	-

Table 2.

46 0860

K_{9E} 5 X 5 TO 1 1/2 INCH • X IN THE HES
KEUFFEL & ESSER CO. MADE IN U.S.A.

PERCENT TRANSMISSION

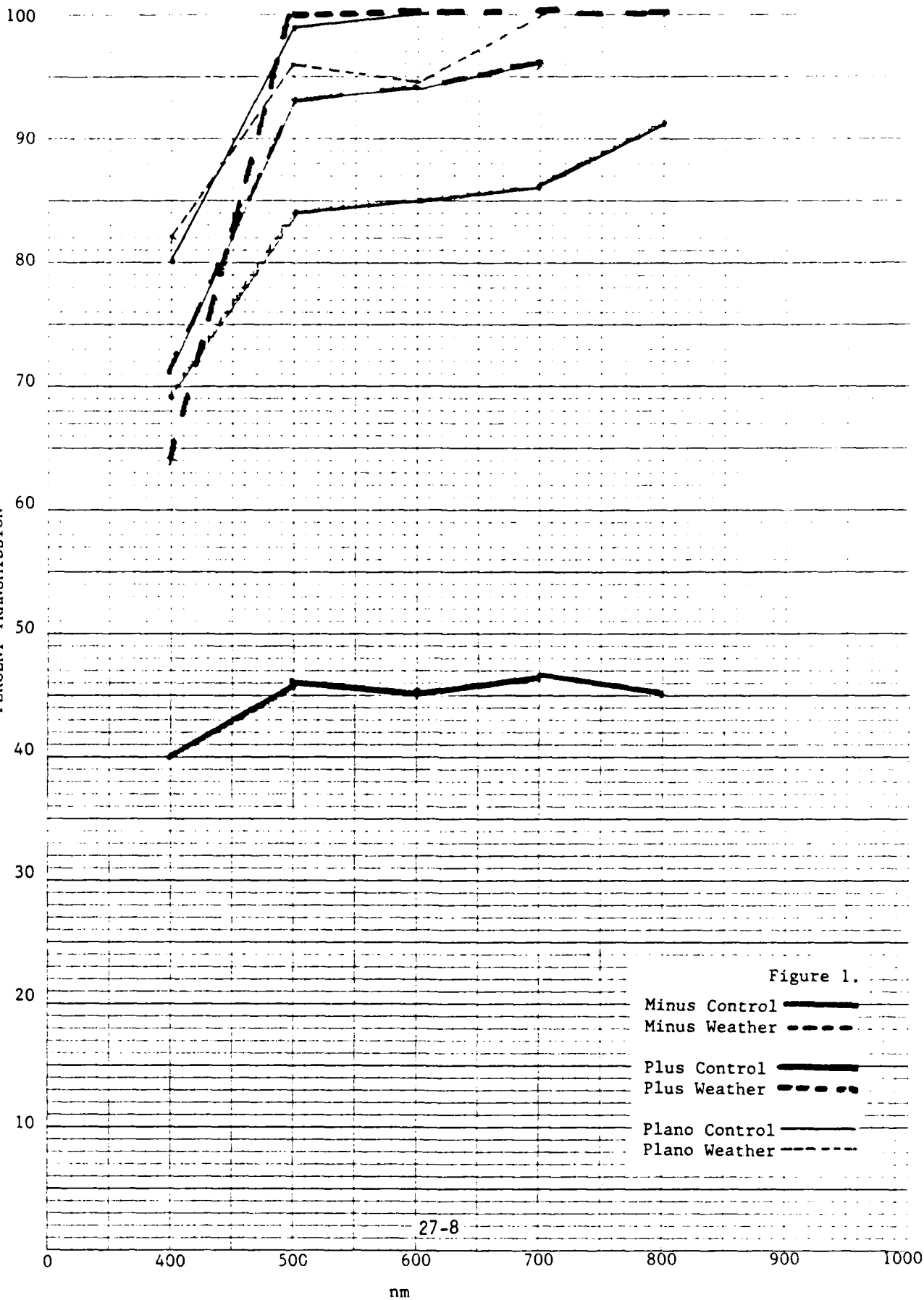


Figure 1.

Minus Control —
Minus Weather - - -
Plus Control —
Plus Weather - - -
Plano Control —
Plano Weather - - -

27-8

nm

27-8

Power of Lens (sphere - cylinder)

<u>LENS NUMBER</u>	<u>CONTROL</u>	<u>WEATHER - EXPOSED</u>
1.	- 1.75	- 1.75
2.	- 2.25 - 0.50	- 2.50 - 0.50
3.	+ 0.25	+ 0.25
4.	+ 2.50 - 0.25	+ 2.50 - 0.50
5.	- 1.25 - 0.25	- 1.25 - 0.25
6.	- 1.25	- 1.50
7.	- 0.50 - 0.25	- 0.75 - 0.25
8.	- 2.00	- 1.75
9.	- 1.50 - 0.25	- 1.50 - 0.25
10.	- 0.75	- 0.75
11.	- 2.25 - 0.25	- 2.50 - 0.25
12.	Plano (0.00)	Plano (0.00)
to	"	"
19.	"	"
20.	- 1.00	- 1.00 - 0.25
21.	- 0.75 - 0.25	- 0.75 - 0.25
22.	- 1.25 - 1.00	- 1.25 - 1.00
23.	- 2.00 - 1.00	- 2.25 - 1.00
24.	Plano (0.00)	0.00 - 0.50
25.	+ 0.25 - 0.75	+ 0.25 - 0.75
26.	+ 0.50 - 0.75	+ 0.50 - 0.75
27.	- 1.75 - 0.50	- 1.75 - 0.25
28.	+ 0.50 - 0.50	+ 0.50 - 0.50
29.	- 0.75 - 0.50	- 0.75 - 0.50
30.	- 0.75 - 1.00	- 0.75 - 1.00

IV. RESULTS

Preliminary

Curvature and spectral measurements are listed in Tables 1 and 2. These values will be compared with follow-up readings to be made at six (6) and twelve (12) months intervals. Photographic slides made showing color - fringe patterns or stress analysis will be maintained in the Aerospace Vision Laboratory.

V. RECOMMENDATIONS

Expectations

Degradation of polycarbonate has been documented in various experimental models. Natural factors such as heat, light and humidity each contribute to the effects of weatherization. Exposure to ultra-violent radiation causes photo-aging, while humidity causes hydrolysis and chemical breakdown. (4) After prolonged exposure, polycarbonates show the effects of erosion due to rain and wind - borne particles. These factors when combined together may contribute to loss of integrity by the lens. (2) Surface flaws which develop may effect optics and the safety factor associated with there usage in glasses and protective shields.

Testing

Spectral analysis is to be done at the six (6) months interval. All previous tests are to be redone after completion of the experiment. Statistical measurement should be done for the completed data. Usage of the Student's t-distribution for both paired and unpaired data should

reveal any major significance between the obtained values. A pneumatic ballistics gun will be used to evaluate impact integrity for control and weathered lens.

Manufacturing

Experimental data collected on polycarbonate recommend a high molecular weight polymer and usage of photo-stabilizers increase the life expectancy. These experiments prefer a polycarbonate with a grade of 3021 or 3021A. They are better able to withstand severe weather conditions and have a survivability of over three (3) years. (1),(4)

References

1. Ram, A., Zilber O., and Kenig, S., "Residual Stresses and Toughness of Polycarbonate Exposed to Environmental Conditions," Polymer Engineering and Science, 25 (1985) 577 - 581.
2. Qayyum, M.M., and White, J.R., "Weathering of injection - moulded glassy polymers: Changes in residual stress and fracture behavior," Journal of Materials Science, 20 (1985) 2557 - 2574.
3. Pakula, T., and Trznadel M., "Thermally stimulated shrinkage forces in oriented polymers: 1. Temperature dependence," Polymer, 26 (1985) 1011 - 1018.
4. Ram, A., Zilber O., and Kenig S., "Life Expection of Polycarbonate" Polymer Engineering and Science, 25 (1985) 535 - 540.
5. Tam E.P., and Martin G.C., "Fatigue Models for Glassy Polymers," Journal of Macromolecular Science and Physics, 23 (1984) 415 - 433.
6. Rickmers, Albert D., and Todd, Hollis N., Statistics: An Introduction, New York, McGraw - Hill Book Company, 1967.
7. Scheie, Harold G., M.D., ScD., F.A.C.S., O.B.E., and Albert, Daniel M., M.D., F.A.C.S., Textbook of Ophthalmology Ninth Edition, Philadelphia, W. B. Saunders Company, 1977.

8. Pryde C.A., "Weathering of Polycarbonates: A Survey of the Variables Involved" Polymer Preparation (American Chemical Society., Division of Polymer Chemistry), 25 (1984) 52 - 53.
9. Walker Jearl, "The Amateur Scientist", Scientific American, 248 (1983) 146 - 152.

1986 USAF-UES SUMMER FACULTY RESEARCH PROGRAM/

GRADUATE STUDENT SUMMER SUPPORT PROGRAM

Sponsored by the

AIR FORCE OFFICE OF SCIENTIFIC RESEARCH

Conducted by the

Universal Energy Systems, Inc.

FINAL REPORT

EFFECTS OF DOBUTAMINE ADMINISTRATION ON
SUSPENSION HYPOKINESIA/HYPODYNAMIA DECONDITIONING IN RATS

Prepared by:	Beverly Elaine Girten
Academic Rank:	Graduate Research Associate
Department and	Exercise Physiology/Physiological
University:	Chemistry, The Ohio State University
Research Location:	Armstrong Aerospace Medical Research Laboratory, BBD, Wright-Patterson Air Force Base, Dayton, Ohio
USAF Researcher:	Clarence M. Oloff
Date:	August 28, 1986
Contract No:	F49620-85-C-0013

EFFECTS OF DOBUTAMINE ADMINISTRATION ON
SUSPENSION HYPOKINESIA/HYPODYNAMIA DECONDITIONING IN RATS

by

Beverly Elaine Girten

ABSTRACT

The primary objective of this study was to determine if the degree of deconditioning commonly seen with suspension hypokinesia/hypodynamia (H/H) in rats could be significantly altered by administration of dobutamine during the suspension. Initial dose finding experiments were conducted, then twenty-four animals were randomly assigned to one of four groups. The four groups were control saline (CON SAL), suspended saline (H/H SAL), control dobutamine (CON DOB) and suspended dobutamine (H/H DOB). The animals were 135 ± 3 days old at the time the treatments were started and the treatments were administered over 14 consecutive days. The data obtained indicate that when actual mass is considered there is significant atrophy of muscle and loss of body weight with H/H suspension. The interactive effect of dobutamine was significant in terms of loss of body mass and loss of soleus mass. When organ and muscle mass were normalized with regard to body weight, there were significant differences between CON SAL and H/H SAL groups with respect to the mass of the heart and adrenals and in three of four hindlimb muscles examined. These results have important implications for formulation of possible interventions with regard to changes brought about by simulated and actual weightlessness. Further investigation into these changes, and the mechanisms involved, appear to be warranted.

ACKNOWLEDGEMENTS

I would like to thank the Air Force Systems Command, the Air Force Office of Scientific Research and the Armstrong Aerospace Medical Research Laboratory for sponsorship of this research. Sincere appreciation and thanks are extended to Leon Kazarian, Robert Hamlin, A. John Merola and, in particular, Clarence Oloff, for providing the opportunity and guidance necessary for completion of this project. In addition, I would also like to acknowledge and thank Emily Morey-Holton (NASA-Ames) for providing advice and details concerning the hindlimb suspension model and for her willingness to allow us to borrow the x-y axis suspension apparatus that were so critical to the study. The efforts of Pat Roberts and the UDRI group with regard to the construction of the suspension cages were also very much appreciated. Special thanks are also extended to all those who provided help and support along the way. Included among those from Wright-Patterson are Marvin Souder, Ed Eveland, Suzanne Smith, James Cooper, Pat Lewandowski, Nadia Greenidge, Gerald Harris and Brian Jenkins. Susan Bloomfield did a great deal to coordinate efforts at Ohio State and included among the others who helped at Ohio State were Peggy Plato, Jamie Hobson, Barb Smith and Jim Schlub. Finally, I would like to thank my mother, Vedna Girtten, and the rest of my family, for their constant support and encouragement during all of my research endeavors.

I. INTRODUCTION

Alterations in the musculoskeletal and cardiovascular systems as a result of the near-weightless environment of space or in simulated weightless conditions are well documented (1,2,3,6). Although general information about the basic physiological and pathological effects of the deconditioning that results from the relative hypodynamic and hypokinesia is abundant (4,5), there is still much to be learned. Investigation of effective countermeasures that might prevent or minimize the alterations that result from deconditioning are being restricted by lack of information on the basic biological mechanisms involved in these changes.

During my employment as a Graduate Research Associate at The Ohio State University, I have been working in the areas of exercise physiology and physiological chemistry for the last three years. Specific areas of study and investigation have involved bioenergetics, sub-cellular enzyme studies and cardiovascular response of exercised animals. My most recent work at Ohio State has centered on changes in oxidative enzymes, antioxidant enzymes and lipids in rats and rabbits undergoing a variety of treatments including long-term exercise training on treadmills. An additional investigation that our laboratory has been involved in deals with alterations of skeletal muscle oxidative enzymes during bedrest. Moderate daily exercise and intravenous infusion of dobutamine, a synthetic catecholamine, served as treatments in the bedrest study. Results indicated that dobutamine was able to decrease the deconditioning effects commonly seen with bedrest in many of the cardiovascular responses studied, as well as some of the skeletal muscle

oxidative enzymes that were examined (7). Since this study was clinical in nature and involved human subjects, the degree to which the bioenergetics and sub-cellular enzyme component could be investigated was severely limited by the small size of the muscle biopsy. So, while the bedrest study did have very definite implications with regard to deconditioning changes seen with the near-weightless environment of space and potential interventions, it generated a number of questions that could best be answered by utilization of an appropriate animal model.

The purpose of the summer research project was to conduct a series of preliminary experiments to provide the information necessary to determine if dobutamine and/or exercise training could significantly alter deconditioning effects in an appropriate animal model that could effectively simulate weightlessness. Investigation into physiological changes induced by hypokinesia/hypodynamia in animals have been conducted at the Armstrong Aerospace Medical Research Laboratory (AAMRL) in the past. Due to the time restraint of the summer project, as well as the above points, a rat hypokinesia/hypodynamia model that was based on a well-established tail suspension protocol was utilized. The past experience of the personnel at AAMRL and the material, equipment and facilities at the laboratory provided an ideal environment for this investigation.

II. OBJECTIVES OF THE RESEARCH EFFORT

The primary goal of this project was to determine if the degree of deconditioning commonly seen with suspension hypokinesia/hypodynamia (H/H) in rats could be altered by administration of dobutamine during the suspension period. Secondary goals were to determine the best methods of

administration and the appropriate amounts of dobutamine to use and to begin to exercise train a group of rats so that the same treatments could be applied to aerobically conditioned animals at a later time. In order to accomplish these overall goals the following specific objectives were formulated:

- Conduct initial dose finding experiments to determine appropriate amounts of dobutamine needed to elicit desired response.
- Determine if subcutaneous pellets designed to release dobutamine over several weeks would be feasible to use.
- Determine which of the above methods of dobutamine administration could best accomplish the major objectives of the study.
- Examine effects of suspension H/H in rats by monitoring food consumption, body weight and activity.
- Determine if administration of dobutamine or suspension H/H over two weeks would have an effect on heart rate, skeletal muscle mass, and organ mass.
- Begin exercise training a group of rats so that the same and additional information could be obtained from them after 10-12 weeks of training.
- Collect and store tissue at sacrifice in such a manner so as to allow detailed biochemical, metabolic and histochemical analysis to be carried out at a later date.

These objectives have all been accomplished. The methods and results that resulted from these goals and objectives are presented in the next two sections of this report. By meeting these objectives, the summer project

has provided preliminary information that is needed for future investigation in this area of research.

III. DOBUTAMINE DOSE RESPONSE

The dobutamine dose response phase of the project was designed to (1) determine the specific amount of dobutamine needed to elicit the optimal response in the experimental animals, and (2) determine if subcutaneous pellets designed to have a controlled dose-dependent rate of release would be feasible to use.

In order to determine the specific amount of dobutamine needed to elicit an optimal response, 12 animals were given a series of subcutaneous (subQ) and intraperitoneal (IP) injections of dobutamine at a variety of dosages. Animals heart rates (HR) were monitored in both the conscious and unconscious states to determine the acute response to the dosages under both conditions.

After two weeks of experimentation, a dose of 1 mg/kg BW injected IP, was found to elicit the desired increase in unconscious HR. Mean values from six animals showed that a mean unconscious HR of 280 ± 18 increased to 424 ± 22 within 9-11 minutes of injection. The HR remained significantly elevated for 35-55 minutes.

A summary of the findings obtained from the first portion of the dobutamine dose response trials include:

1. Use of pentobarbital as an anesthetic agent masked the acute cardiovascular response of dobutamine.
2. IP injections yielded more reliable results than subQ injections.
3. Initial results indicating that relatively low doses could elicit desired responses were not able to be

reproduced with a larger number of animals under more controlled conditions.

4. Efforts to duplicate responses reported by Liang and colleagues were successful. The IP dose used was much larger than that originally tried.
5. Time lines to obtain meaningful electrocardiographic records based on half-life of ketamine/xylazine anesthetic and dobutamine were developed and tested.

The pellet dose response trial was designed to test the feasibility of pellet implants and to determine what dose, if any, would elicit the desired response. This trial utilized 15 animals and tested the effects of 5 concentrations of dobutamine (0, 2.5, 5, 10 and 20 mg/pellet). The major findings resulting from this group of animals are represented by figures 1-3 and table 1.

Figure 1 shows the heart rate response of the groups while the animals were conscious and in a restrainer for 10 minutes, 8 minutes after the anesthetic was administered and the heart rate response up to 32 minutes after the dobutamine pellets were implanted. The heart rate of the conscious animals decreased as expected during the 10 minutes they were restrained. After the conscious baseline heart rates were obtained, the anesthetic was given and the mean heart rate dropped an average of 175 bpm within 8 minutes. The dobutamine pellets were implanted between minute 10 and 12 and as indicated in figure 1, the heart rate increased precipitously in a dose-dependent fashion over the next 8-16 minutes. The dose-dependency was no longer apparent at minute 24 and leveled off at minute 32 with the HR response from all groups (except the placebo group) being approximately the same. Time for the animals to regain consciousness after

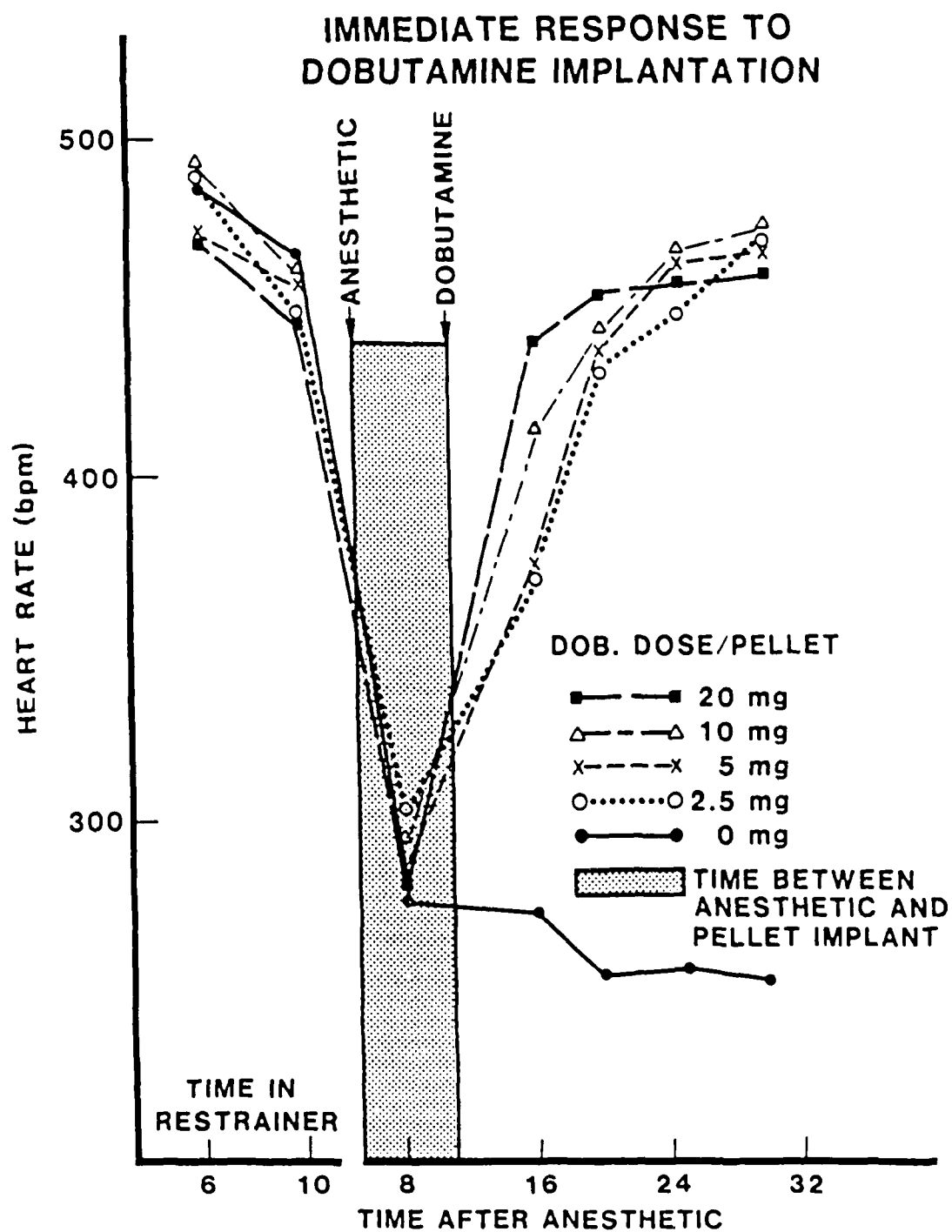


Figure 1.

anesthetic was given also appeared to be dose-dependent as shown in figure 2.

Three days after the pellets were implanted, the animals were weighed. Figure 3 illustrates the mean change in weight over those 3 days. Again, weight change appeared to be dose-dependent, with the placebo group showing a slight increase in weight, while other groups showed a large decrease in weight. This rapid decrease in weight was unexpected, so in an effort to better understand the source of the weight loss the animals were placed in an Optovarimax monitor to determine if there was any difference in the level of activity among the groups. Table 1 shows the means and standard deviations of four activity parameters for the groups. The ambulatory movement parameter was the only one that showed a dose-dependent pattern. It would seem likely that the high ambulatory movement score would account at least in part, for the drastic change in weight. However, food consumption values were not obtained until the fourth day and even though there was no difference in food consumption between groups at this point, conclusions concerning the influence of food consumption on weight change over days 1-3 cannot be made.

Many of the measurements were repeated periodically and by day 5 the effects of the pellets were no longer apparent. Animals in all groups were gaining weight, there was no apparent elevation of unconscious HR, there was no apparent dose-dependency on time to recovery with the anesthetic and the activity levels of all groups were approximately the same as the placebo. At the time of sacrifice, 21 days after the pellets were implanted, the heart weight and heart weight to body weight ratio indicated that there was no cardiac hypertrophy evident at

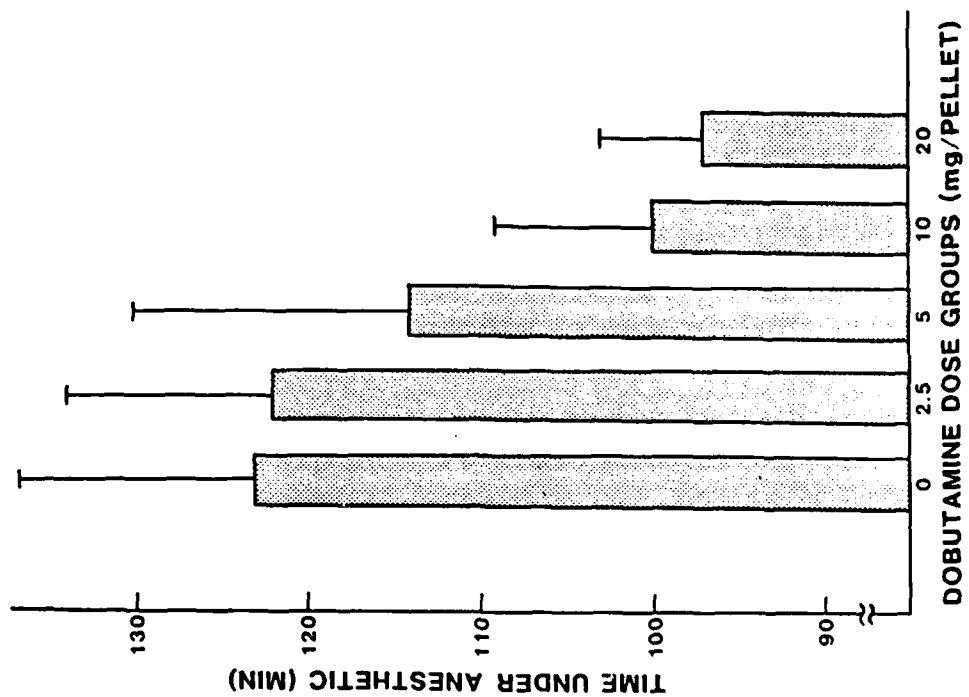


Figure 2.

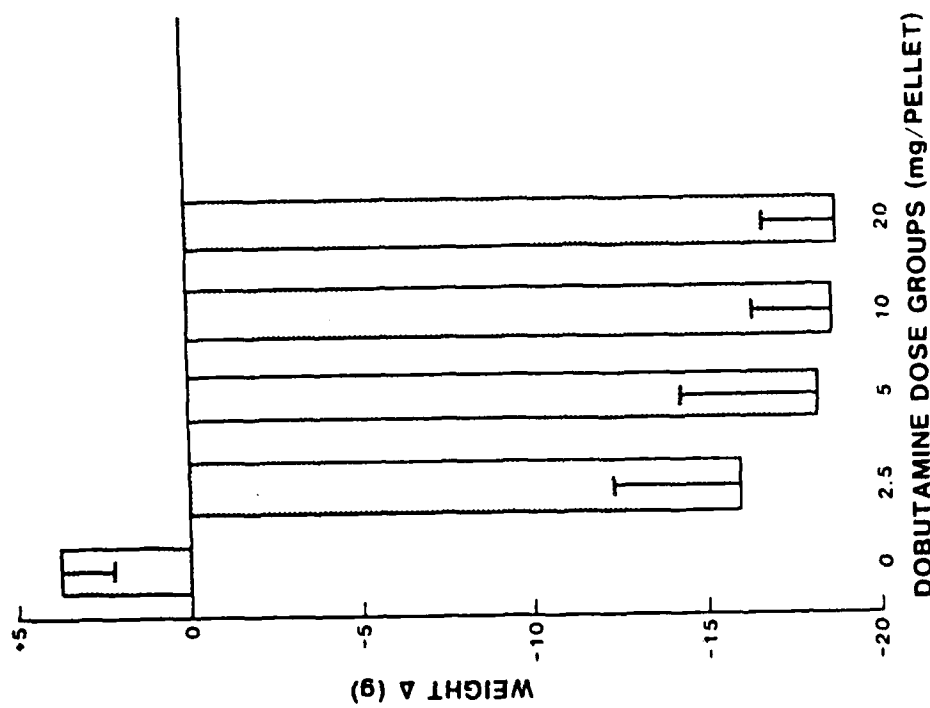


Figure 3.

		DOBUTAMINE DOSE GROUPS (mg/PELLET)				
		0	2.5	5	10	20
ACTIVITY PARAMETERS	AMB	3860	4276	5036	7666	8255
	MOV	±394	±373	±783	±531	±399
	NAMB	1471	1367	1481	839	1156
	MOV	±179	±220	±127	±471	±87
	AMB	160	201	155	99	178
	CTS	±23	±65	±13	±35	±13
	NAMB	130	113	122	80	114
	CTS	±3	±8	±4	±50	±12

Table 1.

		TISSUE WEIGHTS OF SEDENTARY RATS (g)								
		BW	HRT	KID	ADR	SOL	PL	TA	EDL	TRI
TREATMENT GROUPS	SAL	438	1.3663	1.3982	.0318	.1848	.6920	.6117	.1929	2.2480
	CON	±20	±.1193	±.0886	±.0040	±.0114	±.0813	±.0431	±.0423	±.1097
	SAL	381	1.3417	1.2688	.0329	.1056	.5778	.5415	.1174	2.1014
	H/H	±13	±.0731	±.1053	±.0049	±.0083	±.0869	±.0424	±.0284	±.1519
	DOB	417	1.3507	1.2945	.0326	.1705	.7380	.6387	.1997	2.0900
	CON	±17	±.0888	±.0841	±.0017	±.0167	±.0861	±.0952	±.0352	±.1381
	DOB	397	1.4248	1.2852	.0341	.1234	.5149	.5456	.1404	2.0970
	H/H	±16	±.0883	±.0352	±.0044	±.0176	±.0766	±.0855	±.0505	±.1487

Table 2.

any of the dose levels. Histopathological examination (courtesy of C. Hixson, DVM) indicated that remnants of pellet were encompassed by a typical foreign body tissue response--characterized by fibrous connective tissue, macrophages, and foreign-body type multinucleated giant cells. The fibrotic capsule may, in part, account for the apparent failure of the pellets to release the dobutamine over the 21-day period. Further investigation into the feasibility of using dobutamine in pellet form should continue; utilization of pure dobutamine rather than the lyophilized form in mannitol and HCl may be more successful.

IV. H/H SUSPENSION AND DOBUTAMINE TREATMENTS

Four groups of sedentary rats were used in this phase of the study; they were the control saline (CON SAL) group, the suspended saline (H/H SAL) group, the control dobutamine (CON DOB) group and the suspended dobutamine (H/H DOB) group. The animals were 135 ± 3 days old at the time the treatments were started and the treatments were administered over a 14 day period of time. The animals used in this study were older than rats used in most suspension study, and for that reason the information on body weight alterations are of particular interest.

Food consumption and body weights were monitored every day and every other day, respectively. Mean values for the groups are presented in figures 4 and 5. Values for food consumption for all groups, even the nonsuspended groups dropped during the first day. The suspended groups continued to lose weight through the third day. All groups were back to regular levels of consumption by 8 days. The body weights of the suspended animals decreased

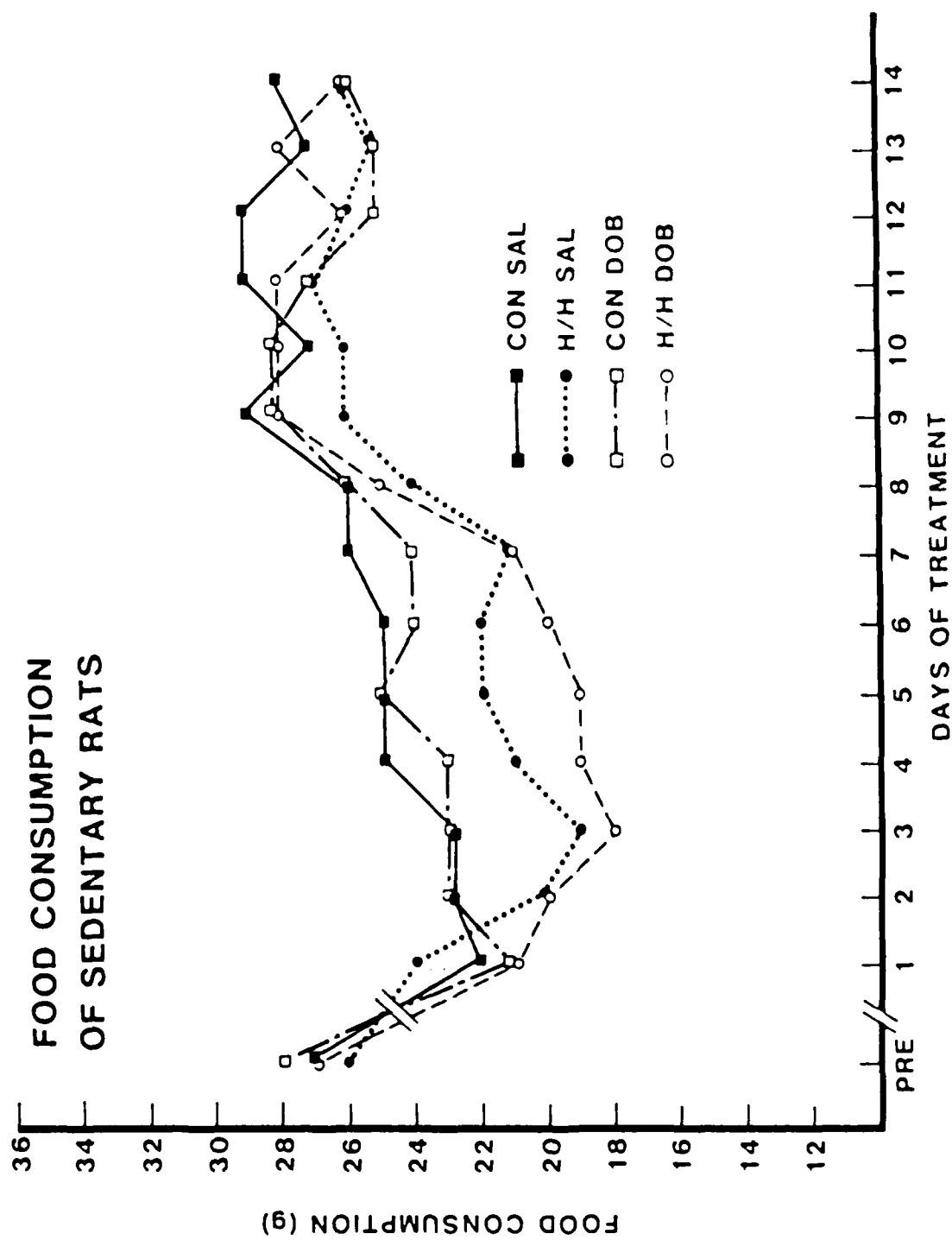


Figure 4.

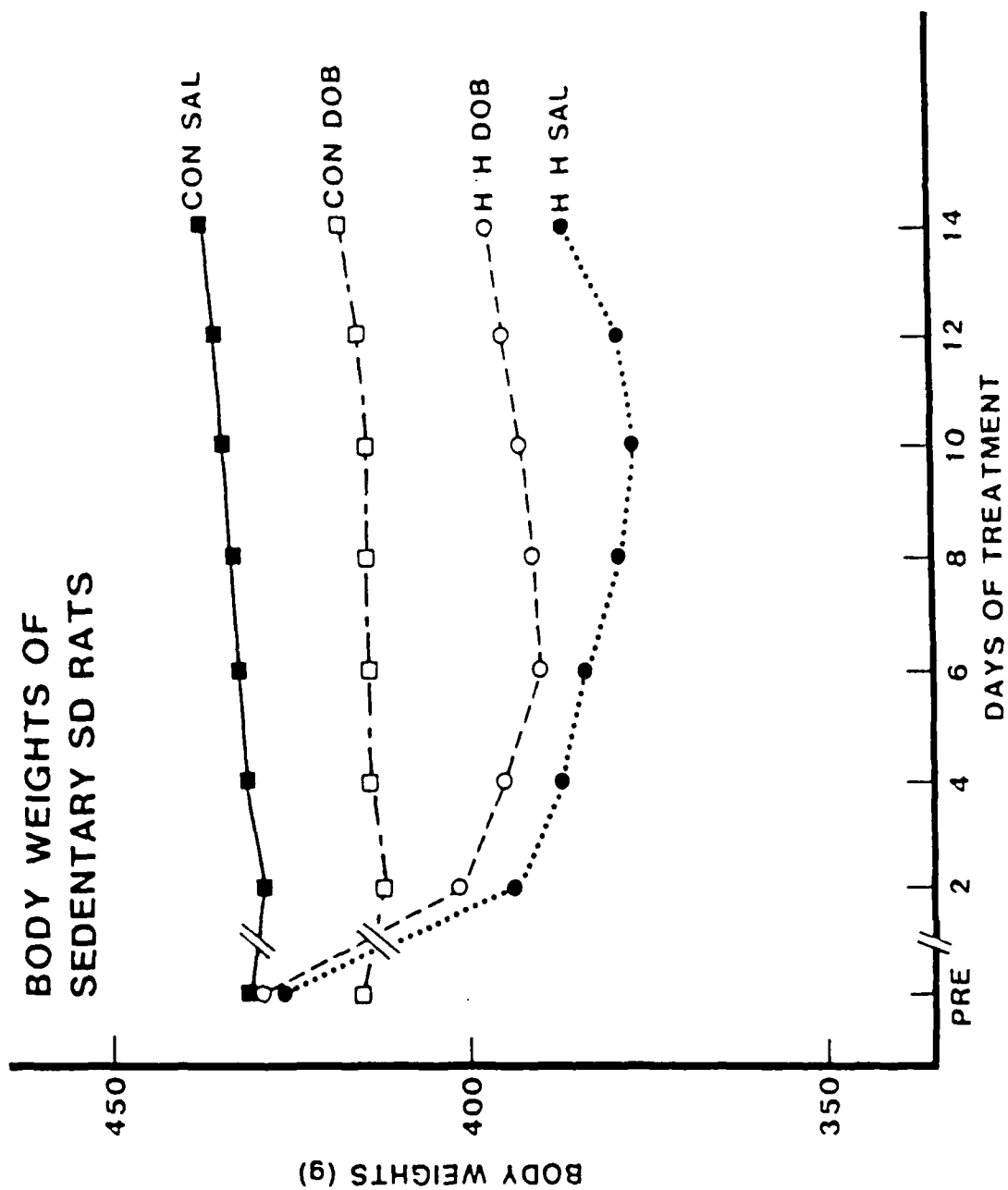


Figure 5.

most severely during the first two days of suspension and continued to drop slightly for several days. The suspended animals receiving dobutamine stopped losing weight four days before the animals that were suspended and were receiving saline did. The nonsuspended animals had minimal weight gains over 14 days.

A select group of muscle and organ weights were also compared. The actual weights are presented in table 2, while the weights which are normalized with respect to body weight are presented in figures 6-13. Two-way analysis of variance (ANOVA) indicated that there were no significant differences between any of the treatment groups with regard to actual weights of any of the three organs examined (see table 2). When the organ weights were normalized with respect to body weight, the ANOVA procedure indicated that there were significant differences ($p < .05$) in the normalized weights of the adrenals and the heart. There were no significant differences in the normalized weights for the kidney. The significant difference ($p < .05$) between groups for the normalized adrenals occurred between the CON SAL vs H/H SAL group indicating a suspension treatment difference. Significant differences ($p < .05$) for normalized heart values occurred between suspension treatment only.

Among the muscles tested, significant differences ($p < .05$) between groups in actual muscle mass were found in the soleus (SOL), the plantaris (PL), and the extensor digitorum longus (EDL). No significant differences were found in the actual muscle mass of the triceps or the tibialis anterior. The differences in the SOL included differences in treatment interaction as well as a significant difference with the suspension treatment. The significant differences ($p < .05$) identified between groups

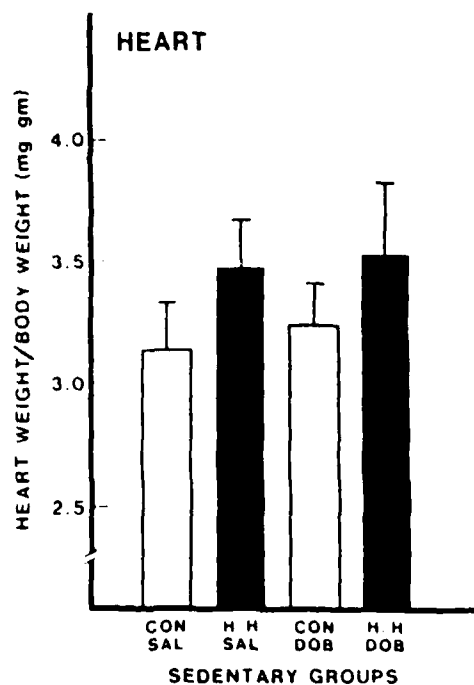


Figure 6.

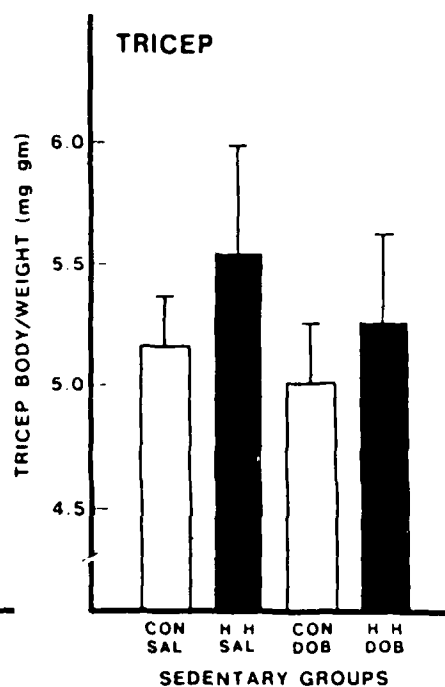


Figure 7.

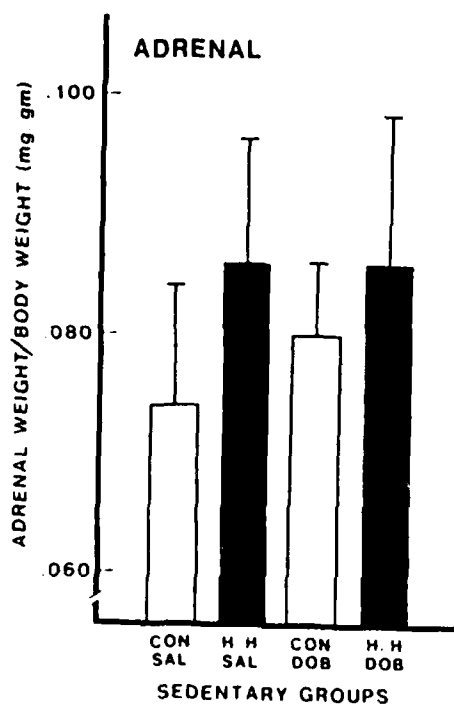


Figure 8.

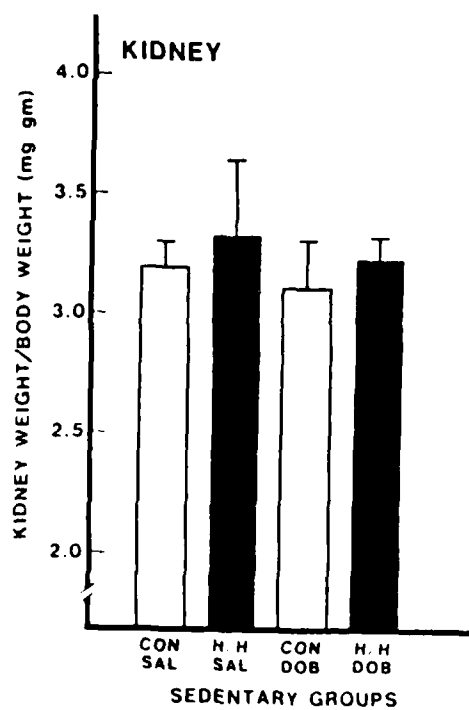


Figure 9.

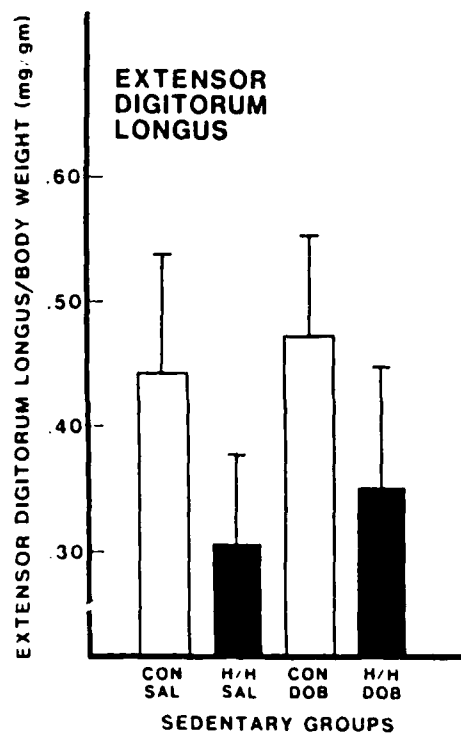


Figure 10.

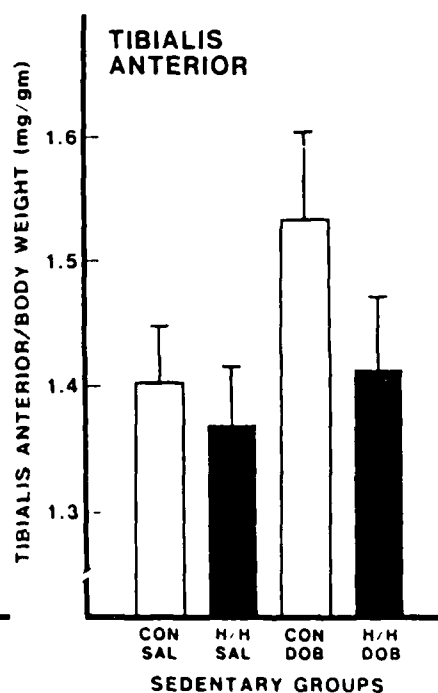


Figure 11.

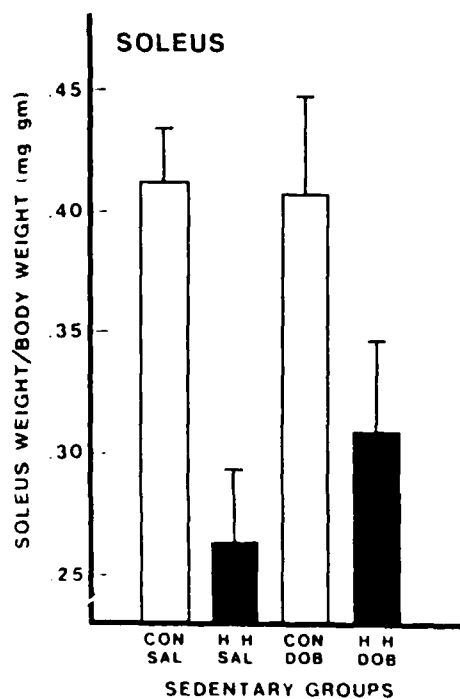


Figure 12.

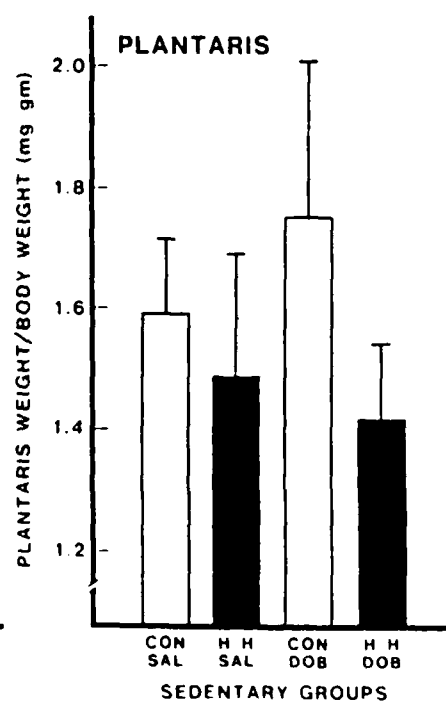


Figure 13.

for actual muscle mass for the PL, and the EDL occurred between the SAL CON and SAL H/H, indicating significant atrophy in these muscles. When the muscle mass was normalized with respect to body weight, significant differences between groups were again found in all muscles except the tricep and the tibialis anterior. The differences were between the CON SAL and H/H SAL, indicating differences as a result of the suspension treatment.

In summary, the suspension treatment resulted in significant loss of muscle mass in the SOL, PL, and the EDL as well as a significant loss of body weight. The interactive effect of dobutamine that significantly altered loss of mass was apparent in the body weight and the soleus. There were no significant differences in organ mass as a result of any treatment. When organ and muscle mass were normalized with regard to body weight, there were significant differences between CON SAL and H/H SAL groups with respect to the mass of the heart and adrenals. Significant differences between groups for normalized muscle mass were found between the EDL, the SOL and the PL, but these differences were limited to those resulting from the suspension treatment; there were no apparent differences relative to dobutamine treatment or the interactive effect of dobutamine and suspension.

These data indicate that when actual mass is considered, there is significant atrophy of muscle and loss of body weight with H/H suspension. Furthermore, the interactive effect of dobutamine appears to have a significance on loss of body weight and loss of mass in at least one muscle (SOL). These results have important implications for formulation of possible interventions with regard to changes in simulated and actual weightless-

ness. Further investigation into these changes, and the mechanisms involved, appear to be warranted.

V. RECOMMENDATIONS

The results that have been obtained to date indicate that dobutamine is able to significantly effect some of the changes induced by H/H suspension in rats. These findings represent the preliminary information needed to formulate testable hypotheses to determine if dobutamine can be used as an effective countermeasure against deconditioning changes seen in both animals and humans during H/H and in the actual weightlessness of space. Further investigation into the mechanisms involved in the observed changes, and the interaction of dobutamine and H/H suspension treatments with prior exercise training, is needed to devise a practical and meaningful program of intervention.

Due to the ten week time limitation of the summer program, it was not possible to complete an investigation into how exercise conditioning prior to treatments with dobutamine and H/H suspension would effect some of the measurements made in this study. This concept was, however, incorporated into the original protocol and a group of animals are currently being exercised trained on a treadmill. These animals will be completing their ten week training program in approximately two weeks and will, at that time, be age-matched with the animals from the summer project. Examination of the same parameters in these animals (in addition to the others) will provide a full complement of experimental groups for a 2³ research design allowing for testing of main and interactive effects of dobutamine, H/H suspension and exercise

training. Also, in keeping with one of the original objectives, the tissue from the animals utilized during the summer (and from the exercised trained animals), has been (or will be) collected and stored in such a manner so as to allow detailed biochemical, metabolic, histochemical and histomorphometric analysis to be carried out at a later date. Details of the additional parameters to be examined, and the specifics of the methods to be utilized, are included in the Research Initiation Proposal that is being submitted.

In conclusion, these results have important implications for formulation of possible interventions with regard to deconditioning changes resulting from simulated and actual weightlessness. Further investigation into these changes, and the mechanisms involved, appear to be warranted.

REFERENCES

1. Booth, F.W., and P.D. Gollnick, "Effects of Disuse on the Structure and Function of Skeletal Muscle," Medicine and Science in Sports and Exercise, 15:5:415-420, 1983.
2. Herbison, G.J., and J.M. Talbot, "Muscle Atrophy During Spaceflight: Research Needs and Opportunities," The Physiologist, 28:6:520-527, 1985.
3. Levy, M.N., and J.M. Talbot, "Cardiovascular Deconditioning of Space Flight," The Physiologist, 26:5:297-303, 1983.
4. Liang, C., R.R. Tuttle, W.B. Wood, et al., "Conditioning Effect of Chronic Infusions of Dobutamine," Journal of Clinical Investigations, 64:613-619, 1979.
5. Popovic, V., "Antiorthostatic Hypokinesia and Circulation in the Rat," The Physiologist, 24:515-516, 1981.
6. Sandler, H., "Effects of Bedrest and Weightlessness on the Heart," In: Hearts and Heart-Like Organs, G.H. Bourne, Ed. New York: Academic, Vol. 2, 1980.
7. Sullivan, M.J., A.J. Merola, A.P. Timmerman, et al., "Drug-Induced Aerobic-Enzyme Activity of Human Skeletal Muscle During Bedrest Deconditioning," Journal of Cardiopulmonary Rehabilitation, 6:232-237, 1986.

1986 USAF-UES SUMMER FACULTY RESEARCH PROGRAM/
GRADUATE STUDENT SUMMER SUPPORT PROGRAM

Sponsored by the
AIR FORCE OFFICE OF SCIENTIFIC RESEARCH

Conducted by the
Universal Energy Systems, Inc.

FINAL REPORT

Experimental Evidence Supporting a Pharmacokinetic Model of
Uptake and Metabolism of Trichloroethylene in the Pregnant
and Lactating rat

Prepared by:	Ellen S. Goldey
Academic Rank:	Master of Science
Department and	Department of Zoology
University:	Miami University
Research Location:	Armstrong Aerospace Medical Research Laboratory, Toxic Hazards Division, Hazard Assessment Branch, WPAFB, OH.
USAF Researcher:	Mr. Jeff Fisher
Date:	September 26, 1986
Contract No.:	F49620-85-C-0013

Experimental Evidence Supporting a Pharmacokinetic Model of
Uptake and Metabolism of Trichloroethylene in the Pregnant
and Lactating Rat

by

Ellen S. Goldey

Abstract

Time pregnant Fisher rats were exposed to Trichloroethylene (TCE) via drinking water, gavage, and inhalation. Dam blood and fetal blood were collected at specified times during pregnancy. Dam blood, dam milk, and pup blood were sampled at different times throughout lactation. These tissue samples were analysed by gas chromatography to determine concentration of TCE and one of TCE's primary metabolites, trichloroacetic acid (TCA). These experimental values were then compared to TCE and TCA concentrations determined by computer simulation using a pharmacokinetic model. In general the experimental values were found to support the accuracy of the model.

Acknowledgments

I'm indebted to Jeff Fisher for providing me with such an exciting research opportunity and for his patient instruction. Thanks to SSgt. Tim Whittaker for his guidance and friendship. I'd like to thank Captain Gary Jepson, SSgt. Barry Hancock and all the other researchers in the Toxic Hazards Branch who helped create such a pleasant working atmosphere. Finally, thanks also goes to Air Force Systems Command, the Air Force Office of Scientific Research and Universal Energy Systems Inc. for providing such a worthwhile program.

I. Introduction

I have recently received my Masters in Zoology from Miami University. My thesis research concerned the effects of trichloroethylene (TCE) on the offspring of rats exposed via the dam's drinking water at TCE concentrations of 312mg/l, 625 mg/l, and 1250 mg/l. I tested the offspring for learning and hormonal effects. Rats exposed to TCE at 625 mg/l revealed heightened performance in an acquisition learning task at 65 days of age and the same treatment group also demonstrated elevated levels of circulating corticosterone at 28 days of age.

Mr. Jeff Fisher at the AAMRL research laboratory is developing a pharmacokinetic model for the uptake, distribution, metabolism, and elimination of TCE and one of its primary metabolites, trichloroacetic acid (TCA), in pregnant and lactating rats (see Fisher, 1985). As in my study, Mr Fisher uses treated drinking water as one method of exposure.

Since Mr. Fisher's study closely corresponds to my thesis work, I felt that I could gain greater insight into my research and to aid Mr. Fisher in his work. Due to our similar interests I was assigned to gather experimental evidence with which to help develop Mr. Fisher's pharmacokinetic model.

II. Objectives of the Research Effort

The overall objective of the project was to develop a pharmacokinetic model that described the complexity of the

interaction of TCE within the body of the pregnant and lactating rat after oral ingestion or inhalation of TCE. This objective can only be achieved by collecting actual experimental data and comparing these results with expected values derived from computer simulation using the model.

The final results of this study may be an invaluable tool for predicting the toxic impact of TCE to the offspring of exposed mothers. Since the pharmacokinetic model can be adapted to many situations by changing the values of selected variables, this model may be applicable to other animal systems to determine the potential toxic insult of TCE and other similar compounds.

My individual objectives were:

1. To acquire proficiency in the use of the gas chromatograph and to use chemical extraction procedures for testing chemical concentrations in biological tissues.
2. To apply the data to the pharmacokinetic model to determine whether the simulated values relate to the actual data.
3. To obtain a better understanding of my thesis research and to develop ideas for my doctoral research.

III. Determination of uptake of TCE via drinking water and gavage

Time pregnant Fischer rats were housed separately in plastic cages with sawdust bedding throughout gestation and lactation. Dams were divided into groups. Each group was treated with TCE via a different route of exposure: drinking water, gavage, and inhalation.

A nominal dose of TCE at 300 mg/l of water was chosen for the drinking water study. It was important to closely monitor concentrations of TCE in the drinking water due to TCE's high volatility. Water bottles were changed daily. Samples of the water were tested for TCE concentration upon filling the bottles and samples from the same bottles were tested at the end of the 24 hour period.

Samples were analysed by mixing one microliter of the water sample in one milliliter of hexane, injecting one microliter of the hexane sample onto the gas chromatograph (GC) and determining the concentration relative to standards. The daily loss rate due to volatilization of the chemical was determined. Dark bottles were used to avoid photoreactions of TCE.

In the gavage study dams were given 1.9 mg/kg body weight of TCE daily. Untreated water was administered in the same manner to control animals.

Prior to my arrival at the lab this summer, some dams had been sacrificed and dam and fetal blood samples had been collected and analysed for TCE and TCA content using gas chromatography. I subsequently aided in collecting tissue samples from animals sacrificed at specified periods throughout lactation.

Dams were anesthetized with 1 ml/kg body weight of a mixture containing 70 mg ketamine and 6 mg xylazine per ml. Lactating rats were also given a .05 ml subcutaneous injection of oxytocin prior to sacrifice. This caused milk let down and allowed for easier milking of the anesthetized

dams. Blood was collected from the dorsal aorta using a heparinized syringe.

Tissue sampling of gavage treated animals occurred within minutes of receiving the dose in order to be able to follow the rapid loss of TCE from the body.

Trichloroethylene concentrations in tissues were not determined for the drinking water study since it was probable that TCE concentrations would be below the limits of detection at the time drinking water animals were sacrificed.

Pups were sacrificed by cervical dislocation and pup blood was collected via heart puncture with a heparinized syringe. In some instances pup blood samples were pooled due to low blood yield.

IV. Analytical chemistry

A Hewlett-Packard 5892A model Gas Chromatograph (GC) equipped with an electron capture detector was used to analyse TCE and TCA samples. Trichloroethylene samples were prepared by adding 100 μ l of blood to 1 ml of hexane and shaking vigorously for 2 minutes. Then 1.0 μ l of the sample hexane was injected into the GC using a gas tight, glass syringe. Three replicate injections were used for each sample.

Blood samples for TCA analysis were added to plasma separation vials and centrifuged. The plasma was then collected and used for subsequent analysis. Because TCA is nonvolatile, a methylation step was required to increase its volatility for analysis by gas chromatography.

Trichloroacetic acid samples were prepared by adding the blood serum or milk to 50 μ l of cold, 3 Normal HCl and methanol, and 1 ml of hexane. The TCA sample was incubated for 30 minutes at 100 C. At the end of the incubation, the hexane layer containing the TCA was removed and placed in sampling vials. Three replicate injections of each hexane sample were analysed by gas chromatography.

Rat TCE and TCA tissue levels(\pm S.D.) for the drinking water and gavage studies are superimposed on pharmacokinetic model simulations (Fig. 1-4). Four to six animals were sacrificed to determine each data point. Graphs are defined as hours into pregnancy or lactation, versus TCE or TCA concentrations in mg/ml.

In the drinking water study TCA concentrations were determined for dam and fetal blood (Fig. 1). During lactation, dam blood, dam milk, and pup blood were also tested for TCA concentration (Fig. 2).

In the gavage study TCA concentrations in dam and fetal blood were determined (Fig. 3A and 3C). Trichloroethylene concentration in the dam and fetal blood was also determined (Fig. 3B). During lactation, TCA concentration was determined for the dam blood, pup blood and milk samples (Fig. 4).

V. Method for determining gastrointestinal uptake and elimination of TCE and TCA

This technique involves in vivo , sequential collection of blood samples. Groups of four to six rats were anesthetized with ketamine-xylazine as mentioned above.

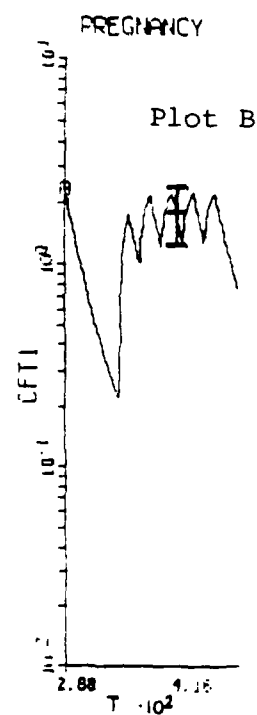
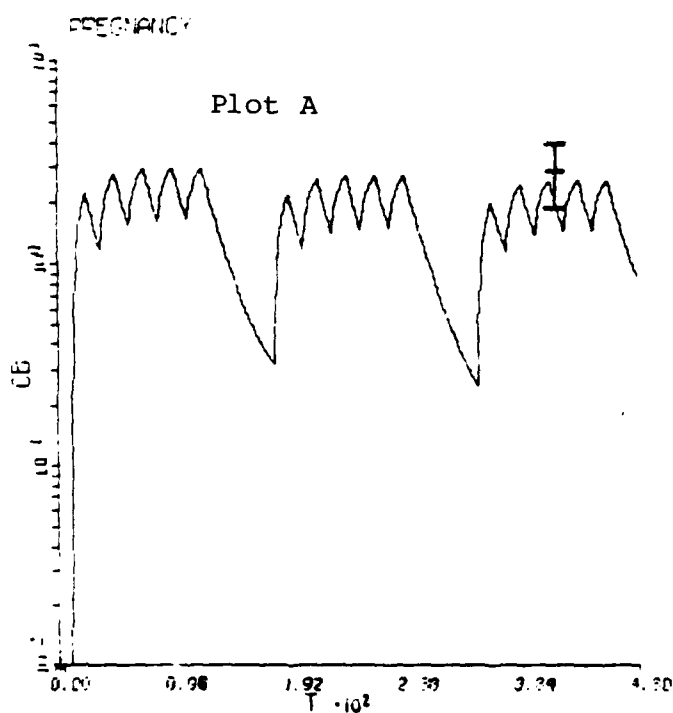


Figure 1: Drinking water study (pregnancy): Plot A represents TCA concentration in dam blood throughout pregnancy. Blood samples were tested at 412.0 hrs. into pregnancy. Plot B represents fetal blood TCA concentration during the final week of gestation. Blood samples were collected at 412.0 hrs.

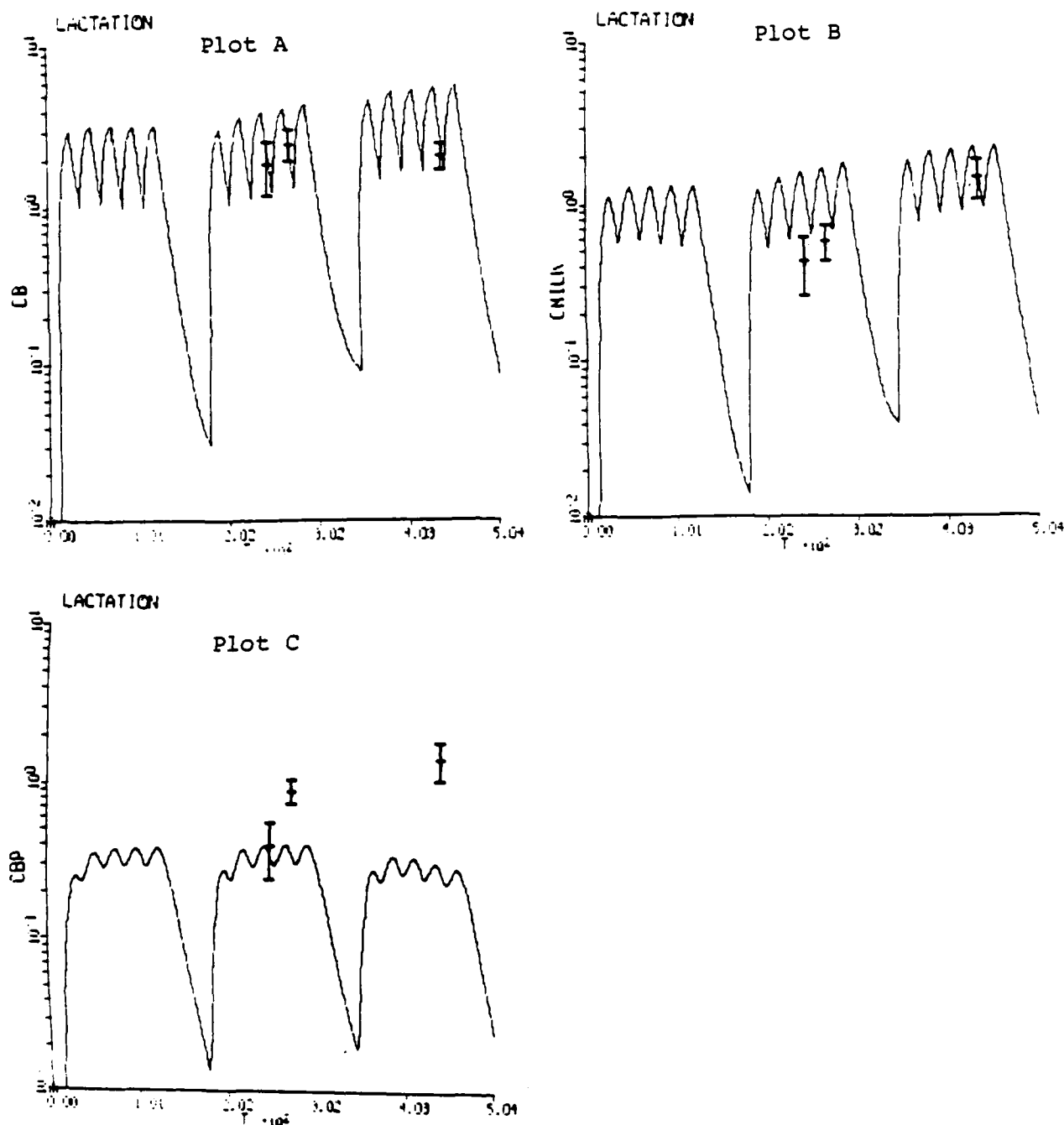


Figure 2: Drinking water study (lactation): Plot A represents dam blood TCA concentration during lactation. Blood samples were tested at 244 hrs., 268 hrs, and 438 hrs. post partum. Plot B represents dam milk TCA concentration throughout lactation. Samples were collected at 244 hrs., 268 hrs., and 438 hrs. Plot C represents pup blood concentration of TCA during 3 weeks post partum. Blood samples tested at 244 hrs., 268 hrs., and 438 hrs.

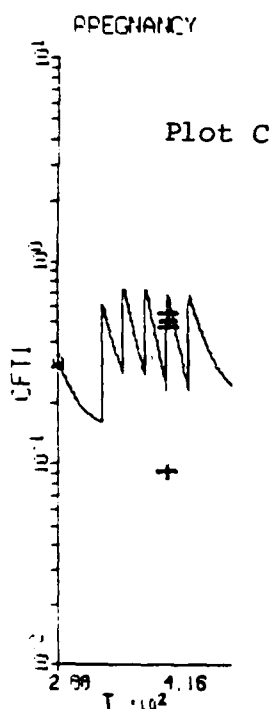
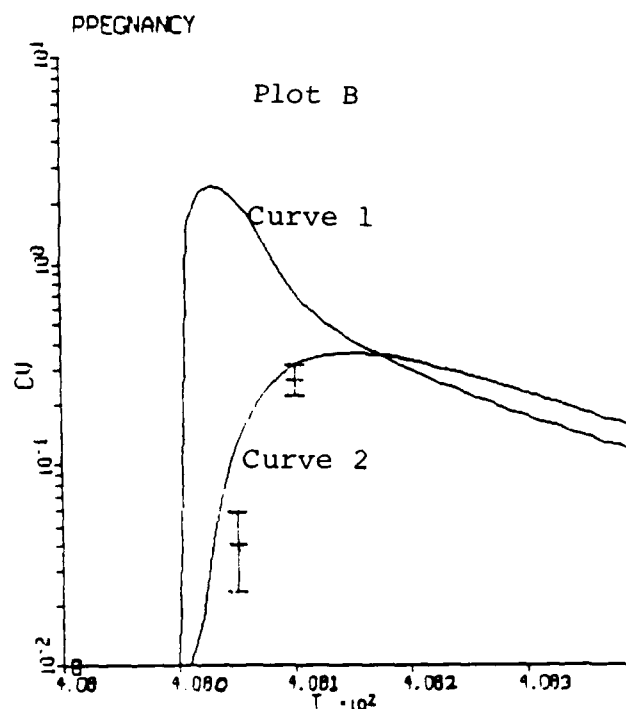
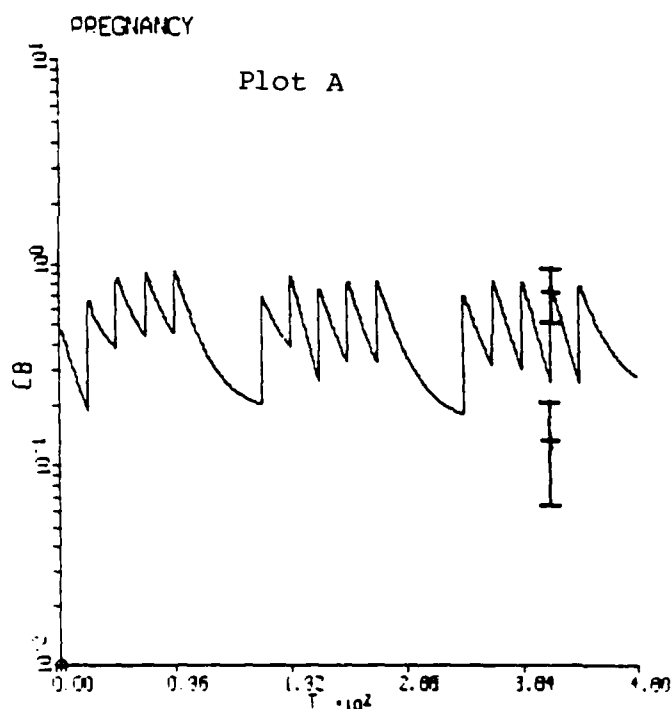


Figure 3: Gavage study (pregnancy): Plot A represents dam blood TCA concentration throughout the 3 week pregnancy with actual samples taken at 408.08 hrs. and 410 hrs. into pregnancy. Plot B represents TCE concentration in dam blood (curve 1) and fetal blood (curve 2) for a 20 minute time interval following an individual gavage treatment (408.0 hrs.). Actual concentrations were determined for dam blood at 408.1 hrs, and for fetal blood at 408.05 hrs. Plot C represents fetal blood TCA concentrations during the final week of pregnancy. Sample values were determined at 408.08 hrs. and 410 hrs.

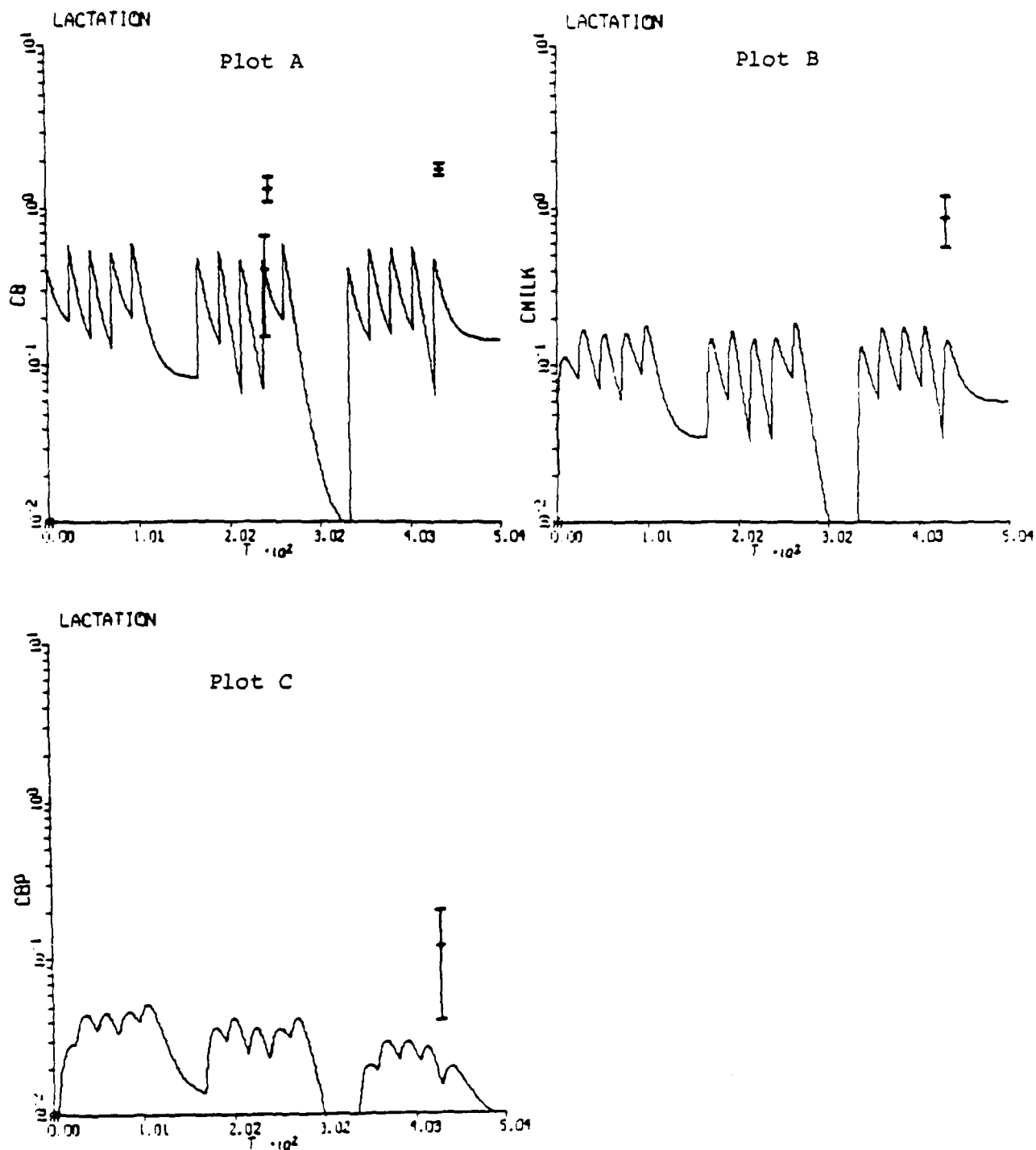


Figure 4: Gavage study (lactation): Plot A represents dam blood TCA concentration throughout the 3 weeks of lactation. Blood samples were tested at 240.08 hrs., 244.0 hrs., and 435.0 hrs. post partum. Plot B represents dam milk TCA concentration throughout lactation. Samples were tested at 435 hrs. Plot C represents pup blood TCA concentration for 3 weeks post partum. Blood samples were tested at 433 hrs.

A 22-gauge polyethylene cannula was inserted into the right jugular vein and threaded under the skin to the exterior at the base of the neck. A harness was fastened around the upper torso of the rats securing the cannula. The next day animals were dosed by gavage with 1.9 mg/kg body weight. Heparinized blood samples were collected at 2 min., 5 min., 10 min., and 18 minutes post gavage. The blood was extracted with hexane and analysed by gas chromatography (McDougall et al., 1985). The pharmacokinetic model for gastrointestinal in vivo uptake of TCE is still under development therefore, the results of this section are not presented.

VI. Determination of uptake of TCE via inhalation

During the last two weeks of my summer program, we began exposure of a new group of time pregnant rats to 600 ppm TCE via inhalation chambers. Rats were exposed for four hours daily. A flame ionization GC monitored TCE concentration in the chambers by automatically sampling at ten minute intervals. A time weighted average was then determined at the end of the daily exposure.

Animals were periodically sacrificed and tissue samples were collected throughout gestation and lactation as in the drinking water and gavage studies. I was not present for the duration of the inhalation study, therefore no final data is presented here.

VII. Recommendations

1. Much work remains to be done on this study before many recommendations can be made. It is important to note at

this point, however, that the experimental values correspond well to the expected values derived from the model. This is especially true of the drinking water study (Fig. 1 and 2). With the model it may be possible to predict the tissue concentration of the chemical at any time throughout the study which is an advantage of using pharmacokinetics. A short term suggestion would be to re-evaluate the model for the gavage study since TCA concentrations in the dam milk and fetal blood may have been underestimated (Fig. 4). It is possible that more TCA is partitioning into the mammary tissue than previously believed. This would also explain the higher concentration of TCA in pup blood.

2. Though it is possible to monitor in vivo uptake and elimination of TCE in adult rats by inserting a jugular cannula as described above, we were unable to monitor pup blood in this manner. One recommendation for adding support to the model is to develop an in vivo testing procedure for pups. One possible method would be to use intravenous injections of TCE and to draw blood periodically to follow its elimination from the body.

3. I firmly believe that the pharmacokinetic model developed by Mr. Fisher represents an accurate and workable method for determining the potential toxic insult of TCE and TCA in pregnant and lactating rats. I recommend that the model be adapted and applied in other animal systems. Through a better understanding of the pharmacokinetic model developed here, it may be possible to determine potential risk factors for pregnant women exposed to TCE and related compounds.

References

1. Fisher, J. W., A deterministic pharmacokinetic oral injection model for trichloroethylene and its metabolite, trichloroacetic acid, in pregnant and lactating rats, Ph.D. Dissertation Research Proposal, AFAMRL/THB Wright Patterson AFB, Ohio (1985) 43 pp.
2. McDougal, J.N., G.W. Jepson, H.J. Clewell, III, and M.E. Anderson. Dermal Absorption of dihalomethane vapors. Toxicology and Applied Pharmacology, 79 (1985) 150-158.

1986 USAF-UES SUMMER FACULTY RESEARCH PROGRAM/

GRADUATE STUDENT SUMMER SUPPORT PROGRAM

Sponsored by the

AIR FORCE OFFICE OF SCIENTIFIC RESEARCH

Conducted by the

UNIVERSAL ENERGY SYSTEMS, INC.

FINAL REPORT

EFFECTS OF ACCELERATION STRESS UPON BLOOD LIPID LEVELS

Prepared by:	Alfred W. Gordon
Academic Rank:	Graduate Student
Department and	Department of Biology
University:	Atlanta University
Research Location:	USAF School of Aerospace Medicine, Brooks AFB, TX, Clinical Sciences Division, Clinical Pathology Branch
USAF Researcher:	Dr. Harvey A. Schwertner
Date:	August 7, 1986
Contract No:	F49620-85-C-0013

EFFECTS OF ACCELERATION STRESS UPON BLOOD LIPID LEVELS

BY

ALFRED W. GORDON

ABSTRACT

Serum total cholesterol and triglyceride concentrations of two individuals were measured after daily exposures to high gravitational forces (+Gz) simulating aerial combat maneuvers. The post-acceleration cholesterol levels were significantly higher (40-95%) than the normal resting levels. Serum cortisol levels were higher than the resting levels. This agrees with previous studies which have shown significant increases in serum cortisol levels after acceleration stress. Cortisol and total cholesterol values were significantly correlated ($r = 0.614$, $p < 0.05$) in one of the individuals of this study. Since cortisol is a hormone which influences lipid metabolism, there may be a causal relationship between the increased cortisol levels produced by acceleration stress and increased lipid levels. The lipid levels in the two subjects after acceleration exceeded the 90th percentile for the population as a whole. As such, they could be at high risk for subsequent coronary heart disease if they are exposed to high G-forces on a frequent basis.

An ancillary study was conducted to develop an electrophoretic method to rapidly separate and quantitate serum high density lipoprotein (HDL) subfractions HDL₂ and HDL₃. Serum levels of one of these subfractions may be a better predictor of coronary heart disease than total cholesterol. Serum α -lipoproteins isolated by affinity chromatography were separated into a number of subfractions by polyacrylamide gel electrophoresis. These subfractions were marked by the usual lipoprotein stains, and by filipin, a fluorescent, naturally occurring antibiotic which, reportedly, binds specifically to cholesterol. Identification and quantification of these HDL subfractions remain to be accomplished.

ACKNOWLEDGMENTS

I would like to thank the Air Force Systems Command and the Air Force Office of Scientific Research for sponsorship of this research. Special thanks to Dr. Harvey Schwertner, my Effort Focal Point, for his generous assistance and guidance. I would like to also thank personnel of the Acceleration Effects Laboratory, Crew Technology Division, the Clinical Radioassay Function, Epidemiology Division, and the Lipids Evaluation Function, Clinical Sciences Division for their support in this research.

I. INTRODUCTION.

I received my B.A. degree from Talladega College in Alabama and a Master of Science degree in Developmental Biology from Atlanta University. I am currently a candidate for the Doctor of Philosophy degree at Atlanta University specializing in Developmental Genetics. One of the short term goals of this research appointment concerned the development of definitive procedures for the separation of serum lipoproteins HDL₃ and HDL₂ from other native lipoproteins. A number of purification techniques (affinity chromatography and electrophoresis) were used. Many of the procedures used during the investigation involved techniques for which I had both professional training and practical expertise.

II. OBJECTIVES OF THE RESEARCH EFFORT.

Pilots flying high-performance aircraft are repeatedly exposed to high sustained G-forces during aerial combat maneuvers. Since both cortisol and physical stress are elevated during high G-forces, and since both cortisol and physical stress have been shown to be associated with elevated lipids levels (1), we sought to determine if lipid levels are elevated in subjects exposed to high G-forces. In addition, we measured serum cortisol concentrations in order to determine if the cholesterol increases are related to the increases in this particular stress hormone.

A complementary goal of this research was to develop an electrophoretic method to rapidly separate serum high density lipoproteins (HDL) into HDL₂ and HDL₃ subfractions, and to rapidly quantitate HDL₂ and HDL₃ cholesterol in these subfractions. The measurement of serum HDL₂ cholesterol may be a better

indicator of coronary heart disease than total HDL (2).

To accomplish these goals, the following objectives were established:

1. Obtain serum samples from individuals prior to and after their exposure to an established protocol of daily +Gz accelerations simulating aerial combat maneuvers.
2. Determine serum cortisol and total serum cholesterol in these serum samples and determine whether the cholesterol levels are related to the cortisol levels. Also, determine whether they increase with increase in G-force.
3. Separate serum high density lipoproteins (HDL) from other serum lipoproteins, and develop an electrophoretic technique to separate the HDL into subfractions HDL₂ and HDL₃. Identify the HDL subfractions with lipid stains or with fluorescent filipin which has been reported to bind specifically to cholesterol (3).

III. +Gz ACCELERATION PROTOCOL AND ANALYTICAL METHODOLOGY.

As part of an ongoing, independent study, two military volunteers were subjected to daily +Gz acceleration on the human centrifuge for a one week training period and for a two week test period. The acceleration protocol included the drawing of a pre-acceleration fasting blood sample on Monday morning prior to acceleration exposure. On Monday, Wednesday, and Friday, volunteers were exposed, unprotected, to rapid and gradual onset of +Gz acceleration to the maximum tolerable +Gz level (4.5-9G). On Tuesday and Thursday, they were exposed, but protected, to more exhaustive aerial combat maneuvers (SCAM, 4.5-9G) and were required to perform specific tracking tasks.

A post-acceleration blood sample was withdrawn from each subject about 15 minutes after each acceleration period. Serum samples were stored at -20°C (about 3 weeks) until analyzed for total cholesterol, triglyceride, and cortisol concentrations. Serum cortisol concentrations were determined by radioimmunoassay. Cholesterol and triglyceride levels were determined by enzymatic methods.

IV. SERUM CORTISOL, CHOLESTEROL, AND TRIGLYCERIDE LEVELS AFTER EXPOSURE TO +Gz ACCELERATION.

In the first subject, a 40-year-old male, serum cholesterol levels increased from a normal 158 mg/dl to 281 mg/dl (approximately 78%) after exposure to +Gz acceleration. The cholesterol remained elevated for the duration of the experiment (Table 1, Fig.1). These elevations are the likely result of the chronic daily exposure to +Gz forces, and are the first reported observations of a rise in serum cholesterol associated with +Gz acceleration. The cortisol levels also appear to be elevated in the first subject, however, cortisol baseline levels were not taken prior to G-force exposure. Previous studies (4, 5) however, have shown that increases in cortisol levels do occur as a result of +Gz acceleration. More importantly, a statistically significant correlation ($r = 0.614$, $n = 11$, $p < 0.05$) was found to exist between cortisol and cholesterol concentrations (Fig. 3). Triglyceride concentrations were also elevated, but varied widely.

The second subject also had elevated cholesterol levels, however, the increases were less pronounced than for the first subject. With this subject, the cholesterol concentration increased from a baseline value of 148 mg/dl to 186 mg/dl after the first acceleration test. The cholesterol values remained

elevated through the completion of the experiment, but were less variable than the values for the first subject (Table 1, Fig. 2). The cortisol levels were also lower than for the first subject. Even though the cortisol and cholesterol levels were elevated after exposure to +Gz forces, there was no significant correlation between them. The differences in absolute cholesterol values between the two subjects could be due to age differences (40 versus 21). Some of the differences could also be due to the fact that some individuals can tolerate stress and others cannot. In other words, some individuals can be classified as responders and others respond to a lesser extent.

V. ELECTROPHORETIC DETERMINATION OF SERUM HIGH DENSITY LIPOPROTEIN (HDL) SUBFRACTIONS HDL₂ AND HDL₃.

Electrophoretic methods were examined for the purpose of developing a rapid clinical method for the analysis of HDL subfractions. Serum samples were fractionated into α -lipoprotein (HDL) and β -lipoprotein (LDL) components with commercially prepared heparin-agarose affinity chromatography columns (Isolab, Inc.). The HDL component was subjected to a number of electrophoretic techniques to separate, identify, and quantitate its subfractions.

A. Agarose Gel Electrophoresis.

Agarose gel electrophoresis has been used to separate serum lipoproteins into patterns showing two lipoprotein bands in the " α zone" of the electrophoretogram (10). The bands were not identified as HDL subfractions. However, we conducted a number of agarose gel electrophoretic analyses of total serum samples and HDL and LDL components isolated by affinity chromatography. Various slab agarose gel plates (0.3 to 2% agarose in Tris barbital buffer, pH 8-9) about 3 mm thick were prepared. Before electrophoresis, serum or lipo-

protein samples were mixed with lipid pre-stains or the fluorescent, natural product filipin, which supposedly binds specifically to cholesterol-containing lipoproteins. The electrophoresis was conducted in closed horizontal chambers in the Tris buffer for 1-2 hours at a constant voltage of 5-6 V/cm. Lipid stained and filipin-treated electrophoretic patterns of α -lipoproteins gave only a single broad band in the HDL region, and even a broad band in the LDL region, which indicates that affinity columns only partially purified the α fraction. We checked the effects of pH between 7.2 and 8.6. In general, the lower pH resulted in slower lipoprotein migration.

B. Polyacrylamide Gel Electrophoresis.

In the polyacrylamide gel studies, a wide range of parameters were modified. The concentration of the acrylamide as well as the degree of cross-linking has been found to be critical. In general, the higher the degree of cross-linking the greater the number of HDL subfractions. A polyacrylamide concentration of 5% with 0.04% cross-linking, and 0.1M sodium phosphate buffer (pH 7.2) gave best resolution of HDL bands. Filipin-treated serum samples were also electrophoresed in slab and tube polyacrylamide gels. However, filipin has not proven to be specific for cholesterol-containing lipoproteins, since fluorescence has appeared in the zone where albumin is expected.

C. Lipid and Lipoprotein Stains.

We have evaluated a number of lipid staining reagents for specificity and sensitivity. Those studied were Sudan Black, Oil Red-O, and filipin. Filipin has been used in anatomical pathology as a fluorescent, cholesterol specific stain. This is the first time it has been used for quantification of lipoprotein cholesterol levels. In these studies, Sudan Black was found to be more specific than Oil-Red-O in that it did not bind to albumin. Filipin

appeared to have sensitivities equal to that of Sudan Black. Some tests were also made to use cholesterol oxidase reagents to specifically stain the lipoprotein cholesterol. This is perhaps the most specific stain.

VI. RECOMMENDATIONS.

In this study, we have shown that exposure to high G-force results in significant increases in cholesterol and triglyceride. In addition, we have provided some evidence that the lipid increases could be the result of increased cortisol levels which accompany the intense physical stress of acceleration. The cholesterol levels of the two subjects studied here had cholesterol levels which exceeded the 90th percentile for their age bracket. With such levels, they are in the high risk group for developing coronary disease.

Since this study involved only two subjects, we feel that further studies should be performed in order to determine whether other individuals exposed to G-forces also experience elevated levels of serum cortisol and cholesterol, and whether there is significant correlation between the two levels.

Since the human centrifuge is capable of producing exact quantifiable levels of G-force, we recommend that further studies be conducted which more closely show the association between G-force, stress intensity, cholesterol concentration, and cortisol concentration. The study would not only have important health implications for pilots of high performance aircraft, but would also be of importance to the population as a whole. Studies identifying changes in individual lipoproteins would also be important, as would studies of other lipid fractions such as the free fatty acids. Other endocrine hormones besides cortisol should also be examined.

It is also recommended that serum high density lipoprotein (HDL), and subfractions HDL₂ and HDL₃ concentrations be determined before and after subjects are exposed to +Gz acceleration. It should be of interest to determine which lipoprotein component is responsible for the observed increases in total serum cholesterol. Studies have suggested that cholesterol associated with these lipoproteins are better indices of the risk of coronary heart disease than total cholesterol (6-9).

Efforts to separate and identify serum high density lipoproteins into subfractions HDL₂ and HDL₃ should continue. Various electrophoretic techniques have been employed, but results have not been consistent. Cellulose acetate electrophoresis on pre- or post-stained slides did not prove promising. Polyacrylamide gel electrophoresis (slabs or tubes) of chromatographically prepared α -lipoproteins produced a number of lipoprotein fractions. Results varied with pH, concentration and degree of cross-linking of the gel. The effect of higher pH (above pH 8) upon resolution of HDL subfractions should be explored. There should also be an examination of the effect of pre-staining upon the separation of HDL into subfractions. Pre-staining may alter migration rates of lipoproteins and, thus, impede their resolution. Finally, an attempt should be made to resolve the α -lipoprotein fraction (isolated on an affinity column) by high performance liquid chromatography (HPLC). This method would permit the evaluation of several parameters in the effectiveness of resolving HDL subfractions.

REFERENCES

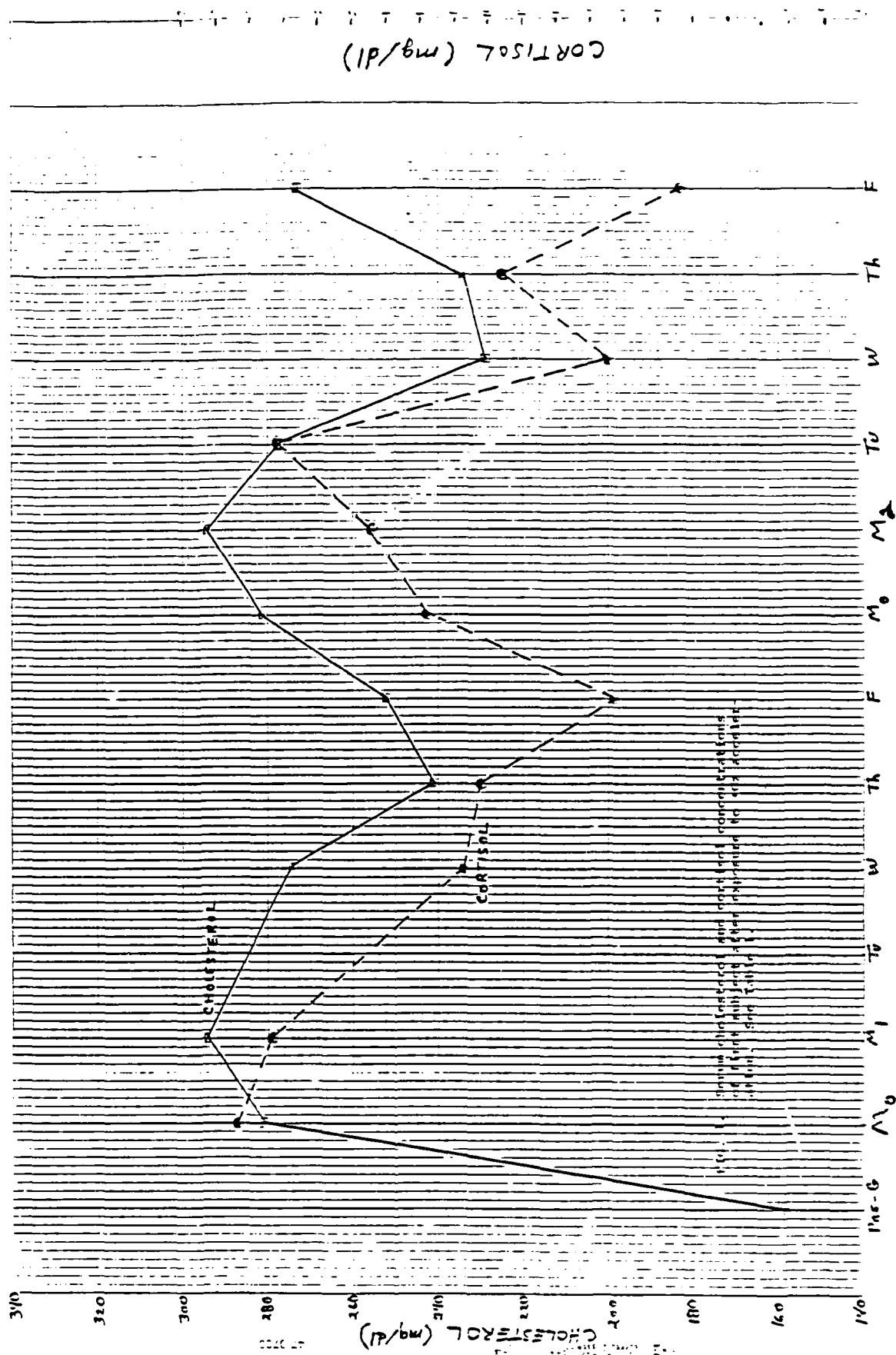
1. Schwertner, H.A. and Torres, Linda, et. al., Clinical Sciences Division, USAF School of Aerospace Medicine, Brooks AFB, Texas 78235-5000.
2. Miller, N.E. and Hammett, F., "Relation of Angiographically Defined Coronary Artery Disease to Plasma Lipoprotein Subfractions and Apolipoproteins," British Medical Journal, 282 (1981) 1741-44.
3. Howard, S.K., "Platelet-Mediated Cholesterol Accumulation in Cultured Aortic Smooth Muscle Cells," Science, 227 (1985) 1243-45.
4. Mills, F.J. and Marks, V., "Human Endocrine Responses to Acceleration Stress," Aviation, Space, and Environmental Medicine, 53 (1982) 537-40.
5. Vernikos-Danellis, J. and Dallman, M.F., "Hormonal Indices of Tolerance to +Gz Acceleration in Female Subjects," Aviation, Space, and Environmental Medicine, 49 (1978) 886-89.
6. Gordon, T., Castelli, et. al., "High Density Lipoprotein as a Protective Factor Against Coronary Heart Disease," American Journal of Medicine, 62 (1977) 707-14.
7. Kannel, W.B., et. al., "Cholesterol in the Prediction of Atherosclerotic Disease. New Perspectives Based on the Framingham Study," Ann. Intern. Med., 90 (1979) 85-91.
8. Tan, M.H., et. al., "Serum High Density Lipoprotein Cholesterol in Patients with Abnormal Coronary Arteries," Atherosclerosis, 37 (1980) 187-8.
9. Miller, N.E., et. al., "Relation of Angiographically Defined Coronary Artery Disease to Plasma Lipoprotein Subfractions and Apolipoproteins," Clinical Chemistry, 282 (1981) 1741-43.
10. Papadopoulos, N.M. and Kintzios, J.A., "Determination of Human Serum Lipoprotein Patterns by Agarose Gel Electrophoresis," Ann. Biochem, 30, (1969) 421-26.

TABLE 1. SERUM CORTISOL, CHOLESTEROL, AND TRIGLYCERIDE LEVELS OF SUBJECTS EXPOSED TO +Gz ACCELERATION

<u>NO.</u>	<u>DATE</u>	<u>DAY</u>	<u>IDENTIFICATION</u>	<u>TOTAL CHOLESTEROL</u>	<u>CORTISOL</u>	<u>TRIGLYCERIDE</u>
0	---	---	Pre-G Baseline	158	---	---
1	5-5-86	Monday	PGB-1G-11 Baseline	281	23.3	206
2	5-5-86	Monday	PGB-1G-11 Post G	294	22.3	223
3	5-7-86	Wednesday	PBG-1G-13 Post G	274	16.7	156
4	5-8-86	Thursday	PBG-1G-14 Post G	241	16.2	307
5	5-9-86	Friday	PBG-1G-15 Post G	252	12.3	117
6	5-12-86	Monday	PBG-1G-21 Baseline	281	17.8	332
7	5-12-86	Monday	PBG-1G-21 Post G	294	19.4	208
8	5-13-86	Tuesday	PBG-1G-22 Post G	277	22.2	233
9	5-14-86	Wednesday	PBG-1G-23 Post G	229	12.5	226
10	5-15-86	Thursday	PBG-1G-24 Post G	234	15.6	163
11	5-16-86	Friday	PBG-1G-25 Post G	273	10.3	273
00	---	---	Pre-G Baseline	148	---	62
12	6-2-86	Monday	PBG-2G-31 Baseline	186	12.3	102
13	6-2-86	Monday	PBG-2G-31 Post G	195	16.6	301
14	6-3-86	Tuesday	PBG-2G-32 Post G	194	6.8	113
15	6-4-86	Wednesday	PBG-2G-33 Post G	195	8.7	198
16	6-5-86	Thursday	PBG-2G-34 Post G	185	-	150
17	6-6-86	Friday	PBG-2G-35 Post G	180	9.4	159
18	6-9-86	Monday	PBG-2G-41 Post G	199	11.0	108
19	6-10-86	Tuesday	PBG-2G-42 Post G	205	13.8	240
20	6-12-86	Thursday	PBG-2G-43 Post G	185	-	95
21	6-13-86	Friday	PBG-2G-44 Post G	175	-	296
22	6-13-86	Friday	PBG-2G-45 Post G	170	12.3	179

a See test for +Gz acceleration protocol. Statistical comparison between serum cortisol and total cholesterol: First subject, $n = 11$, $r = 0.6138$, $p < 0.05$; Second subject, $n = 8$, $r = 0.103$, insignificant.

b mg/dl.



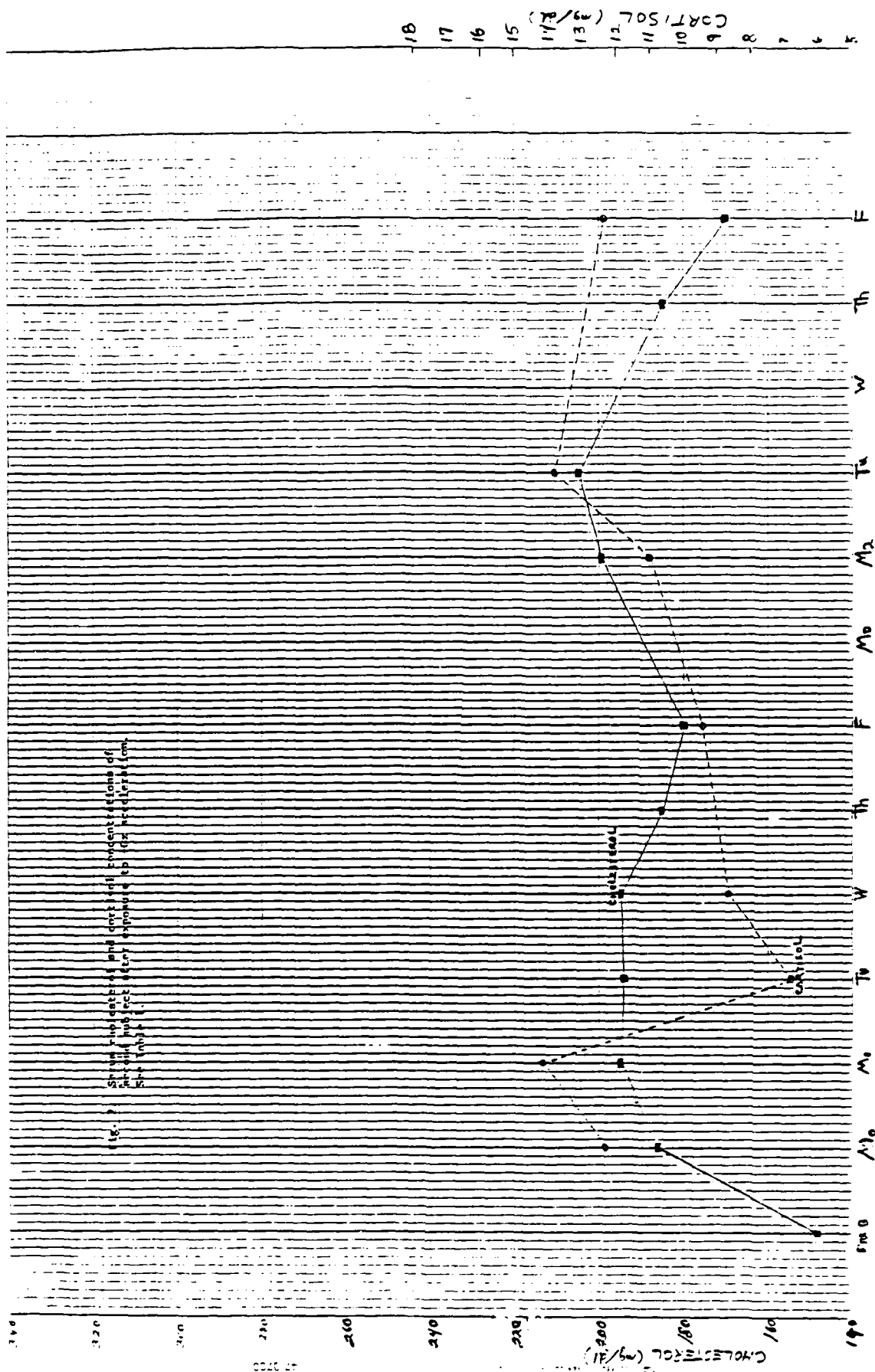
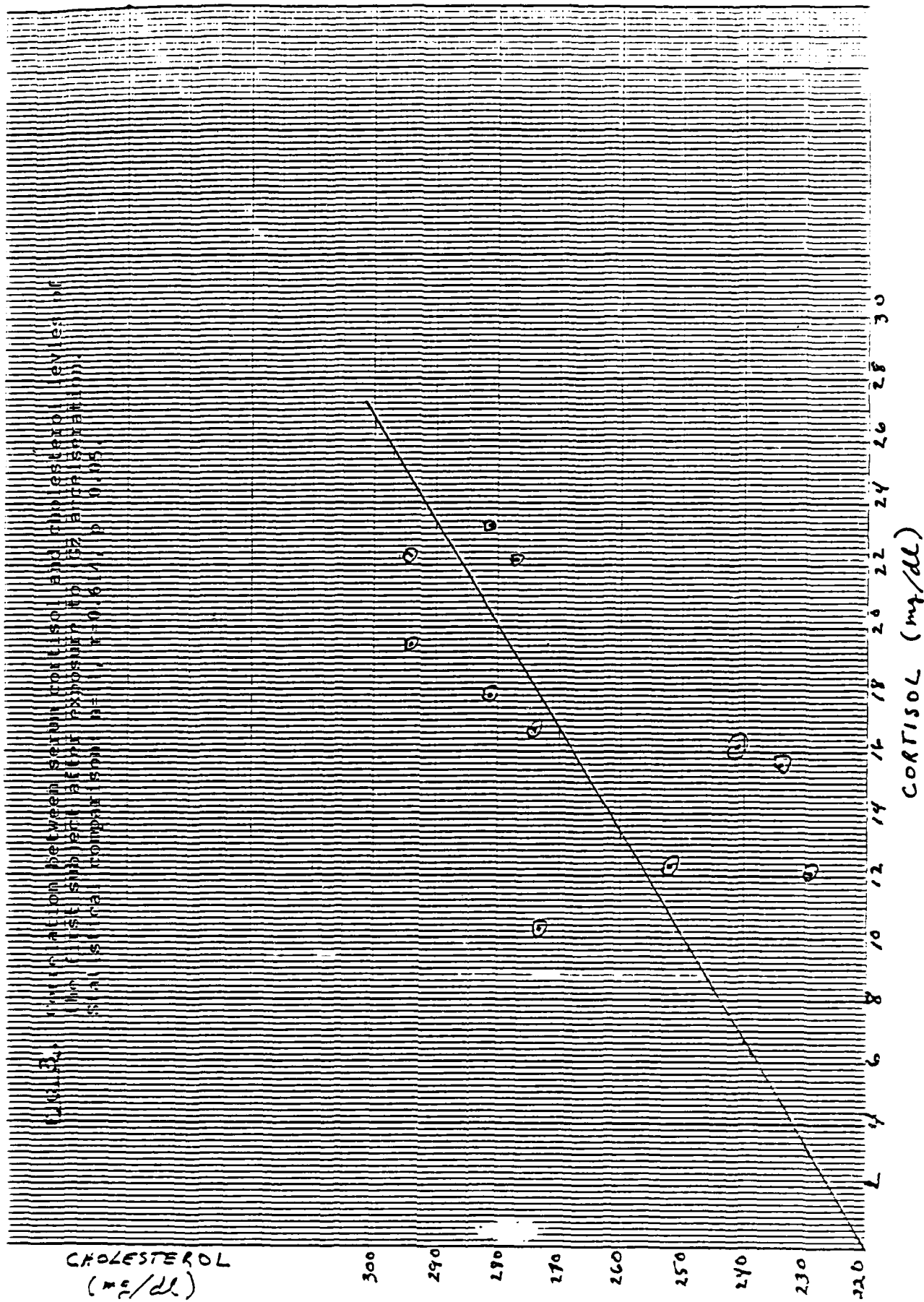


FIGURE 3. Correlation between serum cortisol and cholesterol levels of
 100 subjects after exposure to 152 Rads (sterilization).
 Statistical comparison: $r = 0.61$, $p < 0.05$.



1986 USAF-UES SUMMER FACULTY RESEARCH PROGRAM/
GRADUATE STUDENT SUMMER SUPPORT PROGRAM

Sponsored by the
Air Force Office of Scientific Research

Conducted by the
Universal Energy Systems, Inc.

Final Report

Microfracture Patterns in the Lumbar Vertebrae of Macaca mulatta

Prepared by:	Nadia Clealure Greenidge
Academic Rank:	Graduate Student
Department:	Anthropology
University:	New York University
Research Location:	Aerospace Medical Research Laboratory Biodynamics & Bioengineering Division Biodynamic Effects Branch Wright-Patterson Air Force Base, Ohio
USAF Researcher:	Dr. Leon E. Kazarian
Date:	August 28, 1986
Contract No.:	F49620-85-C-0013

Microfracture Patterns in the Lumbar Vertebrae of *Macaca mulatta*

by

Nadia Clealure Greenidge

ABSTRACT

An experiment was conducted on forty isolated lumbar vertebral bodies excised from ten normal Rhesus macaques. The purpose of this investigation was to evaluate the effects of rate and percentage of vertebral body deformation on the mechanical properties and microfracture distribution in the lumbar vertebrae. Twenty vertebral bodies (L1 and L4) were used as controls. These specimens were disarticulated and examined macroscopically and microscopically to determine normal trabecular anatomy and the incidence of vertebral pathologies. Twenty additional lumbar vertebral bodies (L2 and L3) were disarticulated and mechanically loaded in axial compression within a test range of 10% to 30% deformation, in 5% increments, of the original specimen height. Each vertebral body was individually assigned an ultimate deformation percentage and a rate of deformation of either 5.25×10^{-3} m/min or 25 m/min. The effects of rate and percentage of deformation on the production of vertebral microfracture patterns and several mechanical parameters associated with vertebral injuries were determined.

Acknowledgments

I would like to thank the Air Force Systems Command, Air Force Office of Scientific Research and the Harry G. Armstrong Aerospace Medical Research Laboratory at Wright-Patterson Air Force Base, Ohio. I would also like to extend my thanks personally to Dr. Leon Kazarian, Suzanne Smith, Clarence Oloff, Marvin Souder, Ed Eveland, Lou Muhic, Patrick Roberts, K. C. Smith, D. "Freddie" Hamilton and the staff of UDRI.

I would like to thank my family and the Division of Bioengineering and the Occupational and Industrial Orthopaedic Center of the Hospital for Joint Diseases and the Anthropology Department of New York University for their support and encouragement throughout the summer.

Finally, I would like to thank Lisa Farmer for the typing of this manuscript.

I. Introduction

I received my M.A. degree in Physical Anthropology from New York University studying comparative neurobiology of primates. After completing my Masters degree I expanded my studies to include comparative anatomy and biomechanics of the primate musculoskeletal system. I have recently completed the requirements for a supplementary Masters degree in Occupational Biomechanics, and I am near completion of a Ph.D. in Physical Anthropology. My thesis will consist of a detailed study of the comparative anatomy and kinematics of the hindfoot in Old World Monkeys.

I am currently a research assistant at the Hospital for Joint Diseases, Orthopaedic Institute in the Division of Bioengineering and the Occupational and Industrial Orthopaedic Center. Here I both assist and conduct research projects in clinical orthopaedic biomechanics and comparative primate morphology and biomechanics. The center is currently pursuing various projects addressing the issues of low-back pain including kinematics, injury, anatomy, and rehabilitation.

II. Objectives of the Research Effort

The overall objectives of Biodynamics research are to investigate the responses of the primate musculoskeletal system to mechanical stressors, and to understand the relationship between non-human primate models and human responses. A more detailed understanding of non-human primate vertebral anatomy and its responses to mechanical stressors will greatly assist in the pursuit of these goals.

My individual objectives were:

1. A study of the normal anatomy of the lumbar vertebrae of the Rhesus monkey.
2. Determine the relationship between the rate and percentage of vertebral body deformation to the incidence and patterns of microfractures in the lumbar vertebrae.

III. Lumbar Vertebral Body Anatomy

Externally, the lumbar vertebral body is surrounded by a thin wall of cortical bone. The superior and inferior surfaces are covered with bony cortical and cartilaginous end plates. The anterior and posterior aspects are perforated by channels for the passage of vascular structures. The basi-vertebral vein, which enters the vertebral body via a large funnel-like structure on its posterior aspect, internally traverses throughout the central portion of the body sending branches towards the end plates (figure 1b). Several authors (1, 3, 4, 7, 8) described both the human and nonhuman primate vertebral body as consisting of the following three zones: (a) superior and inferior end zones and (b) central zone. The end zones lie adjacent to the two end plates and consist of uniform, continuous, trabeculae that are oriented perpendicular to the end plates. Transverse trabeculae intersect the main vertical structures at right angles. The marrow spaces in this region are small and uniform. Each of these regions is said to occupy approximately 20% of the vertebral body.

The central zone, which occupies 60% of the vertebral body and houses the main interosseous vascular trunks, consists mainly of thin walls and large irregular marrow spaces. The trabeculae are loosely arranged and large cylindrical plates surround the basi-vertebral veins.

A closer examination of lumbar vertebral anatomy was performed on the excised L1 and L4 control vertebral bodies. These units were cleaned of all soft-tissue, X-rayed, fixed in 70% ETOH and embedded in methylmethacrylate (MMA). One millimeter thick sections were cut in the sagittal and transverse planes for macroscopic and microscopic observations.

The lumbar vertebrae of the Rhesus monkey (and humans) was observed to consist of the following five zones (figures 1 and 2): a) superior and inferior end zones, b) superior and inferior transition zones, and c) central vascular zone.

The superior and inferior end zones are structurally nearly identical and can be described together. They consist of short thick vertical rods oriented perpendicular to the end plates. The transverse trabeculae intersect the main structures at right angles. The marrow spaces are small and uniform, and in cross section have the appearance of a dense spongy lattice-work (figures 1a & c).

The superior and inferior transitional zones are not columnar in appearance as are the end zones. The vertical trabeculae have much thinner walls and are joined by transverse trabeculae at staggered intervals. In cross section the transitional zones have a much more open weaved appearance with the superior zone having catercornered rods and circular canals associated with the pedicles. The cortical bone in the pedicle area increases in thickness away from the central body (figures 1a and d).

The central zone, which contains the major interosseous vascular trunks, consists of large vertically oriented plates in the Rhesus monkey. These plates are intersected by short transverse ties and large vascular canals. Microscopically these structures resemble elongated "T's" and form large irregular marrow spaces. In cross section the central plates are seen to extend throughout the entire depth of the central portion of the vertebral body. These structures lie in close approximation to the lateral and central traversings of the interosseous vascular structures. In humans the central zone trabecular anatomy is very similar to that of the Rhesus but does not include the occurrence of the large vascular plates (figures 1a and e).

IV. Mechanical Test Data

A load-displacement curve was produced during the test procedure. Four test variables were extracted directly from the test curve: ultimate load, energy to ultimate load, yield load, and stiffness. Ultimate load is the maximum compressive load developed by the specimen during testing and indicates the load point at which the specimen has become permanently deformed or structurally damaged. Energy to ultimate load indicates the specimens capacity to absorb or store energy. Yield load marks the point after which permanent deformation or injury occurs. Stiffness represents the loading slope of the test and indicates the deformability of the specimen under the prescribed loading conditions.

Twenty excised L2 and L3 vertebrae from ten healthy male Rhesus monkeys were thawed, disarticulated, X-rayed, and cleaned of all soft tissue. The inferior and superior surfaces were photographed using a standard magnification factor of 3X, and the surface areas calculated using a planimeter (Keuffel & Esser Co., Morristown NJ) and a magnification calibration equation. The lengths of the dorsal and ventral aspects of the vertebral bodies were measured using vernier calipers.

To promote uniform load distribution the superior and inferior surfaces of each L2 and L3 vertebral body were evenly set into an acrylic dental resin (Fastcure, Kerry Laboratory, Romulus, Michigan). Simple axial compression from an electrohydraulic closed-loop test system (Model 810 Material Test System, MTS Systems, Corp., Minneapolis, Minnesota) was performed on each vertebral specimen. Each animal (consisting of an L2-L3 test pair) was assigned to one ultimate deformation value from 10% to 30%, differing in 5% intervals. Each vertebral body was randomly assigned to either 5.25×10^{-3} m/min or 25 m/min deformation rate. Each vertebral body was tested only once at a preassigned ultimate deformation rate and percentage.

The values for average ultimate load and the graph representing average ultimate load to percentage of deformation relative to deformation rate are presented in figure 3. The average ultimate load values at the slow rate of displacement were relatively random, but the fast displacement loads exhibited a trend towards increased ultimate load from 15% to 30% deformation. These results (and the original test curves) seem to indicate that at the slower loading rates ultimate load, per definition, was not reached in many of the specimens tested at the lower deformation percentages.

The values for average energy to ultimate load and the graph representing average energy to ultimate load to percentage of deformation relative to deformation rate are presented in figure 4. The average values for energy to ultimate load were greater for the fast displacement rate tests. The trends were random for both deformation rates, but the patterns were seemingly identical. The greatest energy values for both test rates were observed at 20% and 30% deformation, indicating that closer examination of these two deformation percentages may be valuable.

The values for average yield load and the graph representing average yield load to percentage of deformation relative to deformation rate are presented in figure 5. The average values for yield load were greater for the fast displacement rate tests. The slower rate values were random throughout the test range, but the fast range specimens exhibited an increase in yield load from 15% to 25%, with a plateau from 25% to 30%. Both loading rates follow the same pattern for yield load until they reach 25% where they follow opposite trends. The trends for yield load appear to be rate and deformation dependent. The values for the slower rate do not appear to be significantly different, even though their pattern is relatively random. Further studies with an increased sample size may further define the differences in yield load between loading rate and percentage of deformation.

The values for average stiffness and the graph representing average stiffness to percentage of deformation relative to deformation rate are presented in figure 6. The average stiffness values are greater at the fast load rate. The values are random at the low load rate, but show an almost linear increase from 15% to 25% at the fast rate of deformation. At 25 m/min rate from 25% deformation to 30% there is a slight decrease in stiffness, but this may not be significant. The 10% deformation value at the fast deformation rate is not (apparently) significantly different from the higher stiffness values at this rate, thereby, indicating that a closer examination of the 15% deformation profile for stiffness may prove significant. The slow rate values do not appear to be significantly different even though they exhibit relatively random stiffness trends.

V. Vertebral Microfractures

The lumbar vertebral body of the Rhesus monkey can be divided into 5 individual zones (figure 7a). The works of Vernon-Roberts, Perey, Yabut, Eurell and Kazarian (to mention but a few) have indicated that different patterns of trabecular microfractures are possible under various test conditions. Vernon-Roberts (6) investigated microfracture lesions that result from normal stress fractures observed in human cadaver specimens. His results indicated that stress fractures in vertebrae that are produced from normal daily activities are located primarily in the superior and inferior end zone areas. Perey (5) tested vertebral motion segments under impact loading (10 to 25 kg loads) and observed end zone/end plate fractures in his specimens. Yabut (9) also tested vertebral segments that contained their associated intervertebral disks and posterior elements, but tested his specimens under stimulated fatigue or cyclic loading parameters (600 to 4000 N applied load at .3 Hz). Yabut observed a fracture pattern with a high incidence of superior end zone and transition

zone fractures. Eurell and Kazarian (3), and Kazarian and Graves (4) loaded isolated vertebral bodies to failure at various loading rates (from 8.89 10^{-6} m/sec to 8.89×10^{-1} m/sec). Their observed fracture patterns were in the end and transverse zones, but most predominantly in the central vascular zone. We are met with great difficulty when trying to compare these works because of the differences in specimen preparation and testing methodologies.

Following compression testing of the L2 and L3 vertebral bodies our specimens were X-rayed, fixed in 70% ETOH, embedded in MMA, sectioned and analyzed in the same manner as the control specimens. The trabecular fracture patterns were located and transcribed onto a graphical template of a mock vertebrae. The fractures were characterized by the following fracture types: burst = Δ , transverse = \square , oblique = 0, longitudinal = *, and greenstick = +. Microfractures are not generally described as being of the greenstick type, but the trabeculae which exhibited plastic deformation and splintering without the production of a complete fracture were represented in this manner.

The specimen pre-test X-rays (A-P in position) indicated no gross lesions, fractures or pathologies in the specimens, except for animal number 8 which was later tested at 10% deformation. This specimen possessed grade 1 intermittent osteophytes on the posterior end plate region. Post-test X-rays did not show the production of gross fractures until 25% deformation at 25 m/min deformation rate. Compression damage was apparent at 20% deformation, but no clear fracture lines were visible.

Ten percent deformation fracture patterns are presented in figure 7b and c. The slow deformation rate specimens showed scattered fractures primarily located in the inferior end and transition zones. These consisted of transverse and longitudinal cracks. The fast deformation rate specimens' primary area of damage was the inferior end zone, but scattered fractures were

observed in the superior end zone. The fast rate pattern consisted primarily of burst and greenstick fractures.

Fifteen percent deformation fracture patterns are presented in figures 8a and b. The slow deformation rate specimens exhibited a scattered fracture pattern of all of the fracture types located in the superior end and transition zones. The fast deformation rate specimens show a relatively equal distribution of fracture types throughout the vertebral body, with a small cluster of varied fractures in the anterior, superior end zone.

Twenty percent deformation fracture patterns are presented in figure 8c and d. The slow deformation rate specimens exhibit a clustering of greenstick fractures in the superior end and transition zones, with a scattering of burst and oblique fractures in the more central regions of the transition zone. The inferior end zone shows an anterior and posterior clustering of greenstick and burst fractures. The fast deformation rate specimens show a superior, anterior clustering of primarily burst and greenstick fractures in the superior end and transition zones. The inferior end zone has a scattered pattern of varied fracture types throughout the area.

Twenty five percent deformation fracture patterns are presented in figure 9a and b. This deformation percentage marks the initial point where we observed a persistent incidence of fractures in the central vascular zone. The slow deformation rate specimens show a clustering of all fracture types (mostly burst) in the posterior central zone near the pedical. The fast deformation rate specimens had a densely scattered pattern of all fracture types throughout the central zone, including extensive anterior and posterior damage in this area.

Thirty percent deformation fracture patterns are presented in figure 9c and d. Here both loading rates show massive destruction throughout the vertebral body. The slow deformation rate specimens show extensive burst fracture damage in both superior zones with scattered posterior central zone fractures. The fast deformation rate specimens show extensive overall burst fracture damage with clusters in the central and superior zones. Extensive cortical fractures of the anterior and posterior cortical walls were evident in varying degrees.

The general fracture pattern trends follow from end plate-transitional zone damage at 10% to 20% deformation, to central damage of the vascular areas at 25% to 30% deformation. The majority of fractures present were not detected radiographically.

At the low deformation rate tests there was apparently no direct correlation between the fracture patterns from 10% to 30% deformation and ultimate load, further indicating that many of these test specimens did not reach ultimate load during the test procedure. At fast deformation rates, except for 10% deformation, there was a trend towards increased vertebral body damage with increased ultimate load. The trends exhibited in this study suggest that ultimate load may not be the best indicator for fracture patterns which occur at low deformation percentages under conditions of slow deformation rates.

Energy to ultimate load follows a trend easily correlated to the amount of end plate damage. The lowest energy to ultimate load values were observed in specimens (10% to 20% deformation) with very little end zone damage. The higher energy values were observed in specimens (20% to 30% deformation) with a proliferation of end zone damage.

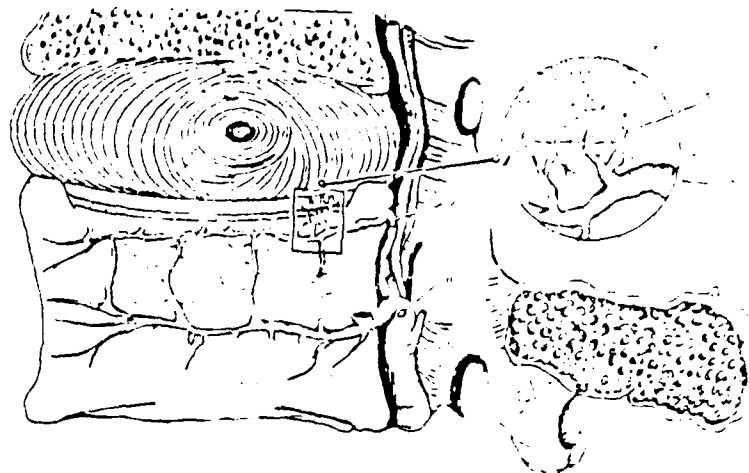
Yield load shows different trends at 25% deformation between the fast and slow deformation rate specimens. The fast rate specimens exhibit massive collapse of the central vascular zone, whereas the slow rate specimens show scattered posterior central zone damage. The fast test rate specimens have an increase yield load relationship with central vertebral collapse. The central zone destruction appears to define the ceiling for yield response, indicated by the plateau reached after 25% fast rate deformation.

Finally, stiffness at the slow rate of deformation does not differ significantly between the deformation percentages. The fast rate specimens (from 15% to 30%) show a good relationship between an increased stiffness profile and a general trend towards an overall increase in vertebral body destruction and incidence of burst fractures.

VI. Recommendations

1. The results of these experiments could be more fully evaluated with an increase sample size so statistical parameters and individual variation could be addressed.
2. A study on the interosseous vascular anatomy of nonhuman primates associated with fracture patterns would help to shed further light on the mechanisms influencing necrosis, osteoporosis, and healing in the primate vertebral system.
3. This experiment, including the aforementioned recommendations, should be repeated on baboon and human vertebral specimens in an effort to further validate our nonhuman primate models for vertebral responses to impact-type loading conditions.

FIGURE(S) # 1 :



B) Vascular anatomy of lumbar vertebrae.
(Taken from: Crock, H & Yoshizawa, H:
The Blood Supply of the Lumbar Vertebral Column.
Clinical Orthopaedics & Related Research. 115:
6- 21, 1976.)

A) Unmascerated section of lumbar
vertebrae 1mm from rhesus monkey
mid-sagittal region.



C) superior end-zone, rhesus



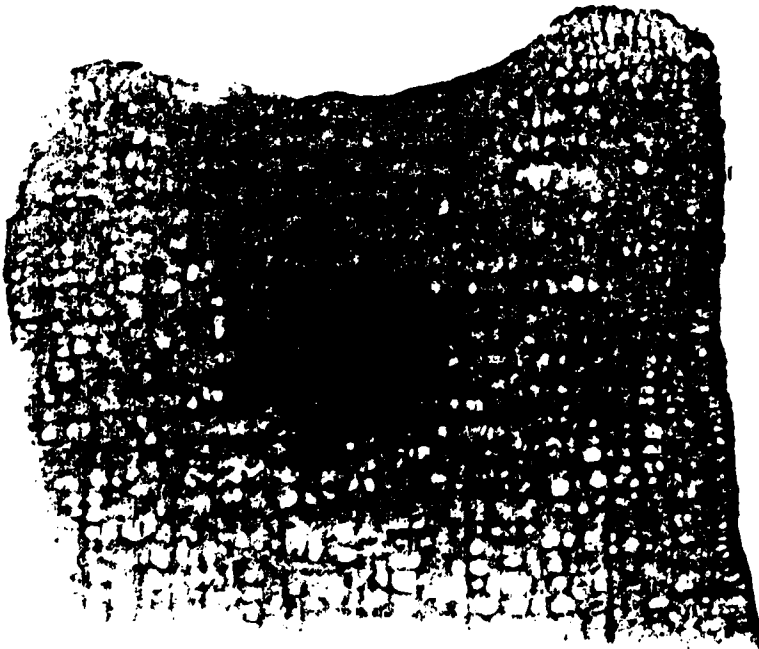
D) transition-zone, superior
rhesus



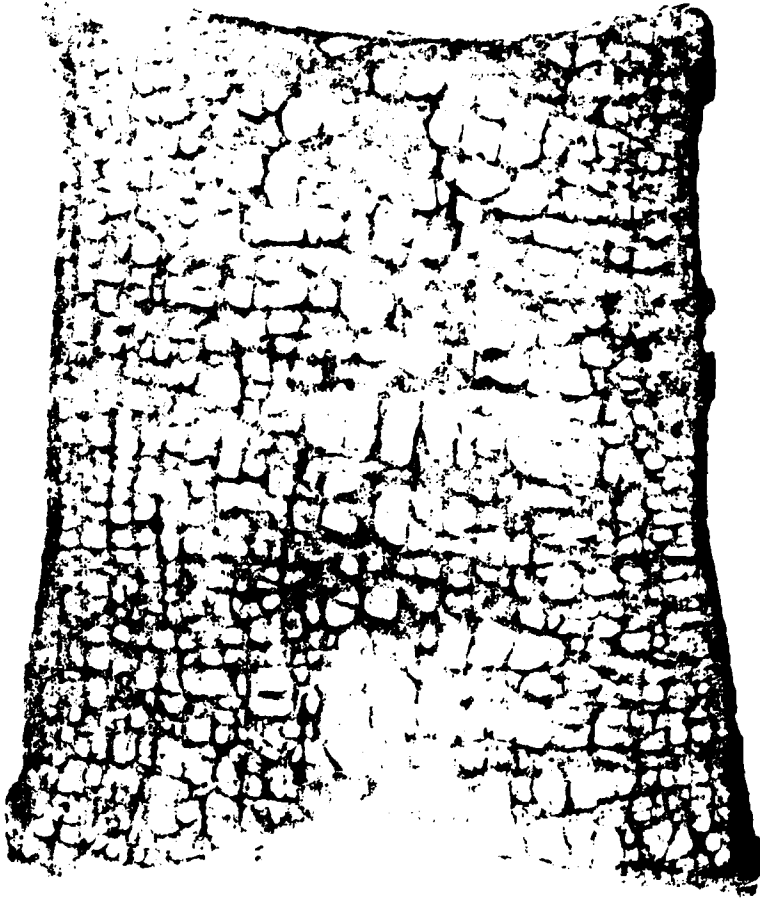
E) central-zone of vascularity
rhesus

FIGURE # 2:

A) Lumbar Vertebral Body: Macaca mulatta



B) Lumbar Vertebral Body: Human



(Taken from; AAMRL-BBD collection of Dr. L.Kazarian)

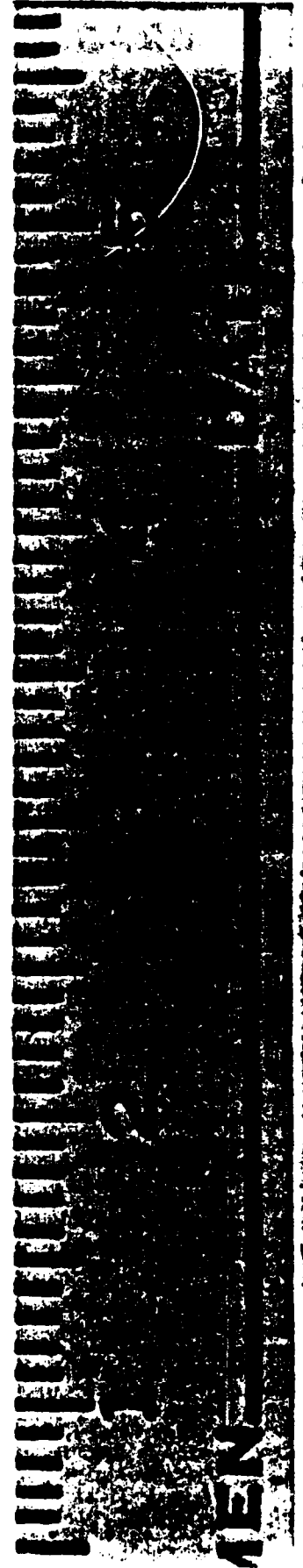
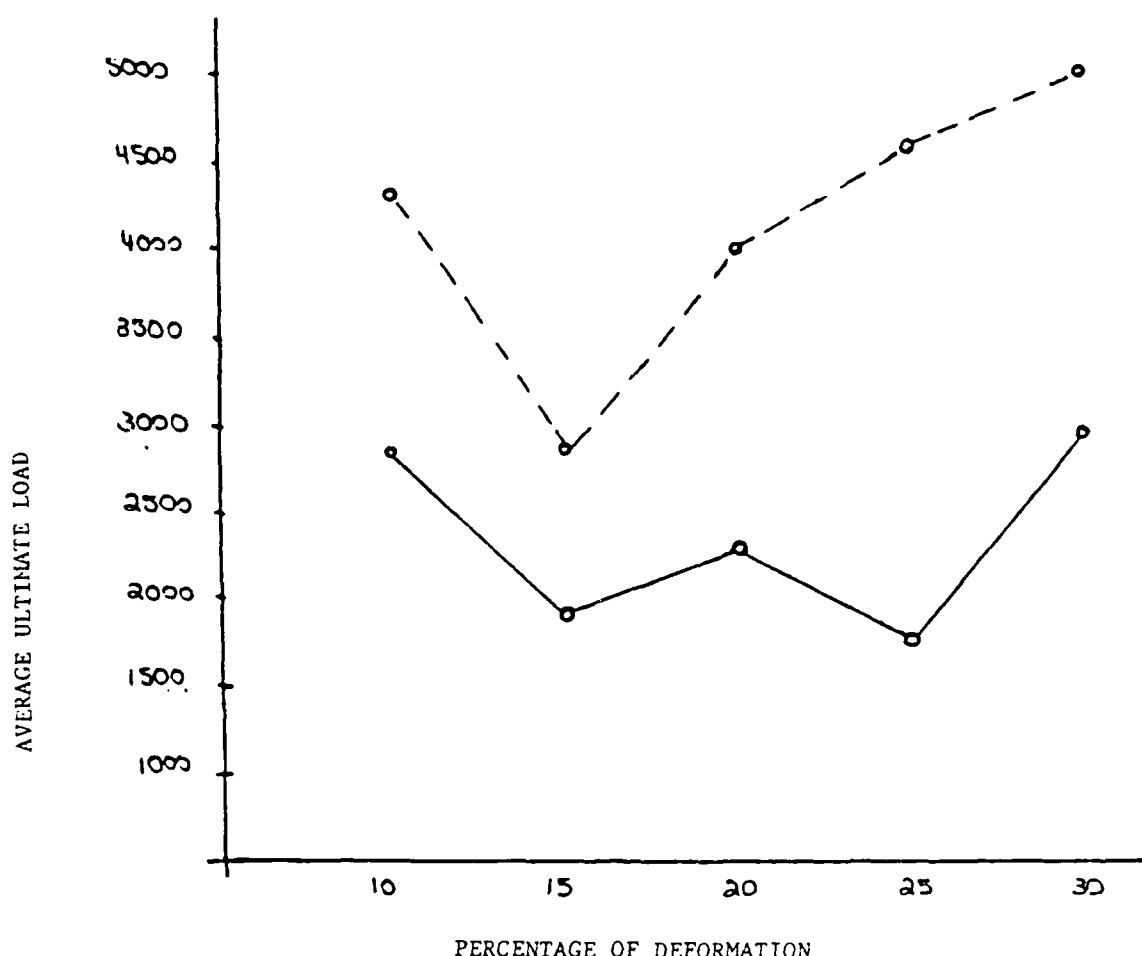


FIGURE # 3:

ULTIMATE LOAD (N)						
RATE	LOCATION	10%	15%	20%	25%	30%
5.25×10^{-3} m/min	L2	2524.24	2235.12	2735.52	1923.75	2891.20
	L3	2852.28	1484.52	1990.48	1556.80	2996.84
	average	2688.26	1859.82	2363.00	1740.28	2944.02
25 m/min	L2	4242.28	2051.64	3869.76	5921.40	5026.24
	L3	4431.22	3725.20	4175.56	3280.40	4981.76
	average	4336.80	2888.42	4022.66	4600.90	5004.00



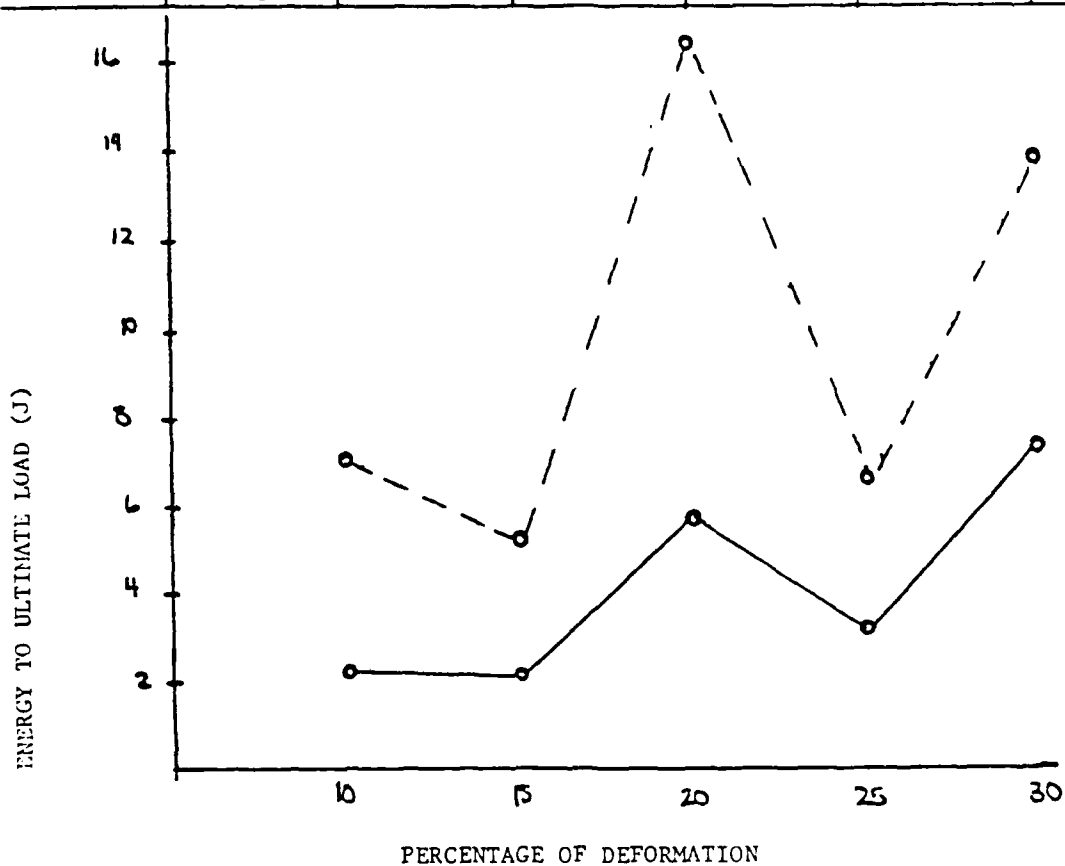
AVERAGE ULTIMATE LOAD TO PERCENTAGE OF DEFORMATION

_____ 5.25×10^{-3} m/min.
 - - - - - 25 m/min

FIGURE # 4:

ENERGY TO ULTIMATE LOAD (J)

RATE	LOCATION	10%	15%	20%	25%	30%
5.25×10^{-3} m/min	L2	1.73	2.28	7.24	3.54	3.72
	L3	2.43	1.86	3.60	missing	11.52
	average	2.08	2.07	5.42	3.54	7.69
25 m/min	L2	5.95	3.89	18.82	7.98	18.95
	L3	8.54	7.71	13.35	5.62	9.13
	average	7.24	5.80	16.08	6.80	13.94



AVERAGE ENERGY TO ULTIMATE LOAD TO PERCENTAGE OF DEFORMATION

————— 5.25×10^{-3} m/min.
 ----- 25 m/min.

FIGURE # 5:

YIELD LOAD (N)

RATE	LOCATION	10%	15%	20%	25%	30%
5.25×10^{-3} m/min	L2	2457.52	2101.68	2296.28	1551.24	2546.48
	L3	2674.36	1395.56	1390.00	missing	2290.72
	average	2565.94	1748.62	1843.14	1551.24	2418.60
25 m/min	L2	3841.96	1845.92	3530.60	5404.32	3758.56
	L3	4142.20	3664.04	2524.24	2868.96	4492.48
	average	3992.08	2754.98	3027.44	4136.64	4125.52

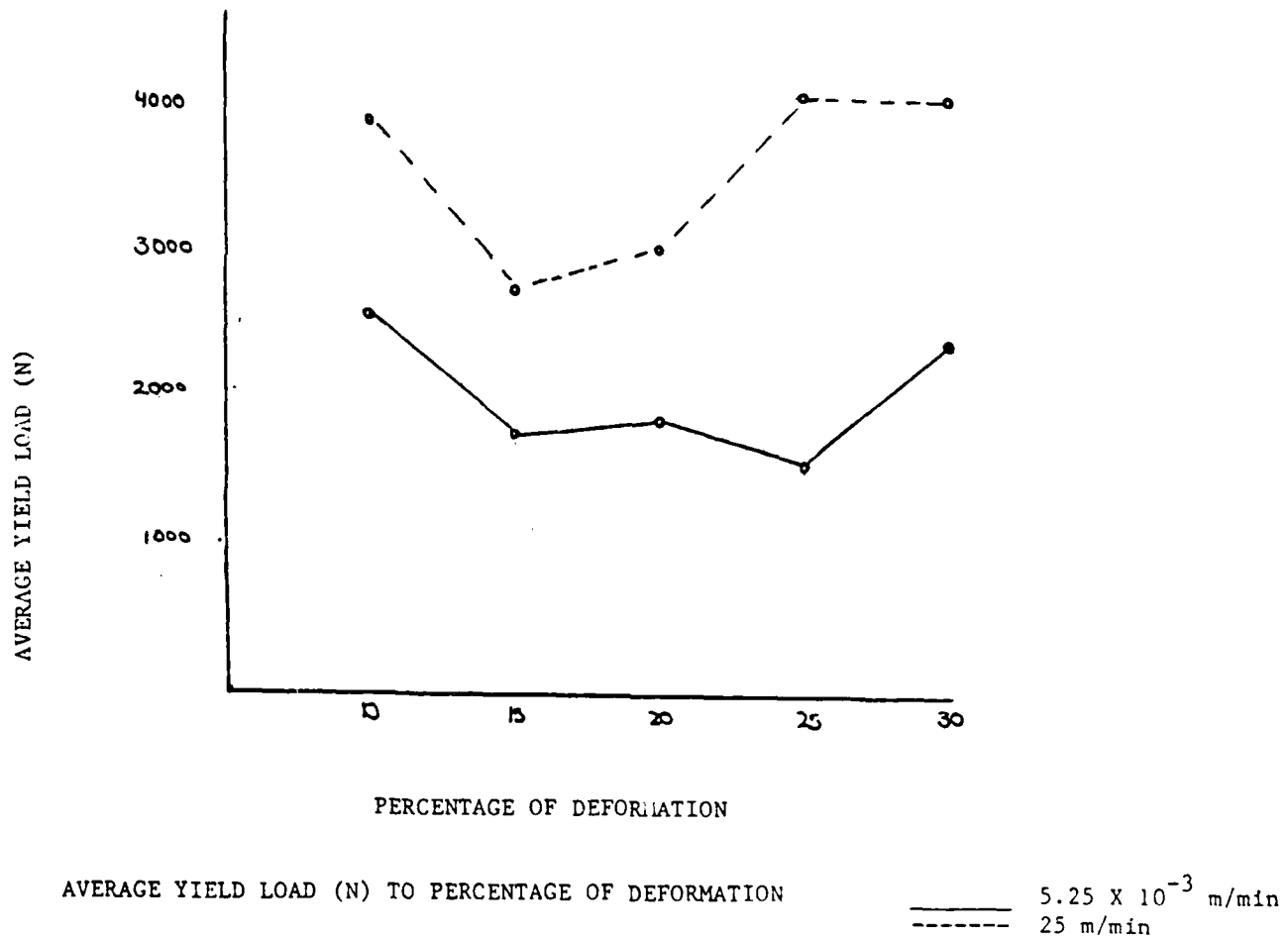
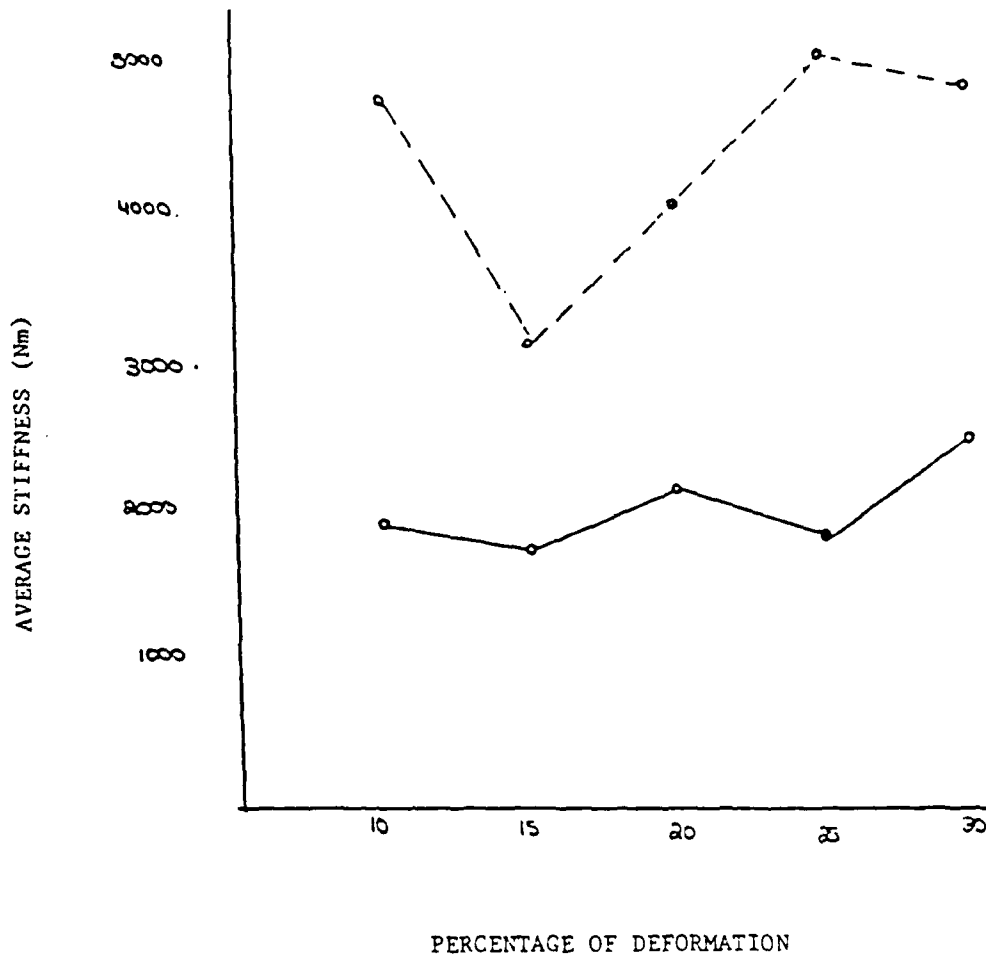


FIGURE # 6:

STIFFNESS (Nm)

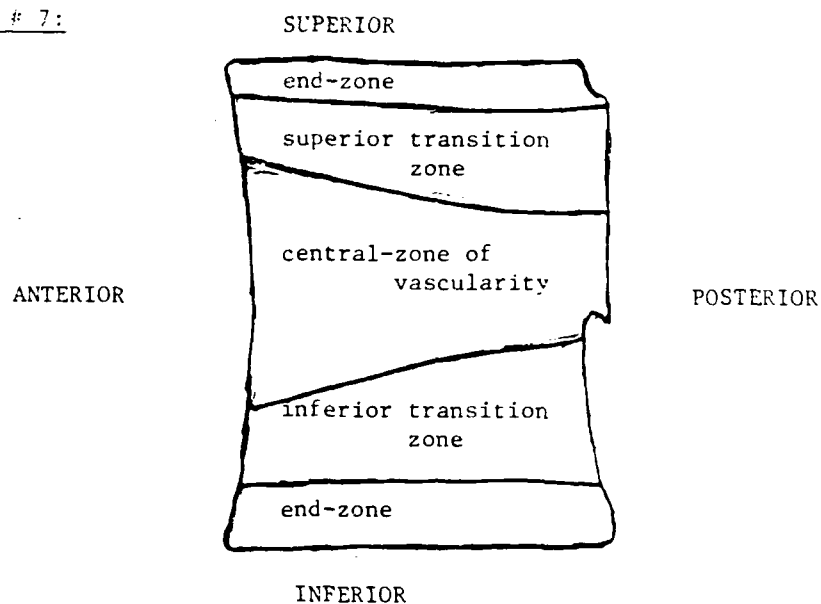
RATE	LOCATION	10%	15%	20%	25%	30%
5.25×10^{-3} m/min	L2	1436	2267	2539	1856	3036
	L3	2392	1323	1768	missing	2051
	average	1914	1795	2154	1856	2544
25 m/min	L2	4607	2164	4087	6363	5027
	L3	4987	4104	4106	3681	4736
	average	4797	3184	4096	5022	4882



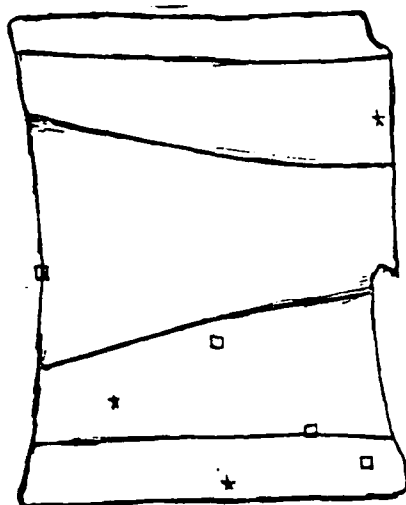
AVERAGE STIFFNESS (Nm) TO PERCENTAGE OF DEFORMATION

— 5.25×10^{-3} m/min
 - - - 25 m/min

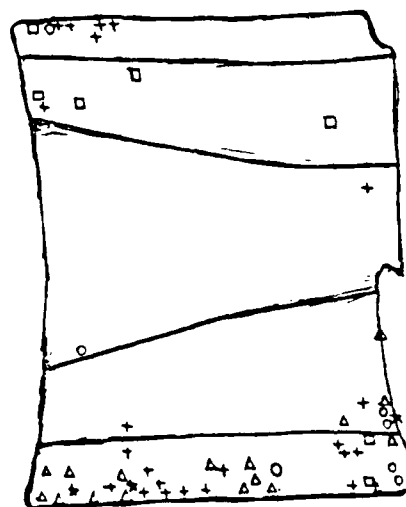
FIGURE # 7:



A) Schematic representing the trabecular compartments of the lumbar vertebral body of the rhesus monkey.

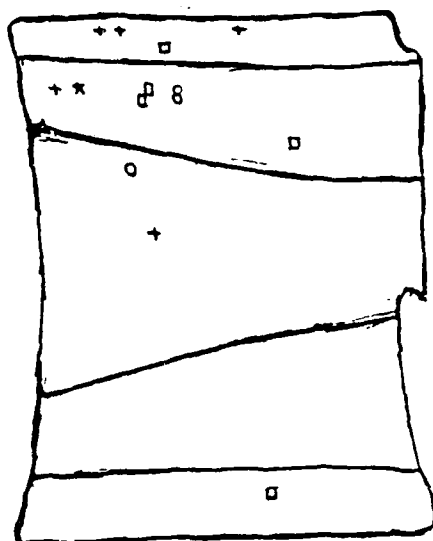


B) Composite of fracture pattern at 10% deformation, 5.25×10^{-3} m/min.

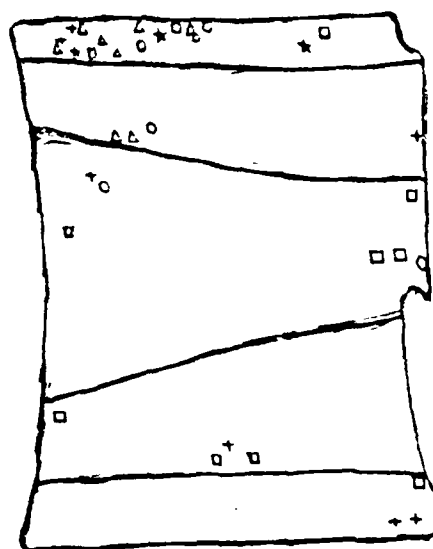


C) Composite of fracture pattern at 10% deformation, 25 m/min.

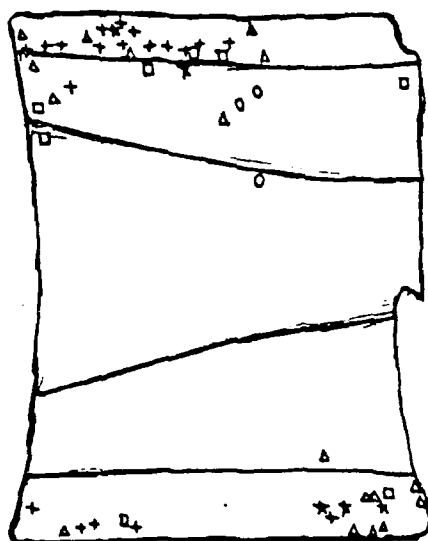
FIGURE # 8:



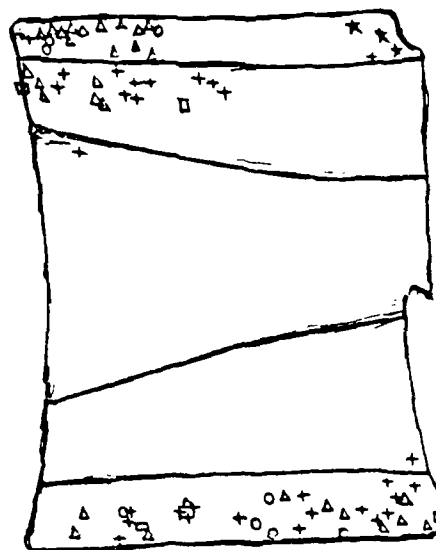
A) Composite of fracture pattern at 15% deformation, 5.25×10^{-3} m/min.



B) Composite of fracture pattern at 15% deformation, 25 m/min.

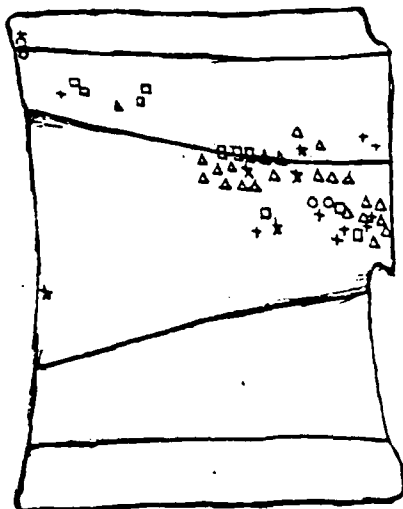


C) Composite of fracture pattern at 20% deformation, 5.25×10^{-3} m/min.

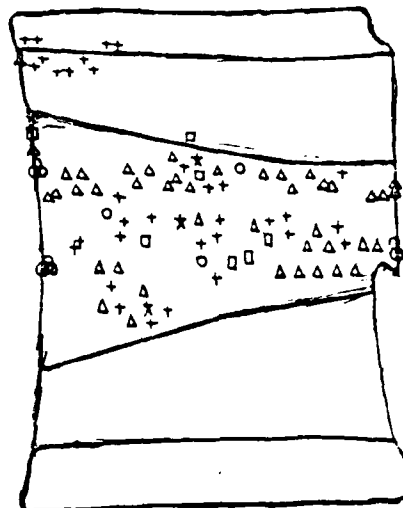


D) Composite of fracture pattern at 20% deformation, 25 m/min.

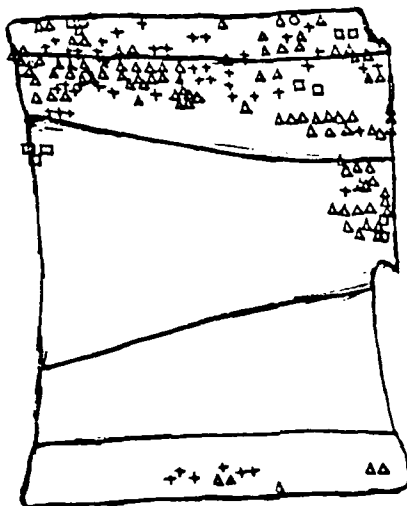
FIGURE # 9:



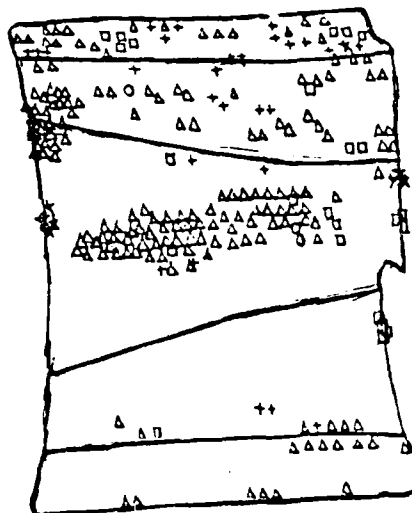
A) Composite of fracture pattern at 25% deformation, 5.25×10^{-3} m/min.



B) Composite of fracture pattern at 25% deformation, 25 m/min.



C) Composite of fracture pattern at 30% deformation, 5.25×10^{-3} m/min.



D) Composite of fracture pattern at 30% deformation, 25 m/min.

References

1. Arnold JS, "Focal Excessive Endosteal Resorption in Aging and Senile Osteoporosis," Osteoporosis. Edited by US Barzel. New York, Grune & Stratton, 1970, pp. 80-100.
2. Crock HV and Yoshizawa H, "The Blood Supply of the Lumbar Vertebral Column," Clinical Orthopaedics and Related Research. No. 115, March - April, 1976, pp. 6-21.
3. Eurell JAC and Kazarian L, "The Scanning Electron Microscopy of Compressed Vertebral Bodies," Spine. 5(7), 1982, pp. 123-128.
4. Kazarian LE and Graves G, "Compressive Strength Characteristics of the Primate (Macaca mulatta) Vertebral Centrum," AMRL-TR-79-8, 1979.
5. Perey O, "Fracture of the Vertebral End-Plate in the Lumbar Spine," ACTA Orthopaedica Scandinavica, Suppl. No. 25, 1957, pp. 5-101.
6. Vernon-Roberts and Pirie CJ, "Healing Trabecular Microfractures in the Bodies of Lumbar Vertebrae," Annals of Rheumatic Diseases, 32, 1973, pp. 406-412.
7. White AA, and Panjabi MM, Clinical Biomechanics of the Spine, J.B. Lippincott Co., Philadelphia, 1978, p. 32-34.
8. Whitehouse WJ, Dyson ED and Jackson CK, "The Scanning Electron Microscope in Studies of Trabecular Bone from a Human Vertebral Body," Journal of Anatomy, 108, 1971, pp. 481-496.
9. Yabut SM, Kummer F, Nordin M, Kahanovitz N, "Radiographic and Histologic Analysis of Fatigue Testing of the Human Lumbar Spine," unpublished Manuscript from the Hospital for Joint Diseases.

1986 USAF-UES SUMMER FACULTY RESEARCH PROGRAM/

GRADUATE STUDENT SUMMER SUPPORT PROGRAM

Sponsored by the

AIR FORCE OFFICE OF SCIENTIFIC RESEARCH

Conducted by the

UNIVERSAL ENERGY SYSTEMS, INC.

FINAL REPORT

Effects of Coherent Scattering on

I R Absorption in Doped Semiconductors

Prepared by:	Peggy Jo Grigsby
Academic Rank:	Graduate Student
Department and	Physics Department
University:	Wright State University
Research Location:	AFWAL Materials Laboratory Electromagnetic Materials Division Laser and Optical Materials Branch
USAF Research:	Gail Brown
Date:	August 15, 1986
Contract No:	F49620-85-C-0013

Effects Of Coherent Scattering
on IR Absorption in Doped Semiconductors

by

Peggy Grigsby

ABSTRACT

The aim of this project was to develop an improved theoretical model for interpreting the excitation spectra from shallow dopants in semiconductors. The research focused on the specific problem of coherent scattering effects (optical channeling). These effects, produced by coherent multiple internal reflection from the plane parallel faces of an optically thin, two-sided polished wafer, compounds the problem of obtaining absorption coefficients, $\alpha(\omega)$ from transmission spectra, $T(\omega)$. The effect occurs in both Si and GaAs. The specific expression for $T(\omega)$ in the presence of channeling was worked out and the inversion of this relation was programmed to obtain $\alpha(\omega)$. When inversion of the coherent scattering formula did not give reasonable values for $\alpha(\omega)$, a combination of coherent and incoherent scattering formulas was used to minimize the spurious oscillations. The program was applied to obtain $\alpha(\omega)$ from FTIR transmission spectra which show channeling effects. This program was then compared to other programs available to eliminate fringes in data.

ACKNOWLEDGMENTS

I would like to thank the Air Force Systems Command, the Air Force Office of Scientific Research and the Laser and Optical Materials Branch of AFWAL Materials Laboratory, Wright-Patterson AFB for the opportunity of spending the summer on this research. I would also like to thank Gail Brown for her encouragement and interest, Dr. Gust Bambakidis for his guidance and Dave Fischer for his support and instruction.

I. INTRODUCTION:

I received my masters degree in mathematics from Wright State University in 1978. Since this time I have been employed by both the mathematics and physics departments at Wright State University to teach various classes and to manage the introductory physics labs. In the latter capacity I have rewritten the physics lab manuals and conducted training sessions for the laboratory instructors. I am currently working on a masters degree in physics at Wright State University.

I began working on the problem of coherent scattering effects last summer. The research this summer was a continuation of work I began then. I was assigned to this project because of my combined experience in physics, mathematics and computer science and my experience on the project last summer.

II. OBJECTIVES OF THE RESEARCH EFFORT:

The overall objective of this research was to develop an improved model for interpreting the excitation spectra in semiconductors. This research focused on the specific problem of coherent scattering effects or optical channeling.

The specific objectives were:

1. To expand upon the computer program I developed last summer to convert transmittance data to absorption coefficients. In order to handle large amounts of data the program needed to:
 - a. continuously adjust the period of the formula to

match the period in the data.

- b. determine the weighting factor to use to average the coherent scattering formula with the incoherent.
 - c. be certain that the real peaks in the data are not confused with the coherent scattering oscillations.
- 2. To use this computer program to actively analyze actual transmittance data taken in lab.
 - 3. To learn to use the experimental apparatus to collect data on samples myself.
 - 4. To investigate other methods of analyzing data containing optical channeling and compare these methods to the one I developed.

III. EXPAND COMPUTER PROGRAM:

The program now in use to convert transmittance data to absorption coefficients assumes completely incoherent scattering. In many cases, however, there is some coherent scattering which obscures the real information. The program I wrote to convert transmittance data to absorption coefficients using the coherent scattering formula also has these oscillations. This can be seen in figure one, where both the coherent formula and the incoherent have been used to transform the same data set to absorption coefficients.

Attempting to account for both coherent and incoherent scattering being present in the same sample, I tried using a linear combination of these two formulas to transform the data set. The result can be seen on figure one. Assuming the scattering is

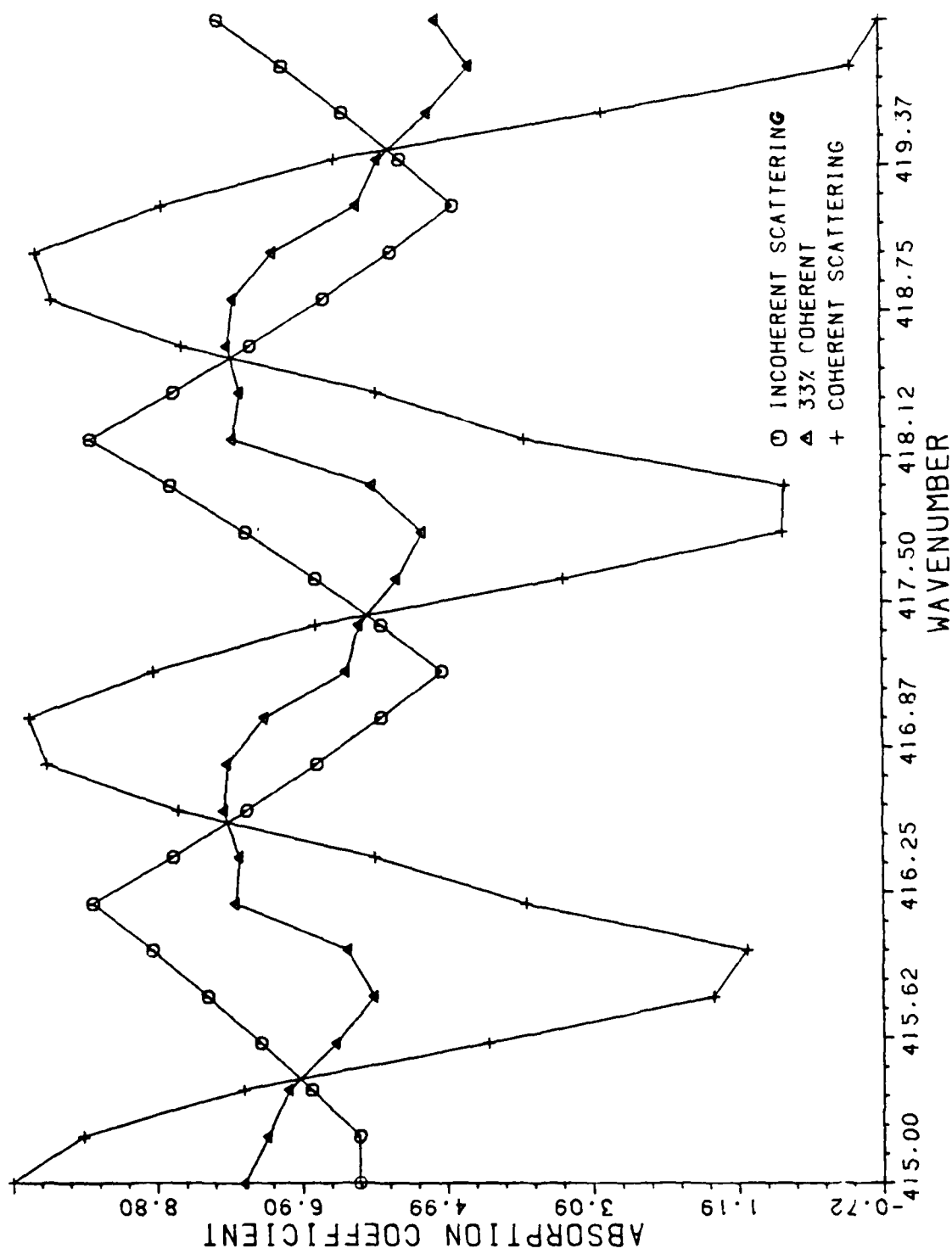


Figure 1: Program does not adjust the period, over small range of wavenumbers.

33% coherent and 67% incoherent results in an absorption coefficient that shows less oscillation. The factor of 33% was obtained by inspection and trial and error.

In addition, the period of these oscillations changes as the wave number changes. As a result, the program works well over a limited range but works progressively less well over an extended range. This can be clearly seen in figure two where the range of the data is much larger than for figure one. An additional complication was that while theoretically, the period should change and the changes can be predicted, the predictions do not match precisely the period on the actual data.

In order to deal with this problem, I revised the program to continually determine the period in the transmittance data by comparing data points to find successive maxima. The program then uses this period in the formula to transform the transmittance data to the absorption coefficient. Comparing figure three to figure one shows that continually readjusting the period results in an absorption coefficient that is more linear. Figure four shows how this revised program works over a larger range.

The 33% weighting factor is still a "guess" however and it varies from sample to sample. To eliminate this guesswork I had the program compare the size of the oscillations in the absorption coefficient from the coherent scattering formula to that from the incoherent scattering formula and determine a weighting factor by averaging over all such oscillations.

To eliminate the chance that the program would interpret an

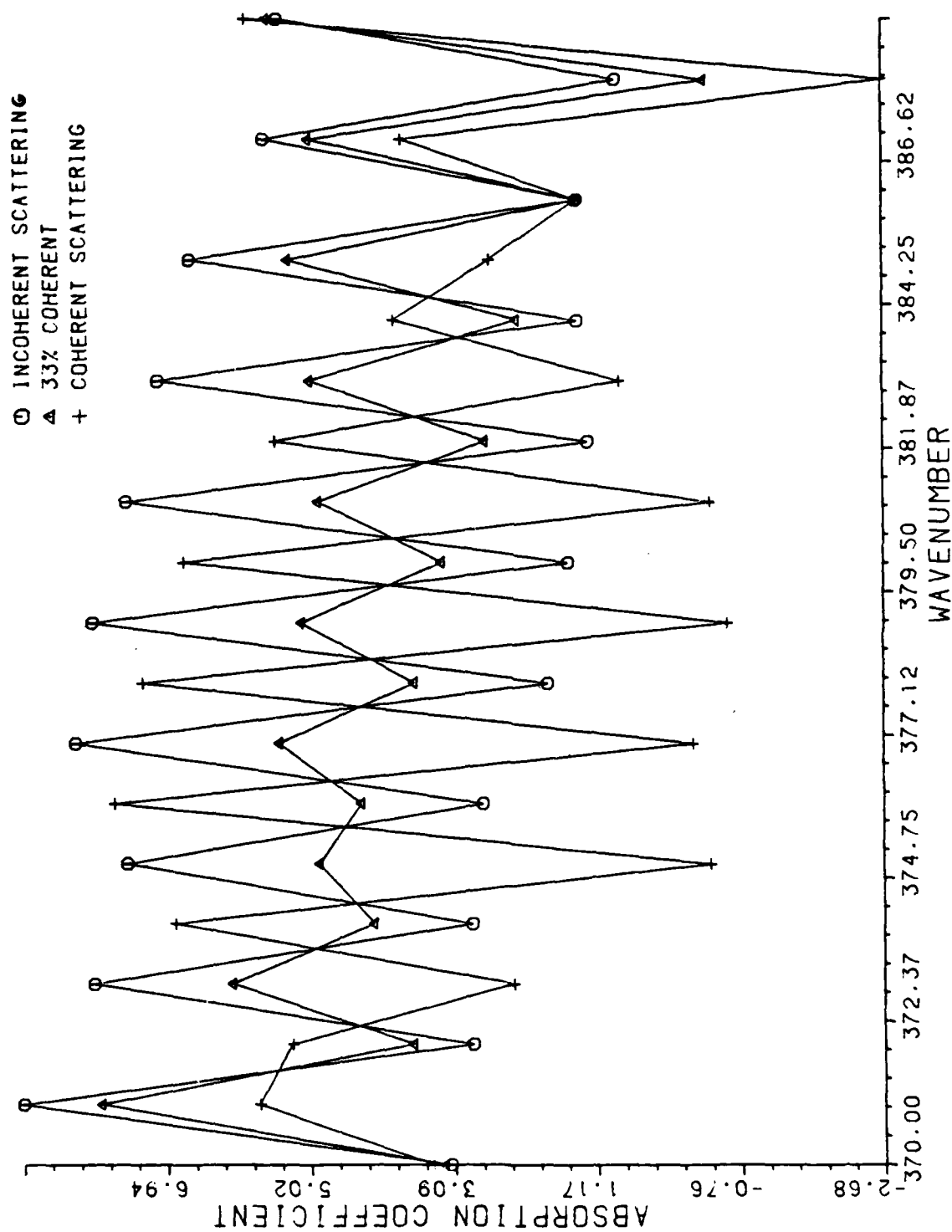


Figure 2: Program does not adjust the period, over large range of wavenumbers.

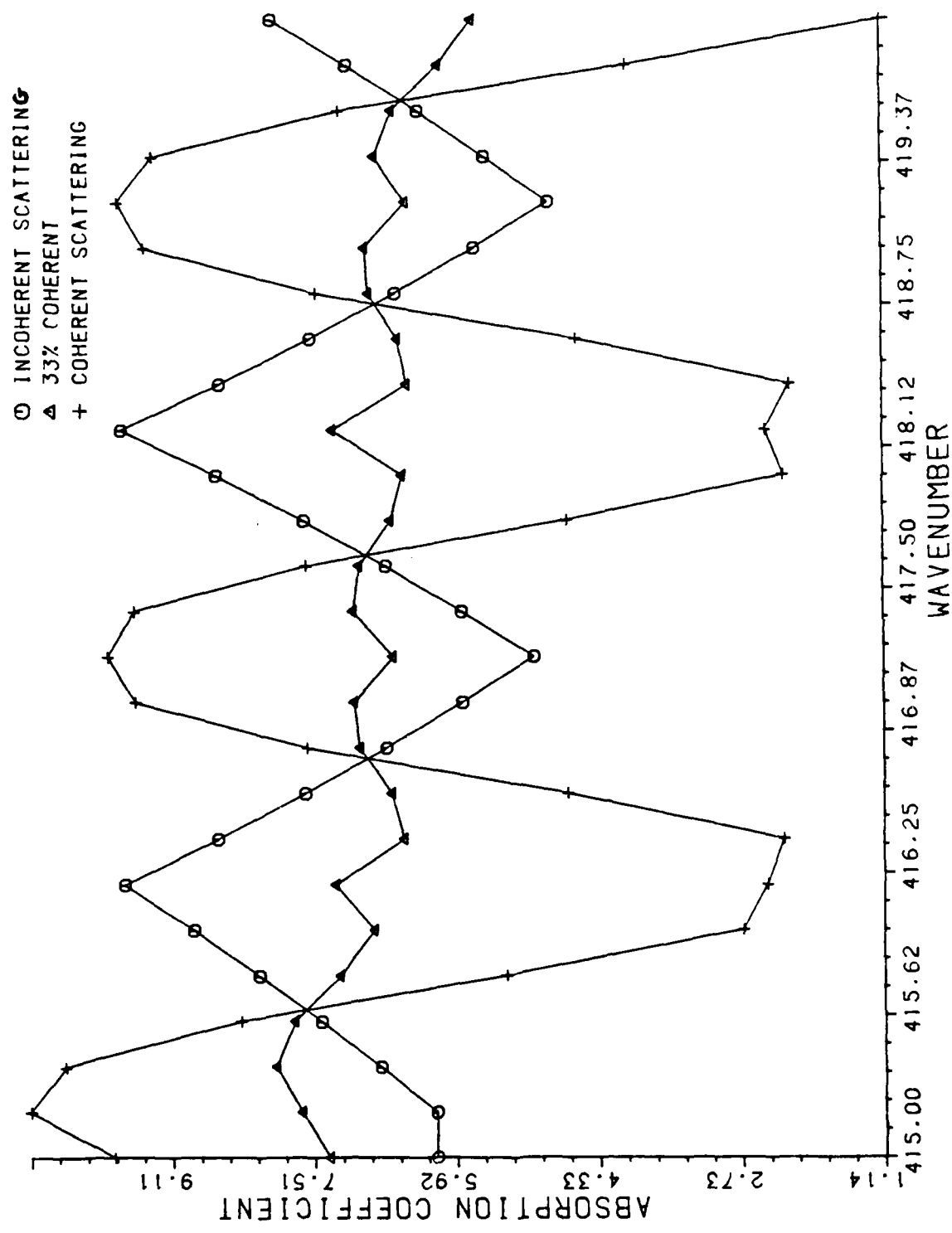


Figure 3: Program adjusting period, over small range of wavenumbers.

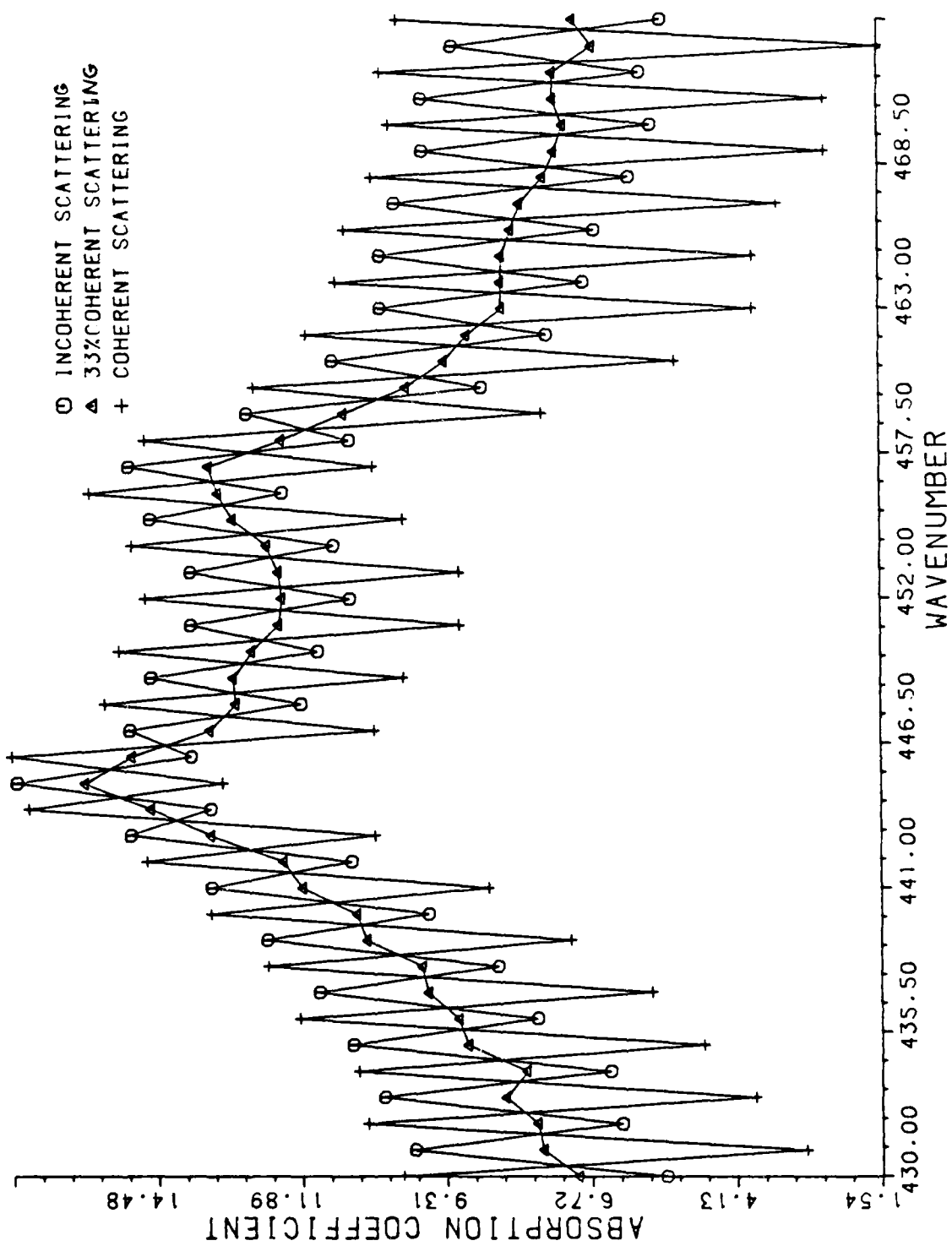


Figure 4: Program adjusting period over large range of wavenumbers.

actual peak as one of these spurious oscillations, I determined the standard deviation of the average and then recomputed the average using only those values within one standard deviation.

The weighting factor determined by this method was surprisingly close to the one determined by "guessing". For example, for the sample 1251 shown in figures one through four, my guess was 33%. The weighting factor determined by averaging the size of the oscillations was 35% and by using only those values within one standard deviation was 36%. Results were similarly close for other samples.

Figure four also shows that the general shape and placement of peaks remains unchanged by this method.

IV. ANALYZING LAB DATA:

In order to see how well my program performed I asked for and obtained transmittance data from any samples run in lab that showed channeling. I concentrated on the region from 300 to 500 wave numbers as this is the region where the channeling is strongest and also the region where features of interest lie and are obscured by the channeling.

I then read the data points from the plots and analyzed the data using my program. I compared the absorption coefficient obtained by using the coherent scattering formula to that obtained using the incoherent formula and also derived the weighting constant for the sample. I then looked at the weighted average of the two formulas.

In the samples I analyzed, using the weighted average made a

significant improvement. It maintained the same general shape, yet did not obscure peaks or information.

In addition, I discovered that this weighting number did not vary significantly over the range of wavenumbers I investigated. The weighting factor did, however, vary considerably from sample to sample. The minimum value was 8% and the maximum was 71%.

V. COLLECT DATA:

In the course of this research, I collected data from samples myself. I learned to operate the spectrometer and use the lab computer to collect and analyze data. I also took the opportunity to learn to use some of the available software to analyze the data.

When I obtained a sample that exhibited extremely strong channeling, I took the interferogram several times, each time analyzing it by one of the different methods available and comparing them.

During this process of familiarizing myself with the equipment and computer I was able to resolve for myself certain questions that had arisen about the data. In addition I was able to formulate new questions and approaches.

VI. COMPARE TO OTHER METHODS:

In order to compare different methods one particularly strong channeling sample was analyzed several different ways.

First I took a set of transmittance data and analyzed it with my program. The results are shown in figure five. The absorption coefficient obtained by using both the incoherent scattering formula as well as the coherent formula are shown as well as the result

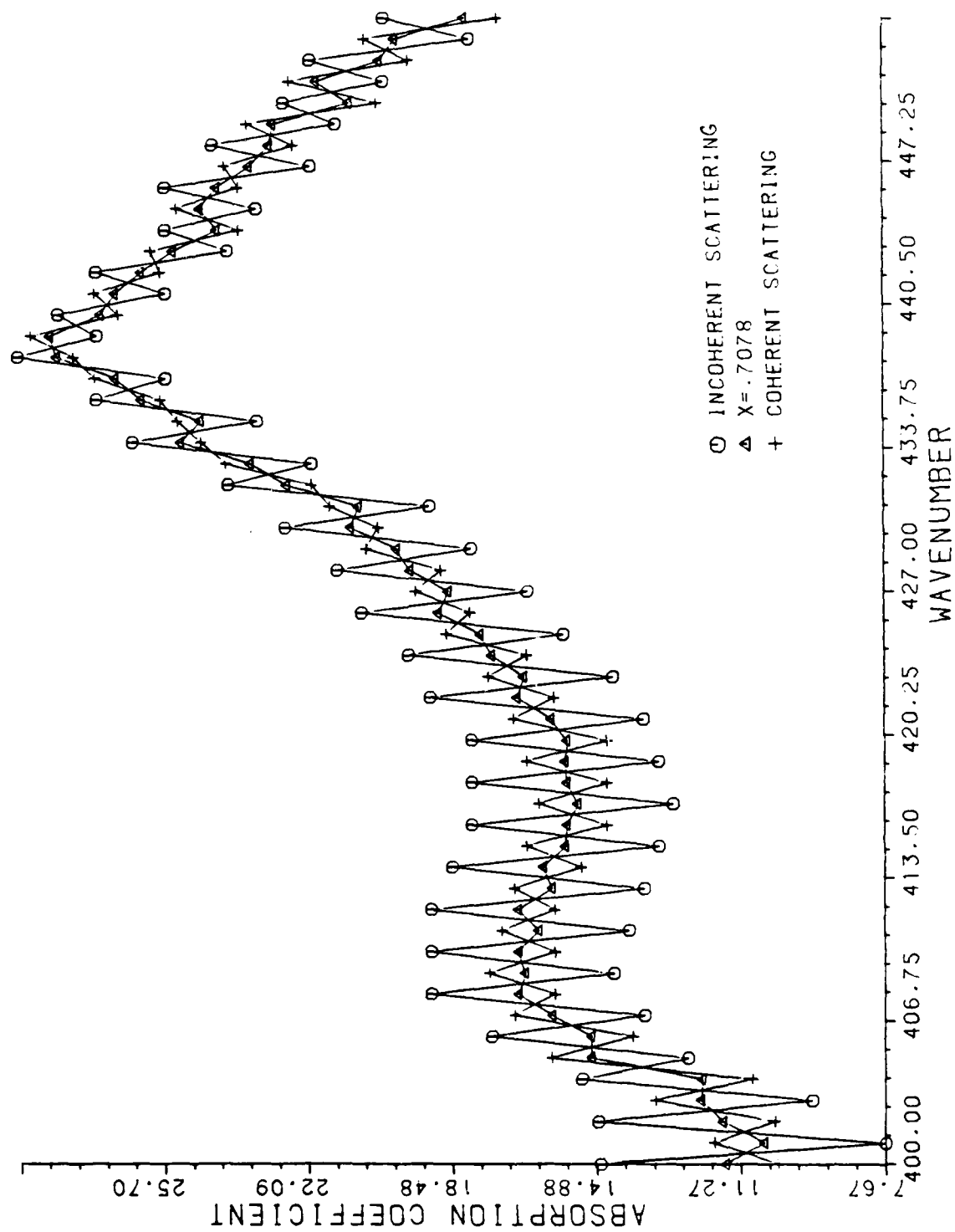


Figure 5: Program adjusting period and determining weighting factor on strongest channeling sample.

obtained by using a linear combination of 71% coherent and 29% incoherent. Using the linear combination is a significant improvement. In fact, merely using the coherent formula instead of the incoherent would provide a significant improvement in strongly channeling samples such as this one.

Next I used an available program called FRINGELIM. This program allows one to change the basic interferogram before the Fourier transform is taken to get the transmittance spectra. The idea is to identify the "glitch" in the interferogram that represents the channeling and then either remove or alter it.

The "glitch" may be;

1. replaced by a straight line connecting the end points of the remaining interferogram.
2. replaced by another section of the same interferogram.
3. replaced by the same section of a reference interferogram.

For each candidate "glitch" I performed all three operations. I then compared the absorption coefficient obtained to that obtained without using FRINGELIM at all. The results can be seen in figure six. For the "glitch" removed here, that between wavepoints 3190 and 3400, no improvement is seen. In fact, the fringing is worse.

I also used a program called SIDEBURST which performs essentially the same operation using a different program. The options here are:

1. replace the section by data points all equal to zero.
2. replace the section by another section of the same interferogram.

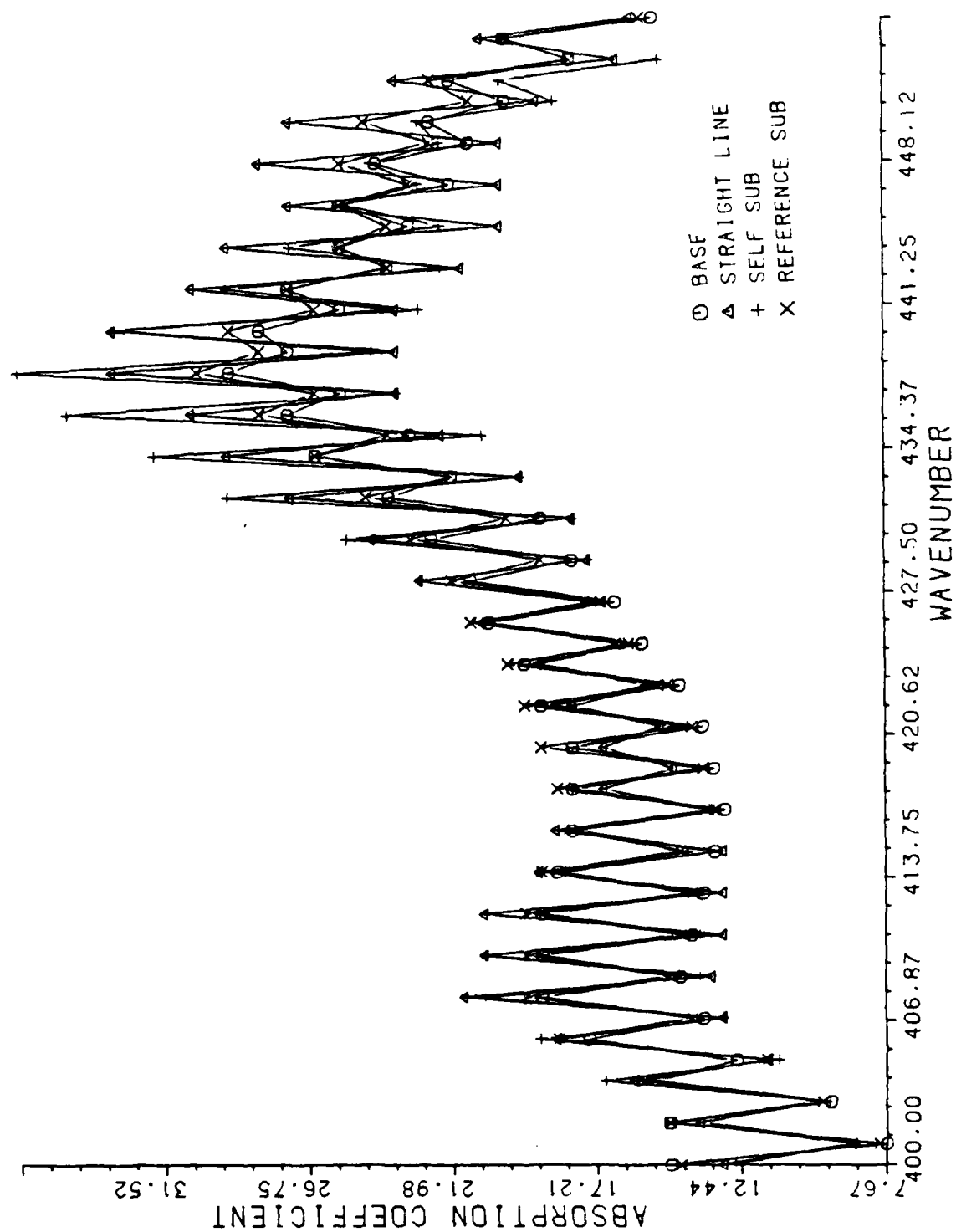


Figure 6: FRINGELIM program.

For comparison I performed these operations on the same section, wave points 3190 to 3400, and compared the results to that obtained without using SIDEBURST. Figure seven shows the results. Once again there is no improvement.

I repeated this procedure for other "glitches" and other sections of the spectrum but the results were substantially the same.

I believe some improvement can be made by using SIDEBURST and FRINGELIM but it requires knowing which "glitch" to remove and determining which one will take experimentation.

VII. RECOMMENDATIONS:

1. One of the time consuming aspects of this project was the fact that data points for the transmittance needed to be read from plots and were not accessible directly from the computer. For this program to be tested extensively data should be accessed directly.
2. This program needs to be tested more extensively:
 - a. the range of wavenumbers needs to be extended and the question of how well this performs on much larger wavenumbers needs to be answered.
 - b. a greater variety of samples should be tested.
3. The coherent scattering formula program should be entered into the permanent software of the system so that when a strongly channeling sample is discovered, the coherent formula could be used in place of the incoherent now in

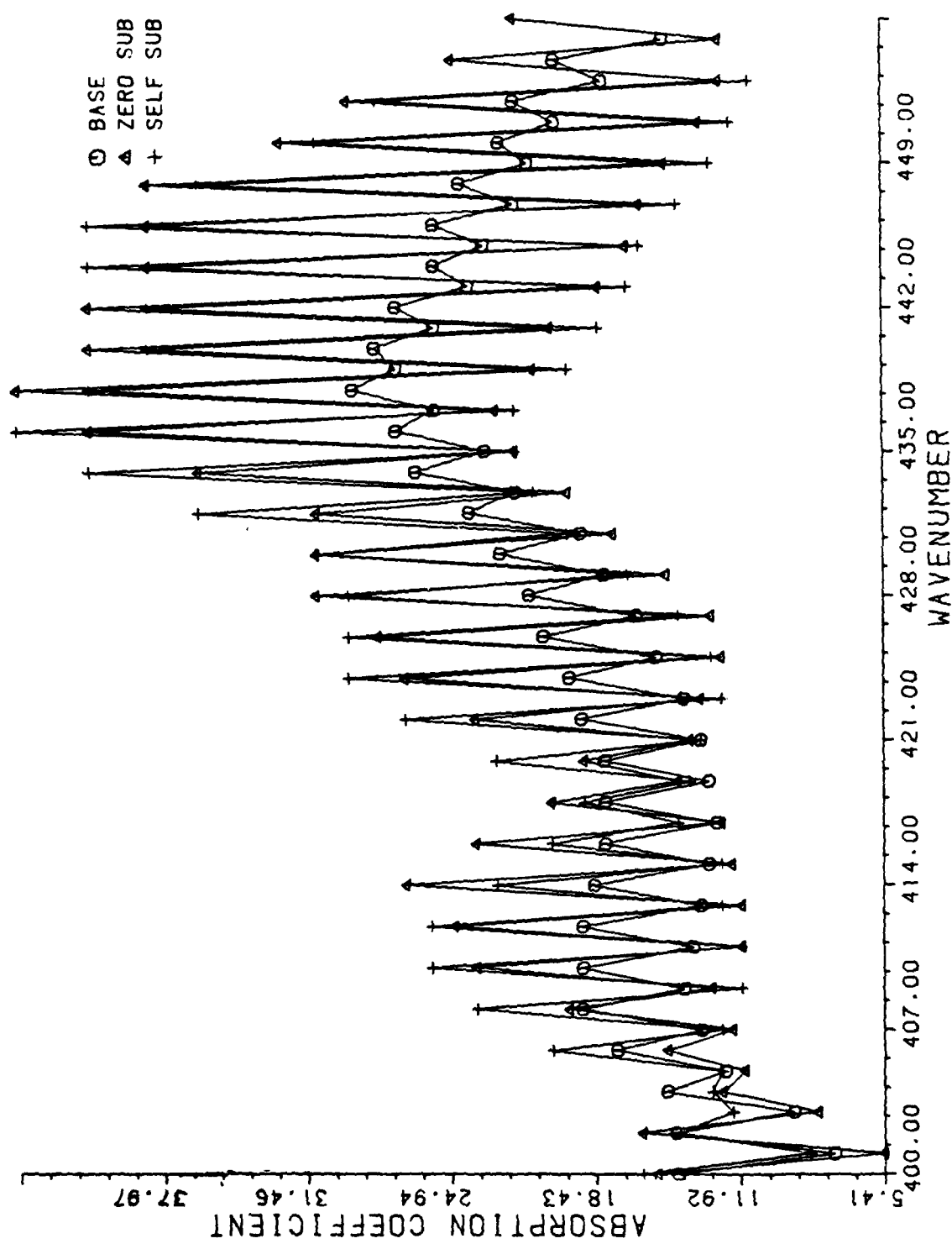


Figure 7: SIDEBURST program.

place.

4. More experience should be gained with the programs FRINGELIM and SIDEBURST so that the "glitch" responsible for the channeling could be identified. These programs may then provide an alternative to the program now in use in some cases.
5. The possibility that there is some relationship between the weighting factor and some physical property of the samples should be investigated.

REFERENCES

1. Born, M., and E. Wolf, Principles of Optics, New York, The Macmillan Company, 1964.
2. Buckley, R. G., and D. Beaglehole, "Absorptance of thin films", Applied Optics, Vol. 16, No. 9, September 1977, pp. 2495-2499.
3. Heavens, O. S., Optical Properties of Thin Solid Films, New York, Dover Publications, Inc., 1965.
4. Loewenstein, E. V., and D. R. Smith, "Optical Constants of far infrared materials. I: Analysis of channeled spectra and application to Mylar", Applied Optics, Vol. 10, No. 3, 1971, pp. 577-583.
5. Motooka, T., "Analysis method for optical properties of thin layers on thick transparent substrates", Journal of the Optical Society of America, Vol. 71, No. 7, 1981, pp. 884-886.
6. Manifacier, J. C., J. Gasiot and J. P. Fillard, "A simple method for the determination of the optical constants n , k and the thickness of a weakly absorbing thin film", Journal of Physics E: Scientific Instruments, Vol. 9, 1976, pp. 1002-1004.

1986 USAF-UES Summer Faculty Research Program/
Graduate Student Summer Support Program

Sponsored by the
AIR FORCE OFFICE OF SCIENTIFIC RESEARCH
Conducted by the
Universal Energy Systems, Inc.

FINAL REPORT

A Modification of the ACSYS Preprocessor Code
for use with the SAMSON2 Finite Element Program

Prepared by: Brad L. Halverson
Academic Rank: Graduate Student
Department and University: Department of Civil and
Environmental Engineering
Washington State University
Research Location: Air Force Weapons Laboratory,
NTE Civil Engineering Research Division,
NTES Applications Branch,
Structural Response Section
USAF Researcher: Mr. Douglas R. Seemann
Date: August 7, 1986
Contract No: F49620-85-C-0013

A Modification of the ACSYS Preprocessor Code
for use with the SAMSON2 Finite-Element Program

by

Brad L. Halverson

ABSTRACT

A finite-element preprocessor code called ACSYS has been modified to be compatible with SAMSON2, a powerful finite-element program owned by the Air Force Weapons Laboratory. This new modified code, known as SAMI, has undergone preliminary testing and appears to work satisfactorily. Because the SAMI code is so dynamic in its operation, all phases of the development of an input file could not be pursued in the ten week time period. There may still be minor errors in the SAMI code. These errors will undoubtedly be discovered as the code is used by AFWL personnel. The long-range objective of the Air Force is to integrate several, multi-purpose preprocessor codes, such as SAMI, into a complete interactive interface for the development of input for a wide range of finite-element programs.

ACKNOWLEDGMENT

In developing a proper acknowledgment, I began to list those that have not only been important in my summer fellowship; but also to those who, through their cumulative effort, have enabled me to receive this opportunity. My list became quite long. I, therefore, present this abridged version.

At the top of the list is Dr. Harold C. Sorensen. He has been my academic benefactor for the last couple of years. A close second, due only to the lack of limelight, are my parents. Their sustaining logistical support has been essential and has often been unrecognized.

Thanks also go to several employees at NTES: Mr. Douglas Seemann and Lieutenant Larry Schoof. Doug gave me the freedom and subtle encouragement to get the project finished, and Larry provided the technical assistance to get me over the occasional obstacles.

Although we have never actually met, I would like to give credit to Mr. Gaymond Yee for developing a very readable program. It made my task significantly easier.

Finally, I would like to thank the Air Force Systems Command, the Air Force Office of Scientific Research, and the Air Force Weapons Laboratory. Without the support and constructive environment of these organizations, none of my efforts could have come to fruition.

To these and many more, I say thank you.

I. Introduction

I am a first year graduate student at Washington State University specializing in structural engineering. I graduated from WSU with a BSCE in December, 1985. While at WSU, I gained computer programming experience in the FORTRAN and BASIC languages.

In the Spring, 1986, Dr. Harold C. Sorensen informed me of a possible internship with the Air Force Weapons Laboratory (AFWL) and a related research project for graduate school. Since I was desirous of an opportunity to advance my education and pursue a position combining my background with computers, I accepted the offer.

The AFWL has a finite-element program called SAMSON2 designed primarily for dynamic analyses of plane and axisymmetric solids. Unfortunately, the input data for this code are cumbersome and require a great deal of time to prepare. AFWL also possesses another finite-element program called DYNA3D for which a convenient preprocessing code, ACSYS, exists. The decision was made by AFWL to modify ACSYS to be compatible with SAMSON2. This would save time in the development of the input file and reduce errors by automatically formatting the data.

II. Objectives

I wanted to accomplish several things during my 10-week tenure at the AFWL. The most important of which was to

complete the necessary modifications to the ACSYS preprocessor code for compatibility with SAMSON2. Once that was completed, I could enhance the code by making it more interactive with the user (i.e. less dependent on the manual) and by installing preventive measures to avoid input errors. The third step was to make the code more clear. This would provide a better understanding of what the program requires and less guesswork by the user. Finally, I wanted to make the program more readable by placing comment statements before procedures into the code. This would make it easier for the individual who might follow up on my work to correct any mistakes that may still exist in the code.

One objective that I was unable to accomplish due to the time element was to make the program usable on all the various terminals in AFWL. As it now exists, the program will only operate on one terminal; namely, the Visual 500.

III. Adaption of the Code to the AFWL System

The ACSYS preprocessor code existed on an IBM compatible floppy disk. Unfortunately, the program was written in FORTRAN77 and could not be compiled on an IBM personal computer. Hence, I transferred the code to AFWL's HP9000 mainframe computer. In the process, due to the speed of the transfer, several lines were partially deleted. These lines had to be located and rewritten.

ACSYS contains a subroutine that allows single character input without a carriage return using the intrinsic functions of the IBM computer. Because FORTRAN77 has no command to do this, Lieutenant Schoof wrote a simple subroutine for me in the C language to accomplish this procedure. There is another subroutine in ACSYS that outputs a character string to the terminal without a carriage return using intrinsic functions. This was easily modified in the FORTRAN language. These two subroutines make the modified code system dependent to the HP9000.

There were several screen controls that ACSYS used in order to interface with the user. One of these, a scrolling region that is used as a window/work area, could only be programmed on one type of terminal available at the AFWL; namely, the Visual 500. Along with the scrolling region, video attributes, such as reverse video and bold type, had to be programmed using Visual 500 escape sequences. Therefore, the modified code is only operable on the HP9000 system in conjunction with the Visual 500 terminal.

IV. Background of ACSYS:

The format of the ACSYS preprocessing code uses a single screen whereby the user can select a menu, select data, or input data. The format of the screen is shown in figure 1. I have used the exact same format in the modification.

Each row or set of rows on the screen has a distinct and

unchanging role. The header line gives the general purpose of the menu that has been selected. The command line is not used in the program and has been installed for future use in ACSYS. A list of selections appears on the menu line including a RETURN option that is always displayed at the far left. In ACSYS, the "=>" and "<=" keys are used to move the cursor to a particular selection which appears in reverse video. The modified code, SAMI, uses the "a" (left) and "f" (right) keys. The menu description lines give an

		Row
	(Header Line)	1
SAMI>	Command Line	2

	Menu Line	4

	Menu Description	6
	Lines	7
=====		
	(Information Line)	9
=====		
		11
		12
		13
		14
		15
		16
	Window/Work Area	17
		18
		19
		20
		21
		22
		23
	Instruction Line	24

Figure 1. Screen Format

expanded explanation of the menu selection. Usually, a short description is presented on row 6 and the record numbers of the affected input file on row 7. The accompanying SAMSON2 users' manual is organized according to these record numbers. The information line is divided into three sections. At the left, the input class (described in section V) that has been entered is shown. The middle of the line will display the mode which is currently active the user is currently in. The three modes are: DEFINE new data, MODIFY old data, and DELETE old data. The title of the input data card appears at the right.

The format of the window/work area and the instruction line will depend on the type of user interface menu. When the user is in the SAMI selection menu, a HELP message will be printed in the window area that will assist the user in the decision making process. The instruction line will indicate which command keys to press: ENTER to activate a selection and TAB to return to the previous menu. For the actual input of data, there are two interface menus: data selection and data entry. The former will list in the work area, in alphabetic sequence, the choices of data from which to select. In the instruction line, there will be a prompt to select a data entry. When an alpha key is entered, the corresponding character will be shown in reverse video by the selected item. Also, it will give instructions for two

command keys. The slash key, "/", will list more data selections if all the items cannot fit on one page. The TAB key will activate the selection (the RETURN will also work but is not shown). In the data entry menu, a list of data value prompts will be displayed in the work area. If the user is in the MODIFY mode, existing values will be shown next to the prompts. Otherwise, the data fields will be left blank. Similar to data selection, the instruction line will give a prompt asking for an item for entry. Once an alpha key is pressed, the cursor will be positioned to the right of the chosen value prompt, waiting for the input of a value or character string. Once the data have been entered for this scrolling region, the TAB key should be pressed to continue.

Examples of this screen format and the three user interface menus are shown in section V.

V. SAMI: The Modified Code

Because I wanted to maintain as much similarity as possible between ACSYS and the new modified code, SAMI, I kept many things the same; such as general procedures and subroutines. For a more in-depth discussion of ACSYS which, in many respects, can be applied to SAMI, see reference 1.

The development of an input file is divided into five independent classes. Each class can be entered in any order by entering the SAMI selection menu (figure 2). Once a class has been chosen, the user can begin to input data. As

```

SELECT AN INPUT CLASS
SAMI>
-----
RETURN: PROBLEM : OUTPUT : MATERIAL : GEOMETRY : BOUNDARY
-----
Return to previous menu.

=====
=====

*****HELP*****

Select the input class for which you want to provide data.
Moving the cursor along the choices will reveal expanded
descriptions of each input class. In general, these classes
have been chosen to reflect physically meaningful data
groupings. All input uses the global data that you provided
at the beginning of the session. Use the "a"(left) and
"f"(right) keys to select the input class that you wish to
enter, strike the "ENTER" key.

ENTER to activate selection  TAB to return to previous menu

```

Figure 2. Main SAMI Selection Menu

mentioned in the previous section, there are two methods in which to do this; data selection and data entry.

As an example problem, assume the user is presently in the main SAMI selection menu and wishes to enter the geometry input class. He/She simply positions the cursor to GEOMETRY and presses the TAB key. A series of menus will be displayed asking for directions or data input. From


```
SELECT POLAR COORDINATE OPTION  
SAMI>
```

```
-----  
      |  DEFINE  |  
-----
```

```
DEFINE new NODAL POINT cards.
```

```
=====
```

GEOMETRY INPUT CLASS	DEFINE
=====	

- A. NO SELECTION
- B. ELLIPTIC INTERPOLATION
- C. LINEAR INTERPOLATION
- D. AVG OF ELLIPTIC AND LINEAR INTERPOLATION
- E. STRAIGHT LINE INTERPOLATION

```
Select item:  Enter / more items  Enter TAB to activate item
```

Figure 3. Data Selection Menu

these, as shown in figure 3, is a data selection menu. At the top of the screen, the header line instructs the user to select a polar coordinate option. The window/work area lists the various choices, including a no selection option, from which the user can select. Once the TAB key is depressed, the associated value of the selection is placed in its proper location in the input file. A sample data entry menu is shown in figure 4. The user can select an item for entry and input a value next to the data prompt. He/She repeats this procedure until he/she is satisfied with the data. Blank

```
ENTER NODAL POINT DATA
SAMI>
```

```
-----
      !  DEFINE  !
-----
```

```
DEFINE new NODAL POINT cards.
```

```
=====
GEOMETRY INPUT CLASS          DEFINE
=====
```

```
A.  NODE NUMBER!I           :
B.  GENERATED COORDINATE SPACING OPTION!I :
C.  X-COORDINATE OF NODE!R   :
D.  Y-COORDINATE OF NODE!R   :
E.  X-COORDINATE OF POLAR COORDINATE ORIGIN :
F.  Y-COORDINATE OF POLAR COORDINATE ORIGIN :
```

```
Select item for entry :
```

```
Enter TAB to continue
```

Figure 4. Data Entry Menu

entries will be entered as zeros in the input file. To exit the menu, the user once again presses the TAB key.

The advantage of the three menu organization is that the format is constant throughout code. The user needs only to learn three menus to execute the entire program. Little time is required for orientation.

At the end of the program, the user can either save the data that were entered in the current session or save the existing input file that was entered at the beginning of the program. There are two safeguards to prevent a mishap at

this point. First, the code will display the name of the input file that is either being defined or modified and ask if this is the correct file name. The second safeguard will inquire whether or not the user intends to overwrite the old file (if it exists) with the new modified file.

VI. Recommendations

The execution of SAMI requires a scrolling region to display help messages and input data. The only terminal on which this scrolling capability was available was the Visual 500. Therefore, the code will only operate on this one terminal.

SAMI has the ability to define, modify, or delete data. Of these three modes, defining has the least chance of error. The data are recorded in the order in which in each particular input class is entered. There is no "shifting" of the data records. In the delete mode, a set of records, is removed from the input file and the remaining cards are shifted to replace the ones deleted. Intuitively, this requires extra programming, but I am confident that the delete mode is error free. The modification of data is where possible errors are most likely to occur. Records can be created or deleted and transferred from one location to another. If one record is put in the wrong place, the remaining records in that input class will be in error.

There are many ways to produce an input file. Not all of the permutations could be tested in the 10 week period. The SAMI preprocessor code will have to stand the test of time in order to become completely debugged.

I strongly suggest that the SAMSON2 user's manual (reference 3) be used simultaneously while operating SAMI. The input data are organized by card numbers in this manual. These numbers are displayed on the screen during execution. The manual also gives an expanded description of the input data and can provide the user with more detailed information.

The SAMSON2 code needs to have two read statements reformatted from '15I5' to '16I5'. The subroutines in SAMI are organized such that long strings of data, such as movie output time steps, are conveniently inputted sixteen at a time.

REFERENCES

1. Yee, Gaymond, Hofmann, Ronald, "ACSYS, A preprocessor for Generically Similar Finite-difference and Finite-element Codes," Science Applications International Corporation, San Leandro, California, March 1986.
2. Hallquist, John O., "DYNA3D Users Manual (Nonlinear Dynamic Analysis fo Solids in Three Dimensions)," Lawrence Livermore National Laboratory, University of California, April 1984.
3. Schreyer, Howard L., Richards, Charles G., Bean, James E., Durka, Georgine R., "SAMSON2, A Nonlinear Two Dimensional Structure-Media Interaction Computer Code: Users Manual (Update)," New Mexico Engineering Research Institute, University of New Mexico, June 1984.

1986 USAF-UES SUMMER FACULTY RESEARCH PROGRAM/
GRADUATE STUDENT SUMMER SUPPORT PROGRAM

Sponsored by the
AIR FORCE OFFICE OF SCIENTIFIC RESEARCH

Conducted by the
Universal Energy Systems, Inc.

FINAL REPORT

Automation of the Method of Optimal Design

Prepared by:	Charles Reif Hammond
Academic Rank:	Ph. D. Graduate Student
Department and	Mechanical and Materials Engineering
University:	Vanderbilt University
Research Location:	Arnold Engineering Development Center
USAF Researcher:	H. LeRoy Henderson
Date:	July 14, 1986
Contract No:	F49620-85-C-0013

Automation of the Method of Optimal Design

by

Charles Reif Hammond

ABSTRACT

The Method of Optimum Design is a systematic, non-numerical approach to constrained, nonlinear, optimization. In this method the mathematical characteristics of the optimization model are studied to determine the optimal solution of the problem. While the optimal solution to the problem is guaranteed to be correct in this method, much work is required of the analyst to develop this solution. This report describes the steps necessary to automate the Method of Optimal Design and the work that has been completed towards this goal. A companion report by Dr. G. E. Johnson presents the work on the automated optimal design of reinforced concrete footings.

ACKNOWLEDGMENTS

The sponsorship of the Air Force Systems Command and the Air Force Office of Scientific Research is gratefully acknowledged. We appreciate the space provided for us in the Design Engineering group of Schneider Systems International at the Arnold Engineering Development Center. Special thanks are due to Mr. Marshall K. Kingery, USAF, for his help and encouragement throughout this summer project.

I.

INTRODUCTION

Mr. Hammond has been involved in the development of nonlinear programming software since 1980 as an undergraduate at the University of Virginia. He has written software for automated signature analysis of mechanical vibrations from anti-friction bearings in paper manufacturing machines and he completed an extensive optimization study of journal bearings as part of his master of science program at the University of Virginia. He is presently working toward a Ph.D. degree at Vanderbilt and his dissertation research project is the development of an automated procedure (based on symbolic manipulation software) to set up and solve nonlinear optimization problems in mechanical design.

We have been assigned to the Design Engineering group (part of Schneider Services International) in the Model Shop at AEDC. This group is production oriented and their mission appears to be to provide support for the physical plant. We are aware of their involvement in the design of foundations, structures, electrical, and HVAC systems. They are currently using some computer based design methods for HVAC work, and they have a computer aided drafting group with several workstations. They may provide design services in other areas as well. We were assigned to this group because of our mutual interest in design and design methodology.

II.

OBJECTIVES OF THE RESEARCH EFFORT

Our goal was to identify some specific design problems at AEDC and to develop computer based design strategies for those problems. The development of an expert system for design was also to be considered. Automation of the Method of Optimal Design[16] involves

the implementation of the knowledge of an expert in a computer program.

III. METHOD OF OPTIMAL DESIGN

The Method of Optimum Design (Johnson's Method) is a systematic, non-numerical approach to constrained optimization. Unlike numerical optimization methods, the Method of Optimum Design results in a general solution to the problem, instead of a local optimal point. This general solution can be used to determine the optimal solution for any numerical case. Thus, once the general problem has been solved, very little effort is required to identify the optimal design for specific cases.

The Method of Optimum Design shares characteristics with the Generalized Reduced Gradient method. The designer must identify a set of "decision variables" (related parameters) to define a suitable space on which to project constraints and conduct the optimization search. The remaining "state variables" (eliminated parameters) are defined in terms of the decision variables. There are a finite number of partitions of the design variable vector and each partition leads to a specific equation system (called a final reduced form) and space for constraint projection.

Each final reduced form has the same solution points as every other possible final reduced form. However, the mathematical properties of the final reduced forms can vary significantly. Accordingly, some partitions can lead to the construction of very simple solution algorithms, while others may prove to be virtually impossible. This results from the fact that some final reduced forms are better behaved than

others. Some final reduced forms may actually provide a convex or even a linear constraint set which can lead to the simple solution algorithms.

In the Method of Optimum Design the designer does the analysis in two distinct steps. In the first step the designer selects the decision and state variables and reformulates the problem so that the state variables are functions only of the decision variables. At this time, any free (unconstrained) variables are treated by substitution or inspection.

In the second step the equations developed in the first step are studied to determine which constraints can be active at the solution. This step is also known as the variational study. The active constraints can then be considered as if they were equality constraints to define possible solution points. This reduces the dimensionality of the problem and can lead to a set of candidate optimal points.

There can be many different final reduced forms since different variables can be selected as the state and decision variables. It is desirable to pick the state and decision variables such that a well behaved final reduced form is obtained to facilitate the variational study. In practice, this can only be done by trial and error, ie., by developing several final reduced forms for comparison. However, much effort is usually required to develop a single final reduced form. Thus, in practice, normally only one final reduced form is considered and the designer will struggle with it instead of deriving another. An automated method of generating the final reduced form would give the designer the ability to generate different final reduced forms until an acceptable formulation is found.

The variational study is not necessary in completely monotonic problems where all of the final reduced forms can be generated. In these problems analysis of each design equation yields a possible solution point. This analysis consists of simply determining whether the magnitude of the design equation increases or decreases with changes in each variable. Analysis of all of the design equations yields all of the possible optimal points. This can be shown with a trivial spring design example.[16]

$$\text{Maximize: } \Delta = R^3 / b \quad \text{Design Equation}$$

$$y = R / b \quad \text{Equality Constraint}$$

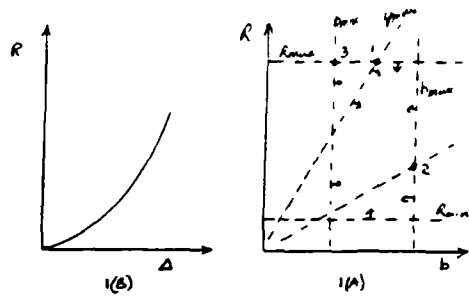
subject to:

$$y \leq y_{\max}$$

$$R_{\min} \leq R \leq R_{\max}$$

$$b \leq b_{\max}$$

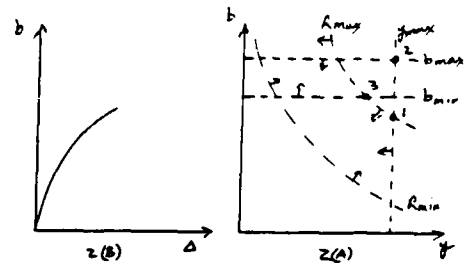
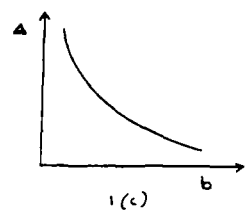
Inspection of the design equation shows that to maximize Delta it is desirable to make R as large and b as small as possible. However, in doing so it is possible to run into the upper limit on R or y. The possible optimal solution points for this problem formulation can be determined with a variational study such as in Fig. 1. Figures 1b and 1c show that when all else is held constant, Delta increases with decreasing b and increasing R. The limits are projected on Figure 1a. Inspection shows that the solution point will be along the line $y=y_{\max}$. Solving $y=R/b$ for R and substituting into $\Delta=R^3/b$ we find that along $y=y_{\max}$, $\Delta=b^2/y_{\max}^3$. Thus to maximize Delta along $y=y_{\max}$, b should be maximized. The two possible solution points are then (1) $y_{\max} R_{\max}$ and (2)



$$\uparrow \Delta = \frac{R^2}{b}$$

$$y = \frac{R}{b}$$

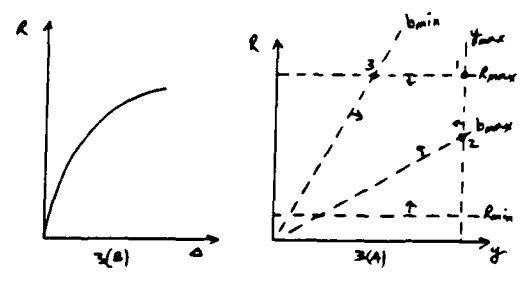
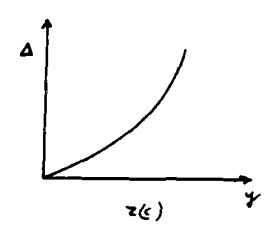
Figure 1.



$$\uparrow \Delta = y^2 b^2$$

$$R = y b$$

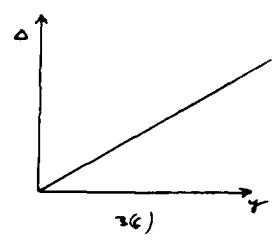
Figure 2.



$$\uparrow \Delta = R^2 y$$

$$b = R/y$$

Figure 3.



$y_{\max} b_{\max}$. If there was a lower limit on b then a third possible point would be (3) $b_{\min} R_{\max}$.

Another partition of the problem would be for y and b to be the decision variables and R to be the decision variable. For this partition, $\Delta = y^3 b^2$ and $R = y \cdot b$. The variational study for this partition is shown in Figure 2 and the analysis is similar to that for the previous partition.

The third partition is when b is the state variable and R and y are the decision variables. In this case, $\Delta = R^2 y$ and $b = R/y$. The corresponding variational study is in Figure 3. This variational study is less difficult than the other two since it is not necessary to determine which way Δ trends along one of the projected constraints.

Comparisons of these three variational studies show that the solution points are the same for each partition, even though the analysis is easier in some partitions than in others. Comparisons of the three design equations brings out an interesting point. The first design equation, $\Delta = R^3/b$, corresponds to point (3), $b_{\min} R_{\max}$. The second design equation, $\Delta = y^3 b^2$, corresponds to point (2), $y_{\max} b_{\max}$. The third design equation, $\Delta = R^2 y$, corresponds to point (1), $y_{\max} R_{\max}$. Thus, it would have been possible to determine the solutions without ever having to plot anything. This holds true for all monotonic problems. Thus, this method can be extended to problems of higher dimensionality that cannot be plotted. The major drawback to the analysis of optimization problems by generating solutions for all of the partitions is the major amount of effort required to do all of the algebra and calculus.

IV.

ANALYSIS BY MULTIPLE PARTITION GENERATION

It is desirable to develop a procedure to automatically generate the reduced form for all partitions. If these could be generated symbolically by a computer then the effort required of the designer would be reduced. Information taken from all of the partitions could be used to solve the problem or to give further insight towards the optimal solution.

A problem that has been transformed into a final reduced form can be further manipulated to produce the other reduced forms. For example:

PROBLEM:

Maximize: $M = x^2 * y$

Subject to:

Equality Constraints: $a = x*y$

$b = y/x$

Trivial Constraints: $a_{\min} \leq a \leq a_{\max}$

$b_{\min} \leq b \leq b_{\max}$

$x_{\min} \leq x \leq x_{\max}$

$y_{\min} \leq y \leq y_{\max}$

This is an imaginary problem with two decision variables, x and y , and two state variables, a and b . There are three distinct steps required to develop all of the final reduced forms:

STEP 1 The first step is to determine the possible partitions of the design space for all other reduced forms.

State	Decision
a b	x y (initial case)
a x	b y
a y	b x
b x	a y
b y	a x
x y	a b

STEP 2 The equations in the system of equality constraints are combined to produce new equations that are in terms of every possible variable combination. For example, if the system of equality constraints is:

$$\begin{aligned} a &= x*y \\ b &= y/x \end{aligned}$$

then

$$\begin{aligned} x &= a/y, & y &= a/x \\ x &= y/b, & y &= x*b \end{aligned}$$

which leads to:

$$\begin{aligned} a/y = y/b &\rightarrow a = y^2/b, \quad b = y^2/a, \quad y = (a*b)^{(1/2)} \\ a/x = x*b &\rightarrow a = x^2*b, \quad b = a/x^2, \quad x = (a/b)^{(1/2)} \end{aligned}$$

These equations are then grouped by partition:

State	Decision	Equality Equations	
a b	x y	$a = x*y$	$b = y/x$
a x	b y	$a = y^2/b$	$x = y/b$
a y	b x	$a = x^2*b$	$y = x*b$
b x	a y	$b = y^2/a$	$x = a/y$
b y	a x	$b = a/x^2$	$y = a/x$
x y	a b	$x = (a/b)^{(1/2)}$	$y = (a*b)^{(1/2)}$

STEP 3 In the last step the equations in STEP 2 are inserted into the design equation to develop the different design equations for each partition:

State	Decision	Design Equations
a b	x y	$M = x^2 * y$
a x	b y	$M = y^3 / b^2$
a y	b x	$M = x^3 * b$
b x	a y	$M = a^2 / y$
b y	a x	$M = a * x$
x y	a b	$M = a^{(3/2)} / b^{(1/2)}$

Thus the equality constraints and design equations have been developed for each partition. The work required to automate STEP 1 was completed previous to the work done at Arnold Engineering Development Center. STEP 2 was automated at Arnold and is discussed in the next section. STEP 3 and analysis of the results will be future work.

V. EQUALITY CONSTRAINT COMBINATION

Our work this summer has involved the development of an automated method to combine the equality constraints to produce all possible equation combinations. This is STEP 2 outlined above.

The first step in the creation of all of the possible final reduced forms from one final reduced form is the combination of the equality design equations in such a way that each variable is expressed in terms of all of the other possible variables. For

example, if the equality design equations in the original final reduced form were:

$$a = f_1(x, y, z) \quad (1)$$

$$b = f_2(x, y, z) \quad (2)$$

$$c = f_3(x, y, z), \quad (3)$$

then the other possible combinations would be:

$$a = f_4(b, x, y) \quad (4)$$

$$a = f_5(c, x, y) \quad (5)$$

$$b = f_6(c, x, y) \quad (6)$$

$$a = f_7(b, x, z) \quad (7)$$

$$a = f_8(c, x, z) \quad (8)$$

$$b = f_9(c, x, z) \quad (9)$$

$$a = f_{10}(b, y, z) \quad (10)$$

$$a = f_{11}(c, y, z) \quad (11)$$

$$b = f_{12}(c, y, z) \quad (12)$$

$$a = f_{13}(b, c, x) \quad (13)$$

$$a = f_{14}(b, c, y) \quad (14)$$

$$a = f_{15}(b, c, z) \quad (15)$$

where f_i is the functional relationship between the variables. Variables a , b , and c are referred to as the state variables in the original final reduced form. Likewise, x , y , and z are referred to as the decision variables. This is a problem in more variables than the previous problems to better show the required steps to combine the equations.

Each of the equations, 1 - 15, are in terms of four variables. For example, equation (4), $a = f_4(b, x, y)$, is in terms of a , b , x , and y . Thus, equation (4) is considered a combination of these four

variables, and can be solved for each of the variables in turn to produce three more equations.

$$a = f_{4a}(b, x, y) \quad (16)$$

$$b = f_{4b}(a, x, y) \quad (17)$$

$$x = f_{4x}(a, b, y) \quad (18)$$

$$y = f_{4y}(a, b, x) \quad (19)$$

These four equations, 16 - 19, are relatively easy to generate, the original equation is simply solved for each variable in turn. The development of equations 4 - 15 is a little more difficult. To determine equation (4), equations (1) and (2) are solved for z and set equal to each other:

$$z = f_{1z}(a, x, y) \quad (20)$$

$$z = f_{2z}(b, x, y) \quad (21)$$

$$f_{1z}(a, x, y) = f_{2z}(b, x, y) \quad (22)$$

Equation (22) is in terms of a , b , x , and y and can be solved for each variable in turn to produce equations 16 - 19. Thus, to develop each of the possible equation combinations, two equations that contain the variables in the desired equation, and a common variable that is not in the desired equation, are solved for that common variable and equated.

The pairs of equations that can be used to generate further equations are determined in advance. The first step is to generate the table of all possible variable combinations. In this case there are six variables taken four at a time (four variables per equation). For six objects taken four at a time,

there are fifteen possible combinations:

$$\frac{N_o!}{N_t! * (N_o - N_t)!} = \frac{6!}{4! (6-4)!} = 15$$

where

N_o = Number of Objects

N_t = Number of Objects at a Time

ROW	SECTION	Combination Variables	Eliminated Variables	From Sections	EQN #	

1	1	[1 4 5 6]	[2 3]	[]	(1)	
		[2 4 5 6]	[1 3]	[]	(2)	
		[3 4 5 6]	[1 2]	[]	(3)	

2	1	[1 2 4 5]	[3 6]	[1]	(4)	
		[1 3 4 5]	[2 6]	[1]	(5)	
		[2 3 4 5]	[1 6]	[1]	(6)	
	+++++					
	2	[1 2 4 6]	[3 5]	[1]	(7)	
		[1 3 4 6]	[2 5]	[1]	(8)	
		[2 3 4 6]	[1 5]	[1]	(9)	
	+++++					
	3	[1 2 5 6]	[3 4]	[1]	(10)	
		[1 3 5 6]	[2 4]	[1]	(11)	
		[2 3 5 6]	[1 4]	[1]	(12)	

3	1	[1 2 3 4]	[5 6]	[1 2]	(13)	
	+++++					
	2	[1 2 3 5]	[4 6]	[1 3]	(14)	
	+++++					
	3	[1 2 3 6]	[4 5]	[2 3]	(15)	

TABLE 1.

Table 1 lists all of the combinations of six objects, 1, 2, 3, 4, 5, 6, taken four at a time. The objects not included in each combination set are in the second column. The last column, From Sections, will be explained later. The From Sections column is generated by taking combinations of the section numbers from the previous row. In the present problem, 1 corresponds to

a, 2 to b, etc. This table has been divided up into rows and sections within the rows. The row number corresponds to the number of the original state variables in the combinations in that row. Each section has a different set of decision variables, but the same sets of state variables.

The first row, ROW 1, contains the equality design equations from the original final reduced form. These equations need only be solved for each of the variables that they contain.

The equations in ROW 2 are generated from the equations in ROW 1. There is only one possible pair of equations that can be combined to form each of these equations. The first two indices in the Combination Variable column refer to the equations in ROW 1 to be combined. To combine two equations a variable must be eliminated, which is the variable contained in the two original equations that does not appear in the resulting equation. This is the second variable listed in the Eliminated Variable set corresponding to the desired equation. For example, the equation (4) is generated by combining equations (1) and (2) with variable number 6, z, eliminated.

While the equations in ROW 2 can only come from the combination of a specific pair of equations, the equations in ROW 3 and higher numbered rows can come from the combinations of many different pairs of equations. For example, let's look at equation number 13. Equation number 13 is a combination of [1 2 3 4]. This combination can come from the combination of any two equations in ROW 2, SECTION 1 with variable 5 eliminated, or any two equations in ROW 2, SECTION 2 with variable 6 eliminated. The third column in Table 1, From Section, lists the sections in

the previous row that the pairs can come from. If there were a fourth row, the From Section column would contain [1 2 3], [1 2 4], [1 3 4], etc. These groupings are generated by taking all of the combinations of the number of sections in the previous row taken the number of section minus one at a time.

The eliminated variable for each section can again be found from the eliminated variable column. The last variable in the list corresponds to the variable eliminated in the first section, the next to last variable corresponds to the variable variable to be eliminated in the next section, and so on.

This method of combining the equality equations is well suited to implementation in a computer algebra system to automate the combinations.

The work required to develop an automated method of generating all of the final reduced forms is approximately halfway complete. The next part of this work should involve the development of an automated method to combine the new forms of the equality constraints with the design equations to produce all of the final reduced forms. Once this has been completed then automated methods should be developed to analyze these new final reduced forms. In addition, methods to automatically convert an initial problem formulation to a final reduced form need to be developed.

In the long term, the development of an automated method to set up and solve nonlinear optimization problems in engineering design is a worthwhile goal. The existence of such software would greatly reduce the effort required to develop optimum design programs for specific mechanical devices and systems. We expect to submit a proposal to continue our work on the expert design system through the mini grant program.

REFERENCES

- 1) Johnson, R. C., "Three Dimensional Variation Diagrams or Control of Calculations in Optimum Design," ASME, Journal of Engineering for Industry, Aug 1967, pp. 391-98.
- 2) Wilde, D. J., "Monotonicity and Dominance in Optimal Hydraulic Cylinder Design," ASME, Journal Engineering Industry, Vol 97, No. 4, Nov 1975, pp 1390-1394.
- 3) Ellis, J., "Johnson's Method of Optimal Design Applied to a Problem with Simple Functional Relationships," Computer Aided Design, Vol. 8, No. 1, Jan. 1976, pp. 9-12.
- 4) Wilde, D. J., "The Monotonicity Table in Optimal Engineering Design," Engineering Optimization, Vol. 2, No. 1, 1976, pp. 29-34.
- 5) Papalambros, P., and Wilde, D. J., "Global Non-Iterative Design Optimization Using Monotonicity Analysis," Journal of Mechanical Design, Vol. 101, Oct 1979, pp. 645-649.
- 6) Johnson, R. C., "A Method of Optimum Design," Journal of Mechanical Design, Vol. 101, Oct 1979, pp. 667-673.
- 7) Papalambros, P. and Wilde, D. J., "Regional Monotonicity in Optimum Design," Journal of Mechanical Design, Vol 102, July 1980, pp. 497-500.
- 8) Ellis, J., "Small-Scale Design Optimization Using an Interactive Minicomputer," Journal of Mechanical Design, Vol 102, July 1980, pp. 524-528.
- 9) Papalambros, P. and Heng Lung Li, "Notes on the Operational Utility of Monotonicity in Optimization," Journal of Mechanisms, Transmissions, and Automation in Design, Vol. 105, June 1983, pp. 174-180.
- 10) Zhou, J. and Mayne, R. W., "Interactive Computing in the Application of Monotonicity Analysis," Journal of Mechanisms, Transmissions, and Automation in Design, Vol. 105, June 1983, pp. 181-186.

- 11) Azarm, S., and Papalambros, P., "A Case for a Knowledge-Based Active Set Strategy," Journal of Mechanisms, Transmissions, and Automation in Design, Vol. 106, Mar 1984, pp. 77-81.
- 12) Azarm, S., and Papalambros, P., "An Automated Procedure for Local Monotonicity Analysis," Journal of Mechanisms, Transmissions, and Automation in Design, Vol. 106, Mar 1984, pp. 82-89.
- 13) Zhou, J., and Mayne, R. W., "Monotonicity Analysis and the Reduced Gradient Method in Constrained Optimization," Journal of Mechanisms, Transmissions, and Automation in Design, Vol. 106, Mar 1984, pp. 90-94.
- 14) Papalambros, P. and Li, H. L., "A Production System for Use of Global Optimization Knowledge," Journal of Mechanisms, Transmissions, and Automation in Design, Vol. 107, June 1985, pp. 277-284.
- 15) Krishnaswami, P., and Bhatti, M. A., "Symbolic Computing in Optimal Design," presented at the ASME Design Engineering Division Conference on Mechanical Vibration and Noise, Cincinnati, Ohio, Sept 10-13, 1985, ASME paper 85-DET-76.
- 16) Johnson, G. E., Strategies For Optimal Design, Ph. D. Dissertation, Department of Mechanical and Materials Engineering, Vanderbilt University, Nashville TN, 1978.
- 17) Johnson, R. C., Optimum Design of Mechanical Elements, John Wiley and Sons, Inc., New York, NY, 1980.

1986 USAF-UES SUMMER FACULTY RESEARCH PROGRAM/

GRADUATE STUDENT SUMMER SUPPORT PROGRAM

Sponsored by the

AIR FORCE OFFICE OF SCIENTIFIC RESEARCH

Conducted by the

Universal Energy Systems, Inc.

FINAL REPORT

Empirical Confidence Intervals for a Validity Coefficient

Under Range Restriction: An Application of the Bootstrap

Prepared by:	Darren E. Hart
Academic Rank:	Doctoral Student
Department and	Department of Psychology
University:	Texas A&M University
Research Location:	Air Force Human Resources Laboratory/MOAE Brooks Air Force Base, TX
USAF Researcher:	Malcolm Ree
Date:	July 11, 1986
Contract No.:	F49620-85-C-0013

EMPIRICAL CONFIDENCE INTERVALS FOR A VALIDITY COEFFICIENT UNDER RANGE

RESTRICTION: AN APPLICATION OF THE BOOTSTRAP

by

Jorge L. Mendoza

with the assistance of

Darren E. Hart and Amy B. Powell

ABSTRACT

Efron's bootstrap procedure was utilized to develop two computer intensive techniques for constructing confidence intervals on the unrestricted correlation parameter under explicit predictor restriction. One procedure bootstrapped the corrected correlation coefficient to obtain the interval, while the other one relied on the frequency distribution of the applicant test scores to generate the bootstrap confidence interval. The techniques were evaluated using a Monte Carlo procedure. The study assessed the techniques under a number of hypothetical selection situations. The results showed that bootstrapping the corrected correlation coefficient is a reliable technique for obtaining confidence intervals for the population correlation under most selection situations.

ACKNOWLEDGEMENTS

We would like to thank the Air Force Human Resource Laboratory at Brooks AFB for sponsoring our research. All laboratory personnel associated with this project went out of their way to accomodate us. The atmosphere at the HRL not only facilitated our research efforts, but also made this summer an enjoyable one. We would also like to thank Malcolm Ree, Toni Wegner, John Welsh, Lonnie Valentine, and Jim Earles for their support and guidance.

I. Introduction

I received a B.S. in psychology from California State University Sacramento in 1984. My undergraduate research interests were focused on interpersonal attraction. I presented a paper entitled "Perception of Individual Traits as a Function of Attire" at the Western Psychological Association Convention in 1985. This paper is currently being revised for submission for publication.

I started the doctoral program in Industrial/Organizational Psychology at Texas A&M University in 1985. During my first year of graduate work, I was exposed to a wide variety of topics in the personnel psychology field. This exposure allowed me to narrow down my interests to personnel selection. I then formulated a thesis proposal which involved the selection of "participative" managers. These interests in personnel selection led me to pursue an internship at the Air Force Human Resources Laboratory.

II. Background

One of the oldest and most common problems in test validation is that of range restriction on the predictor due to explicit selection. Range restriction occurs when predictor and criterion data are available only for the selected group. This is a group that is systematically different from the applicant group mainly because of the organization's selection policy. The restricted variable for which data are missing has generally a restricted variance. Hence, the correlation between the predictor and the criterion in this group underestimates the validity of the test.

Investigators have been concerned with this attenuation problem for some time. Karl Pearson (1903) was the first to provide a

procedure to correct for the bias inherent in the selection process. Lawley (1943) relaxed the assumptions necessary for the correction, and Thorndike (1947) is accredited with bringing the procedure to the attention of psychologists. The Pearson correction formula for explicit selection is

$$r_c = \frac{S_r^2}{S_r^2 + S^2(1 - r)}$$

The " ' " indicates that the test variance and the correlation were computed in the selected group.

The correction procedure makes two assumptions: a) linearity of the regression of the criterion y on the test x , and b) homoscedasticity of the residual variances. Linn (1968) and Lord & Novick (1968) have pointed out that these assumptions are usually not met in practical settings. In general, departures from linearity tend to deflate the corrected correlation, while lack of homoscedasticity tends to inflate it. The correction is robust to lack of homogeneity of variances, but very sensitive to lack of linearity (Greener and Osburn, 1979). Nevertheless, some (Campbell, 1979; Linn, 1968) have suggested that it may be disadvantageous to adjust the correlation under such conditions.

Greener and Osburn (1979) found that while corrected correlations, for moderate to large unrestricted population correlations, are more accurate than uncorrected ones, they become less accurate as the proportion of selected individuals decreases. Using a Monte Carlo procedure, Brewer and Hill (1969) examined the correction under varying degrees of predictor skewness. They found that correction becomes less accurate as skewness and selectivity increase.

Others have investigated the correction under more general conditions. Alexander, et al (1984) have examined the robustness of the correction procedure when both the predictor and the criterion are truncated, and found that the procedure undercorrected in most circumstances. Gross and Fleishman (1983) found that when the selection process is incorrectly assumed to be based solely on the predictor, the corrected correlation is highly positively biased, and it is less accurate than the uncorrected correlation.

Olson and Becker (1983) claimed that the correction has the additional assumption of complete truncation, which is generally not met in applied settings. Complete truncation occurs when all of the observations falling above or below a certain point are lost from the applicant sample. Incomplete truncation or attrition, on the other hand, occurs when "it is possible to observe an individual at any point on the test or job performance distribution, but the probability that an observation is lost from the sample is related to test or job performance itself" (Olson & Becker, 1983, p157). It is likely that incomplete truncation more realistically represents practical situations. Incomplete truncation can appear in situations where there is no strict adherence to a cut off score, and/or when the selection is not based solely on the test score.

Although we know much about the performance of r_c , we know little about its standard error and its sampling distribution. Not knowing the sampling distribution has impeded researchers from testing hypotheses or constructing confidence intervals. The traditional sampling theory for the Pearson product moment coefficient is not appropriate for r_c (Forsyth, 1971).

Given the state of the art, it would be desirable to find either a procedure for obtaining confidence intervals on the unrestricted population correlation ρ , based on r_c , for situations where we know that r_c does a reasonable job and/or establish a procedure for obtaining an estimator of ρ that does not make the assumptions of r_c . Until now, the mathematics necessary for doing such a procedure have been prohibitive. But it can now be attempted using Efron's (1979) bootstrap procedure. In this paper we suggest two bootstrap procedures for setting confidence intervals on ρ and evaluate their effectiveness using a Monte Carlo simulation.

Efron's bootstrap procedure is a computer assisted nonparametric method to evaluate the precision of a statistic. The bootstrap procedure is implemented when parametric assumptions cannot be made regarding the population where the observations were drawn. The central feature of the procedure is the repeated generation of bootstrap samples. A bootstrap sample of size n is obtained by sampling at random and with replacement from one's original sample of size n . Each bootstrap sample is used to estimate the statistic of interest. Efron & Gong (1983) suggest that 200 bootstrap replications are sufficient for most applications. These bootstrap values are then used to estimate population parameters or set confidence interval. Excellent descriptions of the method can be found in Efron & Tibshirani (1984) and Lunneborg (1985). The bootstrap works because the sample data resembles the population from which they were obtained. Its use, of course, requires some degree of confidence in the sample.

III. Objectives

The purpose of the paper is two fold: a) to suggest and evaluate a procedure for constructing confidence intervals on r_c , based on r_c and, b) to suggest and evaluate a parametric free procedure for estimating r_c , which does not depends on r_c .

IV. Bootstrap confidence intervals

Two bootstrap procedures are presented. The first is a procedure for obtaining a confidence interval on r_c using the r_c . The procedure requires two bootstrap samples for each repetition, one from the applicant sample and one from the selected group. The second procedure does not rely on r_c , but instead relies on the applicant frequencies.

Bootstrapping the corrected r

The procedure can be summarized as follows:

- 1) Obtain a bootstrap sample of the applicant sample and compute the test variance S^2 .
- 2) Obtain a bootstrap sample of the selected group and compute the correlation r' between the test and the criterion. Also compute the variance S'^2 of the test.
- 3) Using equation (1) correct r' for range restriction using S and S' to obtain the bootstrap value r_c^* .
- 4) Repeat 1-3 two hundred times to obtain $r_c^{*(1)}$, $r_c^{*(2)}$, . . . , $r_c^{*(200)}$.
- 5) Rank order $r_c^{*(1)}$, . . . , $r_c^{*(200)}$ and count 5 from the top and 5 from the bottom to establish a 95% confidence interval. Efron (1981) calls this method of constructing confidence interval the percentile

method.

Bootstrapping using the applicant frequencies

The procedure is summarized below:

- 1) Obtain the frequency distribution of the test scores for the n applicants. Then, divide the range of test scores the into k equal intervals (e.g., 0-10, 11-20, 21-30, ... ,91-100) and count the number of individuals in each interval.
- 2) Obtain a bootstrap sample of the selected group using the applicant frequencies divided by n . For example, if there are 100 applicants in interval $I(3)$ and 500 in the total sample, then we would sample interval $I(3)$ with probability .20. Once $I(3)$ is selected then each individual in the interval has an equal probability of being selected. For $I(3)$, it would be $1/100$. This is similar to obtaining a quota sample.
- 3) Compute the correlation r^* in the bootstrap sample.
- 4) Repeat 1-3 two hundred times, rank order $r^*(1)$, $r^*(2)$, ... , $r^*(200)$ and construct the confidence interval.

V. THE MONTE CARLO

Under the assumption that the applicant sample resembles a random sample, we wrote a computer program which simulates the hiring process in an organization, to allow us to evaluate the general applicability of the bootstrap procedure to the attenuation problem in the selection paradigm. Given the paradigm, the bootstrap can be applied in a variety of ways. We developed two, both of which utilized information

from the applicant sample. (See the section on bootstrap.)

The Monte Carlo study investigated the behavior of the bootstrap corrected coefficient r_C^* for a number of bivariate distributions that represented the joint distribution of the criterion and predictor in the unrestricted population. The computer program sampled from the bivariate normal distribution, the contaminated bivariate normal (this distribution is symmetric but not normal) and from the bivariate gamma distribution, a skewed distribution.

The program started the simulation by drawing a random sample of size n (200) from a given bivariate distribution with correlation ρ . This random sample represented the sample of applicants. Each applicant had a test score and y (criterion) score. If the individual was selected later by the selection routine, the y score became the criterion score. If, on the other hand, the individual was not selected, the y score for that individual was discarded, resembling the situation where one has only criterion scores for those hired.

The selection routine selected "ns" individuals from the applicant sample according a set of attrition (conditional) probabilities. Table 1 contains the four sets of probabilities used in the study. Note that each set is composed of ten conditional probabilities. These probabilities were chosen to reflect four situations ranging from low-to-high selection and from low-to-high attrition. Next, ten equal intervals were obtained and each interval was then sampled according to its attrition probability. Individuals in the same interval had the same probability of being selected. However, individuals in high-scoring intervals had a higher chance of being selected than those in low-scoring intervals.

After the individuals were selected, the program began the

bootstrapping. The program, first, generated a bootstrap sample from the applicant sample and another one from the selected group. Then, it computed the bootstrap corrected correlation r_c^* . This process was repeated 200 times to generate $r_c^*(1)$, $r_c^*(2)$, ..., $r_c^*(200)$. By rank ordering the correlations and counting 5 from the top and 5 from the bottom, we identified the lower and upper 95% confidence bounds.

The second bootstrap correlation was obtained utilizing the frequency distribution of the applicant sample. The bootstrap sample was drawn so that it resembled the distribution of the test scores in the applicant sample. This was accomplished by creating ten intervals in both samples and counting the number of applicants that fell into each interval. This process yielded ten intervals in the applicant sample and ten corresponding intervals in the selected group. The sampling proceeded as follows. Suppose that out of 200 applicants, interval I(2) in the applicant sample had 20. Then, we would sample from interval I(2) in the selected group with probability .10. We repeated the procedure 200 times and used the median of $r^*(1)$, ..., $r^*(200)$ as the bootstrap estimate of , .

VI. Data Generation

One standard normal and one standard gamma random deviate generator from the Institute of Mathematical Statistical Library (IMSL) were used in the study. The normal routine was used to generate bivariate normal distributions and contaminated normals. We obtained the contaminated normal by mixing two normal distributions with weights .7 and .3. A total of two bivariate normal and two contaminated distributions were utilized in the study. The standard gamma routine was use to generate three standard gamma variables, x_0 ,

x_1 , and x_2 . By forming the variables $x_0 + x_1$, and $x_0 + x_2$, we obtained the bivariate gamma distribution. This distribution has a linear regression of y on x , but the homoscedasticity assumption does not hold. Two gamma distributions were used in the study. By reversing the attrition probabilities when we sample from the bivariate gamma, we simulated the effects of a negatively skewed distribution. Two sets of distributions were used, one set had $\rho = .50$ and the other had $\rho = .33$. We sampled 500 times from each distribution for each situation.

VII. Results

Tables 2 and 3 contain the Monte Carlo results. Each table displays in columns 2, 3, and 4 the average correlation for the restricted correlation, the bootstrap correlation (median r^*), and the corrected correlation, respectively. The number within the parentheses in columns 3 and 4 indicate percentage time that the confidence interval included the unrestricted population correlation. Furthermore, each table displays in column 1 the ratio of the average restricted variance over the average unrestricted variance. The average selection ratio is given in column 5. Table 2 shows the results for $\rho = .33$, and Table 3 gives the results for $\rho = .50$.

Tables 2 and 3 show that overall the corrected correlation r_c estimated the unrestricted population correlation accurately. The r_c tended to overestimate, however, under high-truncation/low-acceptance, and when the samples were drawn from a skewed distribution, corroborating the results of Brewer and Hill (1969).

The r_c -bootstrap confidence interval on ρ performed remarkably well. Even in the worst of the situations, it still included the correlation 89% of the time, rather than 95%. It was somewhat affected by skewness, but overall it was quite robust.

The median r^* generally underestimated the correlation, especially when the correlation was .33. Overall, it performed better than the restricted correlation. The confidence interval based on the r^* 's unfortunately did not perform well.

Selectivity did not seem to play much of a role in the estimation of ρ or the accuracy of the confidence intervals. Both estimators r_c and median r^* performed reasonably well under highly selective situations as can be seen from Tables 2 & 3. This is somewhat contrary to what Greener and Osburn (1979) observe, but they had complete truncation and we did not. It is possible that the r_c is more robust under incomplete truncation than under complete truncation, since under incomplete truncation it utilizes more information.

VIII. Recommendations

The r -bootstrap interval was shown to be robust to incomplete truncation, lack of normality, and lack of homoscedasticity. The study did not investigate, however, the effects of nonlinearity and/or the effects of incorrectly assuming that the selection process is solely based on the predictor. Future studies will have to assess the effects of these conditions on the r_c -bootstrap interval, since these conditions may negatively impact on the stability of the confidence interval. For situations in which these two conditions are not a factor, however, we feel comfortable in recommending the use of the r_c -bootstrap interval. Hence, we recommend that personnel researchers in

the U. S. Air Force and other institutions correct their validity coefficients for range restriction, and obtain a confidence interval on the unrestricted population correlation using the r_C -bootstrap method proposed here.

References

- Alexander, R.A., Carson, K.P., Alliger, G.M., & Barrett, G.V. (1984). Correction for restriction of range when both X and Y are truncated. Applied Psychological Measurement, 8, 231-241.
- Brewer, J.K., & Hills, J. R. (1969). Univariante selection: The effects of size of correlation, degree of skew, and degree of restriction. Psychometrika, 34, 347-361.
- Campbell, J.P. (1976). Psychometric theory. In M. Dunnette (Ed.), Handbook of industrial and organizational psychology. Chicago: Rand McNally.
- Efron, B. (1979). Bootstrap method: Another look at the jackknife. The Annals of Statistics, 7, 1-26.
- Efron, B., & Gong, G. (1983). A leisurely look at the bootstrap, the jackknife, and cross-validation. The American Statistician, 37, 36-48.
- Efron, B., & Tibshirani, R. (1986). Bootstrap methods for standard errors, confidence intervals, and other measures of statistical accuracy. Statistical Science, 1, 54-77.
- Greener, J.M., & Osburn, H.G. (1979). An empirical study of the accuracy of corrections for restriction in range due to explicit selection. Applied Psychological Measurement, 3, 31-41.
- Lawley, D. (1943). A note on Karl Pearson's selection formulae. Royal society of Edinburgh, Proceedings, Section A, 62, 28-30.
- Linn, R.L. (1968). Range restriction problems in the use of self-selected groups for test validation. Psychological Bulletin, 69, 795-801.
- Lord, F.M., & Novick, M.R. (1968). Statistical theories of mental test scores. Reading, MA: Addison-Wesley.

Lunneborg, C.E. (1985). Estimating the correlation coefficient: The bootstrap approach. Psychological Bulletin, 98, 209-215.

Olson, C.A., & Becker, B.E. (1983). A proposed technique for the treatment of restriction of range in selection validation. Psychological Bulletin, 93, 137-148.

Pearson, K. (1903). Mathematical contributions to the theory of evolution XI. On the influence of natural selection on the variability and correlation of organs. Philosophical transactions of the Royal Society, London, Series A, 200, 1-66.

Thorndike, R.L. (1950). The problem of classification of personnel. Psychometrika, 15, 215-235.

Table 1
Attrition Probabilities by Test Intervals

	Test Intervals									
	1	2	3	4	5	6	7	8	9	10
	Low-truncation					Low-acceptance				
p1:	.05*	.10	.15	.20	.25	.30	.40	.40	.40	.35
	Moderate-truncation					Moderate-acceptance				
p2:	.01	.01	.01	.01	.05	.10	.30	.60	.60	.55
	High-truncation					Low-acceptance				
p3:	.001	.001	.001	.001	.001	.001	.003	.28	.39	.39
	Low-truncation					High-acceptance				
p4:	.05	.06	.10	.12	.20	.30	.90	.95	.95	.95

* The probability of being selected (and accepting)
given that an individual falls within the test range

Table 2

Monte Carlo Results for the Eootstrap when $\rho = .33$

The table displays the average correlation and the percent time that the C.I. contains ρ , in parentheses.

Distribution	Mean S Mean S	Restricted Correlation	Eootstrap Correlation	Corrected Correlation	Average Selection Ratio
p1: Low-truncation, Low-acceptance					
Normal	.88	.32	.33 (88)	.34 (93)	.28
Mixed	.86	.31	.32 (90)	.34 (94)	.28
- skewed	.67	.29	.30 (89)	.34 (93)	.36
+ skewed	1.23	.33	.31 (93)	.32 (95)	.19
p2: Moderate-truncation, Moderate acceptance					
Normal	.65	.26	.27 (79)	.33 (93)	.06
Mixed	.73	.27	.29 (85)	.35 (91)	.15
- skewed	.32	.20	.24 (67)	.35 (95)	.38
+ skewed	1.87	.32	.32 (83)	.35 (89)	.05
p3: High-truncation, Low-acceptance					
Normal	.32	.19	.19 (86)	.41 (90)	.09
Mixed	.35	.19	.20 (82)	.44 (90)	.09
- skewed	.25	.19	.20 (83)	.36 (93)	.26
+ skewed	.65	.16	.19 (86)	.48 (88)	.05
p4: Low-truncation, High-acceptance					
Normal	.79	.29	.31 (83)	.33 (94)	.40
Mixed	.82	.29	.31 (84)	.32 (91)	.39
- skewed	.45	.24	.29 (77)	.35 (93)	.73
+ skewed	1.76	.30	.34 (92)	.30 (95)	.18

Table 3

Monte Carlo Results for the Bootstrap when $\alpha = .50$

The table displays the average correlation and the percent time that the C.I. contained ρ , in parentheses.

Distribution	Mean S Mean S	Restricted Correlation	Bootstrap Correlation	Corrected Correlation	Average Selection Ratio
--------------	------------------	---------------------------	--------------------------	--------------------------	-------------------------------

p1: Low-truncation, Low-acceptance

Normal	.87	.46	.46 (89)	.48 (93)	.28
Mixed	.88	.47	.47 (89)	.50 (92)	.28
- skewed	.70	.43	.46 (87)	.50 (94)	.34
+ skewed	1.12	.48	.47 (94)	.47 (92)	.20

p2: Moderate-truncation, Moderate-acceptance

Normal	.69	.37	.41 (93)	.49 (93)	.15
Mixed	.83	.39	.44 (86)	.49 (93)	.13
- skewed	.37	.35	.40 (69)	.52 (91)	.32
+ skewed	1.48	.46	.45 (85)	.47 (89)	.06

p3: High-truncation, Low-acceptance

Normal	.33	.29	.30 (75)	.50 (90)	.09
Mixed	.39	.30	.30 (84)	.52 (89)	.09
- skewed	.28	.32	.33 (72)	.53 (93)	.23
+ skewed	.64	.36	.34 (92)	.53 (95)	.06

p4: Low-truncation, High-acceptance

Normal	.76	.45	.47 (83)	.50 (92)	.39
Mixed	.84	.45	.47 (84)	.49 (94)	.40
- skewed	.49	.40	.46 (73)	.53 (91)	.68
+ skewed	1.49	.51	.49 (90)	.45 (92)	.21

1986 USAF-UES SUMMER RESEARCH PROGRAM/
GRADUATE STUDENT SUMMER SUPPORT PROGRAM

SPONSORED BY THE
AIR FORCE OFFICE OF SCIENTIFIC RESEARCH
CONDUCTED BY THE
UNIVERSAL ENERGY SYSTEMS , INC.
FINAL REPORT

AN ANALYSIS OF RESIDUAL OUTPUT NOISE
FROM THE R.A.D.C. SPEECH ENHANCEMENT UNIT

PREPARED BY:	PETER V. HLINOMAZ
ACADEMIC RANK:	GRADUATE STUDENT
DEPARTMENT AND	DEPARTMENT OF ELECTRICAL ENGINEERING
UNIVERSITY:	UNIV. OF MICH.-DEARBORN
RESEARCH LOCATION:	ROME AIR DEVELOPMENT CENTER/IRAA
USAF RESEARCH:	MR. E.J. CUPPLES
DATE:	24 JULY 1986
CONTRACT NO:	F49620-85-C-0013

AN ANALYSIS OF RESIDUAL OUTPUT NOISE
FROM THE R.A.D.C. SPEECH ENHANCEMENT UNIT

BY

PETER V. HLINOMAZ

ABSTRACT

THE INTELLIGENCE ANALYSIS SECTION (IRAA) OF THE SIGNAL INTELLIGENCE BRANCH OF THE ROME AIR DEVELOPMENT CENTER (RADC/IRAA) HAS DEVELOPED AND IS CONTINUING TO DEVELOP A SPEECH ENHANCEMENT UNIT (SEU) WHICH REMOVES THREE KINDS OF NOISE: WIDEBAND RANDOM (WHITE) NOISE, IMPULSE NOISE, AND STATIONARY AND SWEEPING TONES. ALTHOUGH THE CURRENT WIDEBAND NOISE REMOVAL PROCESS IMPROVES THE SIGNAL BY REDUCING THE NOISE AS MUCH AS 15 DB, THE PROCESS PRODUCES A RESIDUAL NOISE WHICH APPEARS AS PEAKS IN THE OUTPUT SPECTRUM WHICH ARE NOT ASSOCIATED WITH THE SPEECH AND WHICH MOVE AROUND THE SPECTRUM IN A SEEMINGLY RANDOM WAY. TO IMPROVE THE WIDEBAND NOISE REMOVAL PROCESS, THE SEU MUST BE ABLE TO AUTOMATICALLY IDENTIFY AND REMOVE THIS RESIDUAL NOISE.

ACKNOWLEDGMENTS

I WOULD LIKE TO THANK THE AIR FORCE SYSTEMS COMMAND, THE AIR FORCE OFFICE OF SCIENTIFIC RESEARCH AND THE ROME AIR DEVELOPMENT CENTER/INTELLIGENCE RECONNAISSANCE ANALYSIS AND APPLICATIONS BRANCH. I WOULD ALSO IN PARTICULAR LIKE TO THANK MR. JIM CUPPLES, MR. JOHN PARKER, MR. ROY RATLEY, CAPT. WAYNE TODD, AND 2LT. JAMIE FOELKER FOR THEIR INVALUABLE ASSISTANCE WITH MY RESEARCH.

I. INTRODUCTION

I RECEIVED MY BSEE FROM NORTHWESTERN UNIVERSITY WHERE I SPECIALIZED IN COMMUNICATION SYSTEMS. PRESENTLY I AM WORKING TOWARD MY MSEE AT THE UNIVERSITY OF MICHIGAN-DEARBORN, WHERE I AM ALSO SPECIALIZING IN COMMUNICATION SYSTEMS.

MY TASK AT RADC/IRAA WAS TO STUDY THE RESIDUAL NOISE FROM THE SEU, DETERMINE HOW IT DIFFERED FROM SPEECH AND WHITE NOISE, HOW TO CHARACTERIZE IT, AND HOW TO ELIMINATE OR REDUCE IT. THIS INVESTIGATION REQUIRED VARIOUS TIME AND FREQUENCY DOMAIN ANALYSES AND AN UNDERSTANDING OF THE CEPSTRAL DOMAIN. SEVERAL OF THE COURSES THAT I TOOK AS AN UNDERGRADUATE AND GRADUATE STUDENT WERE USEFUL IN CONDUCTING AND COMPLETING THIS RESEARCH EFFORT.

II. RESEARCH OBJECTIVES

THE OVERALL OBJECTIVE OF THIS RESEARCH EFFORT WAS TO INVESTIGATE WAYS TO REDUCE THE RESIDUAL NOISE CREATED BY THE WIDEBAND NOISE REMOVAL PROCESS. THE EFFORT WAS SUBDIVIDED INTO FOUR INDIVIDUAL TASKS: 1. ANALYZE THE RESIDUAL NOISE; 2. CHARACTERIZE THE RESIDUAL NOISE; 3. DEVELOP TECHNIQUES TO REMOVE RESIDUAL NOISE; 4. IMPLEMENT AND TEST NOISE REMOVAL TECHNIQUES.

WHILE AT RADC/IRAA I ACCOMPLISHED THE FIRST THREE INDIVIDUAL TASKS. THE FOURTH TASK WILL REQUIRE FURTHER RESEARCH.

II. BASIC OPERATION OF THE SEU

IN ORDER TO UNDERSTAND THE NATURE OF THIS PROBLEM, IT IS NECESSARY TO UNDERSTAND HOW THE SPEECH ENHANCEMENT UNIT OPERATES. AS STATED PREVIOUSLY, THE SEU SEQUENTIALLY REMOVES THREE TYPES OF NOISE: TONAL, IMPULSE, AND WIDEBAND (IN THIS ORDER). THE SEU DOES THIS WITH SOPHISTICATED DIGITAL SIGNAL PROCESSING ALGORITHMS WHICH ARE

IMPLEMENTED ON A MODIFIED MAP 300 ARRAY PROCESSOR. THE SEU ACCEPTS AND OUTPUTS ANALOG SIGNALS AND HENCE REQUIRES BOTH ANALOG TO DIGITAL (A/D) AND DIGITAL TO ANALOG CONVERSION (D/A). THE DIGITIZED SIGNAL CAN BE PROCESSED BY ANY OR ALL OF THE THREE PROCESSING ALGORITHMS.

THE TONE REMOVAL AND IMPULSE REMOVAL ALGORITHMS ARE ACCOMPLISHED IN THE FREQUENCY AND TIME DOMAINS, RESPECTIVELY. THE WIDEBAND NOISE REMOVAL ALGORITHM IS A CEPSTRAL DOMAIN PROCESS AND PRODUCES THE RESIDUAL NOISE WHICH THIS RESEARCH EFFORT IS AIMED AT REDUCING.

THE LAST NOISE REMOVAL ALGORITHM TO BE PERFORMED (KNOWN AS INTEL) REMOVES WIDEBAND NOISE FROM THE SPEECH SIGNALS. IT DOES THIS BY USING A ROOT CEPSTRAL SUBTRACTION TECHNIQUE. THE ALGORITHM FIRST LOOKS AT A SEGMENT OF THE INPUT SIGNAL (IN THIS CASE A 100 MS OR 200 MS WINDOW) AND CHECKS FOR HARMONIC RELATIONSHIPS IN THE SIGNAL SPECTRUM. IF THE SPECTRUM CONTAINS HARMONICALLY RELATED FREQUENCIES, THE SIGNAL SEGMENT IS ASSUMED TO CONTAIN SPEECH. IF NO HARMONICALLY RELATED FREQUENCIES ARE FOUND, THE SIGNAL IS ASSUMED TO BE NOISE. THE NOISE-ONLY SEGMENTS ARE USED TO COMPUTE A RUNNING AVERAGE OF THE ROOT CEPSTRUM. THE NOISE CEPSTRUM IS THEN SUBTRACTED FROM THE ROOT CEPSTRUM OF THE INPUT SIGNAL WHICH CONTAINS BOTH THE NOISE AND THE SPEECH SIGNAL. THE DIFFERENCE IS THE ROOT CEPSTRUM OF THE SPEECH SIGNAL WHICH IS CONVERTED BACK TO A TIME AMPLITUDE ANALOG SIGNAL. AS TIME GOES ON, THE SEU COMPUTES A INCREASINGLY IMPROVED AVERAGE OF THE NOISE CEPSTRUM. CONSEQUENTLY, THE SIGNAL BECOMES MORE ENHANCED AS TIME PASSES, PROVIDING THAT THE NOISE IS STATIONARY. ALTHOUGH THE ENHANCEMENT PROCESS IMPROVES THE SPEECH SIGNAL BY IMPROVING THE SIGNAL-TO-NOISE RATIO (SNR) AS MUCH AS 15 DB, THE PROCESS PRODUCES A RESIDUAL NOISE WHICH SOUNDS LIKE MANY GARBLED VOICES SPEAKING AT THE SAME TIME.

III. PROCEDURES

TO CONDUCT THIS RESEARCH, STANDARD LABORATORY EQUIPMENT

PLUS TWO SPECIALIZED ANALYSIS TOOLS WERE USED. THE SPECIALIZED INSTRUMENTS USED WERE A SIGNATECTION RESEARCH INC., MODEL ST-701 SPECTRAL CONTOUR PLOTTER AND THE SIGNAL TECHNOLOGIES INTERACTIVE LABORATORY SYSTEM (ILS) SIGNAL PROCESSING SOFTWARE PACKAGE INSTALLED ON A PDP 11/70. THE EQUIPMENT CONFIGURATION IS SHOWN IN FIG.1. BEFORE DISCUSSING THE EXPERIMENTS, A BRIEF DESCRIPTION OF THE SPECTRAL CONTOUR PLOTTER AND THE ILS WILL BE GIVEN.

THE CONTOUR PLOTTER IS AN ANALOG DEVICE WHICH PLOTS THE FREQUENCY SPECTRUM OF A SIGNAL AS A FUNCTION OF TIME. THE PLOTTER PLOTS FREQUENCY ON THE VERTICAL AXIS, TIME ON THE HORIZONTAL AXIS, AND SPECTRAL MAGNITUDE ON THE Z-AXIS AS INTENSITY. THE SPECTRAL PLOTS ARE PRINTED ON THERMAL PAPER 11X17 INCHES IN SIZE. THE Z-AXIS, REPRESENTING SPECTRAL AMPLITUDE, IS REPRESENTED AS A SEQUENCE OF GRAY CONTOUR LEVELS. STRONGER SIGNALS PRODUCE DARKER CONTOUR LEVELS WHILE WEAKER SIGNALS PRODUCE LIGHTER CONTOURS. THUS, THE CONTOUR PLOT OF A SIGNAL RESEMBLES A TOPOGRAPHICAL RELIEF MAP WITH THE STRONG PORTIONS OF THE SIGNAL BEING ANALAGOUS TO MOUNTAINS AND THE WEAKER PORTIONS ANALAGOUS TO VALLEYS. THIS PARTICULAR PLOTTER HAS SEVEN AVAILABLE CONTOURS. EACH CONTOUR REPRESENTS A 6 DB CHANGE IN SPECTRAL AMPLITUDE (FOR THE WORK COMPLETED). THE LOWEST TWO CONTOURS WERE USUALLY SWITCHED OFF SO THAT THE PLOTS WOULD NOT SHOW LOW LEVEL BACKGROUND NOISE. MOST OF THE PLOTS THEREFORE HAD A DYNAMIC RANGE OF 30 DB (6 DB/CONTOUR * 5 CONTOUR LEVELS) . THE CONTOUR PLOTTER CAN STORE MESSAGE LENGTHS OF ONE TO FOUR SECONDS AND CAN PLOT WITH RESOLUTIONS OF 40, 100, OR 300 HZ. MOST OF THE PLOTS USED THE 1 SECOND MESSAGE LENGTH AND THE 100 HZ RESOLUTION SETTING. THE 100 HZ SETTING GAVE A 10 MS (1/100 HZ) TIME RESOLUTION. THE 300 HZ (3.3 MS TIME RESOLUTION) SETTING WAS USED WHEN BETTER TIME RESOLUTION WAS NEEDED AND THE 40 HZ SETTING WAS USED WHEN MAXIMUM FREQUENCY RESOLUTION WAS NEEDED.

THE ILS WAS ALSO USED IN COMBINATION WITH THE CONTOUR PLOTTER. THE ILS IS A DIGITAL PROCESS AND THEREFORE REQUIRES THE ANALOG INPUT SIGNAL TO FIRST BE DIGITIZED (AT A 10 KHZ RATE). THE SAMPLED DATA IS THEN ANALYZED WITH ILS AND THE RESULTS ARE DISPLAYED.

WHEN THE ILS ANALYZES A FILE OF SAMPLED DATA, IT BREAKS THE FILE INTO SMALL SEGMENTS CALLED FRAMES. THE USER SELECTS THE SIZE OF THE FRAMES. AFTER EXPERIMENTING WITH SEVERAL DIFFERENT FRAME SIZES, A 128 POINT FRAME SIZE WAS CHOSEN. THIS GAVE A FRAME LENGTH OF 12.8 MS AND A 78.1 HZ FREQUENCY RESOLUTION ($1/12.8$ MS). THIS FRAME SIZE GAVE TIME AND FREQUENCY RESOLUTIONS COMPARABLE TO THOSE PROVIDED BY THE CONTOUR PLOTTER AND PROVIDED THE BEST TRADE-OFF BETWEEN TIME AND FREQUENCY RESOLUTION. HAMMING WEIGHTING WAS USED TO WINDOW EACH FRAME. EACH WINDOW WAS 25.6 MS LONG AND THEREFORE OVERLAPPED EVERY FRAME BY 50%. THIS WINDOW GREATLY REDUCED HIGH FREQUENCY SIDELOBES AND ALSO PREVENTED INFORMATION FROM BEING LOST.

THE MAIN ILS FEATURES USED WERE THE SMOOTHED 3-D SPECTRAL ANALYSIS PLOT AND THE FORMANT TRACKING PLOT. SEVERAL OF THESE PLOTS ARE INCLUDED IN THIS REPORT.

IV. EXPERIMENTS

FOUR EXPERIMENTS WERE PERFORMED. THE FIRST EXPERIMENT PROCESSED A KNOWN SIGNAL, CORRUPTED BY WIDEBAND NOISE, USING THE INTEL ALGORITHM. THE OBJECTIVE OF THIS EXPERIMENT WAS TO DETERMINE THE LEVEL OF RESIDUAL NOISE PRESENT AFTER INTEL PROCESSING AND TO FIND OUT HOW INTEL PROCESSING AFFECTED THE KNOWN SIGNAL. A 100 HZ GATED SQUARE WAVE WAS USED AS THE TEST SIGNAL. THE GATE WAS ON FOR 32 CYCLES AND OFF FOR 32 CYCLES. THIS GATE PRODUCED A SQUARE WAVE TRAIN THAT WAS ON FOR 320 MS AND OFF FOR 320 MS. THE HARMONIC STRUCTURE OF THIS SIGNAL RESEMBLED THAT OF A ONE SYLLABLE WORD WITH A 100 HZ PITCH RATE AND FREQUENCY PEAKS EVERY 200 HZ. WIDEBAND NOISE WAS ADDED, BY LINEAR MIXING, SO THAT THE SNR WAS 0 DB. THIS TEST SHOWS THAT INTEL PROCESSING REDUCED THE NOISE PEAKS BY 10-15 DB. THESE REMAINING NOISE PEAKS ARE VISIBLE ON THE PLOTS AS GRAY SPOTS LOCATED BETWEEN THE 100 HZ TONES. SINCE FIVE CONTOUR LEVELS ARE DISPLAYED IN THESE PLOTS, ONLY THE STRONGEST RESIDUAL NOISE PEAKS APPEAR IN THE PLOTS.

THE TONE SIGNAL WAS NOT REDUCED. THE STRONGEST PORTIONS OF THE

TONE WERE ABOUT 30 DB STRONGER THAN THE HIGHEST PEAKS OF THE RESIDUAL NOISE. CONSEQUENTLY, SINCE THE PLOTS ONLY PROVIDED A DYNAMIC RANGE OF 30 DB, THE TONE MASKED MOST OF THE RESIDUAL NOISE. THE BEFORE AND AFTER PLOTS ARE SHOWN IN FIG.2.

FOR THE SECOND TEST, PURE WIDEBAND NOISE WAS PROCESSED WITH INTEL AND WAS PLOTTED USING THE 100 HZ BANDPASS SETTING (10 MS RESOLUTION). IT WAS IMMEDIATELY NOTICED THAT THE RESIDUAL NOISE TENDED TO CLUSTER TIGHTLY IN NARROW FREQUENCY BANDS FOR SHORT PERIODS OF TIME AND APPEARED TO MOVE RANDOMLY IN THE FREQUENCY SPECTRUM. THE STRONGEST RESIDUAL NOISE PEAKS HAD SPECTRAL AMPLITUDES 12-15 DB GREATER THAN THE BACKGROUND NOISE. PLOTS OF THE WHITE NOISE AND RESIDUAL OUTPUT NOISE (WITH 100 HZ FILTER) ARE SHOWN IN FIG.3. THIS PLOT WAS ALSO REPEATED USING THE 300 HZ SETTING (FIG.4A) AND THE 40 HZ SETTING (FIG.5A). THE 300 HZ SETTING GAVE IMPROVED TIME RESOLUTION (3.3 MS) WHILE THE 40 HZ SETTING GAVE BETTER FREQUENCY RESOLUTION. TO OBTAIN BETTER TIME RESOLUTION, AN EXPANDED TIME PLOT WAS MADE (FIG.5B) BY TAPING A LENGTH OF RESIDUAL NOISE AND PLAYING IT AT DOUBLE SPEED TO THE PLOTTER. THESE PLOTS CONFIRMED THAT THE RESIDUAL NOISE WAS COMPOSED OF NARROWBAND FREQUENCY PEAKS WHICH REMAINED FIXED FOR ABOUT 20-50 MS BEFORE CHANGING FREQUENCY OR FADING.

THE THIRD EXPERIMENT COMPARED THE NOISE PLOTS TO THOSE OF SPEECH. THE LETTERS "S" AND "A" ($SNR = 0$ DB) WERE PROCESSED WITH INTEL (FIG. 6), AND COMPARED WITH THE PLOTS OF THE WHITE AND RESIDUAL NOISE. THIS EXPERIMENT WAS PERFORMED IN ORDER TO DETERMINE HOW THE RESIDUAL NOISE DIFFERS IN CHARACTER FROM UNVOICED AND VOICED SPEECH. A DIFFERENCE BETWEEN RESIDUAL NOISE AND VOICED SPEECH MUST BE FOUND IF THE RESIDUAL NOISE IS TO BE REMOVED WITHOUT AFFECTING THE SPEECH. THE PLOTS INDICATED THAT THE SPECTRAL PEAK TRACKS OF THE RESIDUAL NOISE LASTED MUCH LONGER THAN SPECTRAL PEAK TRACKS OF THE WHITE NOISE AND UNVOICED SPEECH SEGMENTS, BUT WERE SHORTER THAN THE TRACKS MADE BY VOICED SOUNDS.

THE THIRD EXPERIMENT WAS CONDUCTED ON THE ILS USING THE SPECTRAL PLOTTING AND FORMANT TRACKING ROUTINES. IN THIS CASE, THE ILS

PRINTED 3-D SPECTRAL PLOTS, SPECTRAL PEAKS AND FORMANT (FREQUENCY) TRACKS OF WHITE NOISE, RESIDUAL NOISE, AND THE WORDS "SEVEN", "SISSY", AND "SIX". THIS WAS DONE TO COMPARE THE SPECTRAL PEAKS AND FREQUENCY TRACKS OF RESIDUAL NOISE TO THOSE OF WHITE NOISE AND TO WORDS WHICH CONTAINED BOTH VOICED AND UNVOICED SOUNDS. THEORETICALLY, WHITE NOISE SHOULD NOT LEAVE ANY FREQUENCY TRACKS. THE FORMANT TRACKING ALGORITHM ON THE ILS CAN HOWEVER BE USED TO TRACK GROUPS OF SPECTRAL PEAKS AND DETERMINE HOW LONG THE SPECTRAL PEAKS REMAIN IN A GIVEN FREQUENCY RANGE.

AFTER LOOKING AT THE SPECTRAL PLOTS AND FREQUENCY TRACKS IN FIGS.7-9, IT WAS OBSERVED THAT THE TRACKS FROM THE RESIDUAL NOISE LASTED MORE THAN TWICE AS LONG AS THOSE OF THE WHITE NOISE AND WERE RELATIVELY CONSTANT IN FREQUENCY. THE RESIDUAL NOISE TRACKS WERE SHORTER THAN THOSE TRACKS MADE BY THE VOICED REGIONS OF "SISSEY" AND "SEVEN". THE RESIDUAL NOISE TRACKS DID LAST LONGER THAN THE TRACKS WHICH MAINLY UNVOICED WORDS SUCH AS "SIX" MADE. THE OBSERVED DIFFERENCES BETWEEN THE RESIDUAL NOISE, WHITE NOISE AND VOICED SPEECH APPEARED TO BE SIGNIFICANT ENOUGH SO THAT AN ALGORITHM TO REMOVE THE RESIDUAL NOISE COULD BE DEvised.

V. FINAL CONCLUSIONS

THE EXPERIMENTS DESCRIBED ABOVE DETERMINED THAT INTEL PROCESSING OF WIDEBAND NOISE PRODUCES A RESIDUAL NOISE THAT APPEARS TO BE UNIQUE IN CHARACTER. THE RESIDUAL NOISE APPEARS AS ENERGY PEAKS IN NARROW FREQUENCY BANDS WHICH REMAIN FIXED IN FREQUENCY FOR ABOUT 20-50 MILLISECONDS BEFORE RAPIDLY FADING OR CHANGING FREQUENCY. THESE FREQUENCY PEAKS HAVE SPECTRAL AMPLITUDES OF 12-15 DB GREATER THAN THE PEAKS OF THE REMAINING RESIDUAL NOISE AND ARE ABOUT 30 DB BELOW THE AMPLITUDE OF SPEECH PEAKS (FOR SNR=0 DB). THESE SPECTRAL PEAKS DO NOT SEEM TO BE HARMONICALLY RELATED. THIS ABSENCE OF ANY HARMONIC RELATIONSHIP CLEARLY DISTINGUISHES THE RESIDUAL NOISE FROM VOICED SPEECH WHICH IS HARMONICALLY STRUCTURED. THE FREQUENCY PEAKS OF THE

RESIDUAL NOISE ALSO REMAIN STATIONARY MORE THAN TWICE AS LONG AS THE FREQUENCY PEAKS OF UNVOICED SPEECH. THESE UNIQUE CHARACTERISTICS MAKE IT FEASIBLE TO REMOVE THE RESIDUAL NOISE WITHOUT ADVERSELY AFFECTING THE SPEECH SIGNAL. A POTENTIAL ALGORITHM FOR REMOVING THE RESIDUAL NOISE IS A PROCESS KNOWN AS DIGITAL SPECTRAL SHAPING (DSS) AND IS FULLY EXPLAINED IN THE RADC TECHNICAL REPORT NO.78-232.

RECOMMENDATIONS

1. ONE METHOD FOR ELIMINATING THE RESIDUAL NOISE WOULD BE TO INSERT A MODIFIED DSS ALGORITHM AFTER INTEL. THIS ALGORITHM SHOULD USE 20 MILLISECOND OR SHORTER WINDOWS IN ORDER TO CATCH THE QUICKLY VARYING RESIDUAL NOISE TONES. THE SPECTRUM OF EACH WINDOW CAN THEN BE TESTED FOR TONE PEAKS. IF THESE PEAKS ALSO OCCUR IN NEIGHBORING WINDOWS AND ARE NOT HARMONICALLY RELATED THEN THEY CAN BE REMOVED. THE HARMONICALLY RELATED TONES ARE ASSUMED TO BE THE PITCH AND FORMANT PEAKS AND SHOULD NOT BE PROCESSED.

2. ADDITIONAL RESEARCH SHOULD BE PERFORMED TO DEVELOP A NOISE REMOVAL ALGORITHM BEFORE BUILDING AN ACTUAL RESIDUAL NOISE REMOVER. MOST OF THIS RESEARCH CAN BE CONDUCTED WITH THE CONTOUR PLOTTER AND THE ILS. THE ILS, HOWEVER, NEEDS BETTER DOCUMENTATION AND NEEDS TO BE MADE MORE USER FRIENDLY. A SHORT DOCUMENT WHICH DESCRIBES THE ILS TECHNIQUES USED FOR THIS RESEARCH EFFORT IS BEING PREPARED AND WILL BE AVAILABLE FROM RADC/IRMA IN THE FALL OF 1986.

REFERENCES

TECHNICAL REPORTS:

1. WEISS, MARK, R, AND ASCHKENASY, EARNEST,
"COMPUTERIZED AUDIO PROCESSOR", FINAL
TECHNICAL REPORT:RADC-TR-83-109, ROME AIR
DEVELOPMENT CENTER, GRIFFISS AFB, NY,
MAY 1983.
2. WEISS, MARK, R, AND ASCHKENASY, EARNEST,
"THE SPEECH ENHANCEMENT ADVANCED DEVELOPMENT
MODEL", TECHNICAL REPORT: RADC-TR-78-232,
ROME AIR DEVELOPMENT CENTER, GRIFFISS AFB,
NY, NOVEMBER 1978.

TEXTBOOKS:

3. OPPENHEIM, ALAN, V. AND SCHAFER, RONALD, W,
DIGITAL SIGNAL PROCESSING, ENGLEWOOD CLIFFS,
MICHIGAN,PRENTICE-HALL INC., 1975.

FIG1. EQUIPMENT
CONFIGURATION

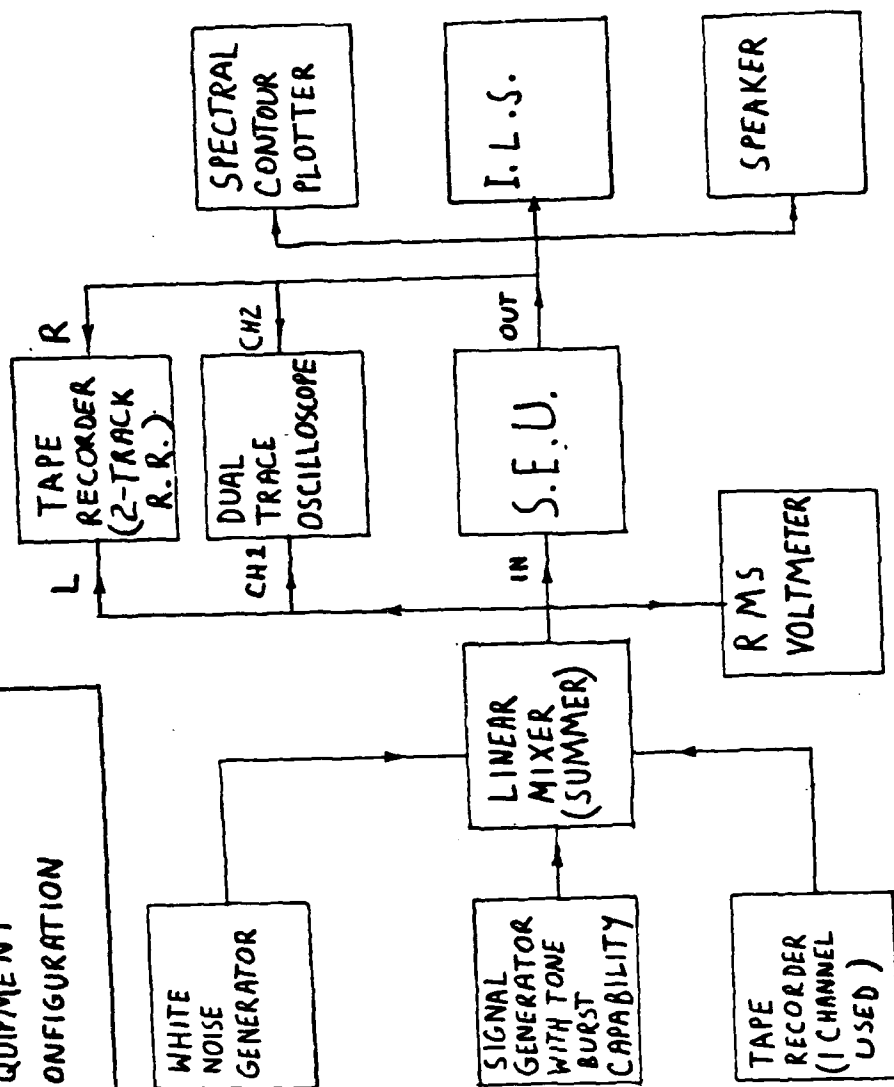
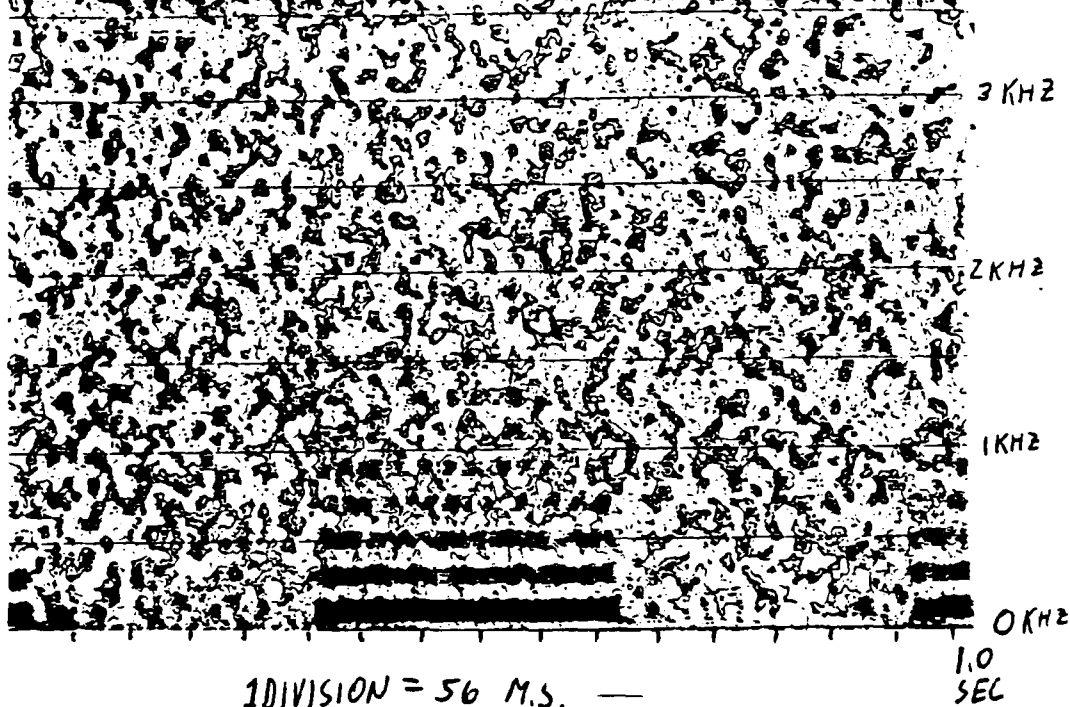
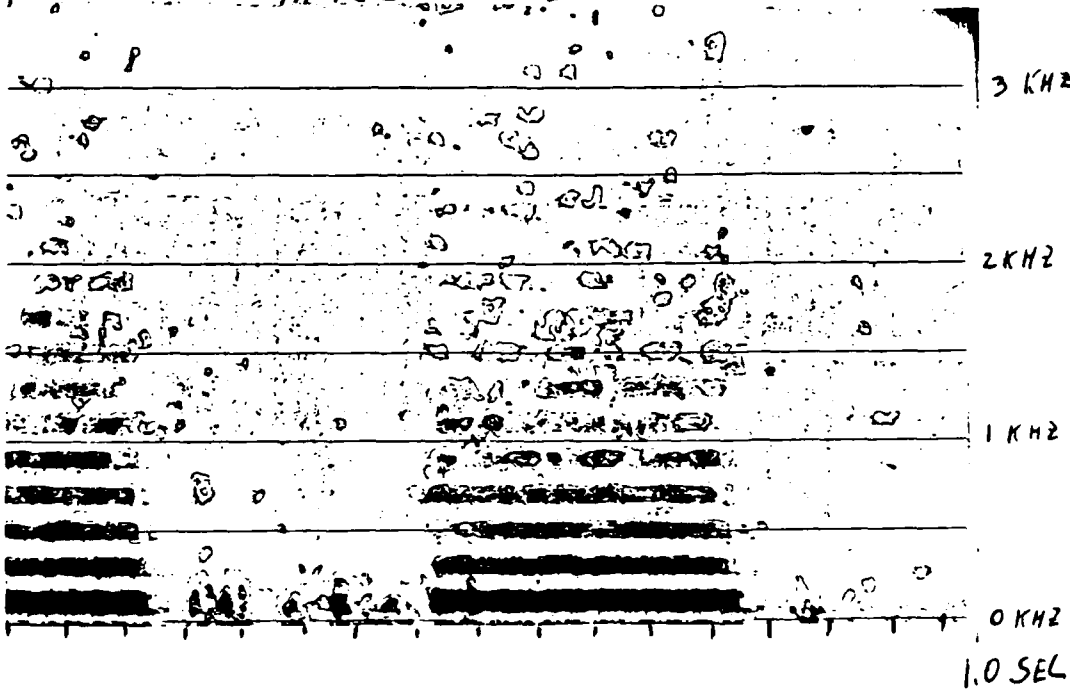


FIG. 2 BEFORE INTEL
 100HZ GATED SQ. WAVE + WIDEBAND NOISE (SNR \leq 0DB, 100HZ FILTER)



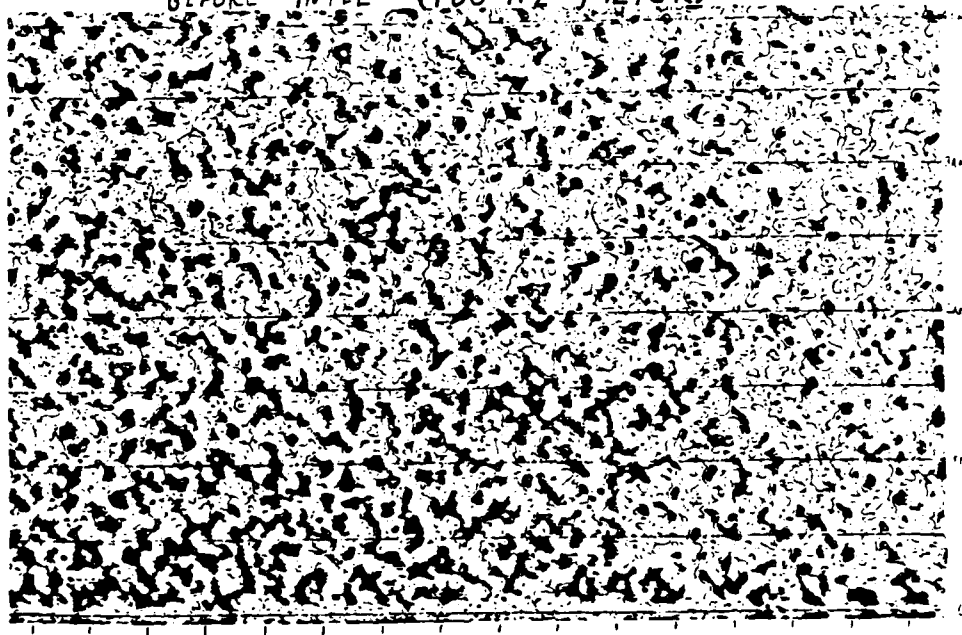
AFTER INTEL



1 DIVISION = 56 M.S.

FIG. 3

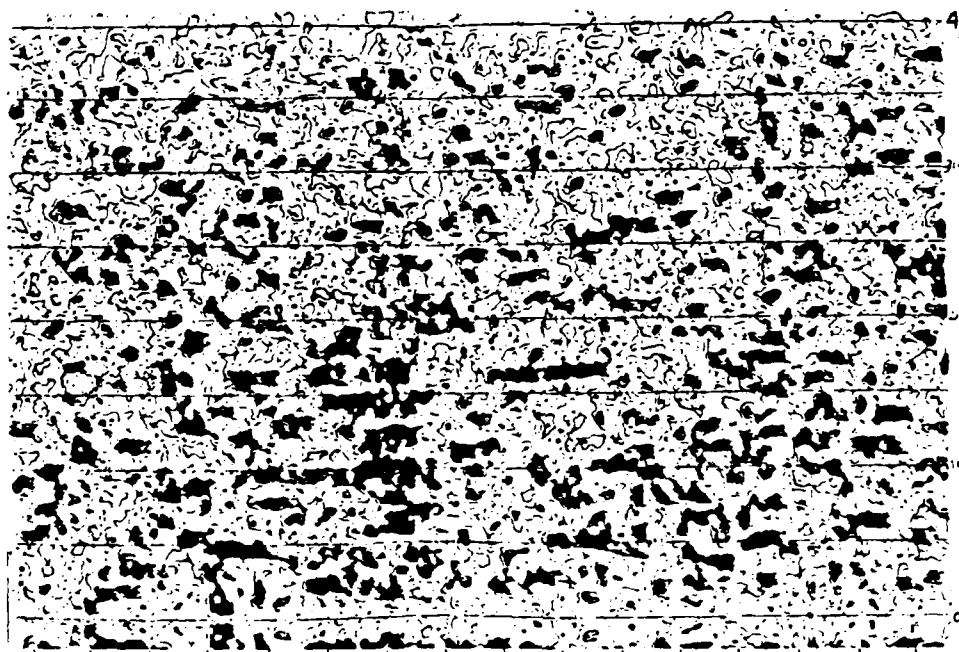
WHITE NOISE INPUT TO SEU
BEFORE INTEL (100 HZ FILTER)



1 DIVISION = 56 m.s.

1.0
SEC

RESIDUAL NOISE AFTER INTEL (100 HZ FILTER)



1 DIVISION = 56 m.s.

1.0
SEC

FIG. 4A

RESIDUAL NOISE PLOTTED WITH 300HZ FILTER

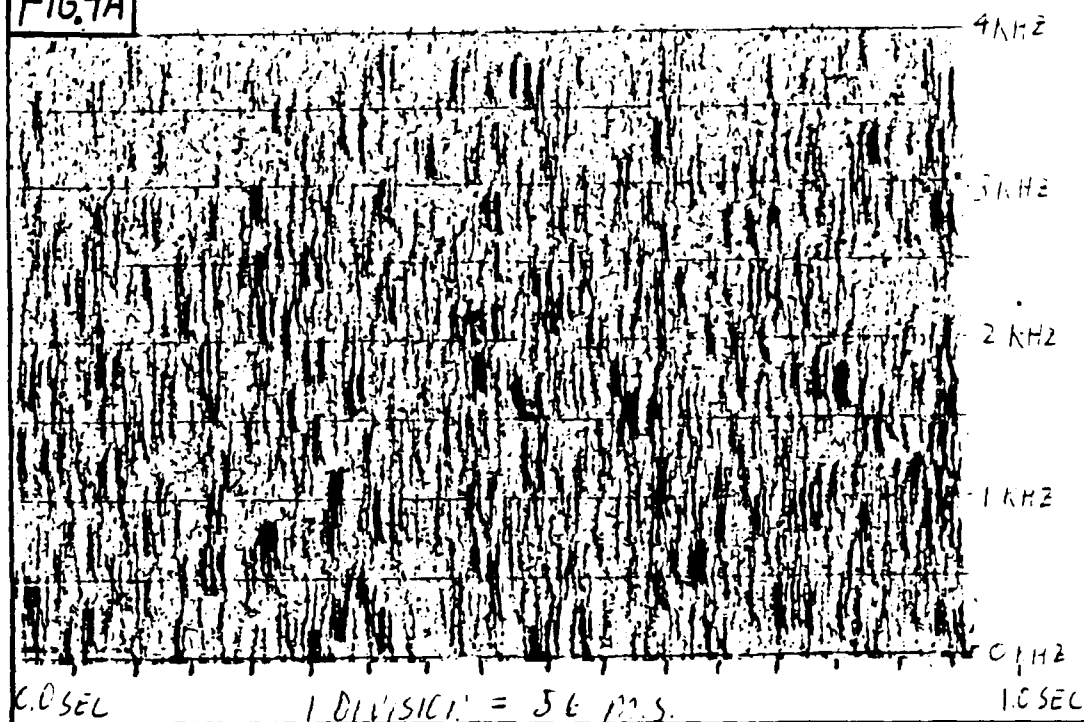


FIG. 4B

RESIDUAL NOISE PLOTTED WITH 100 HZ FILTER

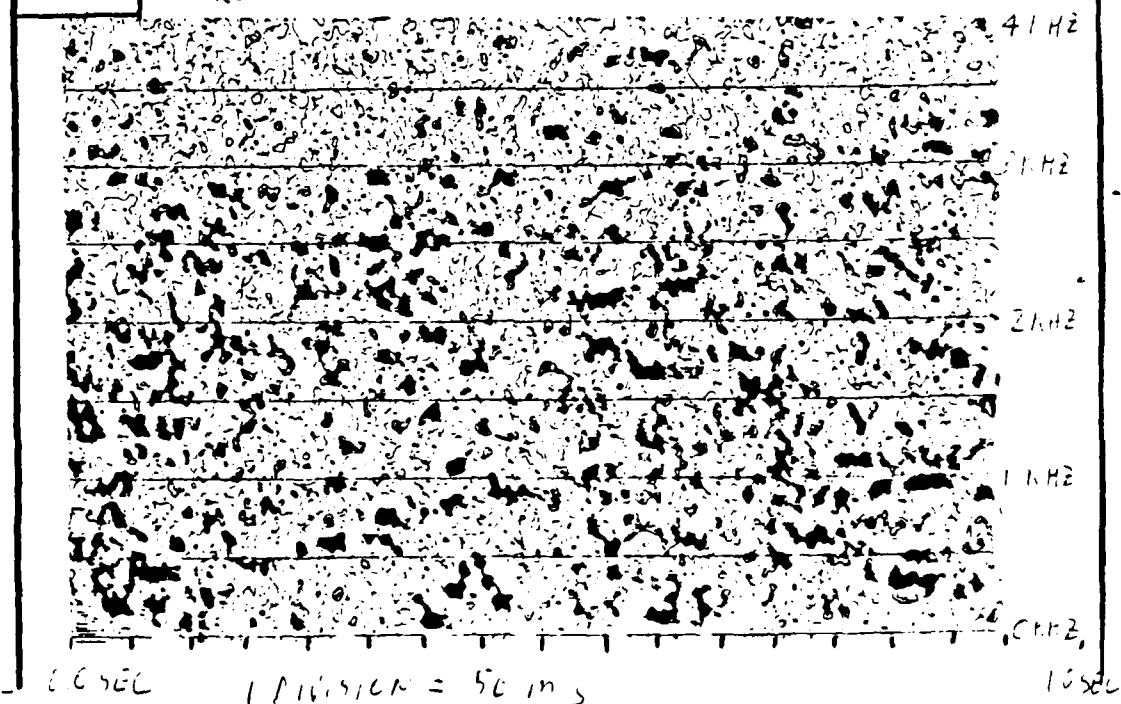


FIG. 5A RESIDUAL NOISE PLOTTED WITH 40 HZ FILTER

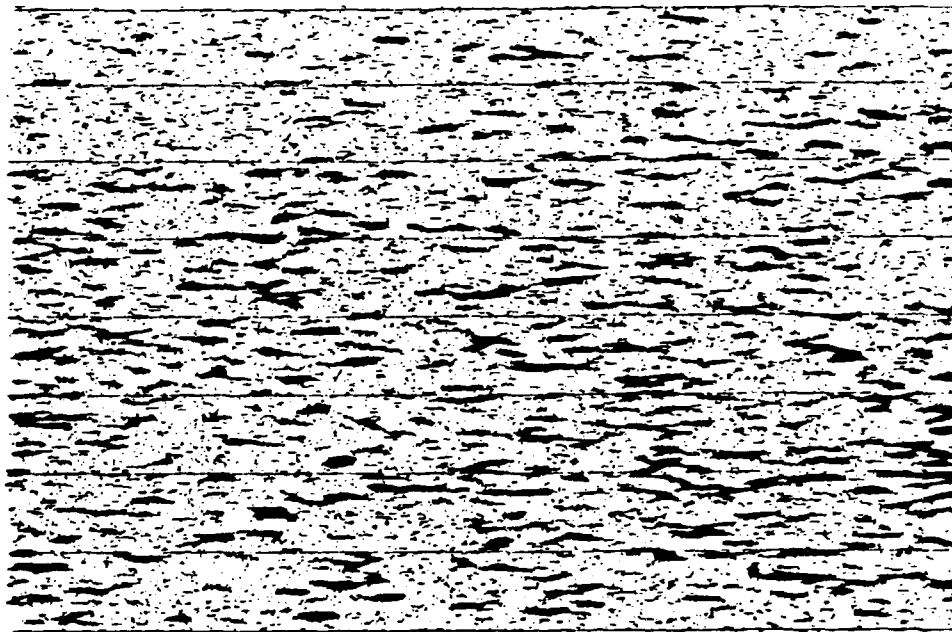
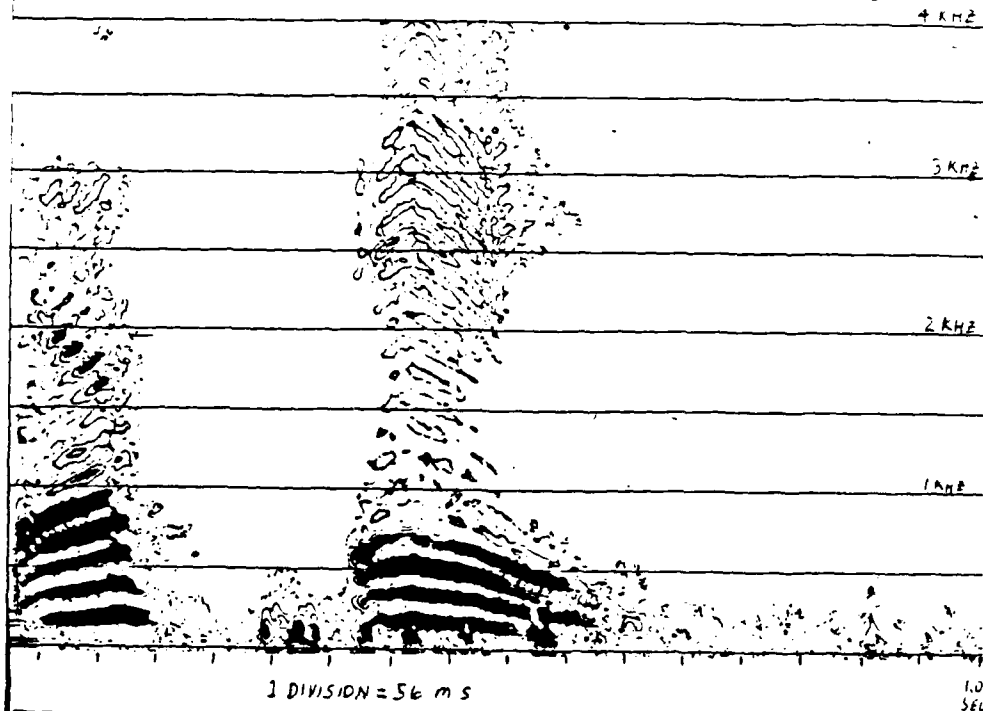


FIG. 5B EXPANDED GRAPH OF RESIDUAL NOISE (100 HZ FILTER)



1 DIVISION = 2.8 m/s

FIG. 6 CLEAN "SA" WITHOUT INTEL (100 HZ FILTER)



NOISY "SA" ($SNR \leq 0dB$) AFTER INTEL (100 HZ FILTER)

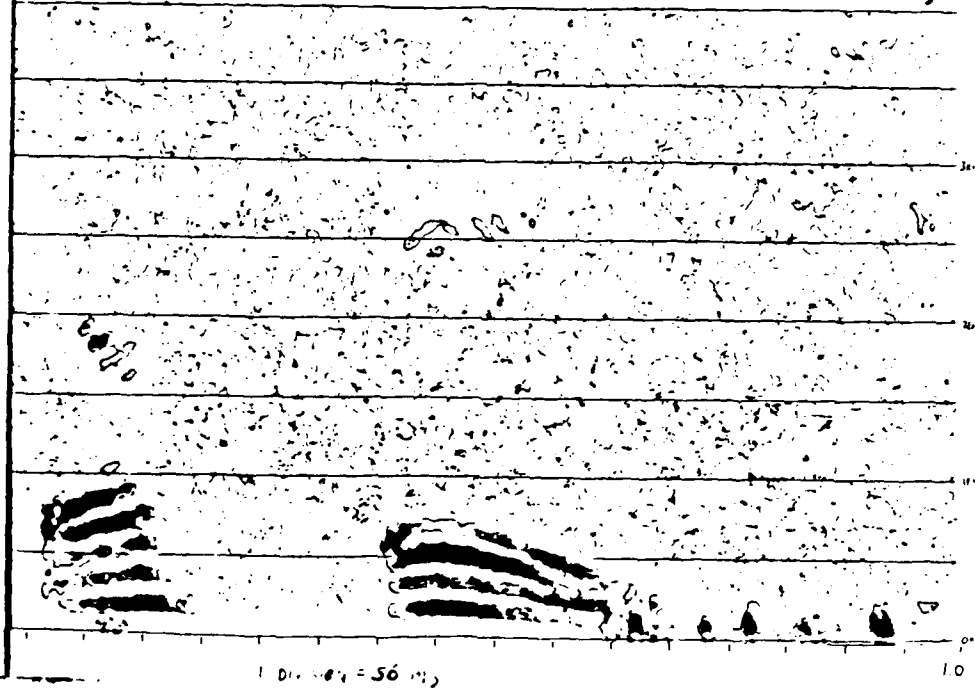
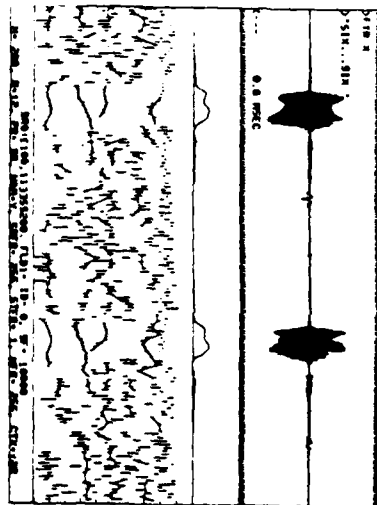
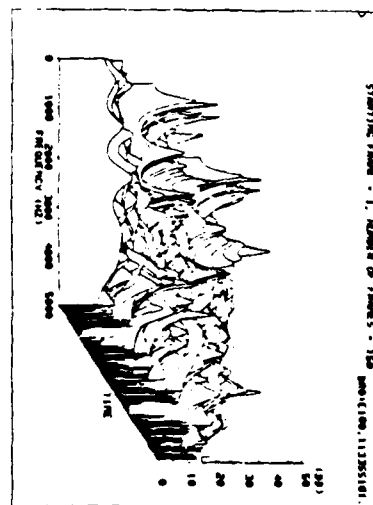


FIG. 8

"SIX SIX"



WHITE NOISE

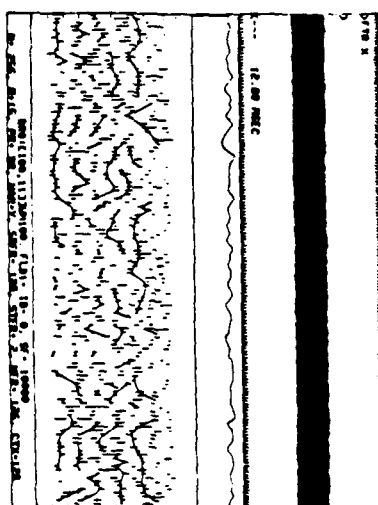
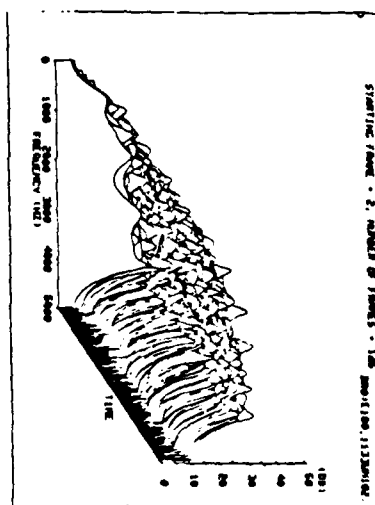
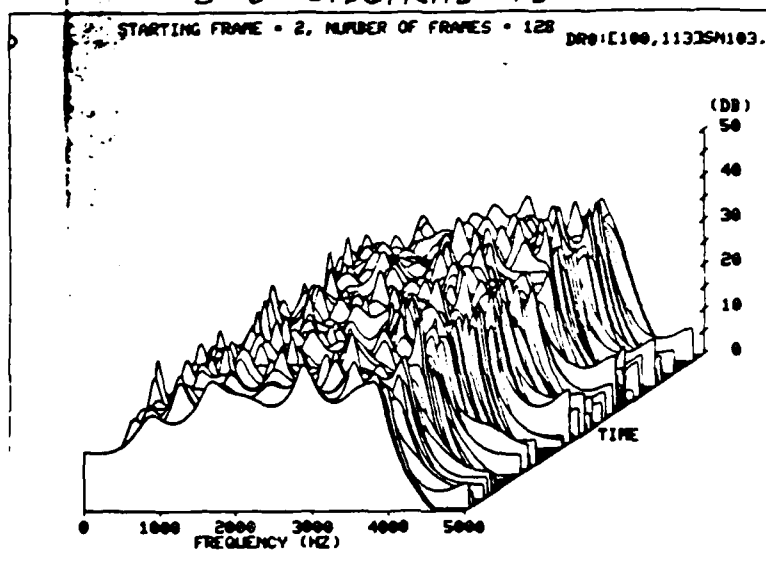


FIG. 7

RESIDUAL SEV. NOISE

3-D SPECTRAL PLOT



TIME DOMAIN SIGNAL, ENERGY VS. TIME, AND FORMANT TRACKING PLOT.

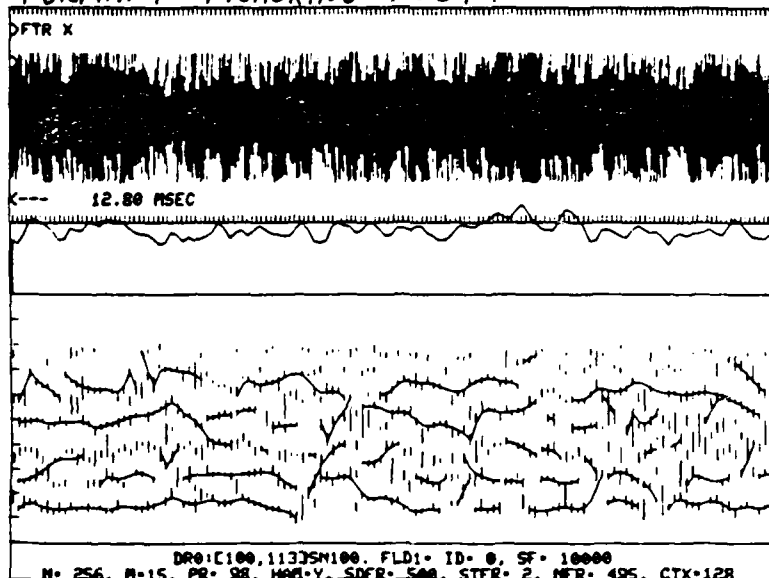
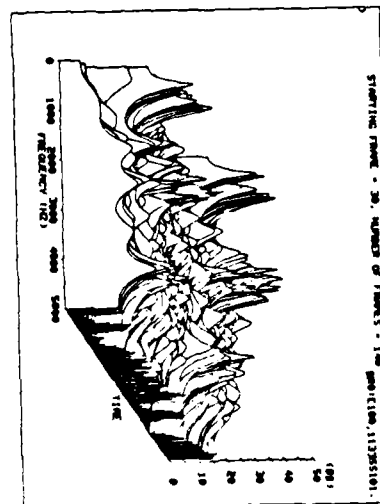
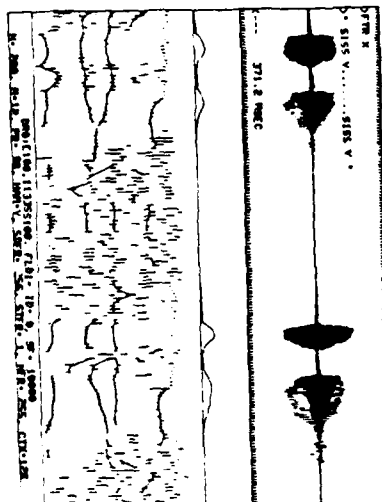
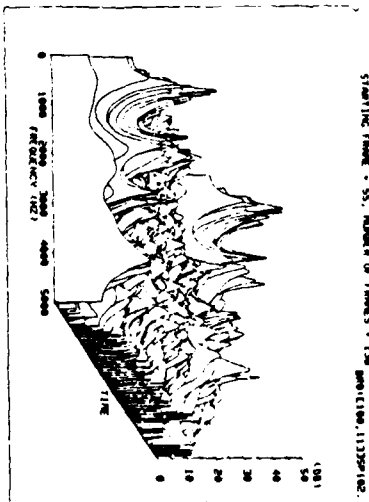
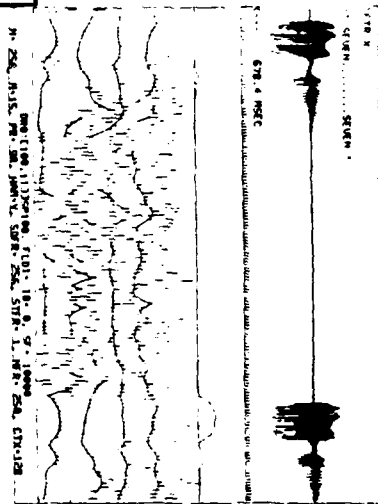


FIG. 9



1986 USAF-UES Summer Faculty Research Program/
Graduate Student Summer Support Program

Sponsored by the
Air Force Office of Scientific Research
Conducted by the
Universal Energy Systems, Inc.
Final Report

Knowledge for the ULCE Expert System

Prepared by:	Stephen Horn
Academic Rank:	Graduate Student
Department and University	Mechanical Engineering Massachusetts Institute of Technology
Research Location:	Materials Research Laboratory, AFWAL/MLTC, WPAFB, Ohio
USAF Research:	Major Steven R. LeClair
Date:	September 12, 1986
Contract No	F49620-85-C-0013

Knowledge for the ULCE Expert System

by
Stephen Horn

ABSTRACT

The knowledge needed for the ULCE expert system was identified and integrated. Boothroyd's assembly and Taguchi's producibility methods were studied for use in integrating manufacturing knowledge into the design knowledge. It was found that the design and manufacturing process operates in an universe of "lities" such as producibility, marketability, supportability, and inspectability. The Ishikawa technique was used to organize the "lities" into cause-and-effect diagrams. These diagrams were used to develop some IF-THEN rules. More work needs to be done in this area.

Acknowledgements

I would like to thank the Air Force Systems Command and the Air Force Office of Scientific Research for sponsorship of my research. The Materials Laboratory provided an intellectually stimulating environment. I would like to thank two members of the MLTC staff, Major Steven R. LeClair and Tom Lagnese, for giving me the opportunity and the guidance necessary for my research.

Finally, I would like to thank David Bridenstine, Gerald Graves, and Patty Evans, for many hours of lively debates about expert systems and artificial intelligence.

I. Introduction

My graduate research at the Massachusetts Institute of Technology is in axiomatic design and manufacturing, knowledge acquisition, and expert system. I have developed expert systems as part of my course work at MIT. The research problem at the AFWAL/MLTC involved the integration of manufacturing knowledge into the design knowledge. The MLTC research is motivated by the following observations:

- In current practice design and manufacturing are considered separately
- Decisions made at the product design stage have a major impact on both product quality and productivity
- Decisions made at the early stage of product conceptualization have the greatest effect on productivity

The integrated knowledge will be used in an expert system for unified life-cycle engineering (ULCE). The research problem under investigation at MLTC was, therefore, very similar to the problems I had studied at MIT. Because of this similarity I was assigned to work on the ULCE knowledge acquisition at MLTC.

II. Objectives of the Research Effort

The stated objective of ULCE is to make tradeoff decisions affecting the product during its entire lifetime while the design begins to take shape and when the investment in the product is small. The incredible complexity of the design process is a cliché, but it is a fact. The analogy for design is a river, the Grand Rapids of Design and Manufacturing (Figure 1). Design decisions made up-stream affect all subsequent outcomes.

The impact of tradeoff decisions can be seen clearly in Figure 2. The cost-time-leverage relationship is illustrated as a curtain. Great leverage can be exercised early in the design process.

There are many models of the design process. The traditional aerospace industry model⁽¹⁾ consists of three design stages: conceptual, preliminary and detailed. The conceptual design stage involves synthesis, the preliminary and detailed design stages analysis. Figure 3 outlines the stages and tasks in the design process. Figure 4 is a storyboard illustrating the synthesis-analysis evolution. In the information age of today a "blackhole analogy" (Figure 5) may be a better representation of integrated design and manufacturing. Declarative and procedural knowledge will be pulled into the design and manufacturing "blackhole" when needed.

My individual objective was to integrate the manufacturing knowledge into the design knowledge. The axiomatic approach to design was used as the starting point. Design and manufacturing methods of Boothroyd and Taguchi were investigated for use in the integration.

III. Design Axiomatics and Corporate Strategy

Two sources of knowledge that can be used at the meta-level of an expert system are design axiomatics and corporate strategy. They can be used to handle the combinatorial problems encountered the expert systems. Axiomatics defines design as the mapping process to transform the functional description of a product into a physical entity⁽²⁾. Figure 6 shows this mapping process. The role of the design axioms for the ULCE expert system is

- To provide the principles for the decision making in the synthesis of products and processes

- To rank quantitatively the alternatives in selecting the best design among several possible designs.
- To facilitate the creative thought process by eliminating irrational designs early in the design process and concentrating only on the best designs

Corporate strategy⁽³⁻⁶⁾ can be used to prioritize desirable characteristics of the production facility. Figure 7 shows the growth opportunities matrix a corporation can use in choosing a competitive strategy. Different "lities" hierarchies (Figures 8 and 9) can develop depending on a corporation's strategy.

IV. The "lities"

The design and manufacturing process (Figure 10) operates in an "universe of lities." There are many more "lities" than shown in Figure 10, and it is difficult to see the relationship of the "lities." A spelling-checker on a PC was used to help brainstorming about the "lities." Over 500 words with the last letters "lity" were located by this spelling-checker. The Ishikawa technique (see section VI) was used to organize these "lities" into diagrams. IF-THEN rules, the integrated knowledge for the ULCE expert system, were developed from examination of these diagrams.

V. Boothroyd and Taguchi Methods

The Boothroyd and Taguchi methods are two bodies of "lities" knowledge. Boothroyd's work⁽⁷⁻⁹⁾ deals with the assemblability of products. He has developed a scheme to decide the best assembly technology to use for any given design. The scheme was derived from empirical data. It is intended for small component assembly. Its use in aircraft design may not be appropriate. In addition supportability, marketability, inspectability etc. are not dealt with in the scheme.

The Boothroyd rules are specialization of the axiomatic corollaries. These corollaries and rules are compared below

Axiomatic Corollaries

Boothroyd Rules

Use standardized or interchangeable parts whenever possible.

Utilize standard components as much as possible.

Utilize standard preshaped workpieces

Use symmetric shapes and/or arrangements if they are consistent with functional requirements.

Attempt to make the parts symmetrical to avoid the need for extra orienting devices and the corresponding loss in feeder efficiency.

Try to facilitate assembly by providing chamfers or tapers.

Integrate functional requirements in a single part or solution if they can be independently satisfied in the proposed solution.

Minimize the number of parts.

Conserve the resources in fulfilling the functional requirements.

Avoid expensive and time-consuming fastening operations.

Employ standard machined features whenever possible.

Utilize raw material in the standard forms supplied

Taguchi's work (10-11) deals with the general producibility of products. His approach is to create a design which is robust via parameter design and he advocates starting design investigations by using low grade raw materials and component parts. The impact of tolerance is measured with the quality loss function.

The knowledge of design and manufacturing can be stated as a theorem as follows:

- Rational production of a product is not possible unless both the design of the products and the design of the processes satisfy functional independence (Suh, 1984)

VI. Ishikawa Diagrams

An Ishikawa⁽¹²⁾ or "fishbone" diagram (often called a "cause and effect diagram") was used to illustrate how the various factors came together to provide the "lity." Figures 11-14 are the Ishikawa diagrams for producibility, marketability, supportability, and inspectability respectively. Some production rules I developed from the four Ishikawa diagrams are

- IF a component requires lots of repair
THEN the problem may be in the training of repair personnel
OR the quality of the replacement part
- IF repairs are needed
THEN try to make them in situ
- IF there are planned maintenance schedules
THEN make the subsystems modular
- IF maintenance is required
THEN make sure repair parts are available
- IF a component cannot be made more reliable
THEN make it easy to get to
- IF the product will need routine inspections
THEN make it easy to disassemble

VII. Recommendations

1. The Ishikawa diagrams for producibility and marketability are almost finished. The experts should review these two diagrams and develop more rules.
2. Much work remains to be done with the Ishikawa diagrams for supportability and inspectability. The experts need to fill in the causes of these "ilities." Rules can then be developed from the diagrams.
3. Develop the ULCE expert system using the above types of knowledge. The architecture might look like Figure 15. The modes of operations are
 - new product design
 - major product design change
 - minor product design change

This expert system can be used on both derivative and future aircrafts. Aircrafts would be arranged by speed ranges (Figure 16). Associated with a speed range would be an aerodynamic shape. The subsystems are organized into a tree such as Figure 17. Portions of this expert system are function and feature driven (Figure 18). The feature driven portions could use the PDDI database.

4. The ULCE expert system can be developed incrementally by building a very simple system first. An example of a simple expert system using some of the above types of knowledge is a material selector. The concept of a template⁽¹³⁾ is used here (Figure 19). This system might be asked to select a cheap material with stiffness and strength constraints. A perceptual map such as Figure 20 might result.

References

1. Integrated Computer-Aided-Manufacturing (ICAM), Architecture Part II/Volumne VIII-Design Product, Report Number AFWAL-TR-81-4023, Volumne VIII, AFWAL/MLTC, Wright-Patterson AFB, Ohio, June 1981
2. Suh, N. "Development of the Science Base for the Manufacturing Field Through the Axiomatic Approach," Robotics and Computer Integrated Manufacturing, Vol. 1, No 3/4, 1984
3. Porter, Michael E., Competitive Strategy, The Free Press, 1980.
4. Skinner, W., "The Focused Factory," Harvard Business Review, May/June 1974
5. Ansoff, H.I., "Strategies for Diversification," Harvard Business Review, September/October 1957.
6. Urban, G.L. and J.R. Hauser, Design and Marketing of New Products, Prentice-Hall, Inc., 1980.
7. Boothroyd, Geoffrey, Fundamentals of Metal Machining and Machine Tools, McGraw-Hill Book Company, 1975.
8. Boothroyd, Geoffrey, C. Poli, and L. E. Murch, Automatic Assembly, Marcel Dekker, Inc., 1982.
9. Boothroyd, G. and P. Dewhurst, Design for Assembly, Boothroyd Dewhurst, Inc., 1983.
10. Taguchi, G. and Y. Wu, Introduction to Off-Line Quality Control, Central Japan Quality Control Association, 1979
11. Taguchi, G., "Quality Engineering in Japan," Proceeding CAD/CAM, Robotics and Automation International Conference, 1985.
12. Ishikawa, K., Guide to Quality Control, Asian Productivity Organization, 1976.
13. Bradberry, M., J. Entekin and D. Jackson, Development and Validation of a Conceptual Aircraft Design Decision Support Problem Template, The Systems Design Group, Department of Mechanical Engineering, University of Houston-University Park, Houston, Texas, May 1986.

Cost-Time - Leverage Relationships

of

Design and Manufacturing Process

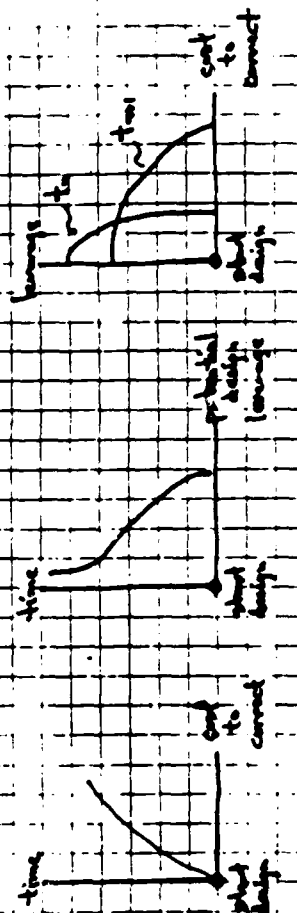
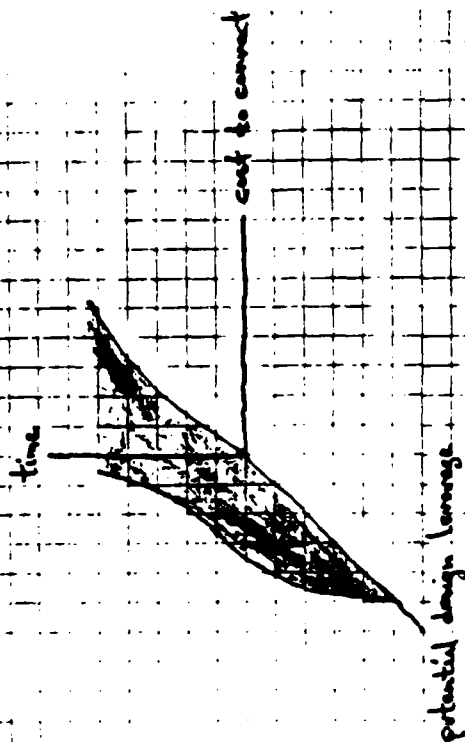


Figure 2
Cost-Time-Leverage

The design decisions made at the upstream of engineering practice affect all subsequent outcomes

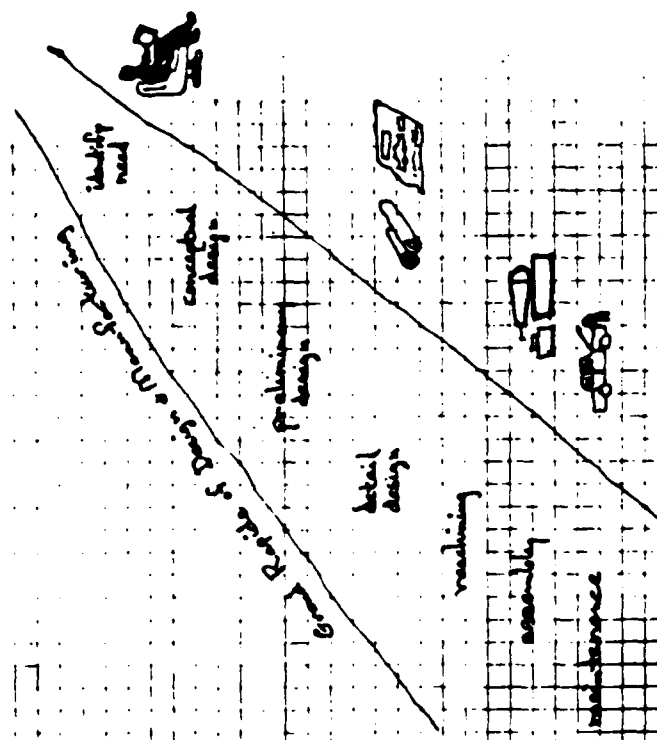


Figure 1
Grand Rapids

The Design Process Stages and Tasks

Conceptual Design Stage

- conduct research
- analyze requirements
- formulate concepts
- select candidate

Preliminary Design Stage

- refine candidate
- select optimum
- review and approve

Detail Design Stage

- develop design layouts
- prepare detail design
- release detail design

Figure 3
Design Process

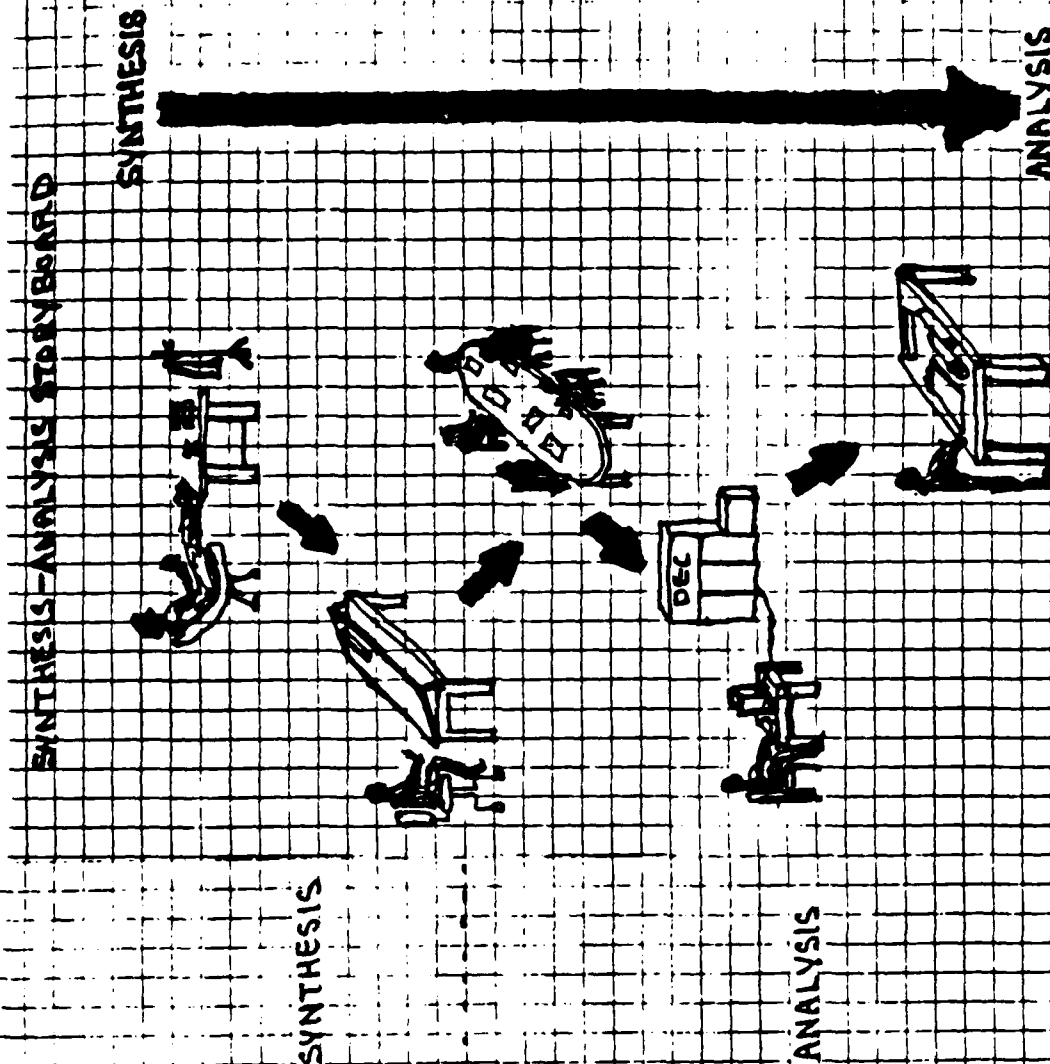


Figure 4
Synthesis-Analysis

Temporal and Spatial Spinal for Design

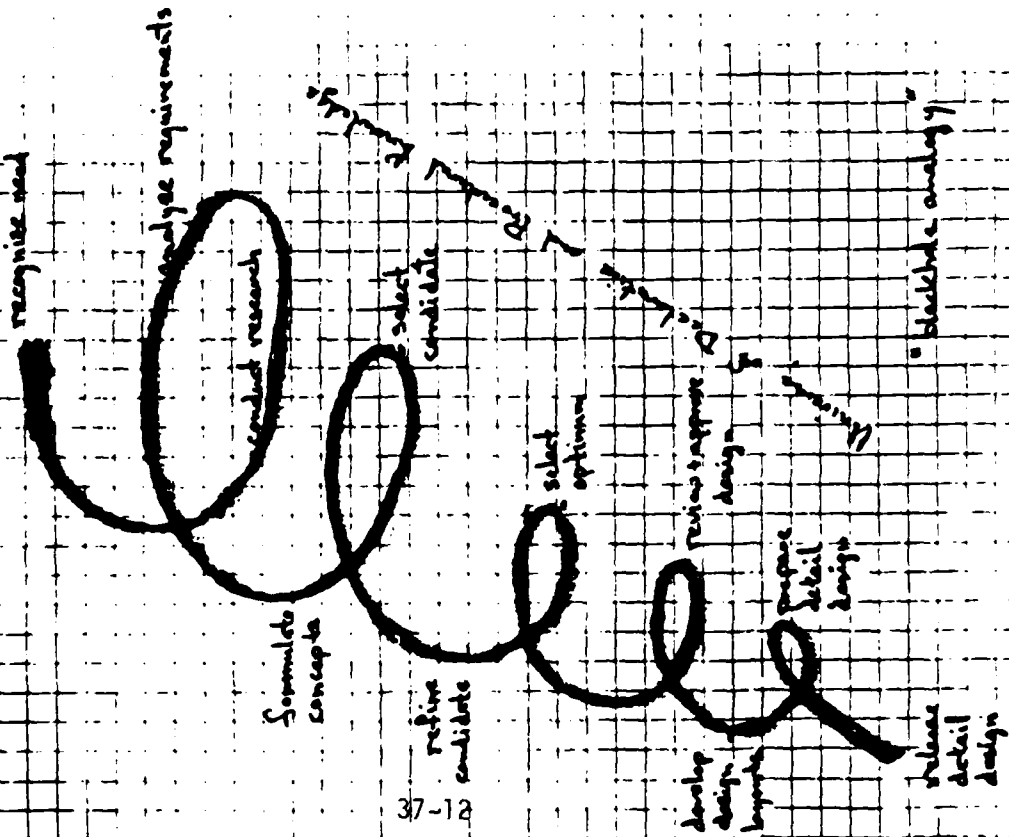


Figure 5
Blackhole

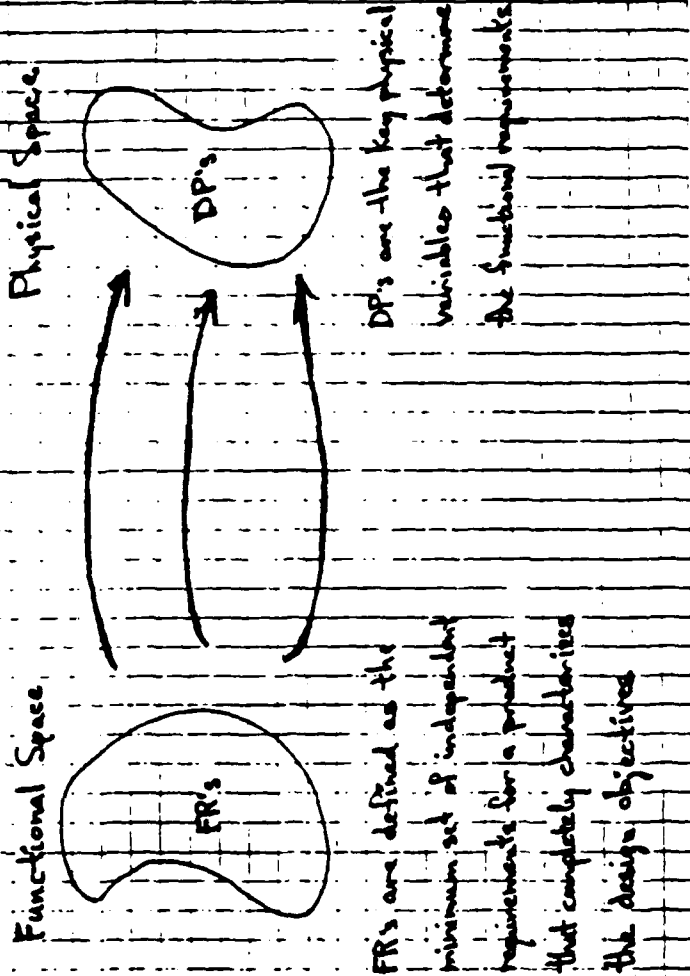


Figure 6
Axiomatic

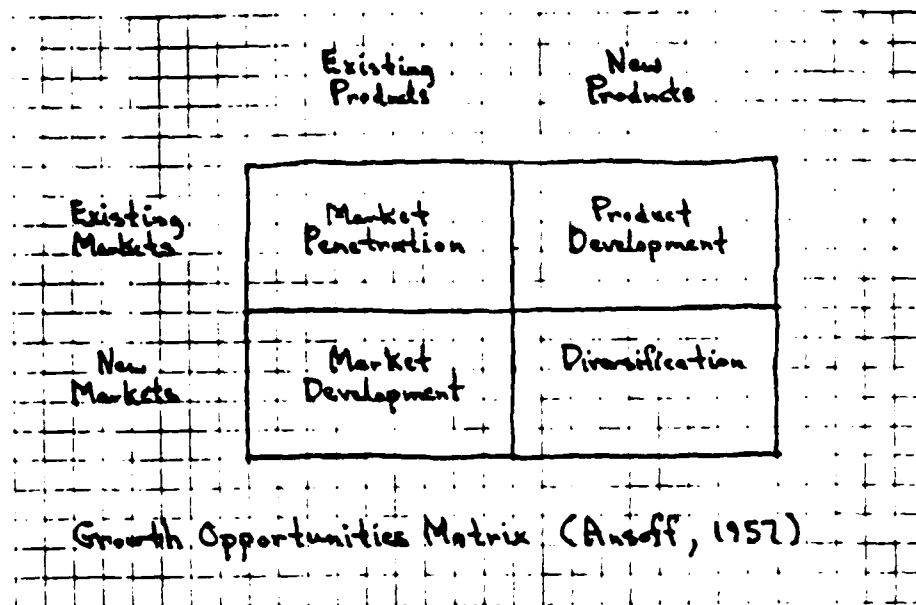
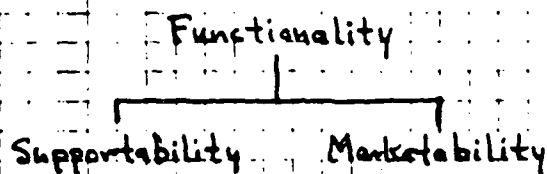


Figure 7
Matrix

Fighter Aircrafts

- Corporate Strategy - technological high risk products
 - low production volume
 - frequent planned changes
 - new products / existing markets

A Hierarchy of "ilities"



* Wickham Skinner, HBS

Figure 8
Fighter Aircrafts

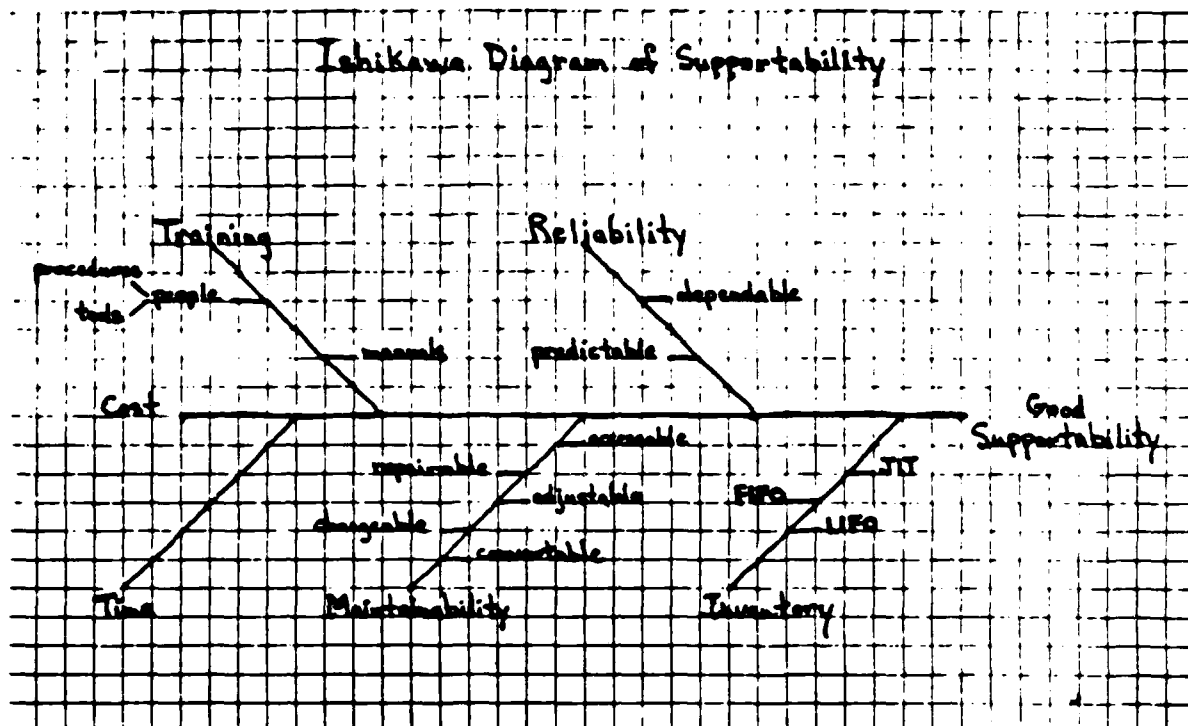


Figure 13
Supportability

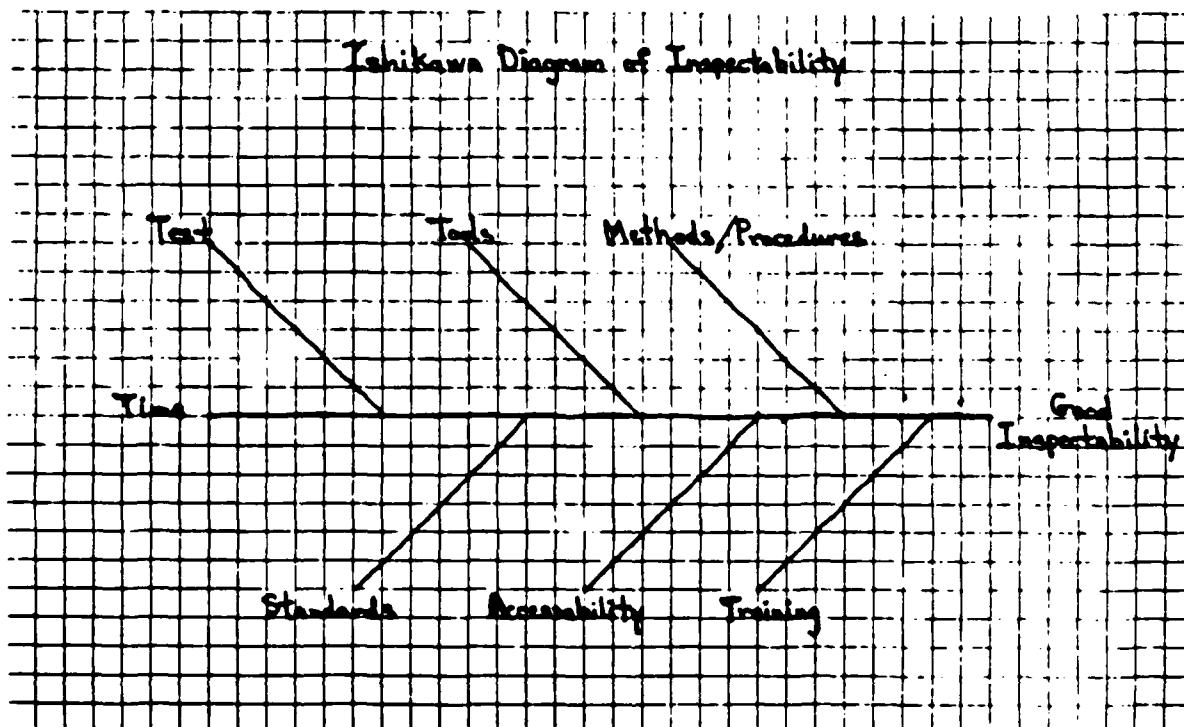


Figure 14
Inspectability

Modes of Operation for Executive Expert System

- Entirely new product design
 - develop conceptual design
 - develop preliminary design
 - develop detail design
- Major product design change
 - develop preliminary design
 - develop detail design
- Minor product design change
 - develop detail design

Figure 15
Expert System

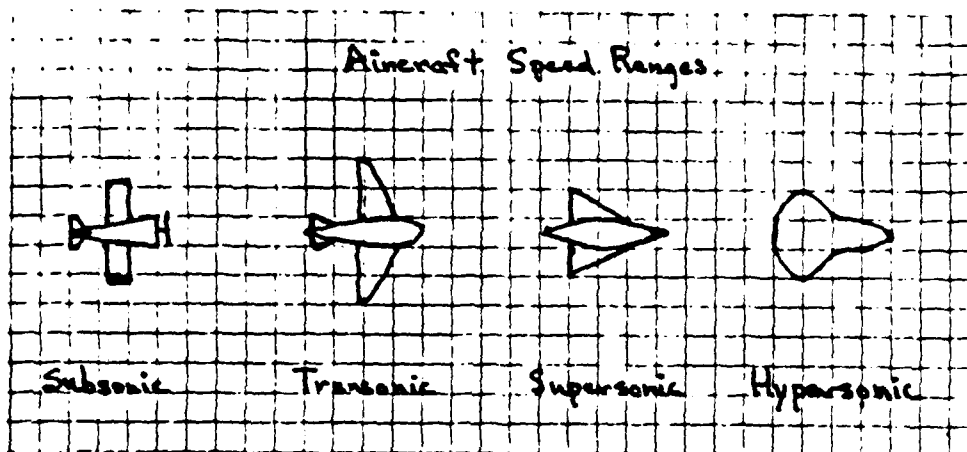


Figure 16
Speed Ranges

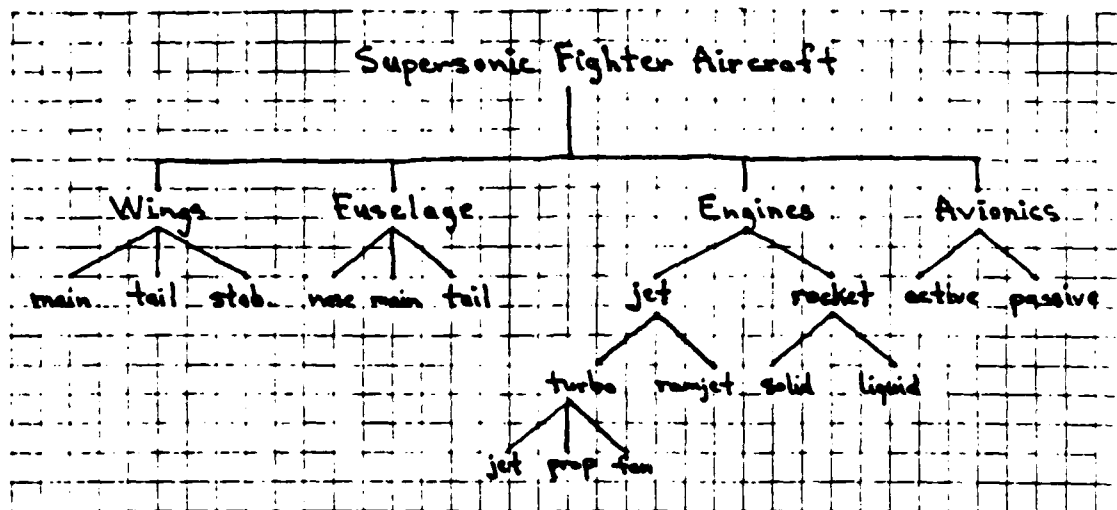


Figure 17
Subsystems

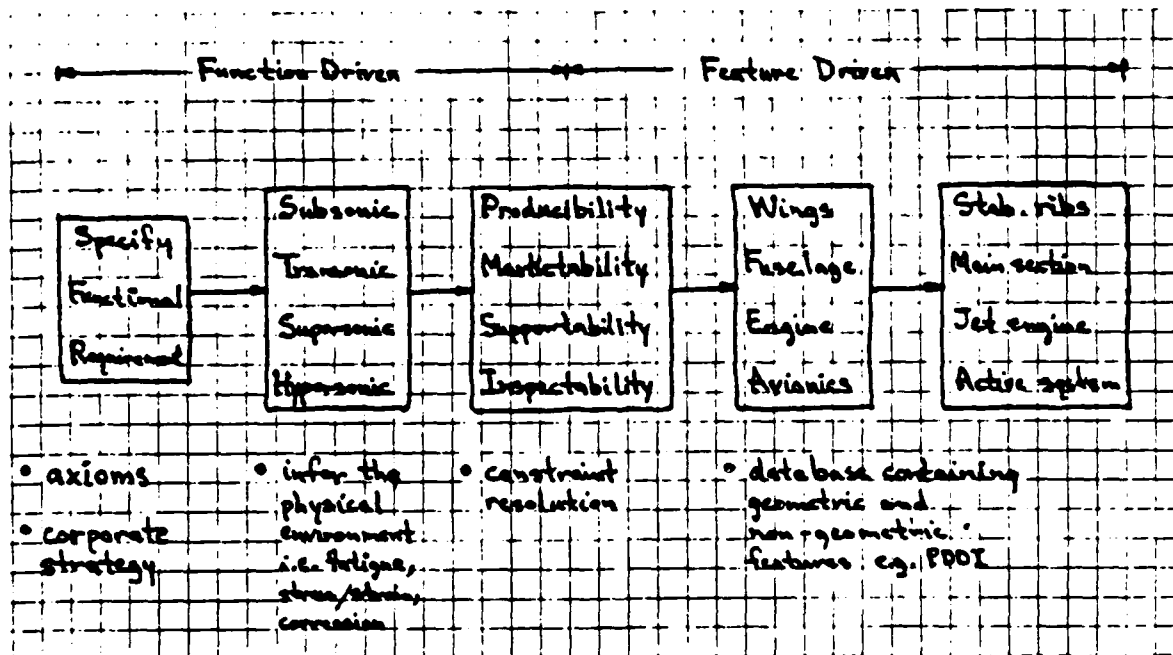


Figure 18
Function/Feature

Template for Material Selection

Problem Type

Strength
Max. Ten. Stress
Fatigue Stress

Stiffness
Modulus
Density

Economics
Cost/Unit
Salvage Value

Constraints

Strength
Max. Allow. Def.

Stiffness
Frequency

Economics
Min. Cost

Parameters

General Dimensions
Length
Dia (or W x H)

Derived
Mom. of Inertia
Cross Sect. Area

Analysis Routines

Analysis
FEA

Optimizer
Linear

Figure 19
Template

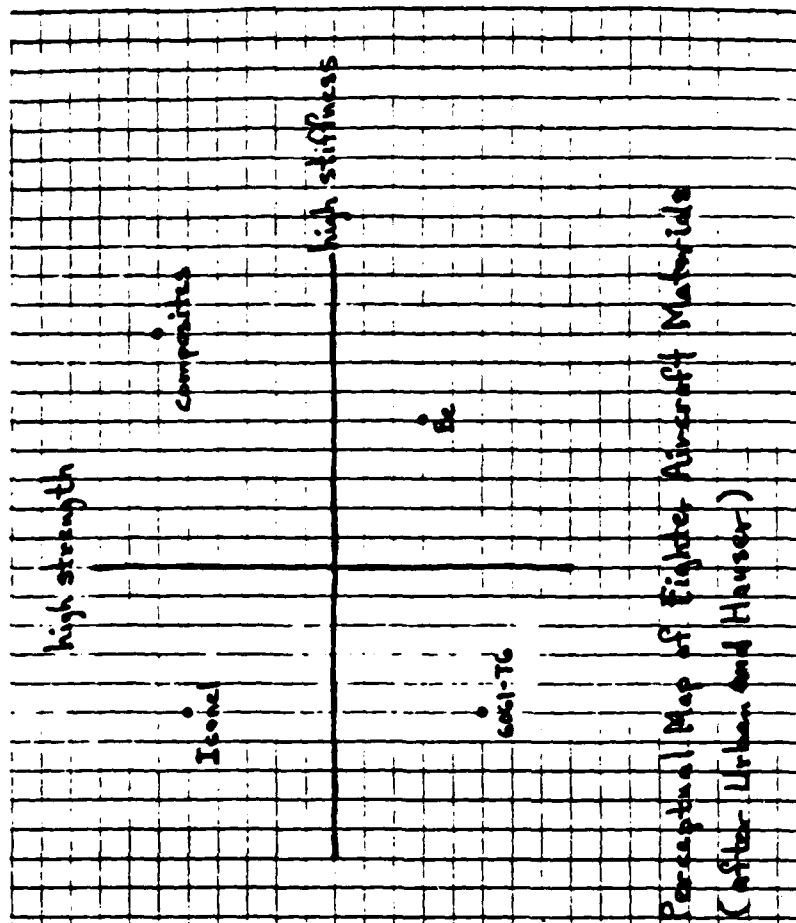


Figure 20
Perceptual Map

Perceptual Map of Fighter Aircraft Materials
(after Urban and Hauser)

1986 USAF-UES SUMMER FACULTY RESEARCH PROGRAM/
GRADUATE STUDENT SUMMER SUPPORT PROGRAM

Sponsored by the
AIR FORCE OFFICE OF SCIENTIFIC RESEARCH

Conducted by the
UNIVERSAL ENERGY SYSTEMS, INC.

FINAL REPORT

AN ANALYTICAL INVESTIGATION FOR DESIGNING AN ENERGY STORAGE
CONTAINER FOR STORING LITHIUM HYDRIDE BETWEEN 300K AND 1200K

Prepared by:	Jamal A. Hussein
Academic Rank:	Graduate Student
Department and	Mechanical Engineering Dept.
University:	University of Toledo
Research Location:	Aero-Propulsion Laboratory, Aerospace Power Division, Power Technology Branch, Nuclear/Thermal Technology Group
USAF Research:	Elliot Kennel
Date:	Aug. 22, 1986
Contract No:	F49620-85-C-0013

An Analytical Investigation for Designing an Energy
Storage Container for Storing Lithium Hydride
Between 300K and 1200K

by

Jamal A. Hussein

ABSTRACT

Stresses on a spherical container was considered for storing lithium hydride between 300K and 1200K. The materials investigated for the container shell were silicon carbide layer sandwiched between two thin layers of molybdenum. Silicon carbide and molybdenum were chosen for their properties at high temperatures. The pressure generated on the shell due to the thermal expansions of lithium hydride was determined using elastic theory. The corresponding container thickness required to withstand this pressure was found as a function of the assumed properties of LiH and sphere radius. Finally, the analysis shows that the ratio of the container thickness to the outer radius is constant ($t/r = 0.11$).

AKNOWLEDGEMENTS

I would like to thank the Air Force Command and the Air Force Office of Scientific Research for sponsorship of my research. I would like to thank several members of the Aero-Propulsion Laboratory, Ms Jill Johnson and Mr. Elliot Kennel, for giving me the guidance necessary for this research.

I. Introduction

Recently, I have graduated with M.S. degree in Mechanical Engineering from the University of Toledo, where I was a lab instructor. The courses I studied were related to the design and thermal science areas.

The research problem at the USAF propulsion laboratory involved a combination of heat transfer and design of a thermal energy storage sphere for storing lithium hydride at a temperature range of 300K-1300K.

The design problem that I was assigned to investigate, is related to my studies at the University of Toledo. Thus, due to the similarities of this research and my area of specialization I was assigned to analyze the stresses in this thermal storage sphere.

II. Objectives of the Research Effort

The main objective of this research is to analyze the stresses on a spherical energy storage device. This device will be used to store lithium hydride (LiH) and receives heat from liquid sodium which flows around its outer surface. The temperature range of the sphere is between 300K and 1300K.

My objectives were:

1. To determine analytically the stresses on a sphere as a function of its internal and external pressures,

temperatures, and radii, also as a function of the materials properties.

2. To investigate the internal pressure caused by the expansion of lithium hydride upon heating.
3. To investigate the stresses caused by the above pressure on the lithium hydride layer that is formed upon heating from 1200K to 300K.
4. To write a computer program to aid in computing the above stresses.
5. Finally, to analyze and compare the above computed stresses, thus to determine the optimum sphere size in terms of its weight and energy storage capacity.

III. Properties of the System Materials

Lithium hydride is proposed as a heat storage medium for its exceptionally high latent heat of fusion, low density, and a convenient melting point (953K). A spherical shaped shell was considered for storing this mixture because of the following:

- a. It gives the lowest stress values.
- b. It contains the largest storage volume with minimum surface area.
- c. It has minimum thickness and surface area. Thus, a sphere could minimize material weight.

The materials considered for this design are silicon

carbide (SiC) sandwiched between two thin layers of molybdenum (Mo). SiC was chosen for its high strength at high temperatures [1], while Mo was chosen for its high corrosion resistance. Both materials have low permeabilities for hydrogen diffusion [2], thus eliminating the hydrogen diffusion problem. Also they both have high thermal conductivities, high melting points, and low coefficients of thermal expansion [3,4].

IV. Effects of Temperature Variation on the System

Due to the high thermal expansion of LiH (table III), some considerations should be taken for increase in volume with temperature (approximately 34%). This is in contrast to the Mo and the SiC shells which have low thermal expansions coefficients (tables I and II).

During the cooling stage, from 1200K to 300K, a void will be formed at the center. The radius of this void can be determined from a mass balance and is equal to 70% of the radius of the LiH sphere. However, when the system is reheated to 1200K, a constant temperature profile will exist in the SiC shell because of its high thermal conductivity, while the temperature differential in the LiH layer will be large because of its low thermal conductivity and high thermal capacity. The maximum temperature difference between the inside and the outside surfaces is expected to be ($T_m -$

Ti); where Tm and Ti are the melting and initial temperatures of LiH respectively. Due to this increase in temperature, both materials (the SiC shell and the LiH) will expand, since the thermal expansion coefficient of SiC is much lower than that of LiH, a pressure on the SiC shell will be generated. If the shell is not thick enough to withstand this pressure the container will rupture.

V. Analysis and Solution

Consider a very thin liquid LiH layer at its outer surface (Fig.1). Let the temperature of this layer be uniform and equal to its melting point. Since this layer is not free to expand at an uninhibited rate, a pressure P will be produced. The corresponding radial and tangential stresses, due to the pressure, on the SiC and LiH shells [5] are:

$$\sigma_{rSiC} = -P \quad \text{---} \quad 1$$

$$\sigma_{tSiC} = Pb/2h \quad \text{---} \quad 2$$

$$\sigma_{rLiH} = Pc^3 (r^3 - \frac{3}{a}) / r^3 (a^3 - c^3) \quad \text{---} \quad 3$$

$$\sigma_{tLiH} = Pc^3 (2r^3 + a^3) / 2r^3 (a^3 - c^3) \quad \text{---} \quad 4$$

The above pressure can be obtained from the elastic behavior of SiC and LiH materials. However; more assumptions are necessary for a closed form solution. These assumptions used are:

1. The container shell is a thin shell made of SiC only and is at a constant temperature.

2. The LiH layer can be treated as a thick shell and has a temperature distribution of the form :

$$T = T_o + [(T_i - T_o) \log(c/r) / \log(c/a)]$$

Where; T_o = surface temperature.

Because of the low thermal conductivity of LiH, the above logarithmic temperature profile was chosen. This profile is expected to give a reasonable approximation of the temperature distribution in the LiH shell.

The radial expansion in the thin liquid LiH layer due temperature rise is the summation of the increase in radii of the SiC and LiH shells. The radial increase for each section can be obtained from equation 263 in ref.5, the boundary conditions ($\sigma_{rLiH} = 0$ for $r=a$, and $\sigma_{rLiH} = -P$ for $r=c$), and the above temperature profile (for the solid LiH layer only). Therefore, the radial change in the liquid LiH layer is:

$$U_{L,L} = [T \alpha_L / 3(1-\nu_L)] [(1+\nu_L)(b^3 - c^3 / b^2) + 3c(1-\nu_L)] \quad - - \quad 5$$

the radial change in the SiC shell is:

$$U_S = \alpha_S T_o + (\sigma_{tsic} b)(1-\nu_S) / E_S \quad - - - - - \quad 6$$

and the radial change in the LiH shell is:

$$U_{S,L} = [T \alpha_L / (3(1-\nu_L))] [(1+\nu_L)(\log c / r) / (\log c / a) + (r^2 - a^2) / (3r^3 \log c / a) - 1] + (2(1-2\nu_L) + a^3 / r^3) (1 / (3 \log c / a) - a^3 / (c^3 - a^3) - 1)] \quad - - - - - \quad 7$$

Where; ν is Poisson's Ratio, E is the modulus of elasticity, and α is the thermal expansion.

The total tangential stresses on the LiH layer due to pressure and temperature rise are:

$$\sigma_{T, LiH} = [\alpha E_L / 3(1-\nu_L)] [2 - (c^3 / (c^3 - a^3)) (2 + a^3 / r^3) + (1/\log c/a) (1 - 2\log c/r)] + \sigma_{tLiH} \quad - - - - - 8$$

VI. Results and Discussion

The primary purpose of this investigation was to develop an analytical relation for determining the required container thickness. The pressure generated due to thermal expansions can be found from equations 5, 6, and 7. Hence:

$$U_{L,L} = U_S + U_{S,L}$$

This pressure is then used in equation 8 to determine the stresses across the LiH sphere shell at different modulus of elasticity values (E_L). It was important to vary E_L , since its exact value is not available. It was found that from 8, the LiH shell is in compression and the generated stress values are much larger than the compressive strength of LiH. Since this pressure is too large, the minimum pressure to cause fracture in the LiH shell was found by substituting the LiH compressive strength in 4. This pressure is then used in 2 to determine the SiC shell thickness.

Figure 2 shows the effects of varying the E_L values on

the internal pressure. This pressure is increasing rapidly with the increase in E_L values. The SiC thickness is dependent on the LiH outer sphere radius (figure 3). The ratio of the required container shell thickness to its internal radius was found to be constant ($t/r = 0.11$). Thus, thickness values, for a corresponding LiH outer radius value, above the ratio line can be considered as a design value. If a factor of safety is required the SiC thickness should be increased appropriately.

VII. CONCLUSIONS

A computer program utilizing the elastic theory was written to determine the generated pressure due to thermal expansions of LiH as a function of the inner radius of the SiC sphere and the properties of SiC and LiH at the maximum temperature difference between the inner and outer surfaces of the LiH shell.

From the computed results it was found that :

1. The ratio of the minimum SiC container thickness to the LiH sphere outer radius is constant and equal to 0.11.
2. The generated pressure "P" increases with the increase in radius, container thickness, and LiH modulus of elasticity.
3. The generated pressure will not effect the thickness to radius ratio for any LiH outer radius.

4. The LiH shell is in compression for any LiH modulus of elasticity value.

VII. RECOMMENDATIONS

1. The obtained results are due to thermal expansion only. If the sphere is in contact with other spheres, a non-uniform pressure distribution will produce an additional compressive stresses on the sphere outer surface which will result in different boundary conditions that should be considered for sizing the sphere.

2. Silicon carbide has exceptional properties at high temperatures. However, if it is used where large temperature fluctuations and a low safety factors are necessary the container shell might fracture due to fatigue. Thus an analysis concerning this fatigue, for sizing the container, should be considered for further investigations.

3. A steady state temperature distribution was used which resulted in large stress values on the LiH shell. However; more accurate relations can be obtained by using a transient temperature distribution.

REFERENCES

1. Weaver, G.Q., and B.A. Olsen, "High Strength Silicon Carbide for Use in Severe Enviroments," Proc. of the Third International Conference on Silicon Carbide, Miami Beach, florida, September 1973, pp. 367-374.
2. Causey, R.A., J.P., Fowler, and C. Ravanbakht, "Hydrogen Diffusion and Solubility in Silicon Carbide," Journal of the American Ceramic Society, Vol. 61, No. 5-6, 1978, pp. 221-225.
3. Kern, E.L., D.W. Hamill, H.w. Deem, and H.D. Sheets, "Thermal Properties of B-Silicon Carbide from 20-2000 C," Bull. Mat. Res., Vol. 4, pp. s25-s32.
4. Northcott, Molybdenum, New York Academic Press Inc. Publishers, 1956.
5. Timoshenko, Goodier, Theory of Elasticity, McGraw-Hill Book Company, 1970.

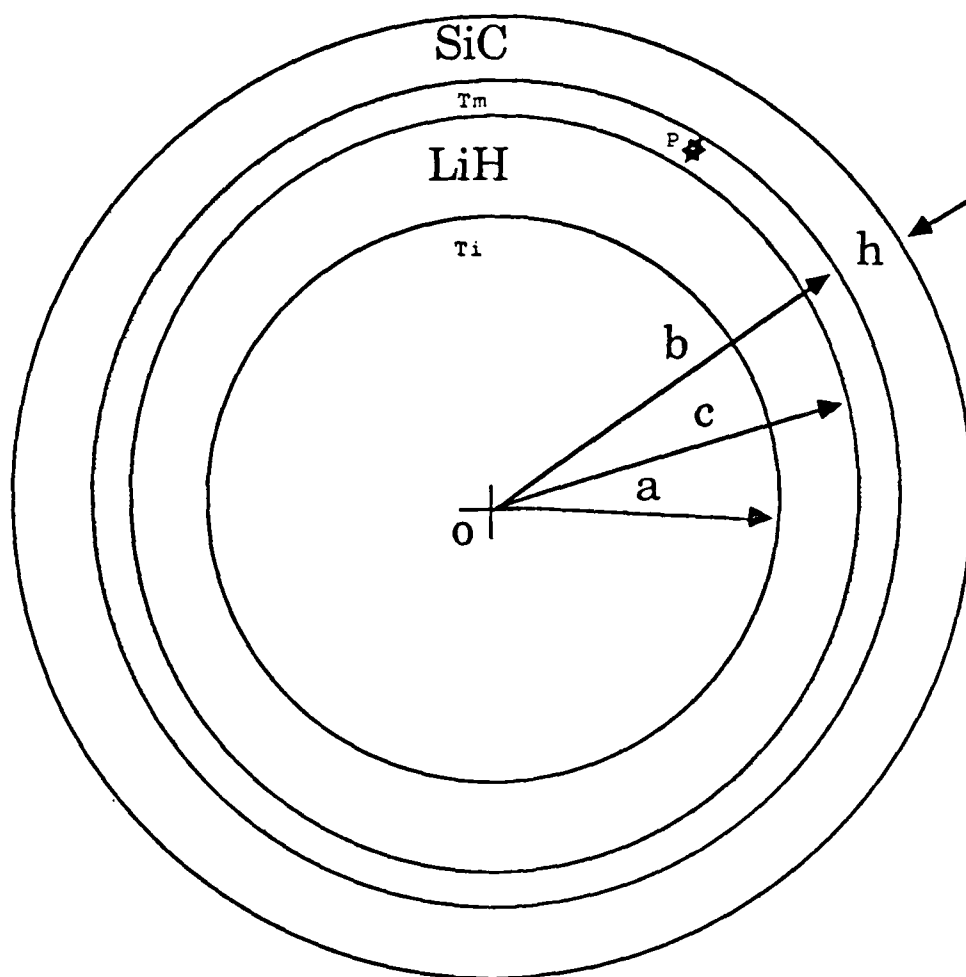


Figure 1

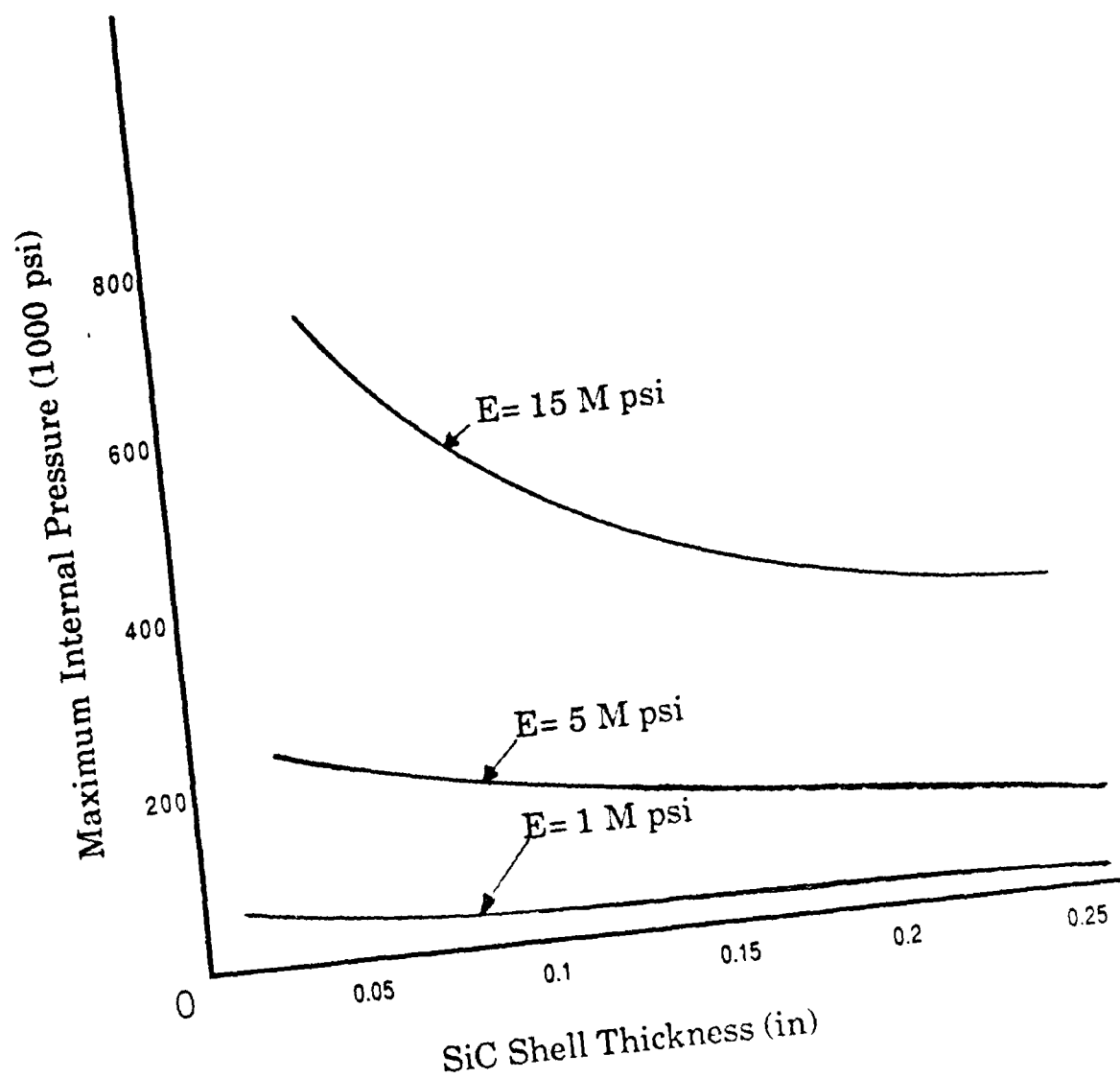


Figure 2

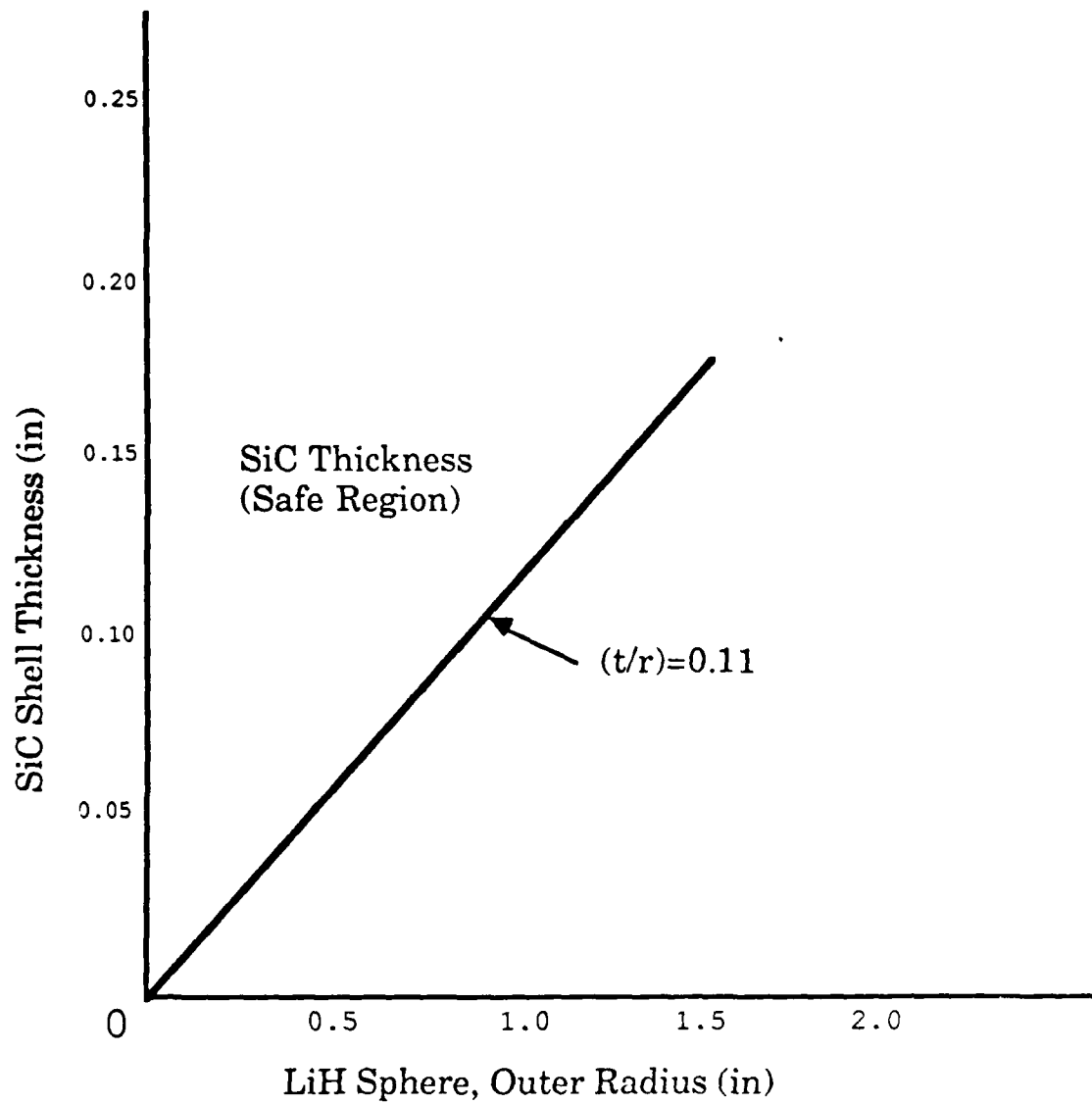


Figure 3

Table I Physical and Thermal Properties of α -SiC

* Temp (T) K	* Coef. Therm. Expan. * $\times 10^{-6}$ /C	* Density * g/cu.cm	* Tensile Strength * MPa	* Comp. Strength * MPa	* E * MPa	* ν *	* K W/m K
* 300	* 3.18	* 3.166	* 207	* 734	* 440,000	* 0.17	* 78
* 1200	* 5.81	* 3.130	* 172	* 586	* 419,000	* 0.18	* 39
* F	* $\times 10^{-6}$ /F	* lb/cu.ft	* psi	* psi	* psi $\times 10^6$	-	* BTU/h ft F
* 80	* 1.77	* 197.7	* 30,000	* 105,000	* 63.8	* 0.17	* 45.0
* 1700	* 3.23	* 195.5	* 25,000	* 85,000	* 60.8	* 0.18	* 28.5

Table II Physical and Thermal Properties of Molybdenum

* Temp. (T) K	* Coef. Therm. Expan. * $\times 10^{-6}$ /C	* Density * g/cu.cm	* Tensile Strength * MPa	* Elastic Limit * MPa	* E * MPa	* ν *	* K W/m K
* 300	* 5.40	* 10.2	* 462-670	* 396	* 317,000	* 0.324	* 132
* 1200	* 6.15	-	* 172-350	* 96	* 269,000	* 0.320	* 93
* F	* $\times 10^{-6}$ /F	* lb/cu.ft	* psi $\times 10^3$	* psi $\times 10^3$	* psi $\times 10^6$	-	* BTU/h ft F
* 80	* 3.00	* 637	* 67-97	* 3	* 46	* 0.324	* 76
* 1700	* 3.42	-	* 25-52	* 4	* 39	* 0.320	* 57

Table III Physical and Thermal Properties of LiH

* temp (T) K	* Coef. Therm. Expan. * $\times 10^{-6}$ /C	* Density * g/cu.cm	* Comp. Streng. * MPa	* Heat of Fusion * J/g	* k W/m K
* 300	* 38.16	* 0.79	* 97-166	* 2532	* 4.0
* 1200	* 45.36	* 0.49	-	-	-
* F	* $\times 10^{-6}$ /F	* lb/cu.ft	* psi $\times 10^3$	* BTU/lb	* BTU/h ft F
* 90	* 21.20	* 48.3	* 14-24	* 1113	* 2.25
* 1700	* 25.20	* 30.6	-	-	-

1986 USAF-UES SUMMER FACULTY RESEARCH PROGRAM/

GRADUATE STUDENT SUMMER SUPPORT PROGRAM

Sponsored by the

AIR FORCE OFFICE OF SCIENTIFIC RESEARCH

Conducted by the

Universal Energy Systems, Inc.

FINAL REPORT

Modeling of Human Body Movement

Prepared by: Patrick R. Hannon
Academic Rank: Associate Professor
Department and Department of Health, Physical
University: Education and Recreation
Northern Arizona University
David Jansen
Graduate Student
Department of Zoology
Washington State University

Research Location: The Harry G. Armstrong Aerospace Medical Research
Laboratory, Biodynamics and Biomedical Engineering: Modeling and Analysis
Wright-Patterson Air Force Base

USAF Researcher: Ints Kaleps-Chief, Modeling and Analysis

Date: September 3, 1986

Contract no: F49620-85-C-0013

Modeling of Human Body Movement

by

Patrick Hannon and David Jansen

ABSTRACT

The Articulated Total Body (ATB) model is used to simulate biodynamic responses due to forces on the human body such as localized contact forces, aerodynamic drag, or internal muscular forces. Validation and possible improvement of the model was investigated through two approaches. A skilled motor performance, the overhand baseball throw was selected as the basis for the validation study, and three-dimensional experimental data from human subjects were obtained. In the first approach, muscle forces derived from the literature were input to the model for the right upper limb. The time courses for the muscle forces were obtained from electromyography studies of overarm throwing. Good statistical correspondence between the experimental data and the output from the simulation resulted. The second approach involved prescribing the motion of a single joint (the right knuckle) and adjusting other parameters of the ATB model to obtain correspondence with the experimental data. No muscular forces were involved in this approach. Significant statistical correspondence resulted, though not as high as with the first approach. Recommendations for further validation and development of the ATB model were made.

ACKNOWLEDGEMENTS

We would like to thank the Air Force Systems Command and the Air Force Office of Scientific Research for sponsorship of our research. The Harry G. Armstrong Aerospace Medical Research Laboratory provided an intellectually stimulating environment. We would like to thank several people on the Biodynamics and Biomedical Engineering/Modeling and Analysis staff, Ms. Louise Obergefell, Dr. Bob Beecher, and Mr. Ric Rasmussen, for giving us the opportunity and the guidance necessary for our research. We would also like to thank Mr. Jim Ryerson of Systems Research Laboratories for his help in smoothing our raw data. A special thanks goes to Branch Chief Dr. Ints Kaleps for his guidance and interest in our project and also for his hospitality during this past summer.

I. Introduction

Patrick Hannon

I received my Ed. D. in Physical Education from the University of Northern Colorado with a major specialization in motor control and a minor specialization in biomechanics in 1980.

My research experience includes working in the Locomotion Laboratory of Northern Arizona University which is jointly operated by Biology and Physical Education. Much of the work done in this facility has been collaborative with Biology and Physical Therapy professors. My faculty exchange experience during the 1984-85 academic year at Montana State University allowed me to work with Dr. Ellen Krieghbaum in biomechanics and Dr. Jim McMillan in neurophysiology.

David Jansen

I am currently a Ph. D. candidate at Washington State University (WSU). My dissertation involves the evolution and biomechanics of the cephalic region of venomous snakes. During my research I employed static analysis to describe the actions of snake jaws. It was also necessary to mathematically model the results, using a microcomputer.

I was also trained in human anatomy while at WSU, having spent five years teaching anatomy of the head, neck and trunk to medical students.

The Armstrong Aerospace Medical Research Laboratory is involved in biomechanical analysis and computer modeling of human movement. The Articulated Total Body Model simulates human movement with a 15 segment model which allows 3-dimensional analysis, incorporating resistive joint

properties and musculature forces. Two current problems being investigated by the Modeling and Analysis Laboratory are human body motion during emergency aircraft ejection and abrupt horizontal deceleration. Although computer modeling of human motion was a new approach for us, our background in biomechanics and human and animal motor control were useful for our selected problem.

II. Objectives of the Research Effort:

The overall objective of our simulation study was to provide information about muscle activity across joints for a selected motor skill, and in turn make comparisons between the ATB model output and the measured 3-dimensional kinematics.

The overarm throwing pattern was chosen for analysis for a number of reasons. First, there exists good descriptive data for this motor skill (specifically x,y,z kinematic data). Secondly, the upper extremity in overarm throwing is a system of three kinetic links with internal muscle torques acting between the segments of the system. This segmental link system is classified as an open kinetic chain where the most distal segment (the hand) is not fixed, but is free to move in space. Therefore, the movement is reasonably but not overly complex. Thirdly, this movement presents similarities to the limb flailing which may occur as a response to aerodynamic drag and lift forces imposed upon a pilot during aircraft ejection.

Individual Objectives:

1. The major purpose of our research effort was to input estimated muscle force data for overarm throwing into the ATB model and compare the model's predicted kinematics with the actual reported three dimensional

kinematic data.

2. A second objective of our research effort was to prescribe limited kinematic data from an overarm throwing movement pattern for the ATB model and simulate the remaining kinematics.

The Articulated Total Body (ATB) model divides the human body into 15 segments linked by 14 diarthrodial joints. The hand and forearm are normally combined into one segment in the ATB model. Our investigation made it necessary to modify the model by resegmenting the forearms and creating right and left wrist joints and hand segments. Body segments of the ATB Model react to input in the form of imposed external forces and to internal (muscular) forces acting across segment articulations.

Recently, reasonably accurate x, y, z kinematic data, with estimated joint centers, has been collected by Feltner (1986). This data was collected on skilled college varsity baseball pitchers at Indiana State University. The reduced data from one right handed male pitcher, age 19, served as the criterion kinematics for the present computer simulations study.

III. Simulation 1

Our first approach involved inputting estimated muscle force data for overarm throwing into the ATB Model in order to compare the model's predicted kinematics with the experimentally collected 3-dimensional kinematic data. We were able to estimate muscle forces from electromyographic (EMG) records of the overarm throwing skill, since electromyographic measures provide a reasonably good within-subject approximation of force production (Bigland-Ritchie, 1981). Therefore, estimated forces from EMG data were used in the ATB model and refined in

an iterative fashion such that appropriate kinematics resulted. The approach that we used was to incorporate EMG on-off times for upper limb musculature during the overarm throwing motion into the modified 17 segment ATB model. The muscle activation patterns during overarm throwing were derived from several sources, including Anderson (1976), Fisk (1976), Jobe, et al. (1983), Jobe et al. (1984). Jobe et al. (1983) and Jobe et al. (1984) were able to estimate from rectified, integrated EMG data the percent of maximal voluntary isometric contraction of active muscles during the time history of the overarm throwing skill. These integrated EMG patterns permitted and led to our development of estimated force curves for agonist and antagonist musculature throughout the throwing sequence. These force curves were based in part on the work of Freivalds (1985). Freivalds (1985) incorporated a number of factors into his program modification of the ATB model (ATBMUS) including the relative percentage of fiber types within a muscle, the percentage of total motor unit recruitment, the parallel elastic component, the length-tension relationship of muscle, and the force-velocity relationship of muscle. Each muscle is assumed to act and react as a restraining belt applying tension to various body segments. Our use of Freivalds work included inputting twelve muscles (belts) in the upper torso, upper arm, and forearm and using his estimates of maximal muscle force production for each muscle as the basis for our force estimates at maximal and submaximal levels. Estimating force production at each interval during the time history was accomplished by calculating the product of the percentage of maximal voluntary isometric contraction and Freivald's estimated maximal force for each muscle. Thus, the musculature was made

active at specific times throughout the motion and the intensity of the activity (magnitude of each belt function) was variable throughout the throwing motion (Table 1). Additionally, Freivalds work supplied the attachment points for each muscle within each affected segment. These points of force application for each muscle were also entered into the ATB Model.

Broer (1969) and Toyoshima et al.(1974) indicate that approximately 50% of the linear velocity of the ball is achieved prior to the upper limb segments coming into play. Cinematography indicates that much of this linear velocity is the result of trunk rotation about the longitudinal body axis. In order to model the overarm throw, we have prescribed the trunk orientation and rotations from the initial x,y,z data. The input of trunk rotations along with muscle activated movement of the upper right limb segments allowed a computer simulation named Torque 1 that approximated the kinematic description of the throwing motion. The right shoulder coordinates along with the trunk rotations were prescribed and should have followed the experimental data for the shoulder. The ATB simulation did follow the trunk rotations, but drift was experienced for the linear position coordinates of the right shoulder throughout the motion. The ATB Model normally will follow prescribed data for a segment's orientation throughout the simulation.

Nevertheless, high correlations for the elbow and wrist points are obtained when the simulated points are plotted against the experimental data. Correlations for the right wrist range from a low of .719 to a high of .944 on the z and x axis respectively (Table 2). In a similar fashion, correlations for the right elbow range from .972 for the z axis

to .988 for the x axis. However, the y coordinates for the wrist and elbow indicate virtually no correlation between the experimental and simulated data points. We feel that some of the error in the y coordinate may be due to the noncompliance of the prescribed right shoulder position imposed by the model. The graphics from this simulation were obtained using the VIEW plotting program and are presented in Figure 1.

IV. Simulation 2

A second objective of this work was to enter a limited amount of prescribed kinematic data from an overarm throwing movement pattern into the ATB model and simulate the remaining body kinematics. In order to accomplish this objective, the hand was forced through the known motion and the joint properties adjusted so that the arm segments matched the kinematic data. First, the right knuckle x,y,z data (Feltner, 1986) was prescribed for the ATB model. Preliminary simulations indicated a need to adjust joint stops and stiffness properties. Through a series of iterations a more accurate simulation and graphic representation labeled Throw 1 resulted (Figure 2). Linear correlations comparing Throw 1 simulation with the experimental data are presented in Table 2. In general this simulation yielded a reasonably good representation of the upper extremity motion performed by the experimental subject. Pearson r values for the wrist x, y, and z values were highest because of the wrist's close proximity to the right knuckle prescribed motion, but these values were also reasonably high for the right elbow and shoulder joints.

A second model (Throw 2) involved moving our simulation performer from the true starting position, with the left foot raised, to a more

stable position with both feet on the ground surface. This adjustment in the starting position was made in order to prevent the performer from falling over during the simulation sequence. Further, a contact force was added between the upper arm and upper torso segments to keep the upper arm and elbow from passing through the upper torso during the latter stages of the simulation. The x,y, and z data correlations for the right wrist, elbow and shoulder are presented in Table 2. In general this new starting position did not result in a closer approximation of the experimental data.

V. Recommendations

1. The use of active muscle elements to drive a motion is a valuable contribution to the Modeling and Analysis Branch effort. The important implication from the first approach is that the ATB program, which incorporates active elements acting at body segments, may be of significant value in the modeling of human motion. In our work, muscular forces were input for the trunk and right upper extremity to drive segments in an appropriate motion that approximated x,y, z experimentally gathered points in a complex motor skill. If this result can be shown to generalize to other types of human motion, then movements which incorporate active musculature would best be modeled using EMG pattern data and the ATB program. Our preliminary work indicates that Frievalds estimation of maximal muscle forces and muscle attachment points may be reasonably accurate. Further, models of high acceleration situations such as high performance aircraft ejections probably involve the pretensing of musculature which can effect the resulting motion. Actions which involve pretensing musculature could be analyzed with

electromyography; then the data could be incorporated into human motion modeling efforts.

2. A second recommendation is that more work is needed to improve the ATB model. We are submitting a mini-grant proposal which will involve the collection of data in three areas: 1) 3-dimensional kinematics, 2) electromyography, and 3) force output measures. The major purpose of this work will be to integrate these measures during elbow flexion and extension motions. This will be accomplished by recording elbow force measures and electromyograms of selected upper arm and forearm muscles coincident with the measurement of 3-dimensional kinematics using a Watsmart analysis system.

3. A final recommendation is made for more work in the area of ATB model validation. This may be accomplished by comparing ATB and ATBMUS simulations with experimentally measured (3-dimensional) motion. In a similar fashion to our present work, a point on the body may be forced through a motion, and the other points can be made to follow this prescribed point during a simulation. What is needed are accurate 3-dimensional experimental data for complex human motions. Then joint stops, joint characteristics may be isolated and varied to successfully approximate the experimentally collected data set.

References

1. Anderson, M.B. (1976) Muscle patterning in the overarm throw and tennis serve: An electromyographic and film study of the skilled and less skilled performance. Ph. D.Thesis, U. of Wisconsin-Madison.
2. Andrews JG (1982) On the relationship between resultant joint torques and muscular activity. Med Sci Sports Exercise 14: 361-367.
3. Atwater, A.E. (1967) What film analysis tells us about movement. Paper presented at the annual meeting of the Midwest Association for Physical Education of College Women, French Lick, Indiana, October.
4. Bigland-Ritchie B (1981) EMG and fatigue of human voluntary and stimulated contractions. In: Human Muscle Fatigue: physiological mechanisms. Pitman Medical, London (Ciba Foundation symposium 82) p. 130-156
5. Chandler RF, Clauser CF, McConville JT, Reynolds HMN Young JW (1975) Investigation of inertial properties of the human body (AMRL-TR-74-137) Aerospace Medical Research Laboratory, Aerospace Medical Division, Wright-Patterson AFB, Ohio (NTIS No AD-A016 485)
6. Crowninshield RD, Brand RA (1981) The prediction of forces in joint structures: distribution of intersegmental resultants. In: Miller DI (ed) Exercise and sport sciences reviews, vol. 9. Franklin Press, Philadelphia pp 159-182.
7. Feltner, M (1986) Dynamics of the Shoulder and Elbow Joints of the Throwing Arm During a Baseball Pitch, accepted for publication, International Journal of Sports Biomechanics.

8. Fisk, C.S. (1976) The dynamic function of selected muscles of the forearm: an electromyographical and cinematographical analysis. Ph. D. Thesis Indiana University-Bloomington.
9. Freivalds, A.(1985) Incorporation of active elements into the articulated total body model. AAMRL-TR-85-061 Wright -Patterson AFB.
10. Jobe, F.W., Tibone, J.E., Perry, J., and Moynes D. (1983) An EMG analysis of the shoulder in throwing and pitching: A preliminary report. The American Journal of Sports Medicine, Vol. 11, 1.
11. Jobe, F.W., Radovich Moynes, D., Tibone, J., and Perry, J.(1984) An EMG analysis of the shoulder in pitching: A second report. The American Journal of Sports Medicine, Vol 12, 3.
12. Lindner, E. (1971) The Phenomenon of the Freedom of Lateral Deviation in Throwing. Medicine and Sport, Vol.6, Biomechanics II, pp.240-245.
13. Tarbell, T. (1971) Some biomechanical aspects of the overhead throw. In J. M. Cooper (Ed.), Selected Topics on Biomechanics. Proceedings of the C.I.C. Symposium on Biomechanics. Chicago: The Athletic Institute, 1971, pp.71-81.
14. Toyoshima, S., Hoshikawa, T., Miyashita, M., Oguri, T. (1974) Contribution of the body parts to throwing performance. Biomechanics IV R. Nelson and C. Morehouse (Ed.) University Park Press: Baltimore, pp. 169-174.

Table 1

MUSCLE-HARNESS FORCES IN POUNDS ENTERED INTO THE ATBMUS OVERARM THROWING
SIMULATION

	SECONDS							
	0	.1	.2	.3	.4	.5	.6	.7
MUSCLES								
Pect. Maj.#1	0	0	0	0	0	149.6	37.4	29.9
Ant. Delt.	20.2	20.2	40.4	0	24.2	80.7	40.4	60.6
Post. Delt.	0	0	0	20.2	0	80.7	60.6	16.1
Infraspinatus	0	0	0	13.2	131.6	98.7	131.6	65.8
Teres Minor	0	0	0	25.9	34.5	8.6	8.6	25.9
Supraspinatus	0	0	0	54.4	72.6	7.3	7.3	72.6
Subscapularis	0	0	0	32.7	217.8	21.8	21.8	217.8
Lat. Dorsi	0	0	0	0	227.7	22.7	227.7	0
Biceps	0	0	0	0	28.1	19.5	19.5	0
Triceps	0	0	0	0	350.5	381	381	0
Pron. Teres	0	0	0	0	0	0	35.4	0
Wrist Flex.	0	0	0	0	0	0	100.0	0

Table 2
Linear Correlation Coefficients for Criterion
Data and Simulations Throw 1, Throw 2, and Torque 1

Throw 1			Throw 2			Torque 1		
			Right Wrist					
X	Y	Z	X	Y	Z	X	Y	Z
.479	.963	.921	.516	.888	.858	.944	-.137	.719
			Right Elbow					
X	Y	Z	X	Y	Z	X	Y	Z
.437	.931	.840	.395	.662	.800	.988	-.151	.972
			Right Shoulder					
X	Y	Z	X	Y	Z	X	Y	Z
.372	.648	.667	.289	.421	.547	.990	.728	.997

Pearson r values for x,y,z coordinates -Critical value .497 $p < .05$
one-tailed test of significance

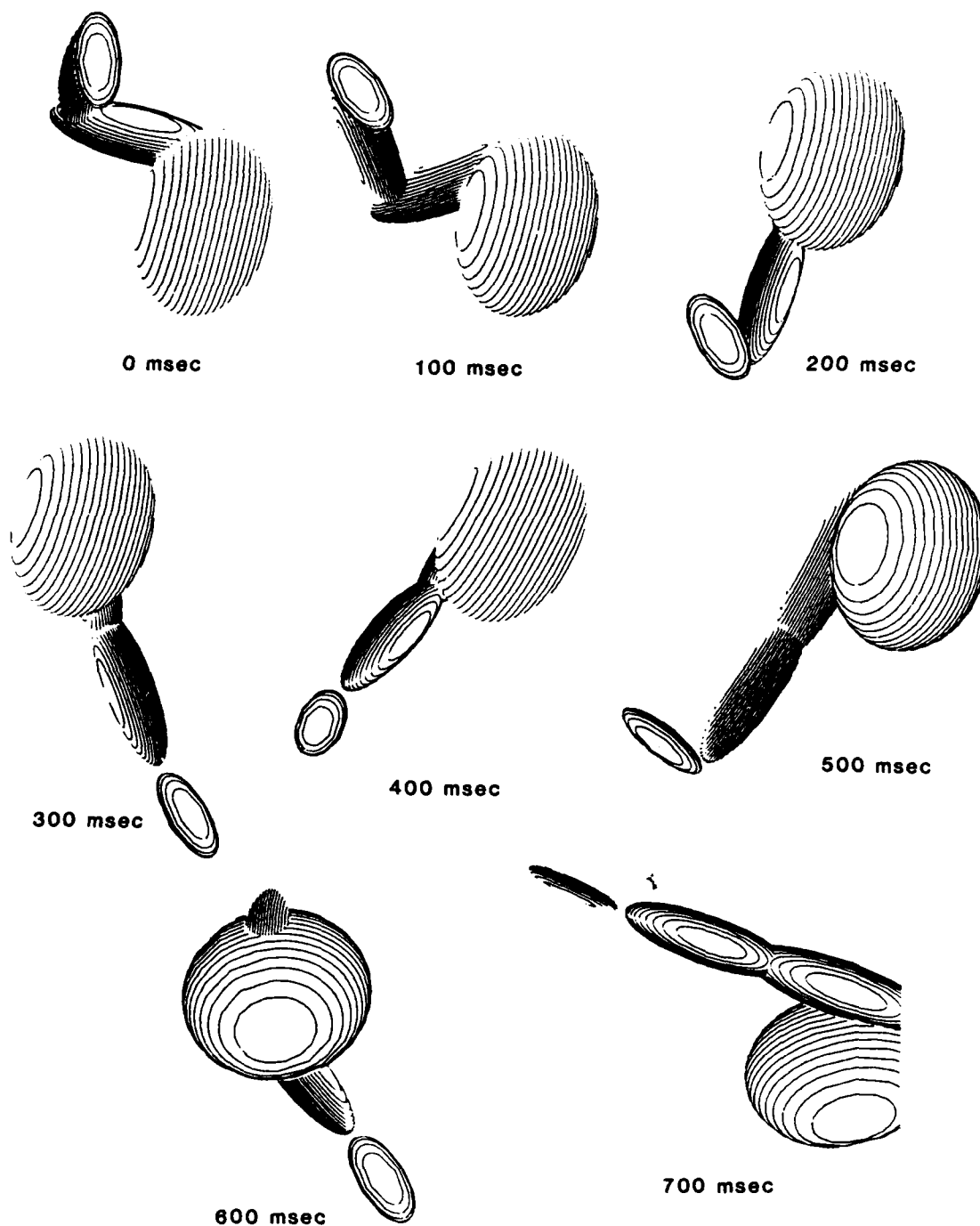


Figure 1. Torque 1 motion simulation of upper torso and right side upper extremity. Movement is the result of inputted muscular forces.

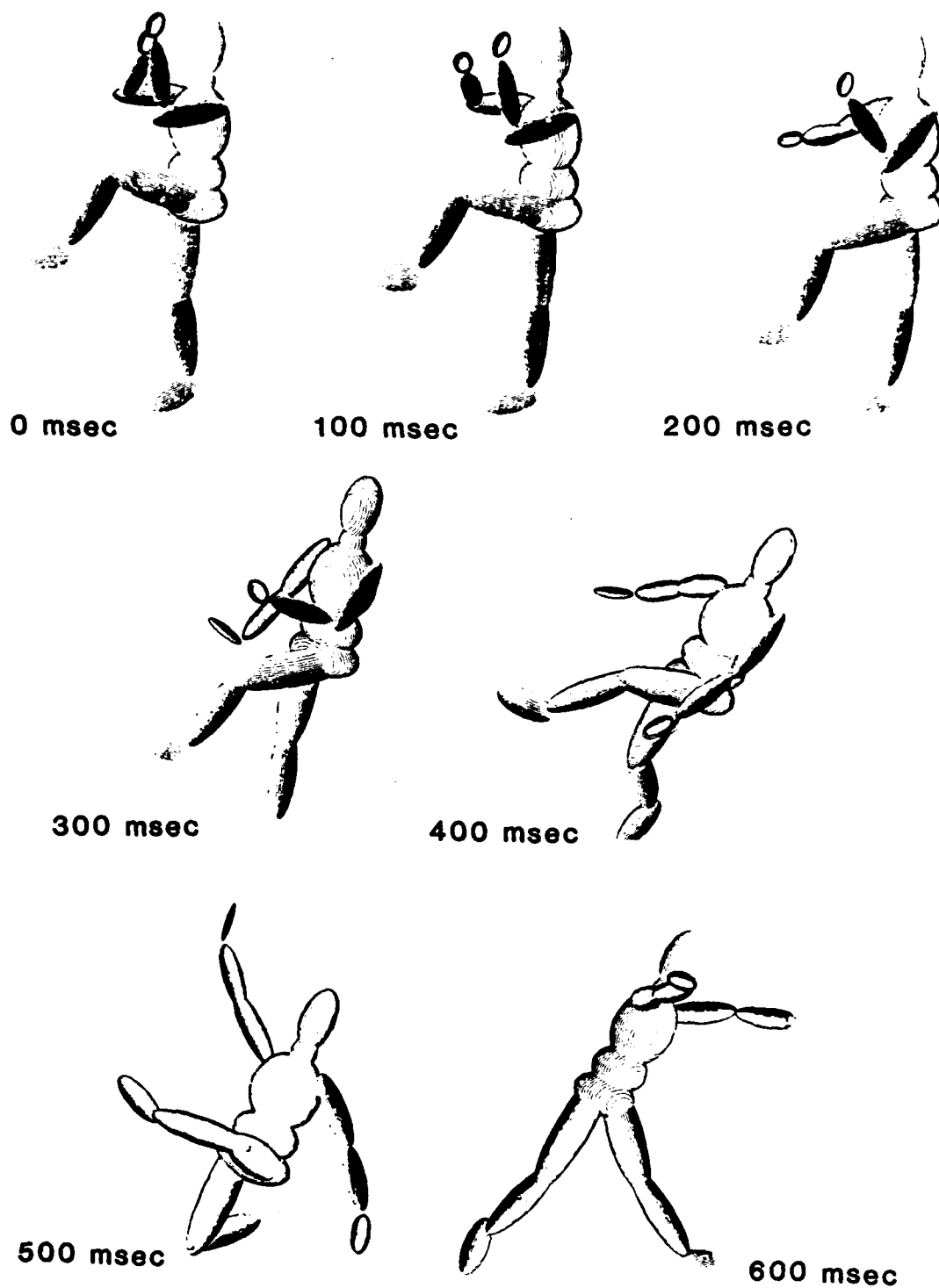


Figure 2. Throw 1 motion simulation based on the prescribed #3 metacarpalphalangeal joint motion of the right hand.

1986 USAF-UES SUMMER FACULTY RESEARCH PROGRAM/
GRADUATE STUDENT SUMMER SUPPORT PROGRAM

Sponsored by the
AIR FORCE OFFICE OF SCIENTIFIC RESEARCH

Conducted by the
Universal Energy Systems, Inc.

FINAL REPORT

NOISE ANALYSIS AND REDUCTION FOR THE AFGL
INFRARED FOCAL PLANE ARRAY SPECTROMETER

Prepared by: Karl Kennedy Klett, Jr.
Academic Department: Physics and Astronomy
University: University of Wyoming
Research Location: Air Force Geophysics Laboratory,
Optical Physics Division, Infrared
Physics Branch
USAF Research
Contact: Dr. Paul D. LeVan
Date: 27 August 1986
Contract No: F49620-85-C-0013

NOISE ANALYSIS AND REDUCTION FOR THE AFGL
INFRARED FOCAL PLANE ARRAY SPECTROMETER

by

Karl K. Klett, Jr.

ABSTRACT

An infrared focal plane array spectrometer has been developed by the Air Force Geophysics Laboratory, sensitive to the 8.0-14.0 micron range of the spectrum for use on the University of Wyoming's 2.3 meter infrared telescope. Due to the low signal/high sky noise ratio expected for the Wyoming telescope at infrared wavelengths, it has been necessary to improve the system to approach the expected level of sky noise. It was determined after testing that improved grounding techniques were required since unwanted digital noise was being introduced into the system signal reference grounds. The separation of digital, analog, and signal reference grounds seemed to reduce the overall system noise. Additionally, the use of coadding was found to greatly improve the signal to noise ratio.

Acknowledgements

I would first like to thank Dr. Gary Grasdalen, my advisor, from the University of Wyoming. Without his effort, I would not have known that this program was available to graduate students. During my summer assignment, I was given advice by Dr. Paul LeVan, my scientific advisor at AFGL, who taught me a great deal about instrumentation and infrared astronomy. I truly value my association with Dr. LeVan, and thank him for a summer well spent. My thanks also go to Mr. Peter Tandy, with whom I had many interesting discussions of a technical nature. Also of special value to me were the many conversations that I had with Dr. Steven Price, the director of the Optical Physical Branch, and Dr. Irene Little, a visiting scientist at AFGL from Wellesley College. They taught me much about working in science and with people that could not be gleaned from textbooks.

Finally, I would like to thank the Air Force Geophysical Laboratory and the Air Force Office of Scientific Research for making programs of this nature available to graduate students like myself.

I. Introduction

The infrared astronomical satellite (IRAS), launched in 1983, provided a sky survey using a scanning detector array and spectrometer. The spectrometer used 5 single infrared detectors, and was sensitive in the 7.8-20.0 micron region of the spectrum. For the last two years, the Air Force Geophysical Laboratory (AFGL) has been building an infrared spectrometer/camera designed for use on the University of Wyoming's 2.3 meter infrared telescope (WIRO). This spectrometer design is complementary to that used by IRAS since it will have a resolution of 0.1 microns. The spectrometer/camera design is centered around a 58 by 62 pixel gallium doped silicon detector chip manufactured by Santa Barbara Research Center (a subsidiary of Hughes Aircraft). The pixels of this array are sensitive to radiation in the 8.0-18.0 micron region of the spectrum, but the Earth's atmosphere limits its use to the 8.0-14.0 micron range. The pixels of the array are bump bonded, using indium, to the address decoder array, which includes two source follower MOSFETs, and the decoder array provides a direct readout capability¹. Each individual pixel has the MOSFET address/reset combination discussed above, and the entire package of pixels and MOSFETs must be cooled to temperatures less than 20 degrees Kelvin for the gallium doped silicon detectors to function properly.

When constructed, this infrared system should produce high quality 8.0-14.0 micron spectral data that can be obtained with ground based systems. The new data from this ground based array will supplement existing IRAS spectral data, will be a key research tool that should lead to improved positions of unidentified IRAS survey sources, and will enhance both AFGL's and WIRO's abilities and those of the infrared astronomical community.

II. Objectives of the Research Effort

The infrared focal plane array requires digital and analog electronic circuitry to address individual pixels, amplify voltages, store pixel signals in RAM, and transfer these data to a PDP 11/34 computer for analysis. Upon my arrival at AFGL, the digital electronics had been tested, along with the interfacing of the array with the RAM and the PDP 11/34 computer. Pixel linearity was also being studied, along with the maximum frequency that pixels could be addressed. After speaking with the principle investigator, Dr. LeVan, it was decided that the next phase of testing should deal with noise reduction of the system electronics. Specifically, it was decided that the dominating source of noise in the system must be determined along with ways of reducing the sources of noise.

III. Direct Readout and Chip Architecture

One of the advantages of this array is the fact that

the individual pixels are read out directly. In arrays where direct readout is not used, accumulation of data is often done in registers, and charge transfer errors often occur when shifting or accumulating registers.

The array may graphically be thought of as a matrix that is divided up into a top half and a bottom half. The individual pixels are addressed from left to right and top to bottom. After a pixel is addressed, sampled, and reset, charge is integrated until addressed again. Each pixel in the array outputs to the gate of a MOSFET, and the gate/source interface of the MOSFETs act as capacitors that store charge (see the cold electronics diagram in figure 4). Integration is twice as long if the whole array is addressed (top/bottom) compared with addressing only the top or bottom of the array, and this feature was exploited during the linearity tests discussed in section V.

The electronics have been designed around the chip architecture, and each pixel in the array is associated with one of four quadrants. This breakdown is as follows.

- Quadrant 1-bottom half of the array/odd pixels
- Quadrant 2-top half of the array/odd pixels
- Quadrant 3-bottom half of the array/even pixels
- Quadrant 4-top half of the array/even pixels

The terminology odd/even pixel relate to the two output lines in the chip architecture, with each valid address for two adjacent pixels on each of the two outputs, and means that in a row of 62 pixels, only the odd or even pixels are sampled.

The array electronics have been built so that single integrations may be examined (coaddition in RAM is suppressed). Single integrations result from addressing each of the pixels once. Multiple integrations may also be collected where the pixels are addressed many times and the values of each integration are added and stored in RAM. I will refer to these as single frame values and coadd values in the remaining discussion. A sky noise subtraction feature is also built into the digital electronics, so that coadds of the sky may be subtracted from coadds of the sky plus source using the chopping feature of WIRO. The analog to digital converter converts 5 volts to 4095 counts. The input gain to the analog to digital converter is approximately 3.6 downstream of the array output. A gain of 0.2 in the source follower circuitry follows the MOSFET that integrates each pixel, and this gain of 0.2 is believed to be due to the falling frequency response of the source follower circuitry. Consequently, an integration node voltage of 7.0 volts would produce a full scale count of 4095 if the pixels responded linearly at all intensities (see section V).

IV. Initial Noise Predictions

The reduction of system noise is critical in the development and testing of the array electronics, since fainter sources can be detected over much shorter integration times for low system noise. This is true until the system noise is reduced to the noise from the

sky and telescope, which is brighter even than the sources to be observed. Four types of noise were initially considered that could cause problems for the array electronics. These possible sources are listed below.

The first possible source of noise is Johnson noise. This noise results from resistances at critical locations in circuits. It may be compared with Brownian motion as a physical analogy, and may be described by the following relations.

$$V_{JN}^2(\text{rms}) = 4kTRB$$

k-Boltzmann's constant

T-degrees Kelvin

R-resistance

B-electronic bandwidth in hertz

Johnson noise has a flat frequency spectrum, which means that the same noise is in each hertz of frequency. Johnson noise also has a Gaussian distribution in amplitude.

A second type of noise that caused initial concern was Shot noise. This type of noise results from the fact that current flow is not a continuous process, but one where electrons with random motions are acting as current carriers. A Brownian motion analogy may again be used. Shot noise is calculated as follows.

$$I_{SN}(\text{rms}) = (2qI_{dc}B)^{0.5}$$

q-charge of electron(1.6×10^{-19} coul.)

B-electronic bandwidth in hertz

Shot noise has a flat frequency spectrum and displays a

gaussian distribution in amplitude, just like Johnson noise².

A third type of noise that was considered was "root-N" noise, where N is a signal detected by the pixels and "root-N" is the noise associated with that signal. This is the noise expected under "background limited" conditions. And finally, there was an initial concern that the digital address and reset switch process that is an internal part of the pixel/MOSFET unit cell would introduce dominant noise into the system, called "read noise". The digital switch closes in a finite time, and since there is a gate-source capacitance of about 0.1 picofarads, it was thought that due to charge transfer resulting from the relation

$$I = CdV/dT,$$

noise would be introduced into the system³.

Regardless of the source noise, it was hoped that it would be gaussian, or symmetrically distributed about the mean since coadding would reduce this kind of noise.

V. Linearity Testing

During this design phase of the the infrared focal plane array, all tests were performed in a single LHe dewar. A heating resistor was used to illuminate the focal plane array. The resistor had a spectral output in the 8.0-18.0 micron range since it could be 'seen' by the pixels, but its spectral characteristics were unknown. Current plans call for transferring the focal plane array after the testing phase to a double dewar

with an LN_2 radiation shield.

Due to the construction of the focal plane array, linearity testing was possible. A top/bottom sampling of radiation would integrate twice as long (two times τ) as a top or a bottom sampling (τ). The individual points (top, top/bottom) correspond to (x,y) values of figure 1 at various heater settings. The top, top/bottom pairs that make up data points are repeated samples of the same pixel. Notice that there is an apparent departure from linearity when the top/bottom values (two times τ) are greater than 3000 counts. This nonlinearity is due to the fact that the pixels have a certain well depth, and at these high values, the pixel wells are filling up. When the nonlinear pixel pairs are removed, the slope of figure 1 is 2.089, close to the expected value of 2.0, proving that pixel response is indeed linear.

If there were no noise at all and the above test is repeated, it would be expected that the points representing repeated pixel samplings would exactly coincide with each other. The introduction of noise or any deviation of test conditions should result in a separation of a repeated measurement. Figure 2 shows three individual pixels that have been tested for linearity twice. Initially, it was thought that the pixel separation caused by repeated measurements represented noise. This is indeed the case, if the

source being observed emits a constant flux. The large y-value separation of pixel pairs in figure 2 probably resulted from not letting the heater resistor stabilize. This is consistent with the order in which the two pairs were sampled: top/bottom, top, top, and top/bottom. In other tests, where the heater resistor was stabilized, the x and y values of the pixel separation were similar, and these separations represented noise.

There was an additional concern that the Datal analog to digital converter (ADC) may not be linear. Figure 3 shows tests of the ADC for the odd output. The fact that the slope is 3.008 indicates that the two operational amplifiers (see figure 4) provide a gain of 3.67.

VI. Initial Noise Testing

After integration, the pixel signal is processed by a signal processing circuit board that consists of digital and analog circuits. On 17 July 1986, when a cold test of the system was performed, it was noticed on an oscilloscope that voltage fluctuations of 100 millivolts (rms) could be observed on the signal reference ground. This observed noise had a period of approximately 10 nanoseconds and decayed after several cycles, characteristic of clock noise.

When the signal processor board was closely examined, it was noted that ground planes for analog and digital grounds were common near the sample hold module, and that an analog ground was also a common ground for

digital clocks that address and sample pixels. This procedure was recommended by the manufacturer. The necessary circuit modifications to improve this situation are discussed in section IX. At this point, it was hoped that the observed noise would display a gaussian or symmetric distribution in amplitude about zero when pixel differences between repeated samplings were averaged. If this condition existed, the signal to noise ratio would improve with increasing coadd number⁴. Shown in figure 5 are single integrations of 30 pixels and the deviation between the initial value and a repeated integration, attributed to noise. Superimposed on this plot is a gaussian for comparison. Sixty-six percent of the figure five pixels were contained in one standard deviation, compared to sixty-eight percent for a true gaussian.

VIII. Noise Statistics

My goal at this point is to determine the amount of "root-N" noise that cannot be 'engineered' out of the system by modifying system electronics. Johnson noise and Shot noise will also be present, but the "root-N" noise will dominate at sufficiently high signal detection levels. The value about to be calculated will also provide a target value from an engineering point of view.

The capacitor that integrates pixel charge has a value of 0.1 picofarads. For one electron, the relation

$V=q/C$ corresponds to 1.6×10^{-6} volts. When the gain of the two operational amplifiers (3.6) is taken into account along with the count/volt ratio of the analog to digital converter (4095 counts=5 volts), one electron equates to 4.8×10^{-3} counts. This means that a full scale analog/digital converter value of 4095 counts corresponds to 8.5×10^5 electrons. It was determined that this value is probably slightly low, since the source follower in the array unit cell MOSFET does not have a gain of exactly 1.0, but is closer to 0.2 due to falling frequency response. A full scale count seems to correspond to 3×10^6 electrons. At a full scale value, the "root-N" signal/noise is 1.7×10^3 . The corresponding noise at the analog to digital converter is

$$4095/1.7 \times 10^3 = 2.4 \text{ counts}$$

Since the electronics of the infrared array have been configured to coadd, the signal to noise level may be improved⁴. Figure 6 shows how the signal to noise ratio improves with coadding. The slope of 0.56 indicates that the noise increases as the square root of the coadded signal. The following table refers to the data in figure 6.

Signal to Noise Improvement due to Coadding

<u># of Coadds</u>	<u>Signal to Noise Ratio</u>
1	29.9
22	110.9
66	129.6
110	283.1

IX. Noise Improvements due to Engineering Techniques

In section VI, I mentioned the analog, digital, and signal reference grounds had common points. This fact has caused problems, since noise in the digital ground busses could feed back into the analog, and ultimately the signal grounds.

The digital clock circuitry has many clock transitions. When an output changes state, both transistors that make up a gate are on, and a 5-20 nanosecond negative pulse is placed in the V_{CC} line. The same type of positive pulse is injected into the digital ground. These spikes due to the common grounds are transferred to the signal and show up as variations in signal values. Even though coadding improves the signal to noise ratio, an even greater improvement may be obtained if noise levels are reduced.

Corrections were made to one of the two signal processor board during a six week period. Analog and digital ground planes near the sample hold module were separated. An analog ground near coaxial cable connections was also serving as a ground for clocks, causing ground loops. This ground was isolated and made a digital ground. Additionally, the signal reference ground was reinforced using #6 gauge wire so that a lower resistance would be encountered by signal ground currents, resulting in lower ground buss noise. It was discovered that the sample hold module as well as the analog to digital converter had common internal

connections between digital and analog ground. These common grounds existed at the chip and board level, even though these devices had separate connections for digital and analog ground.

X. Noise Reduction Resulting From Ground Separation

On 14 August 1986, the even and odd signal processor boards were examined in a cold test. Ground modifications had only been made on the even signal processor board. The use of both boards negated the changes that were made on the even signal processor board, since the odd board introduced noise to the even board through physical connectors. This test would serve as a reference for comparison. On 19 August 1986, only the even signal processor board was tested. An equivalence resistance for the cold MOSFET was used in place of the odd board. In examining the data below, the second set of quadrant 3 and 4 data (even pixels) were used to verify the observed values of standard deviations.

Verification of Noise Improvement by Ground Separation

<u>Type Grounds</u>	<u>Quadrant</u>	<u>Standard Deviation</u>
Common	1	15.17
Common	2	10.99
Separated	3	6.08
Separated	4	8.80
Separated	3	6.55
Separated	4	5.27

The smaller standard deviations indicate that the noise has improved, if the odd and even circuitry can be considered otherwise equivalent.

XI. Recommendations

Since ground noise has been such a problem, it is important that further complications not be added when attaching this instrument to the Wyoming telescope. Although the attachment plate is anodized and non-conducting screws will be used, I would suggest looking at the warm electronics ground before and after attachment to the telescope with an oscilloscope. This simple test should ensure conductive separation.

Not mentioned until now in this report is the fact that the current dewar window is barium fluoride, which has a transmission of 92% at 8.0 microns and only 55% at 14.0 microns. I strongly urge that this material be replaced with zinc selenide coated with the AR#4 coating available from 2-6 Incorporated. Coated zinc selenide transmits 90% at 8.0 microns and 88% at 14.0 microns. Use of this material will more fully utilize the aperture of the Wyoming telescope.

Figure 1-Pixel samples and their repeated values have been plotted after letting the integration time double. Doubling the pixel integration time was accomplished by using the top/bottom, top sampling method described in the text.

Figure 2-Pixel deviations after repeated samplings are plotted in an effort to show deviations that may result from noise or other deviations in test conditions. The large y variations are thought to be due to accidental variations of a source heating resistor.

Figure 3-A linearity plot is shown of the analog to digital converter, showing that the gain of the two operational amplifiers in the signal processor board is 3.67 and that the converter is linear.

Figure 4-A general schematic of the signal processor board is shown, along with block diagrams showing the digital electronics involved downstream of the signal processing board. Also shown in this figure are the necessary modifications that were implemented to eliminate digital ground noise.

Figure 5-Pixel difference counts due to repeated samplings are plotted with a gaussian. The gaussian has been normalized to 6.0, corresponding to the greatest number of counts that were observed in a count difference interval.

Figure 6-Average signal values resulting from thirty one samples are plotted against the standard deviation resulting from pixel difference counts due to repeated samplings. The slope of 0.56 indicated that the noise increases as the

square root of the detected signal. The accumulated signal resulted from coadding.

Figure 1

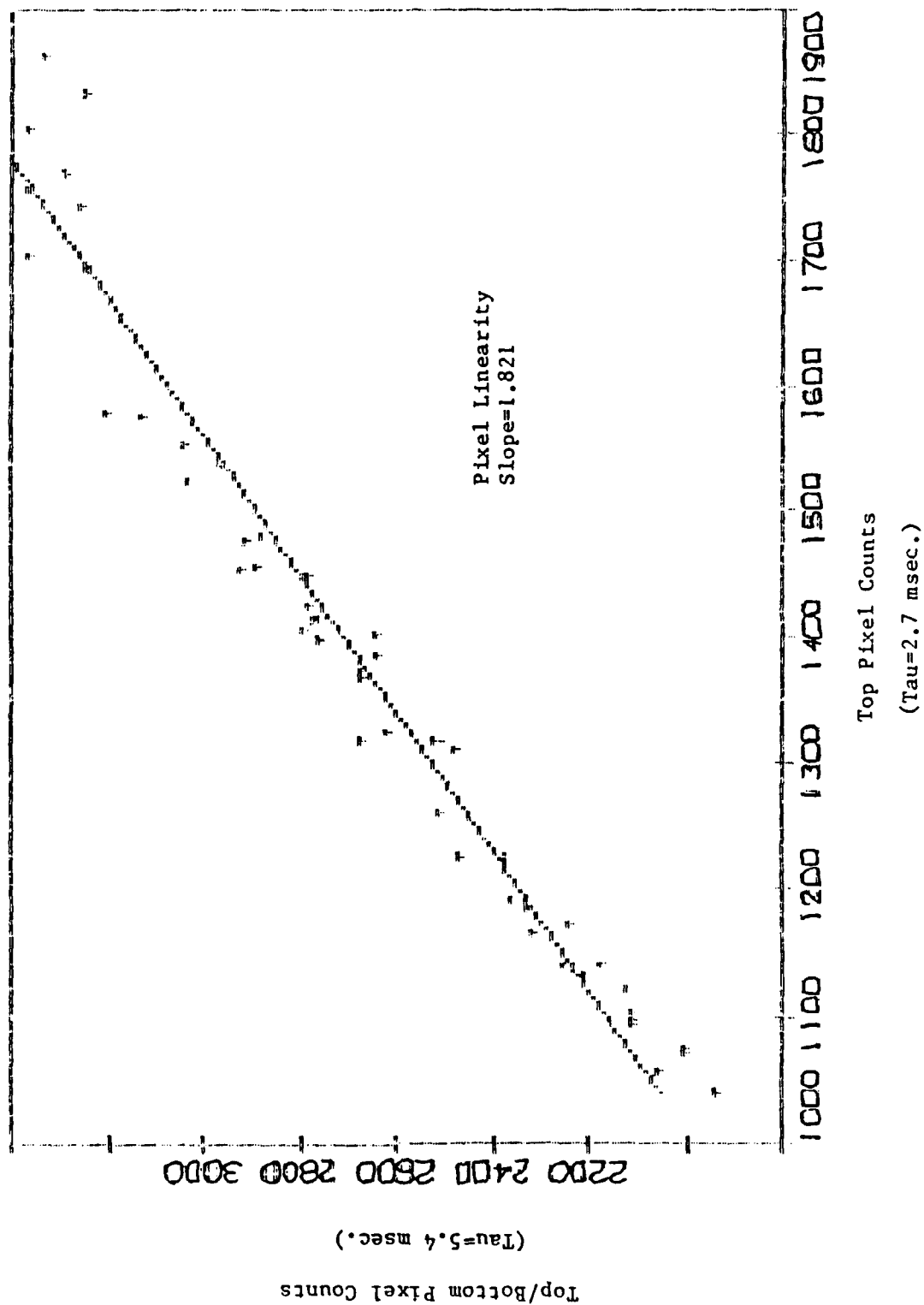


Figure 2

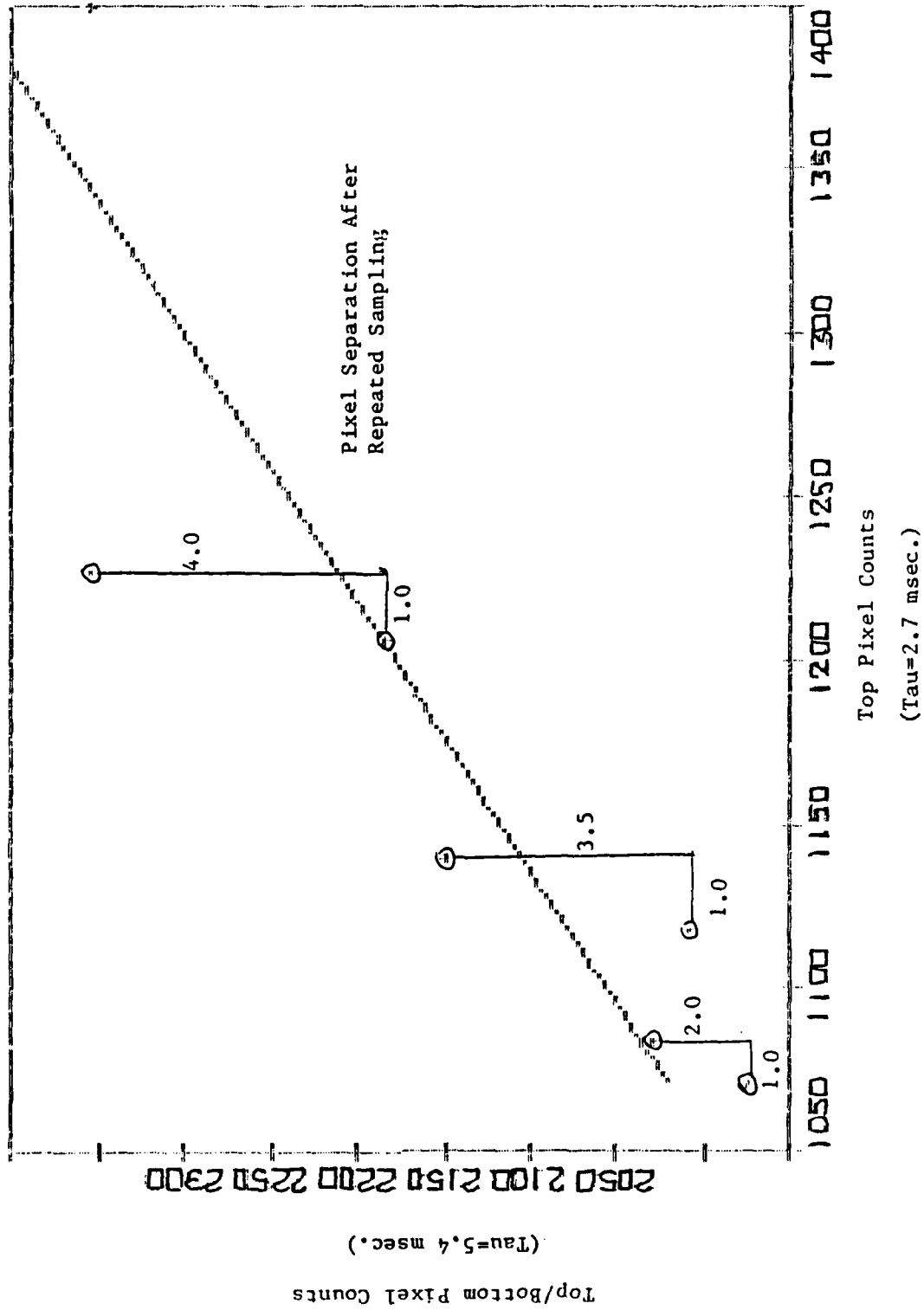


Figure 3

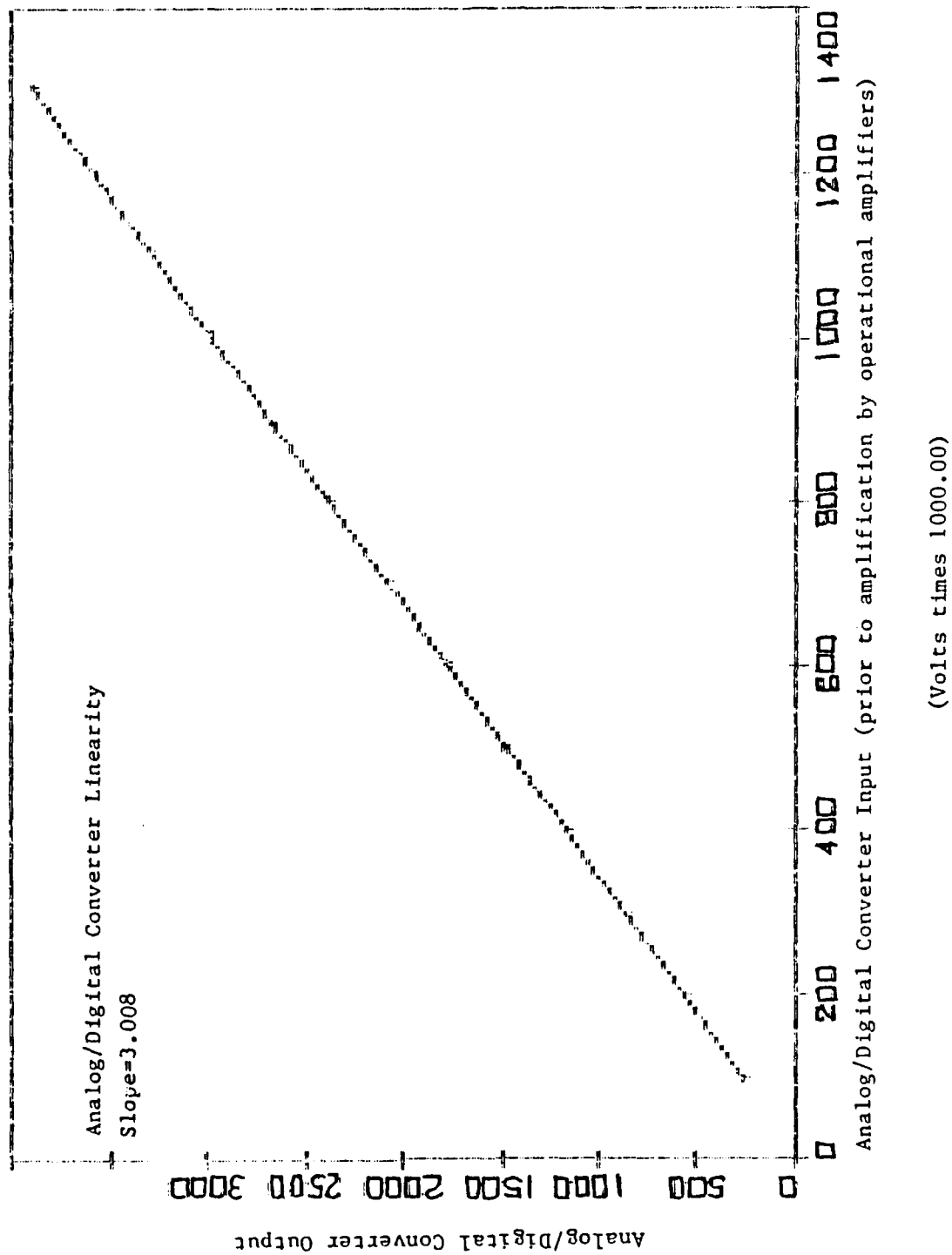


Figure 4

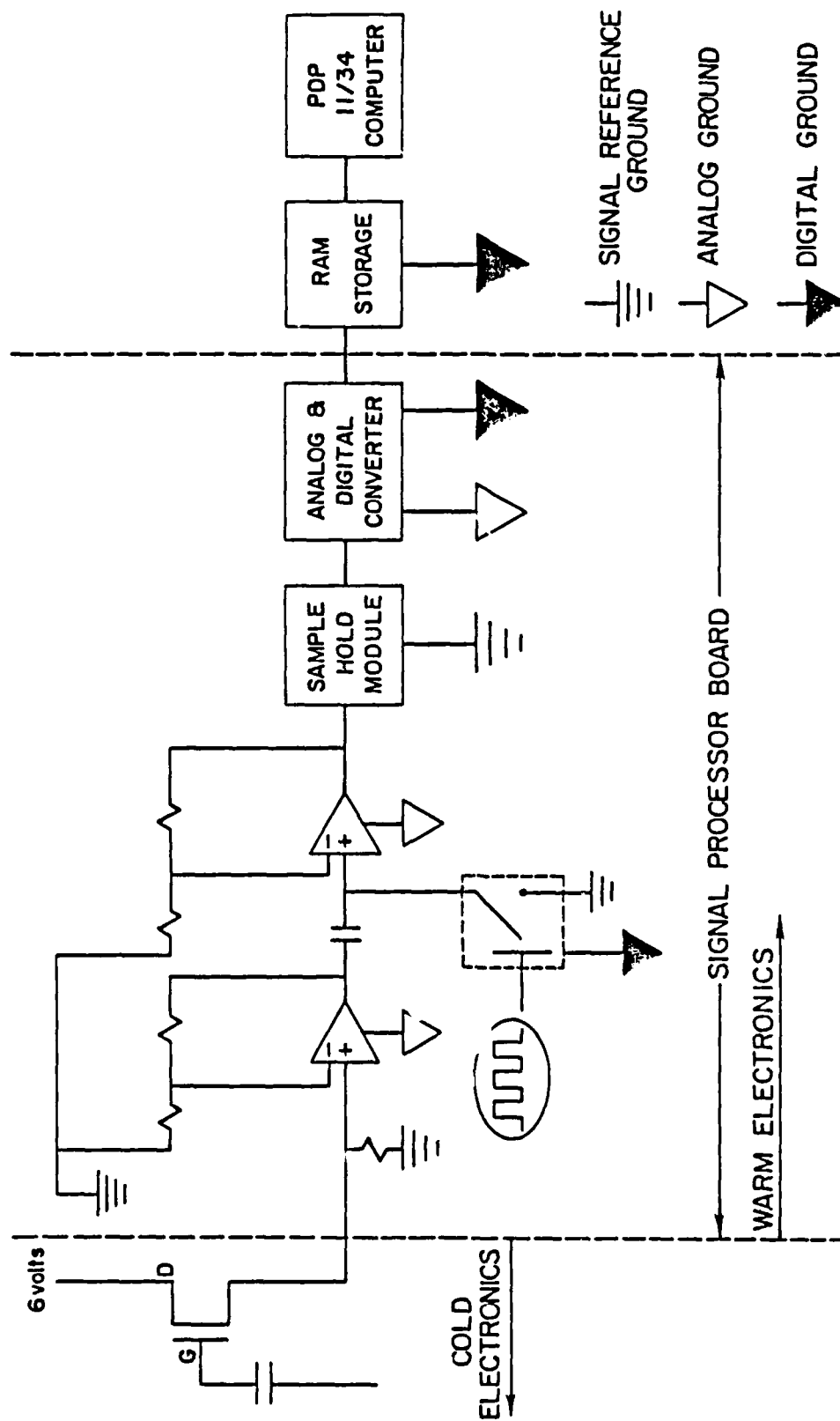


Figure 5

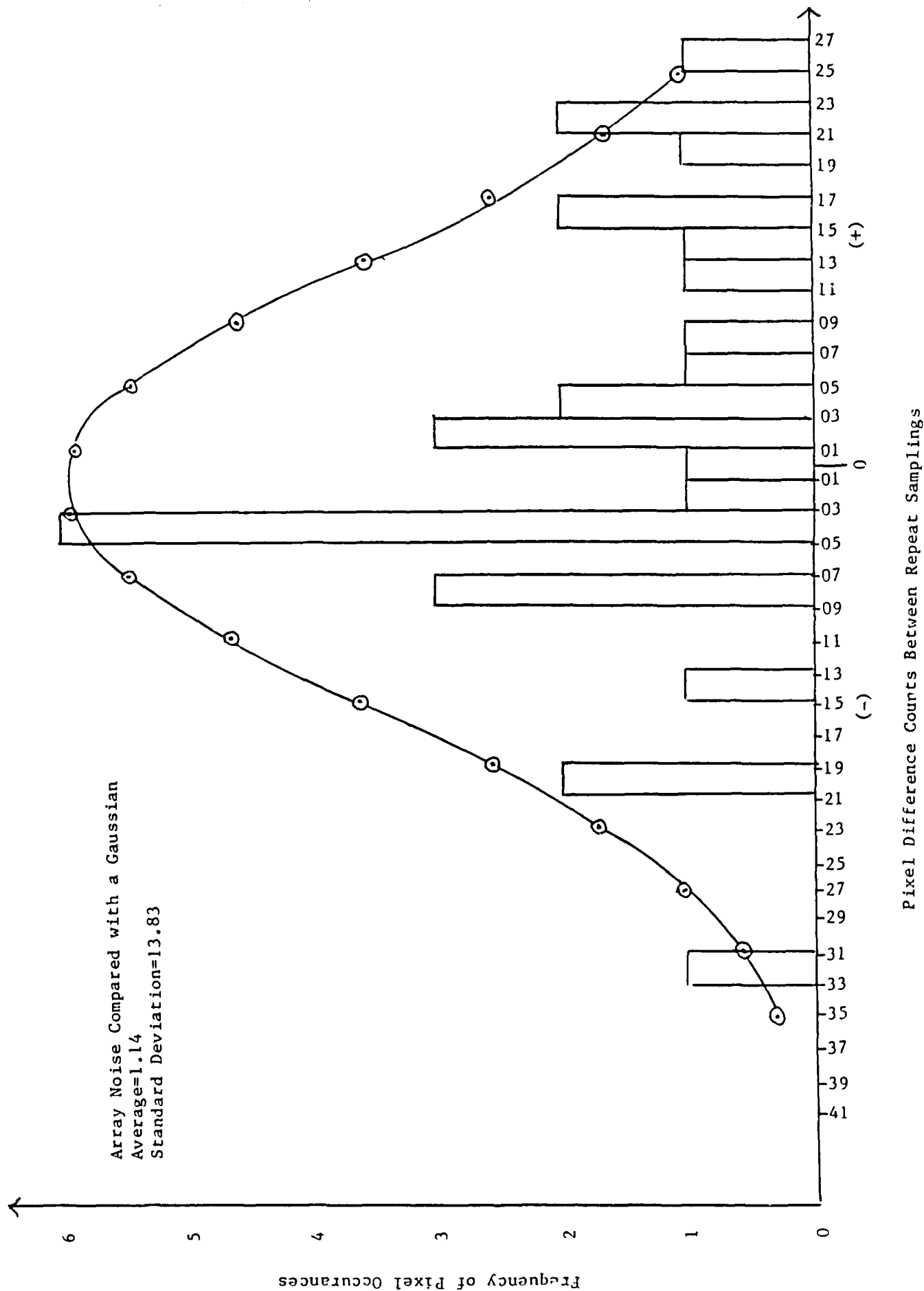
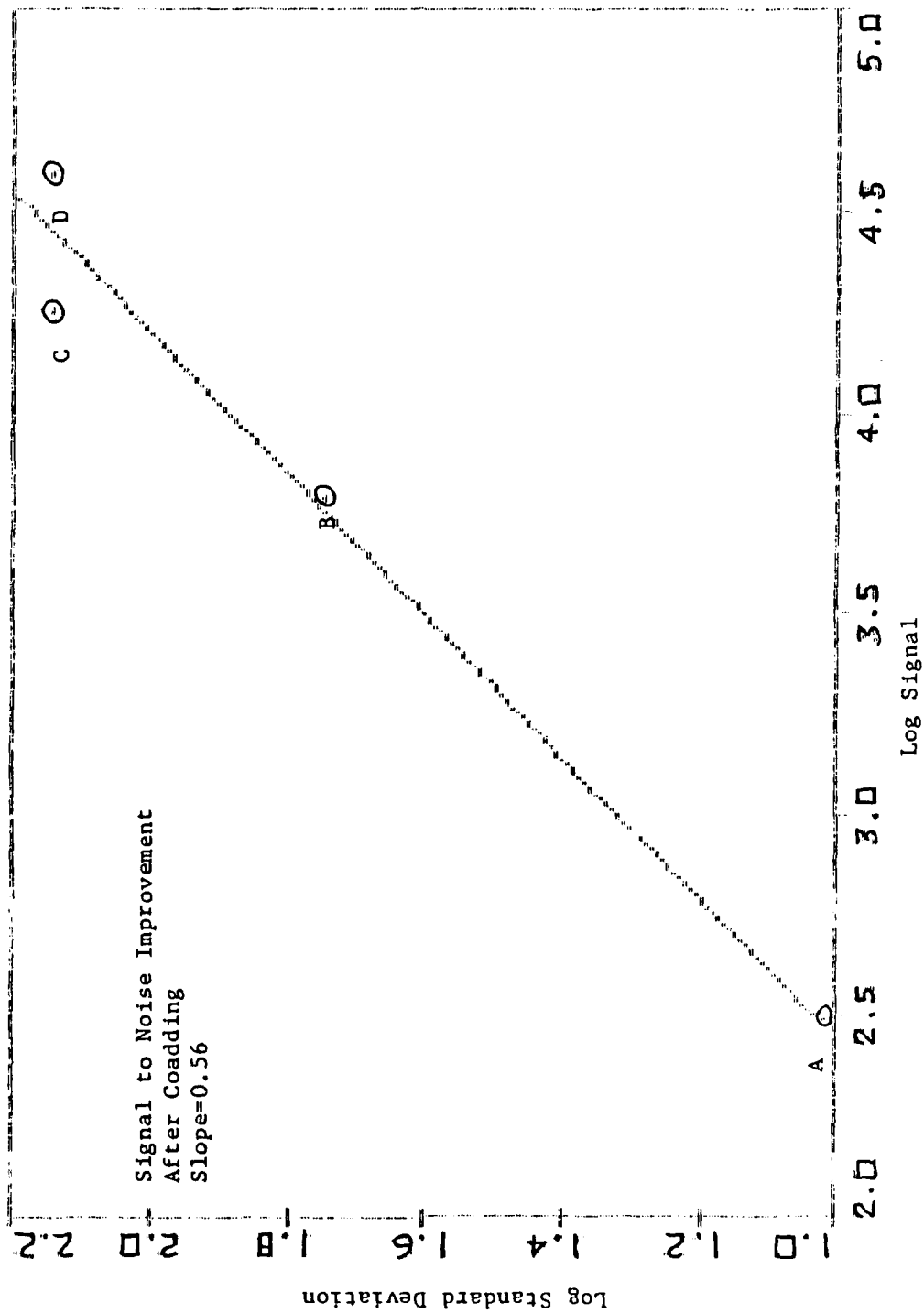


Figure 6



References

1. Edwards, J.M., "Schottky CRC-228 Direct Readout Test Results", Hughes Aircraft Internal Communication, 5 September 1982.
2. Horowitz, P., and W. Hill, The Art of Electronics, (Cambridge University Press, 1984), pp. 228-229.
3. Paul LeVan, Private Communications.
4. Horowitz, P., and W. Hill, pp. 624-625.
5. Ott, Henry W., Noise Reduction Techniques in Electronic Systems, (John Wiley and Sons, 1976), Chapter 3.

1986 USAF-UES Summer Faculty Research Program
Graduate Student Summer Support Program

Sponsored by the
Air Force Office of Scientific Reserach
Conducted by the
Universal Energy Systems, Inc.
Final Report

Structural Optimization Using Bending Elements

Prepared by:	Raymond M. Kolonay
Academic Rank:	Graduate Research Assistant
Department and	Department of Civil Engineering
University:	The Ohio State University
Research Location:	AFWAL/FIBRA Wright-Patterson AFB
USAF Research:	Dr. Vipperla B. Venkayya
Date:	September 2, 1986
Contract No:	F49620-85-C0013

Structural Optimization Using Bending Elements

by

Raymond M. Kolonay

ABSTRACT

Minimum weight design of plane-framed structures subject to stress and displacement constraints is presented. The finite element method is used for the structural analysis while two separate methods are being compared for the optimization algorithm, non-linear mathematical programming and the optimality criterion. The structures being considered are assumed to be linear elastic, composed of isotropic materials, and under static loads. Some differences between the use of membrane elements as opposed to bending elements for structural optimization have also been investigated.

Acknowledgments

I would like to thank the Air Force Systems Command and the Air Force Office of Scientific Research for Sponsorship of my research. Also, I would especially like to thank Dr. Venkayya and all those in the AFWAL/FIBRA group for their help during my stay at the Flight Dynamics Laboratory.

I. Introduction

I received my Bachelor of Science degree from The Ohio State University in the department of Civil Engineering. I am currently enrolled in Ohio State's graduate school pursuing a Masters of Science degree in Civil Engineering. My major area of study is in the field of computer applications to structural analysis and optimization.

The Flight Dynamics Laboratory has been doing a great deal of research in the area of optimization of large scale structures. Much of the lab's work has been concentrated on the use of membrane elements for modeling structures for optimization. Little work has been done on the use of bending elements for structural optimization. In working at the Flight Dynamics Lab I felt that I could gain valuable experience in the optimization field while extending the work done by the lab in the use of bending elements for structural optimization.

II. Objectives of the Research Effort

The overall objective of the research is to produce a computer program that will yield the minimum weight design of large scale structures using frame elements. My individual objectives are:

1. Derive the sensitivity analysis for stress and displacement constraints for planar linear elastic

structures.

2. Derive and compare various relationships between the design variables A and I_z .

3. Write a computer program to optimize plane frame structures under static loads.

4. Compare two different solution procedures, mathematical programming and the optimality criterion.

III. Problem Statement

The purpose of the research is to write a computer program that finds the minimum weight design of large framed structures subject to stress and displacement constraints. The study has been restricted to linear elastic structures composed of isotropic materials under static loads. The problem stated in optimization form reads as follows :

minimize an objective function

$$F(X) = F(X_1, X_2, \dots, X_m)$$

subject to the constraint conditions

$$G_j(X) = G_j(X_1, X_2, \dots, X_m) \leq G_{j0} \quad j=1, 2, \dots, p$$

$$X^{(L)} \leq X \leq X^{(U)}$$

Where $F(X)$ is the weight of the structure and $G_j(X)$ consists of the stress and displacement constraints, with both F and G functions of the design variables (X) . Also, the design variables have upper and lower bounds called side constraints placed on them.

IV. Design Variables

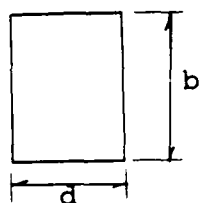
The design variables for the plane frame element are: A ; the cross-sectional area, and I_z ; the moment of inertia about the z axis. The moment of inertia (I_z) and the cross sectional area (A) are not independent. Several different relationships between A and I_z will be considered. One approach that will be tried for I-beams, box beams, and sandwich beams will be to use the radius of gyration (r) to relate I_z to A . It will be assumed that the radius of gyration will remain constant, that is $r^2 = I_z/A = \text{constant}$.

Another approach will be to assume the relation $I = \alpha A^x$. With this assumption and assuming $x=2$ which implies constant shape the following can be found for circular and rectangular cross sections :

rectangular section

$b/d = \text{constant}$

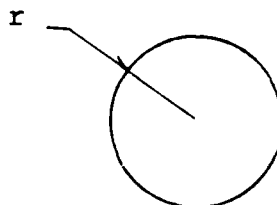
$\alpha = 1/12$



Rectangular Section
Figure 1.0a

circular section

$\alpha = 1/4$



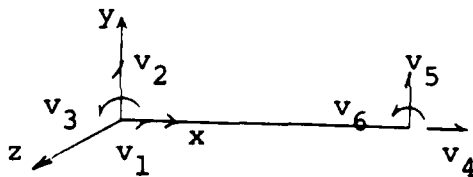
Circular section
Figure 1.0b

The final approach will be to attempt to plot A vs. I for a series of I or C sections from American Institute of Steel Construction (AISC). A curve of the

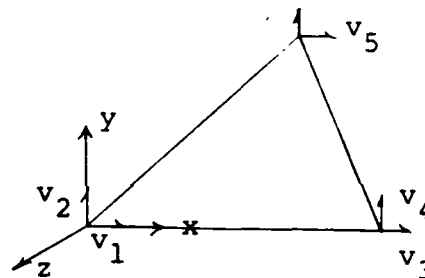
form $I = \alpha A^x$ will be fitted to the points, thus giving a relationship between A and I_z .

V. Frame element

The frame element considered is shown in figure 2.0a. The element has two nodes with three degrees of freedom per node: two translations (x and y) and one rotation about the z-axis. This is compared to the membrane element in figure 2.0b which has three nodes with two degrees of freedom per node: translations in the x and y directions.



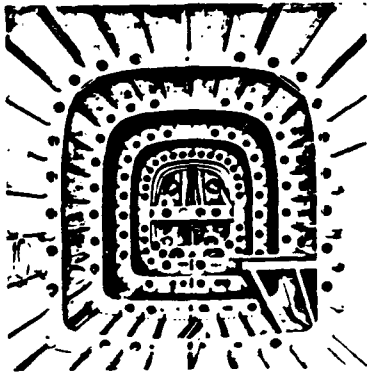
Frame Element
Figure 2.0a



Membrane Element
Figure 2.0b

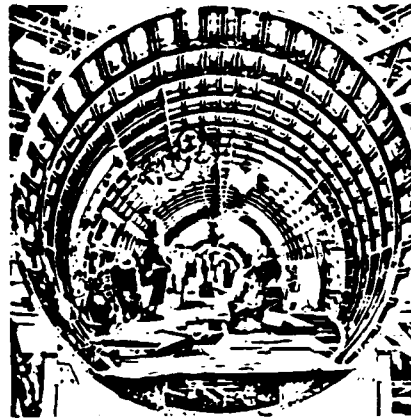
Some modeling applications for the frame element are shown in figure 2.1. Figure 2.1a and 2.1b are fuselages of flight vehicle structures and figure 2.1c and 2.1d show some civil engineering applications. 2.1c is a gabled frame and 2.1d is a multi-story, multi-bayed plane frame.

• Flight Vehicle Structures



Fuselage

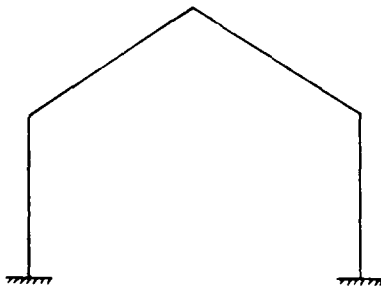
Figure 2.1a



Fuselage

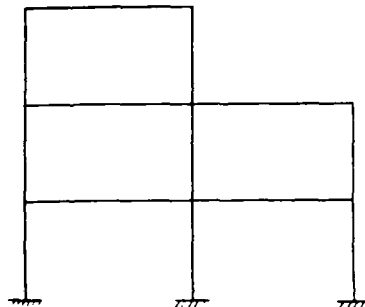
Figure 2.1b

• Civil Engineering Structures



Gabled Frames

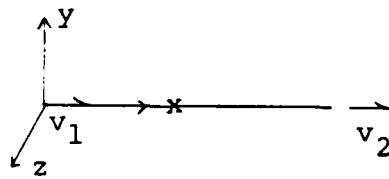
Figure 2.1c



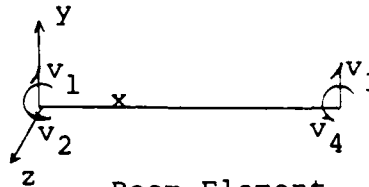
Multi Story
Multi Bay Frames

Figure 2.1d

The frame element can be constructed by superimposing two simpler elements; a truss element and a beam element (figure 2.2). The truss element handles only the axial (x translation) degree of freedom while the beam element handles the bending degrees of freedom (y translation and rotation about the z axis). Throughout this work the frame element will generally be handled by considering the two sub-elements and superimposing the results.



Truss Element
Figure 2.2a



Beam Element
Figure 2.2b

VI. Methods of Solution

There are two methods of solution to the optimization problem being considered: mathematical programming and the optimality criterion. The mathematical programming method used is the method of feasible directions. The optimality criterion is derived based on the Lagrangian formulation of the optimization problem.

The method of feasible directions is a mathematical search based on the iterative equation

$$X_{k+1} = X_k + \alpha_k S_k \quad k=1,2,3,\dots \quad (4)$$

Where α_k is the step size, S_k is the search direction, and $X_i = A_i$ the cross-sectional area. The method of

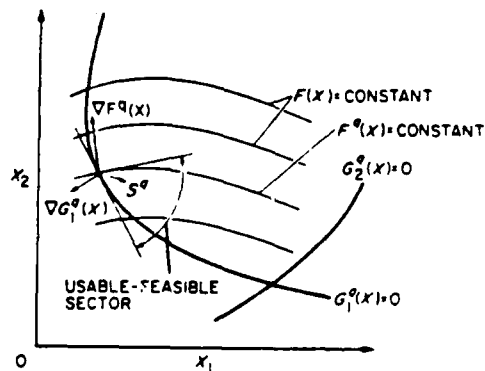
feasible directions requires that the direction (S) be found such that for some small move distance ΔS the objective function is decreased (usable direction) and no constraints are violated (feasible direction). The requirement that S be a usable direction is stated mathematically as

$$\nabla F(X) \cdot S \leq 0 \quad (5)$$

Where $\nabla F(X)$ is the gradient of the objective function with respect to the design variables. The requirement to remain in the feasible region is stated mathematically as

$$\nabla G_j(X) \cdot S \leq 0 \quad j=1, \text{Number of active constraints} \quad (6)$$

Figure 3.0 shows a usable-feasible direction in which equations 5 and 6 are satisfied.



Usable-feasible direction
Figure 3.0

"S" may be found by solving the following problem:

maximize β

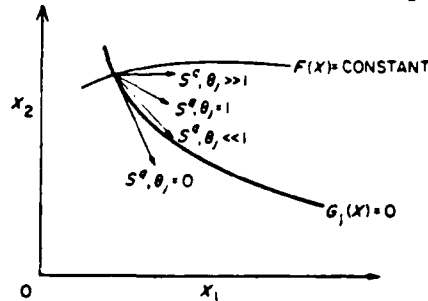
subject to

$$\nabla F(X) \cdot S + \beta \leq 0 \quad (7)$$

$$\nabla G_j(X) \cdot S + \theta_j \beta \leq 0 \quad (8)$$

$$\|S\| = 1 \quad (9)$$

The scalars θ_j are referred to as "push off" factors which effectively "push" the design away from the active constraints. This is shown in figure 3.1.[5]



"push off" factors
Figure 3.1

Once the direction (S) is found then the step length can be found by a one dimensional search bounded by the constraints. The method of feasible directions has been implemented the by the use of CONMIN, a computer program written by G. N. Vanderplatts.

VII. Optimality Criteria

This procedure consists of two steps. The first step is the derivation of a set of necessary conditions that must be satisfied at the optimal design, and the second step, an iterative redesign procedure, is derived to drive the design toward optimality. The optimality criterion is based on the Lagrangian formulation for constrained minimization and is stated as follows:

$$L(X) = F(X) + \sum_{j=1}^p \lambda_j G_j(X) \quad (10)$$

Where $L(X)$ is the Lagrangian function and λ 's are the

Lagrangian multipliers. Minimization of the Lagrangian function with respect to the design variable vector X gives the condition for the stationary value of the objective function with the constraint conditions G .

$$\frac{\partial L}{\partial X_i} = \frac{\partial F(X)}{\partial X_i} + \sum_{j=1}^p \lambda_j \frac{\partial G_j(X)}{\partial X_i} = 0 \quad (11)$$

where $F(X) = A_i l_i \rho_i$ is the weight of the structure.

The optimality condition can be written as

$$e_{ij} \lambda_j = -1 \quad (12)$$

where

$$e_{ij} = \frac{\partial G_j(X) / \partial X_i}{\partial F(X) / \partial X_i} \quad (13)$$

This last equation represents the ratio of constraint to objective function gradients with respect to the design variable. These ratios can be associated with special forms of energy densities depending on the type of constraint functions.

With m design variables and p Lagrangian multipliers, the solution of the optimization problem involves $m+p$ unknowns. The equation $\underline{e} \underline{\lambda} = -1$ only represents m equations. The remaining p equations can be obtained by restating the constraint conditions as follows:

$$\sum_{i=1}^m e_{ij} \rho_i l_i = G_{j0} \quad j = 1, 2, \dots, p \quad (14)$$

Combining equations 12 and 14 gives the necessary conditions for determining the Lagrangian multipliers as follows:

$$H\lambda = G_0 \quad (15)$$

where H is $e^t v e$ and V is a diagonal matrix and its i^{th} diagonal element is given by $V_{ii} = \rho_i l_i$ (l_i is the length of the element). The H matrix cannot be determined explicitly since the e and V matrices are functions of the design variables X which itself is unknown.

Assuming that the problem has only one constraint at a time the values of the Lagrangian multipliers can be found as

$$\lambda_i = \frac{W}{G_{i0}} \quad (16)$$

where W is the total weight of the structure and λ_i 's are used simply as weighting parameters.

From the optimality conditions the element resizing algorithm can be derived. Assuming the cross-sectional area $A = \lambda \alpha$ where λ is a scaling parameter and α is the relative design variable vector the resizing algorithm is:

$$A^{v+1} = A^v \left[\sum_{j=1}^p c_j e_{\lambda_j} \right]^{1/2} \quad (17)$$

where the c_j are weighting parameters which are functions of the Lagrangian multipliers. It is important to note that $A_i = X_i$ the cross-sectional area to clarify some of the notation. [6]

VIII. Approximation Concepts

In order for the method of feasible directions to approach the efficiency of the optimality techniques, Taylor Series approximations are needed. The constraint approximations replace the basic problem with a sequence of explicit problems that preserve the essential features of the original design optimization problem. This approximate problem can then be optimized with appropriate move limits on the design variables to insure that the design does not stray from the region of validity for the approximations. If X_i is the design variable and $d_i = 1/X_i$ (or $1/A_i$) is defined as the reciprocal variable the approximate problem can be stated as

$$\text{Minimize } F(X) = \sum_{i=1}^m \frac{W_i}{d_i} \quad (18)$$

Subject to the approximate constraints

$$G_j(X) = G_{j0} + \sum_{i=1}^m \frac{\partial G_j}{\partial d_{oi}} (d_i - d_{oi}) \quad (19)$$

where W_i is a constant for each design variable equal to $l_i \rho_i$ where ρ_i is the specific weight and l_i is the length of the element. Notice the Taylor series approximation of the constraints is terminated after the first term.[1]

VIIII. Sensitivity Analysis

Both, mathematical programming and optimality criteria require computation of the constraint

gradients. This computation of constraint gradients with respect to the design variables is known as the sensitivity analysis. The Virtual Load Method is used to calculate the gradients of the displacement and the stress constraints.

A. Displacement Constraint Gradient by Virtual Load Method

Write the displacement constraint in the following form:

$$G_j(X) = F^t u - z_j \leq 0 \quad (20)$$

where F is a virtual load vector with $F_l = 0$ $l \neq j$ and $F_l = 1$ $l = j$, u is the global nodal displacement, and z_j is the given constrained displacement.

Differentiation of the constraint gives

$$\frac{\partial G_j(X)}{\partial X_i} = \frac{\partial F^t}{\partial X_i} u + F^t \frac{\partial u}{\partial X_i} \quad (21)$$

Now the derivative of the displacement with respect to the design variable $\partial u / \partial X_i$ is required.

The equilibrium relations for the structure is defined as

$$P = Ku \quad (22)$$

Similarly, f can be defined as,

$$F = Kf \quad (23)$$

where u is the displacements corresponding to load vector P , and f is the displacements due to load vector F . Taking the derivative of equation 22 with respect to the displacement u gives

$$\frac{\partial P}{\partial X_i} = \frac{\partial K}{\partial X_i} u + K \frac{\partial u}{\partial X_i} \quad (24)$$

and solving for the displacement vector derivative gives

$$\frac{\partial u}{\partial X_i} = K^{-1} \left[\frac{\partial P}{\partial X_i} - \frac{\partial K}{\partial X_i} u \right] \quad (25)$$

Substituting equation 25 into 21 and recognizing that $\partial F^t / \partial X_i = 0$ gives the constraint derivative as

$$\frac{\partial G_j(X)}{\partial X_i} = F^t K^{-1} \left[\frac{\partial P}{\partial X_i} - \frac{\partial K}{\partial X_i} u \right] \quad (26)$$

From the equation $F^t K^{-1} = f^t$ the above equation can now be written as

$$\frac{\partial G_j(X)}{\partial X_i} = f^t \left[\frac{\partial P}{\partial X_i} - \frac{\partial K}{\partial X_i} u \right] \quad (27)$$

Assuming that the load vector P is independent of the design variable X_i then equation 27 reduces to

$$\frac{\partial G_j(X)}{\partial X_i} = -f^t \frac{\partial K}{\partial X_i} u \quad (28)$$

B. Stress Constraint Gradients

The stress constraint is written as

$$\sigma - \sigma_{max} \leq 0 \quad (29)$$

Where

$$\sigma = \frac{P}{A} \pm \frac{Mc}{I} \quad (30)$$

P/A is the normal stress due to the axial force and Mc/I_z is the normal stress due to bending. Equation 29 can now be written as

$$[\sigma_a \pm \sigma_b] - \sigma_{max} \leq 0 \quad (31)$$

In order to use the Virtual Load method to find the stress constraint gradients it is necessary to express the stress constraints as a function of the global

displacements u . First, considering only the axial component of the stress σ_a , σ_a can be written as $\sigma_a = E_i \epsilon_x$ where E_i is the material elastic constant and ϵ_x is the normal strain due to an axial force. If $w_i(x)$ is the displacement along the x -axis of a cross section at distance x from end i , the normal strain due to axial forces at the cross section can be represented as a function of the displacement as

$$\epsilon_x = \frac{\partial}{\partial x} w_i(x) \quad (32)$$

$$\text{or } \epsilon_x = D_a w_i(x) \quad (33)$$

where D_a is the differential operator, $\partial/\partial x$ and $w_i(x)$ represents the displacements of the i^{th} element as a function of the local spatial coordinates.

The essence of the finite element method is to approximate the displacements by interpolation functions which express an element's internal displacements as a function of the displacements of the discrete nodes associated with the element. Therefore

$$w_i(x) = \Phi_{ai} u'_i \quad (34)$$

where Φ_{ai} is the shape function whose elements are functions of the spatial coordinates and u'_i is the nodal displacements in local coordinates which is equivalent to $L_a u_i$ where L_a is a direction cosine transformation matrix for the axial degree of freedom (x translation).

Substituting back into equation 33 gives

$$\epsilon_x = D_a \Phi_{ai} L_a u_i \quad (35)$$

and σ_a now can be written in terms of the global displacements

$$\sigma_a = E_i D_a \Phi_{ai} L_a u_i \quad (36)$$

or

$$\sigma_a = F_{ax}^t u_i \quad (37)$$

where F_{ax}^t is the virtual load vector for the normal stress due to axial loading. [1]

When considering the bending component of the normal stress σ_b , writing stress in terms of strain gives

$$\sigma_b = E_i \epsilon_x \quad (38)$$

where axial strain in bending $\epsilon_x = c' / \rho$

where c' is the distance from the neutral axis to the outer-most fiber and ρ is the curvature and is defined as

$$\frac{1}{\rho} = \frac{\left(\frac{d^2}{dx^2} w_i(x) \right)}{\left[1 + \left(\frac{dw(x)}{dx} \right)^2 \right]^{3/2}} \quad (39)$$

Assuming the slope is small (small rotations), the $(dw/dx)^2$ is negligible and $1/\rho$ reduces to $d^2/dx^2 w_i(x)$ and the normal strain due to bending becomes

$$\epsilon_x = c' \frac{d^2}{dx^2} w_i(x) \quad (40)$$

where $w_i(x)$ is the displacements of the i^{th} element as a function of the local spatial coordinates. Using the finite element method $w_i(x)$ can be expressed as:

$$w_i(x) = \Phi_{bi} u_i' \quad (41)$$

where Φ_{bi} is the shape function whose elements are functions

of the spatial coordinates. u_i' is nodal displacements in local coordinates which is equivalent to $L_b u_i$ where L_b is a transformation matrix from global to local coordinates for y translation and rotational (bending degrees freedom). $w_i(x)$ now appears as

$$w_i(x) = L_b u_i \quad (42)$$

Substituting this back into equation 40 the following equation is given

$$\epsilon_x = c' \frac{d^2}{dx^2} \Phi_{bi} L_b u_i \quad (43)$$

and σ_b as a function of global displacements becomes

$$\sigma_b = E_i c' D_b \Phi_{bi} L_b u_i \quad (44)$$

where D_b is the differential operator d^2/dx^2

It is important to note that c' is a function of the design variable x_i .

σ_b can now be rewritten as $F_b^t u_i$. Where $F_b^t u_i$ is the virtual load vector for normal stress due to bending. The constraint can now be written as

$$F_{ax}^t u_i \pm F_b^t u_i - \sigma_{max} \leq 0 \quad (45)$$

Taking the derivative of the above stress constraint with respect to the design variable is done in a similar fashion as taking the gradient of the displacement constraint. The only difference being that there is an additional term because $\partial F_b^t / \partial x_i \neq 0$. This is due to the fact that c' is a function of the design variable.

There are a few assumptions that are being made in the

current study about the stress constraints. The shape function $\bar{\Phi}_{b_k}$ is cubic in terms of the distance along the element and the differential operator D_b is quadratic.[3] This implies that the normal stress due to bending is dependent on the position along the element. For the current work the moments are checked at the two nodal points and at the center of the element and choosing the maximum as the critical case. Also, the stress is dependent on the position within the cross section (c'). This is assumed to be $d/2$ where d is the total depth of the cross section.

X. Recommendations

Currently the completed work consists of all the theoretical derivations. Also, the code for the optimization computer program is in the process of being completed and tested.

Future research should include:

1. Three dimensional structures
2. Anisotropic materials (composites)
3. Dynamic analysis
4. Frequency constraints

References

Canfield R.A., Grandhi R.V., Venkayya V.B., "Comparison of Optimization Algorithms for Large Structures", AFWAL-TM-86-204-FIBR, Flight Dynamics Laboratory, Air Force Wright Aeronautical Laboratories, Wright-Patterson Air Force Base, Ohio, May 1986.

Grierson D.E., "Computer-Automated Design of Building Frameworks", Solid Mechanics Division, University of Waterloo, Canada.

Reddy, J.N., An Introduction to the Finite Element Method, New York, New York, McGraw-Hill Inc, 1984.

Schmit L.A., Hirokazu M., "Approximation Concepts for Efficient Structural Synthesis , NASA Contractor Report NASA CR-2552, NASA, Washington, D.C., March 1976.

Vanderplaats G.N., Moses F., "Structural Optimization by Methods of Feasible Directions , National Symposium on Computerized Structural Analysis and Design, George Washington University, Washington D.C., March 1972.

Venkayya V.B., Khot N.S., Berke L., "Application of Optimality Criteria Approaches to Automated Design of Large Pratical Structures AGARD Conference Proceedings No. 123 Second Symposium on Structural Optimization.

Venkayya V.B., Tischler V.A., OPSTAT-A Computer Prbgram for the Optimal Design of Structures Subjected to Static Loads ,AFFDL-TR-fbr-79-67, Wright-Patterson Air Force Base Ohio, June 1979.

Venkayya V.B., "FRAME: Analysis of Aerospace Structures with Frame Elements".

1986 USAF-UES Summer Faculty Research Program/
Graduate Student Summer Support Program

Sponsored by the
Air Force Office of Scientific Research
Conducted by the
Universal Energy Systems, Inc.

FINAL REPORT

Swirling Flows in Dump Combustors

Prepared by:	Mo Samimy and Craig A. Langenfeld
Academic Rank:	Assistant Professor and Graduate Student
Department and University:	Mechanical Engineering The Ohio State University
USAF Researcher:	Dr. A. S. Nejad
Date:	September 24, 1986
Contract No:	F49620-85-C-0013

Swirling Flows in Dump Combustors

by

Mo Samimy and Craig A. Langenfeld
The Ohio State University
Department of Mechanical Engineering
206 W. 18th Street
Columbus, OH 43210

ABSTRACT

A series of experiments were conducted to study isothermal swirling flows in a dump combustor configuration. A two-component coincident LDV system was utilized for detail mean flow and turbulence measurements in the axial and tangential directions. To have optical access for two-component measurements and to minimize disturbances, a small flat window was used and the inlet to the combustor was moved relative to the combustor by using a novel traversing system. Two constant angle swirl generators with swirl numbers of 0.3 and 0.5 were tested. Only 0.5 swirler generated sufficient axial pressure gradient to produce central recirculation which extended approximately 4.5 times of the step height downstream of the expansion plane. The corner recirculating flows were present in both cases with a smaller recirculating region in the stronger swirler. Very large scale turbulence structure was measured in the central core of both flows; the structure was extremely large in the shear layer between the wake behind the hub and the main flow. The decay of large scale motion was very rapid in the stronger swirler flowfield. While 0.3 swirler flowfield became a single solid-body rotational flow after approximately two combustor diameters, the 0.5 swirler flowfield was combination of solid-body rotation at the central core and constant angle swirl flow outside of the central core even at four combustor diameters downstream.

I. INTRODUCTION

I received my Ph.D. from the University of Illinois at Urbana-Champaign studying applications of optical techniques in fluid mechanics especially flows with high mean velocity and turbulence level. Later as a Visiting Assistant Professor I studied flow-induced unsteady forces acting on the tube-launched missiles.

One of the research programs at the Air Force Wright Aeronautical Laboratories is focused on the experimental study of swirling flows in a dump combustor. The major thrust of the research effort is to obtain detailed mean flow and turbulence data using a two-component coincident laser Doppler velocimeter (LDV). Since I had an extensive experience with LDV, therefore, I was chosen and assigned to work on this project.

My student, Craig Langenfeld, did his undergraduate degree in Mechanical Engineering at the University of Dayton. He finished his degree April of 1986 and he started his Master of Science program at The Ohio State University this fall.

II. OBJECTIVES OF THE RESEARCH EFFORT

The overall objective of the first phase of the research was to design, fabricate, and set up a facility which could be used for a detailed experimental study of swirling flows in dump combustors. The objective for the second phase was to use the facility to study effects of influential parameters on the isothermal swirling flows in dump combustors and also to provide extensive data base for the numerical code development and testing.

The first phase of the research had been completed before the Summer Faculty Research Program. Therefore, our objective was to participate in the second phase of the program to perform the following task:

- a. To conduct preliminary experiment and to check flow quality.

- b. To use the facility to obtain detailed LDV data in two swirling flowfields.
- c. To analyze and interpret obtained data.

III. GENERAL BACKGROUND

The significant effects of imposing a swirl component on a flow have been recognized for many years. Methods of generation, characterization, and applications of swirling flows have been discussed in detail by Beer and Chigier (1) and by Gupta, et al. (2). Swirling flows have significant impact on stability, mixing process, and control of combustors. As a result, swirling flows have been focus of many research efforts in the past few years (3,16). The design and characterization of swirlers with different swirl profile have been examined in detail by Buckley, et al. (3). The characteristics of swirlers have also been studied by Kilik (4).

Confined jet or dump combustor geometry has been studied in detail by Lilley and his co-workers (5). Extensive research effort has been focused on combustor geometry with co-annular swirling flows (6-14). Swirling free jet has also been the subject of some recent studies (15,16).

One can conclude from above referenced papers that even though our understanding of the swirling flows has been improved dramatically in the past few years, still a great deal of work is needed in this area. In Section V, the results of present experiments will be presented and compared with the results of earlier work.

IV. EXPERIMENTAL FACILITIES AND TECHNIQUES

The hot-wire anemometer and pressure probes have been utilized extensively in swirling flows (3,5,6,9,11). This type of flow is sensitive to any probing, there is a great ambiguity in flow direction, and the turbulence intensity is very high. Therefore, accuracy of conventional techniques is questionable. LDV technique could provide detail and accurate results if one

could overcome the problem of optical aberrations by the curved tube in a typical cylindrical combustor geometry (17).

A dump combustor configuration with a 102 mm inlet diameter and 152 mm combustor diameter was utilized in the present experiments. Two swirl generators of axial flow type with 12 curved inlet guide vanes were designed in house (3) and used in these experiments. The vanes of swirler are welded between a 102 mm i.d. outer ring and a 19 mm hub. The swirlers were constant angle swirl generators with 0.3 and 0.5 swirl numbers. The swirler was located approximately 50 mm upstream of the dump plane.

A unique feature of the experimental set up is that the inlet tube can be moved inside the combustor tube and as a result a small flat window of 38 x 38 mm dimensions can be used for two-component coincident LDV measurements with a minimal disturbance to the flowfield. A two-component coincident LDV system was utilized for a detailed mean flow and turbulence measurements in the axial and tangential directions. Titanium dioxide particles of approximately 1 micron diameter were used to seed the flow. In order to reduce statistical uncertainty, 27300 samples were obtained in each location in the flowfield. The constant time sampling method and hold/sample method which uses particle inter-arrival time as a weighting factor were utilized to correct for velocity biasing. There was a good agreement between two methods, but because of larger sample size of the hold/sample method, the results produced by this method will be presented here.

The Reynolds number based on inlet diameter was approximately 120,000. The inlet center line velocity was monitored continuously and kept at 18.9 ± 0.4 m/s. In the following section, the incoming flow, the mean flow, and the turbulence field results will be presented and discussed.

V. EXPERIMENTAL RESULTS

Two-component LDV measurements have been carried out in one upstream location and 13 downstream locations up to 4 combustor diameters. Due to lack of time for appropriate presentation of the results and also due to limit of

number of pages of the report, only some selective results will be presented here.

a) Incoming Flow. The incoming flow data was obtained in a location approximately 75 mm upstream of the swirler. Fig. 1 shows the axial mean velocity, U and the tangential mean velocity, W , profiles. The mean velocities and also turbulence data are non-dimensionalized by the upstream center line velocity which is approximately 18.9 m/s. The axial mean velocity is a typical fully developed pipe flow, but the tangential mean velocity is not zero value perhaps due to the subsonic nature of the flow and the influence from swirler which is located only 75 mm downstream.

Fig. 2 shows turbulence intensities in the axial and tangential directions. The turbulence field is not isotropic, but the ratio of the axial turbulence intensity to the tangential turbulence intensity is approximately 1.25 in each radial location and the turbulence field is quite symmetric relative to the center line.

b) Mean Flow. Mean axial and tangential velocity profiles in selective streamwise locations are shown in Figs. 3-5. The measurements carried out from 0.06 combustor diameter to 4 combustor diameters downstream of the dump plane. The 0.3 swirler didn't generate sufficient axial pressure gradient to produce a central reversed flow. But, there was a central recirculation for 0.5 swirler which extended approximately 4.4 step heights downstream of the dump plane. This swirl induced reversed flow is reported by many researchers in cold flow dump combustor configuration (5), in multiple-stream swirling flows in both cold and hot flows (6-14), and in free jet flows (15,16). The corner recirculation zone extends approximately 4.3 step heights for 0.3 swirler and 3.2 step heights for 0.5 swirler. The shortening of corner recirculation with stronger swirler is consistent with other work (5). By two combustor diameters, the axial velocity for both swirling flows is almost uniform across the combustor diameter.

The tangential velocity shows a central core which behaves as a solid body rotation. While this region extends and covers the entire combustor

diameter by approximately 2 combustor diameters for 0.3 swirler, this region extends and then shrinks very gradually for 0.5 swirlers. At 4 combustor diameters downstream of step, still there is a strong central solid body rotation for 0.5 swirler. This result is consistent with findings of other researchers for stronger swirlers (5).

c) Turbulence Field. Axial and tangential turbulence intensity profiles are shown only at two streamwise locations in Figs. 6 and 7. As shown in Fig. 6, the axial turbulence identifies the extent of the central core and the locations of shear layers. The maximum axial turbulence intensity occurs in the shear layer between the central core and the main flow. Both the axial and tangential turbulence intensities are higher for 0.5 swirler than 0.3 and the turbulence dissipation in streamwise direction is also higher for 0.5 swirler. Very high level of turbulence fluctuation in the central recirculation zone have been also reported for similar configurations (5) and for multi-stream flows (6-8).

At 12 step heights downstream of the dump plane, the axial turbulence intensity is almost uniform for both swirlers, but the turbulence level is higher for 0.3 swirler which is due to lower dissipation rate of turbulence. At the same location, the tangential turbulence intensity is approximately uniform across the combustor for 0.3 swirler, but shows large value for the central core of 0.5 swirler where the mean velocity shows a persistent solid body rotation region. The results at 24 step heights downstream still shows high levels of tangential turbulence intensity for 0.5 swirler. This behavior is also shown in other research work (5).

Shear stress and correlation coefficient profiles at two axial locations are shown in Figs. 8 and 9. Shear stress results show existence of very large scale motion in the shear layer between the core and the main flow in both 0.3 and 0.5 swirler flows and extremely fast decay of large scale structure within a short distance for 0.5 swirler. Experimental results show that it takes approximately 6 step heights for 0.5 swirler and approximately 10 step heights for 0.3 swirler to have almost uniform shear flow across the combustor. These distances correspond to the axial wall pressure relaxation which indicate a

strong correlation between pressure field and large scale structure. Lilley and his co-workers (5) used hot-wire for turbulence data in a similar type of configuration. Their results did show such a high level of shear stress for swirl number much higher than the present experiments but lower shear stress level for those comparable to the present swirl numbers.

Correlation coefficient results shown in Figs. 8 and 9 show very non-uniform turbulence structure in the flowfield. This non-uniformity is still strong at 24 step heights downstream of the dump plane.

Figs. 10 and 11 show distribution of turbulent triple products at 1 step height downstream of the dump plane. Turbulent triple products show the existence of large scale structure not only in the shear layer between the central core and the main flow, but also in the central core itself.

Fig. 10(a) shows that the axial component of turbulent kinetic energy is diffused toward the center line from both edges of the shear layer in the axial-tangential plane. This is similar to subsonic plane shear layers and shear layers formed by separation of boundary layer at a step, but it is opposite to supersonic shear layers (18,19). Fig. 10(b) indicates that the tangential component of turbulent kinetic energy is diffused in the direction opposite to mean tangential velocity direction.

Fig. 11 shows diffusion of turbulent kinetic energy in streamwise direction which is in the positive direction in the central core, but in the negative direction in the shear flows. The magnitude of turbulent kinetic energy diffusion is much smaller in the center line which causes very slow development of the center line mean velocity. Similar to shear stress profiles, the triple products decay much faster for 0.5 swirler than 0.3 swirler.

VI. CONCLUSIONS AND RECOMMENDATIONS

A two-component coincident LDV was used to obtain detailed mean flow and turbulence data in a dump combustor configuration with 0.3 and 0.5 swirl numbers constant angle swirl generator inlet. The data indicated domination

of large scale motion and enhanced mixing by the large scale structure specially for the stronger swirler. The obtained data is a good data base for computational code development and testing. The radial components mean and turbulence data would complement this data and would provide better understanding of the physics of this type of flowfield. From a practical view point, a similar experimental work with much higher Reynolds number would be very beneficial.

ACKNOWLEDGEMENTS

We would like to thank the Air Force Systems Command and the Air Force Office of Scientific Research for sponsoring this program. Any extensive experimental work can be accomplished only by a team of cooperative researchers. The swirl generators designed and fabricated by the experimental group in the Ramjet Technology Branch of APL/AFWAL. The LDV system was initially developed by Dr. Roger R. Craig. The experimental set up was designed and fabricated by Dr. A. S. Nejad. Mr. Kenneth G. Schwartzkopf was very helpful with data acquisition hardware and software. The support and guidance of Dr. A. S. Nejad during the research period are deeply appreciated.

REFERENCES

1. Beer, J. M. and Chigier, N. A., Combustion Aerodynamics, John Wiley and Sons, New York, 1972.
2. Gupta, A. K., Lilley, D. G., and Syred, N., Swirl Flows, Abacus Press, Turnbridge Wells, England, 1984.
3. Buckley, P. O., Craig, R. R., Davis, D. L., and Schwartzkopf, K. G., "The Design and Combustion Performance of Practical Swirlers for Integral Rocket/Ramjets," AIAA Journal Vol. 21, No. 5, May 1983, pp 733-740.
4. Kilik, E., "Better Swirl Generation Using Curved Vanes Swirlers," AIAA Paper-85-0187, 1985.

5. Lilley, D.G., "Swirling Flows in Typical Combustor Geometries," AIAA Paper-85-0184, 1985.
6. Vu, B. T. and Gouldin, F. C., "Flow Measurements in a Model Swirl Combustor," AIAA Journal, Vol. 20, No. 5, May 1982, pp. 642-651.
7. Gouldin, F. C., Depsky, J. S., and Lee, S-OL., "Velocity Field Characteristics of a Swirling Flow Combustor," AIAA Journal, Vol. 23, No. 1, Jan. 1985, pp. 95-102.
8. Ramos, J. I. and Somer, H. T., "Swirling Flow in a Research Combustor," AIAA Journal, Vol. 23, No. 2, Feb. 1985, pp. 241-248.
9. Habib, M. A. and Whitelaw, J. H., "Velocity Characteristics of Confined Coaxial Jets With and Without Swirl," Journal of Fluids Engineering, Trans. of the ASME, Vol. 102, March 1980, pp. 47-53.
10. Brum, R. D., Seiler, E. T., LaRue, J. C., and Samuelson, G. S., "Instantaneous Two-Component Laser Anemometry and Temperature Measurements in a Complex Flow Model Combustor," AIAA Paper-83-0334, 1983.
11. Mattingly, J. and Oates, G., "An Experimental Investigation of Co-Annular Swirling Flows," AIAA Paper-85-0186, 1985.
12. Brondum, D. C., Bennett, J. C., Weinberg, B. C., and McDonald, H., "Numerical and Experimental Investigation of Nonswirling and Swirling Confined Jets," AIAA Paper-86-0040, 1986.
13. Ramos, J. I., "Turbulent Nonreacting Swirling Flows," AIAA Journal, Vol. 22, No. 6, June 1984, pp. 846-848.
14. Kubo, I. and Gouldin, F. C., "Numerical Calculations of Turbulent Swirling Flow," Journal of Fluids Engineering, Trans. of the ASME, Sept. 1975, pp. 310-315.

15. Fujii, S., Eguchi, K., and Gomi, M., "Swirling Jet with and without Combustion," AIAA Journal, Vol. 19, No. 11, Nov. 1981, pp. 1438-1442.
16. Sislian, J. P. and Cusworth, R. A., "Measurements of Mean Velocity and Turbulent Intensities in a Free Isothermal Swirling Jet," AIAA Journal, Vol. 24, No. 2, Feb. 1986, pp. 303-309.
17. Durrett, R. P., Stevenson, W. H., and Thompson, H.D., "Radial and Axial Turbulent Flow Measurements with an LDV in an Axisymmetric Sudden Expansion Air Flow," International Symposium on Laser Anemometry, ASME FED-Vol. 33, 1985.
18. Samimy, M., Petrie, H. L., and Addy, A. L., "A Study of Compressible Turbulent Reattaching Free Shear Layers," AIAA Journal, Vol. 24, Feb. 1986, pp. 261-267.
19. Samimy, M. and Addy, A. L., "Interaction Between Two Compressible, Turbulent Free Shear Layers," to appear in Nov. 1986 issue of AIAA Journal.

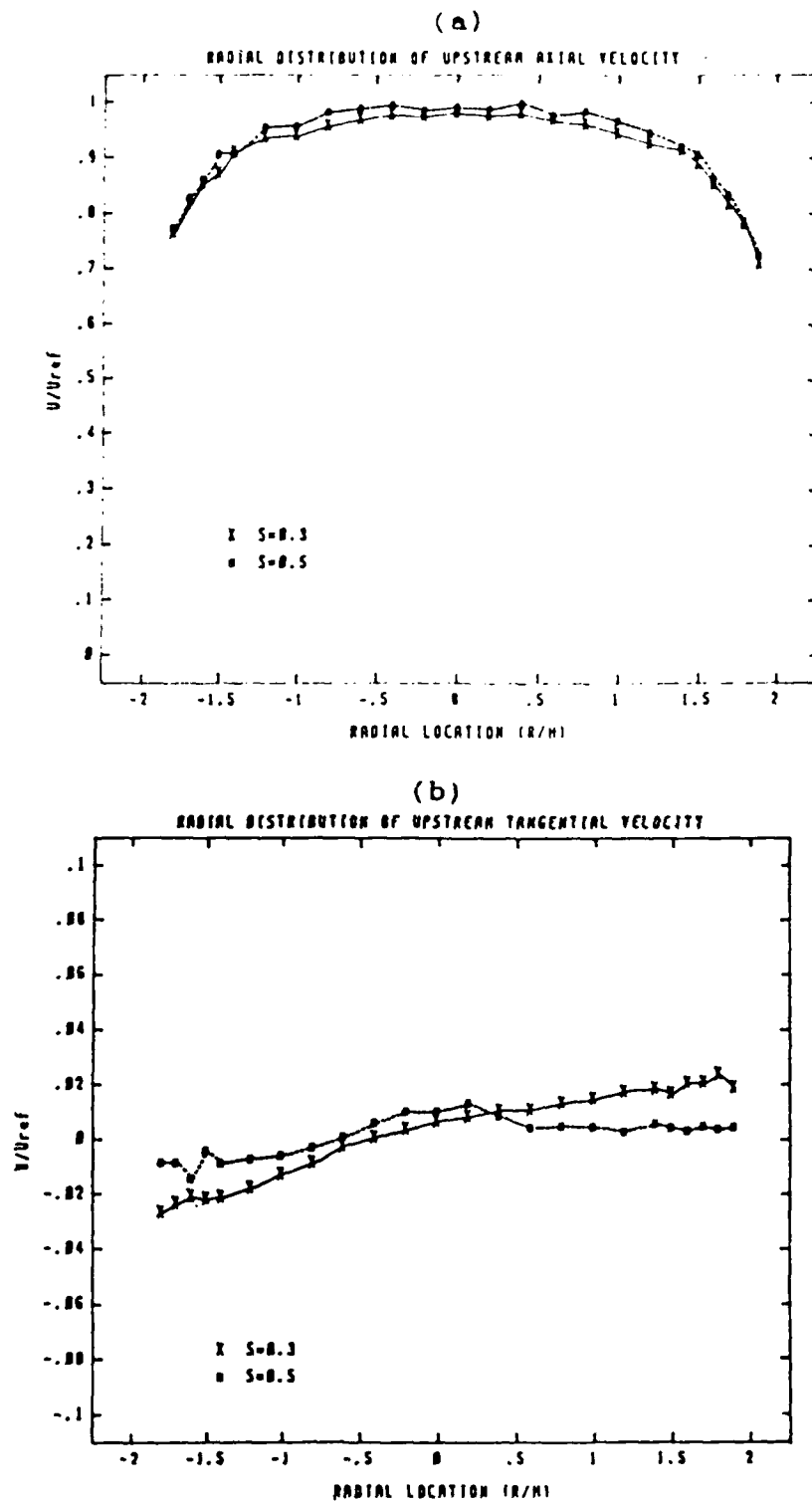


Fig. 1 Incoming axial and tangential mean velocities.
(Approximately 75 mm upstream of swirler)

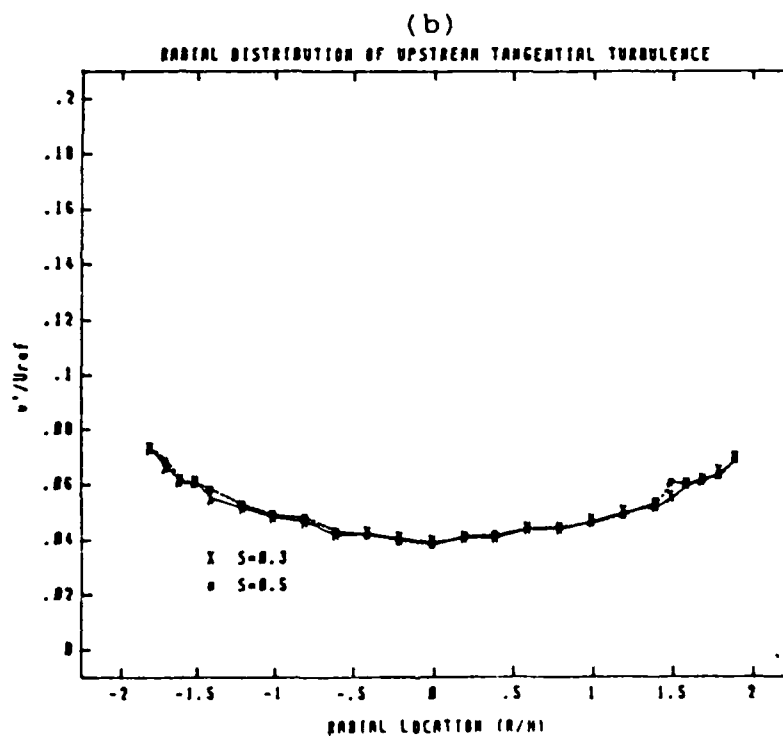
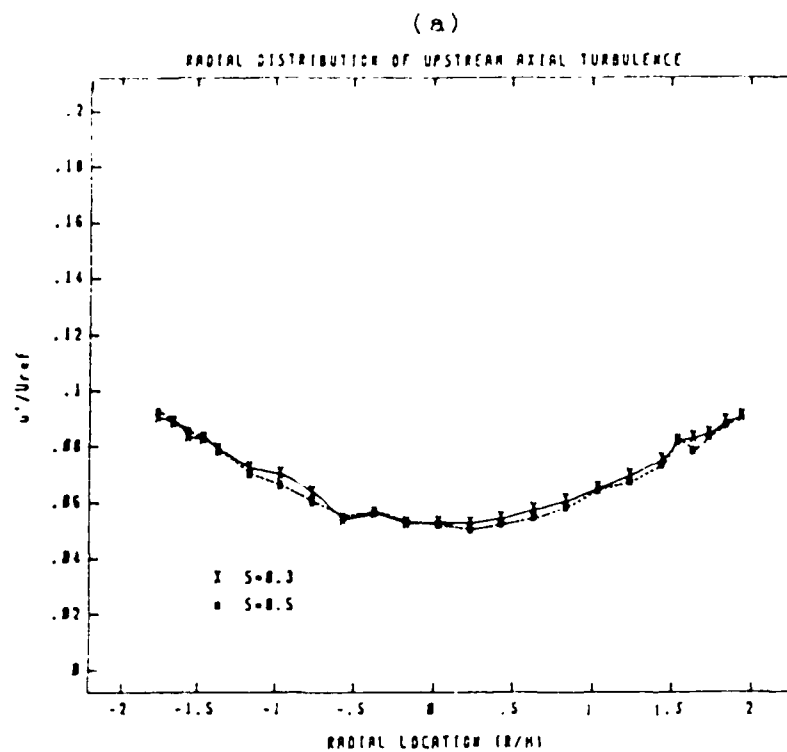


Fig. 2 Incoming axial and tangential turbulence intensities. (u' and w' in Figs. 2, 6, and 7 are standard deviations of fluctuations) 42-12

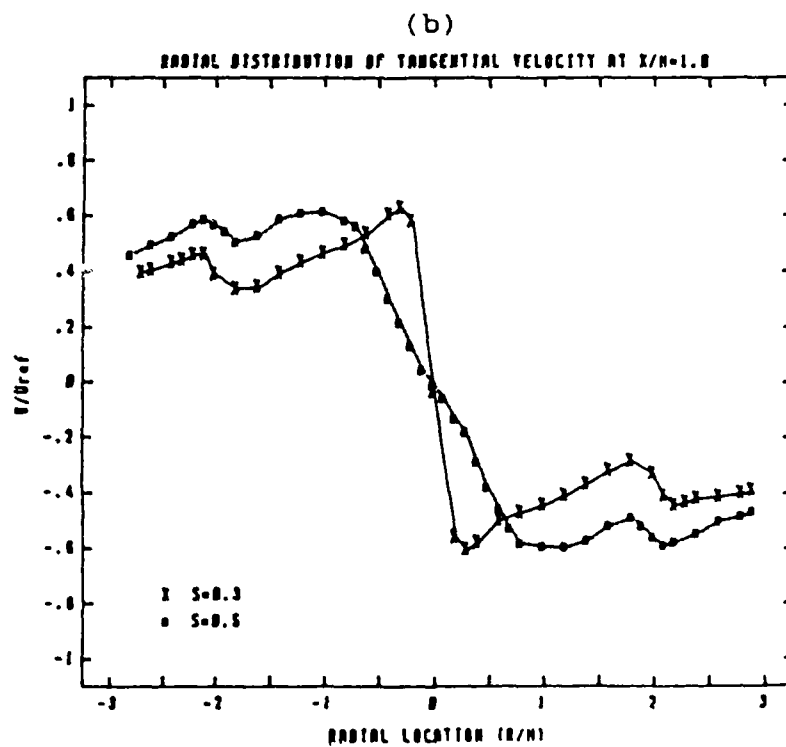
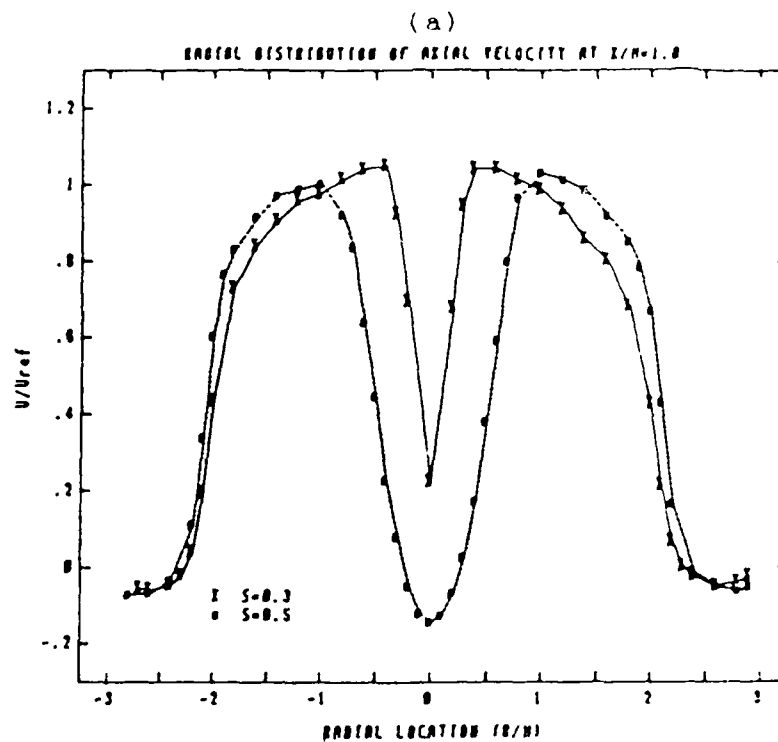


Fig. 3 Axial and tangential mean velocities at $x/h=1$.
(h is step height; 25.4 mm)

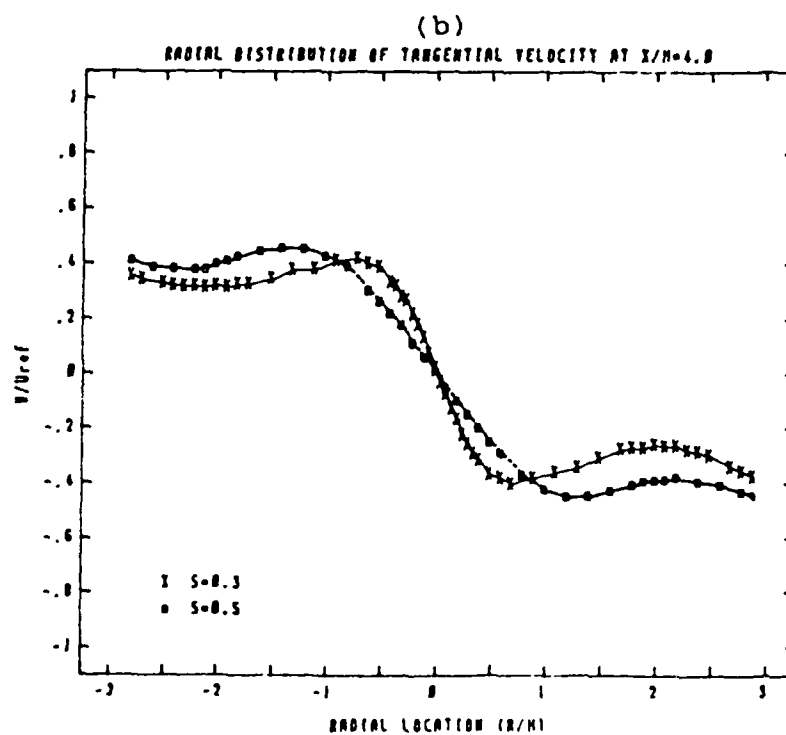
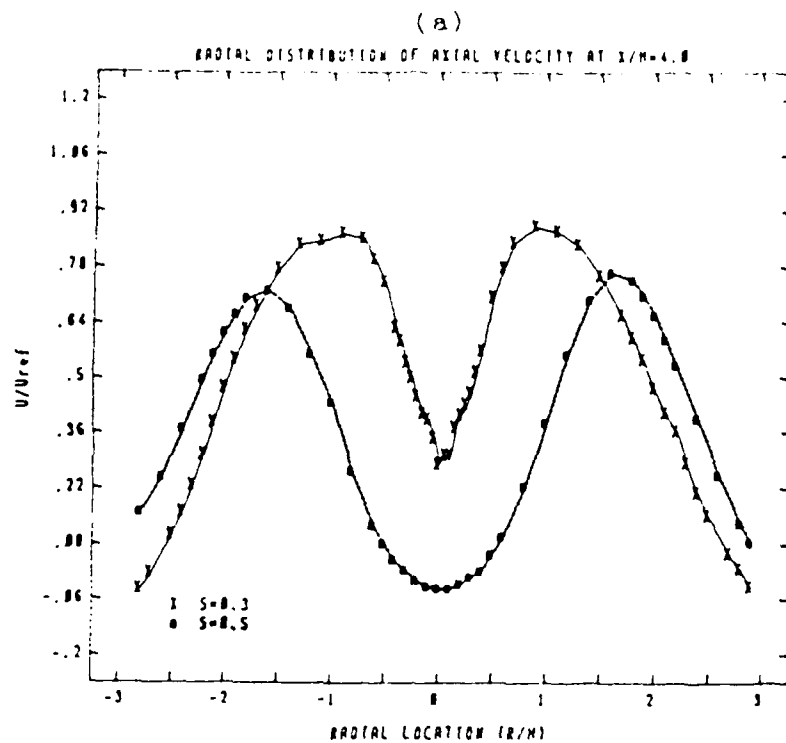


Fig. 4 Axial and tangential mean velocities at $x/h=4$.

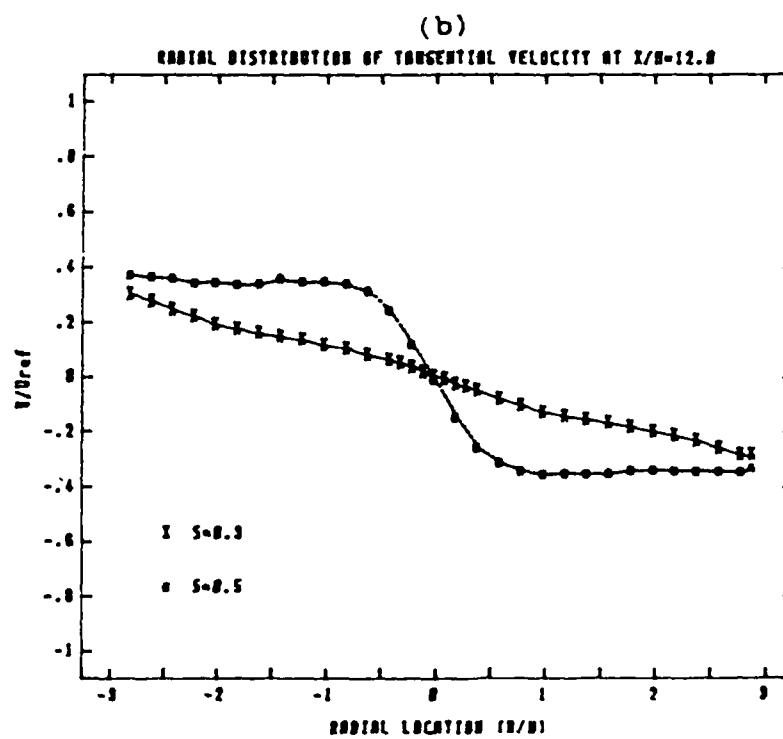
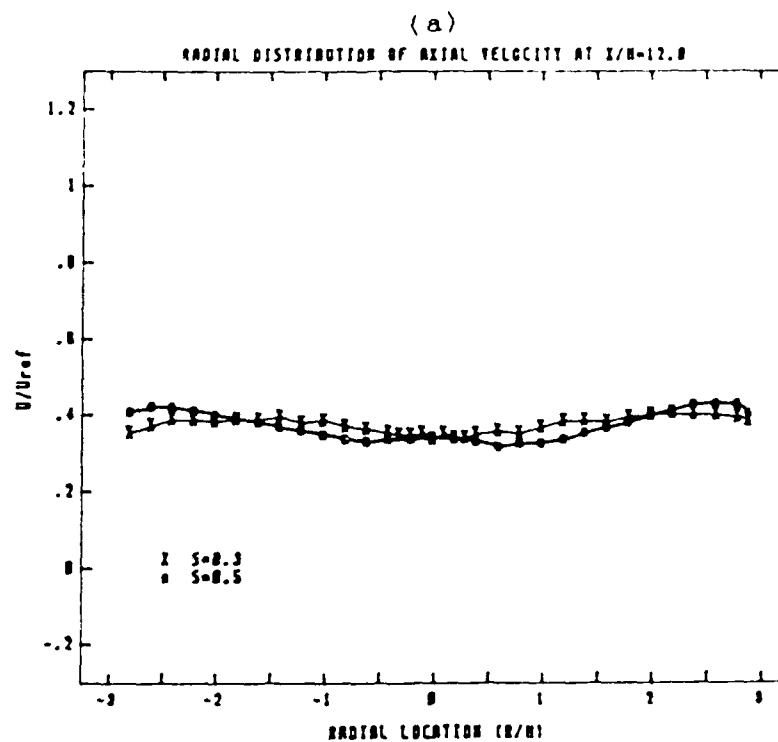


Fig. 5 Axial and tangential mean velocities at $x/h=12$.

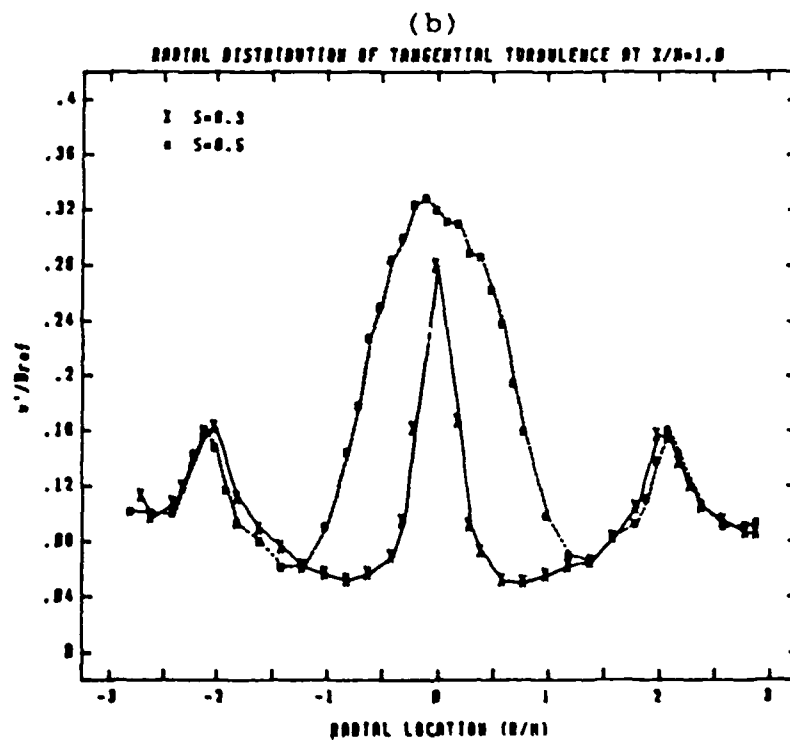
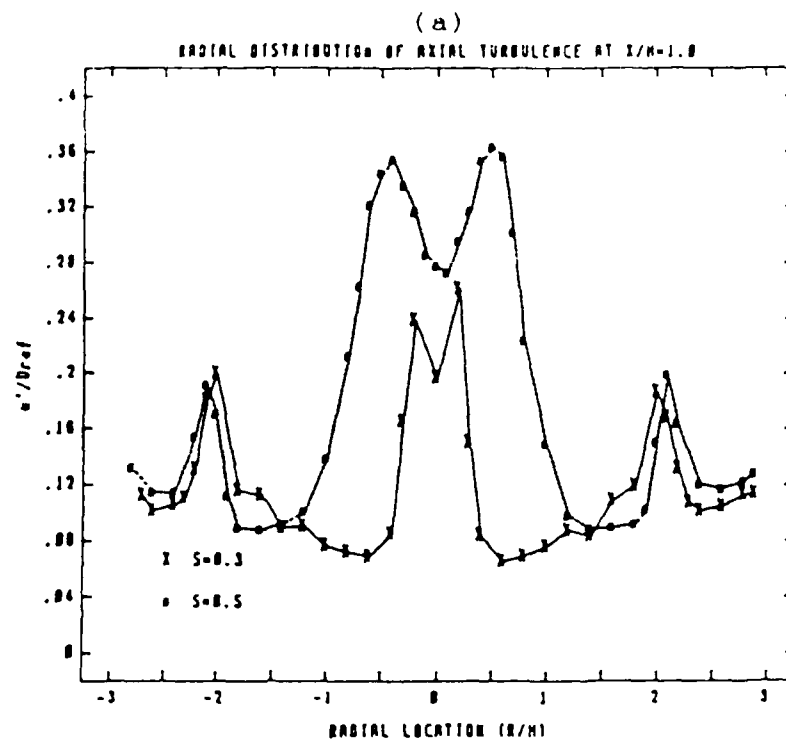


Fig. 6 Axial and tangential turbulence intensities at $x/h=1$.

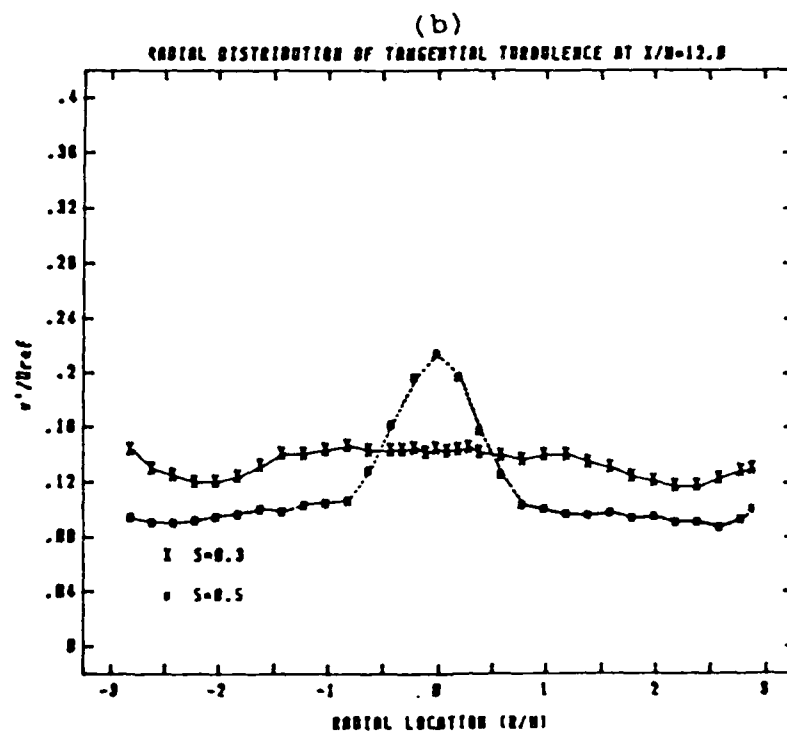
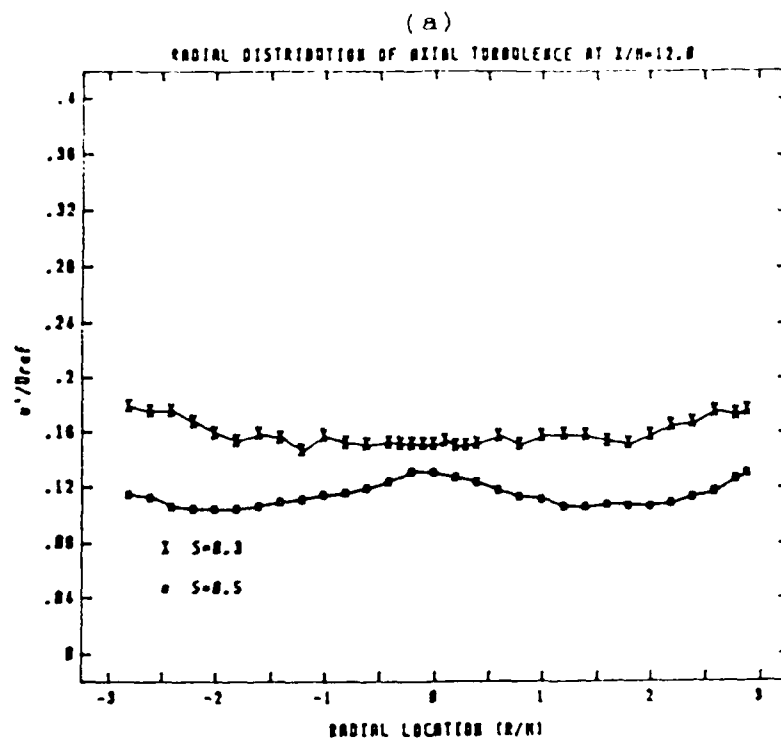


Fig. 7 Axial and tangential turbulence intensities at $x/h=12$.

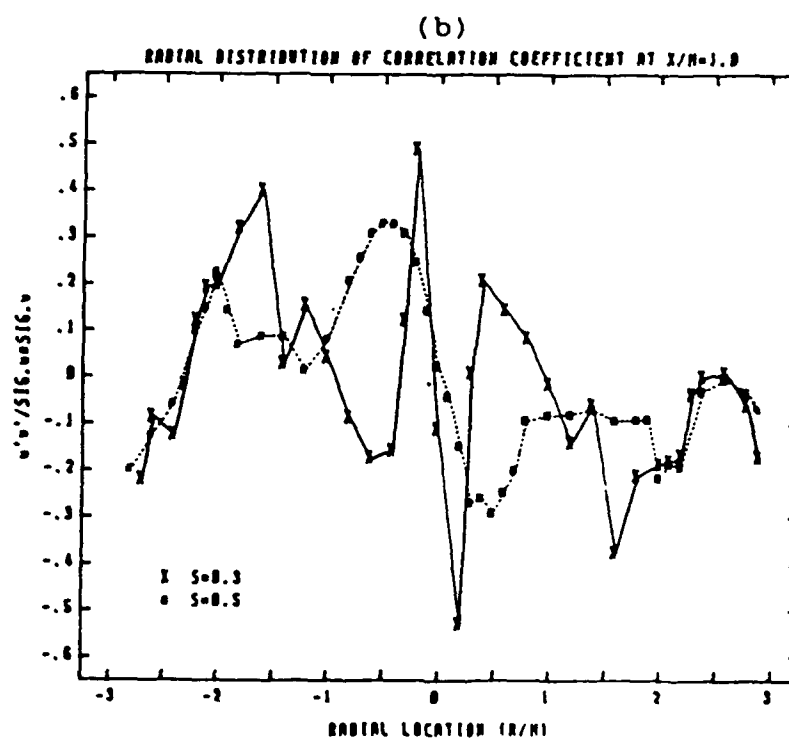
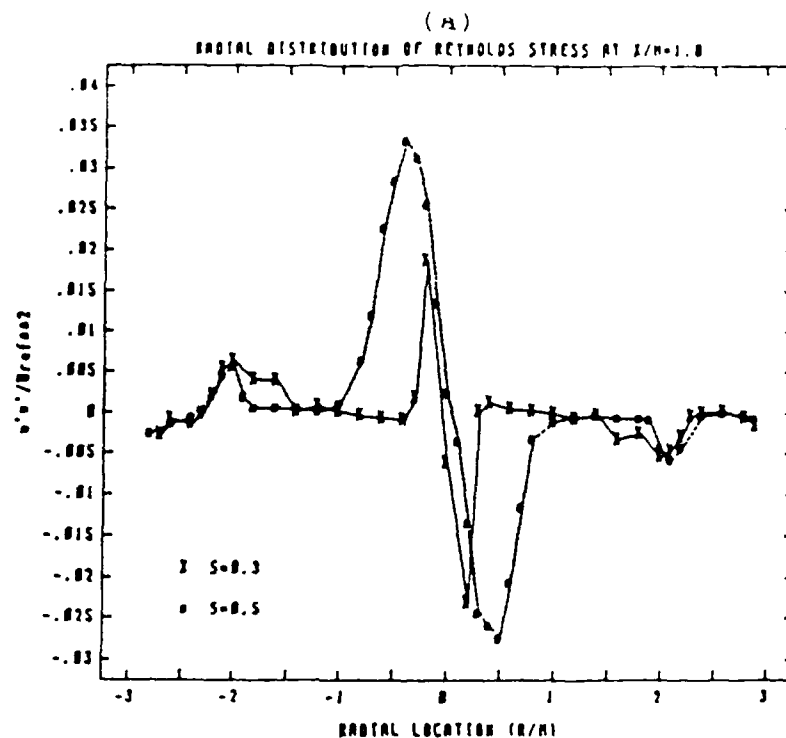


Fig. 8 Reynolds shear stress and correlation coefficient at $x/h=1$.

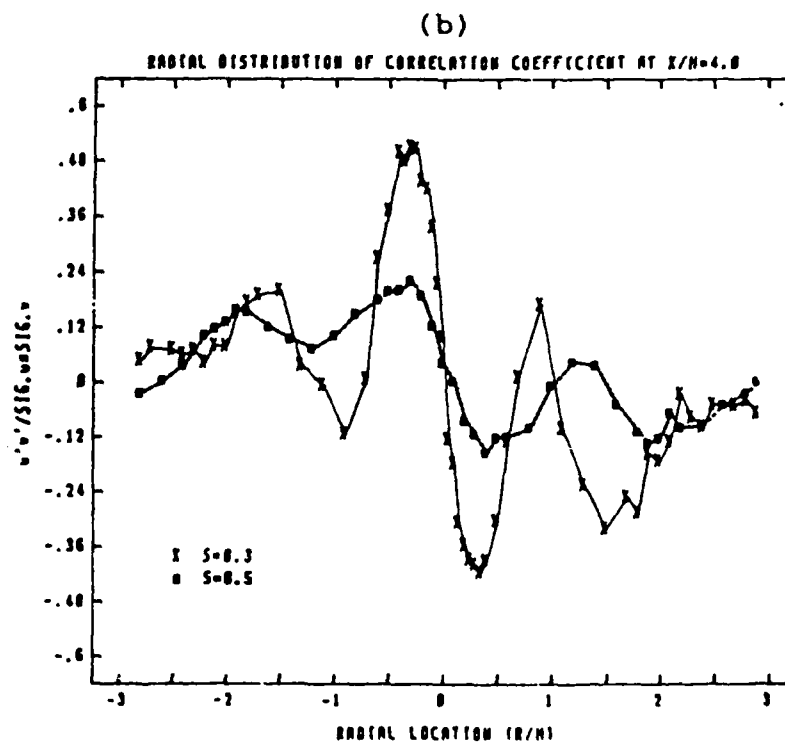
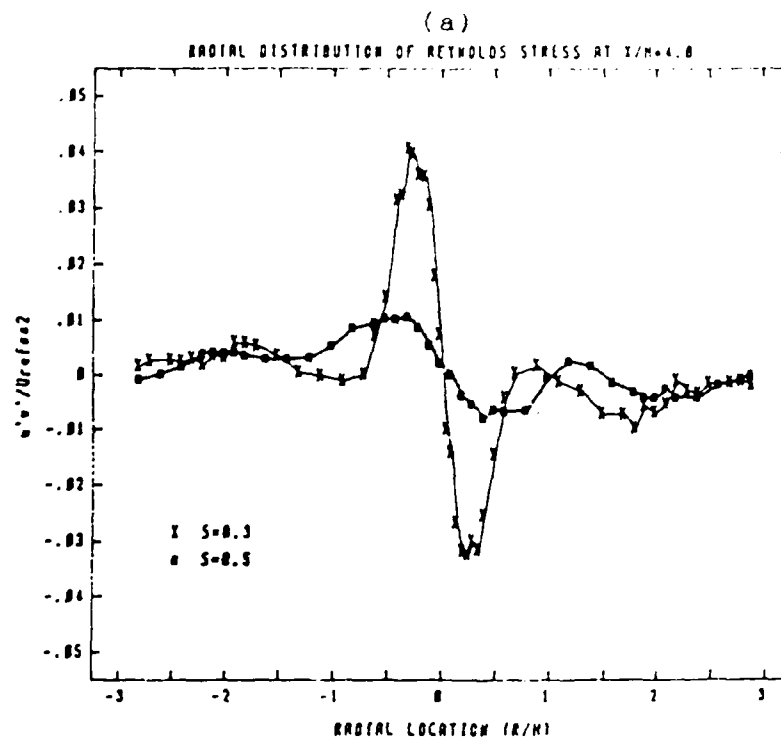


Fig. 9 Reynolds shear stress and correlation coefficient at $x/h=4$.

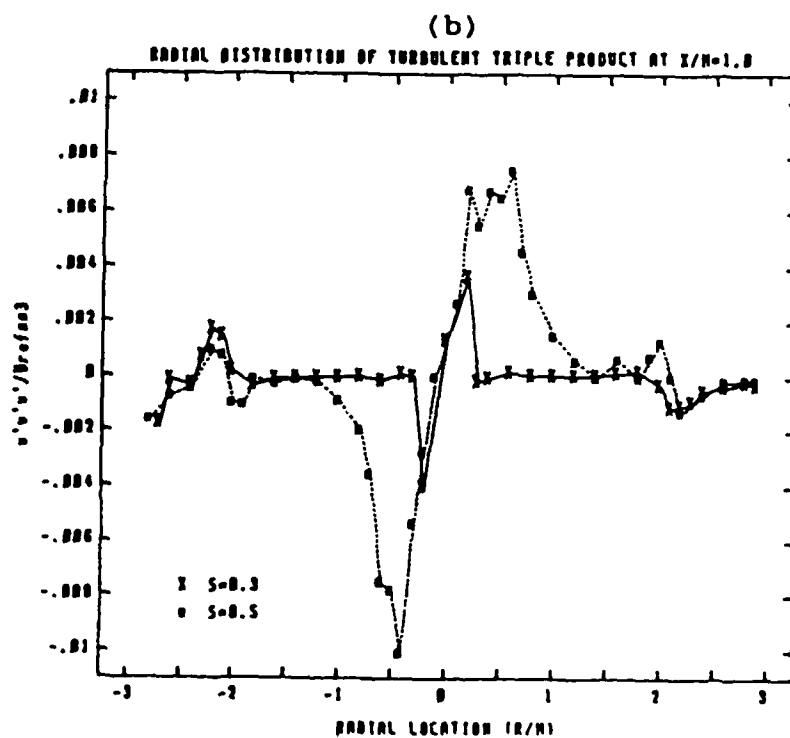
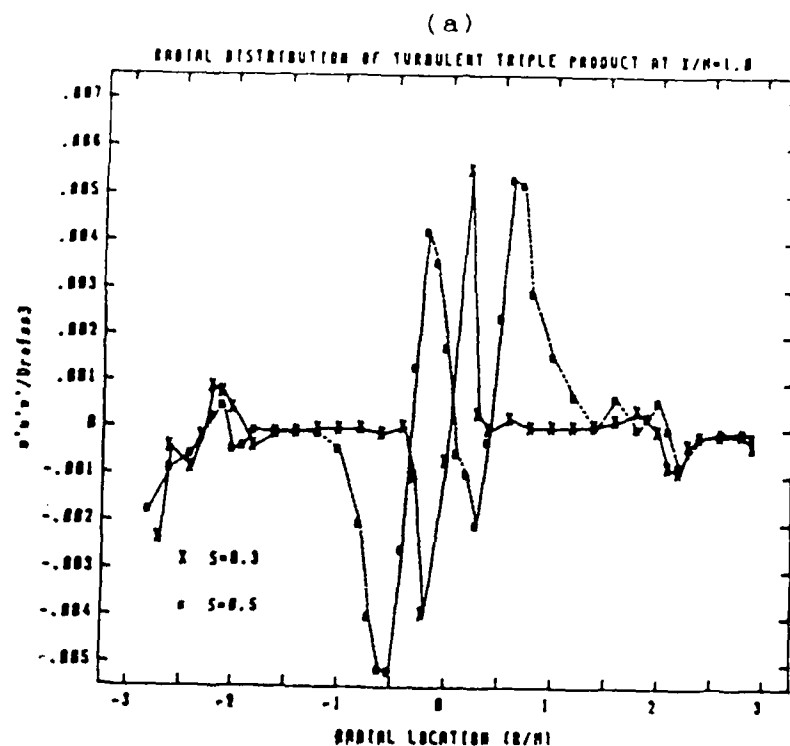


Fig. 10 $u'u'u'$ and $w'w'w'$ components of triple products at $x/h=1$.

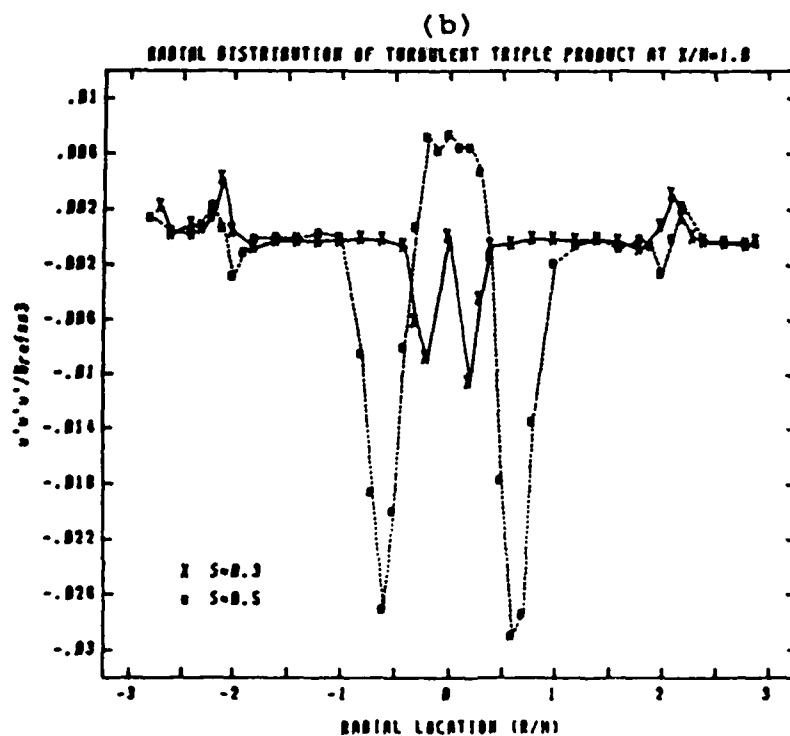
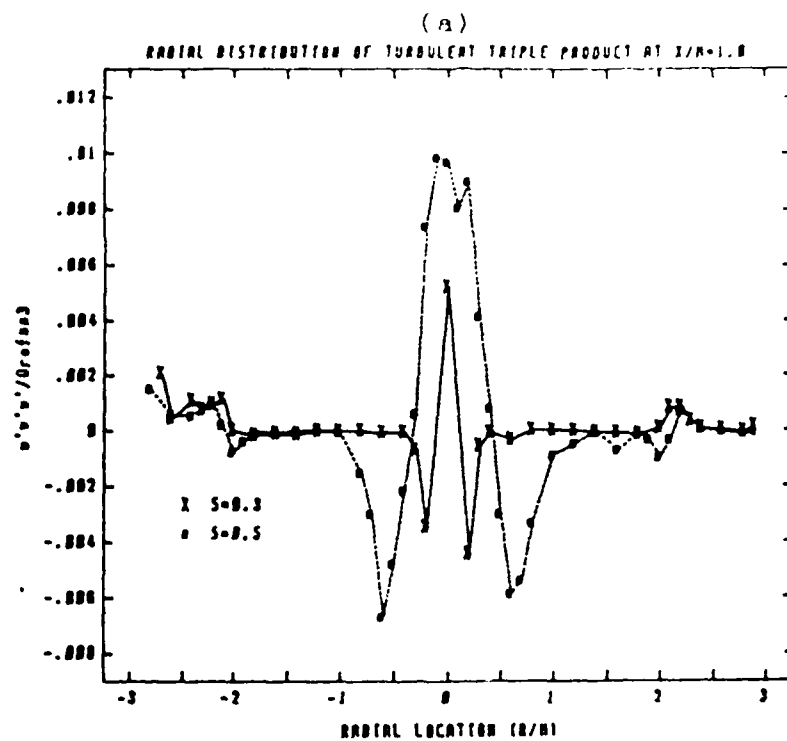


Fig. 11 $u'w'w'$ and $u'u'u'$ components of triple products.

1986 USAF-UES SUMMER FACULTY RESEARCH PROGRAM/
GRADUATE STUDENT SUMMER SUPPORT PROGRAM

Sponsored by the
AIR FORCE OFFICE OF SCIENTIFIC RESEARCH

Conducted by the
Universal Energy Systems, Inc.

FINAL REPORT

THERMAL STABILITY STUDIES OF STRUCTURE-PROPERTY RELATIONSHIP
OF VARIOUS SILAHYDROCARBON LUBRICANTS.

Prepared by :	Tieu-Binh Le	and	Dr. Vijay K. Gupta
Academic Rank :	Graduate student		Professor of Chemistry
Department and	Department of Chemistry		
University :	Wright State University		Central State University
Research Location :	Materials Laboratory (AFWAL/MLBT)		
	Wright Patterson Air Force Base,		
	Dayton, Ohio		
USAF Researcher :	Mr. C.E. Snyder, Jr.		
Date :	September 2, 1986		
Contract No. :	F49620-85-0013		

THERMAL STABILITY STUDIES OF STRUCTURE-PROPERTY RELATIONSHIP
OF VARIOUS SILAHYDROCARBON LUBRICANTS.

by

Tieu-Binh Le and Vijay K. Gupta

Abstract

Thermal stability studies of various silahydrocarbon fluids ($R-Si-(n-C_8H_{17})_3$) were investigated by the micro-thermal stability test followed by GC, GC/MS analysis, kinematic viscosity measurements, and IR spectroscopy analysis. It has been found that saturated substituent in the silahydrocarbon molecule tends to decompose as subjected to thermal stress, whereas the silahydrocarbons with an unsaturated substituent group lead to polymerization under the same conditions. Thermal stability studies of the fluid $CH_3-Si-(n-C_8H_{17})_3$ were performed as a function of temperature and time. It was observed that the above fluid did not decompose significantly up to 725F (385C) for 6 hours stress time, but it decomposed almost completely when stressed for 6 hours at 800F (426.7C).

Acknowledgments

We would like to thank the Air Force Systems Command and the Air Force Office of Scientific Research and the Universal Energy Systems Inc., for sponsorship of this study. We are especially grateful to Mr. Carl E. Snyder Jr. and Ms. Lois Gschwender for their encouragement and helpful suggestions. Also, we are deeply indebted to Dr. Chi Yu who provided GC/MS analysis. Finally, we wish to express our sincere appreciation to the UDRI Lubricants Group for their technical assistance in conducting this study.

I. Introduction

With the increasing demand being placed on lubricants for modern aircraft, much research effort has been devoted to the development of improved lubricants; not only petroleum-based lubricants, but synthetic lubricants, such as silahydrocarbons. Silahydrocarbons are defined as the compounds having the general molecular structure SiR_4 , where the four alkyl groups can be similar or different. Silahydrocarbons are highly thermal stable compounds, and are suitable to use where petroleum-based or synthetic hydrocarbon-based fluids cannot perform due to the thermal deficiency.

The determination of the temperature ranges over which the silahydrocarbons can be used, involves a knowledge of the thermal stability of these fluids. Since the molecular structure of a compound is responsible for its physical properties, a better understanding of the structure-property relationship is also particularly important. For these two reasons, the thermal stability studies for the silahydrocarbon fluids have been conducted. The fluids that have been investigated are shown in table 1.

II. Objectives of the research effort

The primary objective of the study was to determine the structure-property relationship of the silahydrocarbon

fluid to provide a basis for understanding the effect of molecular structure on physical properties. The other objectives of the study were to determine the thermal degradation of the silahydrocarbon fluid $\text{CH}_3\text{-Si-(n-C}_8\text{H}_{17})_3$ as a function of temperature and as a function of time, and to identify the decomposition products in liquid phase and gaseous phase.

III. Experimental

The thermal stability test was conducted according to the micro-thermal stability test method. The procedure was as follows. Approximately 2 cc of the test fluid was added to a 9" long, 0.25" diameter bomb constructed of 304 stainless steel with 316 stainless steel swage-lock fittings on both ends. Nitrogen gas was bubbled through the fluid for 5 minutes to assist in air removal. The bomb was then weighed and placed in an oven at a specific temperature for a specific time period. The bomb was then removed from the oven, allowed to cool to room temperature, and reweighed. If the pre-test and post-test weights differed by more than 0.100g, the test was considered invalid and the test was repeated. The bomb was then cooled to approximately -100F in a dry ice-acetone bath for at least 30 minutes to liquify the gaseous components. The bomb was removed from the cold bath and one of the cap was replaced by a cap with a small hole containing

a septum to facilitate the withdrawal of gaseous sample. The bomb was then allowed to warm to room temperature, and the headspace sample was taken through the septum top with a gas tight syringe and was then analysed by GC. The bomb was opened and the liquid sample was analysed by GC and viscosity measurement.

The gas chromatographic conditions for the analysis was listed in table 8.

IV. Results and discussion

Thermal stability studies for the silahydrocarbon fluid MLO 86-190 were performed. The thermal degradation data of the above fluid as a function of temperature and as a function of time is given in table 2 and 3 and Fig.1 and 2. It is observed that the fluid is quite stable up to 700F (371.1C). It did not show notable decomposition at this temperature up to 24 hours stress time. However, the rate of degradation increases significantly above 700F. The fluid decomposed almost completely in 6 hours when stressed at 800F (426.7C). Viscosity data also show the similar trend for the rate of thermal degradation.

Thermal stability studies of various silahydrocarbon fluids ($\text{R-Si}-(\text{n-C}_{8\text{H}_{17}})_3$) were also investigated. Thermal degradation data of these fluids is given in table 4 and 5. It has been found that saturated substituent in the

silahydrocarbon molecule tends to decompose as subjected to thermal stress, whereas silahydrocarbons with an unsaturated substituent group lead to polymerization. The formation of the polymers is indicated by the significant increase in viscosity of the stressed fluids, and also by the IR spectra. The IR spectra of MLO 86-146 are given in Fig.4 and 5. In the infrared absorption spectrum of the stressed fluid, stretching vibrations owing to the C=C at 1640 cm^{-1} region were not observed indicating that the polymerization has occurred as the fluid is stressed. Similar evidence was found in the IR spectrum of the stressed MLO 86-140 fluid. The rate of production of these addition polymers was related to the position of the double bond in the substituent group on the silahydrocarbon molecule. Significant difference in % change viscosity of the two fluids indicates that the rate of polymerization is more rapid for the silahydrocarbon having a double bond located on the end of the substituent group (MLO 86-146) than the silahydrocarbon with a substituent group having a double bond next to the Si atom (MLO 86-140).

Table 4 shows the thermal degradation data of the saturated substituent silahydrocarbons stressed at 725F (385C) for 16 hours. From the data, it appears that

these fluids decompose almost with the same rate. However, in order to draw the conclusion regarding the structure-property relationship of these silahydrocarbon fluids, further study should be conducted at higher temperature and/or longer stress times.

GC/MS analysis of MLO 86-190 in gaseous and liquid phases stressed at 700F (371.1C) for 120 hours are shown in Fig.6 and 7 respectively. Table 6 and 7 report the gaseous and liquid components of the above stressed fluid. It is observed that hydrocarbons with 1 carbon to 6 carbons are present in gaseous phase, whereas in liquid phase large number of degradation components are found.

V. Recommendations

1. Much work remains to be done with the unsaturated substituent silahydrocarbon fluids. Further thermal stability studies should be conducted. The degree of polymerization needs to be found. Stressed fluids need to be run on GPC and DSC.
2. For the saturated substituent silahydrocarbons, more experiments should be done at higher temperature and/or longer stress times to determine the effect of molecular structure on thermal stability properties of silahydrocarbon fluids.
3. Conditions of the GC should be checked. Some of the

chromatograms obtained during this study showed evidence of sample condensation on the column. Maybe the column temperature was not high enough; replacing the column with higher temperature type column may help.

Table 1. Structures of various silahydrocarbon fluids

MLO No.	Structure
86-20	$n\text{-C}_5\text{H}_{11}\text{-Si-(n-C}_8\text{H}_{17})_3$
86-61	$(\text{CH}_3)_2\text{CHCH}_2\text{CH}_2\text{-Si-(n-C}_8\text{H}_{17})_3$
86-139	$\text{CH}_3\text{CH}_2\text{CH}_2\underset{\text{CH}_3}{\text{CH}}\text{-Si-(n-C}_8\text{H}_{17})_3$
86-166	$\text{CH}_3\text{CH}_2\underset{\text{CH}_3}{\text{CH}}\text{CH}_2\text{-Si-(n-C}_8\text{H}_{17})_3$
86-190	$\text{CH}_3\text{-Si-(n-C}_8\text{H}_{17})_3$
86-140	$\text{CH}_3\text{CH}_2\text{CH}_2\text{CH=CH-Si-(n-C}_8\text{H}_{17})_3$
86-146	$\text{H}_2\text{C=CHCH}_2\text{CH}_2\text{CH}_2\text{-Si-(n-C}_8\text{H}_{17})_3$

Table 2. Thermal Degradation Data of Fluid MLO 86-190 Stressed at 700F (371.1C).

Stressed time (hours)	% concentration of silahydrocarbon	% change conc.	Viscosity (cSt) at 100F (37.8C)	% change visc.
0	99.90	0	7.99	0
6	99.56	-0.34	7.31	-8.51
16	97.82	-2.08	7.19	-10.01
24	96.55	-3.35	7.22	-9.64
48	91.83	-8.08	6.81	-14.77
72	84.15	-15.76	6.74	-15.64
120	51.45	-48.50	5.52	-30.91
168	25.65	-74.32	4.51	-43.55

Fig. 1

THERMAL DEGRADATION OF MLO 86-190

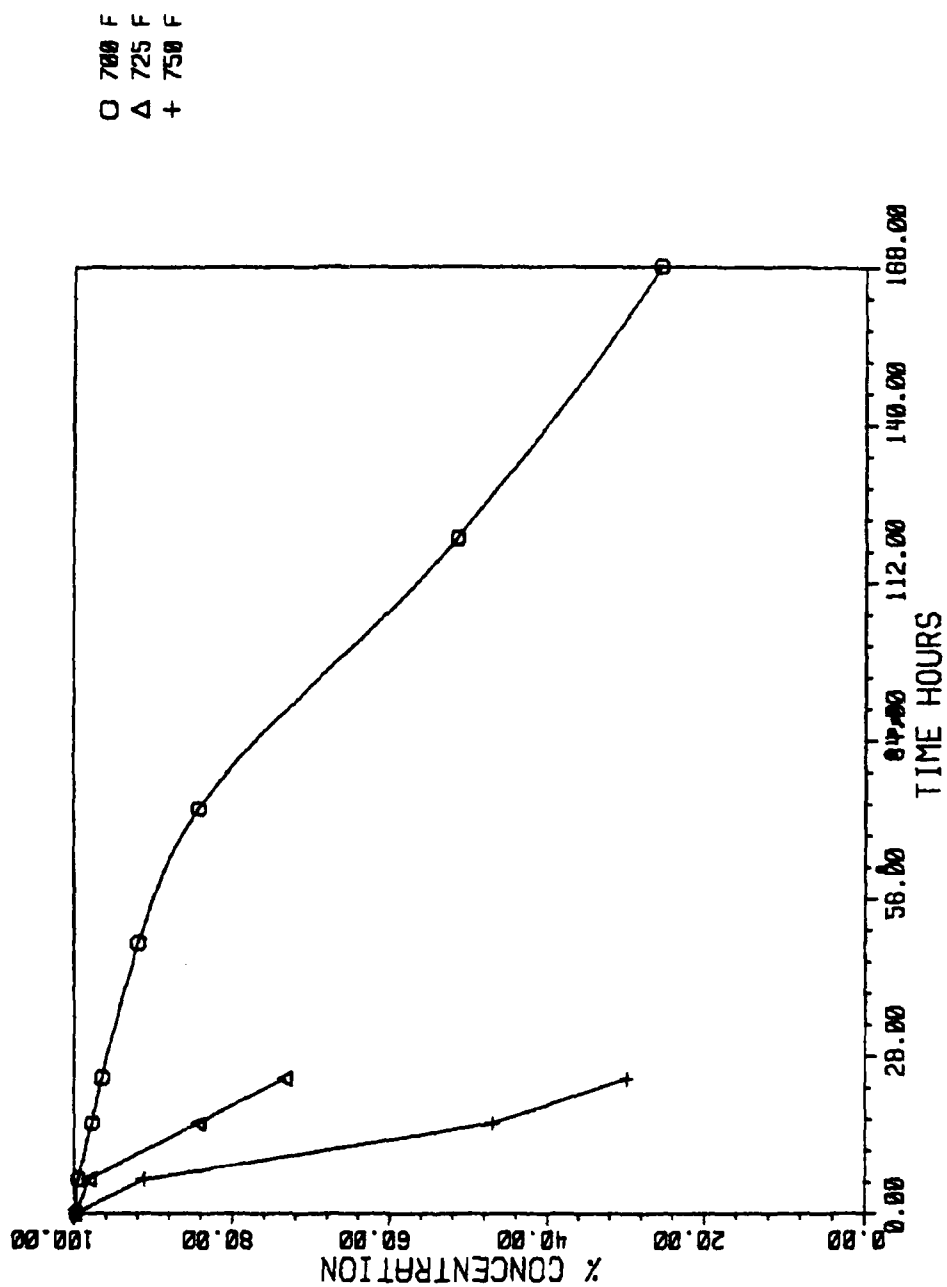


Fig. 2

THERMAL DEGRADATION OF MLO 86-190

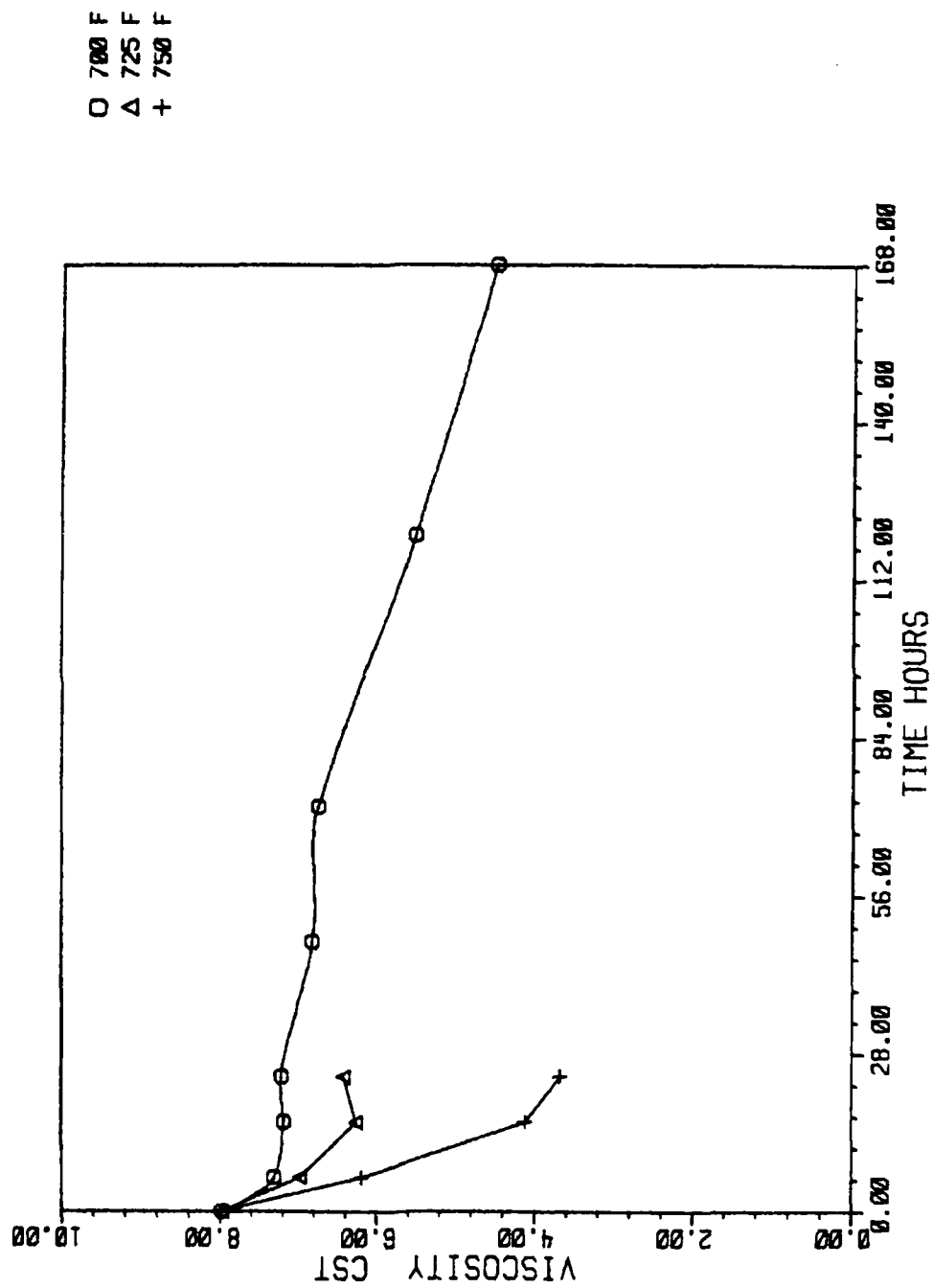


Table 3. Thermal Degradation Data of Fluid MLO 86-190.

Stressed temperature (F)	Stressed time (hours)	% conc. of silahydrocarbon	% change conc.	Viscosity (cSt) at 100F	% change visc.
Unstressed	0	99.90	0	7.99	0
700	6	99.56	-0.34	7.31	-8.51
725	6	98.20	-1.70	6.97	-12.76
725	16	84.35	-15.56	6.25	-21.78
725	24	73.29	-26.64	6.42	-19.65
750	6	91.16	-8.75	6.19	-22.53
750	16	47.04	-52.91	4.12	-48.43
750	24	29.90	-70.07	3.68	-53.94
775	6	55.90	-44.04	5.28	-33.92
800	6	0.63	-99.37	1.63	-79.60

Fig. 3

THERMAL DEGRADATION OF MLO 86-190

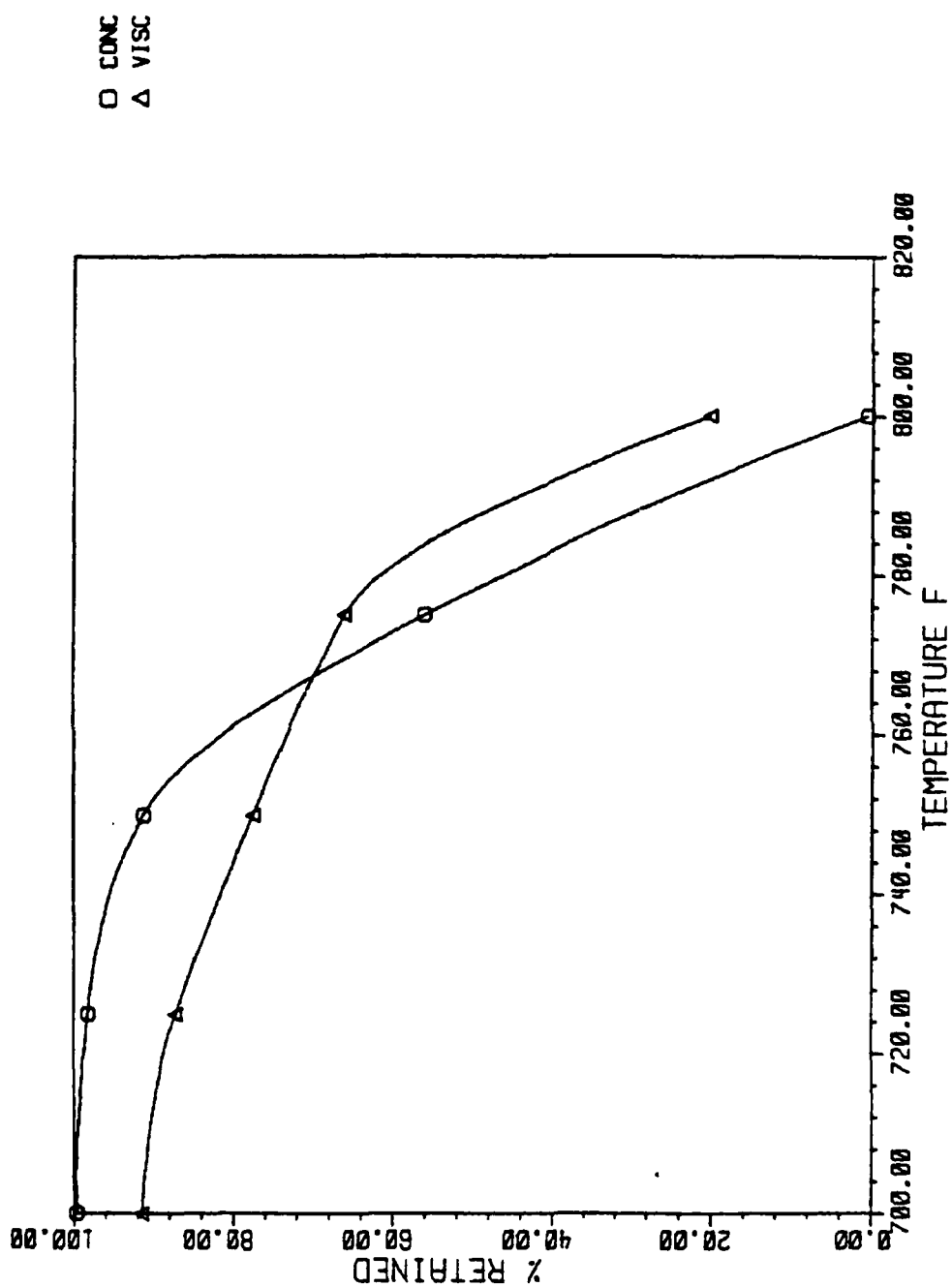


Table 4. Thermal Degradation Data of Silahydrocarbon Fluids Stressed at 725F for 16 hours.

Fluid	<u>% concentration of silahydrocarbon</u>		<u>Viscosity (cSt) at 100 F (37.8C)</u>		% change
	Unstressed	Stressed	Unstressed	Stressed	
MLO 86-20	99.46	78.16	11.36	9.59	-15.58
MLO 86-61	99.68	81.38	12.59	9.57	-23.99
MLO 86-139	99.86	80.44	13.83	9.63	-30.37
MLO 86-166	99.83	82.30	11.95	9.51	-20.42

Table 5. Thermal Degradation Data of Silahydrocarbon Fluid Stressed at 700F (371.1C).

Fluid	Stressed time (hours)	% conc. of silahydrocarbon	% change conc.	Viscosity (cSt) at 100F (37.8C)	% change visc.
MLO 86-140	0	99.84	0	11.09	0
MLO 86-140	16	18.38*	-81.59	13.37	+20.56
MLO 86-146	0	99.88	0	10.72	0
MLO 86-146	6	6.41*	-93.58	80.90	+654.66

* % concentration of silahydrocarbon was measured by using internal standard method.
Tridecane was used as GC internal standard.

Fig.4 I.R. Spectra of NLO 86-146 using 0.025 mm KBr cell.

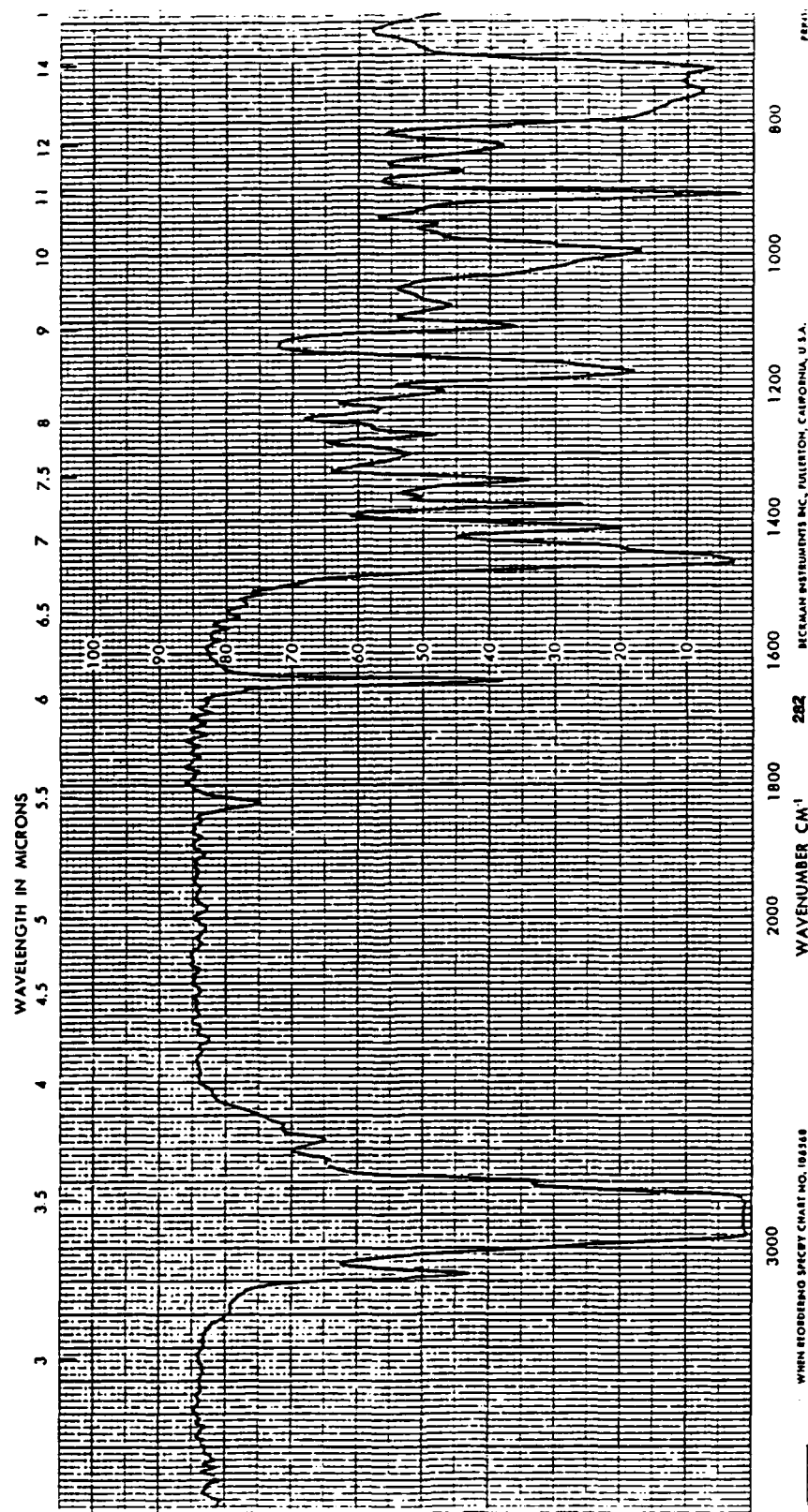
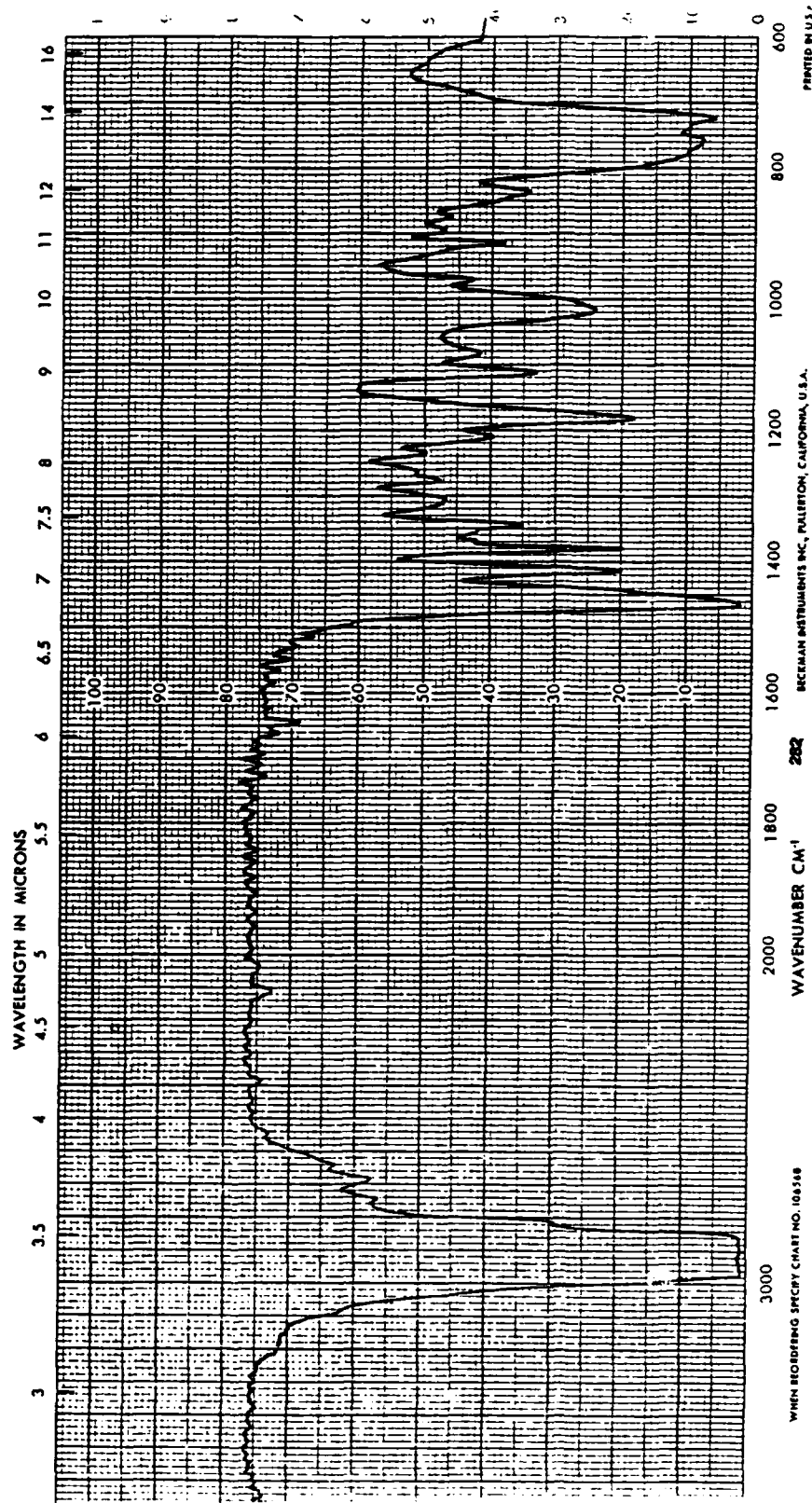


Fig.5 I.R. Spectra of MLO 86-146 Stressed at 700F (371.1C) for 6 hours (0.025 mm KBr cell)



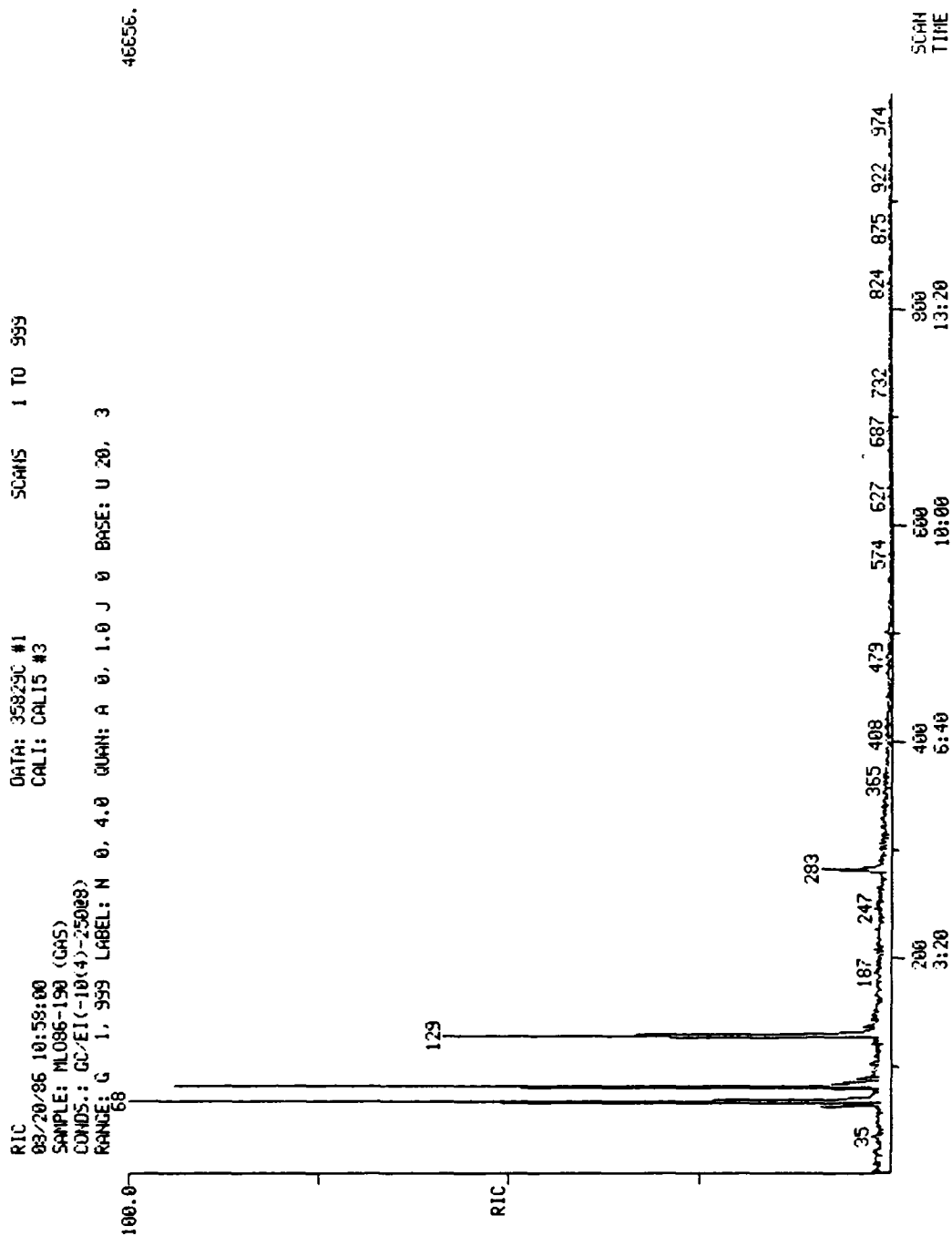


Fig. 6 GC/MS of MLO 86-190 in gas phase stressed at 700F (371.1C) for 120 hours.

Table 6. GC/MS analysis of the gas components of MLO 86-190
stressed at 700F (371.1C) for 120 hours.

Scan No.	Components	No. of C atoms	% concentration
64,68	$\text{CH}_4, \text{C}_2\text{H}_6, \text{C}_3\text{H}_8$	1, 2, 3	55.66
82	C_4H_{10}	4	30.22
129	C_5H_{12}	5	10.03
283	C_6H_{14}	6	2.69

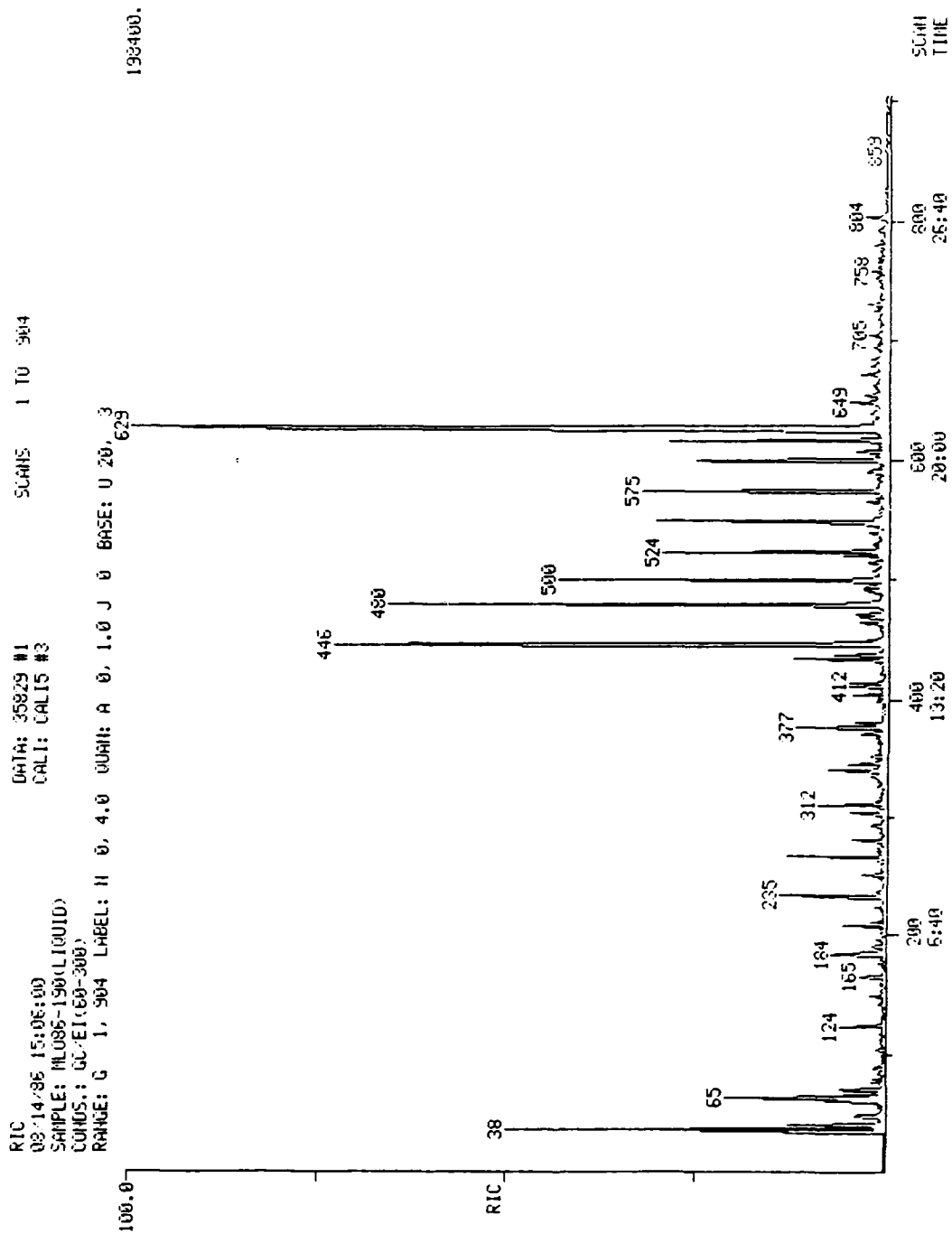


Fig.7 GC/MS of MLO 86-190 in liquid phase stressed at 700F (371.1C) for 120 hours.

Table 7. GC/MS analysis of the liquid components of MLO 86-190
stressed at 700F (371.1C) for 120 hours.

Scan No.	Components	% concentration
36	C_4H_{10}	8.28
38	C_5H_{12}	4.70
42	C_6H_{14}	2.41
62,65,67	C_8H_{16}	7.27
434,438,446	$H-Si-CH_3(C_8H_{17})_2$ and $(CH_3)_2-Si-(C_8H_{17})_2$	7.83
464,469,472,480	$CH_3-Si-C_4H_9C_6H_{13}C_8H_{17}$ and $CH_3-Si-C_3H_7C_7H_{15}C_8H_{17}$ and $CH_3-Si-C_2H_5(C_8H_{17})_2$	4.63
492,494,500	$CH_3-Si-C_5H_{11}C_6H_{13}C_8H_{17}$ and $CH_3-Si-C_4H_9C_7H_{15}C_8H_{17}$ and $CH_3-Si-C_3H_7(C_8H_{17})_2$	2.22
515,521,542	$CH_3-Si-C_5H_{11}C_7H_{15}C_8H_{17}$ and $CH_3-Si-C_4H_9(C_8H_{17})_2$	1.77
540,550	$CH_3-Si-C_5H_{11}(C_8H_{17})_2$	1.62
566,575	$CH_3-Si-C_6H_{13}(C_8H_{17})_2$	1.80
591,601	$CH_3-Si-C_7H_{15}(C_8H_{17})_2$	1.67
608,617,628,629	$CH_3-Si-(C_8H_{17})_3$	51.45

Note : Fragments less than 0.5 % concentration have been
neglected on this table.

Table 8. Gas chromatographic conditions for the analysis of
gases and liquids.

Instrument model : HP5710A

Fused silica capillary column

Length : 12M

Diameter : 0.22 MM

Liquid phase : Methyl silacone carbowax deactivated

Split ratio : 100 to 1

Auxi gas : 40 ml/min

Carrier gas : 1 ml/min

Detector : FID

Attenuation : 10 X 16

Temperature for gas sample : Injector : 200 Deg.C; Detector : 350 Deg.C

Temperature for liquid sample : Injector : 300 Deg.C; Detector : 350 Deg.C

Column temperature for gas sample : -50 Deg.C to 270 Deg.C

Column temperature for liquid sample : 70 Deg.C to 270 Deg.C

Program rate : 8 deg/min

Initial hold : 2 min

Final hold : 32 min

Sample size for gas sample : 1 ml

Sample size for liquid sample : 1 micro-liter

Sample ID : Headspace and Liquid.

REFERENCES

1. Christ Tamborski, Grace J. Chen, Denise R. Anderson and Carl E. Snyder, Jr., " Synthesis and Properties of Silahydrocarbons, A Class of Thermal Stable, Wide Liquid Range Fluids", I & EC Product Research & Development, The American Chemical Society, 22, 172 (1983).
2. Carl E. Snyder, Jr., Lois J. Gschwender, and Christ Tamborski, " Synthesis and Characterization of Silahydrocarbons — A Class of Thermal Stable Wide-Liquid-Range Functional Fluids", ASLE Trans. 25, 299-308 (1981).
3. Carl E. Snyder, Jr. and Christ Tamborski, Lois J. Gschwender and Grace J. Chen, " Development of High-Temperature (-40C to 288C) Hydraulic Fluids for Advanced Aerospace Applications", ASLE Preprint No. 80-LC-1C-1.
4. Gupta, V. K. " Determination of Structure-Property Relationship of Novel Candidate Base Stocks for Advanced Lubricants", Final Report (1985-1986).

1986 USAF-UES SUMMER FACULTY RESEARCH PROGRAM/
GRADUATE STUDENT SUMMER SUPPORT PROGRAM

Sponsored by the
AIR FORCE OFFICE OF SCIENTIFIC RESEARCH

Conducted by the
Universal Energy Systems, Inc.

FINAL REPORT

Computer Software Development in a
Study of Executable Image Efficiency

Prepared by:	Mark Lisee and Martin A. Patt
Academic Rank:	Research Assistant
Department and	Electrical Engineering
University:	University of Lowell
Research Location:	Geophysics Laboratory, Optical Physics Division
USAF Researcher:	Dr. Donald Bedo
Date:	August 12, 1986
Contract Number:	F49620-85-C-0013

Computer Software Development in a
Study of Executable Image Efficiency

by

Mark Lisee and Martin A. Patt

ABSTRACT

Computer software was developed to support a study comparing the efficiencies of executable-image codes generated for a real-time LIDAR application. Programs were compiled and executed under the VMS operating system on a Digital Equipment Corporation VAX-11/780 Mainframe computer. Three languages were tested: C, FORTRAN, and BASIC. Assembly languages software (MACRO) was developed to provide a benchmark.

Acknowledgements

I wish to thank the Air Force Office of Scientific Research and the AFGL for providing this research opportunity. I also wish to thank Martin A. Patt, Associate Professor, University of Lowell for selecting me as his research assistant. In addition, I would like to thank the staff of the OPA division of the AFGL, particularly, Donald Bedo, Robert Swirbalus, Steven Alejandro, Donald Fitzgerald, and Michael Estes.

I. INTRODUCTION:

In August of 1984, a team of dedicated scientists and engineers working out of the Optical Physics Division at AFGL successfully launched a balloon-borne laser radar system for observations of atmospheric backscatter from high altitudes(2). Data acquired during this flight is unique in that it represents the only existing set of high-altitude backscatter data. Simultaneously, under development at AFGL is a ground-based (but mobile), coherent, pulsed, Doppler CO₂ LIDAR system housed in a modified 12m semi trailer. The pulsed Doppler system is designed to evaluate techniques for the acquisition and real time interpretation of atmospheric windfield structure as well as aerosol attenuation and concentrations over long path lengths(1). Experiments simultaneously utilizing both the ground-based and balloon-borne LIDARs are expected to begin as early as the summer of 1987. To facilitate and enhance these combined experiments, a Digital Equipment Corporation VAX-11/730 digital computer will be housed in the semi trailer to perform some real-time signal processing. It has been suggested that this processing time might be reduced by selecting a software source language which bests fits this application.

II. OBJECTIVE OF THE RESEARCH EFFORT:

This summer-research effort has been devoted to a comparative study of the applicability of three source

languages: C, FORTRAN, and BASIC, with the objective of determining which of these may prove most suitable for this signal-processing application. Care has been taken to obtain "best" programs in each of these source languages. Failure to have done so would have resulted in a comparison of the suitability of the programmers rather than the languages. To this end, all source programs have been subjected to careful scrutiny and review by a team of conscientious analytical programmers. In addition, an assembly language (MACRO) program was developed to serve as a benchmark.

III. OVERVIEW OF THE PROCESSING OF THE TELEMETRY DATA:

The processing of the data consists of reading 10 major frames (lidar shots), decrypting the data on a word-by-word basis, checking each word for validity of contents, averaging over time, and cleaning and plotting the results. Each major frame contains five minor frames, with each minor frame consisting of 64 encrypted words. Thus, there are 320 words in each major frame.

A: DECRYPTION: The data words are each 12 bits long, with bit #11 the even parity bit, and bit #10 the good word bit. The remaining 10 bits are the data, with bit #0 the MSB. Each good word that has an even parity must be decrypted by having the 10 bits of the data inverted. At the beginning of program execution, an array is set up. In initializing the array, the 10 bits of the

element number are inverted then shifted left by 1 bit with bit #0 set to obtain even parity. During the remainder of the program execution, the array words are used to look up the correct parity and the decrypted value. This approach was taken to increase the efficiency of the program when five or more major frames of good data are processed.

B: CHECKING: All 64 encrypted words of a minor frame are read and stored in an array. The first four words are decrypted and used to check the validity of the remaining 60 words in the minor frame. The first word of every minor frame is "856" (decrypted), the second word contains the minor frame number ("0" to "4"), if the minor frame number is "0", then the third word contains the major frame number, otherwise it contains a "1", and finally the fourth word always contains a "3". Only the first three words are checked, and if these are correct, the minor frame is considered "good". A "bad" minor frame initiates rejection of the entire major frame.

C: AVERAGING: After the words from all the good major frames have been read and accumulated by range bin in a final array, they are averaged (by range bin). Each element in the total array is divided by the corresponding element in the associated count array.

D: CLEANING: The purpose of cleaning the averaged data is to smooth the resulting plot, by eliminating noise. The

method used in cleaning the data is described in section IV.

E: PLOTTING: After the data has been processed, it is plotted on the screen using the process described in section V.

IV. CLEANING ALGORITHM:

The purpose of any cleaning algorithm is to remove noise. For our demonstration, the values were expected to vary by a maximum of 10% per range bin (the unit of time used). This 10% criteria does not affect the logic of our cleaning algorithm, only the numbers it uses. The cleaning algorithm described here was developed for demonstration purposes only. One should not infer that there is scientific basis for using this particular algorithm.

Since the cleaning algorithm processes each value by comparing it with the values on either side, the first and last counts are not processed. To show the effect of the cleaning, consider three consecutive values A, B, and C. If C varies by a maximum of 20% from A, then B is allowed to vary by a maximum of 10% from the mean of A and C. If B is outside the allowed range, B is given the value of the nearest edge of that region. If C varies from A by more than 20% (see figure 1), then the bounds on the region in which B is allowed to vary are the mean of A and C on one side and one of the bounds of 10% of the mean of A and C brought to its greatest variation of 20% from A. This last

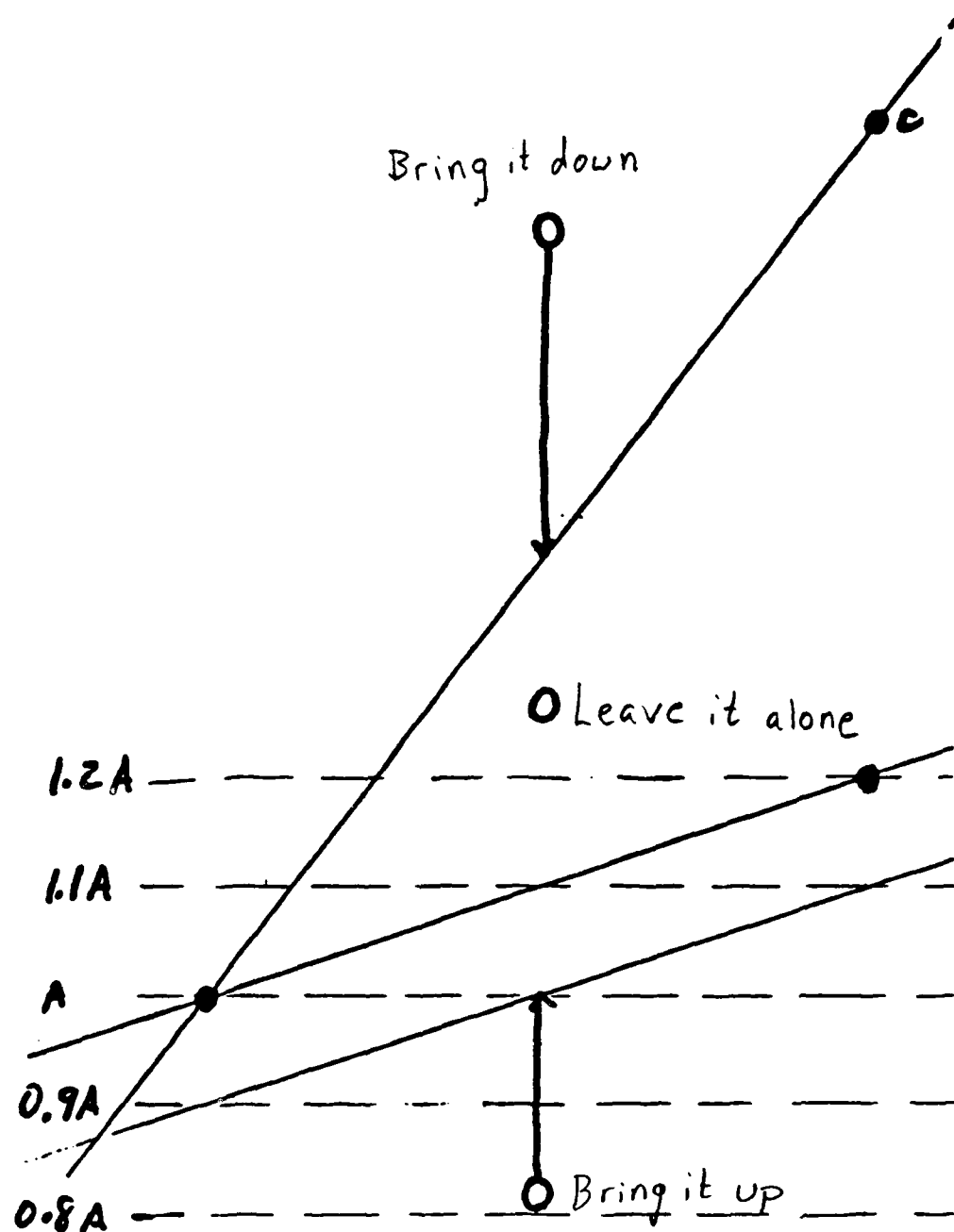


Figure 1

bound is chosen to maximize the allowable region for B. If B is outside this region, it is given the value of the nearest bound to the region.

V. PLOTTING:

The plotting of the resulting graph is done using one screen of text characters. As a result, the resolution is 120 horizontally by 21 vertically. The horizontal axis is the range, which has several points averaged together (the exact number depending on the number of range bins). The vertical axis is the value of the averaged elements. The maximum value on the vertical axis is the smallest number that has only its two left most digits are non-zero, but is greater than or equal to the maximum to be printed. The minimum is the greatest multiple of a power of 10, that is not a non-zero, single digit, and is less than or equal to the minimum to be plotted. The vertical axis is then printed using these and three equally spaced intermediate values. The horizontal axis is printed, the maximum value is the number of range bins, minimum is zero, and with nine intermediate values.

In the process of printing the axes, the remainder of the screen is cleared. The curve itself is plotted using a VT100 escape sequence to position the cursor and print an asterisk for each horizontal element. This approach was taken since it approximately halves the amount of output required by the graph₄₄₋₈ Prior to this "graphics"

enhancement, the FORTRAN software was not competitive with the C, FORTRAN being slower on formatted output.

VI. RESULTS AND CONCLUSIONS:

In tests performed with actual balloon telemetry data, the C ran slightly faster than the FORTRAN, and ran five to six times as fast as the equivalent BASIC software. The assembly language MACRO ran twice as fast as its closest competitor, C. It must be pointed out that the data structure was purposely set up to accomodate FORTRAN, allowing the FORTRAN program to read efficiently from the data file (by structuring one minor frame per record rather than one data word per record). Further, the volume of terminal output was kept as small as possible because the FORTRAN was found to be much slower than C on output. Tests revealed that the C software would have beat the FORTRAN by a factor of two had these concessions not been granted. The apparent superiority of C in this kind of real-time processing is due in part to its inherent efficiency, allowing for better utilization of modern computer architectures.

CPU TIME TO PROCESS TEN LIDAR SHOTS (MAJOR FRAMES)
AS A FUNCTION OF PERCENT-GOOD DATA

<u>Percent-good</u>	<u>MACRO</u>	<u>C</u>	<u>FORTRAN</u>	<u>BASIC</u>
100	1.0	2.1	2.6	12.5
90	1.0	2.0	2.5	12.0
80	1.0	2.0	2.4	11.5
70	1.0	1.9	2.3	10.9
60	1.0	1.9	2.2	10.4
50	0.9	1.8	2.1	9.9
40	0.9	1.7	2.1	9.4
30	0.9	1.7	2.0	8.9
20	0.9	1.6	1.9	8.4
10	0.9	1.6	1.8	7.9
0	0.8	1.5	1.7	7.3

VII. RECOMMENDATIONS:

AFGL maintains a substantial investment in computer hardware. At its main computer center, there is a Control Data Corp. CYBER-750 (Operating System: NOS 2.2) as well as a Digital Equipment Corporation VAX-11/780 (Operating System: VMS 4.4). Although both systems have compilers for both the FORTRAN and Pascal languages, the FORTRAN compilers are used almost exclusively. There is no C compiler available on either CYBER or VAX machines. Both Pascal and C (but not FORTRAN) provide the advantage of speedy software development usually associated with highly

structured languages. Of the two, C is the more versatile language.

It is recommended that:

- (1) A C-compiler be acquired for the VAX-11/780, and that some new AFGL software being developed for the VAX be written in the C-language. Programs written in C for the VAX are readily linked with existing FORTRAN subroutines - users with a substantial investment in existing FORTRAN routines would not be placed at a disadvantage.
- (2) A short course should be taught (possibly by the system programmers as AFGL) to help potential users migrate to the C-language.

REFERENCES

Conferences and Journal Publications:

1. S. B. Alejandro and D. R. Fitzgerald, "AIR FORCE GEOPHYSICS LABORATORY'S (AFGL) MOBILE CO2 DOPPLER LIDAR", Topical Meeting on Optical Remote Sensing of the Atmosphere Sponsored by the Optical Society of America and the U.S. Army Research Office, at Incline Village, Nevada, 1985
2. D. E. Bedo and R. A. Swirbalus, "ATMOSPHERIC BACKSCATTER OBSERVATIONS FROM A BALLOON-BORNE LIDAR", 13th International Laser Radar Conference, Toronto, Ontario, Canada, 1986

Final Reports:

3. Visidyne, Inc., "ABLE INTERFACE CONTROL DOCUMENT/REVISION C", Contract F19628-81-C-0165, Air Force Geophysics Laboratory, 1984
4. M. A. Patt, "Computer Software Executable Image Efficiency in Real-Time LIDAR Applications", Contract F49620-85-C-0013, Air Force Geophysics Laboratory, 1986

Reports:

5. M. A. Patt and M. W. Lisee, "Cleaning Telemetry Data Handbook", Contract F49620-85-C-0013, Air Force Geophysics Laboratory, 1986

1986 USAF-UES SUMMER FACULTY RESEARCH PROGRAM/
GRADUATE STUDENT SUMMER SUPPORT PROGRAM

Sponsored by the
AIR FORCE OFFICE OF SCIENTIFIC RESEARCH

Conducted by the
Universal Energy Systems, Inc.

FINAL REPORT

Optimization of a Material to be used to detect
Incident Microwave Radiation by IR Imaging

Prepared by: Robert K. Littleton
Academic Rank: Graduate Student
Department and Department of Physics
University: University of Colorado - Colorado Springs
Research Location: The Frank J. Seiler Research Laboratory,
United States Air Force Academy
Electromagnetics Laboratory,
University of Colorado - Colorado Springs
USAF Researcher: Professor R. M. Sega
Date: August 21, 1986
Contract No.: F49620-85-C-0013

Optimization of a Material to be used to detect
Incident Microwave Radiation by IR Imaging

by

Robert K. Littleton

ABSTRACT

A material to be used to measure pulsed microwave radiation by means of IR imaging was determined by optimizing various material parameters. The material must absorb as much of the incident power as possible in order for it to heat up during the short duration of the pulse. By use of an existing computer program, the material parameters were varied to give a material with the highest possible absorption, lowest possible reflection, and low thermal mass. However, appropriate samples of the material were not available. A computer program was also developed to calculate the electric field strength inside the material. Also, the response of resistors to known currents was experimentally determined. More experimental work with materials needs to be performed in order to correlate theory with observation.

Acknowledgments

I would like to thank the Air Force Systems Command and the Air Force Office of Scientific Research for their sponsorship of my research. I also want to thank the Frank J. Seiler Research Laboratory for providing space and equipment for my research.

Dr.'s Ron Sega and John Norgard of the Department of Electrical Engineering at UCCS are also deserving of my thanks for letting me carry out my research with them and for pointing me in the correct direction in my research. The other members of the Electromagnetics Lab, Paul Bussey, Jon Zobel, Chad MacAllister, and Alexander Sapp, are also to be thanked for their helpful discussions and assistance with the lab set-up and equipment.

I. Introduction

When an electromagnetic encounters a conductive material, some of the field's power is lost to the material, i.e. the field is attenuated. Through I^2R , or Joule, losses, heat is produced in the material. The induced surface currents of the material are found by:

$$q = J^2/\sigma \quad (1)$$

where J is the surface current, σ is the conductivity, and q is the heat.

This is the basis for the work done by the Electromagnetics Lab at the University of Colorado at Colorado Springs. Components, systems, or detecting materials are placed in a microwave field and viewed with a modern infrared (IR) camera. The greater the temperature increase of an object, the greater the field strength at that point.

The material currently used to detect the free field is carbon paper. This is slightly conductive and does heat up in a microwave field. A better, more efficient detecting material was desired, which I was assigned to come up with. I come to this project from the Physics Department at UCCS, where I am pursuing a Master's Degree. Besides my background in solid state physics and electromagnetism, my research involves solving boundary value problems, which is very relevant to this current problem.

II. Objectives of the Research Effort

The overall objective is to perform high-power pulse microwave experiments at Sandia National Laboratory and the Air Force Weapons Laboratory in Albuquerque.

My contribution to this is to come up with a new detecting material for the pulsed experiments. As the pulses last for only one or two seconds, this new material must heat up very quickly. To do this,

the material must have a low thermal mass (be very thin) and absorb as much of the incident microwave power as possible. But the material must not be too reflective, as microwaves could then be reflected back into the source, causing damage.

My goal was to vary the material parameters to come up with optimum absorption and reflectance and thickness. The parameters to be varied were thickness, permittivity, and conductivity. Once our optimum parameters were determined, samples of materials having these parameters would be evaluated.

Another objective of mine was to map the field inside a material when subject to microwave radiation. This should help us to understand how materials respond in a microwave field

Finally, I was to measure the thermal response of components and materials to a known current, in order to better understand this phenomena.

III. Material Parameter Optimization

PHASEW is a FORTRAN program which calculates the percentage of power reflected, absorbed, and transmitted by a material given the incident frequency, and the material's thickness, conductivity, real and imaginary permittivity, and real and imaginary permeability. The program was developed by Gary Wetlaufer of the UCCS Electrical Engineering Department as part of his thesis research for his Master's Degree.

PHASEW is based upon a three-phase system, where phases 1 and 3 are free space and phase 2 is the detecting material. The percentage of power reflected and transmitted is first calculated by using boundary conditions and the impedance relations for the electric and magnetic fields. Then the power absorbed is found by the conservation of energy:

$$P_{\text{abs}} = P_{\text{inc}} - (P_{\text{ref}} + P_{\text{trans}}) \quad (2)$$

For a fuller discussion of this method, the reader is referred to reference 1.

PHASEW was run many times, keeping the frequency at 3 GHz and assuming the phase 2 material to be non-magnetic. We were told of a company which could dope Mylar with a metal to make it conductive. Mylar has a real permittivity of 2.8, which was put into the program. The only parameters which were then varied were the thickness of the material and its conductivity, which is related to the imaginary permittivity by:

$$\epsilon'' = \sigma/\omega, \quad (3)$$

where ω is the angular frequency of the incident radiation.

Data from many runs was used to make plots of the phase 2 conductivity versus the percentage power absorbed and reflected for several different thicknesses. The most promising of these plots is shown in Figure 1 for a 10 micron film. At low conductivities most of the incident radiation is transmitted through the film. As the conductivity increases, the amount of power absorbed increases faster than the amount of power reflected. But after the amount of power absorbed peaks and declines, the amount of power reflected steadily increases, until at high conductivities virtually all of the power is reflected, as expected.

The company that makes the doped Mylar is Solitron/Microwave in Florida. The thinnest film they make is 12.5 microns, with resistivities ranging from 10 Ω/\square to 50 Ω/\square . Conductivity, σ , and resistivity, ρ , are related by:

$$\sigma = 1/\rho t, \quad (4)$$

where l , w , and t are the dimensions of the film.

PHASEW was run using these parameters. The optimum 12.5 micron film appeared to be that having a resistivity of 18 Ω/\square . This gives a

conductivity of 4,444 mhos/m, with 7% of the power reflected and 51% of the power absorbed.

A 5" by 9" sample was ordered and sent. Unfortunately, the sample did not arrive at UCCS for over a month. When it did finally arrive, the sample appeared to be very metallic, as it was quite reflective. When placed in the test chamber and subjected to microwaves, the sample heated up slowly and unevenly. The edges were hotter than the center, indicating good heat flow, a property of metals.

The sample was measured and found to be 150 microns thick, not 12.5 as ordered, with a resistivity of $64 \Omega/\square$, not the 18 we ordered. This gives a very low conductivity of 107 mhos/m, which is puzzling given the film's apparent properties. A possible explanation for this was found when I scrapped the film and found it to be a piece of Mylar covered by a very thin film of metal. I was unable to measure the thickness of this film. Assuming it to be 3 microns, and given a resistivity of $64 \Omega/\square$, this gives a conductivity of 6,100 mhos/m, which is more in character with the film's appearance. In any event, this material is not suitable for our purposes.

IV. Mapping of Internal Fields

A wave approach was taken to this problem. An incoming free-space wave from the left, described by $Ae^{i(k_1z - \omega t)}$, is incident normally upon the surface of a conductive film at $z=0$. Part of the wave is reflected, given by $Be^{i(-k_1z - \omega t)}$, and part is transmitted into the film and is given by $Ce^{i(k_2z - \omega t)}e^{-k_2''z}$. Because the film is conductive, the propagation constant, k , has an imaginary part, $k = k' + ik''$, with:

$$\begin{Bmatrix} k' \\ k'' \end{Bmatrix} = \left[\frac{1}{2} \epsilon \mu \omega^2 \left\{ \left[1 + \left(\frac{\epsilon''}{\epsilon'} \right)^2 \right]^{\frac{1}{2}} \begin{Bmatrix} + \\ - \end{Bmatrix} \right\} \right]^{\frac{1}{2}} \quad (5)$$

ϵ' is the real permittivity and ϵ'' is the imaginary.

At $z=d$ the wave encounters the other film surface, where part of it is transmitted out into free space and part is reflected back into the film, given by $De^{i(k_2'z-\omega t)}e^{-k_2''(d-z)}e^{-k_2''d}$. When this part of the wave reaches $z=0$, it is totally transmitted and joins with the original reflected wave, $Be^{i(-k_1z-\omega t)}$. This is an approximation, taken for simplicity, as part of the wave would be reflected back into the film, where it would bounce back and forth, being partially transmitted at each boundary.

Now the problem is to solve for the various amplitudes A, B, C, D, and E. The amplitude, A, of the incoming wave is set equal to 1. The appropriate boundary conditions are:

- 1) The tangential components of the electric field are continuous at $z=0$ and d .
- 2) The tangential components of the magnetic field are continuous at $z=0$ and d .

This gives a system of 4 equations with 4 unknowns. A FORTRAN program, WAVE, included in the Appendix, was written to solve this.

At any point, a , inside the film, the amplitude of the electric field is the transmitted wave from the left, attenuated by $e^{-k_2''a}$, plus the reflected wave from the right, attenuated by $e^{-k_2''(d-a)}$. Mathematically:

$$|\vec{E}|_{z=a} = Ce^{ik_2'a}e^{-k_2''a} + De^{-ik_2'(d-a)}e^{-k_2''(d-a)} \quad (6)$$

The phase of the field has been ignored here. The wavelength, λ , inside a conductor is given by $\lambda = 2\pi\delta$, where δ is the skin depth, equal to $(2/\omega\mu\sigma)^{1/2}$. At a frequency of 3 GHz and a conductivity of 10,000 mhos/m, $\lambda = 577$ microns. Since we are dealing with much lower conductivities and films 10-20 microns thick, the phase can be safely ignored.

The program WAVE also calculates and plots the amplitude squared of the electric field for several points inside a film. Figure 2 shows one such plot for a 12.5 micron film with a conductivity of 2,000 mhos/m.

As could be expected, the amplitude inside the film does not decrease much, although close inspection does show that the wave is slightly attenuated.

V. Thermal Response of Components

In an attempt to correlate component heating to current, one resistor was attached to a current source while an identical resistor was left unattached. An inch of styrofoam insulation was placed between them so they would be thermally isolated. The current source was turned on and the temperature of the resistors was measured using the isotherm function on the IR camera at 15 second intervals.

The temperature difference between the two resistors versus time is shown for two different resistors in Figures 3 and 4. The temperature difference rises to a plateau and then decreases as the current is turned off. The highest curve in Figure 4, where the current is 140 mA, is flawed as the current through the resistor decreased as the resistor temperature increased.

The peak temperature difference versus the resistor current is plotted in Figure 5. The relationship is non-linear, which could be expected as the heating is proportional to the power, which is equal to I^2R .

VI. Recommendations

It is recommended that more thin-film, conductive plastic materials be acquired. The properties of these materials should first be predicted by the computer programs PHASEW and WAVE, and then experimentally determined in the microwave test chamber. It would then be known if our theory and understanding of what happens to materials in a microwave field is correct or not.

The temperature increase of different components with a known current passing through them should also be measured. This will give a better understanding of how various components thermally respond to currents.

References

1. Wetlaufer, Gary, Optimization of Thin-Screen Material Used in Infrared Detection of Microwave Induced Surface Currents at 2-3 GHz, University of Colorado, Boulder, 1985
2. Harper, Charles A., Handbook of Materials and Processes for Electronics, New York, McGraw-Hill Book Company, 1970
3. Jackson, J.D., Classical Electrodynamics, New York, John Wiley & Sons, 1975
4. Landau, L.D., Lifshitz, E.M., and Pitaevskii, L.P., Electrodynamics of Continuous Media, Oxford, Pergamon Press, 1984
5. Born, Max, and Wolf, Emil, Principles of Optics, Oxford, Pergamon Press, 1984
6. Bekefi, George and Barrett, Alan H., Electromagnetic Vibrations, Waves, and Radiation, Cambridge, Mass., The MIT Press, 1977
7. Reif, F., Fundamentals of Statistical and Thermal Physics, New York, McGraw-Hill Book Company, 1965

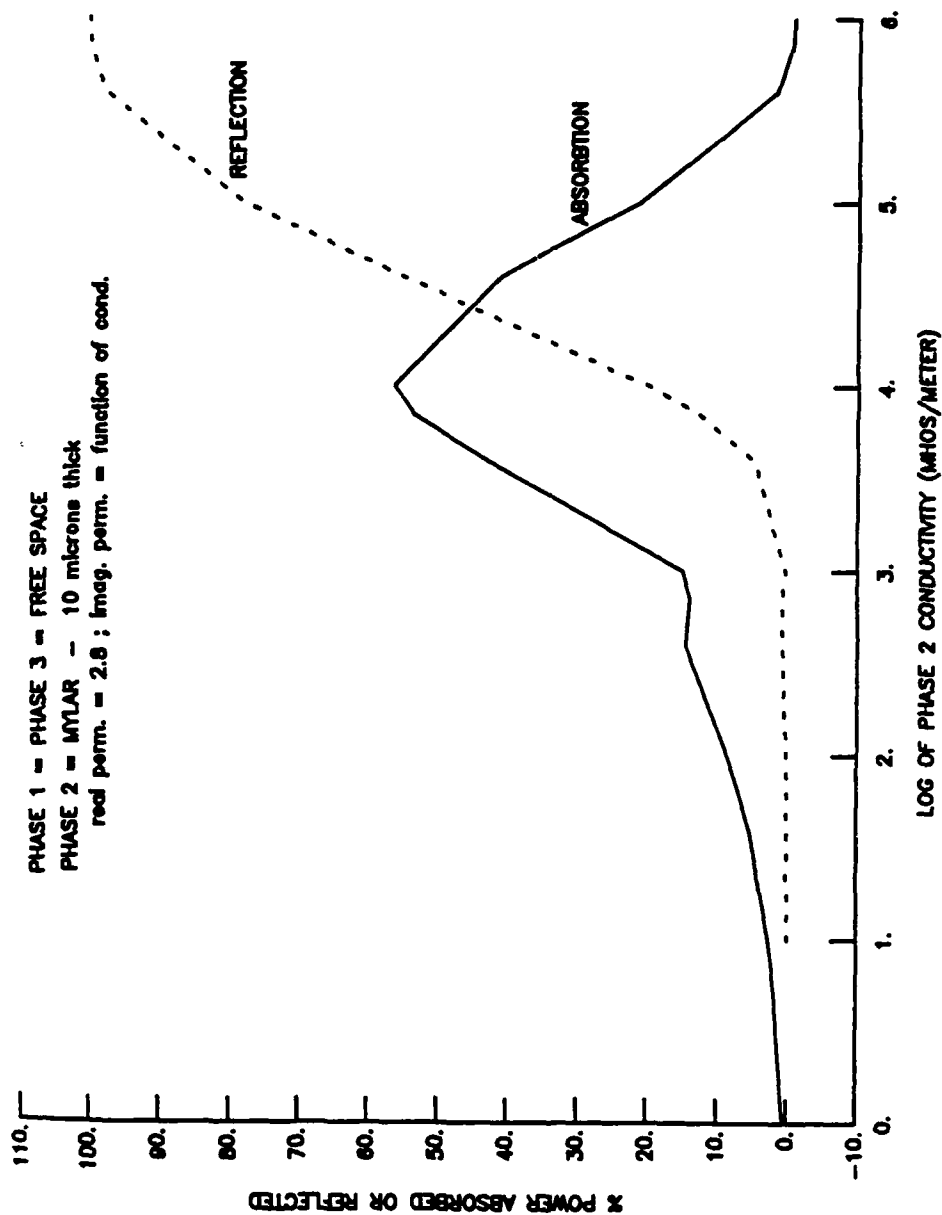


Figure 1. The results from running the program PHASEW used to optimize a detecting material.

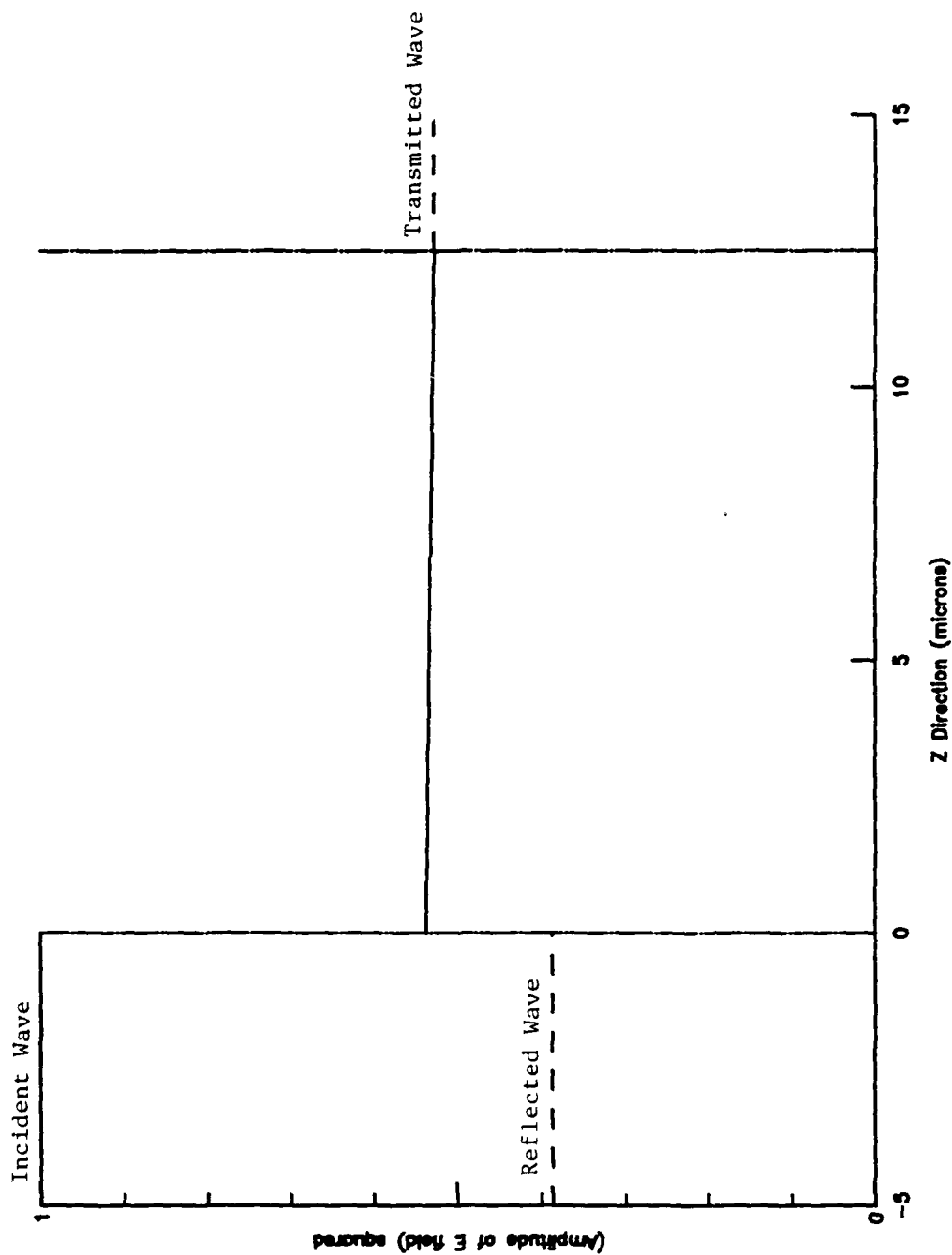


Figure 2. The amplitude squared of the electric field inside a 12.5 micron thick

film. The frequency is 3 GHz, the film is Mylar with a conductivity of 2,000 mhos/m.

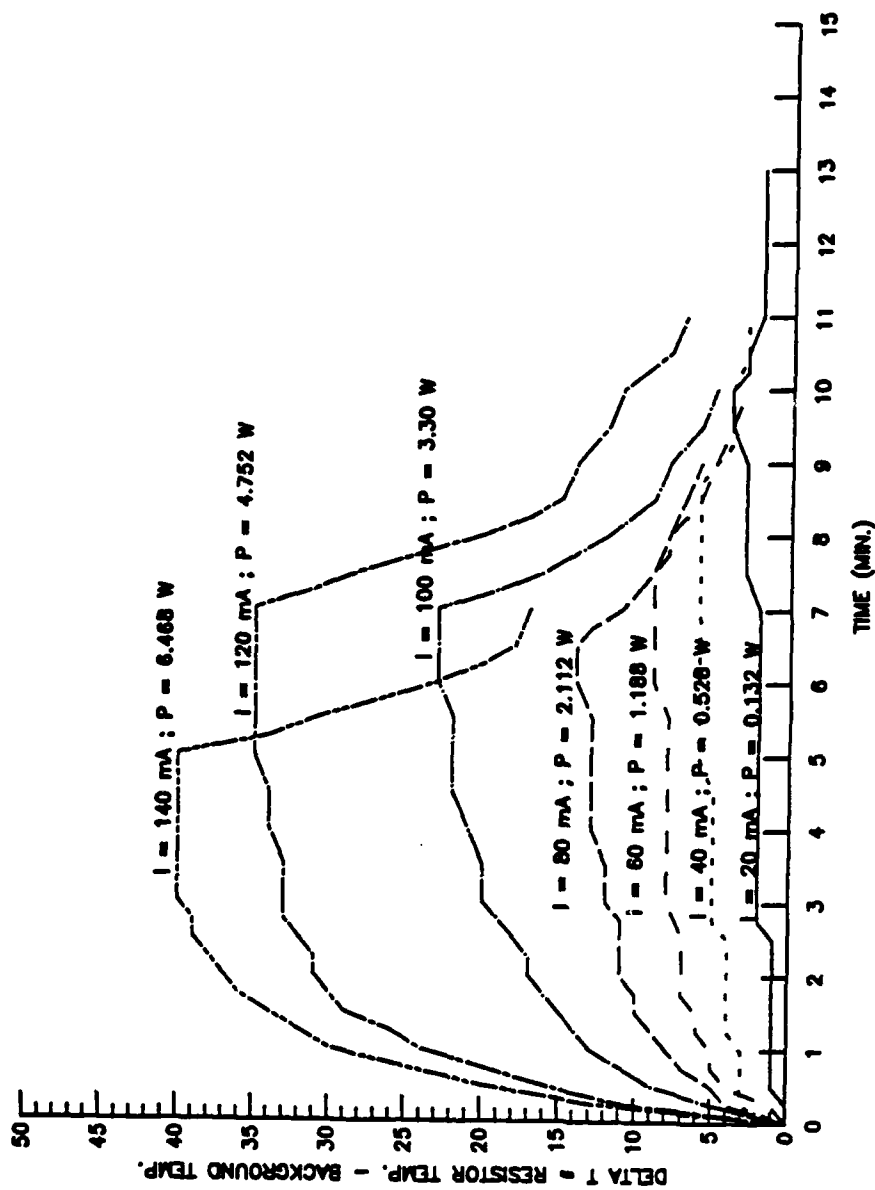


Figure 4. The increase in temperature of a 330 ohm resistor versus time, for several different resistor currents. The top curve is flawed as the current decreased as the resistor got very hot.

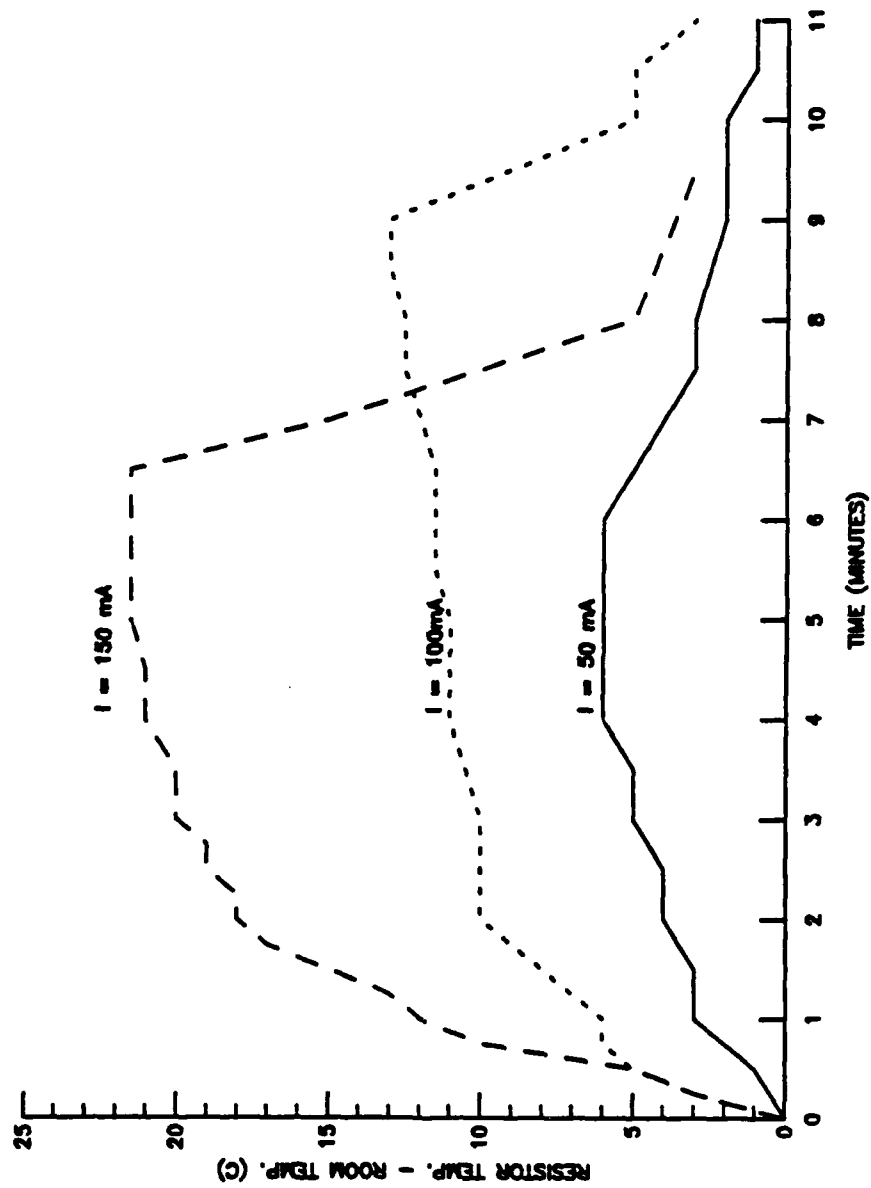


Figure 3. The increase in temperature of a 150 ohm resistor versus time, for several different resistor currents.

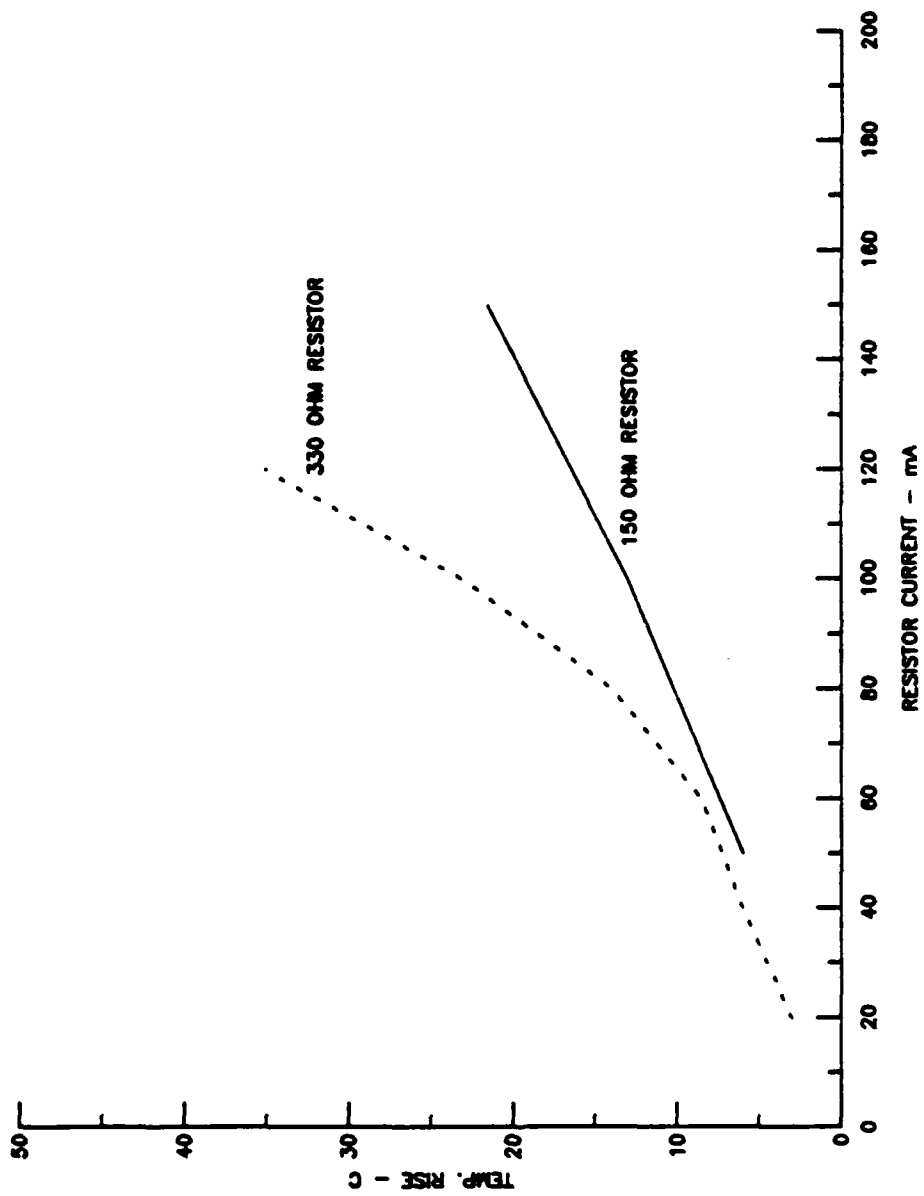


Figure 5. The peak temperature rise, taken from the two previous figures, versus the resistor current.

Appendix A

This appendix consists of the FORTRAN program WAVE, used to calculate the fields inside a film placed in a microwave field.

```
C This program calculates the reflection, transmission &
C absorption coefficients for a 3-media system where the
C first media is free space and the other two can be specified.
C EPSILONREL1 = the real relative permittivity of media 1
C EPSILON0 = the permittivity of free space
C EPSILONRE = the real part of the relative
C permittivity of media 2
C EPSILONIM = the imaginary part of the relative
C permittivity of media 2
C EPSILONREL3 = the relative permittivity of media 3
C KRE = the real part of the wave vector of media 2 (sometimes
C known as alpha)
C KIM = imaginary part of the wave vector of media 2
C (sometimes known as beta)
C K3 = the real wave vector of media 3.
C
C All lengths are in microns.
C
C   INTEGER N,IM,MM,IA,IJOB,ISR
C   REAL*8 EPSILONREL1, EPSILONRE, EPSILONIM, EPSILONREL3
C   REAL*8 EPSILON0, EPSILON1, EPSILON3, MU0, MUREL1, MUREL2
C   REAL*8 MUREL3, MU1, MU2, MU3, KRE, KIM, K3, SIGMA, K1
C   COMPLEX*16 CI, EPSILON2, M(4,4), A(4)
C   REAL*8 PI, OMEGA, F, LAMBDA, WA(4), R, X, Y, Z, T, AA
C   REAL*8 HREF, HTRANS, PREF, PTRANS, PABS, U, EZA, K
C   REAL*8 SKINDEPTH, PINS
C   IM = 4
C   MM = 1
C   IA = 4
C   N = 4
C   IJOB = 0
C
C   CI = (0.0, 1.0)
C   PI = 3.14159
C   EPSILON0 = 8.85E-12
C   MU0 = PI*4E-7
C
C Set the relative permittivity & permeability of media 1
C to those for free space.
C
C   EPSILONREL1 = 1.0
C   MUREL1 = 1.0
C   EPSILON1 = EPSILON0*EPSILONREL1
C   MU1 = MU0*MUREL1
```

```

C
    TYPE*, 'WHAT IS THE FREQUENCY IN HERTZ?'
    ACCEPT *, F
C
C   Calculate the wavelength in microns
C
    LAMDA = 2.998E14/F
C
C   Calculate the real wavenumber in media 1.
C
    K1 = DSQRT(EPSILON1*MU1) * (2*PI/LAMDA)
C
    TYPE*, 'WHAT IS THE REAL RELATIVE PERMITTIVITY OF MEDIA 2 ?'
    ACCEPT *, EPSILONRE
C
    TYPE*, 'WHAT IS THE CONDUCTIVITY OF MEDIA 2?'
    ACCEPT *, SIGMA
C   Calculate the relative imaginary permittivity of media 2.
C
    EPSILONIM = (SIGMA/(2*PI*F)) * 9E9
C
C   Calculate the complex permittivity of media 2.
C
    EPSILON2 = (EPSILONRE + (CI*EPSILONIM)) * EPSILON0
C
C
    TYPE*, 'WHAT IS THE RELATIVE PERMEABILITY OF MEDIA 2 ?'
    ACCEPT *, MUREL2
C
C
    MU2 = MUREL2*MU0
C
C
    TYPE*, 'WHAT IS THE THICKNESS OF MEDIA 2 IN MICRONS ?'
    ACCEPT *, D
C
C
    TYPE*, 'WHAT IS THE REAL RELATIVE PERMITTIVITY OF MEDIA 3 ?'
    ACCEPT *, EPSILONREL3
C
C
    EPSILON3 = EPSILONREL3*EPSILON0
C
C
    TYPE*, 'WHAT IS THE REAL RELATIVE PERMEABILITY OF MEDIA 3 ?'
    ACCEPT *, MUREL3
C

```

```

C
      MU3 = MU0*MUREL3
C
C
C Calculate the real & imaginary wavevectors of media 2.
C
C
      X = 0.5 * EPSILONRE * EPSILON0 * MU2 * (2*PI*F)**2
      Y = (EPSILONIM/EPSILONRE)**2
      Z = DSORT(1+Y)
C
C
      KRE = DSORT(X * (Z+1))
      KIM = DSORT(X * (Z-1))
C
C Convert KRE & KIM from /meters to /microns.
C
      KRE = KRE * 1E-6
      KIM = KIM * 1E-6
C
C Calculate the wavenumber of media 3,
C assuming media 3 is lossless.
C
      K3 = DSORT(EPSILON3*MU3) * (2*PI/LAMDA)
C
C *****
C Now fill up the matrix with the coefficients for the constants
C B (the original reflected field), C (the field transmitted from
C media 1 to 2), D (the field reflected from media 3 back into
C media 2), and E (the field transmitted into media 3).
C
C *****
C
      M(1,1) = -1.0
      M(1,2) = 1.0
      M(1,3) = 0.0
      M(1,4) = 0.0
C
      M(2,1) = DSORT(EPSILON1/MU1)
      M(2,2) = CDSORT(EPSILON2/MU2)
      M(2,3) = (DSORT(EPSILON1/MU1) - CDSORT(EPSILON2/MU2))
      & * DEXP(-2*KIM*D)
      M(2,4) = 0.0

```



```

M(3,1) = 0.0
M(3,2) = CDEXP(CI*KRE*D) * DEXP(-KIM*D)
M(3,3) = CDEXP(-CI*KRE*D) * DEXP(-KIM*D)
M(3,4) = -CDEXP(CI*K3*D)
C
M(4,1) = 0.0
M(4,2) = CDSORT(EPSILON2/MU2)*CDEXP(CI*KRE*D)*DEXP(-KIM*D)
M(4,3) = -CDSORT(EPSILON2/MU2)*CDEXP(-CI*KRE*D) * DEXP(-KIM*D)
M(4,4) = -DSORT(EPSILON3/MU3)*CDEXP(CI*K3*D)
C
C
C Now insert the column vector which consists of the
C coefficients for the constant A, which represents
C the amplitude of the incident wave.
C
C
A(1) = 1.0
A(2) = DSORT(EPSILON1/MU1)
A(3) = 0.0
A(4) = 0.0
C
C
C Call up the IMSL routine to solve for the constants
C B, C, D, & E. They will be named A(1), A(2), A(3),
C & A(4) respectively.
C
C
CALL LEQTIC(M,N,IM,A,MM,IA,IJOB,WA,IER)
C
C
C Calculate the reflection coefficient, R, for the boundary
C between medias 1 & 2, where z = 0.
C
R = A(1) * CONJG(A(1))
& + CONJG(A(1))*A(3)*DEXP(-KIM*D)
& + A(1)*CONJG(A(3))*DEXP(-KIM*D)
& + A(3)*CONJG(A(3))*DEXP(-2*KIM*D)
C
C
C Calculate the transmission coefficient = E x E conjugate.
C
T = A(4) * CONJG(A(4))
C
C Calculate the absorption coefficient, A.
C
AA = 1 - R - T

```

```

C Calculate the % of the incident power which is
C reflected at the boundary between media 1 & 2.
C
      PREF = R * 100.0
C
C Calculate the % of the incident power transmitted
C into media 3.
C
      PTRANS = DSQRT(EPSILONREL3/MUPEL3) * T * 100.0
C
C Calculate the % of the incident power which is absorbed
C in media 2.
C
      PABS = 100 - PREF - PTRANS
C
      TYPE*, ' % of incident power reflected = ', PREF
      TYPE*, ' % of incident power absorbed = ', PABS
      TYPE*, ' % of incident power transmitted = ', PTRANS
C
      TYPE*, ' / '
      TYPE*, ' / '
C Calculate the skin depth for a given frequency & conductivity.
C
      SKINDEPTH = 1E6 * DSQRT(2/(D*PI*F*SIGMA*MU2))
      TYPE*, 'Skin depth in microns = ', SKINDEPTH
C
C Now calculate the electric field inside the absorbing
C media 2, at several points z = a.
      TYPE*, ' / '
      TYPE*, ' / '
C
      TYPE*, 'Enter the # of intervals in media 2 at which'
      TYPE*, 'the electric field will be calculated.'
      ACCEPT*, J
C
C
      DO 19 I = 0,J
C
      EZA = (A(2)*DEXP(-KIM*(I*D/J))
&          + A(3)*DEXP(-KIM*(I*D/J))*DEXP(-KIM*(D-(I*D/J))))
&          * (CONJG(A(2)*DEXP(-KIM*(I*D/J))
&          + A(3)*DEXP(-KIM*(I*D/J))*DEXP(-KIM*(D-(I*D/J))))
C Calculate the time-averaged power inside media 2.
C
      PINS = (DSQRT(EPSILON2/MU2) / DSQRT(EPSILON1/MU1))
&          * (A(2)*CONJG(A(2)) * DEXP(-2*KIM*(I*D/J))
&          + (A(2)*CONJG(A(3)) + A(3)*CONJG(A(2)))
&          * (DEXP(-KIM*(D-(I*D/J)))*DEXP(-KIM*D))
&          + A(3)*CONJG(A(3)) * DEXP(-KIM*(D-(1*D/J)))
&          * DEXP(-2*KIM*D))
C
      WRITE(02,*) I*D/J,EZA
      TYPE*, I*D/J, EZA
C
19 CONTINUE
END

```

1986 USAF-UES SUMMER FACULTY RESEARCH PROGRAM/

GRADUATE STUDENT SUMMER SUPPORT PROGRAM

Sponsored by the

AIR FORCE OFFICE OF SCIENTIFIC RESEARCH

Conducted by the

Universal Energy Systems, Inc.

FINAL REPORT

SYNERGISTIC EFFECTS OF ANITMALRIAL DRUGS AND HYPEROXIA

ON THE GROWTH OF MALARIA PARASITES IN CULTURE

Prepared by:	George Albert Liu
Academic Rank:	Medical Student III
Department and	Physiology Department,
University:	Meharry Medical College
Research Location:	Department of Forensic Pathology, Division of Aerospace Physiology Research, Armed Forces Institute of Pathology, Washington, D.C.
USAF Researcher	Colonel Richard A. Henderson
Date:	25 August 1986
Contract No:	F49620-85-C-0013

SYNERGISTIC EFFECTS OF ANTIMALARIAL DRUGS AND HYPEROXIA

ON THE GROWTH OF MALARIA PARASITES IN CULTURE

by

George Albert Liu

ABSTRACT

We hope to quantitatively determine the effects of oxygen on viability of Plasmodium falciparum growing in continuous culture in human erythrocytes with and without other anti-malarial drug therapy. Three different series of experiments were executed. In the first series of experiments, falciparum cultures were exposed to different pressures and times of hyperoxia. Results were not conclusive and more trials will have to be executed. In the second experiment, parasites were exposed to one atmosphere pressure of oxygen for times ranging from 1 hour to 16 hours. There was marked inhibition of growth after only 4 hours of incubation under one atmosphere pressure of oxygen. This result needs to be reproduced. It might be a possible to use one atmosphere of 95% oxygen to treat malaria in humans in the future. The third series of experiments tried to determine if there is any synergistic action of oxygen and some of the more commonly used antimalaria drugs. No synergy was found, but more trials must be done and other drugs tested.

Acknowledgements

I thank the Air Force Office of Scientific Research and Universal Energy Systems for sponsoring my research this summer. I also thank the Armed Forces Institute of Pathology and the Walter Reed Army Institute of Research, Department of Experimental Therapeutics for permitting me to use their laboratories for my research.

There are also many individuals who made this research possible. I thank Dr. Brice Hartman, Dr. Jim Mrotek, and Sue Espy for enabling me to work in Washington D.C. Major Wilbur Milhous, U.S. Army, and his staff loaned their lab and time to work on the malaria project. Thanks also to Robert Fayer for his help in processing the data for the malaria experiments. Finally, I would like to thank my supervisor, Colonel Richard Henderson--- for his time, effort, teaching, guidance, encouragement and friendship which made my experience at the Armed Forces Institute of Pathology so worthwhile.

I. Introduction:

I received my B.A. in Chemistry from the University of Rochester in 1984. For several summers I have been actively investigating cellular phenomena. I have spent two summers researching receptors of human blood products at the Center for Blood Research in Boston, one summer at the University of Rochester researching exercise training in rats and sympathetic activation using high pressure liquid chromatography, and one summer at the National Institutes of Health, National Heart Lung and Blood Institute, Laboratory of Chemical Pharmacology, researching the toxicity of various drugs on cultured rat hepatocytes.

I am presently a medical student at Meharry Medical College in Nashville, Tennessee. As I have worked, studied and learned at medical school, I wondered if hyperoxia could be used to treat drug resistant malaria. The research at Armed Forces Institute of Pathology and Walter Reed Army Institute of Research investigated the synergistic effects of hyperoxia and drug therapy for Plasmodia falciparum infection. The problem being investigated at Armed Forces Institute of Pathology was very similar to the questions I was asking at Meharry. Therefore, I was assigned to work on the effects of hyperoxia on malaria parasites.

II. Objectives of the Research Effort.

One of the objectives of the Division of Aerospace Physiology Research is to investigate the interaction of oxygen with various life processes at the cellular level in the human body. With a better understanding of the mechanisms of oxygen at the cellular level, the indications and contraindications for oxygen therapy for various diseases may be better delineated.

We hope to quantitatively determine the effects of oxygen on the viability of Plasmodium falciparum growing in continuous culture in human erythrocytes with and without other anti-malarial drug therapy. Other researchers have shown that exposure of infected animals to hyperoxia has cured malaria without other therapy. By showing that in-vitro P. falciparum cultures can be inhibited by high partial pressures of oxygen, it may be possible to use pharmacological doses of hyperbaric oxygen to treat erythrocytic stage human malaria. It may be possible to use hyperoxia as part of a malaria treatment regime in humans in the future.

My individual objectives were:

1. To study the effect of hyperbaric oxygen on growing malaria cultures.
2. To determine the antimalarial properties of oxygen on malaria cultures over time.
3. To study the possible synergistic interactions between oxygen and various chemotherapeutic agents on growing malaria cultures.

IV. Effects of Hyperbaric Oxygen on Growing Malaria Cultures.

It is known that plasmodia parasites are sensitive to oxidant stress. For example, human polymorphism has selected certain types of traits which have evolved a resistance to malaria, such as sickle cell trait, thalassemia and glucose-6-phosphate deficiency. These states are thought to facilitate the production of oxygen radicals in the body which are toxic to plasmodia, thereby protecting humans. Conversely, when states are produced which are clearly anti-oxidant in the body, malaria thrives. We hoped to show that hyperoxia would inhibit Plasmodium falciparum growth in culture.

Over many years of malaria research, investigators at the Walter Reed Army Institute of Research have developed the current state of in-vitro plasmodia culture and antimalarial drug assay techniques. These techniques make this experiment of oxygen effects and interactions with drugs on falciparum infections feasible.

W-6 cultures of P. falciparum were maintained in vitro by a modification of the methods Milhous et al. under an atmosphere of 5% oxygen, 5% carbon dioxide, and 90% nitrogen at a temperature of 37 degrees centigrade.

To measure the effects of hyperbaric oxygen on growing malaria parasites, 25 microliters of RPMI media were combined with 200 microliters of parasites in culture media prepared by the methods of Milhous et al. with a 5% hematocrit and 2%

parasitemia. The samples were incubated at different oxygen pressures of oxygen ranging from one atmosphere to three atmospheres for different amounts of time. Controls were incubated in 5% oxygen, 5% carbon dioxide and 90% nitrogen. After incubation under oxygen, 25 microliters of tritiated hypoxanthine were added to each sample. The parasites were then placed under an atmosphere of 5% oxygen, 5% carbon dioxide and 90% nitrogen overnight. After 16 hours, the parasites were washed with copious amounts of distilled water onto filter paper using a cell harvester. The filter papers were placed into scintillation fluid and counted for radioactive tritium. The number of counts represent uptake of radioactive hypoxanthine by viable parasites. Percentage inhibition was calculated by the following formula:

$$\text{percentage inhibition} = \frac{\text{counts for trial} - \text{counts for control}}{\text{counts for control}} * 100$$

The results of these experiments are shown in table I.

TABLE I

		Run 1	Run 2	Run 3
ONE ATA	HOURS			
	1.00			
	2.00	0.90		7.66
	4.00	13.14	0.00	24.00
TWO ATA				
	1.00		1.14	
	2.00		12.00	
THREE ATA				
	1.00	100.00	9.04	
	2.00		12.01	

Table I represents the percentage inhibition of growth of *P. falciparum* after exposure to hyperoxia.

It is difficult to draw definitive conclusions from this data. In run number one, it is readily apparent that the *P. falciparum* cultures exposed to three atmosphere pressure of oxygen were killed. However in the two subsequent experiments this hyperbaric oxygen effect was not apparent. This series of experiments must be repeated.

IV. Antimalarial Effects of One Atmosphere Oxygen on Malaria Cultures over Time.

Samples were prepared in the same manner as in part III, but 25 microliters of tritiated hypoxanthine was added to each sample before incubation in 95% oxygen. The malaria cultures were then

exposed to 1, 2, 4 or 16 hours of oxygen. Control cultures were incubated in 5% oxygen, 5% carbon dioxide and 90% nitrogen. The percentage inhibition of falciparum culture growth is summarized in table II.

TABLE II

		Run 1	Run 2	Run 3
ONE ATA	HOURS			
	1.00			
	2.00	0.90		7.66
	4.00	13.14	0.00	24.00
TWO ATA				
	1.00		1.14	
	2.00		12.00	
THREE ATA				
	1.00	100.00	9.04	
	2.00		12.01	

Table II. Percentage inhibition of the growth of cultured P. falciparum after exposure to one atmosphere of 95% oxygen for different amounts of time.

It is apparent that after exposure to 100 % oxygen for 16 hours that there is a definite oxygen effect inhibiting the growth of Plasmodia. Several investigators have reported inhibition of malaria parasites at oxygen tensions of 35%. We have used higher pressures of oxygen in our study to demonstrate its antimalarial effects. Should we show more inhibition of malaria by oxygen incubated for extended periods time at one atmosphere in subsequent experiments, oxygen therapy may prove to be clinically useful for the treatment of human malaria infections in the future.

V. Synergistic Oxygen and Antimalarial Drug Effects on the Growth of Malaria Cultures.

Besides the direct anti-malarial effect of oxygen, there is also a demonstrated synergism between oxygen and certain drugs which have been useful against falciparum infections. Some of these antimalarial drugs may act through free radical mechanisms which utilize oxygen radicals, such as para-amino benzoic acid anatagonists and antifolates. Divo, Geary and Jensen showed increased antimalarial effects by several other types of antibiotics after incubation in an atmosphere of 15% oxygen, as compared to incubation in 1% oxygen. Pfaller and Krogstad reported that imidazoles have greater inhibition of malaria grown in a 17-18% oxygen atmosphere, as compared to 3% or 0.3%. Thus, by increasing the amount of oxygen given to the patient to the limits of clinical treatment regimens it may be possible to

augment these chemotherapeutic antimalarial effects. If so, combinations of drug and oxygen therapy may prove more useful against malaria infection in humans than either therapy alone.

We decided to first determine if there was any synergism between the most commonly used antimalarial drugs and oxygen on growing malaria cultures. Thus, we selected the following drugs for the study: chloroquine, quinaesol, quinine, mefloquine, tetracycline, and pyrimethamine.

To assess the possible synergistic effect of oxygen and drugs on growing malaria parasites, 25 microliters of drug at various concentrations and 200 microliters of parasites in RPMI media, 10% plasma, 2% parasitemia and 5% hematocrit were incubated at different oxygen tensions and exposure times. Controls cultures were incubated in 5% oxygen, 5% carbon dioxide and 90% nitrogen. After incubation, the malaria cultures were treated in the same manner as in part III. Concentration-response curves for each drug were measured using uptake of tritiated hypoxanthine as a index of falciparum viability by a method described by Milhous et al. The data were analyzed using computer modeling to determine the concentration of drug which killed 50 percent of the parasites (abbreviated LC50) The LC50 each drug is nanograms/ml of drug. A summary of the experiments is in table 3.

TABLE III

atmospheres hours	1 2	1 4	2 1	2 2	3 1	3 2	control	RUN NUMBER
DRUG								
chloroquine	1.27	1.39 0.25 4.91	4.8	0.41 7.35	0.56 5.46	a,0 0.25 7.2	1.32 0.34	1 2 3
mefloquine	7.53	5.7 3.23 21.8	22	2.03 29.7	1.18 19.2	a,0 0.18 23.3	14.7 3.72 23.8	1 2 3
pyrimethamine	0.59	0.55 0.047 0.059	0.073	0.147 0.117	0.014 0.078	0 ----- 0.078	0.1	1 2 3
quinhaosha	3.19	3.06 0.426 -----	4.1	0.371 5.41	0.146 -----	a,0 0.164 4.83	0.11 ----- 4.61	1 2 3
quinine	8.45	11.39 1.23 18.53	22.43	1.43 21.12	0.136 21.73	a,0 0.939 19.98	9.233 ----- 23.67	1 2 3
tetracycline	1748	1140 239 4685	22816	123 7221	132 5863	a,0 154 3322	1608 172 7429	1 2 3

P. falciparum cultures were exposed to different pressures of oxygen and times. The number given represents the LD50 for each drug in nanograms per milliliter. The LD50 represents the best fit solution of the equation presented in Milhous et al. The curve was calculated from seven successive two-fold dilutions of drug in duplicate.

There appears to be no synergistic or antagonistic effect between oxygen and the various antimalarials tested. However, this does not exclude the possibility that there is synergy between oxygen and drugs. Perhaps there might be other drugs not yet tested that may demonstrate an oxygen-drug effect. The time of incubation with oxygen and the antimalarial compounds may have to be increased before an effect is noticed. Certain metabolites of antimalarials which are not produced in in-vitro studies may work synergistically with oxygen. These possibilities must be explored.

VI. Recommendations:

These series of experiments have proved to be promising but not conclusive. It is important to pursue these series of experiments because of the possible clinical use in the future. Plasmodium falciparum has recently become resistant to many of the more widely used antimalarials, so alternative therapies must be developed.

The first series of experiments, in which malaria parasites were incubated with different pressures of oxygen over time, gave inconsistent results. It is suggested that these experiments be repeated. Should two and three atmospheres pressure of oxygen not be sufficient to produce marked inhibition of malaria cultures, the time of incubation could be increased from the maximum of two hours to at least 4 hours.

In the second series of experiments, in which malaria cultures were exposed to one atmosphere oxygen over a long period

of time to produce a time course, the results were very promising. This experiment should be repeated.

One of the major problems with hyperbaric oxygen treatment of malaria in the future would be the availability of hyperbaric chambers in Third World nations where this disease is endemic. If it is possible to treat malaria with simply one atmosphere of oxygen, this treatment would certainly be more available on a world-wide basis.

The third series of experiments to determine synergistic oxygen-drug effects on the growth of malaria parasites was inconclusive. These experiments should be repeated. In addition, long incubation times should be considered. Also, different drugs should be tried.

References

1. Allison, Anthony C. and Elsie M. Eugui. A Radical Interpretation of Immunity to Malaria Parasites. The Lancet. Dec 25, 1962, 1431-3.
2. J., A. Yayon, S. Friedman and H. Ginsburg. Effects of Mitochondrial Protein Synthesis Inhibitors on the Incorporation of Isoleucine into Plasmodium falciparum in Vitro. Journal of Protozoology. 31-3 (1984) 475.
3. Brewer, George J. Treatment of Acute Rodent Malaria Infections with Hyperoxia. Journal of Laboratory and Clinical Medicine, 72 (5) 1968, 859.
4. Brewer, G. J. and C. C. Coan. Interaction of Red Cell ATP Levels and Malaria, and the Treatment of Malaria with Hyperoxia. Military Medicine---Special Issue, September, 1968, 1056-67.
5. Brewer, George J. and Robin D. Powell. The Adenosine Triphosphate Content of a Glucose-6-Phosphate Dehydrogenase and Normal Erythrocytes, Including Studies of a Glucose-6 Phosphate-Deficient Man with "Elevated Erythrocytic ATP." Journal of Laboratory and Clinical Medicine. 67-5 (1966) 727-741.

6. Brewer, George J. and Robin D. Powell. A Study of the Relationship between the Content of Adenosine Triphosphate in Human Red Cells and the Course of Falciparum Malaria: A New System that May Confer Protection Against Malaria. Proceedings of the National Academy of Sciences, 54 (1965) 741-745.
7. Desjardins, R. E., C. J. Canfield, J. D. Haynes, and J. D. Chulay. Quantitative Assessment of Antimalarial Activity in Vitro by a Semiautomated Microdilution Technique. Antimicrobial Agents and Chemotherapy. 16 (1979) 710-718.
7. Divo, Alan A., Timothy G. Geary and James B. Jensen. Oxygen and Time-Dependant Effects of Antibiotics and Selected Mitochondrial Inhibitors of Plasmodium falciparum in Culture. Antimicrobial Agents and Chemotherapy. 27 (1985) 21.
8. Eaton, John W. and George J. Brewer. Red Cell ATP and Malaria Infection. Nature. 222 (1969) 389-90.
10. Eaton, John W., James R. Eckman, Elaine Berger, and Harry S. Jacob. Supression of Malaria Infection of Oxidant-Sensitive Host Erythrocytes. Nature. 264 (1976), 758-760.

11. Eckman, James R., and John W. Eaton. Dependence of Plasmodial Glutathione Metabolism on the Host Cell. Nature. 278 (1979) 754-6.
12. Fairfield, Alexandra S. and Steven R. Meshnick. Malaria Parasites Adopt Cell Superoxide Dismutase. Science. 221 (1983) 764-6.
13. Friedman, Milton J. Oxidant Damage Mediates Variant Red Cell Resistance to Malaria. Nature. 280 (1979) p. 245-47.
14. Geary, Timothy G. and James B. Jensen. Effects of Antibiotics on Plasmodium in Vitro. American Journal of Tropical Medicine and Hygiene. 32-2 (1983) 221.
15. Gottlieb, S. F. Effects of Hyperbaric Oxygen on Microorganisms. Annual Review of Microbiology, 25 (1971) 111.
16. Gottlieb, Sheldon F. "Oxygen Under Pressure and Microorganisms." In Hyperbaric Oxygen Therapy, J. C. Davis and T. K. Hunt, eds. Undersea Medical Society, 1977, p 79.
17. Haynes, J. D., C. L. Diggs, F. A. Hines, and R. E. Desjardins. Culture of Human Malaria Parasites Plasmodium falciparum. Nature. 263, 1976, 767.

18. Milhous, Wilbur K., Norman F. Weatherly, Jean H. Bowdre, and Robert E. Desjardins. In Vitro Activities of and Mechanisms of Resistance to Antifol Antimalaria Drugs. Antimicrobial Agents and Chemotherapy. 27 (1985) 575.
19. Oelshlegel, Fred J. Jr., Barry J. Sander and George J. Brewer. Pyruvate Kinase in Malaria Host-Parasite Interaction. Nature 255 (1975) 345-7.
20. Pfaller, Micheal A. and Donald J. Krogstad. Oxygen Enhances the Antimalarial Activity of the Imidazoles. American Journal of Tropical Medicine and Hygiene. 32-4 (1983) 660-5.
21. Rencricca, Nicholas J., Robert M. Coleman, Mark D. Altschule, Peter P. Faletra, Alan D. Gray, Paul E. Desrochers and Matthew J. Doyle. Quantification of Hyperbaric Oxygen-Induced Toxicity Utilizing a Malarial System. Aviation, Space and Environmental Medicine. 52-2 (1981) 85-87.
22. Scheibel, Leonard W., Sarah H. Ashton, and William Trager. Plasmodium falciparum: Microaerophilic Requirements in Human Red Blood Cells. Experimental Parasitology. 47 (1979), 410-18.

23. Schiebel, L. W. and G. G. Stanton. New Approaches in Design of Selectively Toxic Antimalarials. IUPHAR 9th International Congress of Pharmacology Proceedings, volume 2, The MacMillian Press Limited, 1984, 385-89.
24. Sherman, Irwin W. Biochemistry of Plasmodium (malaria parasites). Microbiological Reviews 43-4 (1979) p 453.
25. Trager W. M. and James B. Jensen. Human Malaria Parasites in Continuous Culture. Science 193 (1976) 673-75.

1986 USAF-UES Summer Faculty Research Program/
Graduate Student Summer Support Program

Sponsored by the
Air Force Office of Scientific Research

Conducted by the
Universal Energy Systems, Inc.

Final Report

The Metabolism of Isopropylcyclohexan in
Male Fisher 344 Rats

Prepared by:	Isabel Lopez
Academic Rank:	Graduate Student
Department and	Department of Chemistry
University:	Wright State University
Research Location:	WPAFB/AAMRL Dayton, OH
USAF Research:	Major G. Henningson
Date:	September 18th, 1986
Contract No.:	F49620-85-C-0013

THE METABOLISM OF ISOPROPYLCYCLOHEXANE
IN MALE FISHER 344 RATS

By

Isabel Lopez

ABSTRACT

The investigation of the metabolism of isopropylcyclohexane by Fisher 344 male rats was conducted to determine whether a branched chain on a cyclohexane nucleus could alter the non-renal toxicity of cyclohexane. Eight male Fisher 344 rats were dosed by gavage with isopropylcyclohexane on alternate days for 14 days. Urine samples were collected 48 hours after the first administration. Four control rats were dosed with distilled water and their urines also collected. In general, rats exposed to the cyclichydrocarbons exhibited small average weight loss when compared to the control group. Nephropathy was apparent in all rats treated with isopropylcyclohexane. The major metabolites found in the urine samples and kidney extracts were (cis and trans) 4-isopropylcyclohexanol, 2-cyclohexylpropionic acid, 2-cyclohexyl-1,3-propane diol and 4-isopropyl-1,2-cyclohexane diol.

ACKNOWLEDGMENTS

I would like to express my gratitude to Dr. M. P. Servé for giving me the opportunity to take part in this research project and for his helpfulness and guidance throughout this study. I would also like to extend my appreciation to Major G. Henningson, SSgt. B. Hancock, SSgt. T. Whittaker and Mrs. K. O. Yu for their ready and willing assistance and others at the Toxic Hazards Division of AAMRL for making this a friendly and enjoyable working environment. Finally, I would like to thank the Air Force Systems Command and the Air Force Office of Scientific Research and Universal Energy Systems for sponsoring this research.

I. INTRODUCTION

The subject of my Masters thesis included the study of the biological activity of various polymers synthesized from tetrachloroplatinate and biologically active diamines. The bio-assays used in this investigation were performed on 3UR, HeLa and L929 tumor cell lines. Currently, I have enrolled in a doctoral program in Pharmacology and Toxicology. My interest in the field led to an association with Dr. M. Paul Serve (in conjunction with WPAFB/AAMRL Toxic Hazards Division) involving a study on the toxic effects and metabolism of isopropylcyclohexane.

Increase in public and military concern for environmental toxic hazards has stimulated both the U.S. Air Force in collaboration with the U.S. Navy and the Toxic Hazards Research Unit of the University of California and the American Petroleum Institute to engage in extensive studies to determine the toxic and possible carcinogenic potential of current and prospective hydrocarbon containing military fuels as well as other petroleum products, including unleaded gasoline. Results from studies by Halder et al (1) and Alden et al (2) indicate a high incidence of renal toxicity in male rats exposed to various component fractions of unleaded gasoline primarily containing compounds with saturated branched aliphatic chains, as well as to other hydrocarbon containing compounds (including the Air Force Cruise Missile fuel JP-10, a cyclic hydrocarbon, tetralin, cis and trans decalin, Stoddard solvent, methylisobutyl-

ketone, isooctane etc).

Renal toxicity has not been observed in most experimental animals used (dog, monkey, guinea pig, rabbit, female rats) except male rats, thus this species is being employed as a model system to study the mechanism of hydrocarbon nephrotoxicity. Histologic examination of the male rat kidney reveals the main feature of nephrotoxicity to be an accumulation of a proteinaceous material (hyaline droplets) within the lysosomes of the proximal convoluted tubules (PCT) cells. The formation of hyalin droplets may be a manifestation of physiological disruption in the catabolism of proteins to their constitutive amino acids within lysosomes of the male rat PCT cells when exposed to hydrocarbons. Unique to male rats is the presence of protein in the urine of which 50% is attributed to a low molecular weight (16,000-18,000 dalton) protein - α_{2u} globulin. α_{2u} globulin is a sex dependent protein synthesized in the liver under the influence of androgenic hormones (3-5). This protein is readily filtered through the kidney and a large portion reabsorbed in the proximal convoluted tubules of the nephron (5). Its appearance in the urine of male rats has been postulated to be a consequence of the saturation of the reabsorption capacities of the proximal tubules for α_{2u} globulin. Studies by Alden et al (2) using decalin show that the decalin induced hyalin droplets were composed of α_{2u} globulin. These findings suggest an alteration of the renal handling of a male rat specific protein might be

responsible for hydrocarbon induced nephrotoxicity.

Although alpha_{2u} globulin has not been detected in humans, understanding the pathogenesis in male rats will provide a data base for extrapolation to man in safety assessment and for extrapolation to other similar test substances that also appear to induce similar sex/species specific renal pathologic response in biological testing.

There is a growing list of compounds that induce similar morphologic alterations in male rat renal cortices as decalin. Among these compounds are the branched chain hydrocarbons: 2,2,4-trimethylpentane and 2,3,4-trimethylpentane and hydrocarbons which have fused rings: cis and trans decalin (6). Straight chain hydrocarbons such as n-octane and monocyclic molecules such as cyclohexane do not evoke renal damage (1). Of particular interest to this research group is to investigate if placing a branched chain, such as isopropane, on the cyclohexane nucleus alters the non-renal toxicity of cyclohexane. Secondly, since this compound has a high boiling point the animals can not readily ventilate the material thus it must find other means of eliminating it from the body such as metabolizing the molecule. In studying the metabolism of isopropylcyclohexane it may be helpful to note the metabolism of methylcyclohexane as an aid in predicting possible metabolites of isopropylcyclohexane.

Methylcyclohexane is a colorless flammable liquid that occurs in certain crude petroleum oils. It is used as a

solvent and as a starting material in a variety of synthetic processes. Studies by Eliot et al (7) on the metabolism of methylcyclohexane in the rabbit demonstrate several metabolites, the glucuronide of trans-4-methylcyclohexanol being the main metabolite. Methylcyclohexane is of much interest because it contains 1^o, 2^o and 3^o carbon atoms, any of which may be preferentially attacked. Also, if secondary alcohols are formed these can occur as the cis and trans isomers differing in their thermodynamic stability. In the metabolism of steroids it has been observed that the hydroxylation of alicyclic rings occurs through direct replacement of a ring hydrogen by a hydroxyl group (8). Methylcyclohexane has 5 positions where hydroxylation can occur, at the 3^o carbon at position 1, at the 2^o carbons at positions 2, 3 and 4 and at the 1^o carbon in the w position. Table 1 shows the extent of hydroxylation in vivo of various carbon atoms of methylcyclohexane in the rabbit as reported by Eliot et al (7).

Table 1. Extent of hydroxylation in vivo of the various carbon atoms of methylcyclohexane

Position	Hydroxylation (% of dose)		
	Total	cis-Isomer	trans-Isomer
1	0	0	0
2	1.7*	0.5	1.2
3	22.0*	11.5	10.5
4	17.1	2.4	14.7
w	<0.3		

*There are two 2 and two 3 positions.

The results show low values for hydroxylation at the w and the 2 position, this has been attributed to steric hindrance, where as hydroxylation at the 4 position gave the major and more stable metabolite, trans-4-methylcyclohexanol (14.7%). The data thus shows a nonspecific pattern of hydroxylation although steric factors control the extent at each position.

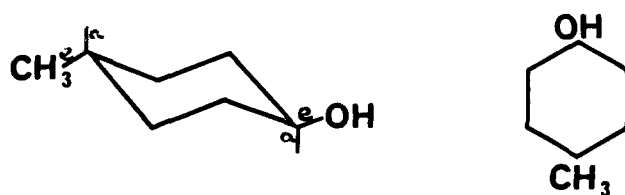
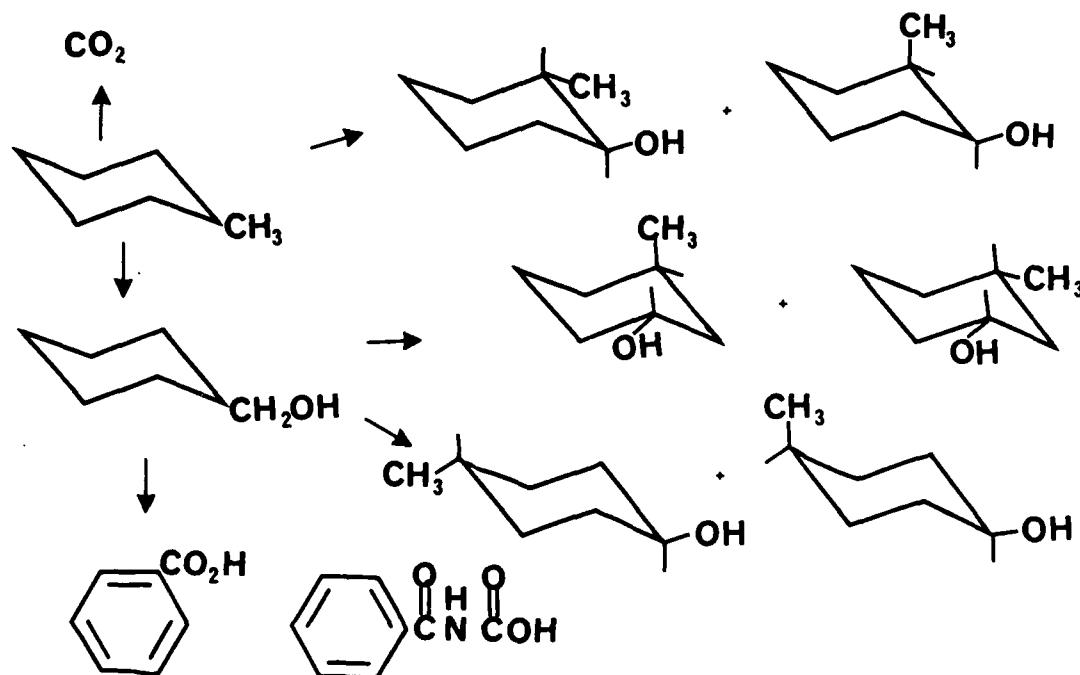


Fig. 1. Metabolism of methylcyclohexane in the rabbit



Isopropylcyclohexane is similar to methylcyclohexane except it has two extra 1° carbons which can be hydroxy-

lated. Like methylcyclohexane steric factors will also play a role in the extent of hydroxylation at each position. It is hoped that a comparison of the urinary metabolite structures of isopropylcyclohexane with those of cyclohexane, methylcyclohexane and the decalins will provide clues as to whether the pathway of metabolism is the determining feature in producing renal toxicity.

II . OBJECTIVES

The overall objectives of this research project were: first, to determine whether a branched chain on a cyclohexane nucleus can alter the non-renal toxicity of cyclohexane. Secondly, to note the favored sites of metabolism on the cyclohexane molecule containing a branched chain hydrocarbon substituent and to determine how it differs from methylcyclohexane. This was accomplished by:

- 1). Dosing 8 Fisher 344 male rats by gavage on alternate days with isopropylcyclohexane and the control group of 4 animals with distilled water.
- 2). Forty-eight hour urine samples were collected and analyzed for the presence of metabolites using gas chromatography.
- 3). On day fourteen the animals were sacrificed and the median lobe of the liver and a kidney were sent to pathology to be histologically examined for toxic effects.
- 4). A kidney sample was homogenized and analyzed

for the presence of metabolites of isopropylcyclohexane using gas chromatography.

III. EXPERIMENTAL

Eight Fisher 344 male rats (average wt. = 307 gr.) were dosed by gavage with 0.30ml isopropylcyclohexane / average kg. body weight. on alternate days for fourteen days and their body weight recorded daily. A control group consisting of four Fisher 344 male rats (average wt. = 302 gr.) was dosed with distilled water and the same regimen as the experimental group followed. Food and water were available ad libitum. The rats were placed in metabolism cages for the first 48 hours following the initial dose, at the end of this time urine samples were collected and frozen for future analysis and the animals housed in regular cages. On the fourteenth day, the rats were sacrificed using Halothan. The median lobe of the liver and one kidney were used for pathologic study; the other kidney was homogenized and analyzed for metabolites using gas chromatography (G.C.).

IV. IDENTIFICATION OF POSSIBLE METABOLITES

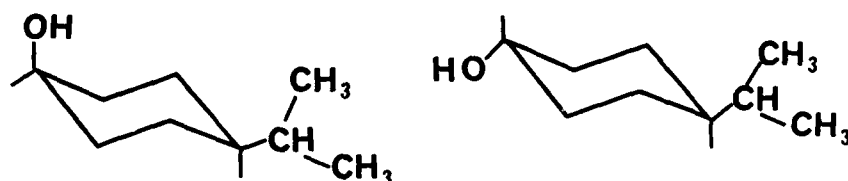
An aliquot from the collected urine was acidified with 5.0N Hydrochloric acid to a pH of 4, to this was added 0.2 ml of glucuronidase/ sulfatase (calbiochem). The solution was placed in a water bath at 37°C and agitated for 24 hours. The solution then allowed to cool to room temperature and filtered through a silica (Clin-Elut) column using

methylene chloride as the eluent. Kidney samples were homogenized with distilled water and treated in the same manner.

The methylene chloride extracts of the urine and kidney were analyzed for the presence of metabolites on a Hewlett-Packard model 5880A - gas-liquid chromatograph (G.C) equipped with a flame ionization detector. A 15m x 0.25mm I.D. carbowax 20M fused silica capillary column. After injecting a sample the oven temperature was maintained at 100°C for 1 minute then raised 5°C / minute to 180°C where it was held for 30 minutes. Injection port and detector temperatures were 200° and 250°C. Helium, with a linear velocity of 35.7 cm / sec and split ratio of approximately 5:1, was used as the carrier gas. Additional varification was obtained by using a Hewlett-Packard gas chromatograph / mass spectrometer model 5985. By comparing the G.C. retention time data of purchased or synthesized possible metabolite standards to those obtained from urine and kidney samples the metabolites were identified.

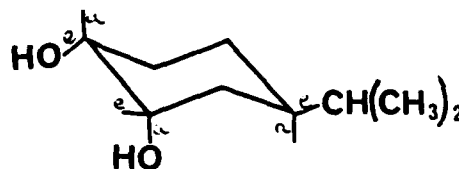
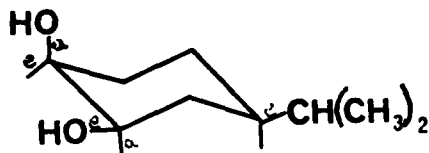
The urinary metabolites of isopropylcyclohexane identified were cis and trans 4-isopropylcyclohexanol, 2-cyclohexylpropionic acid, 2-cyclohexyl-1,3-propane diol and the two cis isomers (with respect to the 1,2 substitution) and the trans isomer (with respect to the 1,2 substitution) of 4-isopropyl-1,2-cyclohexane diol. The results of this experiment are similar to the forementioned results of Eliot et al for the metabolism of methylcyclohexane in the rabbit. The metabolites acquired were methylcyclohexanols varying in

the extent of hydroxylation at different positions, although the main metabolite was 4-methylcyclohexanol. Identification of cis and trans 4-isopropylcyclohexanol was deduced by comparing the G.C. retention times of diluted samples (in methylene chloride) of synthesized standards with the urine spectra of the treated male rats (retention time of standard: 4.16, 4.63 vs 4.14 cis, 4.59 trans isomer). In this study the trans isomer was found to be in greater abundance than the cis. This is consistent with known data of disubstituted cyclohexanes and is in agreement with thermodynamic stabilities (9). It is in the trans position where less interaction will occur between the bulky isopropyl group on C-4 and the hydroxy group on C-1.



Gas Chromatography / Mass Spectral data was employed to varify the presence of 2-cyclohexylpropionic acid and cis (e,a and a,e isomers with respect to 1,2 substitution) and trans (with respect to the 1,2 substitution) 4-isopropyl-1,2-cyclohexane diol. The base peak (relative abundance = 100%) for the acid appears at 112 amu (all single charges are given in terms of m/e) corresponds to the fragment of the acid (m. wt.=156) less CO₂ (m. wt.=44). The ion fragment at 156 amu coincides with the molecular weight of 2-cyclohexylpropionic acid. Of interest was the identifica-

tion of the two cis isomers and the trans isomer (with respect to 1,2 substitution) of 4-isopropyl-1,2-cyclohexane diol with respective G.C. retention times 14.37, 14.75 and 15.66. These retention times were compared to the mass spectral data acquired from the G.C./ Mass Spectral integration of the peaks. Mass Spectral data for the peak with a retention time of 14.37 gives a base peak of 97 amu corresponding to 4-isopropyl-1,2-cyclohexane diol less a water and an isopropyl molecule. The ion fragment at 153 amu (relative abundance = 93%) is derived from 4-isopropyl-1,2-cyclohexane diol less the isopropyl fragment (43 amu, relative abundance = 3.6%). On the other hand the mass spectral data for the peak having a retention time of 14.95 shows a base peak at 115 amu and an ion fragment at 97 amu (relative abundance = 93%) both pertaining to the corresponding ion fragments mentioned above. The trans isomer with a retention time of 15.66 has a base peak of 115 amu and an ion fragment of 97 amu (81.1% rel. abundance) which already has been designated specific fragments. The data discussed indicates isomerism (with respect to the 1,2 substitution) of 4-isopropyl-1,2-cyclohexane diol: trans 1,2 diol and 2 cis isomers differing in the position of the -OH groups (e,a and a,e).



The 2-cyclohexyl-1,3-propane diol metabolite was identified by comparing it with the retention time of a standard sample. Additional evidence was obtained by spiking a urine sample from a treated male rat with 2-cyclohexyl-1,3-propane diol and observing an increase in the size of the presumed peak.

Comparing the results acquired in this study for a branched chain hydrocarbon on a cyclohexane ring in male rats with those reported by Eliot et al (7) for methylcyclohexane in the rabbit, several points may be noted bearing in mind species difference in the methods of metabolizing compounds (branched chain vs a methyl group substituent):

- 1). Metabolism of methylcyclohexane only yielded monosubstituted products: 2,3 and 4 methyl cyclohexanols. Only one monosubstituted isopropylcyclohexane metabolite was obtained, 4-isopropylcyclohexanol.
- 2). No disubstitution was reported for methylcyclohexane but was acquired for isopropylcyclohexane: cis and trans 4-isopropyl-1,2-cyclohexane diol.
- 3). Trace amounts of acid was produced in the metabolism of methylcyclohexane where as the acid appears as one of the major metabolites of isopropylcyclohexane.

Metabolites identified in the kidney homogenates of male Fisher 344 rats are the same as those found in urine

samples except for the appearance of a small peak with a retention time of 3.03. This was identified as 3-isopropylcyclohexanol after comparison with standard metabolites. The minute amount of this monosubstituted metabolite may be due to it being converted into the diol via the kidney microsomal oxidase system.

V. PATHOLOGY

Histologic studies of both liver and kidney tissue of male Fisher 344 rats reveal no microscopic lesions in the liver of either control or treated male rats. However, histologic examination of renal tissue from exposed male rats, even at subgross magnifications, exhibit diffuse and multifocally dilated cystic tubules at the corticomedullary junction and were filled with an eosinophilic debris. In addition to lesions at the corticomedullary junction, diffuse and multifocal occurrence of hyaline droplet formation was noted in proximal tubular epithelial cells throughout the cortex. Further examination revealed mild to moderate multifocal degeneration, sloughing out, of proximal tubular epithelial cells. These microscopic findings confirm hydrocarbon nephrotoxicity and are consistent with histopathologic results acquired by other investigators (10).

VI. RECOMMENDATIONS

The identification of the metabolites of isopropylcyclohexane can serve as a model of how branched chain

hydrocarbons may be metabolized. Also, by comparing the results of this study to those reported for other hydrocarbons, it may be possible to predict the sites on unknown compounds that will undergo metabolism and which of these metabolites (if all or a combination) are responsible for inducing renal toxicity.

A follow up of this study should include testing methylcyclohexane and other hydrocarbons bearing the isopropyl moiety in rats and possibly other species of laboratory animals and comparing the metabolites acquired for possible relationships. This may then be helpful in extrapolating long term exposure of various hydrocarbon fuels and solvents to man.

REFERENCES

- 1). Halder, C.A., Warne, T.M. and Hatoum, N.S (1984).
Renal toxicity of gasoline and related petroleum naphthas in male rats. *Op. cit.* 73-88.
- 2). Alden, C.L., Kanerva, R.L., Ridder, G. and Stone, L.C (1984). The pathogenesis of the nephrotoxicity of volatile hydrocarbons in the male rat. In: Renal Effects of Petroleum Hydrocarbons. M.A. Mehlman, C.P. Hemstreet, J.J. Thorpe and N.K. Weaver, eds., Princeton Scientific Publishers, Inc., Princeton N.J., 107-120.
- 3). Roy, A.K. and Neuhaus, O.W (1966). Identification of rat urinary proteins by zone and immunoelectrophoresis. Proc. Soc. Exp. Biol. Med. 121: 894-899.
- 4). Roy, A.K. and Neuhaus, O.W (1966). Proof of the hepatic synthesis of a sex-dependent protein in the rat. Biochim. Biophys. Acta 127: 82-87.
- 5). Roy, A.K. and Raber, D.L (1972). Immunofluorescent localization of α_{2u} globulin in the hepatic and renal tissues of the rat. J. Histochem. Cytochem.
- 6). Phillips, R.D and Egan, G.F (1984). Toxicol. Appl. Pharmacol. 73: 500-510.
- 7). Elliot. T.H., Tao, R.C.C and Williams, R.T. The metabolism of methylcyclohexane. J. Biochem. 95: 70-76.
- 8). Hayano, M., Gut, M., Dorfman, R.I., Sebek, O.K and Peterson, D.H (1958). J. Am. Chem. Soc. 80: 2336.
- 9). March, J. (ed.), Advanced Organic Chemistry, 3rd

edition, New York, John Wiley and Sons, Inc., 1985.

- 10). Bruner, R.H and Pitts, L.L. Proc. 13th Annu Conf.
Environ. Toxicol., Armstrong Aerospace Medical Research
Lab., Wright Patterson Air Force Base, OH., 1983.

U.S. AIR FORCE
AFRL-WS-88-0013

Contract No. and
AIR FORCE OFFICE OF SCIENTIFIC RESEARCH

Contract No. and
Air Force Office of Scientific Research, Inc.

Contract No.

A Comparative Study and Evaluation of Two Commercial Chemical
Models with Emphasis on Potential Utility in Air Force Research

Prepared by:	Thomas A. Jarney, with Mike Liles
Academic Rank:	Assistant Professor (Graduate Student)
Department and	Meteorology.
University:	Florida State University
Research Location:	Air Force Engineering and Services Center, Environments Division, Tyndall AFB, FL 32407-6111
USAF Researcher:	Captain Lawrence E. Lee
Date:	15 August 1988
Contract No:	F49620-88-C-0013

3. Independent Eval. and Comparison of Four Models and Comparison of the
with Results of Experimental Studies to the Data Available

5.

Thomas A. Jarnev and Michael M. Lives

ABSTRACT

Four models of atmospheric dispersal that might be used for toxic or hazardous chemicals were evaluated and compared to experimental data. The models were evaluated with respect to potential and desirability for use in Air Force applications considering such factors as theoretical foundation, validation history and accessibility of results.

For most general applications, the AFSL AFTOX model is favored; however, the current lack of a module for simulating the behavior of a heavier-than-air-gas (HTAG) in AFTOX favors the use of Radian's CHARM in HTAG situations if limited flexibility in the output format is acceptable.

The models designed for instantaneous or explosive releases, PUFF and TRPUF, are very similar and produce substantially equal results with minimum effort when comparable input specifications are used.

The comparison of these models to two measured releases was used to highlight model features and develop understanding of model operations. The overall performance of the models against the measured data was comparable to previous comparisons and, in general, the model predictions were reasonable and consistent; the few exceptions are noted.

1. The first step is to identify the problem or question that needs to be answered. This involves understanding the context and the specific requirements of the task.

I am deeply grateful for this opportunity to work with the fine staff of the Engineering and Services Center. I would like to thank the Air Force Systems Command and the Air Force Office of Scientific Research for the Summer Faculty Research Program and Universal Energy Systems for conducting it in a commendable manner. In particular, I appreciate the opportunity to bring a graduate student along with me. This has been a valuable experience for the student and the research effort has benefited from his presence.

We appreciate the assistance and hospitality afforded us by the ESO staff and especially by Captain Larry Key who helped formulate the research objectives and worked hard to provide us with the resources needed to complete them. Thanks, also, to Bruce Kunkel of AFSC and Mark Eitgroth of Radian Corporation for their assistance.

I. INTRODUCTION

The announcement of the AFOSR-USF Summer Faculty Research Program (1984) provided an opportunity for research interaction at the Environmental and Services Center at Tyndall AFB, Florida, in the meteorological areas of atmospheric dispersion and modeling. These areas coincide with my present research interests and my professional experience so I was eager to explore this apparent commonality of interest with an Air Force agency located so close to my home institution, Florida State University (FSU).

I joined the faculty at FSU in August, 1984, after spending 17 years working with the development and application of models for the transport and transformation of atmospheric constituents with: the Tennessee Air Pollution Control Division; Brookhaven National Laboratory, operated for the U.S. Department of Energy; NASA's Langley Research Center; and, two privately-owned consulting firms.

Four years of active-duty service as an Air Weather Service officer and six additional years of reserve service with the Tennessee Air National Guard have provided valuable insight to the nature of Air Force operations to augment my professional experience. My Ph.D. was awarded by Saint Louis University in July, 1984, partly for NASA-sponsored research involving the mathematical modeling of the distributions of trace constituents in the lower atmosphere.

For these reasons, I felt I could contribute to and benefit from the related research activities at AFESC and the AFESC personnel involved in the selection process agreed.

II. OBJECTIVES OF THE RESEARCH EFFORT

The following research objectives were formulated with Capt. L. A. ... of the Engineering and Services Center. The objectives were listed as priorities since the proposed research involved tasks with uncertain time factors. The first two priority tasks were completed during this research fellowship. This final report describes the overall accomplishments of this effort. However, some portions of the work are described in further detail in preliminary reports which are hereby referenced here.

Priority #1: Technical review of the CHARM dispersion model for hazardous air pollutants developed under contract for AFESC. The algorithms that adapt the model for use in predicting dispersion of gases that are heavier than air are of particular interest. This review is intended to provide additional insight into model algorithms and can serve as an objective evaluation of the contractor's performance.

Priority #2: Technical and operational evaluations of additional dispersion models either in use by the Air Force or under consideration by AFESC. Models that are based on U.S. Environmental Protection Agency (EPA) standard models will be compared to the appropriate standard model and any differences will be researched and documented.

III. MODEL DESCRIPTIONS

The models examined during this summer fieldwork are listed below:

- 1) The Radian Corporation Chemtrak model - a puff dispersion model with a special algorithm for heavier-than-air-gases (HTAGs).
- 2) The U.S. Air Force Geophysical Laboratory Toxic Chemical Dispersion Model (AFTOX) - a puff dispersion model developed from the Shell Development Company SPILLS code.
- 3) The U.S. Environmental Protection Agency (EPA) PUFF model - a puff model designed to simulate dispersion from "instantaneous releases".
- 4) The Trinity Corporation TRPUF model - an instantaneous release model developed from and similar to the EPA PUFF model.

Brief descriptions of these models are given below. Consult the reference documents for more detailed descriptions.

A. CHARM

Radian's CHARM, as configured for AFESC, is described in the reference documentation (Radian,1985). The HTAG algorithm was reviewed in a preliminary report (Carney,PR1). CHARM includes the evaporation rate module of the SPILLS model with a puff dispersion and advection model after Sheih (1977). Puff dispersion for HTAGs in contact with the ground is based on the Eidsvik (1980) model. A micro-computer version of CHARM was adapted for Air Force use in assessing potential exposure to airborne toxic clouds which might result from accidental releases of toxic compounds.

B. AFTOX

The AFGL AFTOX is, like CHARM, a derivative of the SPILLS model. A

preliminary report discusses the AFTOX simulation of concentrations in the vertical. Turner, 1985). The principal modifications of the Slade model for AFTOX were:

- 1) the technique for specification of the atmospheric stability parameter which determines the extent of plume dispersion at downwind locations; and
- 2) the adjustment of downwind dispersion for the effects of surface roughness.

The reference document for the model provides further details (Turner, 1985).

C. PUFF and TRPUF

PUFF and TRPUF were designed to simulate the dispersion of a neutrally-buoyant tracer released "instantaneously". Of course, real emissions occur over finite intervals of time, however, when the travel time of a puff or plume is long compared to the release time, the release can often be regarded as instantaneous. Puff models are conceptually better representations of such releases than plume models, although the dispersion of both puffs and plumes is often described in models with Gaussian distribution parameters. Theoretically, however, horizontal dispersion in the downwind direction, or σ_{max} , is included in the formulations for puff dispersion. In practice, σ_{max} is usually assumed to be equal to σ_y , since experimental values for σ_{max} are not generally available.

PUFF and TRPUF use the power-law expressions suggested by Slade (1968) for the horizontal and vertical spread parameters. Slade (1969) cautions that the power law expression is applicable only between 100-

4000 m: a significant point which is overlooked in the documentation of these models.

The time series between the PLUFF and TRPUF models are plotted in the user's guide for TRPUF (Trinity, 1985) and were further discussed in a preliminary report (Lukes, PRA). The primary difference involves the specification of the initial puff using either dimensions or a virtual point source approximation. Two versions of the PLUFF model were exercised in this comparison: PLUFFSIG, in which the initial puff size is specified to correspond to the TRPUF virtual source; and, PLUFFDV, in which the virtual distance of the TRPUF model is added to the PLUFF receptor locations.

IV. DESCRIPTION OF COMPARISON DATA SETS

1) The Eagle 3 Experiment

Data from the Eagle 3 field-scale release of nitrogen tetroxide (N_2O_4) performed by Lawrence Livermore National Laboratory for the U.S. Air Force was used for the comparison of models with dispersion of a heavier than air gas (HTAG). This data has been discussed in model comparisons by McRae (1983) and Spicer and Havens (1985). Although there is a considerable degree of uncertainty associated with the source strength and distributions of the plume downwind, this was the best available data set for this comparison since the Air Force is interested in modeling this particular compound and previous comparisons can be referenced.

McRae (1985) presents an extensive analysis of the source strength difficulties. Spicer and Havens (1986) used revised source strengths based on improved understanding of the atmospheric chemistry of N_2O_4 . This study uses source strength estimates developed by Spicer and

Havens, however, it should be noted that many of the uncertainties noted by Hagen (1963) remain associated with the measured values. Table 1 lists pertinent measured physical conditions and model parameters.

II. The Ocean Breeze experiments.

Ocean Breeze was a series of field experiments conducted at Cape Canaveral to establish quantitative diffusion predictions for use as a missile range safety tool (Haugen and Fuquay, 1963). The tests used Zinc Sulfide (ZnS) as the neutrally-buoyant atmospheric tracer. The actual measurements taken were the amounts of mass of a tracer that would accumulate on the filter over the duration of the cloud rather than a time series of concentrations. By definition (Hagen, 1963), dosage (gm) is the product of exposure ($gm \cdot sec/m^3$) and flow rate (m^3/sec) where exposure is the time integral of concentrations at a point. With measured flow rates, exposure was thus determined. This was the form in which the data were reported. For comparison purposes, an average concentration can be approximated by dividing the exposure at a point by the time it takes for the cloud to pass. Neglecting along wind diffusion, the total time of emission can be used for an upper bound on the estimate.

According to the report of the Ocean Breeze experiment (Haugen and Fuquay, 1963) that the vertical temperature difference was the parameter most subject to error and, thus, the accuracy of the stability determination is suspect. The report also notes that stable conditions occur very rarely with on shore winds, so, in the models, all unstable categories along with neutral stability were run for comparative purposes.

1. MODEL EVALUATIONS AND SUMMARY OF COMPARISONS

A. Evaluations

The criteria for the evaluation of the four models described above are based on studies of the model documentation, source listings, reference materials and operational experience gained primarily in exercising the models for comparison to the two aforementioned data sets. The criteria for this evaluation includes the following:

- 1) potential for use in Air Force Operations;
- 2) theoretical foundation and validation history;
- 3) convenience to operate; and
- 4) usefulness of output products.

All of the models considered are based on the Gaussian, or statistical, modeling concept. Gaussian plume models have been validated with substantial documentation for neutrally-buoyant plumes from continuous sources. All of these models use a "puff" concept, and in the cases of CHARM and AFTOX, simulate continuous emissions with a series of puffs. PUFF and TRPUF are meant to be used for instantaneous or "explosive" emissions for which experimental data is very limited, thus the documented validation of these is very sparse.

CHARM includes a HTAG module which has had very limited validation against independent data. Even such limited comparisons with independent data suggests the value of including a model for HTAG behavior when the compound of interest may have a heavier-than-air phase. For that reason, CHARM is superior to AFTOX, the other model in this study designed for general applicability, for HTAG simulations. There is a substantial caveat that must accompany that conclusion however, since this study and the previous comparison of CHARM to the Eagle Series data (McRae, 1985) found CHARM to be rather complicated to use and difficult to interpret.

Later versions of CHARM may have alleviated this problem, but considerable experience with the model seems to be prerequisite to obtaining useful results.

For most applications, we much prefer the AFTOX model. It has most of the useful capabilities of CHARM, without sacrificing operational simplicity. Familiarity with AFTOX, to the point of producing useful dispersion estimates, can be acquired in a fraction of the time necessary for CHARM. This relative ease of access is highly desirable for a model that may be exercised at operational sites by personnel with only limited experience with atmospheric dispersion models. The advantage of CHARM in dense gas situations should be overcome by the planned addition of a dense gas module to AFTOX.

With regard to dense gas modules, a preliminary report (Carney, EFT) concluded that the state-of-art of modeling a dense gas release through its entire atmospheric dispersion cycle is not highly advanced at present. For models like CHARM and AFTOX intended for rather general application (both models have chemical data for over 50 compounds in an input data file), it seems prudent to modify the prediction of HTAG dispersion with a module that describes at least the portion of the HTAG atmospheric cycle where turbulent dispersion is suppressed. The use of the Eidsvik (1980) formulation in CHARM provides an example.

The instantaneous release models are essentially equivalent. We do not share Trinity's (1985) stated preference for the use of a virtual point source configuration for specification of the initial puff. Since EPA is the final arbitrator of many environmental issues of concern here, superficial departures from EPA-developed models are invited headaches that should simply be avoided. We see no particular advantage in

the TRPUP virtual point source specification and the disadvantage of having to show that it is essentially equivalent to the desirable case of PUFF.

With the above exception, PUFF and TRPUP have the same general input requirements. The output of PUFF is less structured but more versatile than TRPUP. The TRPUP output consists of concentration estimates for a number of fixed distances downwind that might require interpolation to distances of particular interest.

The concentration estimates can be in units of ppmv or micrograms per cubic meter in TRPUP, while PUFF output is limited to the latter. Local versions of both models were created that convert the output to ppmv at a specified temperature and pressure.

Since these models are so similar, the choice between them is a matter of convenience for a given application. As suggested above, however, it is much easier to tell EPA that you used their model than to convince them that another model is comparable.

The larger issue with respect to these two models is when to use them. These models are intended for much less general applicability than CHARM or AFTOX. Given the large uncertainties associated with the dispersion parameters for instantaneous releases, it seems likely that predictions from, say AFTOX, could be conservatively adjusted for release, sampling or averaging time differences without significant loss of accuracy compared to the instantaneous models. In fact, an option could quite easily be installed in AFTOX to use the Slade (1968) instantaneous dispersion curves rather than the F-G curves.

B. Comparisons to Eagle 3

The data from the Eagle 3 experiment has been used in model comparison studies by McRae (1985) and Spicer and Havens (1986). Around

300 seconds after the start of the spill, the observed NO_2 value of 500 ppm at a downwind distance of 725 m was reported by McPae et al., (1984) for the lowest receptor. In the model comparisons mentioned above, the actual peak concentration at this distance was estimated as 500-1275 ppm (McPae, 1985) and 500-1040 ppm (Spicer and Havens, 1986).

The results of our models runs for estimates at this distance based on the source strength estimates of Spicer and Havens (1986) are summarized in Table 1. The atmospheric stability for these model estimates was specified to correspond to F-G class D for AFTOX and CHARM and the values for neutral stability are shown for PUFF and TRPUF. In general, the estimates appear to be very reasonable and comparable to results of previous comparisons. Some specific comments with respect to previous comparisons and with respect to each model follow.

In the previous model comparisons, the Gaussian-form model estimates were obtained as representative steady-state estimates, taken well after the start of presumed steady emissions. The estimates shown in Table 3 are taken at 5 minutes after the start of the release which was presumed to last 3 minutes.

For the CHARM estimates, one puff was specified with the initial puff dimensions taken from the spill volume. Other CHARM modes were also run but since they did not allow enough control over puff specification to facilitate output interpretation and assure mass conservation, this option was preferable. In this mode, the CHARM results are more comparable to PUFF and TRPUF than to AFTOX.

Although the input specifications for these runs have been tailored to increase our understanding of the models under evaluation here, it may be of some interest to compare the values in Table 1 to previous

efforts. In general, what such a comparison shows is the importance of the input specifications in determining the modeling results.

The peak concentration from AFTOX, as calculated here, is very close to the measured peak concentration. This value is a linear interpolation of maximum values estimated for: 600 m, five minutes after the instantaneous release; and, 900 m, ten minutes after the release. CHARM computes its own integration timesteps and for this run used 300 s. We did not find a way for the user to control this parameter, which also controls the hardcopy output timesteps.

The AFTOX estimates in Table 3 are considerably higher than estimates from its parent model, the Shell dispersion model, in the McRae (1985) comparison. The McRae results were for 17 minutes after the beginning of a presumed steady release (i.e., a plume estimate). The current estimate attempts to simulate the limited emission period prior to the N₂ purge of the system (McRae et al., 1984). It is clear that the emissions for this release were anything but steady. The temporal variation of the model's prediction is an important indicator of the ability of the model to simulate a real emission event; however, the purge and subsequent outgassing from the ground make it difficult to coordinate model predictions with Eagle 3 results. The maximum concentration from AFTOX after 5 minute elapsed time is considerably higher than the value in Table 3 (~730 ppm, with the roughness correction; ~360 ppm, without) and occurs closer to the release site (375 m). The maximum estimated value reaches 785 m downwind around 7 minutes after the start of emissions.

The AFTOX estimates in Table 3 have been adjusted for surface roughness (see discussion in the model description section above) using 0.5 cm as the representative value. This correction is one of the

significant differences between AFTOX and the Shell dispersion model.

Values from the instantaneous puff models for routine evaluation are also shown in Table 7. These estimates are adjusted by the models to represent a 7 min averaging time. To illustrate the sensitivity of this adjustment, an estimate for a 10 second averaging period is shown for TRPUS.

C. Comparison to Ocean Breeze 2

Table 8 is a summary of the model comparison data to OB2. In addition to the models considered in this evaluation, results from the OB405 regression equation are also shown. In this set of comparisons, the representative sampling time of the model estimates is an important parameter since the measured results are nominal "time averages". The instantaneous puff models have an internal correction for averaging time as previously described. The AFTOX adjustment of the dispersion parameters for averaging time different from 7 min is not applied to a 30 minute release. In the continuous release mode AFTOX and CHARM results at 1.2 and 2.4 km are likely steady-state estimates, which means that time averaging would not be necessary. In the one-puff configurations, however, estimates from CHARM and AFTOX should be regarded as 3-10 minute values (corresponding to P-G curve data). In comparison of these results to the reference data, we must be ever mindful of the particular release scenario used for the model in comparison to the actual release and the uncertainty in the sampling/averaging time for the measured data.

The crosswind spread was computed for OB2 measured data and it is of interest to compare the model computed values with these, again being mindful of the averaging time question. The AFTOX model was run for P-G

classes A and B in addition to the classes shown in Table 4. However, the model-estimated dispersion parameters were large enough relative to the measured spread to eliminate these classes from further consideration.

The surface roughness correction of the AFTOX model and the comparatively smaller spread for the instantaneous puff models discussed above can also be seen in these results. Overall, the model predicted values are reasonable and consistent. Comparing the model estimated concentrations with the "average" value derived from the DB2 experiment, one sees that:

- 1) The instantaneous puff models produce results that are more comparable for unstable conditions than neutral.
- 2) CHARM and AFTOX results are similar with the differences due to instantaneous vs. continuous releases and dispersion adjustments; again demonstrating the importance of the input specifications.
- 3) For each model, results from some configuration of the model are close to the experimental value. This suggests that these models are reasonable to use for modeling the dispersion of passive tracers if the appropriate specifications are made. However, in operational circumstances, where the input specifications depend on our knowledge of a particular event, the important question is: how reliable is the estimate from a model based on the given specifications?

VI. RECOMMENDATIONS

The following recommendations are based on the evaluation described in this report and the conclusions of the evaluation committee.

1) The development of AFTOX as a general applications model to replace the OBVDG model should be continued. In particular, a HTAG module and an optional set of dispersion curves for instantaneous releases would broaden its applicability. The current model is quite sensitive to specification of the roughness length. This correction might be more appropriate as an option, particularly the lateral dispersion correction, to allow user discretion in its application since the empirical evidence for it is not strong.

2) CHARM is currently useful for HTAG simulations for users who are familiar with the operation of the model. Further development or tailoring of CHARM under Air Force sponsorship would not be cost effective, in my opinion, because of the anticipated development of AFTOX.

3) The instantaneous puff models may have some current applicability in contingency planning for explosive releases. Judicious application of AFTOX with adjusted dispersion parameters should be a suitable alternative to those models in the future.

4) Validation of AFTOX with field data should accompany future development. The periodic evaluations conducted by the USDOE Savannah River Laboratory would be useful exercises to test for passive-tracer dispersion capability.

5) The degree of uncertainty associated with model predictions should be quantified, whenever possible. It is highly desirable that dispersion estimates be accompanied by estimates of uncertainty or confidence levels so that responsible use can be made of the results.

TABLE 1

Site: 003 (0.5 m) West Gate 17.1 N 17.1 W
 Date: 7 October 1987 Time: 1648 EDT
 Wind: 3.14 m/s at 2 m Sigma Theta: 13.2 (3-min avg.)
 Temperature: 21.8 C Relative Humidity: 85 %
 Pressure: 907.9 mb Clouds: 95 % at unknown height

Spill Conditions

Volume: 4.2 cu m (6090 kg)
 Rate: 1.4 cu m/min (2030 kg/min)
 Duration: 180 s (3 min)
 Source Strength: 190 kg/min (Spicer and Havens, 1985)

TABLE 2

Data for the Comparison of Models with Ocean Breeze I

Site: Cape Canaveral, FL 28.5N 81W
 Date: 17 May 1961 Time: 1650 EST
 Wind: 3.3 m/s Pressure: 1016 mb
 Temperature: 25.7 C Relative Humidity: 78 %
 Delta T: -.2 C between 54 and 6 ft = -.014 C/m

Spill Conditions

Rate: .989 g/s (.05933 kg/min)
 Duration: 30 min
 Total Emission: 1.78 kg

TABLE 3

Model	Total Emitted (kg)	Emission Time min	Concen- tration microg/m ³	Averaging Time min	Sigma	Sigma- min
CHARM	570	Instan	520	Peak	58	28
AFTOX	570	"	228	"	48	18
PUFFSIG	570	Instan	482	"	28	16
PUFFDV	570	Instan	364	"	18	16
TRPUF	570	Instan	344	"	28	16
TRPUF	570	Instan	2560	0.2	28	16

TABLE 4

Model	Chi1	Sigma --Y--	Sigma --Z--	Chi2	Sigma --Y--	Sigma --Z--
Measured	9.5	87.0	N/A	2.3	95.9	N/A
DB/DG	11.2	N/A	N/A	2.9	N/A	N/A
TRPUF-U	10.7	95.3	93.8	3.3	180.3	155.5
PUFF1-U	10.6	95.4	93.9	3.4	180.4	155.6
PUFF2-U	10.7	95.3	93.8	3.4	180.3	155.5
TRPUF-N	105.2	40.8	21.5	34.9	77.3	34.8
PUFF1-N	105.0	41.0	21.5	34.9	77.4	34.9
PUFF2-N	105.7	40.8	21.5	35.0	77.3	34.8
C-1-C	14.3	121.9	75.5	3.5	228.3	136.4
C-4-C	7.4	"	"	1.4	"	"
A-C3-C	8.1	134.5	71.9	2.3	250.3	135.5
A-C10-C	5.1	171.0	83.8	1.5	319.1	154.3
A-P3-C	30.0	134.8	71.9	3.5	251.1	135.5
A-P10-C	13.0	171.4	83.8	1.5	319.4	154.3
C-1-D	55.4	109.3	36.1	12.4	151.2	56.4
C-4-D	29.2	"	"	5.0	"	"
A-C3-D	25.0	93.7	32.1	8.4	174.8	53.2
A-C10-D	16.0	119.2	37.5	5.5	222.4	60.5
A-P3-D	22.0	94.1	32.1	2.2	175.2	53.2
A-P10-D	8.2	119.6	37.6	.8	227.7	60.5

NOTES:

PUFF1-PUFFDV; PUFF2-PUFFSIG

Chi1 is concentration in micrograms per cubic meter at 1.1 km

Chi2 is the same at 2.4 km

C-1 is CHARM instantaneous release

C-4 is CHARM continuous release

A-C3 is AFTOX continuous release with 3 cm roughness length

A-P10 is AFTOX instantaneous release with 10 cm roughness length

REFERENCES

- Bladon, J.D. 1981: A model for heavy gas dispersion from a rectangular source. *Journal of Hazardous Materials*, 10, 229-237.
- Calder, D.A. and J.D. Calder. 1983: The Great Lakes and the Great Lakes Basin. *Environmental Science and Technology*, 17, 1000-1001.
- Kunkel, B.A.. 1985: Development of an Atmospheric Diffusion Model for Toxic Chemical Releases. Air Force Geophysics Laboratory Environmental Research Paper, No. 85.
- McRae, T.G. 1985: Analysis and Model/Date Comparisons of Large-Scale Releases of Nitrogen Dioxide. ESL-TR-85-05.
- McRae, T.G., R. Cederwall and others 1984: Eagle Series Data Report. UCID-20063, Lawrence Livermore National Laboratory.
- Petersen, W.B.. 1982: Estimating Concentrations Downwind from an Instantaneous Puff Release. USEPA Technical Report Number: EPA 600/3-82-078.
- Radian Corporation. 1985: Emergency Modeling of Hazardous Air Pollutants. AFESC Report No. ESL-TR 84-55.
- Shien, C.M. 1978: A puff pollutant dispersion model with wind shear and dynamic plume rise. *Atmos. Environ.*, 12, 1977-1978.
- Slade, D.H. 1968: *Metereology and Atomic Energy*. TID-24191, U.S. Atomic Energy Commission.
- Spicer, T.O. and J.A. Havens 1986: Development of Vapor Dispersion Models for NonNeutrally Buoyant Gas Mixtures - Analysis of USAF/N 204 Data. AFESC Technical Report.
- Trinity Consultants, Incorporated. 1985: User's Guide for TRPUP-M007. Richardson, TX 75080.

Preliminary Reports

Carney:

1. Evaluation of CHARM Heavier-Than-Air (HTA) Algorithm
2. A Survey of Models for Heavier-Than-Air Gases
3. Preliminary Report on the Air Force Geophysics Laboratory Model

Lukes:

4. Preliminary Comparative Runs Between the EPA PUFF Model and the Trinity Corporation (TRPUP) Puff Model

1986 USAF-UES SUMMER FACULTY RESEARCH PROGRAM/
GRADUATE STUDENT SUMMER SUPPORT PROGRAM

Sponsored by the
AIR FORCE OFFICE OF SCIENTIFIC RESEARCH

Conducted by
UNIVERSAL ENERGY SYSTEMS, INC.

FINAL REPORT

A LOAD-BALANCING MODIFICATION TO A. GEORGE'S INCOMPLETE NESTED DISSECTION
ALGORITHM FOR MAPPING A COMPACT IRREGULAR QUADRILATERAL FINITE-ELEMENT
MESH ONTO THE HYPERCUBE PARALLEL PROCESSING ARCHITECTURE

Prepared By: Wayne R. Lundberg
Academic Rank: Graduate Student
Department and Physics Department of
University: Wright State University
Research Location: Air Force Wright Aeronautical Laboratories
Materials Laboratory (AFWAL/MLLM)
Wright-Patterson Air Force Base, Ohio 45433-6533
USAF Research: Dr. Harold L. Gegel
Date: September 2, 1986
Contract No: F49620-85-C-0013

A LOAD-BALANCING MODIFICATION TO A. GEORGE'S INCOMPLETE NESTED DISSECTION
ALGORITHM FOR MAPPING A COMPACT IRREGULAR QUADRILATERAL FINITE-ELEMENT
MESH ONTO THE HYPERCUBE PARALLEL PROCESSING ARCHITECTURE

by
Wayne R. Lundberg

ABSTRACT

Many types of problems can be analyzed using the Finite Element Method of simulating physical systems. The main emphasis of this work concerns modelling of plastic deformation via ALPID (Analysis of Large Plastic Incremental Deformation). In its current formulation ALPID uses a planar mesh of quadrilateral elements which are analyzed iteratively at each step. Each elemental stiffness matrix is generated and assembled into the global K-matrix, which is then inverted to find nodal velocities. These are compute-intensive steps and thus the total solution time is relatively long on a sequential machine. It is demonstrated herein that ALPID can be modified to process groups of elements, with each group on a separate processor. A general machine algorithm for dividing the mesh is given. It is required to equalize the work done by each processor, and to minimize the inter-processor communications. A resolution of these requirements for any FEM mesh is only possible using a combination of results derived from the references.

ACKNOWLEDGMENTS

Research sponsored by the Air Force Office of Scientific Research/AFSC, United States Air Force, under contract F49620-85-C-0013. The United States Government is authorized to reproduce and distribute reprints for governmental purposes notwithstanding any copyright notation hereon.

I would also like to thank whomever it was that approved my contract, Dr. S. M. Doraivelu and S. Martin for providing references, and Prof. Gegel for allowing me to glimpse the profound depth and diversity of his field.

I. INTRODUCTION:

I received my BS in Physics with honors from Case Institute of Technology, and am currently involved in the Selected Graduate Studies program at Wright State University. My thesis work is on Plasma Anodization of Silicon, and has no bearing on the current effort. I have long maintained an interest in the progress of foundational theoretical physics, and only this year persuaded Nobel Laureate Murray Gel-Mann that a logical connection between Haim Hariri's Rishon model and the Heterotic Superstring Theory must exist. Only a semi-formalized system exists yet, mainly due to severe academic structures and time obligations.

I was hired last year in this branch due to my strong mathematics background, during which I designed and implemented software for digitizing constitutive curves with relative efficiency. This information forms part of the data base for ALPID. This summer's work is ostensibly a continuation of ongoing work to modify and speed up ALPID's execution. Most of this type of work is carried out at Battelle or OSU. The processing group's main concerns are management of contracts to vendor industries and the development and propagation of the Dynamic Material Model under Dr. H. Geigel.

My education in math is of some value since deductive reasoning and graph theory play a vital role in partitioning the FEM mesh. My experience with deformation theory, together with Mr. Martin's knowledge of computational analysis, enabled us to find a workable means of parallelizing ALPID.

II. OBJECTIVES OF THE RESEARCH EFFORT: The work objectives are split in two different areas: assisting Dr. Jain in his work on precision forging; and studying the problems associated with parallelizing ALPID. This latter effort eventually resolved itself into two parts also: discussions with Steve Martin to document the relevant theory and the method of execution of ALPID; and paper simulation of machine-like algorithms for sectioning the FEM mesh. Some background information on other algorithms is provided in the references. I was unable to implement and verify the performance of the resultant decision structure.

III. PRECISION FORGING STUDY: Dr. Jain had designed and fabricated a segmented forging die which is versatile in that several different shapes can be forged. Different inserts are provided for H and T cross-sections. The current need is to run and document several forging trials. Lead billets were used due to the limitations of forging press capacity. We discussed the needs and design of a similar die for use with aluminum, which is the material of prime interest. It is considered that ALPID should be used to simulate aluminum forging to assure an adequate die design, since this is ALPID's function in industrial application. However, good estimates of total forging force in aluminum can be derived from the lead billet trials, since the mechanical properties of each are well known.

Two people are needed to conduct the forging trials. The die segments are bolted together with six large and several smaller bolts, to reduce the extrusion of metal through the joints. The large bolts require two people to tighten and loosen, and there is some time saved by

having two people to tighten the smaller ones. It is also helpful to have two people to observe the trial runs, for safety reasons. I suggested some ways to redesign the die which requires only one person to tighten the large bolts, and also pointed out that lead can be cast into billets more easily than machined to size.

We did some experimentation to find the best way to highlight the inscribed grids in the samples, resulting in the use of resin based graphite and MoS_2 lubricant. It adheres well and provides good contrast for photos. The actual test runs were Dr. Jain's responsibility, but I shall briefly describe how they were conducted. First, the samples were sprayed with Molykote 321R bonded lubricant to study the flow characteristics. The plotter was readied and zeroed, and appropriate settings were made on the control system. Then the sample was inserted in the die and the bolts tightened down. The alignment of the ram was checked; and if it was bad, it was fixed by loosening the die from the ram, inserting the upper die (plunger), tapping the fixture until it aligns, and then tightening. This procedure was rarely necessary. The ram was then raised until contact with the billet was made. Several of the tests were needed to determine a control setting which gives a finished part without overloading the press. Once this was established manually, a full series of tests was conducted automatically. I also photographed the deformed sample grids, as shown in Fig. 1.

Eventually, ALPID was used to simulate the forging trials, Fig. 2. It is difficult to obtain good results in this case due to the large amount of flow localization. The grids used are distorted beyond the

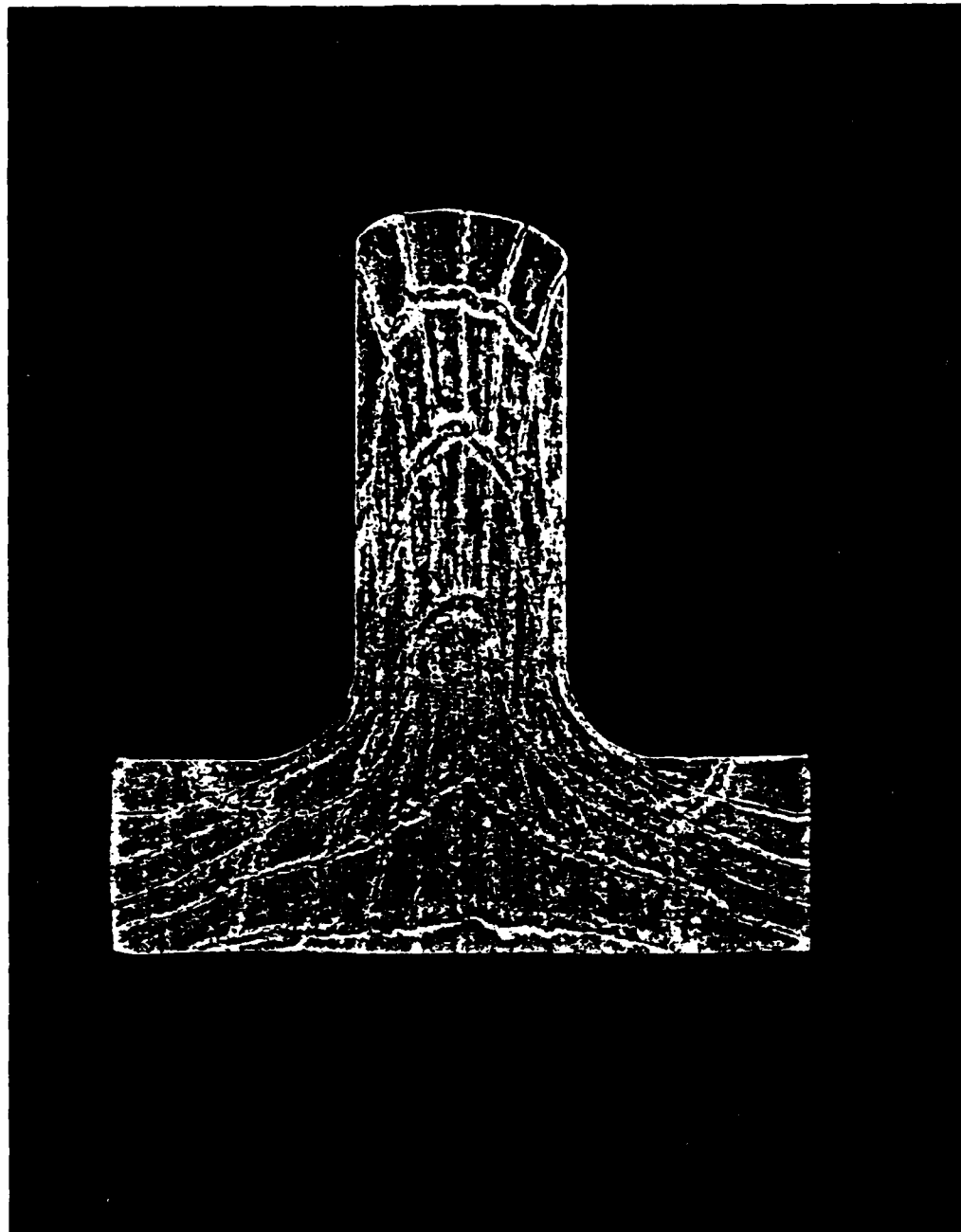


Figure 1. Example of Grid Distortion.

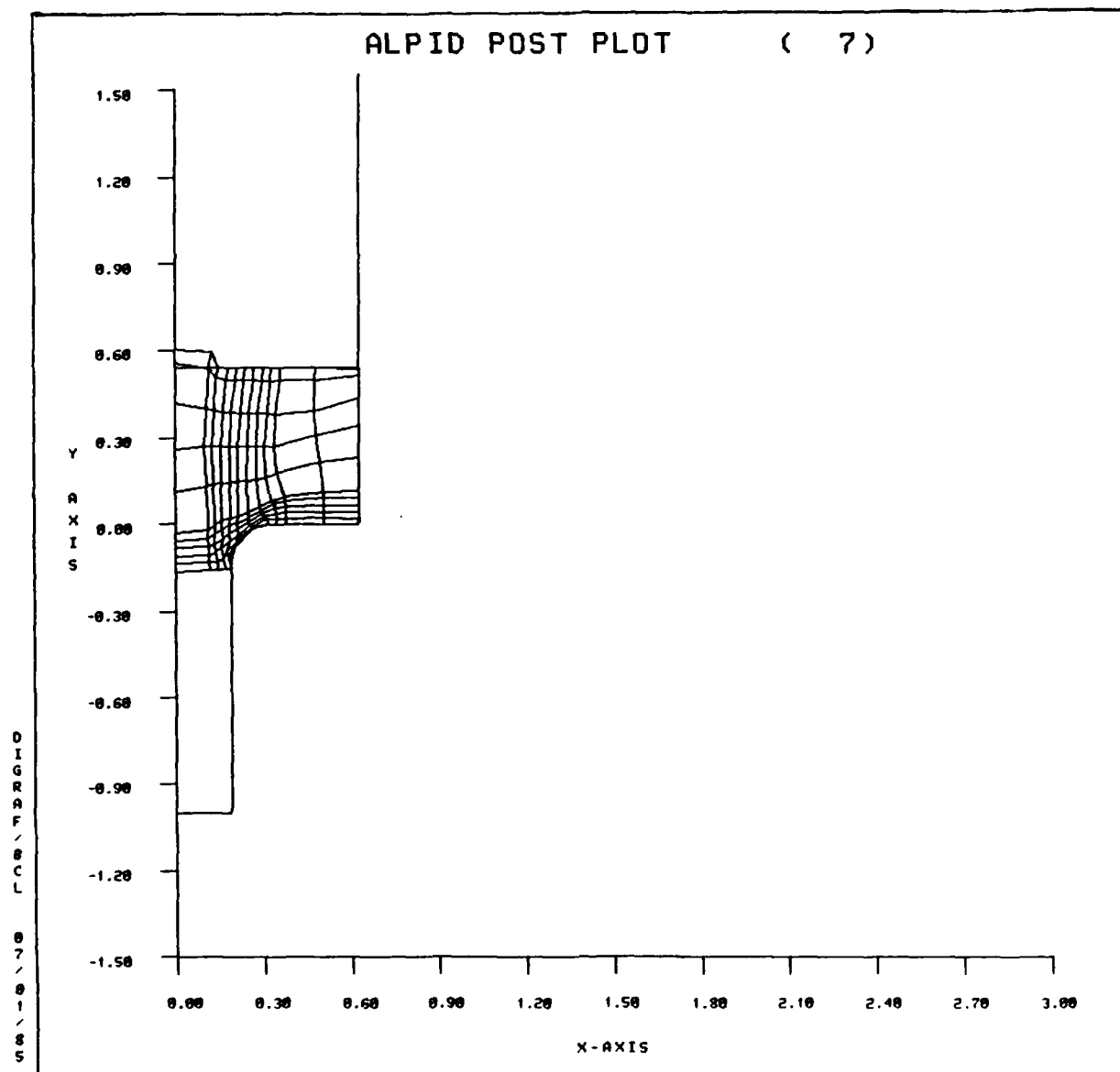


Figure 2. Flow Localization in Simulation.

limits of an accurate simulation. A remeshing routine is needed to extend beyond this limit. It is also projected that a point-tracing routine will be incorporated into ALPID for comparison to the actual deformed grid.

IV. DOCUMENTATION OF ALPID: In order to achieve any parallelization scheme, it is necessary to thoroughly understand ALPID's operation and data structures. Although some documentation exists, it is primarily user oriented and does not provide the information specifically needed. There are three areas which Steve and I concentrated on: flow charts, subroutine functions and data, and finding the places in the subroutines which have a parallel structure. Some (incomplete) flow charts were provided, which were corrected with a compiler listing and a complete record of storage requirements was obtained. Each processor's storage needs is then determinable, given the routines that must reside on every processor. This information is too lengthy to append to this report. Many COMMON blocks of data are used, and so a listing of the sizes of these COMMONs, and all the subroutines which call them, was made by searching through the source code. This list will help prevent any errors in the reorganization of the data structure. There are several important COMMONs which are altered repeatedly as the program progresses, /BLIN/ and / / for example. These were carefully documented by listing their contents, and examining how they are altered in each subroutine.

Each subroutine's function was ascertained, either by inspection or by understanding it's relation to the flow chart and the method used. Doing this gives some insight into how the program evolved, and may allow

some rewriting of the code to give slight improvements in it's sequential processing. In particular, the subroutine SOLVEQ had already been targeted for parallelizing and is under study at UES in Columbus. This involves changing the method used to analyze the K-matrix, from a sequential Gaussian Elimination method to the iterative Preconditioned Conjugate Gradient method (6). Many subroutines were shown to be directly involved in assembling the K-matrix, and so were examined carefully for possible means of parallelization.

It is important to briefly explain how the K-matrix is generated, and what it represents. Each node in the mesh has a strain-rate (velocity) and stress (force) associated with it. Combining the information from each node's nearest-neighbors and the new boundary conditions is required to update the local stress/strain-rate data. Each element has four nodes, which are then assembled into a local K-matrix (dyadic stress and strain-rate). Because of the nonlinearity of the global relationships (including constitutive relations, connectivity, geometry, thermal variations, localized flow, friction, dissipative structures, et al.), these local matrices must be assembled according to a convergent iterative scheme. Once a new global stress/strain-rate field has been arrived at, it is assembled into the global K-matrix. This matrix is very large and contains all the stress, strain-rate, temperature and connectivity information. It is also very sparse since each node is connected only to it's 3, 4, or 5 immediate neighbors.

The iterative procedure for K-matrix generation is contained under the subroutines NONLIN and NONLIB, in similar DO loops which process each

element in turn. Because often two materials are contained in a given extrusion (ex. powder and S.S. can), a provision has been included in the programming for different element groups. This provision will be taken advantage of in order to subdivide the mesh and process many element groups in parallel. For this reason, an accurate understanding of all the subroutines contained in the iterative loops are needed, so that all the appropriate information is available and is processed and distributed correctly. A detailed flow chart with corresponding COMMONs was constructed in order to show how the data is stored and processed. Although, ideally, the separator node information would always be updated before processing is done in an adjoining region; this is not vital, since only when the error norm is small will iteration cease. This may slow convergence slightly, but at least, each processor will not have to wait for new values.

V. SECTIONING THE FEM MESH: At this point, since we knew how the K-matrix was assembled, it is necessary to construct a mapping of the FEM mesh onto the processing architecture. UES had selected the hypercube processing architecture for various reasons, as discussed in (2,5). Several suggested means of mapping regular grids are given there also. The general problem of load balancing and minimizing data communication is not treated thoroughly yet. In (1, 8), nested dissection via the construction of a "level structure" is used in order to find the shortest separator in a general case mesh; which includes appendages, holes, and irregular elements. However, this method is not aimed at producing a balanced load, although in most compact cases it works quite well. Nested dissection is designed to speed up sequential processing by

optimizing the enumeration of nodes. The method developed in this paper might more properly be called "load-balanced incomplete nested dissection", or mesh partitioning. R. J. Lipton (4) has shown that for an N -node 2-D compact graph a separator of order \sqrt{N} is possible, giving two nearly equal pieces. This called the \sqrt{N} separator theorem. He refers to A. V. Aho (7) and the "divide and conquer" idea, which says that load balancing is essential for maximizing computational efficiency. Lipton's algorithm (9) is not altogether similar to the approach taken here. It is substantially more complex since it will handle a more general problem.

Some notation used in graph theory is helpful, but I must take the liberty of defining a few additional concepts. A graph is composed of a vertex set $X=\{x,\dots\}$ and an edge set $E=\{e,\dots\}$, and named $G(X,E)$. In this case, the vertex set is equivalent to the set of nodes, since no nodes will reside on the links between vertices. Since the FEM mesh being used is generated from a known boundary, the boundary nodes are known and named $B_1=\{b,\dots\}$. We shall also need the notation: forbidden node f , separator $S=\{s,\dots\}$. It is convenient to use the notation $\#X=N$ instead of a cardinality symbol. A subgraph of G is defined by $G'=(X',E')$ if and only if $X' \subseteq X$ and $E' \subseteq E$. A series of such subgraphs is called a "rooted level structure" $L(x)=\{L_0(x), L_1(x), \dots\}$ where $L_0(x)=\{x\}$, $L_1(x)=\text{Adj}(L_0(x))$, etc. Each level is comprised of nodes adjacent to the previous level and contains part of the original boundary. For this algorithm, it is necessary to define a "tier structure" in which each tier is comprised of the previous tier graph minus the boundary nodes; $T_2=(T_1-B_1)$, $B_2=\text{Adj}(B_1)$ and $b_2 \subseteq X_1$. This would be termed the "vertex induced subgraph of the

interior vertices" in graph-theoretic terminology. The tier structure is culminated by the uppermost connected tier graph T_m .

Occasionally a disconnected tier may arise, in which case it is easiest to compromise the load-balance by establishing a separator between the components. This situation may be identified by examining the connectivity of the "associated element graph", in which each element is associated with a vertex, and some vertex becomes inaccessible. Only when one component graph is much larger than the other will it be a disadvantage to make such a compromise. On the other hand, using the ultimate tier graph T_u will result in better load balance, but gives a longer, complex separator. Using T_u will not require any tests except for existence, $T_u \neq 0$. In either case, an initial guess at S is provided by Alan George's method (8). Note that the subroutines given may not be compatible with the format of the input mesh.

The following algorithm is essentially heuristic in nature, in that only those situations which occur in a typical ALPID mesh are taken into account. Rules which tend to optimize load balance and do not give long or complicated separators are favored.

1. Generate the tier structure T_1, \dots, T_u and boundaries B_1, \dots, B_u-1 .
2. Estimate T_u separator using George's method.
3. Separate B_n (or T_u), such that nodes on either side are nearly balanced, by number count. $\#X_a - \#X_b$ is minimized.
 - 3a. If no unique S results, compare unit length of S ; $\#S$ is minimized.
 - 3b. If no unique S , compare real path length and minimize.

- 3c. If no unique S , pick new s at random (first in file).
4. Remove gerrymanders, so that no boundary element has four nodes in S .
5. Attach B_n , repeat from 2. If $n=0$ continue.
6. Identify f to be the fourth node of any element which has three nodes in S . Label f such that $s \neq f$.
7. Repeat from 1 for each piece, to give 32 pieces.
8. When complete, assign S nodes to processors to give number balance.

Several paper simulations of this and similar algorithms were carried out, which indicated the need for rules such as the forbidden node rule. This rule prevents the separator from creating an element on one processor which requires that all its nodal information be transmitted from another processor, similar to the situation avoided in step 4. Using the minimum real path length tends to cause the separator to circumscribe regions of dense elements. It is much to our advantage to have regions of localized flow (dense elements) processed on one machine. If the time step used to calculate new deformation is determined by the magnitude of non-linear terms, then regions which undergo slower strain-rate will not require as many iterations to obtain convergence. Thus, if all the processors are kept synchronous, it may be possible to obtain a faster machine time than the 30X speed-up ideally anticipated simply by division of labor.

Since time was limited to examine this method, it is regrettably impossible to demonstrate actual machine operation results, times, or

storage requirements in this report. I would estimate that storage increases by $O(N \log N)$ and time by $O(N^{3/2})$, similar to (1). Resultant separated graphs are appended, showing that load-balancing of $\pm 15\%$ may be expected, Figs. 3, 4.

VI. RECOMMENDATIONS: This algorithm should be applicable to any planar irregular FEM mesh which has no appendages. During the course of my study I have noted the stated interest of the AFOSR in such partitioning methods as fundamental mathematical research. Clearly an extension to three dimensions is an interesting problem. It is also necessary at this point to write software to implement and extend these approaches.

VII. OTHER OBSERVATIONS: Several other possibilities for improving ALPID's applicability have been discussed: Automatic mesh generation is being added, which is already successful in NIKE2D, and SUPERTAB, etc., point-tracing methods for comparison to inscribed grids, etc. I also include the possibility of computing more intensely in high strain-rate regions as described above. Since complete information of constitutive behavior is available through the digitized form of these curves, I would recommend that these curves be used directly via USER6, instead of taking a non-elastic approximation and the added step of finding an equation which reproduces them in HARD1, etc. I also must note that I solicited the funding of rolling simulation studies from a private corporation since they had clearly expressed an interest in such results, in a job interview some months ago.

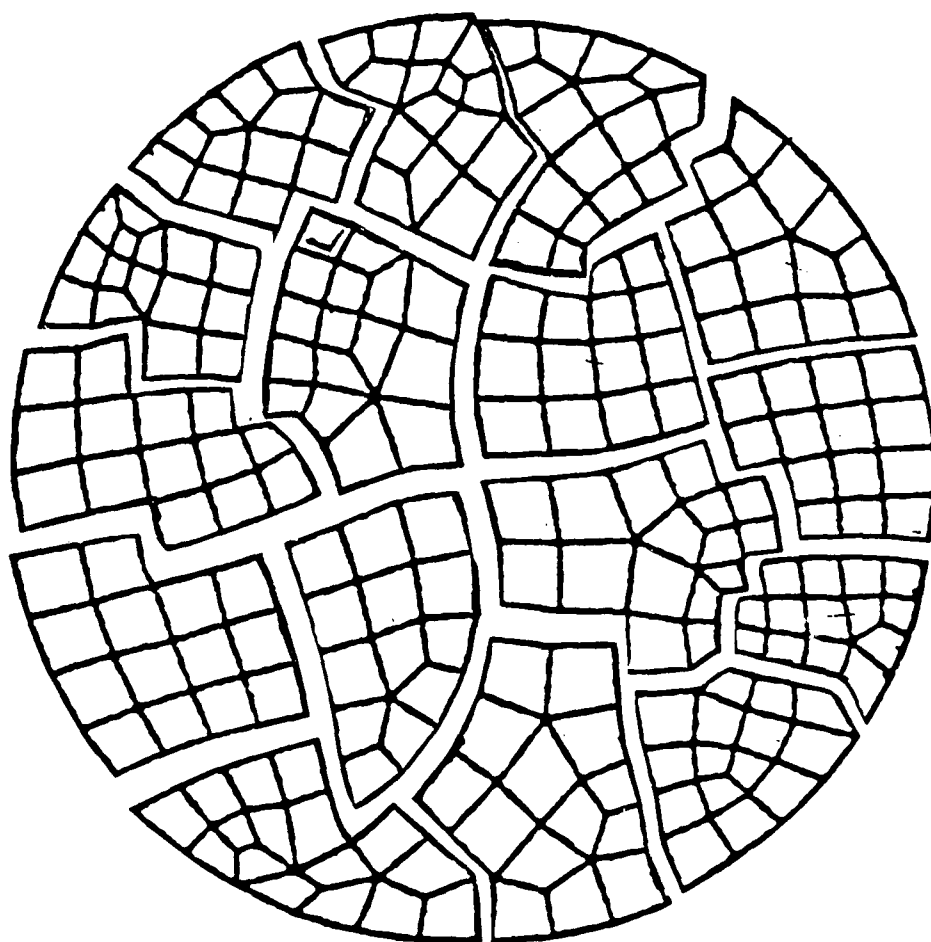


Figure 3. Approximate Result of Dissection Algorithm.

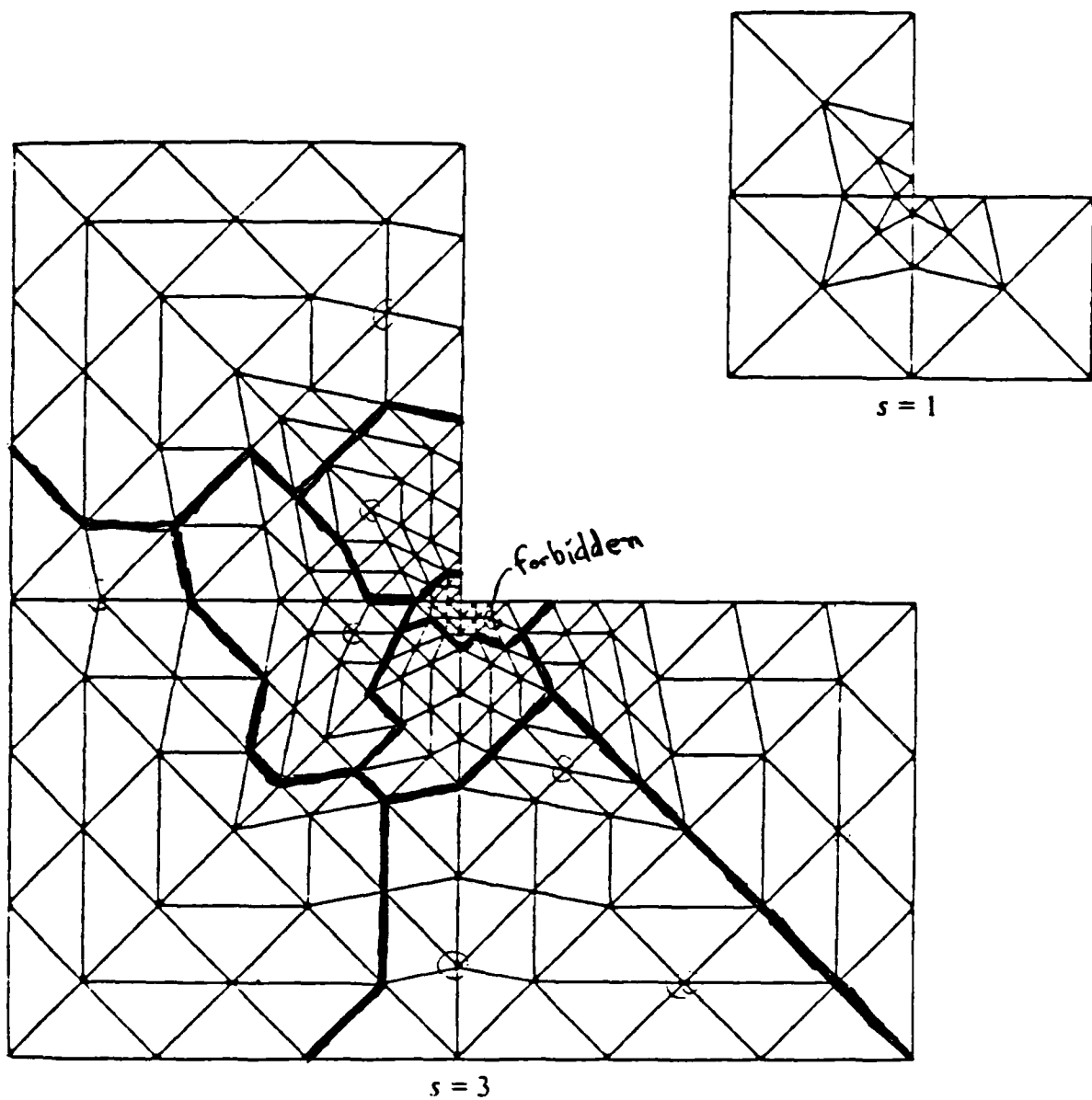


Figure 4. Graded L Mesh with Subdivision Factors $s = 1$ and 3, with an Example of Partitioning.

REFERENCES

1. Alan George and Joseph Liu, "An Automatic Nested Dissection Algorithm for Irregular FE Problems" SIAM J. Numer. Anal. 15(5), 1053 (Oct 1978).
2. F. Ercal, et al.; S. M. Doraivelu, "Parallel Computers for Finite Element Method Analysis," Proceedings 1986 International Joint PVP and Computer Engineering Division Conference and Exhibition July 1986, Vol. 2, p. 43-50.
3. Patrick Henry Winston, Artificial Intelligence, 2nd ed. Addison Wesley, 1984, p. 112.
4. R. J. Lipton, D. J. Rose, and R. E. Tarjan, "Generalized Nested Dissection" SIAM J. Numer. Anal. 16(2), 346 (Apr 1979).
5. S. M. Doraivelu, R. Srinivasan, et al., "Summary of Research Activities to Increase the Computational Performance of the ALPID FE Code" Advanced Simulation Language. for Process Modelling and Process Control of Metal Forming Operation. SBIR, Phase I Final Report, (UES-DoD-MLLM, Contract # F33615-84-C-5098).
6. T. F. Chan and F. Saied, "A Comparison of Elliptic Solvers for General Two-Dimensional Regions" SIAM J. Stat. Comput. 6(3), 742 (July 1985).

7. A. V. Aho, J. E. Hopcraft, and J. D. Ullman, The Design and Analysis of Computer Algorithms, Addison-Wesley, 1974.
8. A. George and J. W. Liu, Computer Solution of Large Sparse Positive Definite Systems, Prentice-Hall (1981) p. 62 and p. 270.
9. R. J. Lipton and R. E. Tarjan, "A Separator Theorem for Planar Graphs," SIAM J. Appl. Math. Vol. 36, No. 2, p. 177 (1979).
10. J. Roman, "Complexity Bounds for a Nested-Dissection Method," Number. Math. Vol. 47, p. 175, (1985).

1986 USAF-UES SUMMER FACULTY RESEARCH PROGRAM/
GRADUATE STUDENT SUMMER SUPPORT PROGRAM

Sponsored by the
AIR FORCE OFFICE OF SCIENTIFIC RESEARCH
Universal Energy Systems, Inc.

FINAL REPORT

Guide to ISPX:

The Interactive Signal Processing Executive

Prepared by: William A. Marty

Academic Rank: Master's Student in Electrical Engineering

Department and University: College of Engineering

School of Electrical Engineering and Computer
Science

The University of Oklahoma

Research Location: AFWAL Avionics Laboratory, AAWP-1

USAF Researcher: Dr James Tsui

Date: 28 July 1986

Contract No.: F49620-85-C-0013

Guide to ISPX:
The Interactive Signal Processing Executive
by
William A. Marty

ABSTRACT

The applicability of several spectral estimation techniques to the Digital Receiver problem was studied. Software tools for comparison of the characteristics of the different techniques were developed. Specifically, the Interactive Signal Processing executive was developed. ISPX was then used to run a large number of test cases on the various methods, and plot the results. Based on plots of these preliminary test cases, the kernel of a strategy for optimum detection and frequency estimation was developed. More work, using this kernel as a basis, will likely yield a more practical solution of the detection and estimation problem.

Acknowledgements

I would like to thank the Air Force Systems Command and the Air Force Office of Scientific Research for sponsorship of my research. To be most effective, research must be conducted in a proper environment, with the proper tools. The AFWAL Avionics Laboratory provided just such an environment. I would particularly like to thank Dr. James Tsui, Captain Thomas Vermillion, and Mr. Gerd Schrick of AFWAL/AAWP-1 for their guidance and friendship.

Finally, I would like to thank Dr. John Cheung, my graduate advisor, for many things. Among these are this patience and companionship. My summer would not have been the wonderful experience that it was without him.

I. Introduction

I received my B.S. in Electrical Engineering from the University of Oklahoma. I am currently studying towards an M.S. in E.E., with emphasis on signal processing, adaptive signal processing, and possible applications of artificial intelligence to problems in signal processing. Based on the recommendation of Dr. John Cheung, my graduate advisor, I was selected to work on the Digital Receiver problem with Dr. James Tsui of the Avionics Laboratory.

II. Objectives

The basic objective of my summer's research was to aid Dr. John Cheung in a preliminary study of the suitability of various spectral estimation techniques for the Digital Receiver problem.

My individual objectives were:

1. Develop software tools for generating data sets and applying these techniques.
2. Using these software tools, study the characteristics of the various techniques.
3. Recommend a possible solution of the detection and frequency estimation problem in the Digital Receiver.

III. Results

My main contribution was the development of the Interactive Signal Processing Executive software package. In order not to duplicate efforts with Dr. Cheung, his final report will discuss the findings of our preliminary study of spectral estimation techniques, and mine will cover the ISPX software package (see "A Preliminary Study of the

Characteristics of Various Digital Signal Processing Techniques in Receivers", 1986 USAF-UES Summer Faculty Research Program). In documenting ISPX, I produced an ISPX manual in two parts: User's Manual, and Programmer's Manual. I will present the User's Manual as my final report.

ISPX Manual

Introduction

The Interactive Signal Processing Executive (ISPX) software package is a flexible framework allowing the user to generate data sets, apply a variety of signal processing techniques to the data, and view the results graphically. As such, it provides a valuable tool for studying the characteristics of the techniques and their responses to particular classes of signals. The ISPX package also provides a kernel which can easily be expanded to include more techniques, as necessary.

This manual is divided into two segments. The first is a User's Manual which explains the operation of the program. The second segment is a Programmer's Manual describing the structure of the software and the steps necessary for addition or modification of subroutines. It is hoped that the ISPX software will continue to grow and become more comprehensive.

User's Manual

1.0 Getting Started:

The ISPX software currently resides on the AFWAL EWI VAX in the directory of Dr. James Tsui. After logging into Dr. Tsui's directory, type 'ispix' to run the program. The ISPX command screen should come up.

OPERATIONS	+ DATA ARRAYS	
a) Generate Data Arrays	+ 0)	
b) Choose PSD Method	+ 1)	
c) Plot an Array	+ 2)	
d) Print an Array	+ 3)	
e) File I/O	+ 4)	
f) Data Windowing	+ 5)	
g) Exit	+ 6)	
+++++	+ 7)	
	+ 8)	(Storage array info
	+ 9)	area)
	+ 10)	
(Operator Information Area)	+ 11)	
	+ 12)	
	+ 13)	
	+ 14)	
	+ 15)	
	+ 16)	
=====	+ 17)	
	+ 18)	
	+ 19)	
(Command Area)	+ 20)	

Figure 1. ISPX Command Screen

There are seven basic operations, labeled a-g, which are selected by typing their label in response to the 'Command?' prompt. Below the operation list is the operator information area. Information on program defaults, choices available to the operator, and error messages will appear in this area. Below the operator information area is the command area. The program will prompt the operator for input here.

Information on the data arrays is presented on the right side of the screen. Data arrays are the basic units on which ISPX operates. Each

data array is a structure with four fields: length, label, kind, and data. For example,

'0) one sine 64 cmplx'

indicates that array zero contains 64 complex data points, and has the label 'one sine'. The operator may work with any array at any time, or write over old arrays as needed.

ISPX is configured to run on two work stations, the VT100 and the VISUAL 102. After the command screen is established, the operator will be prompted for a terminal type, and should respond with a one-letter label as listed in the information area. To get hard copies of plots or printouts of data files, the operator should work on a VT100 terminal equipped with an LA50 printer.

Some of the signal processing algorithms in ISPX were written by Dr. Steven Kay. He has provided two data files, one real and one complex, to test his algorithms. These files are read into arrays 19 and 20 on program execution.

Once a terminal type has been chosen, the 'Command?' prompt will appear, and data processing may begin. Every attempt has been made to prevent an operator error from causing a fatal error which would halt execution. Generally, the best course following an error is to continue through to the end of the current sequence and then try again. In order to reduce input errors and operator tedium, ISPX incorporates a system of default values for common operations. In the course of performing an operation, the default values for that operation are written to the operator information area, and the prompt, 'Do you want to change any

default values?', is given. To leave the values unchanged, type 'n'. To change a default value, type its number, and following the prompt, 'New Value?', type its desired new value.

Each of the operations is described below.

2.0 Generating Data Arrays

ISPX allows the operator to generate data sets to simulate a wide variety of 'real' environments. To enter the data generation sequence, type 'a' (the quotes are to separate the character, do not type them) in response to the 'Command?' prompt. Following the prompts, enter an array number in which to store the data, and a label for the array. Then enter the desired number of data points. After the first time through the data generation sequence, the operator will have a choice of generating a new signal or taking more samples of the current signal. The data generation defaults will appear in the operator information area.

DATA GENERATION DEFAULTS

1	Waves:	1.0000
2	Complex Data:	0.0000
3	Sample Freq:	1.0000
4	Noise Amp:	0.0000
5	Overlap:	0.0000
6	Bits:	8.0000
7	Reference Amp:	1.0000
8	Quantize?:	1.0000

FOR WAVE 1

1	Frequency:	0.2000
2	Amplitude:	0.8000
3	Delay:	0.0000
4	Duration:	64.0000
5	Period:	128.0000
6	Chirp Rate:	0.0000

The first default is the number of waves. The operator may specify up to five waves. Each wave has its own set of default values, which will be covered below. Real data is generated by default, but complex data may be specified by changing the value of the complex data default to 1. The real data corresponds to the cosine of an angle, while the imaginary part corresponds to the sine of the same angle. The sample frequency may be

set to any real value. A value of 1.0 for the sample frequency allows the operator to deal in normalized frequency.

The noise amplitude default value controls the amplitude of white Gaussian noise in the signal. For a desired input signal to noise ratio, the noise amplitude required may be calculated as follows:

$$\text{NOISE AMP} = \frac{\frac{\sqrt{2}}{2} \text{ SIGNAL AMP}}{10^{\text{SNR}/20}}$$

Once a signal has been established, through the data generation sequence, more samples of that same signal may be taken. The overlap default controls overlapping of successive samples of the signal. If the overlap of the current signal is set to 32 points, and the operator asks for 64 points, the last 32 points of the last sample will be reproduced as the first half of the new sample, followed by 32 new points.

Defaults 6, 7, and 8 relate to quantization of the signal. If the quantization default is set to 1, then the signal values are quantized

according to the number of bits and reference amplitude specified. If it is set to 0, no quantization takes place. The quantizing routine divides the + reference amp to - reference amp range into $(2^{**} (\text{bits} - 1) - 1)$ intervals. The quantized data sample value is the center point of the interval into which the actual data sample value falls.

For each wave specified in default 1, a set of wave defaults appears in the operator information area. The first two of these, frequency and amplitude, may be set to any real value. Delay, duration, and period have to do with the pulse characteristics of the wave, as shown below. These also may be set to any real value. The period should be larger than or equal to the duration.

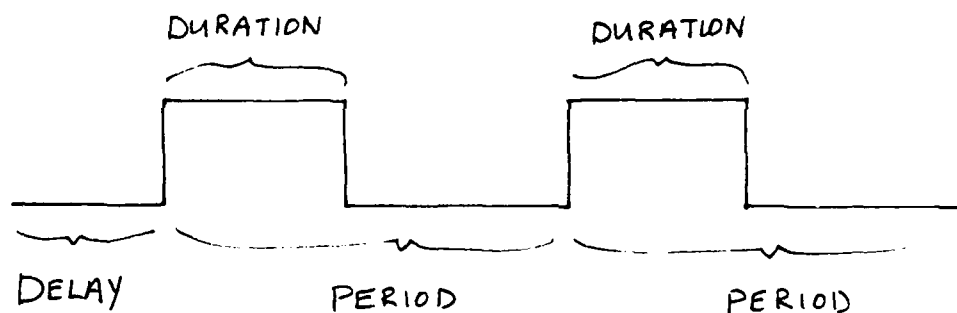


Figure 1. Pulse Specification

Lastly, the chirp rate may be specified. With a chirp rate of zero, the wave is a sinusoid. Care must be taken that the chirp rate and number of samples taken do not result in an end frequency greater than half the sampling frequency. When the chirp rate is non-zero, ISPX displays the effective end frequency of the signal in the operator information area before generating the data array. Hit return to continue. If the effective end frequency is greater than 0.48 times the

sampling frequency, the message 'Warning: Aliasing present' is displayed.

After all the defaults have been set, a white Gaussian random phase is selected for each wave, and the signal is generated.

3.0 Choosing a Power Spectral Density (PSD) Method

To choose a PSD method, type 'b' in response to the 'Command?' prompt. Currently, three categories of methods are available: Fourier, ARMA, and Adaptive.

3.1 Fourier Methods

METHODS

- a) Periodogram
- b) Blackman-Tukey

The choices here are the Periodogram and the Blackman-Tukey. The periodogram is a straight Fast Fourier Transform, while the Blackman-Tukey performs the FFT on the windowed autocorrelation sequence.

Defaults for the Periodogram are number of frequency samples and windowing. The number of frequency samples may be set to any integral power of two, larger than or equal to the length of the data sample, and less than or equal to 512. If larger than the data sample, the data array is padded with zeroes. By setting the windowing default to 1, the data set may be windowed. The window needs to have been previously established by the windowing option, and needs to be the same length as the data sample. Windowing occurs before padding with zeros.

There are three defaults for Blackman-Tukey: frequency samples, mode, and largest lag. Setting the mode to 0 gives the unbiased autocorrelation estimate, while 1 gives the biased estimate. The

operator may specify the number of lags used in calculating the autocorrelation estimate. Blackman-Tukey calls the windowing routine to get a window for the autocorrelation function. The operator may choose the window type and parameter, if any. For the number of points on the window, the operator should enter $2M+1$, where M is the number of lags used in BT.

3.2 ARMA Methods

METHODS

- a) Correlation
- b) Autocorrelation
- c) Covariance, Modified Covariance
- d) Burg
- e) RMLE
- f) ARMA PSD

A thru e are the AR methods currently available. ARMA PSD is the routine to generate the Power Spectral Density plot from the AR coefficients. At this point, since they are less desirable for the digital receiver, no MA or ARMA methods have been implemented.

The AR model order is a default for all the AR methods. It should be set to the largest lag desired in computing the AR coefficients. For the correlation and autocorrelation methods, the mode allows the operator to select either biased (1) or unbiased (0) estimates. For the covariance methods, the mode selects between covariance and modified covariance. The default is 1 for the modified covariance method.

With the standard PSD default set to 1, the AR coefficients generated are automatically fed to ARMA PSD. The number of frequency samples is set as above.

3.3 Adaptive Methods

METHODS

- a) ALC
- b) SER

The adaptive methods currently are Adaptive Line Cancellation and Sequence Regression. For both, the mode default selects either the enhancement mode (0), or the cancellation mode (1). Generally, the cancellation mode is more reliable, so the default is set to 1. The model order refers to the AR model order, as above. The constant default provides a convergence rate. Larger constants lead to faster convergence, but also to more error. A typical value is 0.01. The standard PSD and frequency samples defaults are the same as above.

4.0 Plotting Arrays

The most useful facet of ISPX is the plotting utility. The operator can plot any of the 20 arrays, or overlay plots of up to 4 of the arrays on a single plot. This is particularly useful for making comparisons between the various methods, or differing parameters within the same method. See the example plots at the end of the User's Manual.

PLOTTING DEFAULTS:

1	Top Half Only?	1.0000
2	Graphs?	1.0000
3	Set Range?	0.0000
4	Print Plot?	0.0000
5	PSD Scaling?	1.0000

In working with PSDs of real data, the graph is symmetric about zero frequency, so an option has been incorporated to plot only the top half of the frequency scale, thus giving twice the resolution. This is

selected by setting the top half only default to 1. The second default is the number of graphs to be displayed simultaneously. Up to four graphs may be displayed at once. To do this, however, the data arrays to be graphed must all be of the same length.

The plotting utility scans the data arrays, picking out extreme values to set the range of the y-axis. The operator may, if desired, override this and fix the range by setting the set range default to 1. To get a printout of the plot, the operator must be at a workstation equipped with an LA50 printer, and must set the print plot default to 1. Two types of x-axis scaling are available. For PSD plots, the x-axis scaling runs from -0.5 to +0.5 normalized frequency (analogous to $-\pi$ to $+\pi$). For any other type of plot, the x-axis is scaled for the number of points in the array. The default is set to 1 for PSD scaling.

After the default values have been adjusted as necessary, ISPX prompts the operator for the array(s) to be plotted. If there is more than one array to be plotted, enter the array numbers separated by commas. Next, the operator will be given the choice of linear scale or log scale for the dependent variable. Choose one or the other by entering its one letter label. For complex data, the complex absolute value is plotted.

If the operator has chosen to set the range, ISPX will ask for the max and min values of y. If the plot is to be printed out, ISPX will ask for a title for the plot and labels for the x and y axes. These titles may each be as long as 45 characters. If no titles are desired, respond to the prompts with carriage returns.

ISPX will clear the screen and plot the requested arrays on the screen. After examining the plots, hit the return key to move on. If

the operator has specified a printout of the plot, it will be dumped to the printer after this carriage return. If, for some reason, the plot on the screen is not as desired, type 'abort' before the carriage return. This will prevent the plot from being dumped to the printer.

5.0 Printing Arrays

To see the contents of any of the data arrays, select the 'Print an Array' operation by typing 'd' in response to the 'Command?' prompt. Arrays may be printed to the screen, or to an LA50 printer. Enter the one letter label of desired print destination. After printing to the screen, ISPX will wait for a carriage return before clearing the screen and re-establishing the command screen.

6.0 File I/O

A provision has been made to allow the operator to write a data array out as a file, or to read in a file as a data array. To do either of these, enter an 'e' in response to the 'Command?' prompt. Choose read or write by entering the corresponding one letter label displayed in the operator information area. Then enter the file name, with extension, and the array number. If the file to be read in wasn't generated by ISPX, care must be taken to put the data into the correct format. ISPX expects the data in complex format (a1, f10.7, a1, f10.7, a1).

7.0 Data Windowing

WINDOWS AVAILABLE:

- a) Kaiser-Bessel
- b) Hamming
- c) Cosine

Typing 'f' in response to the 'Command?' prompt invokes the windowing operation. Two modes are available. In the first, a window is generated and stored in an array. Then that window is applied to a specified data array and the result is stored in another array. The PSD methods may then be applied to this windowed array. In the second mode, the window is generated and stored in the specified array only. The first mode is the default mode. If the second mode is desired, set the window only default to 1.

Each window requires the user to specify the length. The Kaiser-Bessel and Cosine windows also require a parameter. For the KB window, alpha may be any real value (the suggested range is 3.0 to 10.0). As the value of alpha gets larger, the main lobe of the window gets wider and the highest sidelobe falls off farther. The parameter for the Cosine window should be an integer from 1 to 4. The value of alpha is the exponent of the cosine operation. For instance, the common cosine squared window is selected by entering an alpha of 2. The window array and the PSD of the window array may also be plotted.

8.0 Exiting

When processing is completed, respond to the 'Command?' prompt by typing 'g'. This returns control to the VMS operating system.

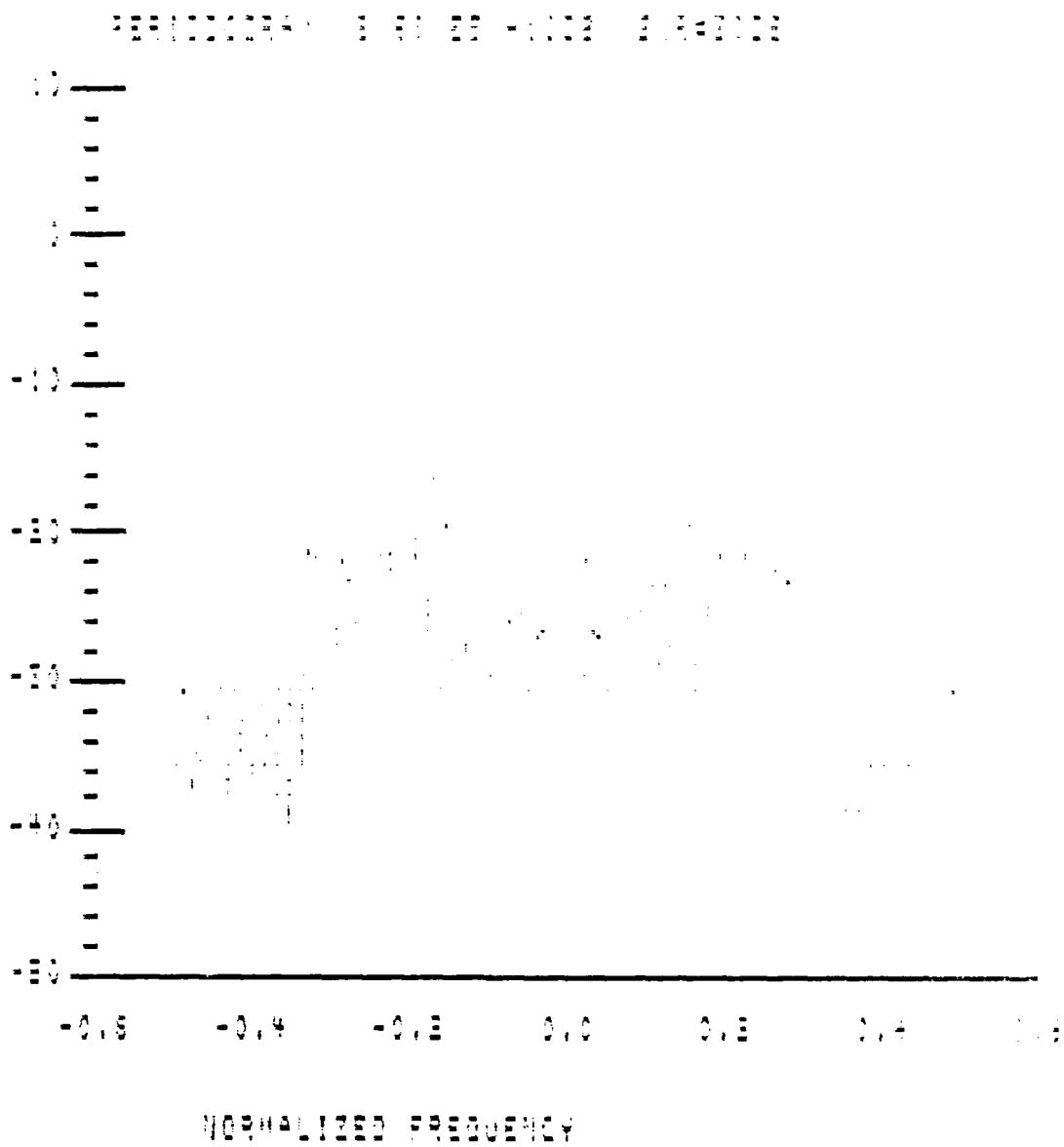


Figure 3. Example plot.

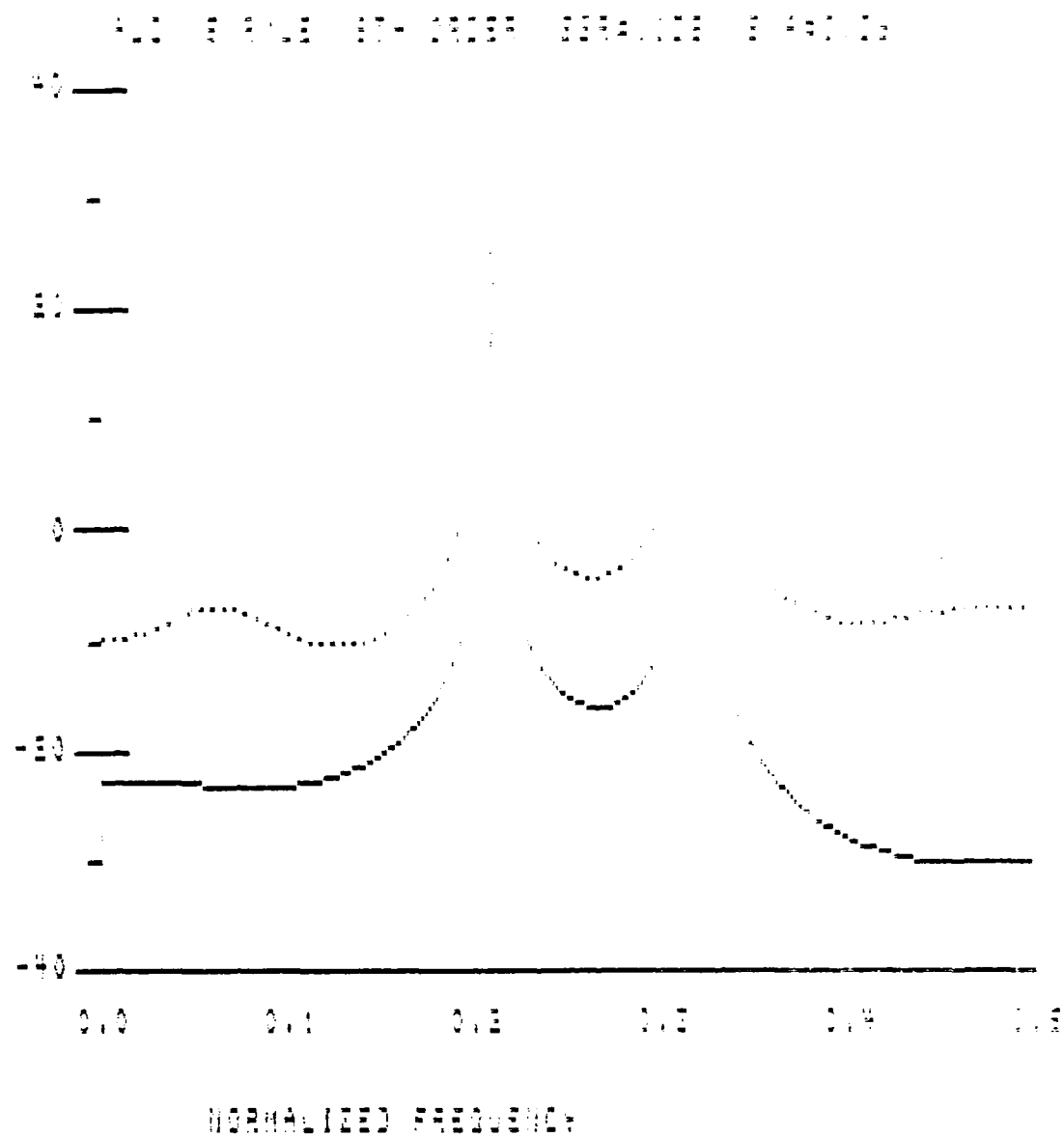


Figure 4. Example plot.

IV. Recommendations

A. ISPX is a useful tool for basic research into signal processing techniques. I feel that it should be augmented to keep pace with research on the Digital Receiver problem. To this end, I have written a programmer's manual which details the structure and contains pseudo-code listings for all the subroutines. Once a subroutine for a new algorithm has been written and tested, it is a simple matter to insert it in the ISPX framework.

B. A fundamental problem of the Digital Receiver is how to set a detection threshold. Dr. Cheung and I recommend an alternate approach. With AR methods, pole locations are assigned to periodicities in the input signal. As the model order rises beyond the number of distinct frequencies in the input, remaining poles are placed at random locations. By comparing pole locations of successively higher order methods, the poles corresponding to frequencies in the input signal remain in fairly constant locations, while the excess poles wander over the inside of the unit circle. Based on this, it should be possible to develop a highly reliable detection method. This would be an excellent area for further research.

V. References

Harris, Frederick J., "On the Use of Windows for Harmonic Analysis With the Discrete Fourier Transform", Proceedings of IEEE, Vol. 66, No. 1, January 1978, pp. 51-83.

Kay, Steven M., Modern Spectral Estimation: Theory and Application, Vol. 1, 1986 draft to be published by Prentice Hall.

Kay, Steven M., and Marple, Stanley Lawrence, Jr., "Spectrum Analysis - A Modern Perspective", Proceedings of IEEE, Vol 69, No. 11, November 1981, pp. 1380-1419.

Oppenheim, Alan V., and Shafer, Ronald W., Digital Signal Processing, (1975: Bell Telephone Laboratories and Prentice Hall).